

Metabolic fluxes of the model crop rice

Technological development and biological applications

Dissertation

zur Erlangung des Grades

des Doktors der Ingenieurwissenschaften (Dr.-Ing.)

der Naturwissenschaftlich-Technischen Fakultät III

Chemie, Pharmazie, Bio- und Werkstoffwissenschaften

der Universität des Saarlandes

von

M.Sc. Lisa Maria Dersch

aus Battenberg (Eder)

Saarbrücken, 03.05.2016

Tag des Kolloquiums:	26. August 2016
Dekan:	Prof. Dr.-Ing. Dirk Bähre
Berichterstatter:	Prof. Dr. Christoph Wittmann Prof. Dr. Elmar Heinzle Prof. Dr. Michael Schroda
Vorsitz:	Prof. Dr. Gert-Wieland Kohring
Akad. Mitarbeiter:	Dr. Björn Becker

Peer-reviewed publications:

Partial results of this thesis have been published in advance in the following papers and manuscripts. This was authorized by the Institute of Systems Biotechnology, Saarland University, represented by Prof. Dr. Christoph Wittmann:

1. Dersch, L.*, Beckers, V.*, Wittmann, C. (2015) Green pathways: Metabolic network analysis of plant systems. *Metabolic Engineering*, **34**: 1-24.
2. Dersch, L., Beckers, V., Rasch, D., Melzer, G., Bolten, C., Kiep, K., Becker, H., Bläsing, O. E., Fuchs, R., Ehrhardt, T., Wittmann, C. (2016) Novel Approach for High-Through-out Metabolic Screening of Whole Plants by Stable Isotopes. *Plant Physiology*. **171**: 25-41
3. Beckers, V., Dersch, L., Lotz, K., Melzer, G., Bläsing, O. E., Fuchs, R., Ehrhardt, T., Wittmann, C. (2015) *In silico* metabolic network analysis: Properties and natural boundaries of the plant *Arabidopsis thaliana*. *BMC Systems Biology*, submitted.
4. Beckers, V.*, Dersch, L.*, Rasch, D., Bläsing, O.E., Chen, X., Völler, G., Lotz, K., Fuchs, R., Ehrhardt, T. and Wittmann, C. (2015) Elucidating herbicide effect on rice crop metabolism by isotopically non-stationary ¹³C metabolic flux analysis. To be submitted.

Patent application:

Fuchs, R., Woiwode, O., Peter, E., Schön, H., Wittmann, C., Rasch, D., Beckers, V. and Dersch, L. (2014) Method and device for marking isotopes, WO2014/079696 A1.

Vorwort

Mein besonderer Dank gilt meinem Doktorvater Herrn Prof. Dr. Christoph Wittmann für die Überlassung des spannenden Themas, die zielführende wissenschaftliche Betreuung, die stetige Diskussionsbereitschaft, die vielen guten Ideen, Tipps und Ratschläge und den mitreißenden Enthusiasmus.

Herrn Prof. Dr. Elmar Heinzle danke ich für das Interesse an meiner Arbeit und die Zweitbegutachtung meiner Dissertation. Ein Dankeschön gilt auch Herrn Prof. Dr. Gert-Wieland Kohring für die Übernahme des Prüfungsvorsitzes, sowie Dr. Björn Becker als Vertreter des akademischen Mittelbaus.

Des Weiteren möchte ich mich ganz herzlich bei Veronique Beckers für die gute Zusammenarbeit während des Projekts, die Hilfe bei der Planung und Durchführung der Markierungsexperimente, sowie der mathematischen und visuellen Auswertung der Daten bedanken. Dein analytisches Denken, das „auf dem Boden bleiben“ und deine Zielstrebigkeit habe ich oft bewundert. Besonders bedanken möchte ich mich für das immer offene Ohr, die angenehme gemeinsame Zeit in Berlin und die vielen Diskussionen, die das Projekt sehr voran gebracht haben.

Ein großer Dank geht auch an Detlev Rasch für die Konstruktion der Markierungskammern, ohne die diese Arbeit nicht möglich gewesen wäre, sowie für die aktive Unterstützung bei den Markierungsexperimenten. Die scheinbar unendliche Fülle an Ideen und deren kreative Umsetzung haben diese Arbeit sehr bereichert.

Yvonne Göcke danke ich für die Hilfe bei der Methodenentwicklung und für die Beantwortung aller labor- und gerätetechnischen Fragen.

Ganz besonderer Dank gilt meinen Bürokollegen Bo, André, Rudolf, Anna und Veronique für die angenehme Arbeitsatmosphäre, die Hilfe bei großen und kleinen Problemen, die fachlichen und außerfachlichen Diskussionen, das gemeinsam Lachen und gegenseitig Aufmuntern und die Versorgung mit Kaffee, Energy Drink, Studentenfutter und Keksen.

Dem gesamten Team des IBVT und ISBio danke ich für die supertolle Arbeitsatmosphäre und die unvergessliche Zeit. Durch die vielen gemeinsamen Aktivitäten von Teamevent über Unisport bis Festival sind viele Freundschaften entstanden. Ihr habt die Zeit der Promotion zu einer der schönsten meines Lebens gemacht.

Dr. Thomas Ehrhardt und Dr. Ralf Looser danke ich für die Möglichkeit bei der Metanomics GmbH arbeiten zu können, für ihr Interesse am Projekt, ihren kritischen Input und das entgegengebrachte Vertrauen.

Besonderer Dank gilt Dr. Regine Fuchs für die Betreuung während des gesamten Projekts, insbesondere während meines Aufenthalts bei der Metanomics GmbH. Ich bedanke mich für die Gespräche auf Augenhöhe, das Interesse an meiner Person, die vielen Ideen und Ratschläge, die tatkräftige Unterstützung bei allen Experimenten und den Einsatz für mich. Deine Begeisterungsfähigkeit, deine positive Art, die hohe Problemlösefähigkeit, der wertschätzende Umgang mit Mitarbeitern und dein außergewöhnliches Engagement sind mir ein großes Vorbild.

Dr. Ginka Völler danke ich für die nette und unkomplizierte Aufnahme in ihre Arbeitsgruppe, die Diskussionsbereitschaft und die GC-MS Messungen.

Für die Mithilfe bei den Markierungsexperimenten danke ich Dr. Regine Fuchs, Marcel Schink, Detlev Rasch, Olaf Woiwode und Veronique Beckers. Bei Olaf Woiwode möchte ich mich zudem für das Sprühen während der Herbizidversuche bedanken. Marcel Schink danke ich für die netten Gespräche, die Hilfsbereitschaft und die vielen kreativen Ideen.

Für die Pflanzenanzucht und die Beantwortung aller, die Phytohalle betreffenden Fragen, bedanke ich mich ganz herzlich bei Olaf Woiwode und Florian Hundert. Bei Dr. Enrico Peter bedanke ich mich für den Input bezüglich des experimentellen Designs und der Hilfe beim Troubleshooting.

Für die GC-MS Messungen und Auswertungen bedanke ich mich bei Dr. Ginka Völler, Antje Bollwahn und Peter Driemert. Für die LC-MS/MS Analytik danke ich Dr. Jonny Nachtigall und Janine Notzke. Des Weiteren danke ich Georg Richter und Martin Dostler für die Hilfe bei der LC-MS/MS Methodenentwicklung. Dr. Jürgen Kastler und René Müller, sowie Horst Becker von der BASF SE in Limburgerhof danke ich für die IRMS Messungen. Bei Peter Eilert möchte ich mich für die Hilfe bei der Inbetriebnahme des Online-MS bedanken.

Ich danke dem gesamten Team der Probenvorbereitung für die große Hilfsbereitschaft, die vielen Tipps und die Mithilfe.

Allen Mitarbeitern der Metanomics GmbH danke ich ganz herzlich für die Integration in das Team, die gute Arbeitsatmosphäre, das Interesse an meiner Arbeit und die uneingeschränkte Hilfsbereitschaft. Vielen Dank an das Team der GC für die nette Aufnahme in ihre Arbeitsgruppe und die Bereitstellung des Arbeitsplatzes.

Meiner Familie danke ich dafür, dass sie immer an mich geglaubt und mich bei allem unterstützt hat. Vielen Dank für die aufmunternden Worte, die unendliche Geduld und das Erden.

Nico, dir danke ich dafür, dass du immer für mich da warst, mich in allem unterstützt, immer an mich geglaubt und oft zurückgesteckt hast. Deine positive und ruhige Art hat mich oft auf den Boden der Tatsachen zurückgeholt.

Table of contents

Summary	1
Zusammenfassung	2
1 Introduction	3
2 Objectives	5
3 Theoretical Background	6
3.1 Green biotechnology - towards improved plant lines.....	6
3.2 Model crop rice (<i>Oryza sativa</i>)	9
3.2.1 Growth and development	10
3.2.2 Morphology	12
3.2.3 Metabolic routes in central carbon metabolism.....	14
3.2.4 Stress resistance.....	18
3.3 Isotopic labeling studies for plant flux analysis.....	20
3.3.1 Experimental considerations for plant cell and tissue cultures	23
3.3.2 Experimental considerations for whole plants.....	25
3.3.3 ¹³ C Labeling analysis.....	26
3.3.4 Assimilation, translocation and biosynthetic fluxes	28
3.3.5 Intracellular fluxes in heterotrophic plant systems	29
3.3.6 Intracellular fluxes in autotrophic plant systems.....	31
4 Materials and Methods	33
4.1 Chemicals.....	33
4.2 Plant growth	33
4.2.1 Plant material	33
4.2.2 Media	33
4.2.3 Growth conditions	33
4.3 Isotopic labeling experiments with ¹³ CO ₂	34
4.3.1 Pulse-chase labeling experiments.....	35
4.3.2 Dynamic labeling experiments.....	36
4.4 Analytics.....	38
4.4.1 EA-C-IRMS and C/N elemental analysis of whole plant material	39
4.4.2 GC-C-IRMS for isotopic enrichment detection.....	39
4.4.3 LC-MS/MS analysis of sugar phosphates and organic acids	41
4.4.4 GC-MS analysis of sugars, sugar phosphates, amino and organic acids.....	42

4.4.5	Determination of biomass composition	42
4.5	Calculation and data processing	44
4.5.1	Calculation of ¹³ C and ¹⁵ N enrichment	44
4.5.2	Data correction for natural isotopes	44
4.5.3	Calculating the absolute isotopic enrichment.....	45
4.5.4	Determination of C/N elemental composition.....	45
4.5.5	Determination of root-to-shoot ratio and translocation flux.....	45
4.5.6	Determination of biomass formation rate	46
4.5.7	Determination of carbon export to the root	47
4.5.8	Statistical analysis.....	47
4.5.9	Metabolic network reconstruction and flux calculation	47
5	Results and Discussion	49
5.1	Pulse-chase experiments as fast screening tool for plant phenotypes	50
5.1.1	Reactors for pulse-chase labeling studies	50
5.1.2	Quantification of ¹³ C and ¹⁵ N amino acid enrichment using GC-C-IRMS	54
5.1.3	Carbon and nitrogen metabolism in rice seedlings	55
5.1.4	Carbon and nitrogen metabolism in adult rice plants	64
5.2	Non-stationary metabolic flux analysis of illuminated rice seedlings.....	71
5.2.1	Automated flux box for dynamic labeling studies	71
5.2.2	Data acquisition and assessment of data quality	75
5.2.3	Anabolic nature of rice seedling metabolism displays high demand for building blocks, supporting growth and development.....	99
5.2.4	Imazapyr-destructive effect due to altered carbon/nitrogen metabolism with a supposed regulatory role of intracellular pyruvate	106
6	Conclusions and Outlook	116
7	Abbreviations	118
8	References.....	120
9	Appendix.....	142

Summary

Metabolic engineering of plants to ensure global food supply and to produce valuable compounds is challenging as plant metabolic networks are highly complex and cellular functions largely unknown. In the present work, a comprehensive labeling-based flux analysis toolbox was established for *in vivo* analysis of whole plant metabolism under physiologically relevant conditions. This method was used to analyze the metabolism of rice, an agriculturally relevant crop plant. The studies revealed fundamental characteristics of photoautotrophic metabolism, specific features of salt stress response and the mode-of-action of a broad-spectrum herbicide. The analysis of untreated rice seedlings emphasized the anabolic nature of photosynthetic metabolism and revealed a necessity for futile cycling to dissipate excess energy. The herbicide imazapyr was found to inhibit the biosynthesis of branched-chain amino acids and caused accumulation of storage carbohydrates, increased protein turnover and enhanced futile cycling. Decreased flux into biomass suggests a switch from anabolic growth to metabolic maintenance for plant survival. This study revealed the incredible potential of the established toolbox to examine metabolic phenotypes at the systems level and therefore is of considerable interest for plant physiologists and green biotechnology.

Zusammenfassung

Metabolic Engineering von Pflanzen zur Sicherung der Nahrungsmittelversorgung und zur Wertstoffsynthese ist anspruchsvoll, da metabolische Netzwerke von Pflanzen hochkomplex und zelluläre Funktionen weitgehend unbekannt sind. In der vorliegenden Arbeit wurde ein umfassender Ansatz der metabolischen Flussanalyse zur *in vivo* Untersuchung ganzer Pflanzen unter physiologisch relevanten Bedingungen etabliert. Die Technologie wurde eingesetzt um den Stoffwechsel von Reis, einer bedeutenden Nutzpflanze, zu untersuchen. Die Studien legten grundlegende Eigenschaften des photoautotrophen Stoffwechsels, spezifische Eigenschaften der Stressantwort, sowie den Wirkmechanismus von Herbiziden offen. Die Analyse unbehandelter Reiskeimlinge zeigte eine anabole Form des lichtabhängigen Stoffwechsels und die Notwendigkeit für Substratkreisläufe zur Umwandlung überschüssiger Energie. Es konnte beobachtet werden, dass das Herbizid Imazapyr die Biosynthese verzweigtkettiger Aminosäuren inhibierte und zu einer Akkumulation von Speicherkohlenhydraten, gesteigerten Proteinumsatzraten und erhöhten Flussraten durch Substratzyklen führte. Der verminderte Fluss in die Biomasse spricht für einen Wechsel von anabolem Wachstum hin zum Erhalt lebenswichtiger Stoffwechselfunktionen. Diese Studie zeigte das außerordentliche Potenzial des etablierten Ansatzes für die Analyse metabolischer Phänotypen auf Systemebene und ist deshalb von erheblichem Interesse für Pflanzenphysiologen und die grüne Biotechnologie.

1 Introduction

Genetic engineering of crop plants allows to enhance plant resistance towards different biotic and abiotic stresses, and is applied to improve nutrient quality and quantity, which is particularly important considering the increasing global demand for food, feed and fiber. Beyond, engineered plants are also useful sources to derive valuable compounds such as biofuels (Furtado et al., 2014), spider silk (Weichert et al., 2014) and bioplastics (Bohmert-Tatarev et al., 2011), as well as high-value vaccines, hormones and antibodies for therapeutic use (Basu et al., 2010; Ahmad et al., 2011). Plants as production system bear several attractive properties, including low production cost, easy scale-up and product safety, which is mainly due to the fact that they can live on carbon dioxide and sunlight as sole substrates and possess the ability to synthesize glycosylated proteins (Fischer and Emans, 2000; Sharma and Sharma, 2009).

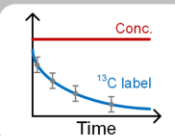
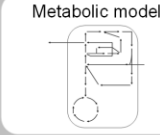
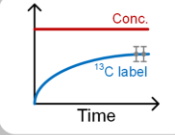
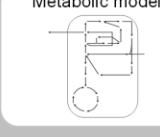
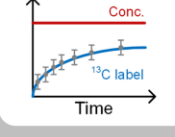
Type of analysis	Calculations	Isotopic and metabolic stationarity	Advantages	Disadvantages
Pulse-chase	Algebraic equations $\delta = \left(\frac{R_{\text{sample}} - R_{\text{standard}}}{R_{\text{standard}}} \right) \cdot 1000$ $AP = \frac{100 \cdot R_{\text{sample}}}{1 + R_{\text{sample}}}$		<ul style="list-style-type: none"> - suitable for autotrophs - fast screening - no computation - little experimental effort 	<ul style="list-style-type: none"> - no deduction of fluxes - not predictive
¹³ C MFA	Metabolic model 		<ul style="list-style-type: none"> - high accuracy - predictive - resolution of reversible fluxes - large networks 	<ul style="list-style-type: none"> - only applicable to heterotrophic cultures - time-consuming
¹³ C INST-MFA	Metabolic model 		<ul style="list-style-type: none"> - detailed information - predictive - suitable for autotrophs - short experiments 	<ul style="list-style-type: none"> - high computational/ experimental effort

Figure 1. 1 Approaches for label-based plant metabolic analysis

Principal characteristics of different label-based approaches for the analysis of plant metabolism, ranging from simple pulse-chase experiments for qualitative studies to isotopically non-stationary metabolic flux analysis for more comprehensive investigations.

Without doubt, tailored engineering approaches require a good knowledge of the underlying plant metabolic pathways and regulatory processes of plant biochemistry. Due to their highly complex, compartmented metabolic networks, many plant cellular functions are still unknown. This explains the strong interest in tools and technologies to analyze plants on the systems level. Particularly, plant analysis on the level of metabolic pathways and intracellular fluxes,

has predictive power regarding potential targets for metabolic engineering (Kruger and Ratcliffe, 2009; Shachar-Hill, 2013). Isotopic tracers are used since decades to track metabolite flow *in vivo*, thereby elucidating fundamental plant metabolic functions. Tracer experiments can greatly differ in complexity, ranging from simple pulse-chase studies to advanced dynamic approaches (Figure 1. 1). Simple tracer studies require less time and computational effort than model-based approaches and are very potent as fast screening tool (Schwender, 2008). More comprehensive approaches integrate isotope labeling studies with network modeling, thereby allowing for plant metabolic fluxes to be inferred with high precision and resolution. The most widely used technique is ^{13}C metabolic flux analysis (^{13}C MFA), in which fluxes are deduced from an isotopic steady-state labeling pattern after metabolic stationarity has been reached. This technique is, however, only applicable to heterotrophic organisms, as photoautotrophs assimilate carbon from the one carbon source CO_2 . Labeling to isotopic steady-state would hence result in uniform and uninformative labeling (Nöh and Wiechert, 2011). Isotopically non-stationary approaches were developed to overcome the described shortcomings of steady-state MFA in autotrophic organisms (Allen et al., 2009a). In such approaches, labeling time-courses are monitored following a change from unlabeled to labeled substrate (Roscher et al., 2000), while the system is at metabolic steady-state. Two recent studies with whole *Arabidopsis* plants reveal that non-stationary MFA approaches are a very promising tool to investigate photoautotrophic metabolism under physiologically relevant conditions in order to gain deeper insight into plant metabolic functions and thereby help to guide rational engineering for improved plant performance (Szecowka et al., 2013; Ma et al., 2014).

2 Objectives

The aim of the present work was to establish a comprehensive ^{13}C -based metabolic flux analysis toolbox for detailed *in vivo* analysis of whole rice (*Oryza sativa*) plants under physiologically relevant conditions. The toolbox should consist of a pulse-chase approach for fast screening of metabolic phenotypes, and a more sophisticated isotopically non-stationary metabolic flux analysis workflow for detailed analysis of the most promising phenotypes. Special emphasis should be given to the development of the experimental setup, involving challenges associated with the autotrophic nature of plants, i.e. $^{13}\text{CO}_2$ tracer application at natural abundance and subsequent analytics with high precision and sensitivity.

The developed toolbox should subsequently be applied to elucidate specific features of rice plant metabolism. Pulse-chase studies should be conducted to compare rice plants of different developmental stages, concerning assimilation, translocation and incorporation of label into protein amino acids after single or double labeling with $^{13}\text{CO}_2$ and $^{15}\text{NH}_4\text{NO}_3$. Thereby, the interaction of C/N metabolism and relevant sink:source relations of individual plant organs should be described. Furthermore, stress-induced phenotypes should be investigated by exposing rice seedlings to high salinity and a broad-spectrum herbicide. Untreated and herbicide-treated rice seedlings should furthermore be analyzed by the more comprehensive ^{13}C INST-MFA approach to provide a detailed flux map of shoot metabolism under normal growth conditions and in response to herbicide stress. The latter should elucidate the mode-of-action of the applied herbicide at the systems level, thereby enhancing the understanding of herbicide-induced plant death.

The present work ultimately aimed at providing plant metabolic engineers with a flexible, sophisticated toolbox to analyze plant metabolism.

3 Theoretical Background

3.1 Green biotechnology - towards improved plant lines

Plants played a key role in the evolution of life on earth by enriching the atmosphere with oxygen in a process called photosynthesis. Hereby, carbon dioxide and light energy are converted into oxygen and carbohydrates, which makes plants the ultimate source of energy and organic material. Plants and their products are used as origin of food, feed and fiber and furthermore provide mankind with fossil fuels and medicine. Plants are cultivated since 8000 BC (Zohary et al., 2012) and conventional breeding as well as genetic engineering have since been extensively used to boost productivity and enhance plant fitness (Harlan and Zohary, 1966; Fraley et al., 1983). Conventional breeding, i.e. the hybridization of two varieties carrying useful gene alleles, brought about many new cultivars superior to wild types in terms of stress resistance and yield potential. However, such complex multigenic traits are often difficult to address by conventional breeding. In addition, the technique is limited by the availability of desirable genes in crossable gene pools (Basu et al., 2010). The directed transfer of desired traits via genetic engineering allows the use of genes from intra-kingdom species and even non-plant species as well as synthetic genes (Takeda and Matsuoka, 2008). Due to extensive research, today, all major crop plants can be genetically modified (Ji et al., 2013).

The most important desire for agriculture is yield increase. The consistently growing world population and limited arable land cause a major threat to adequate food supply and call for improved crops to optimize the use of existing crop areas and efficiently utilize wastelands (Khush, 2003; Takeda and Matsuoka, 2008; Ahmad et al., 2011). During the last 50 years, the world cereal production has increased by 190% (FAO, 2015a) while the arable land only expanded by 9% (FAO, 2015b). This yield increase, in the course of the so called 'green revolution', was only possible by introducing semi-dwarf cultivars combined with high applications of fertilizers and pesticides, which caused severe ecological problems. These approaches of the green revolution are currently reaching their biological limits (Long et al., 2015), while the world population continues to grow by almost 80 million people per year, of which 95% are caused by developing countries (UN Department of Economic and Social Affairs, 2015). Due to rising standards of living, especially in Asia, more meat, eggs and milk are consumed, which further enhances the demand for grains as livestock feed (Khush, 2003). Until 2050, the world population will have reached 9.1 billion, raising the global food demand by 60% (Alexandratos and Bruinsma, 2012).

The genetic yield potential (Y_p) of a crop plant under optimal environmental conditions is the product of the radiation received over the growing season (Q), light interception efficiency (ϵ_i), photosynthetic efficiency (ϵ_c) and harvest index (ϵ_p):

$$Y_p = Q * \epsilon_i * \epsilon_c * \epsilon_p \quad (\text{Eq. 3. 1})$$

During the green revolution, conventional breeding enhanced light interception efficiency and harvest index to almost reach their biological limits through modification of the canopy architecture and by the introduction of dwarfing phenotypes, respectively (Long et al., 2015). Photosynthetic efficiency, however, remains at a low level, which makes it a promising target to further increase yield using genetic engineering (Long et al., 2006; Peterhansel et al., 2008; Zhu et al., 2010). Research in this field is mainly focused on introducing a CO₂ concentrating mechanism (CCM), e.g. C4 photosynthesis (Karki et al., 2013) or cyanobacterial and algal CCMs (Price et al., 2013; Rae et al., 2013; McGrath and Long, 2014), into C3 crops to enhance the efficiency of ribulose 1,5-bisphosphate carboxylase/oxygenase (RuBisCO) and reduce carbon and energy loss by photorespiration. Furthermore, modification of RuBisCO (Lin et al., 2014), introduction of a photorespiratory bypass (Kebeish et al., 2007), the overexpression of sedoheptulose 1,7-bisphosphate (Rosenthal et al., 2011) and the enhanced synthesis of starch as transient sink (Gibson et al., 2011) resulted in enhanced photosynthetic efficiency.

In addition to directly enhance crop yields, efforts have been made to reduce yield loss. Due to biotic and abiotic stresses, crop losses are reaching 30-60% each year (Dhlamini et al., 2005). Present-day crop protection strategies involve genetic modification of plants towards enhanced resistance against unfavorable environmental conditions, thereby reducing the need for fertilizers, improving yields and reducing economic loss. A prominent example is the transfer of endotoxin-coding genes from the soil bacterium *Bacillus thuringiensis* (Bt) into crop plants to provide them with resistance against insect predation (Betz et al., 2000). Furthermore, plants have been engineered to withstand the infection by fungi (Chen et al., 2010; Brunner et al., 2011; Mao et al., 2013), viruses (Cao et al., 2013; Shimizu et al., 2013; Chen et al., 2014) and bacteria (Tian and Yin, 2009; Schoonbeek et al., 2015), as well as several abiotic stress factors like drought (Vendruscolo et al., 2007; Liu et al., 2009; Jeong et al., 2010), salinity (Hoang et al., 2015; Wang et al., 2015), flooding (Xu et al., 2006), extreme temperature (Sui et al., 2007; Byun et al., 2015) and oxidative stress (Long et al., 2014; Han et al., 2015).

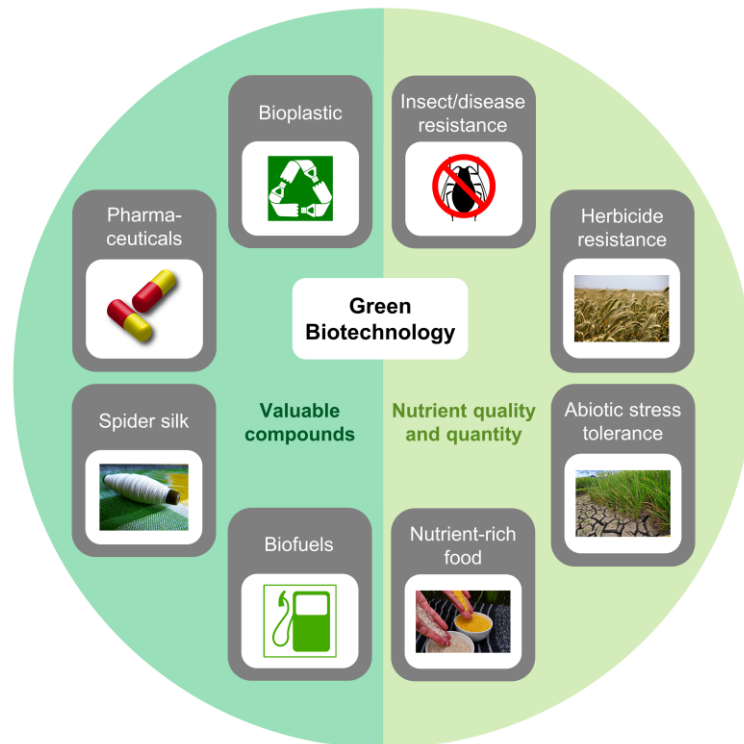


Figure 3. 1 Fields of application of green biotechnology

Fields of application of green biotechnology can be subdivided into the production of valuable compounds and the enhancement of nutrient quality and quantity. Valuable compounds produced in plants are, for example, bioplastics, biofuels, pharmaceuticals, like vaccines, hormones and antibodies, as well as spider silk, used as source of clothing and textiles. Yield increase is achieved by mediating insect/disease and herbicide resistance, as well as abiotic stress tolerance. Nutrient quality is enhanced through biofortification of food crops with essential micronutrients. (Figure licenses: 'Golden Rice' and 'CHR_0516, Drought research at IRRI' by International Rice Research Institute (IRRI), licensed under CC BY 2.0. 'Bug icon - Noun project 198' by The Noun Project, licensed under CC BY 3.0 via Wikimedia Commons. All others are created by pixabay.

Biofortification, the improvement of the nutritional content of crops, is another anticipated goal of plant genetic engineering. Staple crops are a major food source of mankind, but are usually deficient in micronutrients. Rice endosperm, for example, is deficient in iron, folate, provitamin A and vitamin E. Vitamin A plays an important role in vision, immune response, reproduction and development (Beyer, 2010). Worldwide, 250 million preschool children and a substantial number of pregnant women suffer from vitamin A deficiency, leading to eye defects, followed by blindness or even death, if untreated (WHO, 2015). As the genes, encoding the vitamin A biosynthetic pathway, are not available in the rice gene pool, conventional breeding is no option to fortify rice with vitamin A (Beyer, 2010). Genetic engineering was therefore applied to create a rice line, capable to accumulate high amounts of provitamin A in the endosperm, giving it a yellow color, hence called 'golden rice' (Ye et al., 2000; Beyer et al., 2002). Because rice is grown and consumed worldwide, golden rice has the power to reach many people, even those who cannot afford other sources of vitamin A. To

alleviate malnutrition, crops have furthermore been nutritionally enhanced with micronutrients like folate (Storozhenko et al., 2007), iron (Borg et al., 2012; Masuda et al., 2013) and zinc (Johnson et al., 2011) as well as with essential amino acids (Lee et al., 2003; Huang et al., 2006; Wakasa et al., 2006; Houmard et al., 2007).

Besides enhancing nutrient quality and quantity, engineered plants are also valuable sources to derive high-value recombinant proteins like vaccines, hormones and antibodies for therapeutic use (Basu et al., 2010; Ahmad et al., 2011). Compared to mammalian and bacterial cell systems, the production of pharmaceuticals in plants, called biopharming, bears several advantages. Plants can produce a vast variety of recombinant molecules and possess a complex eukaryotic protein synthetic machinery. Plants, just as mammalian cells, are able to glycosylate and thus stabilize proteins, whereas bacterial cells are not (Fischer and Emans, 2000). Glycosylation is important for the right folding of proteins, thereby determining their function and activity. Compared to mammalian cells, that are easily contaminated by human pathogens, such undesired entities are absent from plant tissues (Commandeur et al., 2003) making them safer. Plant-derived pharmaceutical products do furthermore not require extensive purification and processing (Twyman et al., 2003). In this regard, oral administration of vaccines through edible transgenic plant parts is desired. Vaccines produced in storage tissues like cereal seeds do not need refrigeration and can be applied without injection needles (Nölke et al., 2003). In addition, transgenic plants offer a unique potential for scalability, providing the opportunity for almost unlimited production. Several plants have been used for the production of biopharmaceuticals including leafy crops, cereals, vegetables, legumes and fruits. Genes encoding antigens against HIV (Ramírez et al., 2007; Cueno et al., 2010; Rubio-Infante et al., 2015), hepatitis B (Kumar et al., 2005; Lou et al., 2007; Youm et al., 2007), rabies (McGarvey et al., 1995; Ashraf et al., 2005; Perea Arango et al., 2008) and cholera (Arakawa et al., 2001; Kim et al., 2006; Nochi et al., 2007; Sharma et al., 2008; Soh et al., 2015), etc. have been successfully expressed in different plant species (Tiwari et al., 2009).

The described examples show the vast potential of genetic engineering to provide plants with desirable traits (Figure 3. 1). Without doubt, tailored engineering approaches require a good knowledge of the underlying plant metabolism. In many cases this knowledge is still lacking or incomplete, which is why elucidation of plant metabolic functions is one of the main aims of plant research today.

3.2 Model crop rice (*Oryza sativa*)

Rice is one of the most important crop plants in the world, since it is the staple food for more than half of the world's population (IRRI, 2015a). About 3.5 billion people depend on rice for

more than 20% of their daily caloric intake. Rice is especially important for human nutrition, as it is directly consumed, whereas maize and wheat are mainly taken for animal feed (Khush, 2003). Rice is furthermore unique, as it can grow in wet environments that other crops cannot survive in (GRiSP, 2013). Rice is the seed of the monocot annual grass *Oryza sativa* (Asian rice) or *Oryza glaberrima* (African rice) which, together with 25 other species, form the genus *Oryza* (GRiSP, 2013). *Oryza* belongs to the family Poaceae or true grasses (Shimamoto, 1995) in the class of angiosperms, i.e. flowering plants producing seeds enclosed in an ovary. *Oryza sativa* is growing in tropical and subtropical areas on every continent except Antarctica (Toriyama et al., 2004). There are two subspecies of *Oryza sativa*, the sticky short-grained *japonica* species, which are typically cultivated in dry fields of upland Asia and the non-sticky long-grained *indica* varieties, growing submerged throughout tropical Asia (Garris et al., 2005; Molina et al., 2011). The genome of *Oryza sativa* consists of 430 Mb across 24 chromosomes and is the smallest among cereal crop plants (Sasaki et al., 1996; Goff, 1999). Among the latter, it has been the first to be completely sequenced (International Rice Genome Sequencing Project, 2005) and shows high synteny with other grasses used as crops, like wheat, barley and maize (Ahn and Tanksley, 1993; Kurata et al., 1994; Shimamoto, 1995). It is furthermore renowned for being easy to genetically modify (Hiei et al., 1994; Shimamoto, 1994). The importance for human consumption, small genome size and availability of straightforward transformation techniques make rice a widely used model species for cereal genomics.

3.2.1 Growth and development

Rice development is divided into three main phases, (i) the vegetative phase comprising germination, seedling and tillering stages, (ii) the reproductive phase including panicle initiation and heading stages and (iii) the ripening phase (Figure 3. 2) (Wang and Li, 2005). Depending on growth duration, rice species are categorized into two groups: short-duration varieties, which grow for 105 to 120 days to reach maturity and long-duration varieties, which mature over 150 days. The vegetative phase is comparatively long, constituting about half (ca. 60 days) of the whole growth period in a 120-day variety. Reproductive phase and ripening phase each take approximately 30 days, one quarter of the whole growth period (Yoshida, 1981).

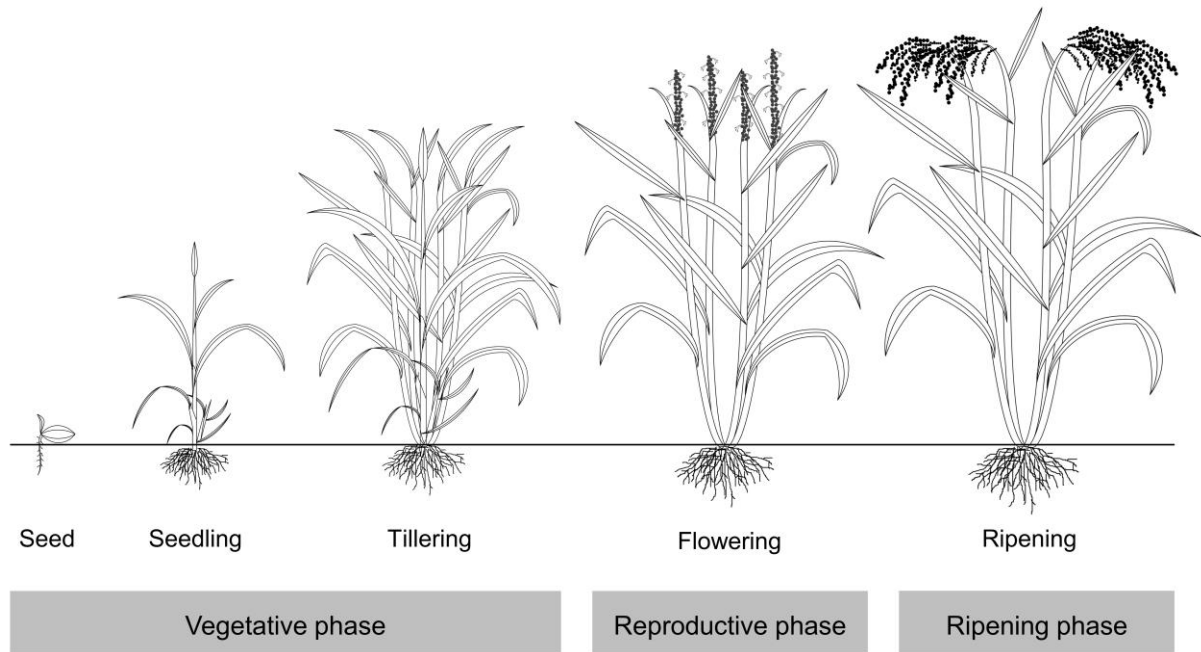


Figure 3. 2 Rice developmental stages

Rice development is subdivided into three main phases: vegetative, reproductive and ripening phase. The vegetative phase comprises germination and tillering, the reproductive phase includes panicle initiation, booting, heading and flowering and the ripening phase is characterized by maturation of the seeds.

The **vegetative stage** starts with germination. To break dormancy, seeds have to absorb a specific amount of water, called imbibition, and be exposed to temperatures between 10-40 °C (Yoshida, 1981; Bewley, 1997). These conditions initiate the emergence of the first shoot (coleoptile) and root (radicle). This is directly followed by the seedling stage or early vegetative stage, during which seminal roots and the first five leaves develop, largely dependent on the seed reserve (Yoshida, 1981). The late vegetative stage begins when the first tiller (side branch) appears, usually in the 5th leaf stage, and lasts until the maximum number of lateral shoots is reached. Tillering is an agronomic trait, as it determines the number of culms and thereby the number of panicles, a major determinant of grain yield (Li et al., 2003; Yang and Hwa, 2008; Wang and Li, 2011). Stem elongation begins late during vegetative stage and ends just before panicle initiation. The beginning of the **reproductive stage** is characterized by a bulge at the base of the flag leaf sheath, harboring the developing panicle. This so-called 'booting' stage occurs shortly after flag leaf emergence and is characterized by the panicle pushing up through the flag leaf sheath. During further development the panicle continues to grow and in the 'heading' stage fully emerges from the leaf sheath (Moldenhauer and Slaton, 2001). Shortly after panicle exertion, spikelet anthesis or flowering begins, during which flow-

ers open and spread their pollen (Yoshida, 1981). Rice is largely self-pollinated and the number of spikelets per panicle, another yield trait, is determined by the number of flowers that are fertilized (Moldenhauer and Slaton, 2001). Pollination is very sensitive to environmental factors like high temperature and drought stress, which might significantly reduce kernel number. During the **ripening stage**, the grains increase in size and weight by accumulation of sugar, starch and storage protein, called grain filling (Moldenhauer and Slaton, 2001). As kernel size and weight are determined during this stage, the grain filling period is critical for the production of high yields. Ripening can be subdivided into milky, dough, yellow-ripe and mature stage, based on the texture and color of the developing grains. At the milky stage the kernel is green, soft and has a high moisture content. As it ripens it turns yellow, the moisture content decreases and the kernel gets hard and firm. Ripening is accompanied by senescence of leaves, which translocate proteins, sugars and starch to younger leaves and to the grain (Yoshida, 1981).

3.2.2 Morphology

Higher plants are compartmentalized at the organ, tissue and subcellular level, leading to interconnected pathways, nutrient transport and cell signaling (O'Grady et al., 2012). Compartmentation concentrates enzymes in specific compartments and separates incompatible metabolic processes. The macroscopic morphology of the rice plant is constituted by its main organs: root, stem, leaves and panicle (Figure 3. 3).



Figure 3. 3 Morphology of an adult rice plant

A rice plant consists of the main organs root, stem, leaves and panicle. The panicle is the inflorescence of the plant, carrying several spikelets, i.e. single florets. The uppermost leaf on a culm is called flag leaf.

The sparsely branched seminal roots of the seedling are later replaced by secondary adventitious or nodal roots. The round, hollow, jointed culms are made of a series of nodes and internodes, each node bearing a leaf and a bud, which may give rise to a tiller. Rice leaves consist

of the sheath, which envelops the culm, and the flat and sessile blade which bears stomata on the lower and upper epidermis. The uppermost leaf on a culm is called flag leaf. The terminal shoot is the panicle, the inflorescence of the plant, carrying the spikelets (Chang and Bardenas, 1965). *Oryza sativa* can form up to 30 erect culms, bearing one slender panicle each (Yoshida, 1981). With approximately 150 spikelets per panicle, one plant can carry up to 4500 grains (Itoh et al., 2005).

The described organs are constituted of distinct tissues and cell types which perform specialized tasks, e.g. water and nutrient uptake by root hair cells (Gilroy and Jones, 2000) and photosynthesis by palisade cells (Figure 3. 4). The subcellular organization of the different cell types is, however, largely conserved.

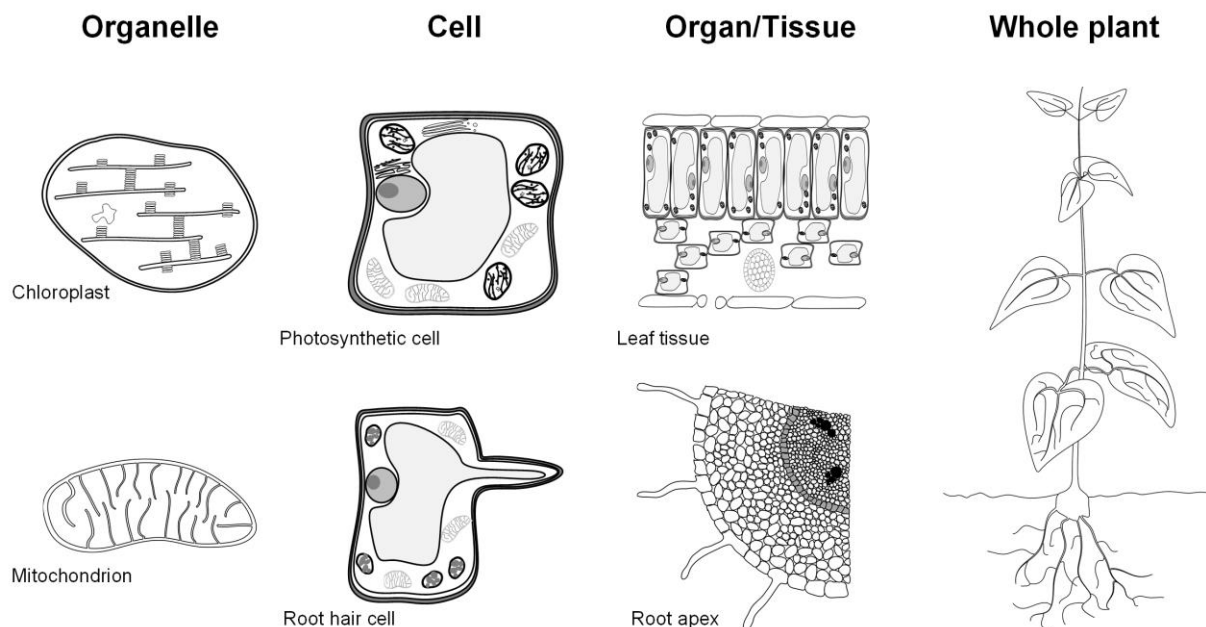


Figure 3. 4 Degree of compartmentalization of higher plants

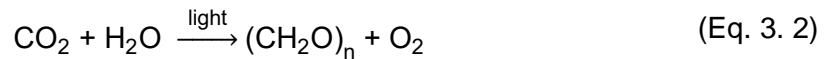
Plants are compartmented into specialized organs/tissues, different cell types and subcellular organelles, reflecting the complexity of plant metabolism. Photosynthetic cells are characterized by large vacuoles and the presence of many chloroplasts and mitochondria, whereas root hair cells have 'hair-like' outgrowths and can, next to a vacuole and nucleus, contain amyloplasts and mitochondria. Figure taken from Dersch et al. (2015).

Plant cells exhibit membrane-bound organelles, locally separating specific metabolic functions (Lunn, 2007; Sweetlove and Fernie, 2013). The DNA is organized in chromosomes, located in a nucleus (Guo and Fang, 2014). Chloroplasts and mitochondria are important organelles of a plant cell, as they are the energy-producing sites, performing photosynthesis and respiration, respectively (Bogorad, 1981; Jensen and Leister, 2014; Schertl and Braun, 2014). Peroxisomes take part in photorespiration and the detoxification of reactive oxygen species (Hu et

al., 2012). The vacuole sequesters waste products and stores water to maintain cell turgor (Zhang et al., 2014). Plant cells are surrounded by the cell membrane and a second, more robust layer, the cell wall (Keegstra, 2010).

3.2.3 Metabolic routes in central carbon metabolism

Photosynthesis is the most important biogeochemical process in the world. It catalyzes the conversion of solar energy into chemical energy, stored as carbohydrate.



Photosynthesis takes place in the chloroplasts, which are most abundant in leaf cells. Hereby, light energy is absorbed by reaction centers that contain the green pigment chlorophyll, giving leaves their green color. Photosynthesis is subdivided into light-dependent reactions and light-independent reactions. The light-dependent reactions use solar energy to split water, thus producing reduced nicotinamide adenine dinucleotide phosphate (NADPH) and adenosine triphosphate (ATP), whereby oxygen is generated as waste product (Arnon, 1971). The light-independent reactions of photosynthesis, also called Calvin-Benson-Bessham (CBB) cycle, use NADPH and ATP from the previous reaction to reduce CO_2 , thereby producing carbohydrate, subsequently stored as starch and sucrose, respectively (Figure 3. 5). In the first step of the CBB cycle, ribulose 1.5-bisphosphate (RBP) is carboxylated by the enzyme RuBisCO, generating two molecules of 3-phosphoglycerate (3PG). These are reduced in a two-step process to form glyceraldehyde 3-phosphate (GAP). In the third part of the cycle, the carbon acceptor molecule RBP is regenerated, which uses up five GAP molecules (Calvin, 1962). Three successions of the cycle are therefore necessary to yield a net gain of one molecule of GAP, which is subsequently used for conversion into hexose sugars. The regeneration of RBP is tightly intertwined with the non-oxidative pentose phosphate pathway, using the same phosphate sugar intermediates to recycle GAP by successive transketolase and transaldolase reactions (Berg et al., 2006).

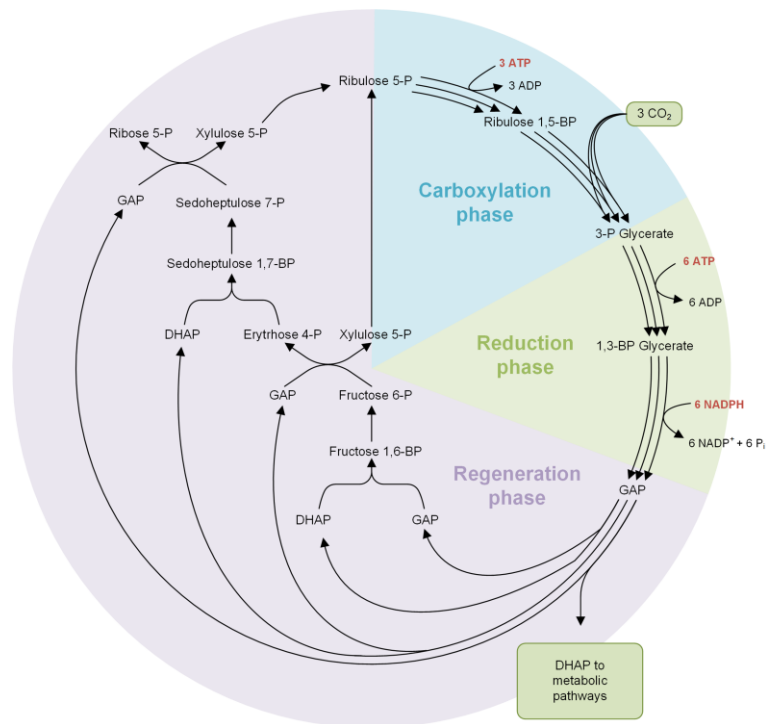


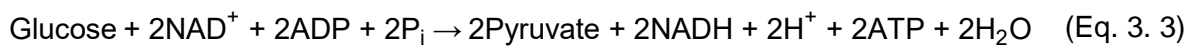
Figure 3. 5 The Calvin-Benson-Bessham cycle

The Calvin-Benson-Bessham cycle can be subdivided into three parts: carboxylation phase, reduction phase and regeneration phase. Three molecules of CO_2 have to be assimilated by three successions of the complete cycle to yield one molecule of triose phosphate for subsequent incorporation into hexose sugars. Figure taken from Beckers (2015).

RuBisCO is the most abundant protein in the world. It is the key enzyme of photosynthesis, but unfortunately an extremely inefficient catalyst, which is why it is present in a vast amount, constituting about 50% of the leaf soluble protein (Ellis, 1979). It furthermore wastefully reacts with oxygen, generating 2-phosphoglycolate. In a process called photorespiration, toxic 2-phosphoglycolate is salvaged by a series of enzymatic reactions involving chloroplast, mitochondrion and peroxisome. As the recovery of 2-phosphoglycolate is accompanied by a considerable loss of previously fixed CO_2 and energy, photorespiration is a main target for crop improvement (Schneider et al., 1992; Bauwe et al., 2010).

Further central metabolic pathways in plants are the pentose phosphate (PP) pathway as well as the Embden-Meyerhof-Parnas (EMP) pathway and the tricarboxylic acid (TCA) cycle (Figure 3. 6). PP and EMP pathway enzymes are duplicated in chloroplast and cytosol, which is a unique feature of plants (Plaxton, 1996; Kruger and Von Schaewen, 2003). Exchange of phosphate sugars between these two compartments is accomplished via specialized transporters located in the plastidic envelope (Eicks et al., 2002; Flügge et al., 2011; Weber and Linka, 2011). The PP pathway is subdivided into an oxidative branch and a reversible non-oxidative

branch. In the oxidative branch, glucose 6-phosphate (G6P) is converted into ribulose 5-phosphate (Ru5P), generating the reductant NADPH, which is further used for fatty acid synthesis and to prevent oxidative stress. The non-oxidative branch generates pentoses for the production of nucleotides and aromatic amino acids (Kruger and Von Schaewen, 2003). While the enzymes of the oxidative part are found in the cytosol and in the chloroplast stroma, the enzymes of the non-oxidative part are predominantly located inside the plastids. The EMP pathway occurs parallel to the PP pathway and yields ATP and reduced nicotinamide adenine dinucleotide (NADH) through catabolic degradation of sucrose and starch, called glycolysis. It furthermore produces building blocks for anabolism, as well as pyruvate, thereby fueling plant respiration (Plaxton, 1996).



The conversion of hexoses into pyruvate can independently occur in the cytosol and in the plastid, mainly degrading sucrose and starch, respectively (Dennis and Miernyk, 1982; Givan, 1999). The EMP pathway is furthermore amphibolic, as it can work in reverse to yield hexoses from low-molecular-weight compounds by energy-demanding gluconeogenesis (Plaxton, 1996). The coenzyme NAD^+ is the oxidizing agent of the glycolysis and it has to be regenerated to maintain glycolytic activity. In plants, this is achieved via the complex mechanisms of cellular respiration, involving the TCA cycle, the mitochondrial electron transport chain (miETC) and molecular oxygen as final electron acceptor. In the first step, pyruvate from glycolysis is transported to the mitochondrion where it is decarboxylated to yield acetyl-CoA (AcCoA). Acetyl-CoA enters the TCA cycle, where it is completely oxidized to carbon dioxide and water, producing NADH. NADH is subsequently oxidized to NAD^+ via the miETC located in the inner mitochondrial membrane, thereby generating a proton gradient, which is used to produce ATP in a process called oxidative phosphorylation. The processes of respiration hence consume oxygen and produce carbon dioxide as waste product. TCA cycle intermediates serve as precursors for secondary metabolites, isoprenoids, fatty acids and amino acids. Anaplerotic reactions are required to replenish the TCA cycle intermediates, withdrawn for anabolism (Ferne et al., 2004; Plaxton and Podestá, 2006). Moreover, the respiratory pathway participates in pivotal metabolic processes, like nitrate assimilation, redox homeostasis, as well as maintenance of high levels of photosynthesis (Dutilleul et al., 2003; Scheibe et al., 2005; Noguchi and Yoshida, 2008; Nunes-Nesi et al., 2008; Sienkiewicz-Porzucek et al., 2010).

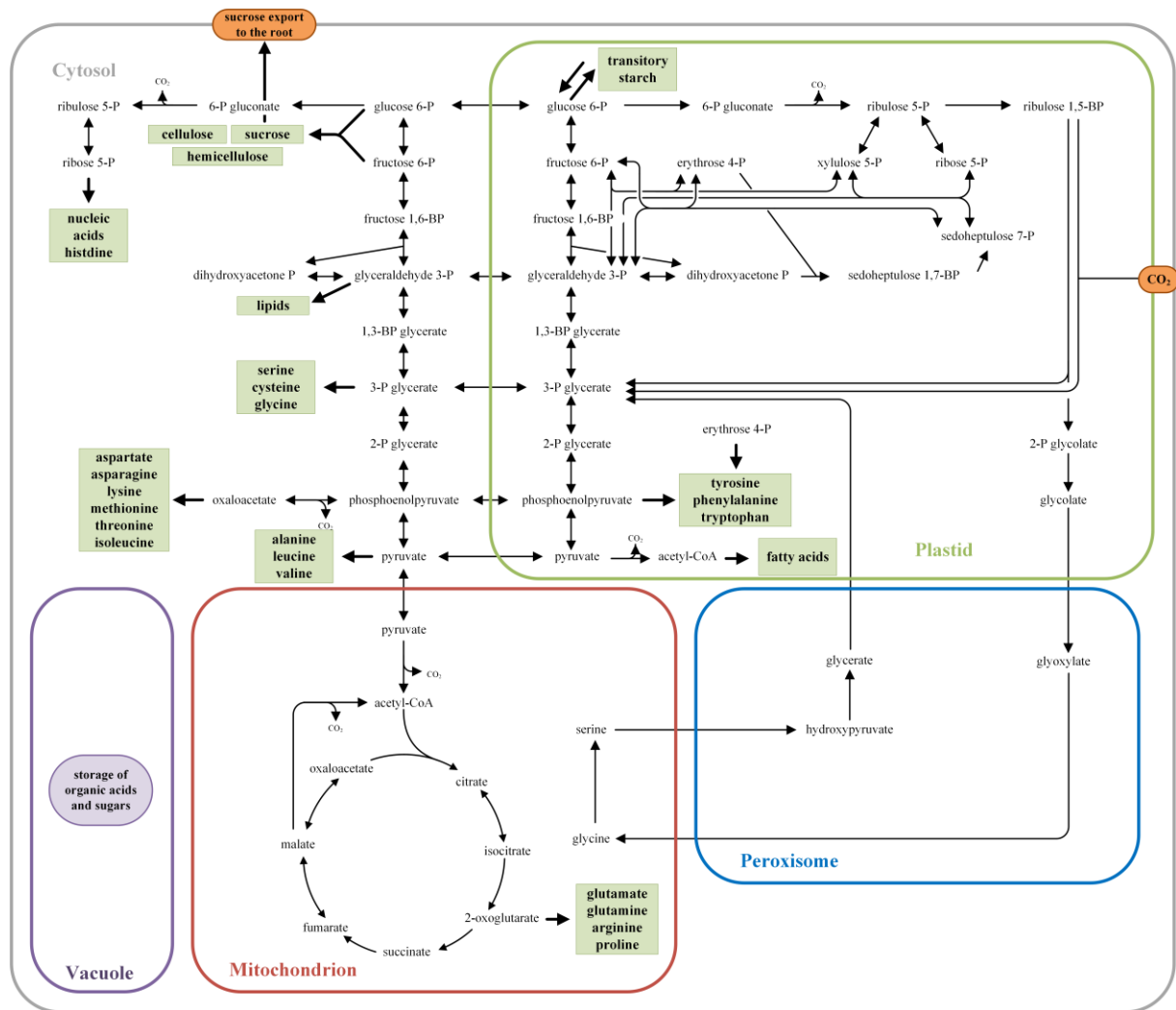


Figure 3. 6 Central carbon metabolism of a photoautotrophic plant leaf cell

Metabolic pathways of central carbon metabolism, comprising cytosolic and plastidic EMP and oxidative PP pathway, plastidic CBB cycle and non-oxidative PP pathway, mitochondrial TCA cycle and the reactions of photorespiration, located in plastid, peroxisome and mitochondrion. Anabolic precursors are highlighted in green. Figure taken from Dersch et al. (2015).

Compared to other organisms, plants have evolved alternative enzymes, bypassing the conventional reactions of cytosolic glycolysis, the TCA cycle and the miETC, thereby providing plants with metabolic flexibility that mediates the adaptation to environmental stress and enables plants to survive in an ever-changing environment (Givan, 1999; Plaxton and Podestá, 2006).

Despite great research effort, plant metabolic networks are still not fully understood. This is mainly due to the complex nature of plant metabolic pathways and the high degree of compartmentation, which gave rise to a myriad of transport reactions interconnecting the different compartments and to a specific regulatory machinery tightly modulating opposing processes

like photosynthesis and respiration as well as duplicate pathways, like glycolysis located in cytosol and stroma.

3.2.4 Stress resistance

Plants, as sessile organisms, experience a multitude of stresses, considerably influencing plant metabolism, performance and growth. The term 'stress' is not uniformly employed, definitions ranging from very broad to narrow concepts. A reasonable definition describes stress as unfavourable condition, exceeding a certain, organism-specific threshold (Lichtenthaler, 1998; Munns et al., 2006). Stress can further be divided into biotic and abiotic stress. Biotic stressors are living organisms, like insects, nematodes, fungi and weeds. Abiotic stress refers to unfavourable environmental factors, e.g. high salinity, drought, cold, heat and micronutrient-deficient soils. Plant stress response involves a multitude of interconnected pathways and a myriad of genes, and is not yet fully understood (Chinnusamy et al., 2005; Bohnert et al., 2006; Sahi et al., 2006; Sreenivasulu et al., 2007; Ahmad et al., 2011). To improve stress tolerance, there is a strong need to elucidate underlying mechanisms of stress response in plants.

3.2.4.1 Abiotic stress – high salinity

Salt stress affects 20% of the irrigated land worldwide and causes an economic loss of \$11 billion every year (FAO, 2015c). All major crop plants belong to the salt sensitive group of glycophytes, rice being the most sensitive among them (Maas and Hoffman, 1977; Salt Tolerance Database on USDA-ARS, 2015). Therefore, salinity is one of the greatest threats to crop production worldwide. Salt stress leads to membrane damage, ion imbalance, the production of reactive oxygen species and finally to growth arrest and diminished grain yield (Kumar et al., 2013). Plants sense high salt concentrations in the soil through osmotic and ionic perturbation (Kader and Lindberg, 2010). Ion tolerance is achieved by reduced uptake of toxic Na^+ and Cl^- ions into cells, called ion exclusion. If this mechanism fails, excess ions are sequestered into the vacuole and older tissues (Wang et al., 2012a; Roy et al., 2014). This causes osmotic pressure, which is balanced by the accumulation of compatible solutes like proline and soluble sugars in the cytosol (Munns and Tester, 2008). These osmoprotectants detoxify reactive oxygen species (ROS) and stabilize the quaternary structure of proteins (Kumar et al., 2013). Salt stress furthermore leads to abscisic acid (ABA) synthesis in roots, which, as a signalling molecule, triggers stomatal closure, resulting in reduced photosynthesis and growth (Wilkinson and Davies, 2002). To improve yield under salinity stress, it is important to understand the metabolic mechanisms behind salt tolerance, which is a quantitative trait, controlled by several genes (Chinnusamy et al., 2005). Traditional rice cultivars and landraces, like Pokkali, Nona Bokra and Bura Rata, exhibit a higher salt tolerance than cultivated species.

Pokkali has therefore been extensively employed in metabolic studies to enhance the understanding of salt tolerance mechanisms (Kawasaki et al., 2001; Pattanagul and Thitisaksakul, 2008; Jiang et al., 2013; Soda et al., 2013; Yamada et al., 2014; Ferreira et al., 2015). Extensive research including quantitative trait loci (QTL) (Koyama et al., 2001; Lin et al., 2004; Wang et al., 2012b) and transcriptional analysis (Theerawitaya et al., 2012; Wu et al., 2015), as well as genomics (Sahi et al., 2006; Kumar et al., 2013) and proteomics studies (Abbasi and Komatsu, 2004; Kim et al., 2005; Dooki et al., 2006; Parker et al., 2006; Chitteti and Peng, 2007; Sarhadi et al., 2012; Liu et al., 2014), identified a myriad of signal transduction pathways, ion transporters and osmoprotectants conferring salt tolerance in rice (Kumar et al., 2013). The acquired knowledge was used to genetically modify rice plants for improved salt tolerance, e.g. by targeting signal transduction (Saijo et al., 2000; Campo et al., 2014; Kusuda et al., 2015), transcription factors (Zheng et al., 2009; Chen et al., 2015), osmotic (Sakamoto et al., 1998; Su et al., 2006) and ionic (Ohta et al., 2002; Obata et al., 2007) homeostasis, antioxidant machinery (Tanaka et al., 1999; Singla-Pareek et al., 2008) and heat shock proteins (Zou et al., 2012; Liu et al., 2013).

3.2.4.2 Biotic stress - weeds

Weeds pose considerable stress to crop plants by competing with them for resources, like nutrients, light and water (Basu et al., 2004). Therefore, weeds are considered a pest in agriculture, causing an annual, worldwide reduction in crop productivity of up to 10% (Oerke, 2006). In order to control weeds and diminish their destructive effect on crop yield, there is a need for safe, potent herbicides. The discovery and development of new herbicides is a long and trying endeavour. They should not cause animal or crop injury, but show a selective mode of action (MoA) for weeds (Casida, 2009). The MoA is the overall mechanism by which an herbicide affects a plant at the tissue or cellular level. The evolution of herbicide resistant weeds is increasingly rapid as there are only about 20 different mechanisms of action that are targeted by herbicides today. Due to increased developmental effort and cost, no herbicide with a new MoA was introduced to the market since 20 years (Duke, 2012). The discovery of novel target sites is based on the application of structurally diverse compounds to whole plants, followed by precise characterization of the induced phenotype. Phenotyping is the first level of a three-tiered approach of MoA identification proposed by Tresch, further involving genetic and biochemical screens (Tresch, 2013). Phenotyping includes intensive physiological profiling, called physionomics (Grossmann et al., 2012), as well as other omics technologies like transcriptomics and metabolomics. Almost 70% of the compound classes known today were identified by phenotyping (Tresch, 2013). A well-described herbicide family is represented by the imidazolinones, a group of acetohydroxyacid synthase (AHAS) inhibitors. AHAS is the enzyme

catalyzing the first step during biosynthesis of the branched-chain amino acids valine, leucine and isoleucine (Shaner and Reider, 1986; Shaner and Singh, 1991). Imidazolinone-resistant rice varieties were obtained through conventional breeding and were commercialized in 2002 under the name Clearfield® rice. Genetically engineered rice varieties resistant to glufosinate (Liberty Link® rice) and glyphosate (Roundup Ready® rice) are also available, but have not yet been commercialized (IRRI, 2015b).

Technological development provides new possibilities to further augment the success of phenotyping methods to identify novel target sites. In comparison to traditional omics technologies, the emerged field of fluxomics is particularly promising, regarding its ability to provide direct functional information about metabolic phenotypes (Kruger and Ratcliffe, 2009). Fluxomics, as complementary set of information within systems biology approaches, might help to provide a holistic picture of plant response to synthetic compounds.

3.3 Isotopic labeling studies for plant flux analysis

As exemplified above, the still limited understanding of plant metabolic networks hampers successful plant modification towards improved performance. Plant metabolic networks are far more complex than those of other organisms. This is due to prominent plant characteristics: being sessile, photoautotrophic and possessing a vast amount of secondary metabolites. Furthermore, plants consist of different organs and specialized cell types with a high degree of subcellular compartmentation, leading to interconnected pathways of nutrient transport and cell signaling. The high degree of connectivity between pathways is the main reason why plant metabolic engineering was often unsuccessful, especially considering single gene alterations (Allen et al., 2009a). Since tailored engineering approaches have to build on understanding, there is a strong need to elucidate cellular functions at the network level. As cellular functions are closely related to intracellular fluxes, i.e. the fluxome, metabolic flux analysis is a promising tool to provide systems-level understanding and predict potential targets for metabolic engineering (Kruger and Ratcliffe, 2009; Kohlstedt et al., 2010).

The exploration of microbes probably displays the pioneering and most stimulating application of isotopic tracers for the identification (Barker et al., 1940; Barker and Kamen, 1945) and quantification (Wang et al., 1958) of metabolic pathway fluxes. Physiologists adapted such approaches from early on to study the metabolism of plants (Calvin, 1962). In short, tracer-based studies involve labeling experiments, in which an isotopically enriched tracer substrate is metabolized by the cells to be examined (Figure 3. 7). This is coupled to subsequent analytics of the label distribution in the studied cells using scintillation counting for radioactive tracers (Tanaka and Osaki, 1983; Sun et al., 1988; McNeil et al., 2000) or nuclear magnetic

resonance (NMR) (Dieuaide-Noubhani et al., 1995; Szyperski, 1998; Cegelski and Schaefer, 2006; Williams et al., 2008) and mass spectrometry (MS) (Antoniewicz, 2013; Godin et al., 2007; Hasunuma et al., 2010; Huege et al., 2007; Meier-Augenstein, 1999; Wittmann and Heinzle, 1999; Yuan et al., 2010) for stable isotopes, respectively. Finally, flux information is extracted from the data, either via simple algebraic equations or with the help of more comprehensive models. Generally, the experiments can vary greatly in terms of complexity, from rather simple pulse-chase studies to highly advanced and precisely controlled dynamic approaches.

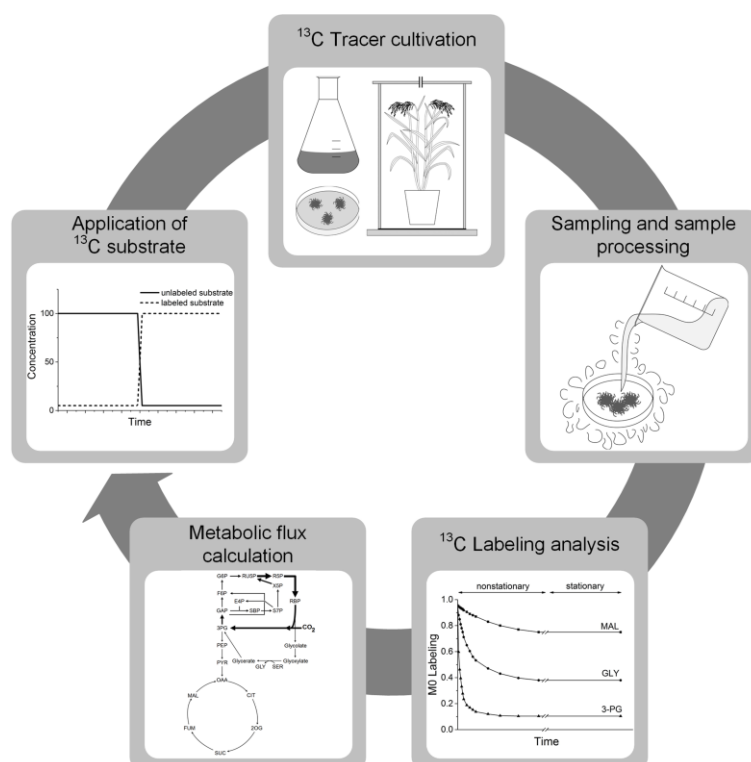


Figure 3.7 Workflow of tracer studies

Tracer studies consist of five major handling steps: Application of tracer, cultivation on labeled substrate, sampling and sample processing, measurement of isotopic distribution and data interpretation. Although these steps are common to every tracer study, details can differ tremendously, concerning type of cultivation and labeled substrate, the amount and type of metabolites to be measured, the analytics used and the form of data evaluation, either by applying simple algebraic equations or by performing network modeling. Figure adapted from Dersch et al. (2015).

Since carbon is a universal component of all organic metabolites and molecules, carbon isotopes are preferred tracers for mapping central carbon metabolism in plants (Ratcliffe and Shachar-Hill, 2006; Young et al., 2011). The stable isotope ^{13}C is most often used. In addition, ^{15}N (Harada et al., 2006; Schwender et al., 2006), ^2H (Boatright et al., 2004; Matsuda et al., 2005; Colón et al., 2010), ^{33}P (McNeil et al., 2000) and ^{35}S (Osaki and Shinano, 2001) tracers,

or even tracer combinations (Schwender et al., 2006) have been applied. The choice of labeled substrate determines the quality of information for a given question. Therefore, selecting the most appropriate tracer is an important aspect. Computer-based experimental design is performed to predict the tracers best suited (Libourel et al., 2007; Nargund and Sriram, 2013). Differentially labeled tracers (Schwender et al., 2003; Alonso et al., 2007a) or tracer combinations (Cliquet et al., 1990; Dyckmans et al., 2000; McNeil et al., 2000; Schwender et al., 2004) can help to enhance flux resolution. From the experimental point of view, steady-state approaches with organic tracer substrates such as sugars or amino acids enable the analysis of metabolic fluxes in heterotrophic plant systems. In steady-state ^{13}C -MFA, isotopic labeling patterns are measured after the system has reached a metabolic and isotopic steady-state (Figure 3. 8). These labeling patterns of metabolic intermediates are used to back-calculate the flux through the respective pathway. The underlying models can handle large networks with reversible steps, cyclic fluxes and subcellular compartmentation (Ratcliffe and Shachar-Hill, 2006), and do not require additional information on pool sizes or pathway kinetics (Wiechert and De Graaf, 1996). However, it cannot be applied to study photoautotrophic metabolism under physiological conditions (Roscher et al., 2000), which has stimulated the development of dynamic approaches, which can resolve fluxes in CO_2 -provided whole plants.

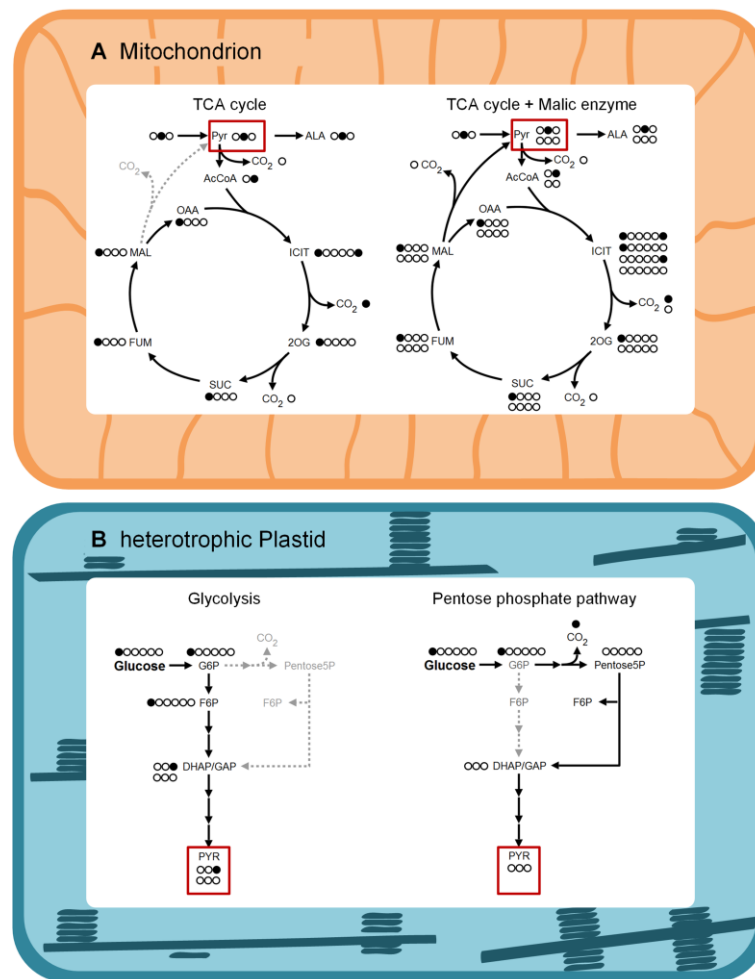


Figure 3. 8 From labeling data to fluxes

Exemplary labeling pattern of central carbon metabolites of heterotrophic plant tissue after labeling with $1[^{13}\text{C}]$ -glucose. The labeling pattern of pyruvate differs, dependent on the activity of the tricarboxylic acid (TCA) cycle and/or malic enzyme and glycolysis or the pentose phosphate pathway (PPP). The ratio of the unlabeled (M0) to singly labeled (M1) pyruvate can be used to back-calculate the flux through the respective pathway. Figure taken from Dersch et al. (2015).

3.3.1 Experimental considerations for plant cell and tissue cultures

Heterotrophic plant cell (Kruger et al., 2007a) and tissue cultures (Sriram et al., 2007a; Koubaa et al., 2012) have been extensively studied on the flux level. They are typically cultivated in shake flasks, and bioreactors, similar to microorganisms (Rontein et al., 2002; Baxter et al., 2007; Kruger et al., 2007a; Williams et al., 2008; Young et al., 2011). Plant cells are much more shear-sensitive than microorganisms and therefore require optimized impeller systems when cultivated in a bioreactor (Georgiev et al., 2013; Georgiev and Weber, 2014). They might additionally require specific light regimen in order to achieve optimum growth conditions. Light-emitting diodes (LEDs) that emit white light are most often applied at a low irradiance of 100 to 200 $\mu\text{mol m}^{-2} \text{s}^{-1}$ to avoid photoinhibition (Wienkoop et al., 2010; Young et al., 2011; Kliphuis

et al., 2012; Martzloff et al., 2012). LEDs are available in certain commercial incubators and bioreactors and are easy to add to existing equipment. The plant culture medium is typically based on the Murashige-Skoog medium (Murashige and Skoog, 1962), which contains several essential macro- and micronutrients, as well as vitamins, amino acids, phytohormones, like naphthaleneacetic acid, kinetin and indole 3-acetic acid and a carbon source, usually sucrose or glucose. For labeling of cell and tissue cultures, amino acids or sugars are replaced by their isotopically labeled equivalent (Rontein et al., 2002; Schwender et al., 2006; Baxter et al., 2007; Kruger et al., 2007a; Williams et al., 2008). Cultures can furthermore be supplied with the labeled form of metabolic intermediates to address specific questions. Radiolabeled gluconate was, for example, used to more directly and sensitively examine flux through the oxidative pentose phosphate pathway (Garlick et al., 2002). A combination of tracers further enhances resolution and the confidence in estimated fluxes (Schwender et al., 2004; Schwender et al., 2006; Alonso et al., 2007a; Allen et al., 2009b; Allen and Young, 2013). Therefore tracer combinations can be applied to address nontrivial questions, like the elucidation of subcellular OPPP activity, which was found to be most prominent in the cytosol (Masakapalli et al., 2010). This and subsequent studies, considering the impact of nitrogen and phosphorus starvation on the interaction between cytosolic and plastidic metabolism, revealed the limitation of the OPPP to meet the NADPH requirements of biosynthetic processes in heterotrophic plant cell metabolism, which highlights the contribution of non-plastidic processes to provide reducing power for the plastid (Masakapalli et al., 2010; Masakapalli et al., 2013; Masakapalli et al., 2014a).

Studies with heterotrophic cell and tissue cultures are performed at metabolic steady-state. After harvest and dissection from their original plant environment, tissue cultures are immediately supplied with the labeled substrate in which they are further cultivated for several days. Cell cultures are typically cultivated for approximately 4 to 7 days to reach steady-state conditions (Garlick et al., 2002; Rontein et al., 2002; Alonso et al., 2007a; Baxter et al., 2007; Iyer et al., 2008; Williams et al., 2008; Masakapalli et al., 2010) and are subsequently labeled for several hours or days, depending on the purpose of the study. For metabolic pathway elucidation, shorter labeling periods are sufficient (Garlick et al., 2002; Baxter et al., 2007), whereas stability of metabolism was typically examined in long-term labeling experiments (Rontein et al., 2002; Williams et al., 2008). One important point to notice is the extremely divergent turnover rates of intracellular plant metabolites. In isotope studies, metabolites of central carbon metabolism are labeled within seconds to hours, whereas storage molecules have half-lives of several days (Rontein et al., 2002; Schwender et al., 2003; Alonso et al., 2007a; Troufflard et al., 2007). Therefore, it might be reasonable to simulate the metabolite turnover rates *in silico*, prior to the experiment, to know how long the labeling has to proceed (Hasunuma et al., 2010).

Alternatively, an *a priori* experiment to measure labeling time-courses can be performed, to estimate when isotopic stationarity is reached (Kruger et al., 2012).

3.3.2 Experimental considerations for whole plants

A major focus of flux studies in plants is given to the analysis of whole plants under physiological conditions, i.e. growing photoautotrophically on isotopically labeled carbon dioxide, their natural substrate. Specially designed enclosures are applied to incubate plant parts or entire plants in a defined atmosphere containing isotopically labeled carbon dioxide. Such enclosures range from freeze clamps (Hasunuma et al., 2010) and single leaf chambers (Schaefer et al., 1980) over simple plastic bags (Tanaka and Osaki, 1983) to more advanced chambers with humidity, temperature and CO₂ control (Andersen et al., 1961; Nouchi et al., 1994), like the commercially available Biobox (Huege et al., 2007; Römisch-Margl et al., 2007). The use of labeled carbon dioxide, however, results in an isotopic steady state where all carbon atoms are uniformly labeled, thus lacking information about internal fluxes (Allen et al., 2009a). To circumvent this, the isotope experiments can be conducted as pulse-chase and as transient labeling studies, examples being investigations of single leaves (Schaefer et al., 1980; Osaki and Shinano, 2001), as well as of whole, intact plants (Römisch-Margl et al., 2007; Chen et al., 2011; Szecowka et al., 2013; Ma et al., 2014). Hereby, labeling time-courses are monitored over time, after a change from unlabeled to labeled substrate (Roscher et al., 2000), while the system is at metabolic steady-state. Suitable monitoring of kinetic labeling patterns requires a set of about 20 samples taken over a rather short period of time. Many samples should be taken directly after the onset of labeling, whereas sampling frequency can be decelerated towards later sampling time points. Typically, labeling profiles of central carbon metabolites are determined, as these provide fast enrichment due to their high turnover rates. This drastically decreases labeling time of dynamic experiments as compared to its steady-state variant. It might furthermore be reasonable to consider additional labeling data of e.g. amino acids, fatty acids and sugars as well as other anabolic building blocks, since every additional constraint potentially enhances flux resolution and confidence in the determined fluxes (Ratcliffe and Shachar-Hill, 2006). In addition, pool size measurements are in most cases required. As the metabolism of the studied system is at steady-state, it is sufficient to measure pool sizes in one sample, e.g. before the onset of the labeling change (Shastri and Morgan, 2007). Alternatively, unknown pool sizes can be estimated from the measured data by parameter fitting, typically of the full set of mass isotopomer distributions (MIDs), (Young et al., 2011). The obtained labeling and pool size data can later be processed by two different computational approaches, isotopically non-stationary metabolic flux analysis (Young et al., 2011; Ma et al., 2014) and kinetic flux profiling (McNeil et al., 2000; Boatright et al., 2004; Matsuda et al., 2005; Baxter et

al., 2007; Colón et al., 2010; Szecowka et al., 2013). Today, isotopically non-stationary labeling approaches are best suited to analyze small-scale networks, as analysis is getting more complex with every reaction step and the computational burden explodes rapidly. Therefore, they are particularly suitable for the analysis of peripheral metabolic pathways, e.g. secondary metabolism (Boatright et al., 2004; Matsuda et al., 2005; Ratcliffe and Shachar-Hill, 2006; Colón et al., 2010).

3.3.3 ^{13}C Labeling analysis

NMR and MS are the two main approaches, used to measure isotopic enrichment after stable isotope labeling in plants (Ratcliffe and Shachar-Hill, 2006) (Figure 3. 9). Both are complementary techniques that, when used synergistically, can maximize the information gain and the confidence in the measured fluxes (Kleijn et al., 2007). In brief, NMR yields information about positional labeling of metabolites (Figure 3. 9) and can be applied to monitor metabolism in living cells on-line (Roscher et al., 1998). The extension to multinuclear and multidimensional NMR spectroscopy increases the information content substantially, up to the level of entire sets of positional isotopomers (Fan and Lane, 2008). As example, NMR studies of maize root tips revealed the ^{13}C enrichment of specific carbon atoms in amino acids and carbohydrates, used to elucidate steps of sucrose metabolism (Dieuaide-Noubhani et al., 1995) as well as *in vivo* unidirectional steady-state reaction rates of enzymes in their cellular environment (Roscher et al., 1998). MS provides information about the number of heavy isotopes in a molecule and is mainly applied to assess mass isotopomer distributions (Figure 3. 9). It is suitable for the measurement of less abundant metabolites (Wittmann and Heinzle, 1999), due to higher sensitivity as compared to NMR (Pan and Raftery, 2007). It is routinely coupled to gas chromatography (GC) or liquid chromatography (LC) to separate the metabolites of interest in the complex sample background prior to detection. MS labeling analysis has been extensively used in tracer experiments in plants (Boatright et al., 2004; Roessner-Tunali et al., 2004; Matsuda et al., 2005; Baxter et al., 2007; Colón et al., 2010; Chen et al., 2011; Young et al., 2011; Szecowka et al., 2013; Ma et al., 2014). More recently, isotope ratio mass spectrometry (IRMS) (Griffiths et al., 2004; Wu et al., 2009; Soong et al., 2014) has been introduced to quantify extremely low ^{13}C and ^{15}N enrichments (Figure 3. 9). It exhibits a much higher precision (0.0002 atom%) than conventional mass spectrometry (0.05 atom%) (Meier-Augenstein, 1999b), based on triple quadrupole technology, enabling the use of small amounts of tracer in isotope labeling experiments. This is particularly useful for plant labeling experiments using physiological tracer concentrations (Cliquet et al., 1990; Dyckmans et al., 2000; Griffiths et al., 2004; Leake et al., 2006; Wu et al., 2009). The IRMS unit can be coupled to an elemental

analyzer (EA) (Griffiths et al., 2004; Wu et al., 2009; Soong et al., 2014) or a gas chromatograph. The latter enables the labeling analysis of individual compounds in complex matrices (Molero et al., 2011). Other useful instrumentations include capillary-electrophoresis coupled to mass spectrometry (CE-MS) (Monton and Soga, 2007).

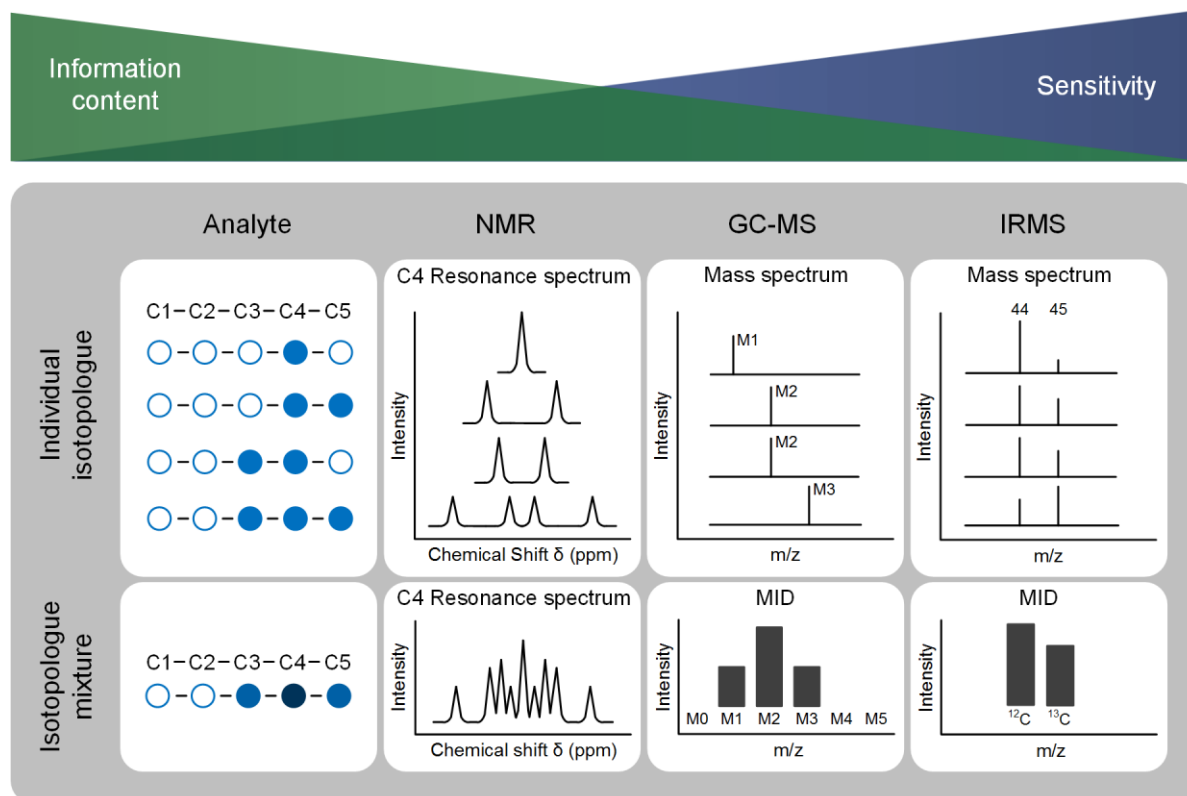


Figure 3. 9 Analytics for flux analysis

Comparison of NMR, GC-MS and IRMS analysis, concerning information content after detection of spectra for individual isotopologues and the isotopologue mixture. NMR analysis of the C4 resonance elucidates the positional labeling of the C4 atom and its neighboring atoms C3 and C5. With GC-MS analysis, individual isotopologues can be detected and quantified, but it is not possible to differentiate between isotopic positional isomers. IRMS measurements yield a ratio of ^{13}C over ^{12}C , relative to an international standard ($\delta^{13}\text{C}$), expressed as per mill enrichment. MID – mass isotopomer distribution. Figure taken from Dersch et al. (2015).

In order to tackle intracellular complexity and scalability of plants, there is a particular need to improve the resolution of ^{13}C -based plant flux studies. Subcellular compartmentation is one of the main challenges for high flux resolution (Fernie and Morgan, 2013). Compartment-specific labeling information can be gained by non-destructive methods such as *in vivo* metabolic imaging, using MS (Hölscher et al., 2009; Jun et al., 2010; Matros and Mock, 2013), NMR (Kim et al., 2011; Borisjuk et al., 2012) or fluorescence resonance energy transfer-based techniques (Lalonde et al., 2005; Okumoto et al., 2008). Other methods refer to the use of reporter metabolites, specific as readouts for particular compartments. Not only fatty acids (Allen et al.,

2007) and amino acids (Sriram et al., 2004; Masakapalli et al., 2010), but also protein glycans (Sriram et al., 2007b), cell wall components and starch (Allen et al., 2007) have been used to estimate the flux contribution of duplicate plastidial and cytosolic pathways. Recent developments in this field comprise amino acid labeling analysis of protein subunits, synthesized in different compartments (Allen et al., 2012), as well as the determination of isotopic labeling in peptide fragments (Allen et al., 2014; Mandy et al., 2014). Another, recently advanced technique, yielding considerable compartment-specific flux information is non-aqueous fractionation (Gerhardt and Heldt, 1984; Farré et al., 2002; Benkeblia et al., 2007; Klie et al., 2011; Tiessen et al., 2012). Non-aqueous fractionation, combined with labeling analysis, was recently used to distinguish between plastidic and cytosolic pools of sugar phosphates, which enhances the resolution of starch and sucrose synthesis by adding further constraints to the metabolic model (Szecowka et al., 2013).

3.3.4 Assimilation, translocation and biosynthetic fluxes

Whole plant isotopic pulse-labeling is particularly suitable, if the assimilation of nutrients, and the interaction of different plant parts is to be examined, e.g. source-sink relations (Tanaka and Osaki, 1983) as well as interactions between plants and soil microorganisms (Griffiths et al., 2004; Leake et al., 2006; Wu et al., 2009). The underlying tracer studies require less time and computational effort than model-based approaches and are potent for the use as fast screening tool (Schwender, 2008). They do not per se provide quantitative intracellular fluxes through individual reactions and pathways, but gross metabolic activities, i.e. flux profiles or fingerprints, respectively. Pulse-chase studies in plants revealed the metabolic structure of lipid biosynthesis (Bao et al., 2002), glycine metabolism (Cegelski and Schaefer, 2005) and lysine degradation (Araújo et al., 2010), leading to an enhanced understanding of the plant metabolic network. Combined ^{13}C and ^{15}N labeling studies (Soong et al., 2014) allow for simultaneous investigation of C and N dynamics in plants, especially uptake and allocation of assimilates (Cliquet et al., 1990; Dyckmans et al., 2000) leading to deeper insights into C and N metabolic routes (Cegelski and Schaefer, 2005). Monitoring the kinetic decay from ^{13}C to ^{12}C under ambient conditions, enables sampling with minimal disturbance. Turnover of metabolite pools was monitored by isotope dilution experiments after maximum labeling with ^{13}C (Huege et al., 2007; Chen et al., 2011). This method is, however, very cost-intensive because plants have to be raised in a $^{13}\text{CO}_2$ atmosphere. An alternative to pulse labeling for the examination of whole plants is the recently developed approach of measuring labeling time-courses. Transient metabolite labeling profiles can be detected to determine metabolite turnover rates, thereby identifying rate-limiting steps in specific metabolic pathways (Hasunuma et al., 2010).

3.3.5 Intracellular fluxes in heterotrophic plant systems

Excised tissue or cell suspension cultures grown on isotopically labeled substrates, mostly ^{13}C -labeled sugars and amino acids, are often used to study heterotrophic metabolism of plant systems. These systems are cultured under controlled conditions for extended time periods under metabolic and isotopic steady-state (Ratcliffe and Shachar-Hill, 2006). A pioneering study in maize root tips provided 20 fluxes of central carbon metabolism in three subcellular compartments (Dieuaide-Noubhani et al., 1995). The study revealed two parallel routes for fueling of the TCA cycle by triose phosphate: the phosphoenolpyruvate branch and the pyruvate kinase branch. In addition, sucrose cycling was identified to be the largest flux, consuming about 70% of the ATP produced by respiration (Dieuaide-Noubhani et al., 1995). These implausibly high estimates are probably an artefact of the assumption that the labeling of the extracted glucose represents the labeling of the cytosolic pool, thereby ignoring the vacuolar glucose pool. Sucrose cycling can only be reliably quantified by steady-state MFA if the isotopic enrichment of cytosolic and vacuolar glucose is known, an information that is not easy to obtain (Kruger et al., 2007b).

As cell suspension cultures are very versatile, they have been used to study the metabolic flux phenotype of e.g. *Arabidopsis* (Williams et al., 2008; Masakapalli et al., 2010; Masakapalli et al., 2013; Masakapalli et al., 2014a) and tomato cells (Rontein et al., 2002). Tomato cell suspensions in different stages of the cell cycle revealed that fluxes through key pathways, like glycolysis, PPP and TCA cycle remained constant relative to total glucose influx, whereas anabolic fluxes were found to be variable throughout the culture cycle (Rontein et al., 2002). The central reactions hence displayed metabolic stability, whereas anabolic pathways seemed flexible, depending on growth demand (Rontein et al., 2002). Most MFA studies in plant tissue have, however, focused on seeds, due to their economic relevance and metabolic amenability (Schwender et al., 2003; Schwender et al., 2004; Sriram et al., 2004; Schwender et al., 2006; Spielbauer et al., 2006; Alonso et al., 2007a; Lonien and Schwender, 2009; Allen et al., 2009b; Alonso et al., 2010; Alonso et al., 2011; Allen and Young, 2013; Schwender et al., 2015). These studies considerably enhanced the understanding of metabolic pathways in storage tissue. High carbon use efficiencies were discovered for green seeds, e.g. seeds of soybean (Allen et al., 2009b), maize (Alonso et al., 2010; Alonso et al., 2011) and *Brassica napus* (Schwender et al., 2003; Schwender et al., 2004; Schwender et al., 2006), as compared to non-green seeds, e.g. seeds of sunflower (Alonso et al., 2007a). This is attributed to the light-driven provision of ATP and reductant for fatty acid biosynthesis in green seeds by operation of the RuBisCO bypass, which allows the more efficient conversion of hexose to oil (Schwender et al., 2004; Allen et al., 2009b; Schwender et al., 2015). The RuBisCO bypass eliminates the need for significant TCA cycle flux and provides 3-phosphoglycerate as main carbon source for fatty

acid synthesis in developing *Brassica napus* embryos. Plastidic pyruvate entering the fatty acid synthesis is mainly derived via pyruvate kinase activity (Schwender et al., 2006; Schwender et al., 2015). Compared to *Brassica napus* seeds, soybean metabolism provides sufficient reductant, but requires large amounts of ATP for protein and oil biosynthesis. Flux through RuBisCO is lower than in oilseed rape, probably due to the conventional operation of the TCA cycle, which provides most of the required ATP (Allen et al., 2009b). Besides sugars, glutamine can serve as carbon source for fatty acid biosynthesis in soybean. Modulation of pyruvate kinase and malic enzyme activities coordinate glycolysis with amino acid uptake (Allen and Young, 2013), and hence carbon partitioning into protein and oil (Iyer et al., 2008). In non-green sunflower embryos, the demand for ATP and NADPH for fatty acid synthesis is met by high fluxes through the TCA cycle and the OPPP, pathways that release a lot of CO₂. Other than in green tissue, the emitted CO₂ in non-green embryos cannot be refixed by RuBisCO, thus lowering the carbon conversion efficiency (Alonso et al., 2007a). The studies indicate, that the importance of the TCA cycle in providing ATP for oil biosynthesis is inversely related to the ability to harness light. In maize embryos, hexose-P is the main carbon source for fatty acid biosynthesis, a minor contribution being made by malate. The reductant NADPH is mainly supplied by the OPPP, which is, however, not able to cover the whole demand. Hence, NADP-dependent malic enzyme is important to provide additional reductant. The ATP demand is completely covered by the activity of plastidic pyruvate kinase and phosphoglycerate kinase (Alonso et al., 2010). Compared to the maize embryo, the endosperm mainly produces starch. Therefore, it has a decreased demand for NADPH and hence a lower flux through the OPPP, as compared to other heterotrophic plant tissues (Alonso et al., 2011).

To enhance understanding about metabolic regulation, MFA has been used to investigate metabolic effects of genetic and environmental perturbations (Spielbauer et al., 2006; Iyer et al., 2008; Williams et al., 2008; Lonien and Schwender, 2009; Allen and Young, 2013; Masakapalli et al., 2014b). *Arabidopsis* cell suspensions exposed to elevated oxygen concentrations, revealed no change in relative fluxes through central metabolic reactions (Williams et al., 2008). Neither did transgenic tobacco hairy roots, engineered for enhanced geraniol production, which displays the robustness of central carbon metabolism (Masakapalli et al., 2014b). Only perturbations that alter biomass composition are likely to affect central carbon metabolism (Spielbauer et al., 2006; Iyer et al., 2008). Soybean cotyledons were exposed to high temperature, resulting in biomass accumulation and carbon partitioning to lipids (Iyer et al., 2008). The elucidation of fluxes of developing maize kernels by proton-decoupled ¹³C NMR spectroscopy and GC-MS revealed a significant increase in hexose cycling in starch-deficient mutants (Spielbauer et al., 2006).

In addition, transient labeling studies with kinetic flux calculations were conducted in heterotrophic plant cultures: cell suspensions (Baxter et al., 2007), as well as excised plant organs like leaves (McNeil et al., 2000; Boatright et al., 2004; Colón et al., 2010) and tubers (Matsuda et al., 2005). The studies focused on the kinetics of secondary metabolism (McNeil et al., 2000; Boatright et al., 2004; Matsuda et al., 2005; Colón et al., 2010) and dynamic stress responses (Baxter et al., 2007). Kinetic studies proved valuable to examine the flexible nature of plant metabolism and to predict rational targets for metabolic engineering. The examination of ^{13}C -labeling kinetics of *Arabidopsis* cell suspensions in response to oxidative stress demonstrated that the imposed stress significantly altered fluxes through central metabolic pathways by inhibiting the TCA cycle and amino acid biosynthesis (Baxter et al., 2007). Under stress conditions, carbon was rerouted to glycolysis and to the oxidative PP pathway. The detected switch from anabolism to catabolism was hypothesized to help maintain the cellular ATP level (Baxter et al., 2007). Kinetic modeling of radiotracer data revealed that the main pathway of choline biosynthesis in tobacco leaf discs is at the phosphor-base level and allowed the prediction of phosphoethanolamine *N*-methyltransferase as rational target for enhancing the flux towards choline, the precursor of glycine betaine synthesis (McNeil et al., 2000). Labeling with phenyl-*d*5-alanine and subsequent analysis of labeling kinetics by GC-MS and LC-MS was used to study the phenylpropanoid pathway in wound-healing potato tubers (Matsuda et al., 2005), as well as to analyze the benzenoid network of *Petunia* petals (Boatright et al., 2004; Colón et al., 2010). The analysis of benzenoid metabolism revealed a two times higher contribution of the non- β -oxidative pathway compared to the β -oxidative pathway (Boatright et al., 2004). Metabolic control analysis furthermore revealed phenylacetaldehyde synthase to be the major controlling enzyme of the phenylacetaldehyde branch of the benzenoid network (Colón et al., 2010).

3.3.6 Intracellular fluxes in autotrophic plant systems

To date, three pioneering studies describe isotopically non-stationary flux analysis of photoautotrophic organisms. The first one investigated the unicellular cyanobacterium *Synechocystis* (Young et al., 2011), whereby the calculations solely based on intracellular labeling data, without necessity for measured pool sizes. *Synechocystis* cultures were transiently labeled with $\text{NaH}^{13}\text{CO}_2$ and isotopic labeling profiles of several central carbon metabolites were detected by GC-MS and LC-MS/MS. The rates of Calvin cycle reactions, photorespiration and several side reactions were quantified with high precision. The results indicated a suboptimal carbon conversion efficiency in photoautotrophically grown cells, due to a loss of carbon through the oxidative pentose phosphate pathway (Young et al., 2011). In a more recent study, the flux phenotype of wild type and high-light acclimated intact *Arabidopsis* plants was assessed (Ma

et al., 2014). Labeling with $^{13}\text{CO}_2$ and subsequent analysis of labeling trajectories by GC-MS and LC-MS/MS resulted in the estimation of 54 free fluxes using INST-MFA, thereby providing a comprehensive description of the metabolic network. This is a great accomplishment, considering the estimation of only four free fluxes using kinetic flux profiling, as discussed below (Szecowka et al., 2013). Model-based estimates of inactive pools and subcellular compartmentation were used to fit the measured data to the model. Increased photorespiratory carbon loss was detected after acclimation to high light, which was associated with a repartitioning of photosynthetic carbon to promote growth. Whole *Arabidopsis* plants were additionally examined by an extended KFP approach after transient labeling with $^{13}\text{CO}_2$ and enrichment detection by GC-TOF-MS and LC-MS/MS (Szecowka et al., 2013). Isotopic labeling data and directly measured pool sizes were used as model constraints, including the results of non-aqueous fractionation to distinguish between cytosolic, vacuolar and plastidic pools (Szecowka et al., 2013). The method of isotopically non-stationary metabolic flux analysis shows high potential for accurate computation of individual reaction fluxes in complex metabolic networks and paves the way for extended kinetic studies of plant dynamic phenotypes.

4 Materials and Methods

4.1 Chemicals

For isotopic studies, $^{13}\text{CO}_2$ (> 99 atom% ^{13}C) was purchased from Eurisotop (Saarbrücken, Germany). Labeled ammonium nitrate ($^{15}\text{NH}_4\text{NO}_3$, > 98 atom% ^{15}N) was obtained from Sigma-Aldrich (Steinheim, Germany). If not otherwise specified, remaining chemical components were purchased from Sigma Aldrich (Steinheim, Germany), Merck (Darmstadt, Germany) or Carl Roth GmbH (Karlsruhe, Germany) and were of analytical grade.

4.2 Plant growth

4.2.1 Plant material

Seed material of *O. sativa* L. ssp. *japonica* Nipponbare was obtained from CropDesign N.V. (Zwijnaarde, Belgium).

4.2.2 Media

Plants were grown either on soil (Einheitserde Type-GS90, 70% organic fiber peat, 30% clay, pH 5.5-6, Einheitserde- und Humuswerke Gebr. Patzer, Altengronau, Germany) or on hydroponic medium, containing 1.43 mM ammonium nitrate, 1 mM calcium chloride hexahydrate, 0.18 mM magnesium sulfate heptahydrate, 1.32 mM potassium sulfate, 0.32 mM monosodium phosphate, 1 mM Fe-ethylendiaminetetraacetic acid, 8 μM manganese (II) chloride tetrahydrate, 0.15 μM zinc sulfate heptahydrate, 0.15 μM copper (II) sulfate pentahydrate, 0.075 μM ammonium heptamolybdate and 1.39 μM boric acid (Ritte, 2010). In isotope experiments, naturally labeled NH_4NO_3 was replaced by an equimolar amount of $^{15}\text{NH}_4\text{NO}_3$.

4.2.3 Growth conditions

Rice seeds were germinated on moist filter paper in a Petri dish for four days at 26 °C in the dark. Seeds were then transferred into light (500 $\mu\text{mol m}^{-2} \text{s}^{-1}$ photosynthetically active radiation (PAR)), one day before they were either transplanted into 0.7 dm³ pots used for further cultivation on soil or into hydroponic boxes. Prior to sowing, pots were soaked with deionized water, containing 0.15% of the fungicide proplant (Stähler, Stade, Germany) and seeds were subjected to hot water treatment (60 °C, 10 min) to prevent sheath rot. Rice plants were grown under 13/11 h day/night cycles at an average irradiance of 500 $\mu\text{mol m}^{-2} \text{s}^{-1}$ PAR during the light phase (Powerstar HQI-BT 400W, Osram, Munich, Germany), temperature cycles of 26/21 °C and a relative humidity of 60%. During the first 14 days of development, plants were

irrigated two times per day with deionized water. During the first three weeks, plants were watered via top-irrigation, later via sub-irrigation. Between weeks three and ten, plants were fertilized with 'Hakaphos-Blau' solution (0.3% in deionized water, Compo, Münster, Germany) twice per week, replacing one deionized water treatment, respectively. Plants in different developmental stages were used for $^{13}\text{CO}_2$ labeling experiments. Rice seedlings were used for experimental purposes after 12 to 15 days of cultivation. Plants of the flowering, as well as the early and late grain filling stages were examined at an age of 68 days, 75 and 88 days, respectively. Alternatively, plants were grown in hydroponic containers (27 x 17 x 12 cm), covered with a perforated styrofoam plate. Plastic meshes were placed inside the holes (2 cm diameter) on which pre-germinated seedlings were cultivated with their roots freely suspended in hydroponic medium, which was replaced once per week. The hydroponic cultures were incubated under the same conditions regarding light, temperature and humidity as soil-grown plants.

4.2.3.1 High salt treatment

In salt stress experiments, hydroponically growing seedlings were subjected to high salt treatment for six days, by adding 100 mM NaCl to the growth medium.

4.2.3.2 Imazapyr treatment

Prior to the labeling experiment, soil-grown seedlings were subjected to herbicide treatment using imazapyr, a non-selective herbicide of the imidazolinone group. The imazapyr solution (0.3 mM imazapyr (BASF SE, Ludwigshafen, Germany), 0.1% (v/v) dimethyl sulfoxide (DMSO), 0.1% (v/v) adjuvant Dash E.C. (BASF SE, Ludwigshafen, Germany)) was applied with an airbrush, reflecting common doses of 62.5 g ha⁻¹ (Johnson et al., 1999). Control plants were subjected to a reference treatment (0.1% (v/v) DMSO, 0.1% (v/v) Dash E.C.). Labeling experiments were conducted four hours after herbicide application.

4.3 Isotopic labeling experiments with $^{13}\text{CO}_2$

All described experiments, except for those concerning method development, were performed under the following conditions: 400 $\mu\text{L L}^{-1}$ $^{13}\text{CO}_2$ was applied in the time frame of four to eight hours after sunrise. Pulse-chase experiments were performed with 12 day old seedlings. For dynamic labeling studies, 15 day old seedling were chosen, as more plant material was necessary for comprehensive analytics.

4.3.1 Pulse-chase labeling experiments

The labeling experiments were conducted in specifically constructed labeling reactors (Figure 5. 1). These reactors were designed and constructed by Detlev Rasch (Institute of Biochemical Engineering, Technical University Braunschweig, Germany). A large tube reactor (0.5 m diameter, 1.3 m height, 255 L volume) was designed for $^{13}\text{CO}_2$ isotope experiments with soil-grown, adult plants (Figure 5. 1 A), and a small tube reactor (0.5 m diameter, 0.5 m height, 98 L volume) served for $^{13}\text{CO}_2$ isotope experiments at the seedling stage (Figure 5. 1 B). The tube reactors were built from Plexiglas[®] acrylic sheets (5 mm thickness, Hans Keim Kunststoffe, Rottweil, Germany). The material allowed full spectral transmission of sunlight at wavelengths between 400 nm and 900 nm, containing the essential spectral interval for plant growth (Figure 5. 2). EPDM rubber (ethylene propylene diene monomer, Mercateo, Munich, Germany) was used as sealing material, because of its high flexibility and endurance. The rubber sealing was agglutinated to the plexiglas or polycarbonate sheets with solvent-free glue (Loctite 406 Henkel, Düsseldorf, Germany). The tube was conglutinated to the lid with a two-component adhesive (Pattex Stabilit, Henkel, Düsseldorf, Germany). For maintenance of a constant temperature, a cooling system with a water-cooled ventilator (peltier cooler/heater, 380W, 24V, Uwe Electronic, Unterhaching, Germany), connected to an external cryostat (Lauda RMT20, Lauda Dr. R Wobser, Lauda-Königshofen, Germany) was installed. The ventilator and the connectors were attached to the bottom plate of the reactor. To keep the humidity level at or above 60% of saturation during the experiments, water-soaked cloth was placed in a glass beaker inside the enclosure. Temperature and relative humidity were monitored on-line by a humidity and temperature logger (Voltcraft DL-120 TH, Conrad Electronic SE, Hirschau, Germany). The CO_2 concentration was measured once by a carbon dioxide gas analyzer at the beginning of the experiment (Voltcraft CM-100, Conrad Electronic SE, Hirschau, Germany). All reactors contained two perforated pipes, one in the upper back part (exhaust air) and one in the lower back part (supply air). These were connected to a CO_2 adsorption unit, consisting of a high power pump (6000 L min^{-1} , Bravo 2000, 220V, Scoprega Spa, Cassano d/Adda, Italy), a fine dust filter (Filter Cartridge A Kärcher, Gelsenkirchen, Germany) and a CO_2 adsorber (5 L, Dräger-sorb[®] 800+, Drägerwerk, Lübeck, Germany). All power supplies, except for the external adsorber pump, had 24V D.C. to allow safe handling. All labeling reactors were installed inside a phyto chamber (Svalöf Weibull, Malmö, Sweden), directly beside lab benches, where rice plants were grown at ambient air prior to and after the labeling experiments, respectively. For labeling studies, plants were placed inside the enclosure. In order to avoid that CO_2 released from the soil altered the composition of the well-defined gas atmosphere, pots were covered with plastic wrap. Ambient CO_2 was removed ($< 20 \mu\text{L L}^{-1}$) by adsorption for a short time period of about 30 seconds, as described above. Immediately after purging, the desired amount of

$^{13}\text{CO}_2$ was injected through a valve (screw cap with silicone diaphragm), positioned in the lid of each enclosure and the plants were then incubated for a defined labeling period. Afterwards, the plants or specific parts of it were directly harvested or further cultivated in the phyto chamber at ambient air, prior to analysis. All harvested plants or plant tissues were immediately deep-frozen in liquid nitrogen to stop metabolic activity. At each sampling time point, at least three biological replicates were obtained. In the case of seedling experiments, the whole shoot was harvested. Roots were collected from hydroponically grown plantlets and treated equally. Of a full-grown plant, five tillers were harvested, whereby flag leaf, leaf, stem and panicle were separated, followed by immediate quenching in liquid nitrogen. The 'leaf' was defined as whatever leaf on the tiller except the flag leaf. The individual tissues originating from the five tillers were pooled. The outermost, photosynthetically active leaves were removed from the stem prior to further treatment. Experiments were generally performed in the timeframe of four to eight hours after sunrise.

4.3.1.1 Combined ^{13}C and ^{15}N labeling experiment

A box reactor (C/N reactor, 0.5 x 0.5 x 0.5 m, 125 L volume) was developed for combined $^{13}\text{CO}_2$ and $^{15}\text{NH}_4\text{NO}_3$ labeling of hydroponic rice cultures (Figure 5. 1 C). The reactor was built from polycarbonate (5 mm thickness, Hans Keim Kunststoffe, Rottweil, Germany), which allowed full spectral transmission of sunlight (Figure 5. 2). Plants were pre-grown in the phyto chamber as hydroponic cultures. Prior to the experiment, cultures were transferred from naturally labeled growth medium to a container with $^{15}\text{NH}_4\text{NO}_3$ medium. The container was then placed inside the reactor on a perforated plate (polyvinylchloride, 5 mm, Hans Keim Kunststoffe, Rottweil, Germany) and the enclosure was closed tightly via fixation clamps. Immediately afterwards, the $^{13}\text{CO}_2$ pulse was applied, as described above. Monitoring and control of temperature, humidity and $^{13}\text{CO}_2$ level was done as described for the tube reactors (see above). At the end of the labeling incubation period, the box reactor was opened to ambient air and the plants were either directly harvested or re-transferred into naturally labeled growth medium after washing the roots with the latter. Sampling and sample processing was done as described above.

4.3.2 Dynamic labeling experiments

A sophisticated, gas-tight and largely automated flux incubator (0.75 x 0.75 x 1.1 m, 620 L volume) was constructed for dynamic labeling experiments, allowing the incubation of seedlings, as well as adult plants (Figure 5. 14). The reactor constructed by Detlev Rasch (Institute

of Biochemical Engineering, Technical University Braunschweig, Germany) consisted of a detachable upper part and a movable lower part and was installed inside a phyto chamber to provide equal growth and labeling conditions concerning light intensity and quality.

The detachable plant incubator unit was built from polycarbonate (8 mm thickness, Hans Keim Kunststoffe, Rottweil, Germany), allowing full spectral transmission of light. The polycarbonate sheets were connected by a housing frame made of duralumin (item Industrietechnik GmbH, Solingen, Germany). To permit easy transfer of the plant pots to the incubator unit, one of the housing walls was constructed to be an operable door that could be tightly closed by fixation clamps. As for the above-described reactors, EPDM rubber (Mercateo, Munich, Germany) seals were attached, using the solvent-free glue Loctite 406 (Henkel, Düsseldorf, Germany). The incubator unit was further equipped with a sampling port (Figure 5. 16 A), allowing the fast harvest of individual plants without disturbing the reactor atmosphere. The sampling port consisted of an opening in one of the housing walls, covered by flexible rubber straps (THERABAND, The Hygenic Corporation, Akron, OH, USA). A polycarbonate plate (5 mm, Hans Keim Kunststoffe GmbH, Rottweil, Germany) was magnetically attached to the port during adsorption and in between sampling to completely seal up the incubator unit. For flexible positioning of individual plants in front of the sampling port, the reactor was further equipped with a polyvinylchloride (5 mm, Hans Keim Kunststoffe, Rottweil, Germany) turning table, operated by an external chopper transistor (Transistor-Gleichstromsteller Typ GS 24 S, EPH elektronik, Besigheim-Ottmarsheim, Germany). Specially designed scissors were used to quickly harvest individual plants. Therefore, foam rubber pieces (Meteor Gummiwerke, Bockenem, Germany) were attached to the blades of gardening scissors (Classic Anvil Secateurs, GARDENA, Ulm, Germany). These foam rubber pieces fixed the cut plant, allowing it to be safely and single-handedly transferred through the sampling port (Figure 5. 16 B).

The regulatory unit in the lower part of the reactor comprised an automated temperature-regulating and air-humidification system, as well as a ventilating system to ensure sufficient air circulation for fast mixing of the injected $^{13}\text{CO}_2$ with the reactor atmosphere (Figure 5. 14 C-E). The temperature was regulated by a peltier cooling/heating element (UETR-PT24V16A, uwe electronic, Unterhaching, Germany) with integrated temperature sensor, mediating the switch from cooling to heating by a change in polarity. The humidifier consisted of a 1.5 L reservoir for deionized water and a submerged piezoceramic transducer (Conrad Electronic SE, Hirschau, Germany), nebulizing the water by mechanical oscillation of the ceramics at 3 MHz. A constant air flow from the inside of the incubator through the peltier element and the humidifier back into the plant chamber, was enabled by strong ventilators ($170 \text{ m}^3 \text{ h}^{-1}$, 4312 NGN and

5 m³ h⁻¹, 4312 NGN, ebm-papst, Muldingen, Germany). An injection valve (screw cap with silicone diaphragm) in the incubator wall enabled the application of the ¹³CO₂ gas, thereby starting the labeling experiment. An online CO₂ monitoring system, in form of a quadrupole mass spectrometer (Pfeiffer Vacuum GmbH, Asslar, Germany), allowed for the discrimination of ¹²CO₂ and ¹³CO₂, recording their respective concentration throughout the experiment. The HiQuad mass spectrometer (100-240 V, 50/60 Hz) was able to detect masses in a range of 1 to 512 amu. The capillary of the mass spectrometer was inserted into the incubator via a pinhole in one of the incubator walls, sealed by a cable fitting. A CO₂ adsorption unit, connected to a high power pump (1.8 m³ min⁻¹, BRAVO 2000, Scoprega, Cassano D'Adda, Italy) allowed for the removal of up to 96% of the atmospheric CO₂ within one minute. The air from the inside of the chamber was pumped through 15 L of soda lime pellets (Drägersorb® 800+, Mercateo, München, Germany) and CO₂ depleted air was returned into the incubator after passing a fine dust filter. A vacuum valve with adsorber material and a fine dust filter, as well as a pressure relief valve were integrated to compensate for low and gauge pressure during and right after adsorption, respectively.

Prior to labeling, 15 soil-grown rice seedlings were placed in the flux incubator and atmospheric CO₂ was removed (< 20 µL L⁻¹) by adsorption for 60 seconds. Immediately after adsorption, ¹³CO₂ was injected with a gas-tight syringe (500 mL, Hamilton Company, Reno, NV, USA) to reach a concentration of 400 µL L⁻¹. The first time point was sampled directly after injection. In total, 15 samples were collected over a 30 minute interval at the following time points: 0, 10, 20, 30, 40, 50, 60, 90, 120, 150, 180, 300, 420, 600, 1800 seconds. The entire shoot was harvested and immediately quenched in liquid nitrogen. The sampling process was performed in one to two seconds. Additionally, root material was collected at the following time points: 300, 600 and 1800 seconds. The root was extracted from the soil, immediately after shoot harvest, and washed in deionized water. The seed and all remaining green tissue were cut off the root, which was subsequently deep-frozen in liquid nitrogen to stop metabolic activity. Five replicate experiments were conducted per studied condition, each including a total of 75 rice seedlings.

4.4 Analytics

Analytical processing was performed in collaboration with Metanomics GmbH (Berlin, Germany), if not specified otherwise. EA-C-IRMS and GC-C-IRMS measurements of pulse-chase studies, were performed in collaboration with BASF Agricultural Center (Limburgerhof, Germany), as indicated below. Prior to the following sample processing and analytical steps, the

harvested plant material was freeze-dried (Christ Gamma 2-16 LSC, Martin Christ Gefriertrocknungsanlagen, Osterode am Harz, Germany) and ground to fine powder in a ball mill (3-5 min, 30 Hz, Retsch MM300, Retsch, Haan, Germany).

4.4.1 EA-C-IRMS and C/N elemental analysis of whole plant material

EA-C-IRMS analyses were performed to determine the ^{13}C and ^{15}N uptake of rice seedlings. Therefore, the total ^{13}C and ^{15}N enrichment of seedling samples from a typical labeling experiment (4.3.2) was measured. Five biological replicates were analyzed. Additionally, EA-C-IRMS was used to measure the C/N ratio of unlabeled plant material to determine their protein content. Three biological replicates were analyzed. For both analyses, an amount of 0.8 to 0.9 mg dried plant material was transferred into a tin capsule (3.5 x 5 mm, HEKAtech, Löbau, Germany). EA-C-IRMS analyses were performed at 1020 °C on a FLASH HT Plus elemental analyzer (Thermo Fisher Scientific, Bremen, Germany) run in the single reactor combustion mode. The dedicated reactor sections comprised layers of Cr_2O_3 for combustion, of reduced Cu for reduction and of silvered cobaltous/cobaltic oxide to remove halogens and sulfur.

Measurement of samples from pulse-chase experiments (4.3.1) was performed in collaboration with BASF Agricultural Center (Limburgerhof, Germany) with the following alterations to the above described protocol:

The isotopic enrichment of the dried plant material was determined using an elemental analyzer (FLASH 2000 Elemental Analyser, Thermo Scientific, Waltham, USA-MA) coupled to an isotope-ratio mass spectrometer (Delta V Plus Isotope Ratio MS, Thermo Scientific, Waltham, USA-MA). The gas flow was set to 300 mL min⁻¹ and the column temperature was kept at 41 °C. Three biological and two technical replicates were analyzed.

4.4.2 GC-C-IRMS for isotopic enrichment detection

4.4.2.1 Proteinogenic amino acids

The isotopic enrichment of protein-bound amino acids was measured by GC-C-IRMS. Protein extraction was carried out as described previously (Hurkman and Tanaka, 1986), involving the modifications outlined below. An amount of 5 mg dry plant material was mixed with 400 µL extraction buffer (0.175 M tris(hydroxymethyl)aminomethane/HCl, pH 8.8, 5% (w/v) sodium dodecylsulfate, 15% (v/v) glycerol, 0.3 M dithiothreitol) and clarified by centrifugation (13,000 xg, 10 min, room temperature). The supernatant was mixed with 1.6 mL ice-cold acetone and incubated for precipitation of cell protein (1 h, -20 °C). Precipitated protein was collected by centrifugation (13,000 xg, 10 min, 4 °C), washed two times with 80% acetone, air-dried and

then hydrolyzed into amino acids (125 μL , 6 M HCl, 100 $^{\circ}\text{C}$, 12 h). The hydrolyzate was clarified from solids (Millipore, Ultrafree-MC, Durapore-PVDF 0.22 μm , Sigma-Aldrich, Steinheim, Germany) and evaporated under a nitrogen stream. Amino acids were derivatized by addition of pyridine and N-methyl-N-*t*-butyldimethylsilyl-trifluoroacetamide (MBDSTFA, Macherey-Nagel, Düren, Germany), followed by incubation for 1 hour at 80 $^{\circ}\text{C}$ (adapted from Heinzle et al., 2008). Labeling measurement was conducted on a GC-C-IRMS instrument (Trace 1300 gas chromatograph, TriPlus RSH autosampler, GC Isolink (with a NiO combustion tube in combination with NiO and CuO wires set to 1000 $^{\circ}\text{C}$), ConFLO IV interface, Delta V Advantage isotope ratio mass spectrometer, Thermo Fisher Scientific, Bremen, Germany). Water, generated in the combustion reactor, was removed by passage of the combustion products through a water permeable Nafion membrane. The GC was operated in the splitless mode (injection volume 1 μL). Separation was conducted on a DB-5 column (30 m x 0.25 mm, 0.25 μm , Agilent Technologies, Santa Clara, CA, USA), with helium as carrier gas set to constant flow (2.3 mL min^{-1}). The following temperature program was applied: 1 min at 70 $^{\circ}\text{C}$, 8 $^{\circ}\text{C min}^{-1}$ to 280 $^{\circ}\text{C}$, 50 $^{\circ}\text{C min}^{-1}$ to 340 $^{\circ}\text{C}$ and 3 min at 340 $^{\circ}\text{C}$. Five biological replicates were analyzed.

Measurement of samples from pulse-chase experiments (4.3.1) was performed in collaboration with BASF Agricultural Center (Limburgerhof, Germany) with the following alterations to the above described protocol:

Isotopic composition of proteinogenic amino acids was measured by GC-C-IRMS (Trace GC Ultra Gas Chromatograph, Delta V Plus Isotope Ratio MS, Thermo Scientific, Waltham, USA-MA). A sample volume of 0.5 μL was injected via the PTV-inlet (250 $^{\circ}\text{C}$) at a split ratio of 1:20. Helium was used as carrier gas at a constant flow rate of 1 mL min^{-1} . Analytes were separated on a fused silica capillary column (HP-5MS, 30 m x 25 mm, 0.25 μm , Agilent, Waldbronn, Germany) and then transferred to an oxidizing combustion reactor (1000 $^{\circ}\text{C}$). The initial oven temperature of 120 $^{\circ}\text{C}$ was kept for 2 minutes. Afterwards, temperature was increased at a rate of 8 $^{\circ}\text{C min}^{-1}$ until 200 $^{\circ}\text{C}$. In a second gradient step, temperature was raised to 300 $^{\circ}\text{C}$ at 10 $^{\circ}\text{C min}^{-1}$, followed by a temperature hold for 5 minutes. The GC-C-IRMS profile of MBDSTFA-derivatized amino acids was obtained in selective ion monitoring (SIM) mode via the mass isomers of formed CO_2 (m/z 44, 45, 46) and N_2 (at m/z 28, 29) at their corresponding retention time, respectively. Metabolite identification was achieved by GC-MS (7890A GC-System, 7000 GC/MS Triple Quad, 7693 Autosampler, Agilent Technologies, Waldbronn, Germany) measurements of single amino acids and their mixture (10 μM each) in full-scan acquisition mode, followed by a NIST mass spectral search (NIST MS search 2.0) and comparison of the chromatographic pattern with the one of the corresponding GC-C-IRMS measurement.

Data acquisition and evaluation was conducted using the Software Isodat NT (Thermo Scientific, Waltham, USA-MA). Analytical accurateness was a precondition for further data evaluation. Data points, for which peak integrity was corrupted, e.g. seedling, tyrosin, t0, were therefore omitted from graphical data representation. Three biological and two technical replicates were analyzed.

4.4.2.2 Free amino acids and sugars

The isotopic enrichment of free amino acids, soluble sugars and malate was measured by GC-C-IRMS (Table 5. 2). Metabolite extraction was carried out, using 5 mg lyophilized and ground plant material, extracted with cold methanol/water/formic acid (80/20/1 (v/v/v)) using a ball mill (30 seconds, 30 Hz, Retsch MM300, Retsch, Haan, Germany). After centrifugation (13,000 xg, 10 min, 4 °C) the supernatant was subjected to solid phase extraction (Oasis MCX, Waters, Eschborn, Germany). Therefore, it was loaded onto the conditioned and equilibrated sorbent material and washed with methanol/water/formic acid (80/20/1 (v/v/v)). The flow-through, containing free sugars, was collected and dried down. The dried residue was redissolved in 50 µL methoxyamine hydrochloride in pyridine (20 mg mL⁻¹) and derivatized for 90 minutes at 60 °C, followed by a second derivatization step (50 µL MSTFA, 30 minutes, 60 °C). Amino acids, bound to the solid phase, were subsequently eluted with 5% ammoniumhydroxid in acetonitril, dried down and derivatized for 60 minutes at 60 °C in pyridin and MBDSTFA (Macherey-Nagel, Düren, Germany). Labeling measurements were according to 4.4.2.1 with the following changes of injection volumes and temperature profiles. For analysis of free amino acids: 1 µL injection volume, 2 min at 100 °C, 10 °C min⁻¹ to 280 °C, 50 °C min⁻¹ to 340 °C and 1 min at 340 °C. For analysis of soluble sugars: 0.5 µL injection volume, 1 min at 100 °C, 50 °C min⁻¹ to 140 °C, 5 °C min⁻¹ to 190 °C, 40 °C min⁻¹ to 340 °C and 2 min at 340 °C. For analysis of sucrose: 0.5 µL injection volume, 2 min at 200 °C, 50 °C min⁻¹ to 340 °C and 2 min at 340 °C. Five biological replicates were analyzed.

4.4.3 LC-MS/MS analysis of sugar phosphates and organic acids

The mass isotopomer distribution (Table 5. 2), as well as the concentration (Table 5. 3) of sugar phosphates, organic acids and amino acids was determined by LC-MS/MS analysis. Metabolite extraction was performed as described previously (Balcke et al., 2011) with the following modifications. An amount of 5 mg dried plant material was extracted with 900 µL of ice cold dichloromethane/ethanol (2:1) and 150 µL 1.5 M ammonium acetate by bead milling (6.5 m s⁻¹, 30 s, FastPrep24, MP Biomedicals, Eschwege, Germany). After centrifugation (14.000 xg, 2 min, 0 °C), 100 µL of the polar phase was collected in a centrifugal filter unit

(Millipore, Ultrafree-MC, Durapore-PVDF 0.22 μm , Sigma-Aldrich, Steinheim, Germany). Extraction and centrifugation was repeated with 150 μL 1.5 M ammonium acetate. An amount of 200 μL of the polar phase, combined with the first extract, was purified through filter units (14.000 $\times\text{g}$, 2 min, 0 $^{\circ}\text{C}$). The entire extract was lyophilized and resuspended in 100 μL deionized water. Mass isotopomer distributions were determined applying an acquisition method corresponding to Balcke et al. (2011). To quantify pool sizes, an external calibration series was used for each individual metabolite. A list of isotopomer transitions and additional acquisition parameters, used for the analyses, can be found in Table A9. 14. Five biological replicates were analyzed.

4.4.4 GC-MS analysis of sugars, sugar phosphates, amino and organic acids

The mass isotopomer distribution (Table 5. 2), as well as the concentration (Table 5. 3) of amino acids, organic acids, soluble sugars and sugar phosphates was determined by GC-MS analysis. Intracellular metabolites were extracted from 5 mg lyophilized tissue with 800 μL polar (80% (v/v) methanol) and nonpolar (methanol/dichloromethane, 2:3) solvents, using a ball mill (3 min, 30 Hz, Retsch MM300, Retsch, Haan, Germany). The polar phase was dried down and subjected to derivatization followed by GC-MS analysis as described by Walk et al. (2007) with the following modifications. In brief, the polar fraction was derivatized with O-methyl-hydroxyamine hydrochloride to convert oxo-groups to O-methyloximes and subsequently with a silylating agent (N-methyl-N-(trimethylsilyl) trifluoroacetamide) before GC-MS analysis (6890 GC coupled to a 5973 MS-System, Agilent Technologies, Waldbronn, Germany). Each sample was analyzed twice by two different SIM methods with split ratios reflecting the analyte concentration. A list of mass fragments, used for analyses, can be found in Table A9. 13. Quantitative measurements of the compounds of interest were performed using an external calibration. Five biological replicates were analyzed for the determination of mass isotopomer distributions and the quantification of pool sizes.

4.4.5 Determination of biomass composition

Sucrose and starch levels were determined from 10 to 20 mg of lyophilized plant material, extracted with 1.5 mL 80% (v/v) ethanol using a ball mill. The samples were cooled to 4 $^{\circ}\text{C}$ and starch was separated by centrifugation (12.000 $\times\text{g}$, 5 min, 4 $^{\circ}\text{C}$). An amount of 200 μL of supernatant, containing free sugars, was dried down. The dried residue was redissolved in 50 μL methoxyamine hydrochloride in pyridine (20 mg mL^{-1}) and derivatized for 90 minutes at 60 $^{\circ}\text{C}$, followed by a second derivatization step (50 μL MSTFA (Macherey-Nagel, Düren, Germany), 30 minutes, 60 $^{\circ}\text{C}$). The pellet was washed with 1.5 mL 80% (v/v) ethanol and dried down. The dried pellet was incubated at 55 $^{\circ}\text{C}$ with 850 μL buffer (100 mmol L^{-1} imidazole

(Sigma-Aldrich, Steinheim, Germany) and 5 mmol L⁻¹ MgCl₂ x 6 H₂O (Roth, Karlsruhe, Germany), pH 7.0), 75 µL α-amylase (25 units, Sigma-Aldrich, Steinheim, Germany) and 75 µL amyloglucosidase (25 units, Sigma-Aldrich, Steinheim, Germany) at 1.400 rpm using a Thermomixer comfort (Eppendorf, Hamburg Germany). After 24 hours the samples were centrifuged (12.000 xg, 5 min, 25 °C) and 100 µL of the supernatant was used for analysis of free sugars as described above. Measurements were performed using an Agilent MSD instrument. The GC was equipped with a split/splitless injector (split 15:1; injection volume 0.5 µL for sugar analysis) and a RXI-XLB column (20 m, 0.18 mm I.D., 0.18 µm film thickness (Agilent Technologies, Santa Clara, CA, USA), with helium as carrier gas set at constant flow (1.3 mL min⁻¹). The following temperature program was applied: 1 min at 70 °C, 120 °C min⁻¹ to 120°C, 18°C min⁻¹ to 220°C, 45°C min⁻¹ to 350°C, 2 min at 350°C. Quantitative measurements of the compounds of interest were performed using an external calibration. Three biological replicates were analyzed.

Fatty acid methyl esters (FAMES) were quantified in samples of approximately 25 mg plant dry weight. First, fat was extracted by mixing plant material with 1 mL of methyl-*tert*-butyl-ether (MTBE) in a ball mill (5 min, 30 Hz, 5 mm steel ball, Retsch MM300, Retsch, Haan, Germany). After centrifugation, 10 µL trimethylsulfonium hydroxide (TMSH) solution (0.25 mol L⁻¹ in methanol) was added to 200 µL of extracted fat to hydrolyze the latter and concurrently esterify free fatty acids. Triheptadecanoin (C17:0) was used as internal standard. After 20 minutes of incubation at room temperature, samples were analyzed by GC-MS (6890 gas chromatograph, 5973 inert MS detector, EI, scan 50 – 400 amu, Agilent Technologies, Waldbronn, Germany). The GC was operated in the split mode (1:75, injection volume 0.5 µL) and a MXT-WAX column (10 m x 0.18 mm x 0.2 µm) Restek, Bad Homburg, Germany), with helium as carrier gas, was set at constant flow (0.5 mL min⁻¹). The following temperature program was applied: 0.5 min at 140 °C, 20 °C min⁻¹ to 240 °C and 2.5 min at 240 °C. Three biological replicates were analyzed.

The protein content of unlabeled whole plant material was determined by C/N elemental analysis as described in 4.4.1. Citrate, succinate and malate were quantified by GC-MS, as described in 4.4.4. Proteinogenic amino acids were quantified by UPLC-UV with adaptations based on the AccQTag analysis kit (Waters Corp, Milford, MA, USA). An amount of 4.5 mg of lyophilized plant material was hydrolyzed for 24 hours at 110 °C in 450 µL 6 M HCl, including 45.8 mg L⁻¹ norvaline as internal standard and 50 µL 100 mM sodium dithionite. An aliquot of 50 µL was dried under vacuum and derivatized for 15 min at 55 °C with 80 µL borate buffer and 20 µL reagent solution, supplied by the AccQTag analysis kit. The sample was filtered and subjected to UPLC-UV analysis as described by the instructions of the kit.

4.5 Calculation and data processing

4.5.1 Calculation of ^{13}C and ^{15}N enrichment

The δ values (‰), received after EA-C-IRMS and GC-C-IRMS analysis, are expressed relative to international standards as:

$$\delta = \left(\frac{R_{\text{sample}} - R_{\text{standard}}}{R_{\text{standard}}} \right) * 1000 \quad (\text{Eq. 4. 1})$$

where R is the ratio of $^{13}\text{C}/^{12}\text{C}$ or $^{15}\text{N}/^{14}\text{N}$. The ^{13}C and ^{15}N measurement was calibrated against Vienna Pee Dee Belemnite (VPDB) and atmospheric nitrogen, respectively, using the international reference materials cellulose (IAEA-CH-3) and ammonium sulphate (IAEA-N-1) as secondary standards. Typical values for $\delta^{13}\text{C}$ of unlabeled C3 plant material are between -34 and -22‰ (Meier-Augenstein, 1999a; Richter et al., 2010).

4.5.2 Data correction for natural isotopes

IRMS data of the pulse-chase studies were corrected for naturally occurring isotopes of the analyte and, in the case of GC-C-IRMS, additionally of derivative groups (Wittmann, 2007). Data correction was done corresponding to Docherty et al. (2001). In brief, δ values for labeled whole plant material and labeled amino acids were normalized to their respective unlabeled equivalents by subtracting values of the unlabeled control from the corresponding value of the labeled sample:

$$\delta_{\text{corr}} = \delta_{\text{sample}} - \delta_{\text{control}} \quad (\text{Eq. 4. 2})$$

where δ_{corr} is the labeled compound, δ_{sample} is the derivatized labeled compound and δ_{control} is the derivatized unlabeled compound. For each experiment, unlabeled control plants were harvested (at least three biological replicates) that were exposed to the exact same growth conditions as the labeled plants, i.e. that were grown on the same batch of soil or hydroponic medium, respectively. Furthermore, unlabeled controls were subjected to the same sample processing steps like labeled samples.

For amino acid pathway illustrations, corrected δ values were normalized to 100%. Therefore, the highest δ_{corr} value of the respective data set was identified and set 100%. The normalized value of any number x (X_{norm}) of the original data set was calculated by the following equation:

$$X_{\text{norm}} = \frac{x * 100}{\delta_{\text{max}}} \quad (\text{Eq. 4. 3})$$

where δ_{max} is the highest δ_{corr} value.

Dynamic experimental data were corrected for natural labeling of the derivatizing agent by the method described by Heinzle et al. (2008). Natural labeling of the oxygen atoms of CO₂ was corrected for by applying the method provided in INCA (Isotopomer Network Compartmental Analysis) (Young, 2014).

4.5.3 Calculating the absolute isotopic enrichment

As described above, the δ notation describes isotopic enrichment as a ratio of the abundance of heavy and light isotopes, relative to an international standard. Isotopic enrichment can, however, also be expressed as absolute value, called atom percent excess (APE). Calculating the absolute isotopic enrichment is necessary where the degree of ¹³C and ¹⁵N enrichment is to be directly compared, like in Figure 5. 7. First, atom percent (AP), i.e. the percentage of ¹³C or ¹⁵N atoms relative to the total amount of C or N atoms in the sample was determined via (Eq. 4. 4):

$$AP = \frac{100 * R_{\text{sample}}}{1 + R_{\text{sample}}} \quad (\text{Eq. 4. 4})$$

Atom percent excess was subsequently calculated by subtracting the enrichment of the control from the enrichment of the sample:

$$APE = AP_{\text{sample}} - AP_{\text{control}} \quad (\text{Eq. 4. 5})$$

To be comparable in absolute terms, ¹³C and ¹⁵N enrichment values were furthermore corrected for the C/N ratio of the sample or compound, by multiplying the APE value with the number of C or N atoms present in the molecule, respectively.

4.5.4 Determination of C/N elemental composition

Protein, a major portion of the cellular composition was quantified by determination of the C/N ratio of unlabeled plant material, analyzed by EA-C-IRMS. C/N elemental composition was performed by Isodat 3.0 software (Thermo Fisher Scientific, Bremen, Germany), with acetanilide being used for calibration of the instrument. The software allows calculating C/N elemental composition, both based on the data of the integrated thermal conductivity detector (TCD) and on the mass spectral data. In the latter case, N₂ is measured with the Faraday cups set to *m/z* 28 and 29.

4.5.5 Determination of root-to-shoot ratio and translocation flux

To set up a flux map for a rice seedling, it was important to derive the root-to-shoot ratio of the analyzed plantlets. It was assumed that the decrease of ¹⁵N enrichment in the root within two

hours of tracing is only due to translocation of label to the shoot. With this assumption, the root-to-shoot ratio was derived via the following formula:

$$M_{\text{shoot}} * (\delta^{15}\text{N}_{\text{shoot}, t_2} - \delta^{15}\text{N}_{\text{shoot}, t_0}) = M_{\text{root}} * (\delta^{15}\text{N}_{\text{root}, t_0} - \delta^{15}\text{N}_{\text{root}, t_2}) \quad (\text{Eq. 4. 6})$$

where M is the mass of shoot and root, respectively. A root:shoot ratio of 1:6 was obtained for twelve day old seedlings. This value was used to estimate the percent enrichment of individual plant parts after two hours of tracing. Considering that shoot biomass was six times as much as root biomass, it follows that ^{15}N enrichment of the shoot was diluted by a factor of six, upon translocation to the shoot, whereas ^{13}C enrichment accumulated 6-fold upon translocation to the root. Accordingly, $\delta^{15}\text{N}$ values of the shoot were multiplied by six, whereas $\delta^{13}\text{C}$ values of the root were divided by six. Shoot and root enrichment values of ^{13}C , as well as ^{15}N labeling at time point zero were summed, displaying 100% uptake, respectively. On this basis, ^{13}C and ^{15}N percent enrichments were estimated for root and shoot. The amount of ^{13}C labeling that could not be recovered in plant tissue was assumed to be lost by respiration.

4.5.6 Determination of biomass formation rate

The biomass formation rate, used as constraint in the modeling procedure of the INST-MFA approach, was calculated from the growth rate and CO_2 uptake rate of soil-grown rice seedlings at the age of 15 days. The growth rate was determined gravimetrically. The logarithm of measured weights was plotted against the harvest time in hours. The slope of the resulting regression represents the specific growth rate of the rice seedlings in 1 h^{-1} . In order to determine the CO_2 uptake rate, a $^{13}\text{CO}_2$ labeling experiment (4.3.2) was performed, followed by EA-IRMS enrichment detection and C/N elemental analysis (4.4.1). The ^{13}C enrichment of total plant material, detected as δ -value, was subsequently converted into isotopomer distributions (M0 and M1) by (Eq. 4. 1). The carbon percentage of biomass was determined by C/N elemental analysis for each sample. Additionally the dry weights of the harvested shoots were measured gravimetrically. The amount of ^{13}C in gram per gram biomass (BM) was calculated by (Eq. 4. 7),

$$\frac{\text{g } ^{13}\text{C}}{\text{g BM}} = (M1_{t_n} - M1_{t_0}) * \frac{\% \text{C (w/w) BM}}{100} * m_{t_x} (\text{g}) \quad (\text{Eq. 4. 7})$$

where M1 is the singly labeled mass isotopomer ^{13}C , t_0 to t_n are the sampling time points, %C (w/w) BM is the carbon fraction of the biomass and m_{t_x} (g) is the mass of the weighed seedlings in gram at time point x. The resulting values were subsequently transformed into mmol ^{13}C by (Eq. 4. 8).

$$\text{mmol } ^{13}\text{C} = \frac{\text{g } ^{13}\text{C}}{\text{g BM}} * \frac{13 (\text{g mol}^{-1}) * 1000}{m_{\text{tn}} (\text{g})} * \frac{\% \text{C (w/w) BM}}{100} \quad (\text{Eq. 4. 8})$$

The values for ^{13}C enrichment in mmol were plotted against time, yielding a linear regression. To determine the biomass yield, the daytime growth rate was divided by the CO_2 uptake rate (Eq. 4. 9).

$$\text{BM Y (g DW (100 mmol CO}_2\text{)}^{-1}) = \frac{\text{g DW h}^{-1}}{\text{mmol } ^{13}\text{C h}^{-1}} * 100 \quad (\text{Eq. 4. 9})$$

4.5.7 Determination of carbon export to the root

In order to analyze how much carbon is exported from shoot to root in form of amino acids and sucrose, the concentration of the respective analyte was integrated with its isotopic enrichment. The isotopic enrichment was determined via GC-C-IRMS analyses, the concentration of amino acids and sucrose was quantified by GC-MS. The basis of carbon export analyses is the assumption that roots themselves do not fix CO_2 . Hence, all labeled carbon in the root comes from $^{13}\text{CO}_2$ previously assimilated by the shoot. The amount of exported carbon was calculated via (Eq. 4. 10):

$$C_{\text{exp}} (\text{C mmol (g DW}_{\text{root}}\text{)}^{-1} \text{ h}^{-1}) = A (\text{mmol (g DW}_{\text{root}}\text{)}^{-1}) * n_{\text{C}} * \Delta^{13}\text{C} * \text{h}^{-1} \quad (\text{Eq. 4. 10})$$

where C_{exp} is the amount of exported carbon in $\text{C mmol (g DW}_{\text{root}}\text{)}^{-1} \text{ h}^{-1}$, A is the analyte in $\text{mmol (g DW}_{\text{root}}\text{)}^{-1}$, n_{C} is the number of carbon atoms of the analyte and $\Delta^{13}\text{C} * \text{h}^{-1}$ is the increase in isotopic enrichment per hour.

4.5.8 Statistical analysis

The statistical significance of differences between mean values were determined using Student's t-test or one-way ANOVA followed by a post-hoc Tukey's test (Köhler et al., 2012; Timischl, 2013). According to a 95% confidence interval, differences were considered significant when the P -value was below 0.05 (Vaux, 2014).

4.5.9 Metabolic network reconstruction and flux calculation

Metabolic network reconstruction and flux calculation was performed by Veronique Beckers (Institute for Systems Biotechnology, Saarland University, Germany).

4.5.9.1 Metabolic network reconstruction for *Oryza sativa* seedling shoot metabolome

A genome-based metabolic network of central carbon metabolism of an autotrophic rice seedling shoot was constructed as basis for subsequent flux modeling (Beckers, 2015). The network consisted of the main pathways of photosynthesis and respiration, e.g. the Calvin cycle, EMP pathway, TCA cycle and PP pathway and considered biomass formation and experimentally determined composition, as well as sucrose export to the root. Carbon dioxide served as external carbon source. The metabolic model was compartmentalized, comprising cytosol, plastid, mitochondrion and peroxisome. The transport of specific metabolites between these compartments was accounted for by integrating transport reactions between cytosol and mitochondrion and between cytosol and plastid, respectively. Anabolic pathways for the production of amino acids, soluble sugars, starch and fatty acids were integrated and assigned to their respective compartments. The complete metabolic network comprised 75 reactions and 65 metabolites (Beckers, 2015).

4.5.9.2 Flux calculation using Isotopomer Network Compartmental Analysis (INCA)

In brief, non-stationary ^{13}C metabolic fluxes were calculated using the software INCA (Young, 2014), implemented in Matlab (R2012b, The Mathworks Inc., Natick, MA, USA). A Levenberg-Marquardt algorithm was used to vary fluxes and pool sizes, thereby minimizing the sum of squares error between measured and simulated mass isotopomer distributions (Young et al., 2008). Parameter estimation yielded the best fit estimate after 50 runs starting from random initial values. To assess the goodness of fit of the simulated fluxes, statistical evaluation using the χ^2 -test and parameter continuation was performed. The latter was applied to all net fluxes to estimate 95% confidence intervals (Antoniewicz et al., 2006).

5 Results and Discussion

Quantitative analysis of pathway function and regulation is a key to understand and engineer plant physiology (Maliga and Graham, 2004). This, however, is demanding, due to the high complexity and connectivity of plant metabolic networks. Here, a comprehensive approach was developed to assess whole plant metabolic fluxes. In a first step, $^{13}\text{CO}_2$ and $^{15}\text{NH}_4\text{NO}_3$ pulse studies under precisely controlled physiological conditions were coupled with an ultra-sensitive GC-C-IRMS method for parallel ^{13}C and ^{15}N labeling analysis in different plant tissues and even individual molecular compounds to elucidate plant metabolic traits. Different tube reactor layouts enabled $^{13}\text{CO}_2$ isotope experiments with soil grown seedlings and adult plants, up to an height of about one metre (Figure 5. 1 A, Figure 5. 1 B), whereas parallel $^{13}\text{CO}_2$ and $^{15}\text{NH}_4\text{NO}_3$ labeling of hydroponic plant cultures could be conducted in a specific box reactor (Figure 5. 1 C). In contrast to previous techniques (Tanaka and Osaki, 1983; Nouchi et al., 1994; Römisch-Margl et al., 2007), the methodology minimized potential alterations of the studied plant during the experiment due to an atmosphere with ambient CO_2 levels, controlled temperature, humidity and illumination, as well as incubation times of only 10 minutes. The careful experimental layout provided data with high precision and reproducibility among replicates, independent of the developmental stage of the analysed plants. Assimilation and translocation of carbon in different tissues (Figure 5. 10) and even individual molecules (Figure 5. 11) could be quantified at deviations below 20% for adult plants. Given the fact that plants in advanced developmental stages are rather complex and subject to a certain biological variation, due to differentiation into specific organs and cell types, precision and reproducibility can be regarded excellent. For seedlings, they were partially even higher (Figure 5. 5, Figure 5. 7). This allowed to accurately discriminate metabolic properties, even if they differed only slightly, which seems a valuable characteristic of our approach.

In a second step, time-course ^{13}C labeling experiments were conducted and coupled with *in silico* modeling to yield a comprehensive flux map of a rice seedling. For this purpose, a largely automated flux incubator was constructed, allowing precise control of ambient conditions as well as fast harvest of individual plants without disturbing the reactor atmosphere. Furthermore, the reactor enabled joint incubation of all plants belonging to one experiment run, which is of great value to the quality of dynamic labeling data. A comprehensive set of analytical tools, like EA-C-IRMS, GC-C-IRMS, GC-MS and LC-MS/MS, was deployed to determine the MID, pool size and biomass share of 40 different metabolites. The obtained data was fitted to a reaction network of central carbon metabolism of a seedling shoot, using the software INCA. Compared to previous studies (Szecowka et al., 2013; Ma et al., 2014), a larger network, ad-

ditionally comprising fatty acid and amino acid biosynthetic pathways, and a more comprehensive data set were used to quantitatively describe leaf metabolism. Furthermore, a crop plant was used for the first time to perform isotopically non-stationary metabolic flux analysis under photoautotrophic conditions.

5.1 Pulse-chase experiments as fast screening tool for plant phenotypes

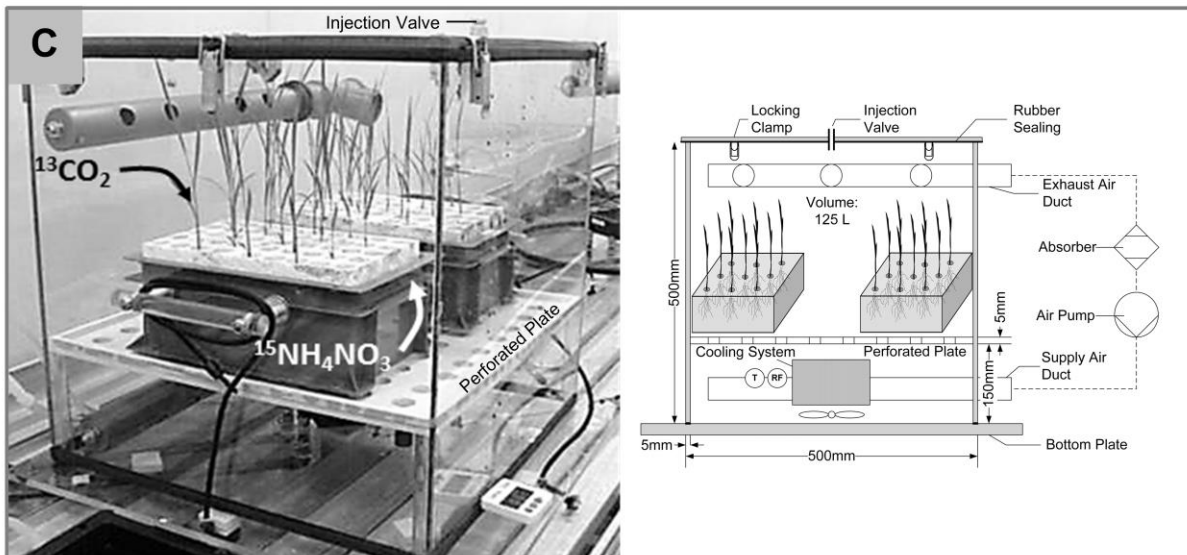
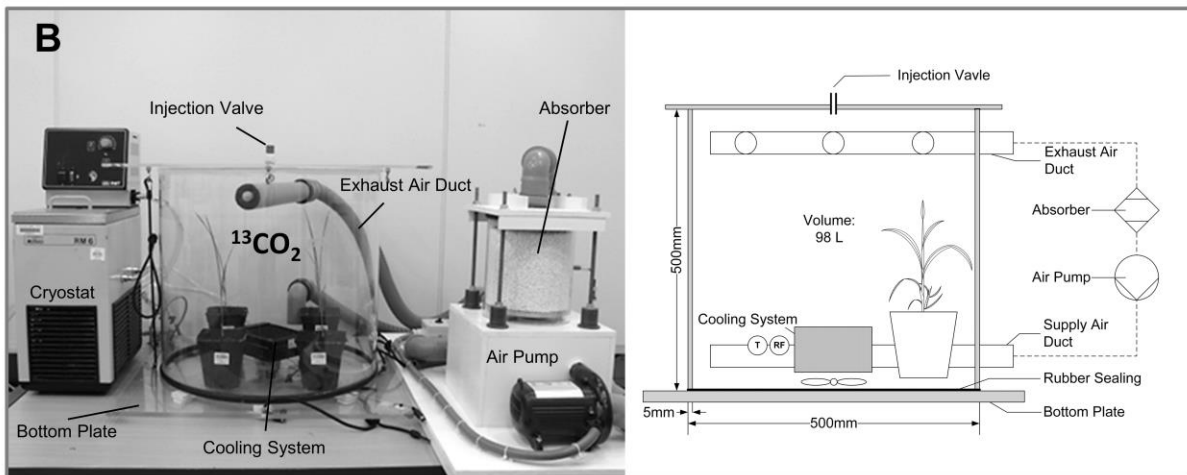
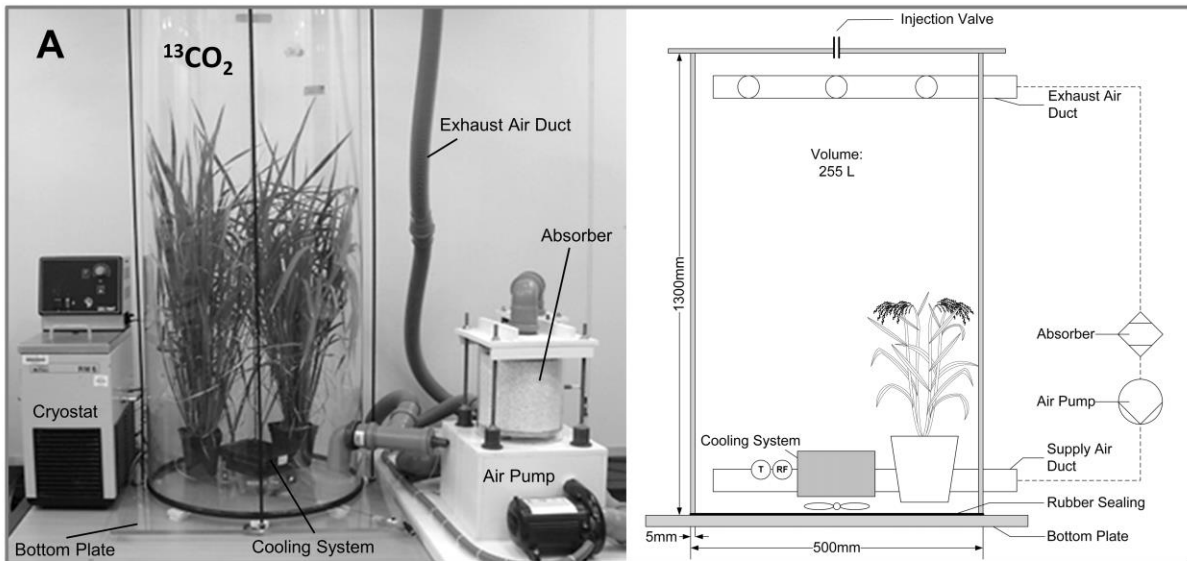
In order to elucidate physiological features of rice seedlings, pulse-chase experiments with $^{13}\text{CO}_2$ and $^{15}\text{NH}_4\text{NO}_3$ were performed, assuming that intracellular metabolite levels and metabolic fluxes are not perturbed by replacement of the naturally labeled substrate with an isotopically labeled one. Generally, ^{13}C and ^{15}N enrichments could be quantified with excellent reproducibility, particularly considering the high complexity of the studied plant system.

5.1.1 Reactors for pulse-chase labeling studies

Three sizes and types of labeling reactor were designed, constructed and validated to evaluate their suitability for *in vivo* ^{13}C labeling studies (Figure 5. 1): two tube reactors for $^{13}\text{CO}_2$ studies with soil-grown adult plants (255 L) and seedlings (98 L), respectively, and a box reactor for combined $^{13}\text{CO}_2$ and $^{15}\text{NH}_4\text{NO}_3$ labeling studies with hydroponically grown seedlings (125 L). For all reactors, the used wall material allowed full transmission of light (Figure 5. 2) and temperature and humidity could be maintained at desired values (Figure 5. 3 A-C). Hence, the reactors allowed plants to be labeled under the same light, temperature and humidity regimen that they were exposed to during growth in an enclosed research plant growth cabinet (phyto chamber). For more detailed information about reactor specifications, please refer to chapter 4.3.1.

Figure 5. 1 (next page) Equipment designed and constructed for *in vivo* ^{13}C and ^{15}N labeling studies

Large tube reactor (0.5 m diameter, 1.3 m height, 255 L volume) for $^{13}\text{CO}_2$ labeling of soil-grown adult rice plants (A); Small tube reactor (0.5 m diameter, 0.5 m height, 98 L volume) for $^{13}\text{CO}_2$ labeling of soil-grown rice seedlings (B); Box reactor (0.5 x 0.5 x 0.5 m, 125 L volume) for simultaneous $^{13}\text{CO}_2$ and $^{15}\text{NH}_4\text{NO}_3$ labeling of hydroponically grown rice seedlings (C). All reactors were equipped with a temperature control, comprising a water-cooled ventilator at the bottom plate of the reactor and an external cryostat. In addition, an external CO_2 adsorption unit consisted of a high power pump, an adsorber and a fine dust filter. Prior to the experiments, the chosen plants were placed inside the reactor, which were then closed gas tight by a rubber sealing. Ambient CO_2 was removed from the reactor within 30 seconds. Experiments were started by injecting desired amounts of $^{13}\text{CO}_2$ through an injection valve in the lid of each reactor.



Immediate replacement of ambient CO₂ by an equimolar level of ¹³CO₂ was realized by an absorber unit connected to the reactor. A first set of experiments with soil-grown rice seedlings was conducted to identify the optimum conditions regarding supply of tracer (400 μL L⁻¹, 700 μL L⁻¹ ¹³CO₂) and the time period of incubation with ¹³CO₂ (10, 60, 180 min) (Figure 5. 3 D). Short incubation times of 10 minutes at ambient levels of ¹³CO₂ (400 μL L⁻¹) were sufficient to allow precise estimation of assimilated carbon, due to the high sensitivity of the EA-C-IRMS measurement. Labeled under these conditions, the shoot of rice seedlings showed marked ¹³C enrichment, i.e. a delta value of 170 ± 6‰. The low deviation underlines that the assimilation was quantified with excellent reproducibility, particularly considering the high complexity of the studied plant system. Enrichment values were in an equal range after simultaneous labeling of one, three, six or twelve plants in the same reactor for 60 minutes, indicating that even larger sets of plants and longer incubation times did not result in CO₂ limitation (Figure 5. 3 E).

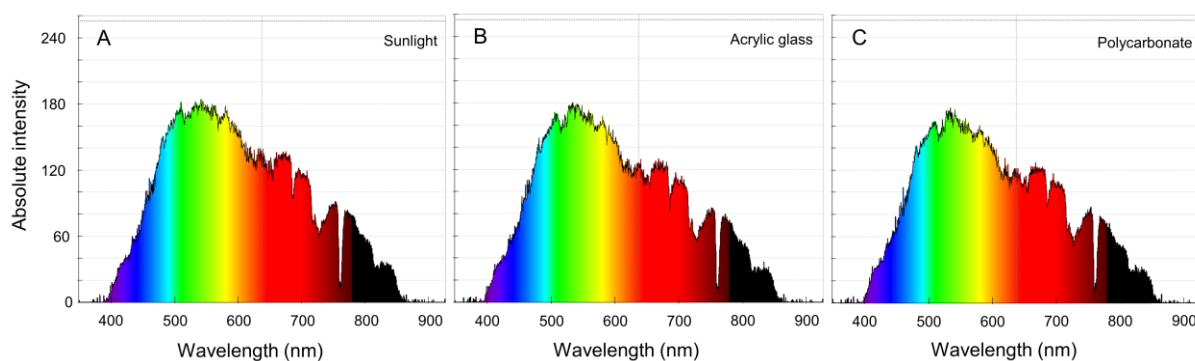


Figure 5. 2 Absorption spectra of sunlight at midday

Absorption spectrum (A) without deflection, (B) through acrylic glass and (C) through polycarbonate, measured by the spectrometer Spektra SN 3K 8116 (Spektra Schwingungstechnik und Akustik GmbH, Dresden, Germany). Acrylic glass and polycarbonate do not inhibit transmission of light between 400 and 900 nm, the essential wavelengths for plants.

In order to examine diurnal effects on photosynthesis and CO₂ assimilation, isotopic labeling studies with seedlings were conducted every hour in the timeframe of 2.5 to 9.5 hours after sunrise. Labeling of plants at different daytime did not reveal significant difference from plants labeled at midday (6.5 hours after sunrise) (Figure 5. 3 F). Accordingly, the routine workflow was as follows: *Oryza sativa* plants were grown in a phyto chamber under ambient air, until they were placed inside the enclosure shortly before the labeling experiment. Ambient CO₂ (400 μL L⁻¹) was then removed from the reactor within 30 seconds and replaced by an equimolar amount of ¹³CO₂. After 10 minutes of incubation in this atmosphere, plants were removed from the reactor and either directly harvested for assessment of carbon assimilation or cultivated further on in the phyto chamber for assessment of carbon translocation, respectively. For simultaneous tracing of ¹⁵N, roots of hydroponically grown seedlings were supplied with

$^{15}\text{NH}_4\text{NO}_3$. The isotopic enrichment of harvested plant material and extracted amino acids was determined using EA-C-IRMS and GC-C-IRMS, respectively.

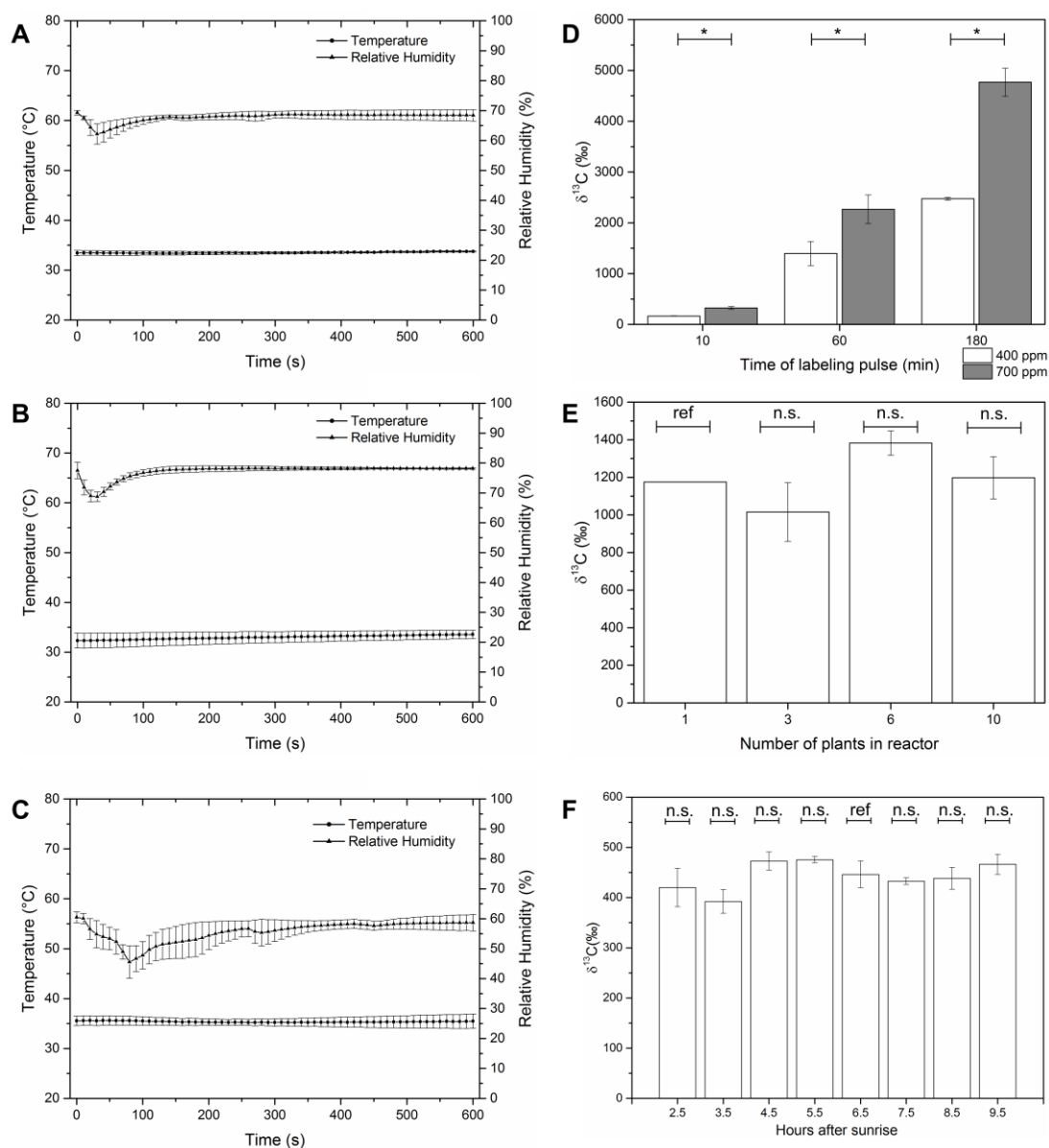


Figure 5.3 Reactor and labeling characteristics

Profiles of temperature and relative humidity inside (A) the tall tube reactor, (B) the small tube reactor and (C) the C/N reactor throughout the experiment. Mean values \pm SD ($n = 3$) are shown. Ambient CO_2 was absorbed from the reactor for 30 seconds, leading to a decrease of relative humidity, which quickly got back to start conditions after absorption. Temperature remained constant throughout the entire experiment. Influence of (D) magnitude and duration of $^{13}\text{CO}_2$ labeling pulse, (E) number of plants in the enclosure and (F) daytime on the enrichment of seedlings. Soil-grown seedlings (12 days) were labeled with (E) $400 \mu\text{L L}^{-1} \text{ }^{13}\text{CO}_2$ for 60 minutes and (F) $700 \mu\text{L L}^{-1} \text{ }^{13}\text{CO}_2$ for 10 minutes, respectively. Plants were harvested immediately after the pulse and ^{13}C enrichment of the freeze-dried plant material was determined by EA-C-IRMS. Mean values \pm SD ($n = 3$ to $n = 10$) are shown. Asterisks indicate significant differences between mean values at $P \leq 0.05$, as determined by (D) Student's t-test and (E,F) one-way ANOVA followed by Tukey's test. n.s., not significant. ref, reference against which means were tested for statistical significance. The full data set is given in Table A9. 2.

5.1.2 Quantification of ^{13}C and ^{15}N amino acid enrichment using GC-C-IRMS

Using GC-C-IRMS, the measurement of labeling enrichment was extended to amino acids. For each amino acid, eluting from the GC column, the ^{13}C and ^{15}N enrichment was given by the ion intensity at a mass to charge ratio of $m/z = 45$ and $m/z = 29$, reflecting $^{13}\text{CO}_2$ and $^{14}\text{N}^{15}\text{N}$, respectively, formed by combustion in the instrument. For 16 amino acids, satisfying signal quality was generally obtained and provided precise estimates of their labeling status. Hereby, the amino acid pairs glutamate/glutamine and aspartate/asparagine were each quantified as lumped pools, due to conversion of the carboxamides asparagine and glutamine into their corresponding acids during the protein hydrolysis step of sample processing (Wittmann, 2007). Four amino acids were not accessible, because they were degraded (cysteine, methionine, tryptophan, arginine) during this treatment (Wittmann, 2007). Generally, 5 mg of lyophilized material was sufficient to provide high quality data, independent from the type of tissue processed. The conditions used for extraction, precipitation and derivatisation of protein from lyophilized plant material was crucial with regard to yield and purity of the obtained amino acids. In contrast to extraction in TRIS buffer (pH 8.8), extraction in hot water (100 °C, 15 min) did yield much less protein (data not shown). Similarly, precipitation of the extracted protein in ice-cold 10% TCA was less efficient than precipitation in ice-cold acetone (data not shown). Additional tests with alternative derivatisation agents, revealed that tri-methyl-silyl derivatives of the amino acids, obtained e.g. with trimethylsilyl-trifluoroacetamide, were not fully separated by gas chromatography. Even a set of variations in the temperature profile did not allow full baseline separation for the amino acids methionine/aspartate, isoleucine/proline and glutamate/phenylalanine. Full baseline separation was, however, necessary as the combustion of analytes into CO_2 and N_2 prior to detection does not allow to discriminate between overlapping analyte peaks. Derivatisation with methyl-*t*-butyldimethylsilyl-trifluoroacetamide into *t*-butyl-dimethyl-silyl derivatives finally led to full baseline separation of the target analytes. Some of the seedling samples, however, did not provide an unambiguous signal for tyrosine, probably due to matrix overlay. Due to the fact that interference with background noise or matrix effects may lead to false results in isotope experiments (Wittmann, 2007), this amino acid was partly excluded from further interpretation. It also turned out that the addition of dimethylformamide, commonly used to process microbial samples (Wittmann, 2007), was not compatible with the used GC-C-IRMS instrument, because solvent was largely transferred into the combustion chamber. Accordingly, derivatisation was conducted without addition of the solvent. Tests with different incubation times (30, 60, 90, 120 min) and temperatures (80, 90, 100 °C) revealed that the combination of 60 minutes and 80 °C provided the optimum signal-to-noise ratio (Figure 5. 4).

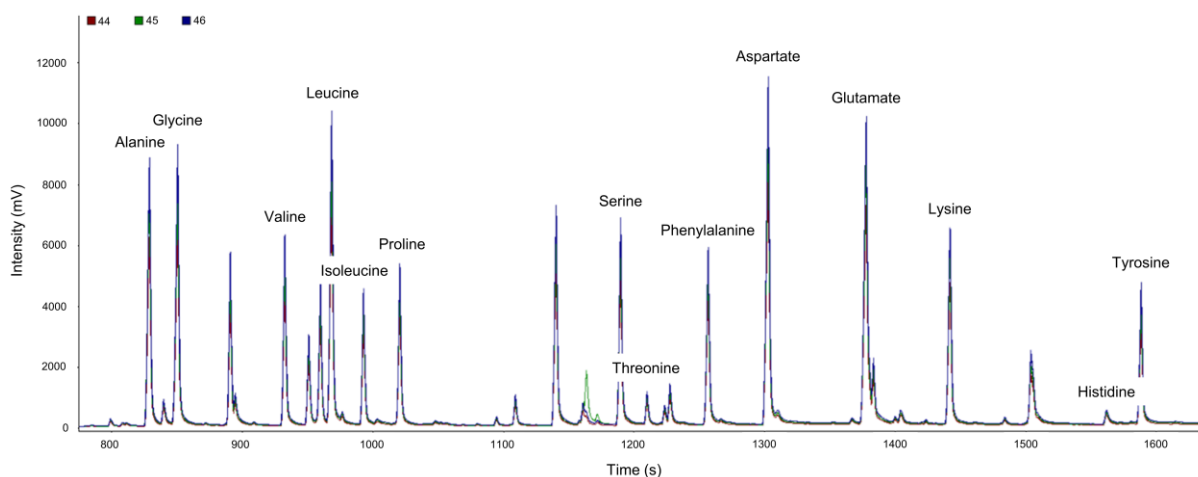


Figure 5. 4 GC-C-IRMS spectrum of proteinogenic amino acids

Spectrum of protein-bound amino acids of the flag leaf of a soil-grown rice plant in the late grain filling stage (88 days old), at time point zero. The established protocol for protein extraction and precipitation, derivatization of amino acids and measurement by GC-C-IRMS yields good baseline separation of all desired metabolites, as well as a high signal/noise ratio.

5.1.3 Carbon and nitrogen metabolism in rice seedlings

Combined labeling studies with $^{13}\text{CO}_2$ and $^{15}\text{NH}_4\text{NO}_3$ are interesting due to the close connection of carbon and nitrogen metabolism in plants, but have been conducted only rarely (Cliquet et al., 1990; Dyckmans et al., 2000). Therefore, in this study, carbon and nitrogen metabolism of illuminated rice seedlings was examined in the untreated plantlets, as well as in seedlings exposed to high salinity and the broad-spectrum herbicide imazapyr. Salt stress and herbicide treatment were used as case study to demonstrate the great potential of the established technology to elucidate gross metabolic activities, thereby supporting the identification of stress response mechanisms and herbicide modes-of-action.

5.1.3.1 Intracellular distribution of newly assimilated carbon and nitrogen is fast

Plant growth and development depend on the interaction of carbon and nitrogen metabolic pathways. Therefore, understanding carbon-nitrogen interactions is a cornerstone to increase plant productivity (Gauthier et al., 2010). In order to reveal specific features of carbon and nitrogen metabolism, combined $^{13}\text{CO}_2$ and $^{15}\text{NH}_4\text{NO}_3$ labeling of hydroponically grown rice seedlings was performed (Figure 5. 5).

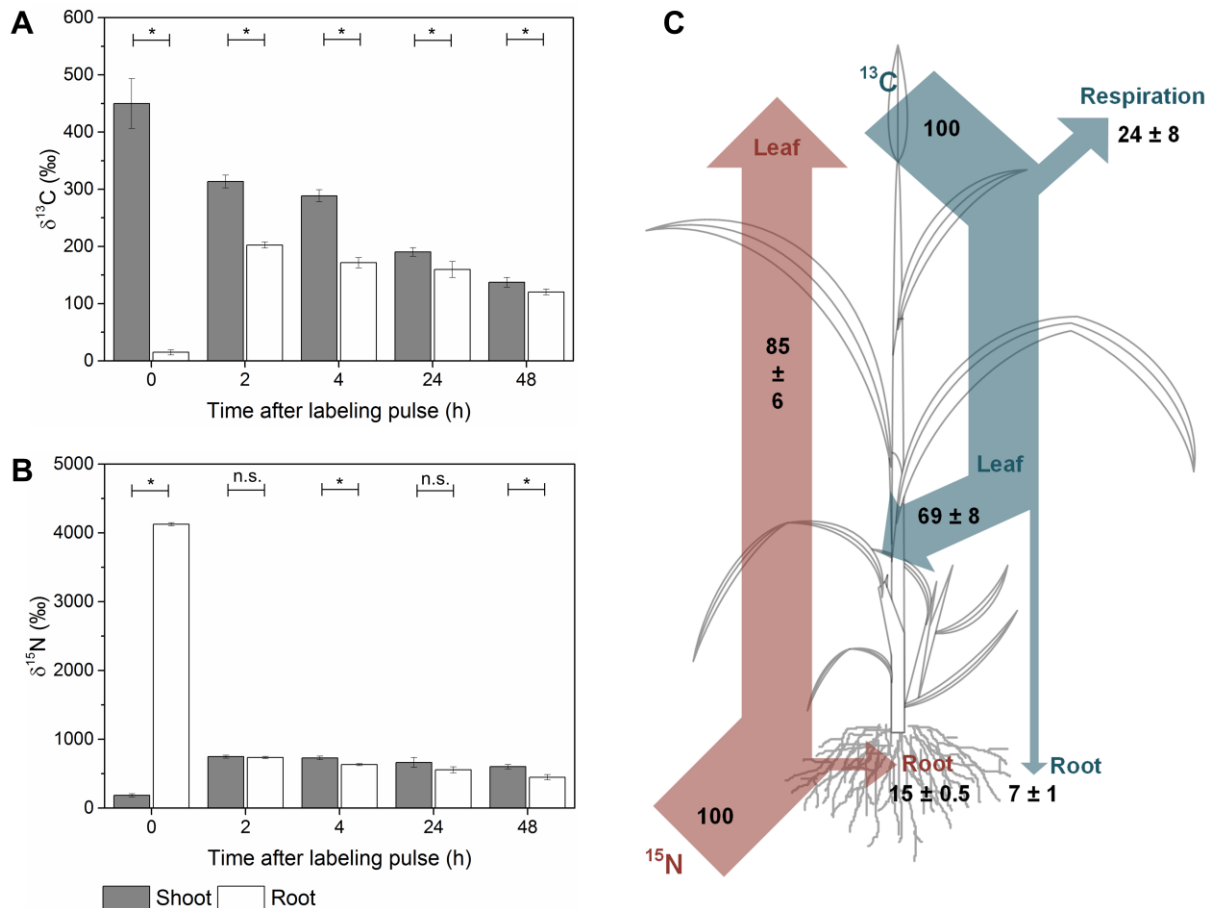


Figure 5.5 Combined ^{13}C and ^{15}N pulse labeling of hydroponic rice cultures

Time resolved shoot and root enrichment patterns of a hydroponically grown rice seedling (12 days) after simultaneous labeling with (A) $^{13}\text{CO}_2$ ($400 \mu\text{L L}^{-1}$) through the reactor gas phase and (B) $^{15}\text{NH}_4\text{NO}_3$, (1.43 mM), supplied via the hydroponic growth medium. The labeling pulses were applied for 10 minutes, after which plants were either directly harvested to assess assimilation, or were further cultivated at ambient air and in non-labeled medium for 48 hours, respectively, for tracing of label translocation. The ^{13}C and ^{15}N enrichment of freeze-dried plant material was analyzed by combustion isotope ratio mass spectrometry, coupled to elemental analysis. Mean values \pm SD ($n = 3$) are shown. Asterisks indicate significant differences between mean values at $P \leq 0.05$ (Student's t-test). n.s., not significant. In (C), the relative reallocation of assimilated carbon and nitrogen is displayed. A root-to-shoot ratio of 0.173 was calculated from the ^{15}N label distribution after two hours of tracing, using (Eq. 4.4) and (Eq. 4.6). Based on this ratio, the percent distribution of label between shoot and root was determined. The total amount of assimilated carbon and nitrogen at time point zero was set to 100% carbon and nitrogen uptake, respectively, in order to provide relative data. The full data set is given in Table A9.3.

Isotopically labeled ammonium nitrate was provided to the roots, while at the same time, $^{13}\text{CO}_2$ was supplied to the shoot, using the designed box reactor (Figure 5.1 C). Immediately after the pulse, maximum ^{13}C enrichment was detected in the shoot ($450 \pm 45\text{‰}$) (Figure 5.5 A), while ^{15}N labeling was highest for the root ($4130 \pm 25\text{‰}$) (Figure 5.5 B). However, transport of carbon and nitrogen seemed fast, as significant ^{15}N enrichment at this time point was already found in the shoot ($190 \pm 25\text{‰}$) (Figure 5.5 B). Likewise, the root contained slight amounts of

^{13}C ($15 \pm 5\text{‰}$) (Figure 5. 5 A). Within two hours after assimilation, ^{15}N and ^{13}C levels were evenly equilibrated. During the ongoing chase period, ^{13}C and ^{15}N enrichments continuously decreased in root and shoot. By integration of the measured ^{13}C and ^{15}N enrichment data, it was now possible to determine the percent reallocation of label within two hours after the labeling pulse (Figure 5. 5 C), thereby providing fast and quantitative access to relative carbon and nitrogen fluxes in rice seedlings. The root-to-shoot ratio, calculated from the labeling data via (Eq. 4. 6) was 0.173. This seemed a proper estimate according to previously reported values for rice between 0.05 – 0.3 (Yoshida, 1981). The majority of assimilated nitrogen (85%) was transported to the shoot (Fig. 3A), whereas only 15% remained in the roots. Regarding assimilated carbon, the major fraction (69%) was retained in the shoot, whereas only 7% was translocated into the roots. A total of 76% of assimilated carbon was thus recovered inside the seedling, two hours after assimilation, which indicated a loss of 24% via respiration. The retention of carbon in the shoot was slightly higher than that for maize plants, in which 53% of ^{13}C is recovered inside the shoot at elongation (Meng et al., 2013). The same calculation, using labeling data from samples, taken 24 hours after the pulse, i.e. including a dark period, revealed an increased loss of carbon through respiration by 52% (data not shown), which agreed well with corresponding data obtained from the measurement of dry matter production, photosynthesis and respiration (Tanaka and Yamaguchi, 1968).

The study highlights fast interorgan distribution of carbon and nitrogen in seedlings, whereby the shoot operated as major sink and exhibited a ten-fold and 6-fold higher demand for carbon and nitrogen compounds, respectively, as compared to the root (Figure 5. 5 C), which reflects sufficient supply with water and nutrients, especially nitrogen (Wilson, 1988; Peuke et al., 1994). Obviously, the examined seedlings received all essential macro- and micronutrients, and were exposed to optimal growth conditions, concerning light, temperature and humidity, so that carbon and nitrogen were mainly used for shoot growth and development.

Incorporation of ^{13}C into proteinogenic amino acids is uncoupled from nitrogen metabolism

Amino acids are the analytes of choice for microbial pathway analysis, because they are much more abundant in cell extracts and protein than their precursors and provide extensive labeling information (Wittmann, 2007). On basis of the underlying biosynthetic precursor amino acid relationship it is easy to deduce the labeling patterns of the precursor metabolites from the patterns of the corresponding amino acids. Amino acid enrichment patterns were equal for soil-grown and hydroponically grown rice seedlings (Figure 5. 6), indicating that hydroponic cultivation did not significantly influence at least this part of metabolism.

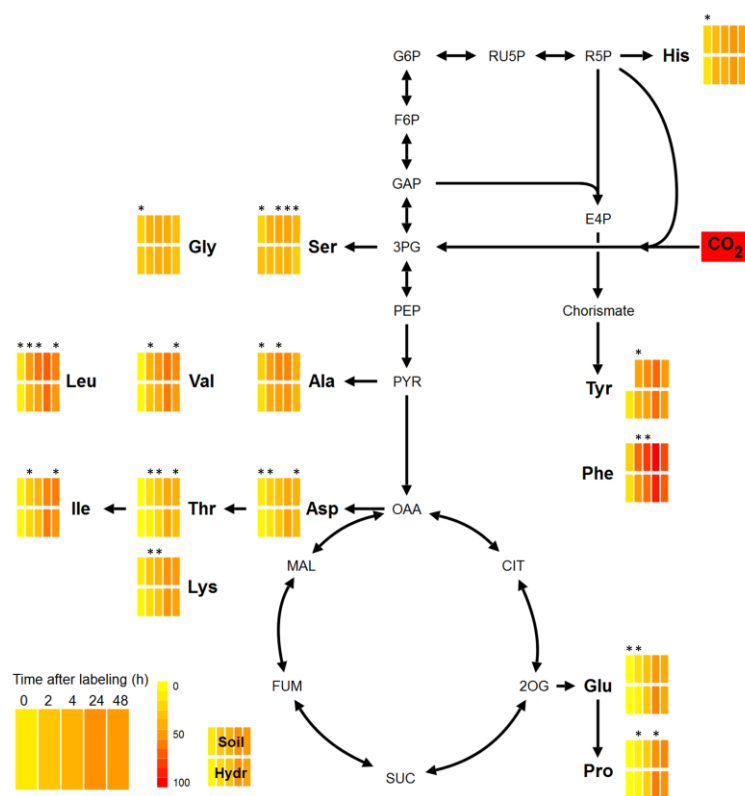


Figure 5. 6 Simplified pathway illustration of amino acid ^{13}C enrichment of soil and hydroponically grown rice seedlings

Seedlings were labeled with $400 \mu\text{L L}^{-1} \text{ }^{13}\text{CO}_2$, applied to the shoot for 10 minutes. Enrichment of extracted proteinogenic amino acids was analyzed by GC-C-IRMS. Mean values ($n = 3$) are plotted as atom percent excess (APE), corrected for natural isotopes. The degree of enrichment is displayed by color: yellow - no enrichment, red - 100% enrichment, corresponding to the highest APE-value of the data set. Asterisks indicate significant differences between mean values at $P \leq 0.05$ (Student's t-test). Abbreviations: Soil (soil grown plants), Hydr (hydroponically grown plants). Amino acid abbreviations are according to the three-letter code, all others can be found in Table A9. 1. The full data set is given in Table A9. 4.

Enrichment increased with time, as ^{13}C was incorporated into cell protein. Amino acids strongly differed with regard to label incorporation, which seemed to correlate to their biosynthetic origin. Particularly, tyrosine and phenylalanine, originating from intermediates of the EMP pathway (phosphoenolpyruvate) and of the non-oxidative PP pathway (erythrose 4-phosphate), were enriched rather fast and to a greater extent than all other amino acids, contributing up to 9% and 15% of the entire enrichment, respectively (Figure 5. 6). Immediately after the pulse, significant ^{13}C incorporation was also observed for amino acids deriving from pyruvate, another intermediate of the EMP pathway, i.e. alanine, serine, glycine, valine and leucine. In contrast, enrichment was delayed for amino acids synthesized from 2-oxoglutarate and oxaloacetate, intermediates of the TCA cycle. Generally, highest enrichments were detected 24 hours after the labeling pulse. After 48 hours, the enrichment declined for most amino acids, probably due to a dilution with $^{12}\text{CO}_2$ taken up during the post-labeling incubation. The ^{13}C labeling profile of

glycine and serine was similar, indicating that they originate from the same metabolic precursor, 3-phosphoglycerate (Wittmann, 2007). The same trend was also found for other amino acid families, like the aspartate family of amino acids with threonine, lysine, isoleucine and aspartate itself.

Although the applied technique does not directly provide quantitative flux rates, the ^{13}C enrichment data reveal a fast and strong influx of ^{13}C into the EMP pathway and the non-oxidative PP pathway, indicating high activities of these routes. The rather low enrichment of TCA-cycle related amino acids most likely reflects a downregulation of the cycle in the light (Tcherkez et al., 2005). In addition, the slow dynamics could be an indication, that glutamate, aspartate and amino acids derived therefrom, are not formed in the shoot, but are rather synthesized in the root, followed by transport into the shoot. This is indeed taking place, which is discussed below on basis of integrated ^{13}C and ^{15}N labeling data (Figure 5. 7).

Subsequently, amino acids of the shoot were analyzed for their ^{13}C and ^{15}N enrichment, from combined $^{13}\text{CO}_2$ and $^{15}\text{NH}_4\text{NO}_3$ labeling experiments with hydroponically grown rice seedlings (Figure 5. 7). For six selected amino acids, i.e. alanine, glycine, proline, serine, aspartate and glutamate, root-based data with satisfying quality could be derived, which allowed a tissue-specific examination, at least for these molecules. Immediately after labeling, strong ^{15}N enrichment was detected for serine, aspartate and glutamate of root protein (Figure 5. 7 C). At the same time, alanine, glycine and serine, extracted from shoot protein, revealed significant ^{13}C enrichment (Figure 5. 7 B). Within two hours, labeled compounds were distributed inside the plant, leading to ^{13}C and ^{15}N enriched amino acids in shoot and root. Although all amino acids exhibited significantly different ^{13}C and ^{15}N enrichment, strongest differences were found for shoot amino acids. Alanine, and serine exhibited higher ^{13}C enrichment, whereas proline, aspartate and glutamate were more strongly enriched with ^{15}N . Four hours after the labeling pulse, similar amino acid enrichment patterns of shoot and root indicated the equilibration of label between these organs (Figure 5. 7).

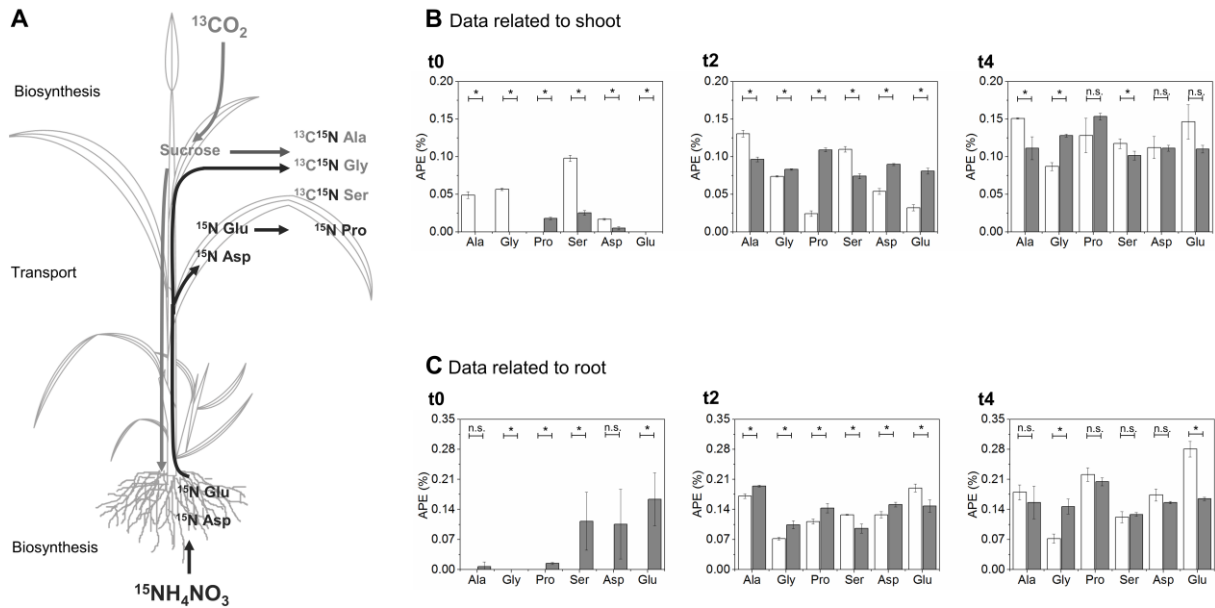


Figure 5.7 Carbon and nitrogen metabolic routes displayed by amino acid enrichment

Integrated analysis of carbon and nitrogen metabolism by combined labeling of hydroponically grown rice seedlings with $^{13}\text{CO}_2$ and $^{15}\text{NH}_4\text{NO}_3$. Tissue specific enrichment of extracted amino acids was quantified by GC-C-IRMS. Integrated view on transport and biosynthetic routes of Ala, Gly, Ser, Glu/Gln, Asp/Asn and Pro regarding assimilated ^{13}C (light grey) and ^{15}N (dark grey) labeling (A), assessed in shoot (B) and root (C), represented by bar graphs over the first four hours of tracing. The data reflect mean values \pm SD ($n = 3$). At the age of 12 days, rice seedlings were simultaneously labeled with $400 \mu\text{L L}^{-1}$ $^{13}\text{CO}_2$ and 1.43 mM $^{15}\text{NH}_4\text{NO}_3$ for 10 minutes and then either harvested directly for assessment of label assimilation, or further cultivated at ambient air for 2 to 4 hours for assessment of label translocation. Asterisks indicate significant differences between mean values at $P \leq 0.05$ (Student's t-test). n.s., not significant. The full data set is given in Table A9. 5.

Combined ^{13}C and ^{15}N labeling of hydroponically grown rice seedlings showed an immediate occurrence of ^{15}N labeled glutamate/glutamine and aspartate/asparagine in the root, whereas the ^{13}C labeled forms appeared much later (Figure 5.7 C). Obviously, these amino acids were formed from carbon precursors in the root through $^{15}\text{NH}_4$ assimilation and transamination (Lam et al., 1995), which explains the exclusive enrichment with ^{15}N (Figure 5.7 A and Figure 5.7 C). Subsequently they were transported into the shoot (Funayama et al., 2013) to serve as amino group donors for the biosynthesis of other amino acids (Kiyomiya et al., 2001). Glutamate with its rather high ^{15}N and low ^{13}C enrichment, synthesized in the root and transported to the shoot (Figure 5.7 B, 2 hour time point) is the precursor for *de novo* synthesis of proline, exhibiting a similar labeling pattern.

The immediate ^{13}C enrichment (Figure 5.7 B, time point zero) indicates a fast biosynthesis of alanine, glycine and serine in the shoot. For glycine and serine this may be due to photorespiration, which typically leads to high turnover rates for these amino acids (Gauthier et al., 2010). Overall, this provides a spatially resolved picture of amino acid metabolism (Figure 5.7 A), which explains the different dynamics of ^{13}C and ^{15}N enrichment. From similar effects after

simultaneous labeling of rape plants with ^{13}C and ^{15}N it has been hypothesized that the incorporation of assimilated ^{13}C into amino acids is not tightly connected to nitrogen assimilation (Gauthier et al., 2010). This seems to also hold for rice.

5.1.3.2 Salt stress affects nitrogen metabolism, leading to an altered sink:source relation

Salt stress, a major abiotic factor affecting growth and productivity of salt sensitive crops (Roy et al., 2014), resulted in strong perturbation of nitrogen uptake by the root and transport to the shoot of rice seedlings. Carbon assimilation and translocation, however, was not significantly affected (Figure 5. 8 A, Figure 5. 8 C). Hydroponically grown rice seedlings were exposed to 100 mM sodium chloride for six days, prior to the labeling experiment. Untreated plants served as a control. Immediately after the labeling pulse, root ^{15}N enrichment was $4190 \pm 25\%$ in the control plant and only $2490 \pm 160\%$ in the stressed plant, corresponding to a decreased ammonium uptake of 40% (Figure 5. 8 D). In addition, the translocation of nitrogen from root to shoot was strongly impaired, leading to significantly less enrichment in the shoot of stressed plants (43% to 62%), compared to control plants, at all sampling time points. In contrast, carbon assimilation in the shoot was unaltered (Figure 5. 8 A).

As described above for untreated control plants (Figure 5. 5 C), the distribution of carbon and nitrogen was inferred for a stressed seedling by integrating ^{13}C and ^{15}N labeling data. The shoot-to-root ratio estimated via (Eq. 4. 6) was only slightly increased under stress conditions (0.165 ± 0.01 for control plants compared to 0.173 ± 0.03 for stressed plants). Relative carbon distribution did not change in seedlings exposed to stress (Figure 5. 5 C, Figure 5. 8 E). Nitrogen distribution, however, changed significantly, leading to the recovery of 30% of the assimilated nitrogen in roots, compared to 15% in control plants. The amount of labeled nitrogen transported to the shoot was accordingly decreased, resulting in 69% compared to 86% in control plants (Figure 5. 5 C, Figure 5. 8 E). This means that stressed plants kept relatively more nitrogen in the root, as compared to non-stressed plants, probably to support the supply with N-containing compatible solutes (Wang et al., 2012a). Enhanced retention of nitrogen compounds inside the root might furthermore be due to adaptive mechanisms to ensure adequate water and nutrient acquisition from the rhizosphere (Sharp et al., 2004).

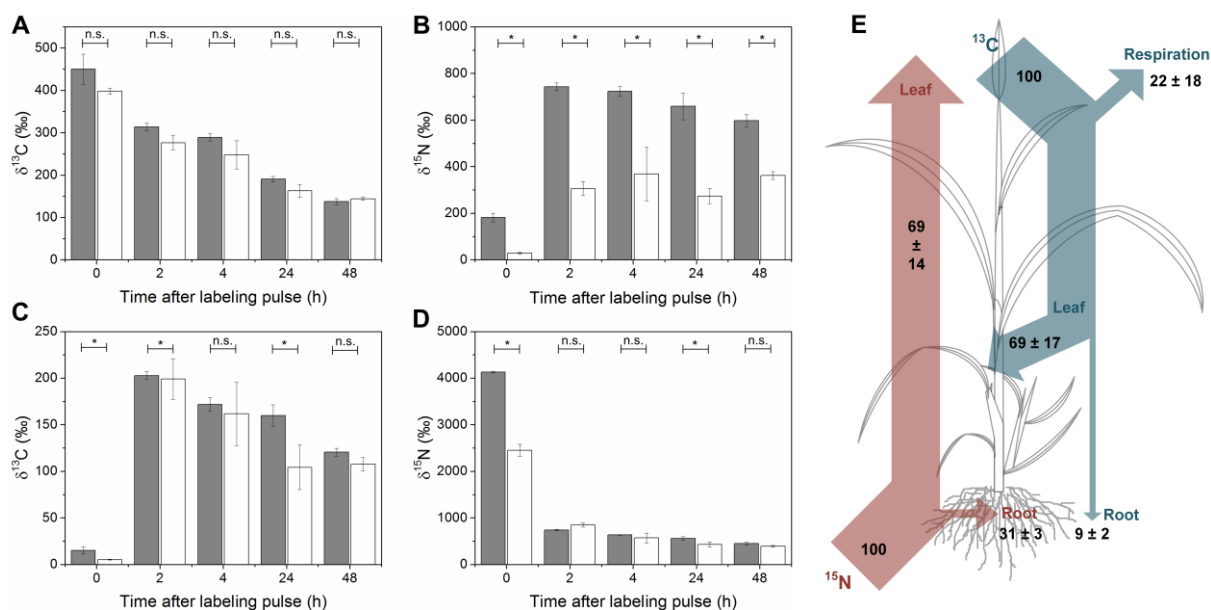


Figure 5.8 Effect of salt stress on assimilation and translocation of metabolic tracers

Impact of salt stress on carbon and nitrogen assimilation and translocation of hydroponically grown rice seedlings. The data reflect ^{13}C (A) and ^{15}N enrichment (B) in the shoot, and ^{13}C (C) and ^{15}N enrichment (D) in the root. The data comprise mean values \pm SD ($n = 3$) for stressed seedlings (100 mM NaCl for six days, white bars) and untreated controls (grey bars). In (E), the percentage reallocation of assimilated carbon and nitrogen is displayed, as calculated from ^{13}C and ^{15}N enrichment data. A root-to-shoot ratio of 0.165 was calculated from the ^{15}N label distribution after two hours of tracing, using (Eq. 4. 6). Based on this ratio, the relative reallocation of label between shoot and root was determined. The total amount of assimilated carbon and nitrogen at time point zero was set to 100% carbon and nitrogen uptake, respectively. At the age of 12 days, rice seedlings were simultaneously labeled with $^{13}\text{CO}_2$ (400 $\mu\text{L L}^{-1}$) through the reactor gas phase and with $^{15}\text{NH}_4\text{NO}_3$ (1.43 mM), supplied via the hydroponic growth medium. The labeling pulses were applied for 10 minutes, after which plants were either directly harvested to assess assimilation, or were further cultivated at ambient air and in non-labeled medium up to 48 hours, respectively, for tracing of label translocation. The ^{13}C and ^{15}N enrichment of freeze-dried plant material was analyzed by combustion isotope ratio mass spectrometry, coupled to elemental analysis. Asterisks indicate significant differences between mean values ($P \leq 0.05$, Student's t-test). n.s., not significant. The full data set is given in Table A9. 3.

The relative flux maps for carbon and nitrogen, giving the relative distribution among the different tissues on basis of the isotope enrichment data, provide a straightforward snapshot of plant metabolism (Figure 5. 5 C, Figure 5. 8 E). Given the available instrumentation, such insights can be easily provided within one day after an isotope experiment and thus allow for a fast evaluation, e.g. to study environmental stresses as demonstrated for salt-stressed rice (Figure 5. 8). In light of breeding stress tolerant plant lines, an important area of application is metabolic phenotyping in order to identify protective mechanisms (Cramer et al., 2011) and changes in sink-source relations (Roitsch, 1999; Albacete et al., 2014). Our data reflect these features for plants exposed to high salinity.

5.1.3.3 Immediate response to imazapyr comprises impaired biosynthesis of branched-chain amino acids

Herbicide treatment was used as proof of concept to demonstrate the potential of the established technology for mode-of-action studies (Figure 5. 9). Imazapyr was chosen as a widely used herbicide. The experiments have been performed during the initial phase of toxicity (four hours after herbicide application), not compromising plant viability. To correct for metabolic effects of the solvent DMSO and the adjuvant Dash® E.C., control plants were treated with a solution containing only DMSO and Dash® E.C., but not the active ingredient imazapyr.

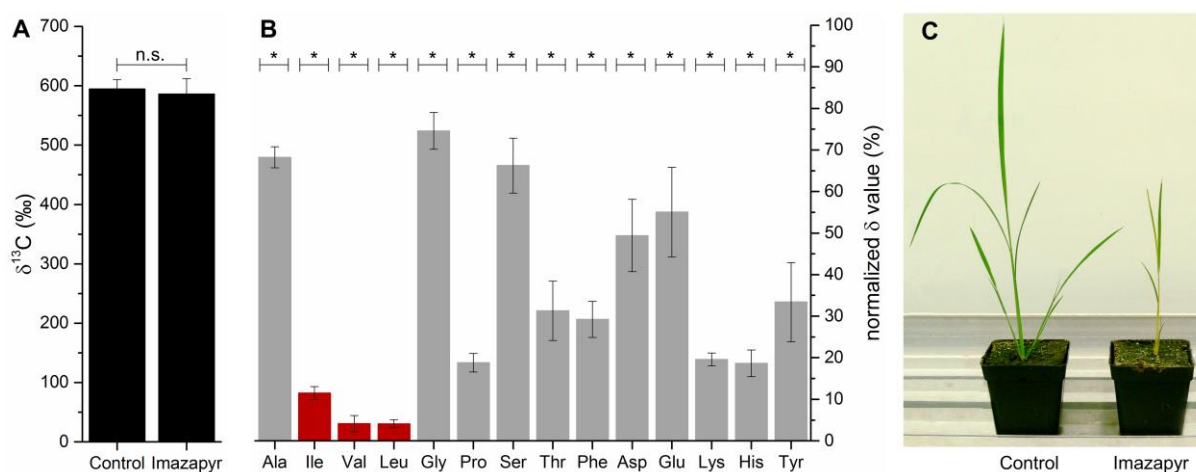


Figure 5. 9 Effect of imazapyr on rice seedlings

Mode-of-action analysis on the effect of the herbicide imazapyr on rice seedlings using $^{13}\text{CO}_2$ labeling in combination with EA-C-IRMS to assess carbon assimilation (time point zero) (A) and with GC-C-IRMS to assess ^{13}C enrichment of extracted proteinogenic amino acids (time point 2 hours) (B). The experimental set-up contained seedlings at the age of 12 days, subjected to imazapyr (62.5 g ha^{-1} active ingredient) and control treatment (62.5 g ha^{-1} control solution). Four hours after the treatment, seedlings were labeled for 10 minutes with $400 \mu\text{L L}^{-1} \text{ }^{13}\text{CO}_2$. The assimilation of ^{13}C , determined immediately after the labeling pulse from freeze-dried plant material, is expressed as $\delta^{13}\text{C}$ (‰), corrected for natural isotopes. The enrichment of extracted amino acids was determined after two hours of further cultivation at ambient air. The $\delta^{13}\text{C}$ -values of the amino acids of imazapyr-treated rice seedlings were normalized to those of the control seedlings. The phenotype of rice seedlings, seven days after treatment with the control solution (left plant) and the imazapyr solution (right plant) is shown in (C). Asterisks indicate significant differences between mean values of imazapyr-treated and control plants at $P \leq 0.05$ (Student's t-test). n.s., not significant. Mean values \pm SD ($n = 3$) are shown. The full data set of (A) and (B) is given in Table A9. 6 and Table A9. 7, respectively.

For pulse-chase studies, 12-day old, soil-grown rice seedlings were exposed to imazapyr treatment or a control treatment. Plants were pulse-labeled with $^{13}\text{CO}_2$, four hours after herbicide application. At the time-point of the labeling experiment, no phenotypic alterations of plant morphology, as compared to control plants, were observed (data not shown). The overall carbon assimilation at this time point was not disturbed, as indicated by equal ^{13}C shoot enrichment of stressed and control plants, namely $586 \pm 26\text{‰}$ and $595 \pm 16\text{‰}$, respectively (Figure

5. 9 A). However, strongly diminished label incorporation was detected in proteinogenic amino acids, which was particularly pronounced for branched-chain amino acids (BCAAs), 2 hours after the labeling pulse (Figure 5. 9 B). Amino acid enrichment of stressed plants reached 19 to 75% of the enrichment detected in control plants, except for the branched-chain amino acids, which did only reach 4 to 11%. The observed phenotype perfectly matches with the known mode-of-action of imazapyr. The herbicide is highly target-specific, inhibiting the enzyme acetohydroxyacid synthase, a key step in branched-chain amino acid biosynthesis (Tan et al., 2005). Our analysis further demonstrated that metabolic changes at this early time point were not restricted to branched-chain amino acids as primary target. In fact, metabolism was affected much more globally. Newly assimilated ^{13}C was incorporated into protein to a lesser extent in herbicide-treated plants than in control plants (Figure 5. 9 B), which may be due to increased turnover of existing protein to recycle branched-chain amino acids. In this regard, our profiling toolbox appears valuable to study the mode-of-action of synthetic compounds at the initial level of plant phenotyping, the first level of a three-tiered approach for mode-of-action identification (Tresch, 2013).

In the longer term, imazapyr causes dysfunction of cell growth, as well as disruption of DNA synthesis (Shaner and Reider, 1986b; Scarponi et al., 1995; Royuela et al., 2000). Accordingly, observable phenotypic effects became evident only seven days after imazapyr application and comprised inhibition of growth, chlorosis of aboveground plant parts, as well as a dieback of young leaves (Figure 5. 9 C). This indicates a slow rate of plant death, which is related to the amount of intracellularly stored amino acids (Shaner and Singh, 1991).

5.1.4 Carbon and nitrogen metabolism in adult rice plants

The transfer of the established methodology to older plants is challenging, as plants in advanced developmental stages are more complex, due to differentiation into specific organs and cell types. Furthermore, sampling is more difficult, as the harvested tiller has to be disassembled into individual organs prior to quenching in liquid nitrogen. Many plant characteristics can, however, only be investigated using adult plants, especially considering flowering and grain filling, two important developmental stages determining grain yield.

5.1.4.1 During grain filling, leaves are the main carbon provider of the panicle

Grain yield, the most prominent characteristic of crop plants, is strongly dependent on the source-sink relationship between plant parts (Kato et al., 2004), whereby the operational mode of a distinct plant organ, as source or sink, changes throughout development (Meng et al., 2013). Pioneering studies with rice plants, using radioactive $^{14}\text{CO}_2$ at high dosage had revealed translocation of assimilated carbon into the panicle during grain filling (Cock and Yoshida,

1972). This was quantitatively assessed here, however, by much safer and easier handling using stable $^{13}\text{CO}_2$. We furthermore extended the study of Cock and Yoshida by specific examinations, which assessed the capture and distribution of carbon at different growth stages and in individual tissues. In flowering and grain-filling stage, rice plants exhibit different leaf types, i.e. normal leaves and flag leaves, the flag leaf being the uppermost leaf on a culm (Rawson and Hofstra, 1969). Assimilation patterns of plants in different developmental stages, sampled immediately after a 10-minute labeling pulse, were compared (Figure 5. 10 B). Plants in the flowering stage showed similar ^{13}C enrichment in normal leaves ($260 \pm 40\text{‰}$) and flag leaves ($240 \pm 50\text{‰}$). This was also observed for the early grain-filling stage. During later grain filling, the flag leaf became more important for the assimilation of $^{13}\text{CO}_2$, indicated by significantly higher enrichment ($170 \pm 10\text{‰}$ in normal leaves, compared to $270 \pm 30\text{‰}$ in flag leaves), which is similar to previous findings for wheat (Rawson and Hofstra, 1969) and consistent with its function as major source organ for carbon transport into the panicle. During development from flowering to late grain filling, the relative contribution of different leaves to carbon assimilation probably corresponds to changing metabolic requirements (Meng et al., 2013). During late grain filling, the lower activity of carbon assimilation in mature leaves, relative to the flag leaf, indicated mechanisms of senescence (Figure 5. 10 B). In senescing leaves, the RuBisCO content and, as a consequence hereof, the photosynthetic activity rapidly decreases. Therefore, mature leaves cannot assimilate as much CO_2 as younger leaves (Makino et al., 1984). Immediately after the labeling pulse, the stem was not enriched with ^{13}C , in none of the examined developmental stages, while the panicle showed low ^{13}C accumulation during grain-filling ($10 \pm 5\text{‰}$).

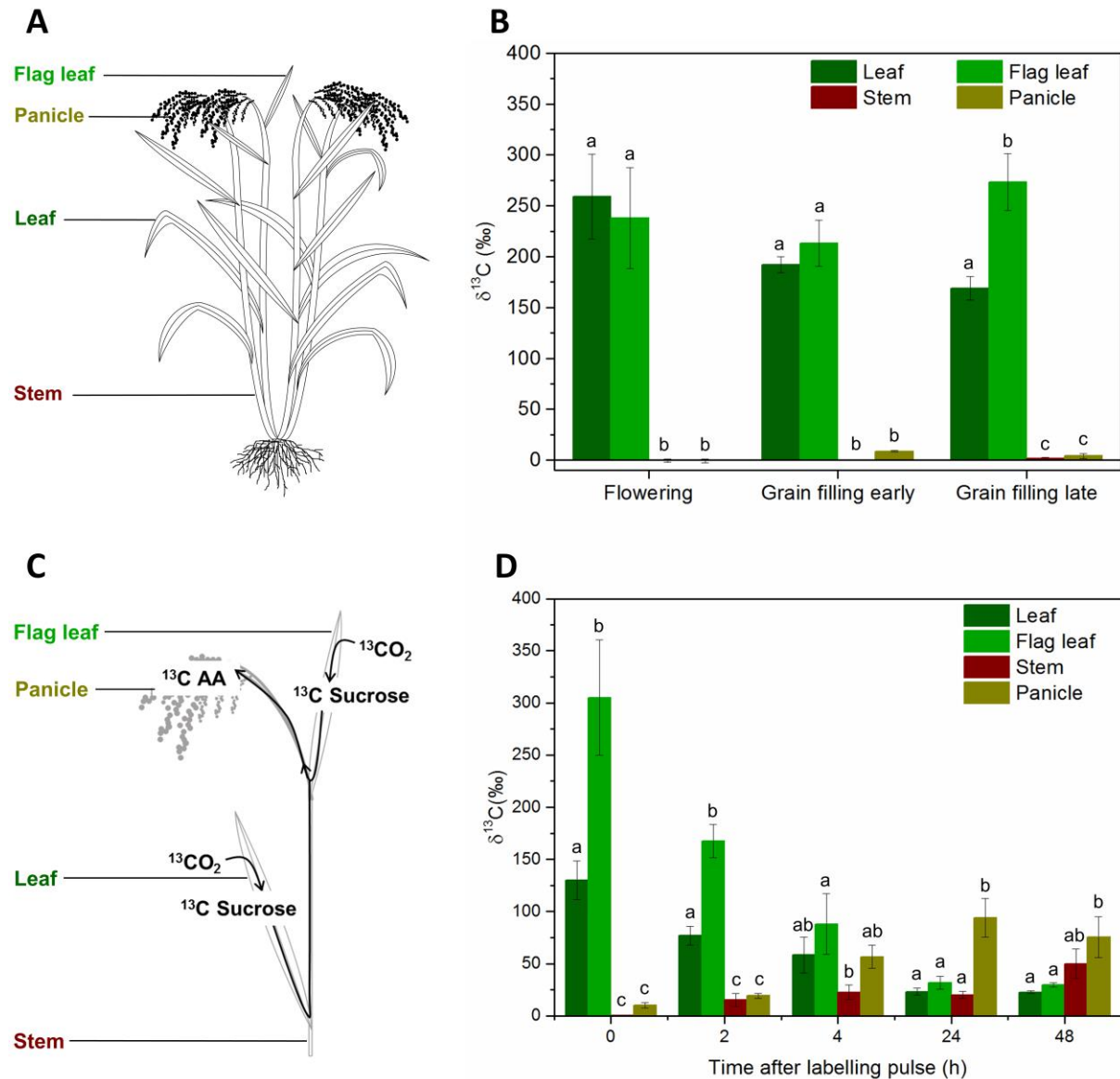


Figure 5. 10 Carbon assimilation and translocation in adult rice plants

Carbon assimilation and translocation in adult rice plants, assessed by $^{13}\text{CO}_2$ isotope experiments and labeling analysis by combustion isotope ratio mass spectrometry, coupled to elemental analysis. Morphology of the studied plants with sampled leaf, flag leaf, stem and panicle (A); Tissue-specific ^{13}C assimilation of rice at flowering stage (68 days), at early grain filling stage (75 days) and at late grain filling stage (88 days), for which soil-grown plants were labeled with $400 \mu\text{L L}^{-1} \text{ }^{13}\text{CO}_2$ for 10 minutes and directly harvested for assessment of ^{13}C enrichment (B); Morphology of the studied plants with identified carbon assimilation routes (C); Time-resolved carbon assimilation and translocation of rice plants at late grain filling stage (88 days), for which soil-grown plants were labeled with $400 \mu\text{L L}^{-1} \text{ }^{13}\text{CO}_2$ for 10 minutes and directly harvested, or further cultivated at ambient air for 2, 4, 24 and 48 hours prior to harvesting (D). In all cases, ^{13}C enrichment of freeze-dried plant material is displayed as $\delta^{13}\text{C}$ (‰), corrected for natural labeling. Mean values \pm SD ($n = 3$) are shown. The letter coding (a, b, c) indicates significant differences between means ($P \leq 0.05$, one-way ANOVA with Tukey's test) of sampled organs at the respective time points. The full data sets of (B) and (D) are given in Table A9. 8 and Table A9. 9, respectively.

In order to assess carbon translocation, plants were post-cultivated in the phyto chamber after a labeling period of 10 minutes. Samples taken after distinct chase periods provided a time-resolved ^{13}C sequestration pattern. Immediately after the $^{13}\text{CO}_2$ pulse, most of the label was recovered in the leaves (Figure 5. 10 D). Within two hours of further growth, the ^{13}C enrichment of flag leaves and normal leaves declined by 45% and 41%, respectively, while the enrichment of stem and panicle increased. This trend continued until a maximal enrichment was reached after 24 hours for the panicle ($100 \pm 20\%$) and after 48 hours for the stem ($50 \pm 15\%$). Generally, a strong decrease of ^{13}C was detected in the assimilating tissue during the first 24 hours of the chase period. This decrease amounted to almost 90% in plants of the late grain filling stage, which is in the range of values reported for other plants (Leake et al., 2006). Most of the labeled carbon was translocated to the major sink, the panicle. At night, ^{13}C was further lost by respiration. Additional carbon loss might have resulted from a combination of translocation to tissues not analyzed, e.g. the roots of plants grown on soil, and dilution of the label by overall plant biomass increase during the experiment (Leake et al., 2006).

5.1.4.2 Protein biosynthesis is most active in growing and developing tissues

The ^{13}C enrichment of protein amino acids inside the different organs of a full-grown, reproducing plant was examined to elucidate the molecular interaction between plant tissues and obtain insights into their specific function. In comparison to rice seedlings, the general amino acid enrichment was, on average, eight times lower in the leaf of an adult plant during the late grain filling stage (Figure 5. 11), which was interesting to note, as the total assimilation of carbon of both tissue types was in the same range (Figure 5. 3 D, 400 ppm, 10 minutes and Figure 5. 10 B). This perfectly matches with the changing role of leaves as strong sink during development to their function as major source during reproduction (Thrower, 1962; Turgeon, 1989), assimilating but not incorporating carbon dioxide.

The ^{13}C labeling of amino acids differed largely between individual tissues. For rice at late grain filling, low enrichment was equally observed for normal leaves ($60 \pm 10\%$ total amino acid enrichment), the flag leaf ($70 \pm 10\%$ total amino acid enrichment) and the stem ($40 \pm 25\%$ total amino acid enrichment) within one day of label translocation (Figure 5. 12). In contrast, the panicle of adult rice plants was much more active regarding amino acid metabolic pathways ($280 \pm 30\%$ total amino acid enrichment). Here, highest enrichment was detected for phenylalanine ($39 \pm 3\%$) and tyrosine ($30 \pm 2\%$), followed by alanine ($28 \pm 4\%$), glutamate ($23 \pm 2\%$) and leucine ($22 \pm 3\%$), which was in accordance to the pattern detected for rice seedlings. The other amino acids showed lower enrichment.

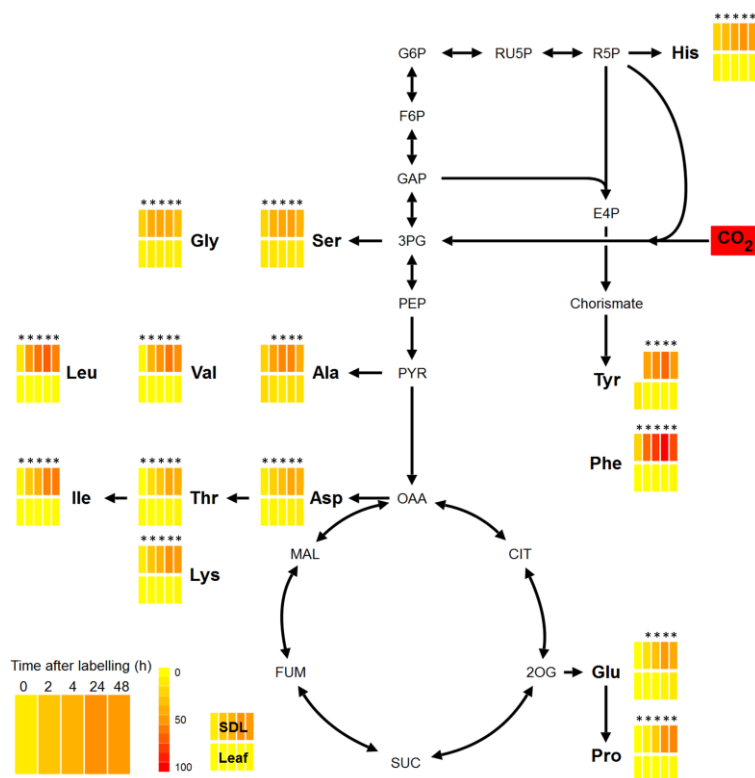


Figure 5. 11 Amino acid ^{13}C enrichment of a rice seedling in comparison to the leaf of a rice plant in the late grain filling stage.

Incorporation of ^{13}C into protein amino acids upon $^{13}\text{CO}_2$ labeling. Enrichment of extracted amino acids was analyzed by GC-C-IRMS. Time-resolved pattern of a rice seedling (upper panels, age of 12 days) and an adult rice plant at late grain filling (lower panels, age of 88 days), for which soil-grown plants were labeled with $400 \mu\text{L L}^{-1} \text{ }^{13}\text{CO}_2$ for 10 minutes and then directly harvested, or further cultivated at ambient air for 2, 4, 24 and 48 hours prior to harvesting. Statistical analysis was conducted using the Student's t-test, whereby significant differences ($P \leq 0.05$) between seedling and adult leaf are marked with an asterisk. The enrichment data are provided as mean values ($n = 3$) and reflect atom percent excess (APE), corrected for natural isotopes. To facilitate comparison, the data are normalized for the highest enrichment of the data set, which was set 100% and visualized by a color code between yellow (0%) and red (100%). Abbreviations: SDL (seedling shoot). Metabolite abbreviations can be found in Table A9. 1. Amino acid abbreviations are according to the three letter code. The full data set is given in Table A9. 10.

Leaves and flag leaves, assimilated the provided $^{13}\text{CO}_2$ (Figure 5. 10) but incorporated only little of it into protein (Figure 5. 12). In fact, most of the assimilated carbon was translocated to the panicle, where it was incorporated into proteinogenic amino acids. The panicle exhibited an active *de novo* protein biosynthesis, reflecting filling of the grains with a strong demand for protein precursors (Cock and Yoshida, 1972).

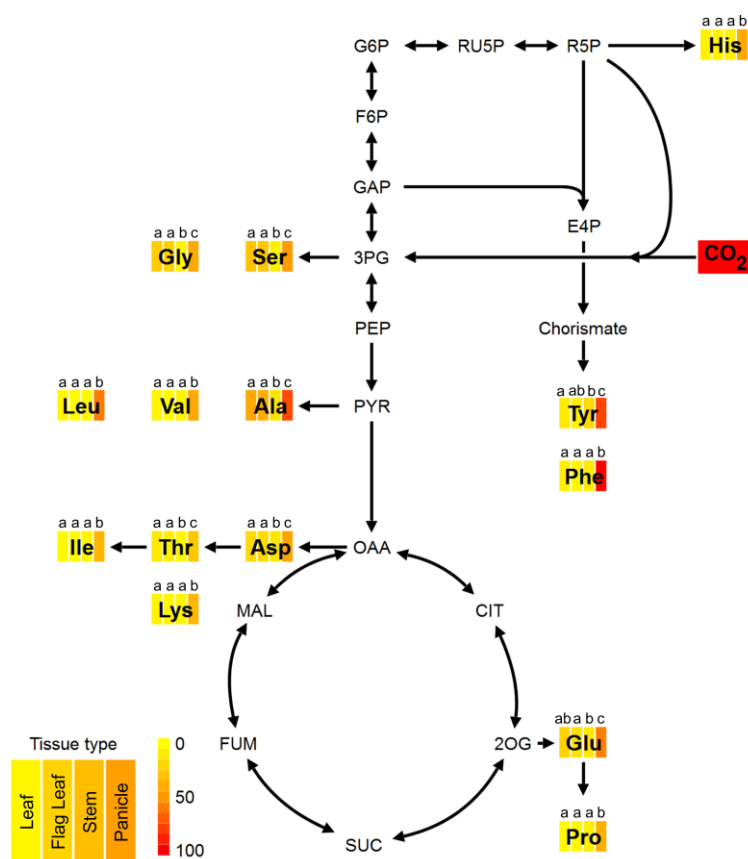


Figure 5. 12 Amino acid ^{13}C enrichment of rice plant organs in the late grain filling stage.

Tissue-resolved pattern of an adult rice plant at late grain filling (88 days), for which plants were labeled with $400 \mu\text{L L}^{-1} \text{ }^{13}\text{CO}_2$ for 10 minutes, followed by 24 hours of further cultivation at ambient air prior to harvesting of leaf, flag leaf, stem and panicle. Statistical analysis was done by one-way ANOVA with Tukey's test ($P \leq 0.05$), whereby different letters (a, b, c) indicate significant differences between means of the different tissues. The enrichment data are provided as mean values ($n = 3$) and reflect atom percent excess (APE), corrected for natural isotopes. To facilitate comparison, the data are normalized for the highest enrichment of the data set, which was set 100% and visualized by a color code between yellow (0%) and red (100%). Metabolite abbreviations can be found in Table A9. 1. Amino acid abbreviations are according to the three letter code. The full data set is given in Table A9. 11.

A compound-oriented view, based on statistical significance of labeling patterns, groups amino acids into colored ellipses according to their labeling similarity (Figure 5. 13). This immediately highlights specific metabolic fingerprints for all tissues of rice. Leaf and flag leaf differed only in a few amino acids, whereas stem and panicle revealed drastically altered patterns and evidence for a tissue-specific carbon metabolism. This type of visualization further highlighted strong differences between the carbon metabolism of an adult leaf and a young shoot.

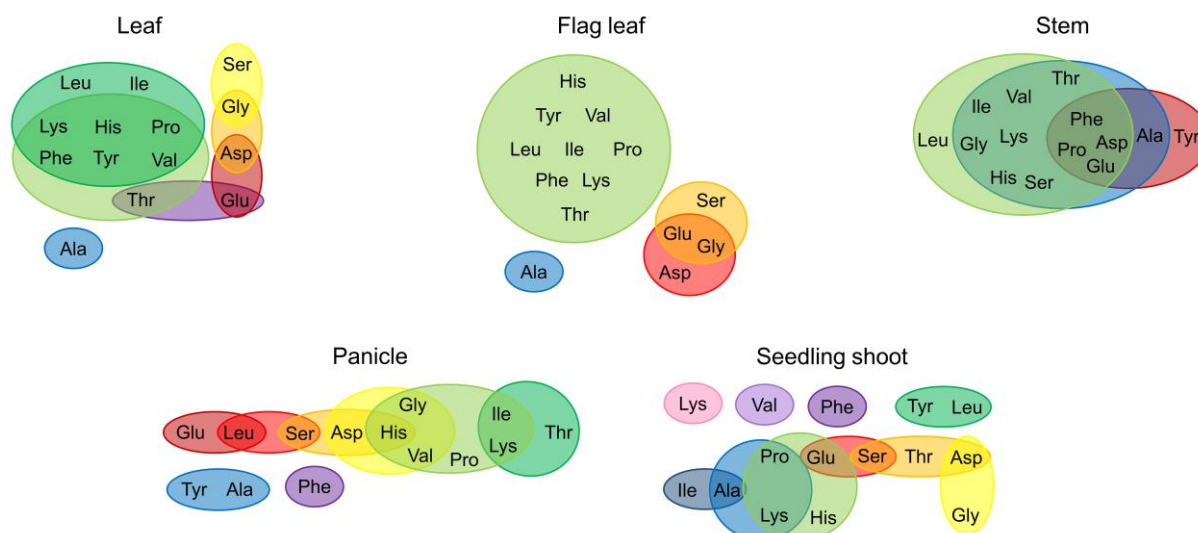


Figure 5.13 Tissue-specific amino acid ^{13}C enrichment of rice plant organs

Tissue-specific amino acid metabolism, visualized as Venn diagram, which displays the relation of amino acids, based on the statistical significance between measured ^{13}C enrichments. Soil-grown plants (12 days) were labeled with $400 \mu\text{L L}^{-1} \text{ }^{13}\text{CO}_2$ for 10 minutes and further cultivated at ambient air for 24 hours prior to harvesting. Significant differences between means of amino acid ^{13}C enrichments ($P \leq 0.05$) were determined by one-way ANOVA with Tukey's test. Amino acids that do not show significantly different ^{13}C enrichment, are located in equally colored ellipses. Amino acid abbreviations are according to the three letter code. The full data set is given in Table A9.12.

Grain yield of crop plants is largely determined during flowering and grain-filling stages of development. Therefore, elucidating metabolic traits of these developmental stages may greatly contribute to successful genetic engineering of crops for higher yield. The pulse-chase experiments conducted to examine rice metabolism during flowering and grain-filling stages show the high potential of this cost-effective and high-throughput screening tool. Complementing the pulse-chase studies by the developed isotopically non-stationary MFA approach would be the next step to gain deeper insight into metabolic functions of the individual organs of the rice plant. This could significantly enhance current knowledge about the interplay of different plant organs and the metabolic alterations that plants perform during development.

5.2 Non-stationary metabolic flux analysis of illuminated rice seedlings

Dynamic labeling experiments with $^{13}\text{CO}_2$ were combined with *in silico* flux calculations to fit the measured data to a comprehensive metabolic network model in an approach called isotopically non-stationary metabolic flux analysis. INST-MFA provides the possibility to map the fate of carbon in autotrophic metabolic networks and was therefore used to get deeper insight and a more comprehensive picture of rice seedling shoot metabolism. Metabolic flux maps are broad descriptions of metabolism as they usually integrate a myriad of experimental data, e.g. mass isotopomer distribution and pool sizes of intracellular metabolites, as well as biomass formation rate and biomass composition with a stoichiometric network model. The integration of isotopic labeling with network modeling increases precision and confidence in calculated fluxes and enhances flux identifyability, as it allows the resolution of fluxes through parallel and cyclic pathways or bidirectional enzymes (Wiechert, 2001). Compared to the fast and simple pulse-chase experiments, INST-MFA provides much more information at the cost of extensive experimental and computational effort. A prerequisite for INST-MFA studies was that intracellular metabolite levels and metabolic fluxes remain constant throughout the labeling experiment and were not disturbed by the replacement of $^{12}\text{CO}_2$ with $^{13}\text{CO}_2$. To perform INST-MFA with whole rice plants, several preconditions had to be met. First, a gas-tight reactor was built for labeling of plants with $^{13}\text{CO}_2$. The constructed reactor provided a highly controlled environment with tracer concentrations equimolar to those of ambient CO_2 . As advantageous feature, the reactor comprised the possibility for combined labeling of plants belonging to one experimental run, thereby decreasing the inter-experimental error. The fast sampling of individual plants at previously defined time-points provided a good coverage of fast and slowly labeled metabolites.

5.2.1 Automated flux box for dynamic labeling studies

To perform *in vivo* transient ^{13}C labeling experiments, a specialized flux incubator was constructed (Figure 5. 14). As the labeling experiments should be possible with $^{13}\text{CO}_2$, the reactor had to be gas-tight and had to enable fast replacement of unlabeled by ^{13}C labeled carbon dioxide. This was achieved by a CO_2 adsorption unit, featuring a high power pump to remove ambient CO_2 to values below $20 \mu\text{L L}^{-1}$ within one minute. Strong ventilators with a per minute gas-exchange capacity, four times that of the chamber volume, provided fast distribution of the subsequently injected $^{13}\text{CO}_2$.

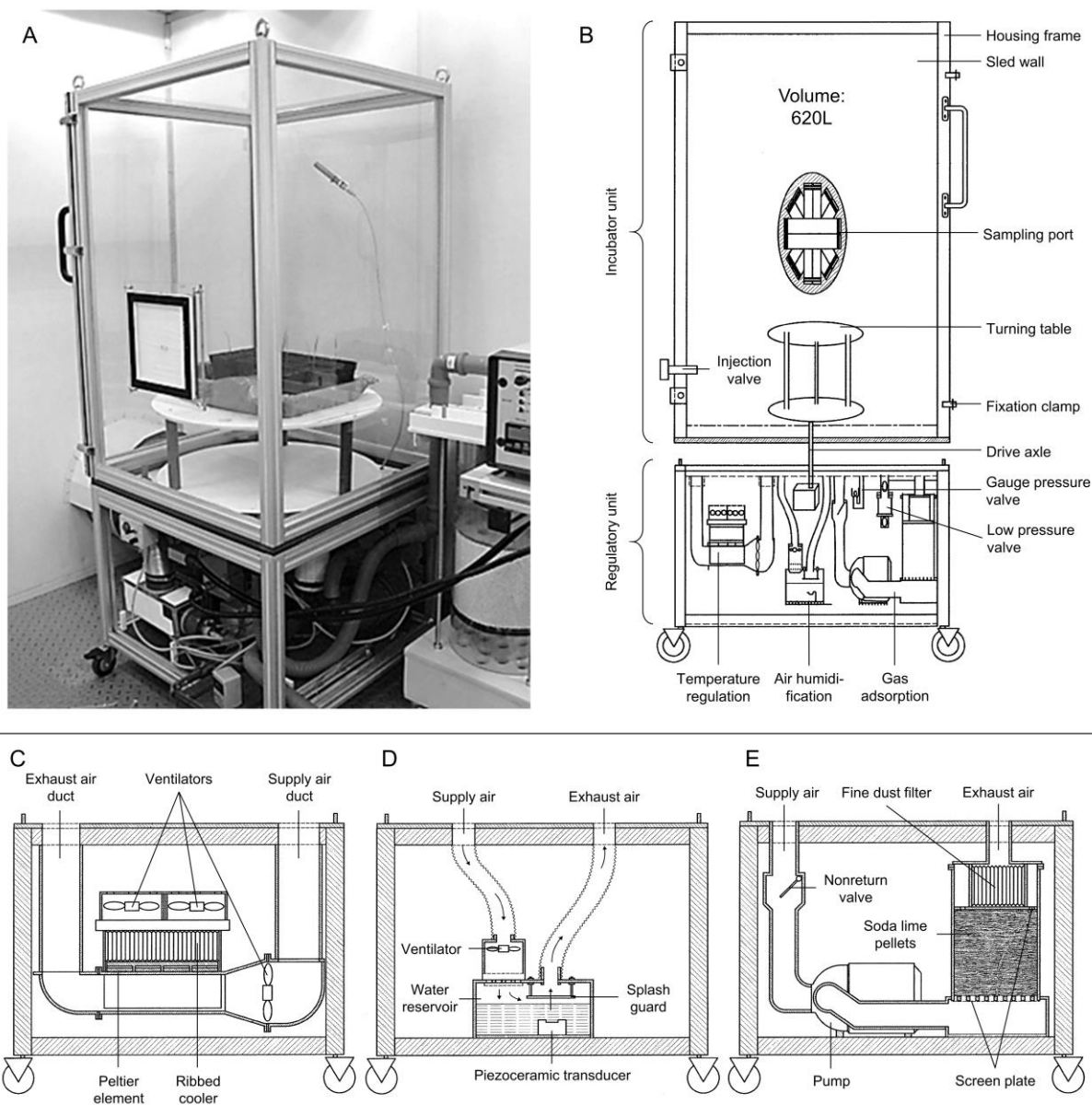


Figure 5. 14 Automated flux reactor used for isotopically non-stationary metabolic flux analysis

Flux reactor constructed for *in vivo* dynamic labeling of rice plants with $^{13}\text{CO}_2$. (A) Photo of the flux reactor inside the phyto chamber. (B) Sketch of the flux reactor consisting of a detachable incubator unit and a movable regulatory unit, comprising a (C) temperature-regulating system, (D) air-humidification system and (E) adsorption unit (Patent WO 2014/079696 A1).

A highly sensitive online quadrupole mass spectrometer, capable to distinguish between $^{12}\text{CO}_2$ and $^{13}\text{CO}_2$, recorded the CO_2 composition inside the reactor throughout the experiment (Figure 5. 15 A, Table A9. 15). The incubator furthermore featured well-defined, automatically controlled environmental conditions considering temperature and humidity. Ambient parameters were maintained at desired values (27 ± 1 °C and $70 \pm 10\%$ relative humidity) and were recorded online by a temperature and humidity logger (Figure 5. 15 B).

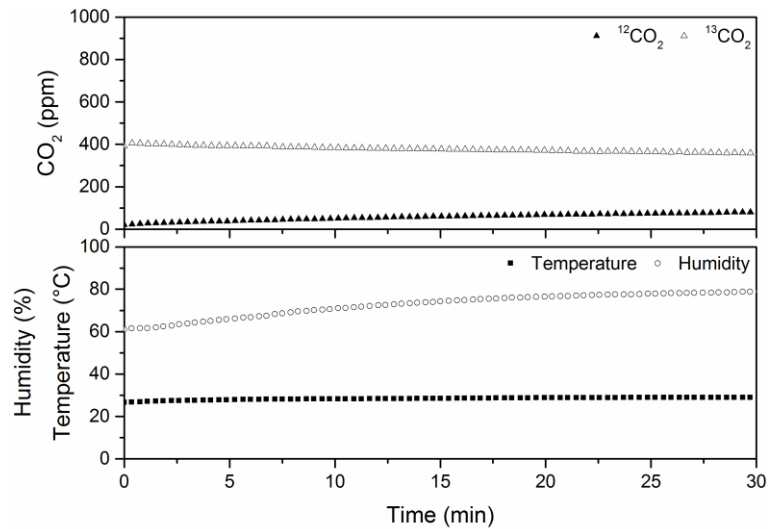


Figure 5. 15 Atmosphere inside the flux incubator during a labeling experiment

(A) After adsorption, the concentration of $^{13}\text{CO}_2$ decreased as it was assimilated by plants, whereas $^{12}\text{CO}_2$ concentration increased. (B) The temperature was maintained at 27 °C, whereas humidity constantly increased throughout the experiment due to plant transpiration.

Constant atmospheric conditions were of major importance for meaningful flux results, as fluctuations in environmental parameters otherwise could have influenced metabolite levels and hence fluxes. The flux incubator was therefore particularly designed to minimize intra-experimental errors, as it allowed the simultaneous labeling of all plants belonging to one replicate experimental run. This was made possible by integrating a sampling port in one of the reactor walls (Figure 5. 16 A), enabling fast sampling of individual plants throughout the experiment with minimal perturbation of the controlled atmosphere. This was a major advantage compared to previous studies, where individual plants were labeled separately for distinct time periods (Szecowka et al., 2013; Ma et al., 2014). The approach significantly enhanced throughput and eliminated the risk of exposing the plants to variable ambient conditions, at least for the samples of one experimental run. For more detailed information about reactor specifications, please refer to chapter 4.3.2.

Specially designed scissors served for single-handed sampling, minimizing the risk of disturbing the reactor atmosphere (Figure 5. 16 B). A turning table allowed for exact positioning of the plants in front of the sampling port, thereby enhancing sampling frequencies. A tailor-made syringe with a stop mechanism was used to aspirate an exact volume of labeled carbon dioxide prior to each injection (Figure 5. 16 C).

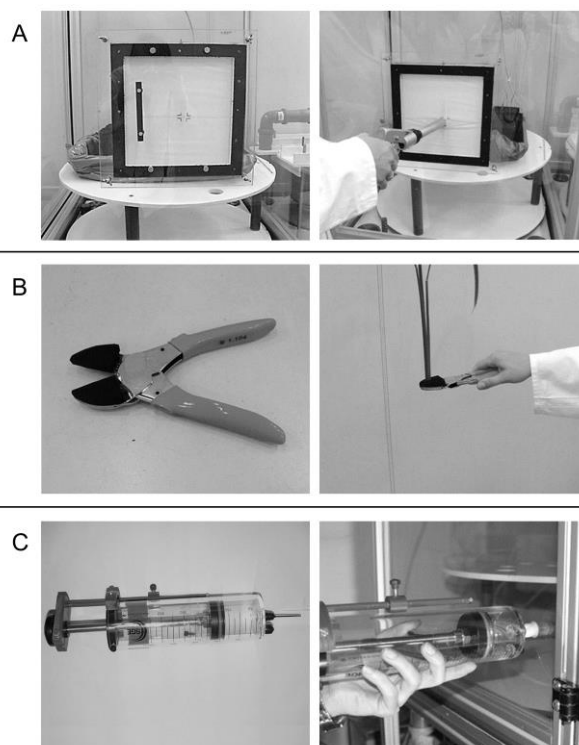


Figure 5. 16 Experimental equipment

(A) Sampling port covered by flexible rubber straps to allow plant harvest without disturbing the tightly controlled reactor atmosphere. (B) Scissors with foam rubber pieces attached to the blades for safe and single-handed sampling. (C) Custom-made syringe (500 mL) for injection of an exact amount of $^{13}\text{CO}_2$.

The wide range of covered metabolite concentrations (Table 5. 3) was linked to strong differences between respective enrichment rates (Figure 5. 22). To assure a high mass isotopomer resolution for both fast and slowly labeled metabolites, optimal sampling time points were calculated by computer simulations. A random, stoichiometrically possible flux distribution was taken as basis for the simulation of isotopomer distributions, i.e. labeling profiles. Based on these simulated labeling profiles, sampling intervals were chosen to be short at the beginning of the labeling experiment, increasing with time. Rice seedlings, pre-grown in the phyto chamber at ambient air, were transferred to the flux incubator, just before the start of the labeling experiment. Atmospheric CO_2 was removed by adsorption, followed by the injection of $^{13}\text{CO}_2$ ($400 \mu\text{L L}^{-1}$). During a 30 minute labeling experiment, 15 samples were taken at defined time points (0, 10, 20, 30, 40, 50, 60, 120, 150, 180, 300, 420, 600, 1800 seconds). Samples were immediately deep-frozen in liquid nitrogen and analyzed by a diverse set of analytical techniques, comprising IRMS, GC-MS and LC-MS/MS analytics, to determine the MIDs and pool sizes of intracellular metabolites, as well as biomass composition and growth rate.

5.2.2 Data acquisition and assessment of data quality

The measurement of intracellular fluxes is nontrivial, as there is no easy way of monitoring the interconversion of metabolites or the intracellular activity of enzymes. Today, intracellular fluxes in plant metabolic networks are determined by stable isotope labeling experiments in an approach called metabolic flux analysis. Metabolic flux analysis requires knowledge about (i) the redistribution of label through the network, (ii) a sophisticated network model, (iii) a fitting procedure to determine a set of metabolic fluxes and (vi) statistics to assess the reliability of flux estimates (Kruger and Ratcliffe, 2015). The reconstructed, compartmented metabolic model of *Oryza sativa* comprised pathways of central carbon metabolism, e.g. EMP and PP pathway, CBB and TCA cycle, as well as the reactions of photorespiration, and anabolic pathways, like sucrose and starch synthesis, as well as fatty acid and amino acid biosynthesis (Beckers, 2015). The experimental data supplied to the model consisted of enrichment data, i.e. mass isotopomer distributions, pool sizes of intracellular metabolites, uptake and production rates and biomass composition (Figure 5. 17, Table 5. 1).

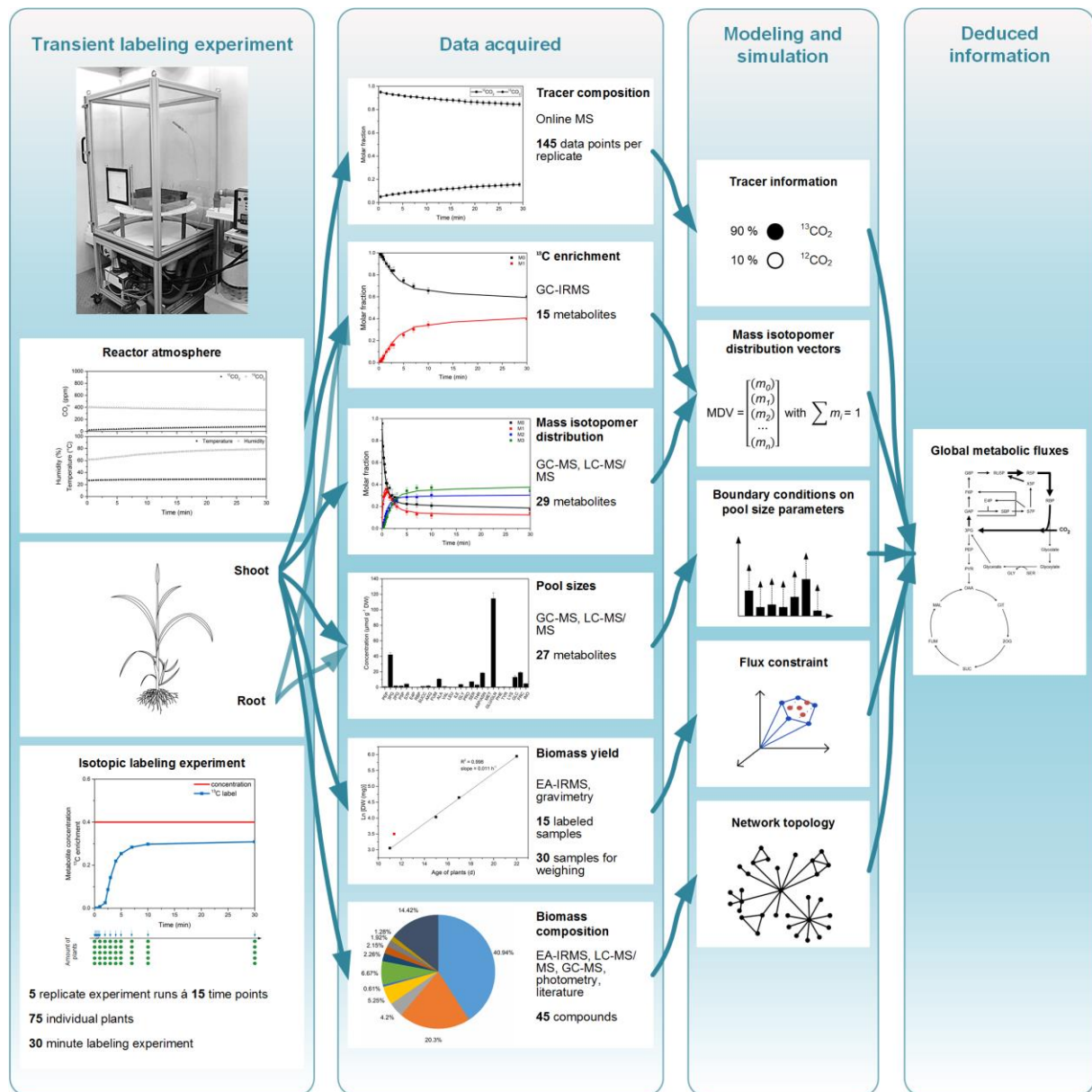


Figure 5. 17 Overview of experimental design, acquired data, computational analysis and information flow in non-stationary metabolic flux analysis

The transient labeling experiments yielded a high amount of measured data that were subsequently used as basis for computational modeling and simulation of metabolic fluxes, displayed in form of a comprehensive flux map.

To determine metabolic fluxes, these experimental data were fitted to the network model. A variety of different analytical techniques was used for data acquisition, as listed in Table 5. 1.

Table 5. 1 Overview of experimental data integrated for metabolic flux analysis

The metabolic network model was provided with a vast amount of experimental data to constrain the solution space of the flux calculation. The tracer composition inside the plant reactor during the experiment, mass isotopomer distributions of a multitude of chemically different intracellular metabolites, their corresponding pool sizes, the cellular composition, as well as uptake and production rates were integrated for flux calculations. The table lists the type of data integrated into the model, as well as the analytical technique used to measure the respective metabolites and parameters.

Type of data	Analytics	Measured metabolites/ parameters
Tracer composition	Online MS	$^{12}\text{CO}_2$, $^{13}\text{CO}_2$
^{13}C enrichment	GC-IRMS	amino acids, organic acids, soluble sugars
Mass isotopomer distribution	LC-MS/MS GC-MS	amino acids, organic acids, soluble sugars, sugar phosphates
Pool sizes	LC-MS/MS GC-MS	amino acids, organic acids, soluble sugars, sugar phosphates
Biomass yield	EA-IRMS	^{13}C enrichment
	gravimetry	shoot dry weight
Biomass composition	EA-IRMS	C/N ratio (protein content)
	LC-MS/MS	amino acids, organic acids
	GC-MS	soluble sugars, organic acids, fatty acids, starch and sucrose
	literature	organic acids, pigments, cell wall components, nucleotides
Carbon export to the root	GC-IRMS	amino acids, soluble sugars
	GC-MS	amino acids, sucrose

5.2.2.1 Tracer composition

Isotopomer incorporation into metabolites largely depended on the concentration and composition of the applied tracer. Therefore, $^{12}\text{CO}_2$ and $^{13}\text{CO}_2$ concentration was recorded by an online quadrupole mass spectrometer throughout the labeling experiment (Figure 5. 15 A). Recording the concentrations both of $^{12}\text{CO}_2$ and $^{13}\text{CO}_2$ was crucial, as these data were used to determine the substrate concentration and composition, even considering changes in composition due to CO_2 assimilation and respiration by the plant. Furthermore, the measurement of $^{13}\text{CO}_2$ provided the possibility to control the injection of the labeled CO_2 gas. The latter was

a great advantage, as it ensured that the desired amount of $^{13}\text{CO}_2$ was actually injected. In addition, the response time of the mass spectrometer was extremely short and accuracy was high, allowing for very precise time-resolved measurements. The possibility to monitor the $^{12}\text{CO}_2$ and $^{13}\text{CO}_2$ signals on-line, enabled the adjustment of the $^{13}\text{CO}_2$ concentration or the abortion of the experiment in case of incorrect injection. The use of quadrupole mass spectrometry is a great improvement as compared to widely-used infrared gas analyzers (IRGAs), as the latter are insensitive to $^{13}\text{CO}_2$ (Bromand et al., 2001), hence underestimating its real concentration (Bromand et al., 2001). The used quadrupole mass spectrometer was especially suitable for residual gas analysis under high vacuum. It was able to scan over a wide mass range (1 to 512 amu) with high sensitivity and measuring rate. Before starting the measurement of an unknown gas mixture, the following tune and calibration tasks had to be accomplished: (i) tuning of the ion source parameters, (ii) offset calibration, (iii) mass scale adjustment, (iv) background determination and (v) gas specific calibration. The ion source was tuned, regarding maximum intensity, high resolution and optimal peak shape. The offset calibration defined the noise signal of the preamplifier at closed gas inlet. The mass scale was adjusted, so that the peak maxima was exactly matching the expected mass. The background, determined with helium gas, was subtracted from following measurements, as it displayed the presence of molecules and ions that are carried with the gas flow but do not belong to the actual quantity to be measured. The gas specific calibration of the instrument was non-trivial and required three individual adjustments. As the share of $^{12}\text{CO}_2$ and $^{13}\text{CO}_2$ in air should be quantified, the first calibration was performed with air (78 % N_2 , 20.9 % O_2 , 0.9 % argon, 0.04 % CO_2 , 0.6 % H_2O), setting calibration factors for all components. The amount of H_2O in air is dependent on the relative humidity and the temperature and was determined with the aid of the Molier h-x diagram. As the composition of air inside the phyto chamber may be different from that of outside air, the second calibration was performed with a defined calibration gas (10% O_2 , 0.05 % CO_2 , 89.95 % N_2), thereby enhancing the accurateness of the calibration factors determined for O_2 , CO_2 and N_2 . The third calibration was performed to calibrate the $^{13}\text{CO}_2$ signal (2 % $^{12}\text{CO}_2$, 1 % $^{13}\text{CO}_2$, 97 % N_2). The calibration factors are overwritten by the subsequent calibration. Finally, a test gas (0.075 % $^{12}\text{CO}_2$, 0.075 % $^{13}\text{CO}_2$, 98.5 % N_2) was measured to check the accuracy of the calibration. The calibration was checked daily prior to the experiment and was repeated if necessary. Tuning of ion source, offset, mass scale and

background was repeated when, after gas specific calibration, measured values were still deviating from those of the defined test gas.

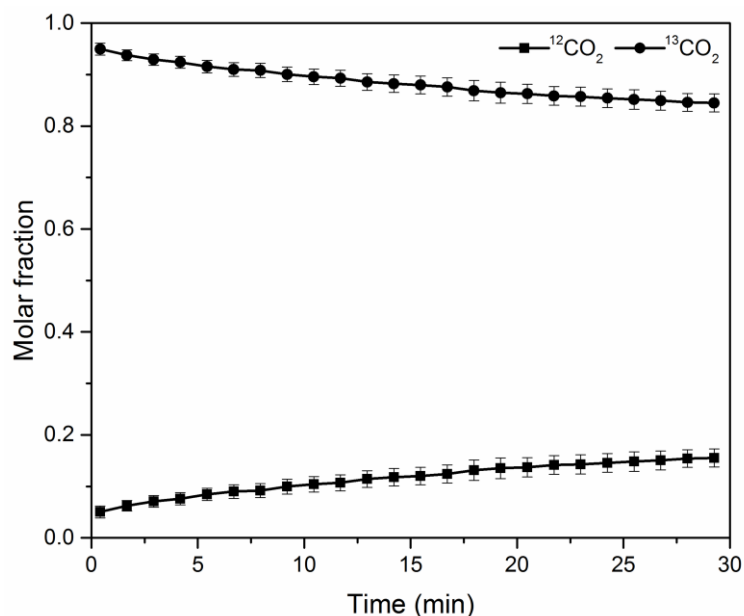


Figure 5.18 Mass isotopomer profile of CO_2 present in labeling reactor throughout experiment

Molar fractions of $^{12}\text{CO}_2$ and $^{13}\text{CO}_2$ as measured by online mass spectrometry throughout a 30 minute labeling experiment inside the flux reactor. The reactor housed 15 untreated, soil grown rice seedlings at an age of 15 days. Mean values \pm SD ($n = 5$) are shown.

Immediately after adsorption of atmospheric CO_2 and subsequent injection of the labeled tracer, $^{12}\text{CO}_2$ concentration was as low as $20 \mu\text{L L}^{-1}$, whereas $^{13}\text{CO}_2$ concentration was at the desired $400 \mu\text{L L}^{-1}$. Throughout the 30 minute experiment, the $^{12}\text{CO}_2$ content steadily increased reaching $80 \mu\text{L L}^{-1}$, while the $^{13}\text{CO}_2$ level decreased to $360 \mu\text{L L}^{-1}$, which was due to plant respiration and assimilation, respectively. As the change in tracer composition influences transient mass isotopomer distributions (Wiechert and Nöh, 2013; Antoniewicz, 2015), this change was included as parameter in the modeling procedure. The CO_2 composition, as measured in the flux reactor, was converted into an isotopomer profile: $^{12}\text{CO}_2$ reflecting the M0 mass isotopomer, $^{13}\text{CO}_2$ reflecting the M1 mass isotopomer. The sum of $^{12}\text{CO}_2$ and $^{13}\text{CO}_2$ concentrations equaled the total amount of CO_2 present in the reactor (Figure 5.18). A dummy reaction was used to model a mixture of $^{12}\text{CO}_2$ and $^{13}\text{CO}_2$. These values had to fit the isotopomer profile measured inside the reactor.

5.2.2.2 Mass isotopomer distributions

Mass isotopomer distributions are of major importance for flux calculations. As there is no direct technique for measuring the *in vivo* flow of metabolites, fluxes are determined indirectly from measurable information. Compared to methods that are solely based on extracellular fluxes, the complementation of such studies with intracellular isotopic labeling information is much more reliable (Wiechert and Nöh, 2013). The mass isotopomer distribution of intracellular metabolites was determined by GC-MS, LC-MS/MS and GC-C-IRMS. A variety of amino acids, organic acids, soluble sugars and sugar phosphates were analyzed, resulting in excellent coverage of central metabolism (Table 5. 2). The detected MIDs of all metabolites are listed in Table A9. 16 to Table A9. 65. The EMP pathway intermediates dihydroxyacetone phosphate and glyceraldehyde 3-phosphate were not detectable in plant extracts, probably due to very low concentrations. The TCA-cycle intermediate oxaloacetate was highly unstable and degraded during sample processing and mass spectrometry (Zimmermann et al., 2014).

Table 5. 2 List of analytes for which mass isotopomer distributions were obtained

The use of different analytical techniques allowed the isotopic enrichment to be measured for a vast amount of chemically diverse compounds. Mass isotopomer distributions were determined for the listed intracellular metabolites, comprising sugar phosphates, organic acids, amino acids and soluble sugars. The measurement of compounds with more than one analytical platform enhances validity of the measured data and yields additional labeling information.

Compound class	Metabolite	GC-C-IRMS	GC-MS	LC-MS/MS
Sugar phosphates	Pentose 5-phosphate			x
	Sedoheptulose 7-phosphate			x
	Fructose 6-phosphate			x
	Glucose 6-phosphate		x	x
	Fructose 1,5-bisphosphate			x
	Ribulose 1,5-bisphosphate			x
Organic acids	Succinate		x	
	α -Ketoglutarate		x	
	Fumarate		x	
	Phosphoenolpyruvate			x
	Pyruvate		x	x
	3-Phosphoglycerate			x
	2-Phosphoglycerate			x
	6-Phosphoglycolate			x
	Malate	x	x	
	Citrate		x	
	Glycerate		x	
	Glycolate			x
Amino acids	Alanine	x	x	
	Valine	x	x	

Compound class	Metabolite	GC-C-IRMS	GC-MS	LC-MS/MS
	Leucine		x	
	Isoleucine		x	
	Glycine	x		
	Proline		x	
	Serine	x	x	
	Threonine		x	
	Aspartate	x		
	Asparagine	x	x	
	Glutamate	x	x	
	Glutamine	x		
	Phenylalanine		x	
	Tyrosine	x		
	Lysine	x		
Soluble sugars	Sucrose	x	x	
	Glucose	x		
	Fructose	x		
	Inositol	x		

Optimization of GC-MS analyses

The power of GC-MS analysis arises from the high sensitivity of the mass spectrometer and its selectivity owing to two separation steps. The first step occurs chromatographically by separation of molecules according to their chemical and physical properties. The second separation takes place inside the mass spectrometer, where molecules are ionized, fragmented and subsequently separated according to their mass to charge ratio (Karasek and Clement, 2003). In this study, GC-MS analyses were performed according to Walk et al. (2007) to measure amino acids, organic acids, soluble sugars and sugar phosphates. To enhance sensitivity for target analytes the mass spectrometer was operated in selected ion monitoring (SIM) mode. In SIM mode, only the most indicative ion of a substance is measured, hence increasing the dwell time for that ion, as the mass spectrometer is set to measure on specific mass. Matrix interferences are furthermore eliminated by the high selectivity of selected ion monitoring, as unwanted ions are being filtered. Hence, the most prominent fragment ion was selected for each metabolite of interest. All possible ^{13}C mass isotopomers of the selected fragment were included as individual masses into the SIM methods (Table A9. 13). Two separate SIM measurements were performed, which allowed to adjust a split ratio according to the amount of metabolite in the sample.

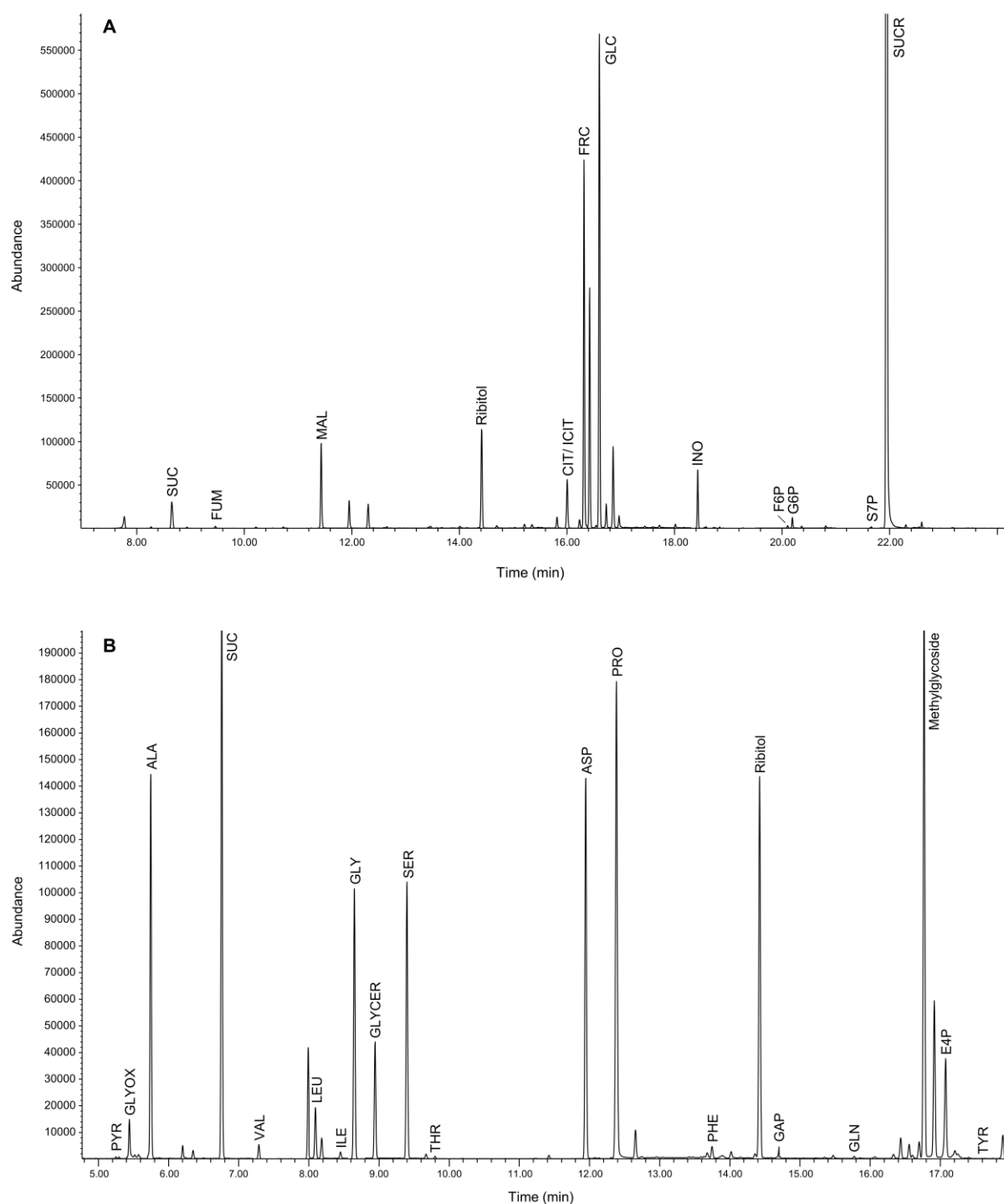


Figure 5. 19 GC-MS chromatogram of sugars, amino acids, organic acids and sugar phosphates

Chromatogram of soluble sugars, free amino acids, organic acids and sugar phosphates extracted from the shoot of a 15-day old, soil grown rice seedling at time point zero. The split ratio was 30:1 (A) and 2:1 (B) to account for divergent concentrations of the different metabolites. The established protocol for metabolite extraction, derivatization and measurement by GC-MS yields good baseline separation and a high signal to noise ratio. Ribitol and methylglucoside were used as internal standard. Metabolite abbreviations can be taken from Table A9. 1.

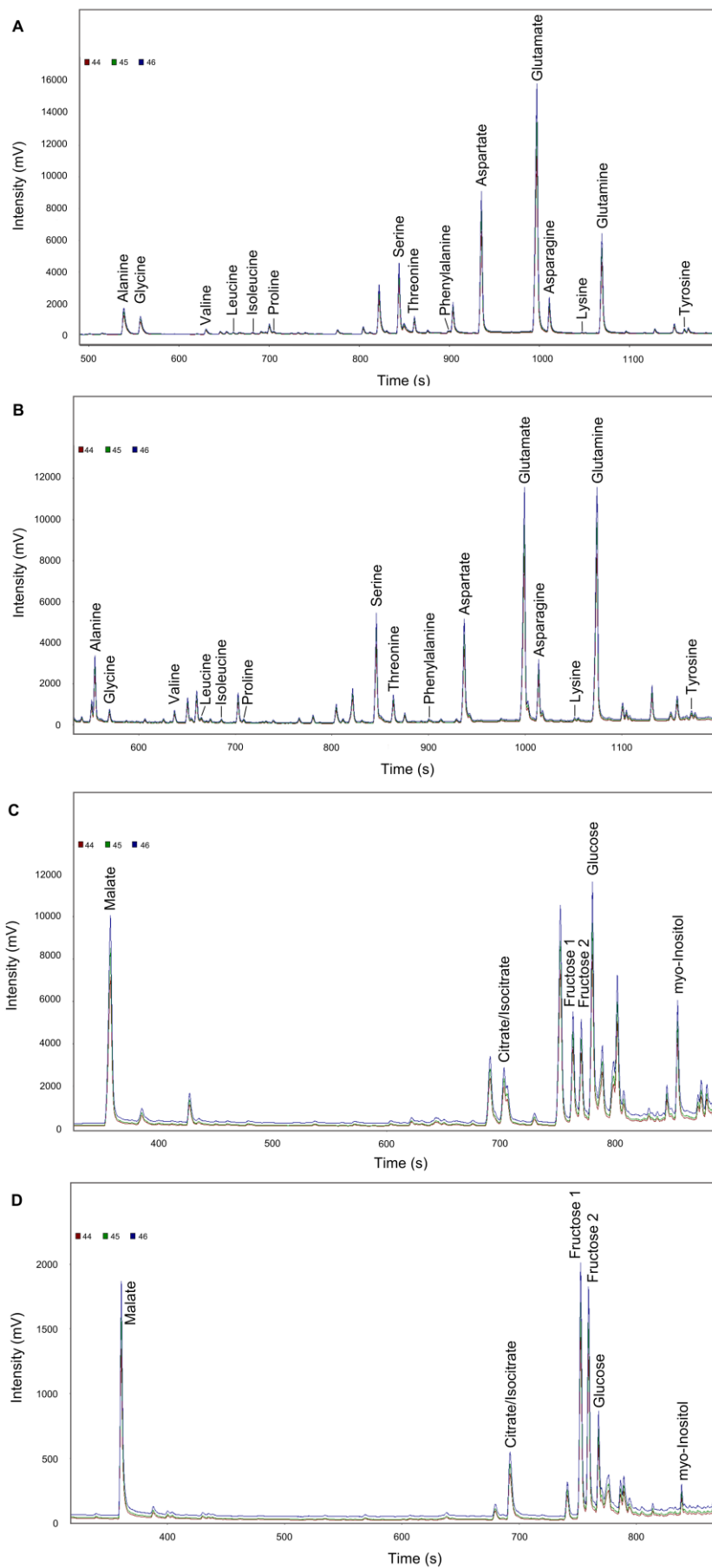
The applied GC-MS method yielded baseline separation of all target analytes, except for the organic acids citrate and isocitrate, which were measured as pool (Figure 5. 19). Citrate and isocitrate are structural isomers, meaning that they exhibit the same molecular formula, but differ in their three-dimensional orientation in space. Although structural isomers may in general have different physicochemical properties, it was not possible to chromatographically separate citrate and isocitrate. As the latter furthermore have the same fragmentation pattern, they could not be separated according to their mass to charge ratio.

Optimization of GC-C-IRMS analyses

Isotope ratio mass spectrometry yielded enrichment data (quantitative information) instead of isotopomer distributions (structural information), which is less informative, concerning the actual isotopomeric composition of the metabolite (Figure 3. 9). However, as GC-C-IRMS is highly precise, it was possible to even detect the enrichment of slowly labeled metabolites, like lysine, tyrosin, glycine, fructose and glucose. Compared to conventional GC-MS, GC-C-IRMS lacks mass selectivity, as there is only one separation step, i.e. the chromatographic separation. Chromatographic baseline separation is hence crucial for precise isotope ratio mass spectrometry. Peak overlap or peak distortion has a detrimental effect on accuracy and precision of isotope ratio analysis (Meier-Augenstein, 1999a). After chromatographic separation, the substances eluting from the column were converted into CO₂ and N₂ inside a combustion chamber before entering the ion source. The mass spectrometer in isotope ratio MS distinguished between $m/z = 44$ (¹²C¹⁶O¹⁶O), 45 (¹³C¹⁶O¹⁶O and ¹²C¹⁶O¹⁷O) and 46 (¹²C¹⁸O¹⁶O) for CO₂, as well as between $m/z = 28$ (¹⁴N¹⁴N) and 29 (¹⁴N¹⁵N) for N₂, respectively. The isotopomers were simultaneously detected by multiple Faraday cups, one for each isotopomer. The high precision of IRMS even allows to measure isotopic enrichment at natural abundance level (Meier-Augenstein, 1999a). GC-C-IRMS analyses were performed according to 4.4.2. Free amino acids and soluble sugars were measured in two runs after individual sample preparation, allowing the separation of both groups. Combined analysis does not allow for baseline separation due to the number and elution pattern of the analytes. The temperature profile for the two compound classes was adjusted to reach optimal peak separation (4.4.2.2, Figure 5. 1).

Figure 5. 20 (next page) GC-C-IRMS chromatogram of free amino acids and soluble sugars/organic acids

Chromatogram of free amino acids in shoot (A) and root (B) and soluble sugars/organic acids in shoot (C) and root (D) of a 15-day old, soil grown rice seedling at time point zero. The established protocol for metabolite extraction, derivatization and measurement by GC-C-IRMS yields good baseline separation for most metabolites, as well as a high signal to noise ratio.



Optimization of LC-MS/MS analyses

Liquid chromatography is especially suitable to separate heat labile or high molecular weight compounds, as it provides less harsh conditions than gas chromatography. Compared to GC-based techniques, analytes do not need to be derivatized prior to liquid chromatography, which simplifies sample preparation and enhances throughput. The isotopic precision of LC-MS is in the same range as for GC-MS (Godin et al., 2007). However, coupled to tandem mass spectrometry, liquid chromatography provides higher specificity, higher sensitivity and the ability to determine multiple analytes, when compared to GC-MS. LC, coupled to a triple quadrupole mass spectrometer (MS/MS) provides three analytical filters: (i) the LC unit separates the analytes according to their physicochemical properties, (ii) the first quadrupole of the MS/MS isolates ions of a specific mass to charge ratio, which are subsequently fragmented in the second quadrupole, followed by the isolation of characteristic product ions in (iii) the third quadrupole. The first mass filter, provides high selectivity by differentiating among ions formed from co-eluting analytes. The second mass filter provides enhanced specificity, as only fragment ions of the desired precursor ion are measured, even when mass interferences are selected with the precursor ion inside the first mass filter. Sensitivity, defined as limit of detection (LOD) and quantitation (LOQ), is related to specificity, as the mass-differentiation between different analytes also occurs between an analyte and chemical noise. Hence, analyte ions can be detected in the presence of a complex biological matrix (Winnik and Kitchin, 2008). In this study, LC-MS/MS analyses were performed according to Balcke et al. (2011) to measure sugar phosphates and organic acids (Figure 5. 21). For each analyte, the precursor ion, as well as the most prominent product ion were selected. Parameters, characteristic for each analyte, were optimized, particularly collision energy (CE). The collision energy is the amount of energy that precursor ions receive as they are accelerated into the collision cell, which determines the degree of fragmentation. All possible ^{13}C isotopomers of an analyte were considered by mass transitions, yielding 126 mass transitions for 18 metabolites. All mass transitions were individually checked for background noise, overlap with matrix components and cross-talk. Cross-talk may occur when several mass transitions with the same product ion are acquired. If the collision cell is not completely emptied within the short time between two transition settings, signals will appear in the following mass transition trace (Vogeser and Seger, 2010).

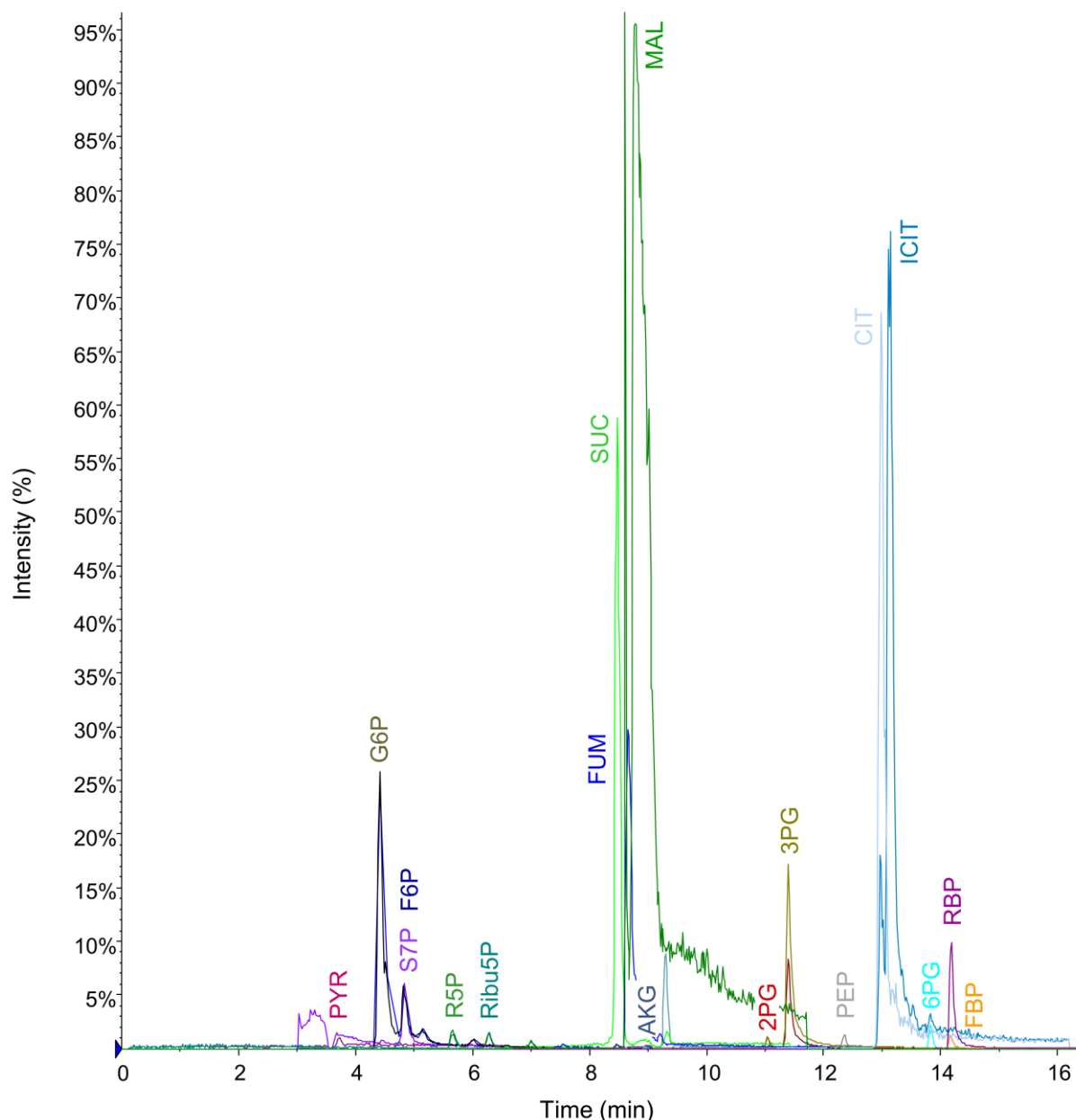


Figure 5. 21 LC-MS/MS chromatogram of sugar phosphates and organic acids

Chromatogram of sugar phosphates and organic acids of an unlabeled, 15-day old, soil grown rice seedling. LC-MS/MS analysis allows to differentiate between analytes that are not baseline separated by characteristic mass transitions, e.g. S7P and F6P, CIT and ICIT, as well as FUM, MAL and SUC. Metabolite abbreviations are listed in Table A9. 1.

As different sugar phosphates were measured by LC-MS/MS, several mass transitions exhibited the same product ion, i.e. 97 or 79, displaying $[H_2PO_4]^-$ and $[PO_3]^-$, respectively (Table A9. 14). To avoid cross-talk, the interscan delay time, or pause time, was adjusted. Additionally, to get an optimal signal to noise ratio, the dwell time was adjusted, which is the time spent to acquire a specific mass transition during each cycle.

Overall, the obtained labeling profiles showed small error bars and a good reproducibility among replicates, especially considering the high complexity of plants (Figure 5. 22). Furthermore, the data showed a good fit with simulated mass isotopomer distributions. A total of 37 metabolites was measured per sample, comprising 35 mass isotopomer distributions and 18 enrichment detections. For each sample, more than 200 individual peaks were edited, summing up to 15.000 individual spectra for one experiment with 15 sampling time points and 5 replicate repeats. Intermediates of EMP and PP pathway, as well as from photorespiration, displayed fast enrichment, whereas those of the TCA cycle, as well as soluble sugars and most amino acids exhibited slower label incorporation. Of the latter, only sucrose, alanine, serine, glycine, aspartate and phenylalanine showed noteworthy enrichment (data not shown). This is in accordance to results obtained from pulse-chase studies (5.1.3.1) and other previous examinations (Szecowka et al., 2013; Ma et al., 2014), supporting the validity of the measured data and indicating a high robustness of central carbon metabolism. The rate of isotopomer enrichment of intracellular metabolites generally depends on three factors: (i) their respective metabolic proximity to the $^{13}\text{CO}_2$ entry point, (ii) their respective pool sizes, as well as (iii) flux rates and flux directions in the network. The first stable compound of CO_2 assimilation is 3-phosphoglycerate (3PG). This compound is in metabolic equilibrium with the displayed 2-phosphoglycerate (2PG) (Figure 5. 22). Although more distant to 3PG, sedoheptulose 7-phosphate (S7P) showed faster label incorporation than 2PG (Figure 5. 22). Considering the pool sizes, one would expect S7P to have a slower enrichment rate, as its pool size was more than two times that of 2PG (Table 5. 3). This discrepancy was due to the directionality and rate of metabolic flux at the 3PG node (Figure 5. 27). The flux from 3PG towards S7P was almost four times as high as the flux from 3PG to 2PG, explaining the higher enrichment rate of S7P.

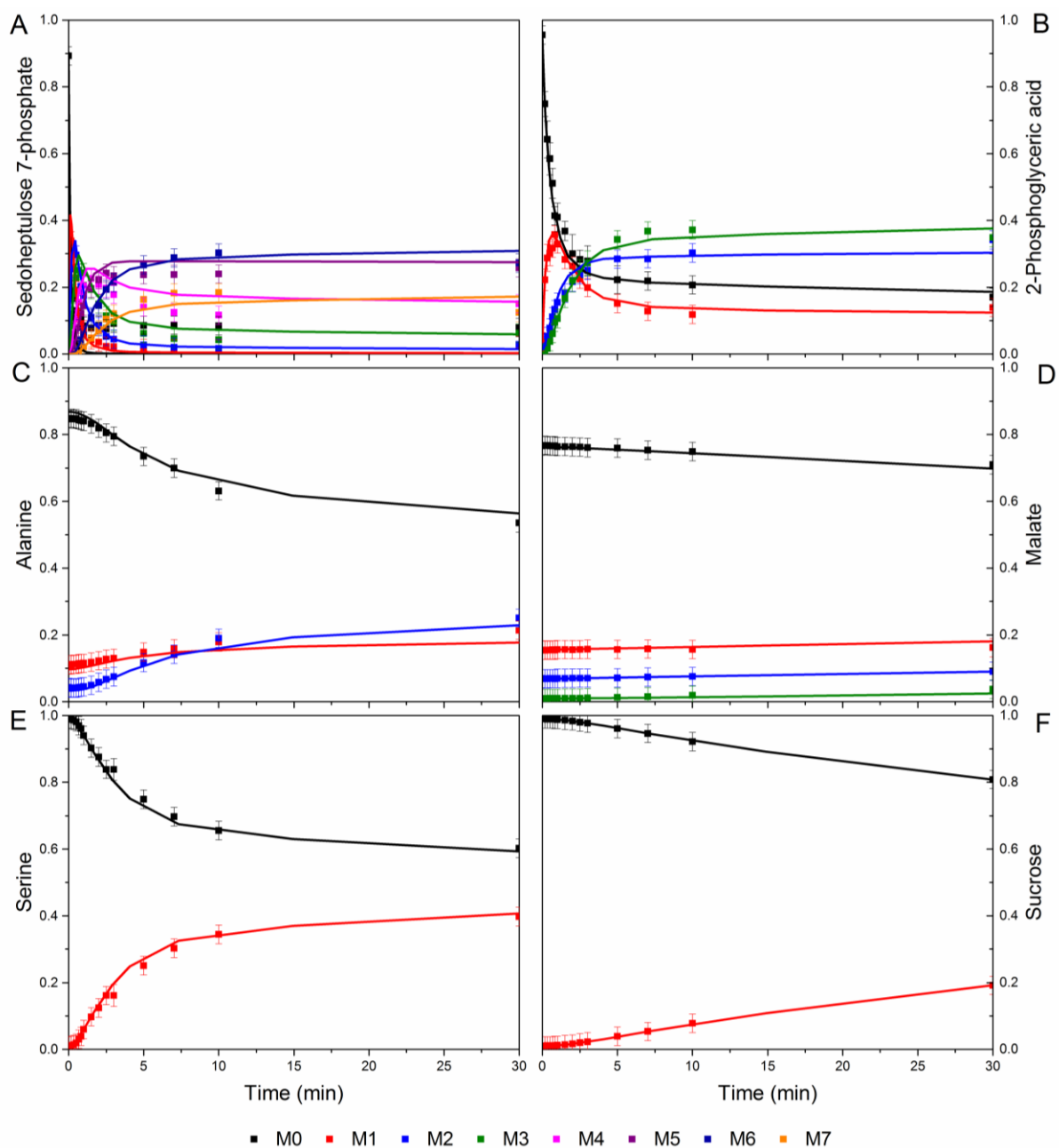


Figure 5.22 Transient ^{13}C labeling profile of selected intracellular metabolites

Experimentally measured (data points) and simulated (solid line) transient mass isotopomer distribution for metabolites determined by (A, B) LC-MS/MS (sedoheptulose 7-phosphate, 2-phosphoglycerate), (C, D) GC-MS (alanine, malate) and (E, F) GC-C-IRMS (serine, sucrose). Sedoheptulose 7-phosphate, alanine and serine show fast label incorporation, 2-phosphoglycerate, malate and sucrose are labeled more slowly. Data points show mass isotopomer data corrected for natural isotope abundance as mean values \pm SD ($n = 5$). Soil-grown rice seedlings (15 days) were labeled with $400 \mu\text{L L}^{-1} \text{ }^{13}\text{CO}_2$ for the following time periods: 0, 10, 20, 30, 40, 50, 60, 90, 120, 150, 180, 300, 420, 600 and 1800 seconds. (M0-M7 – mass isotopomers. The raw data of the measured MIDs of (A), (B), (C), (D), (E), and (F) are given in Table A9.54, Table A9.60, Table A9.52, Table A9.42, Table A9.23, Table A9.24, respectively.

5.2.2.3 Pool sizes

Pool sizes inform on the abundance of intracellular metabolites, influence labeling time-courses and allow to estimate absolute fluxes (Amaral et al., 2011; Heise et al., 2014). Hence, pool sizes represent a valuable additional model constraint, maximizing flux identifiability, although they are not necessarily required for INST-MFA. Accurate quantification of intracellular metabolites is easily compromised by metabolite losses during quenching and extraction, thereby underestimating the actual metabolite concentration (Young et al., 2011). Therefore, all measured pool sizes were incorporated into the model as lower boundary and were fitted during the flux estimation procedure. This means, that pool sizes were allowed to be equal or higher than the measured value, in order to find the optimal fit during flux estimation. Pool sizes of chemically diverse central metabolites were quantified, using GC-MS and LC-MS/MS (Table 5. 3, Figure 5. 23).

Table 5. 3 Pool sizes of intracellular metabolites

Pool sizes of soil-grown, unlabeled rice seedlings, at the age of 15 days, were determined by GC-MS and LC-MS/MS. EMP and PP pathway intermediates, as well as TCA cycle metabolites (PEP, AKG, P5P, S7P, SUCC, 2PG, FUM, E4P, RBP) exhibited small pool sizes, except for 3PG. Soluble sugars (inositol, glucose, fructose) had pool sizes between 5 to 20 $\mu\text{mol g}^{-1}$ DW. All amino acids, except for alanine, serine, glycine and threonine showed concentrations below 2 $\mu\text{mol g}^{-1}$ DW. DW – dry weight.

Pathway	Metabolite	Pool size ($\mu\text{mol g}^{-1}$ DW)	Analytics
EMP pathway	Phosphoenolpyruvate	0.92 ± 0.06	LC-MS/MS
	3-Phosphoglycerate	42.02 ± 2.88	LC-MS/MS
	2-Phosphoglycerate	1.88 ± 0.14	LC-MS/MS
PP pathway	Pentose 5-phosphate	1.80 ± 0.27	LC-MS/MS
	Sedoheptulose 7-phosphate	4.21 ± 0.16	LC-MS/MS
	Erythrose 4-phosphate	0.20 ± 0.06	LC-MS/MS
	Ribulose 1,5-bisphosphate	0.15 ± 0.03	LC-MS/MS
TCA cycle	Succinate	1.23 ± 0.06	GC-MS
	α -Ketoglutarate	1.83 ± 0.28	GC-MS
	Fumarate	0.43 ± 0.02	GC-MS
Amino acids	Alanine	10.70 ± 0.82	GC-MS
	Valine	1.11 ± 0.03	GC-MS
	Leucine	0.41 ± 0.03	GC-MS
	Isoleucine	0.31 ± 0.03	GC-MS
	Glycine	3.60 ± 0.28	GC-MS
	Proline	0.69 ± 0.03	GC-MS
	Serine	7.27 ± 0.18	GC-MS
	Threonine	3.08 ± 0.18	GC-MS
	Aspartate/Asparagine	18.43 ± 0.39	GC-MS
	Methionine	0.33 ± 0.02	GC-MS

Pathway	Metabolite	Pool size ($\mu\text{mol g}^{-1} \text{DW}$)	Analytics
	Glutamate/Glutamine	114.55 ± 7.33	GC-MS
	Phenylalanine	0.41 ± 0.00	GC-MS
	Tyrosine	0.62 ± 0.08	GC-MS
	Lysine	0.42 ± 0.07	GC-MS
Soluble sugars	Glucose	13.07 ± 2.17	GC-MS
	Fructose	19.02 ± 1.08	GC-MS
	Inositol	4.65 ± 0.27	GC-MS

Some metabolites could not be quantified with the applied mass spectrometric techniques. The EMP pathway intermediates dihydroxyacetone phosphate and glyceraldehyde 3-phosphate were not detectable in plant extracts, probably due to very low concentrations. The TCA-cycle intermediate oxaloacetate was highly unstable and degraded during sample processing and mass spectrometry (Zimmermann et al., 2014). The pool sizes of fructose 1,6-bisphosphate, fructose 6-phosphate and glucose 6-phosphate were not used for flux simulations, as there were two separate pools of these metabolites, one in the plastid and one in the cytosol/plastid. These separate pools could not be distinguished, as total pool sizes were measured. To separate such pools, compartment specific pool size quantification would be necessary. Citrate and isocitrate were not separated analytically, hence being treated as one pool as well.

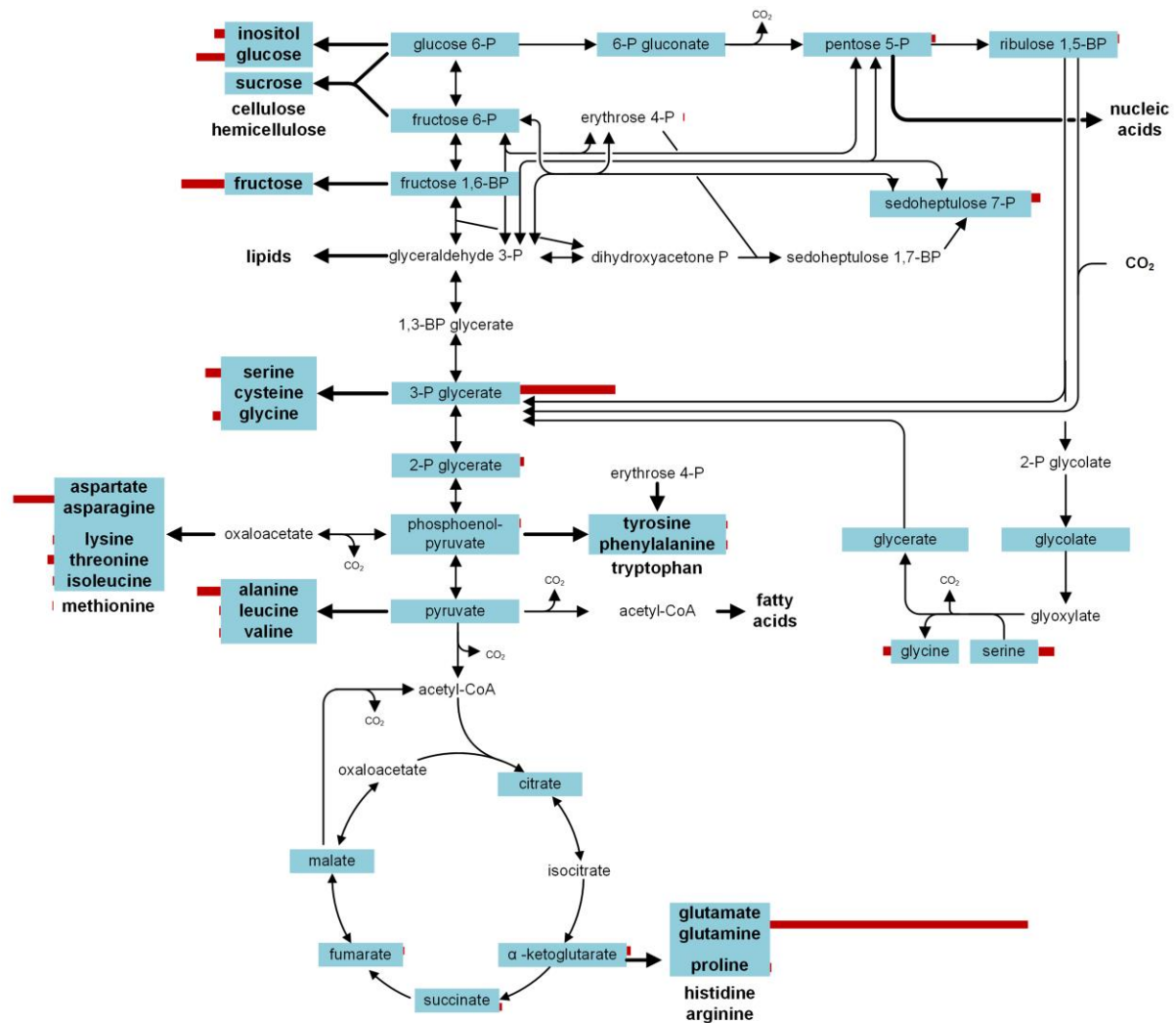


Figure 5. 23 Excellent coverage of central metabolism by measured mass isotopomer distributions and pool sizes

The mass isotopomer distribution of compounds, displayed in light blue, were measured by GC-MS, GC-IRMS and LC-MS/MS. Soil-grown rice seedlings at an age of 15 days were labeled with $400 \mu\text{L L}^{-1}$ $^{13}\text{CO}_2$ for 30 minutes. Samples were taken at the following time points: 0, 10, 20, 30, 40, 50, 60, 90, 120, 150, 180, 300, 420, 600 and 1800 seconds. Pool sizes, displayed as red bar, were determined by GC-MS and LC-MS/MS analyses from soil grown, unlabeled rice seedlings at the age of 15 days. The size of the bar represents the respective pool size. Bold arrows and metabolites represent fluxes towards biomass components.

The analytical determination of mass isotopomer distributions, as well as pool sizes yielded an excellent coverage of central metabolism (Figure 5. 23). Metabolites of PP and EMP pathway exhibited very small ($< 5 \mu\text{mol (g DW)}^{-1}$) pool sizes, except for 3-phosphoglycerate ($42 \pm 3 \mu\text{mol (g DW)}^{-1}$), which matches with its role as first stable product of carbon assimilation (Calvin, 1956). The abundance of soluble sugars was between 5 to $20 \mu\text{mol (g DW)}^{-1}$. Amongst amino acids, highest concentrations were detected for glutamate/glutamine ($115 \pm 7 \mu\text{mol (g DW)}^{-1}$) and aspartate/asparagine ($18 \pm 0.5 \mu\text{mol (g DW)}^{-1}$). In leaves these amino acids are the primary product of nitrogen assimilation. Therefore, their pools are large, especially in the light

(Lam et al., 1995). Alanine, serine, glycine and threonine, which are easily interconverted by the activity of aldolases and aminotransferases, exhibited concentrations between 3 to 10 $\mu\text{mol (g DW)}^{-1}$. Serine, glycine and alanine metabolism is associated with photorespiration (Liepman and Olsen, 2003; Häusler et al., 2014). The *de novo* biosynthesis of serine was furthermore found to be highly active in proliferating tissues, such as meristems of developing leaves (Benstein et al., 2013). All remaining amino acids, as well as the intermediates of the TCA cycle showed smaller pool sizes ($< 2 \mu\text{mol (g DW)}^{-1}$) (Table 5. 3, Figure 5. 23). The ratio of amino acid pools, detected in this study, was also found for developing *Arabidopsis* leaves (Watanabe et al., 2013; Hildebrandt et al., 2015), indicating reliability of the measured data. In general, small pool sizes were detected for central carbon metabolites, except for 3-phosphoglycerate, whereas biomass components, like sugars and amino acids, exhibited larger pools. This suggests that seedling metabolism works anabolically during the light phase, and indicates a tight regulation of central carbon metabolism with no need for large pools of specific compounds, due to fast metabolite conversions.

5.2.2.4 Cellular composition of rice seedling shoots

Biomass composition is a very important, further model constraint, as it determines the anabolic demand for metabolic precursors. The extent to which changes in biomass composition require changes in intracellular fluxes was highlighted by Schwender and Hay (2012). The cellular composition of rice was determined by quantifying protein-bound amino acids, organic acids, soluble sugars and starch by GC-MS and LC-MS/MS. Lipids were quantified as fatty acid methyl esters by GC-MS, according to 4.4.5 (Figure 5. 23).

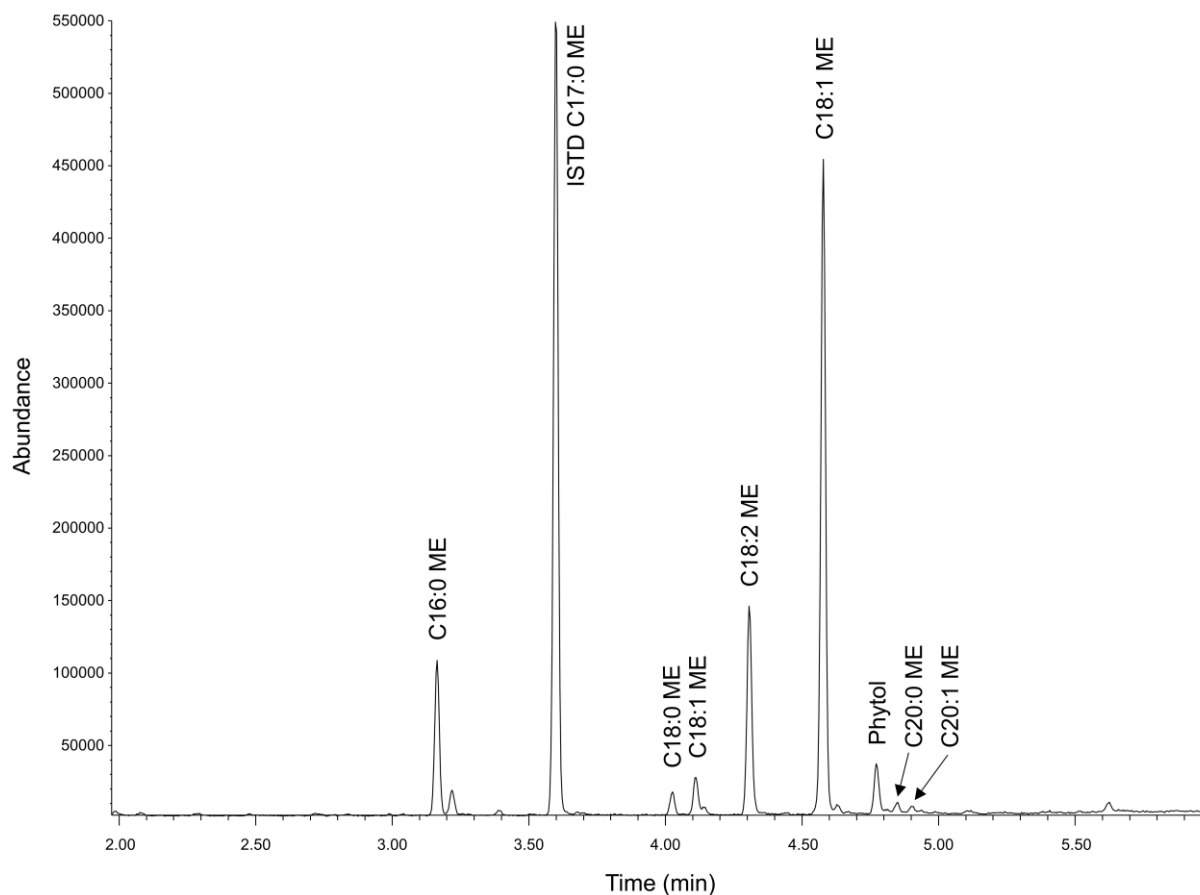


Figure 5. 24 GC-MS chromatogram of fatty acid methyl esters

Chromatogram of fatty acid methyl esters of an unlabeled, 19-day old, soil grown rice seedling. The established protocol for extraction of fat, subsequent hydrolyzation into fatty acids followed by esterification and measurement by GC-MS yields good baseline separation of fatty acid methyl esters, as well as a high signal to noise ratio. Fatty acids with C16, C18 and C20 chain length were quantified, using C17:0 as internal standard (ISTD).

Values for carbohydrate, cellulose, lignin, pigment and nucleotide content were taken from literature (Table 5. 4). The cellular composition and precursor demand of a 15-days old rice seedling is displayed in Table 5. 4.

Table 5. 4 Biomass composition of rice seedlings and corresponding precursor demand

Cellular composition of a soil grown rice seedling shoot at the age of 15 days in mg (g DW)⁻¹ and the metabolite precursor demand for the anabolic building blocks that make up the cell in mole precursor per mole building block. The cellular composition was determined by LC-MS/MS and GC-MS analyses, as well as by quantitative starch, sugar and fatty acid methyl ester measurement. Values for hemicellulose, cellulose, lignin, pigments and nucleotides were taken from literature. DW - dry weight. Metabolite abbreviations are given in Table A9. 1.

Metabolite	Amount (mg g ⁻¹ DW)	Precursor demand (mol mol ⁻¹)																	
		ACCOA.p	PYR.cp	CO2.p	PEP.cp	AKG.m	P5P.p	E4P.p	OAA.c	3PG.cp	GAP.cp	F6P.cp	G6P.cp	FUM.m	MAL.m	CIT.m	SUCC.m	Starch.p	Phenylalanine
Amino acids [A, B]																			
Alanine	19.3	1																	
Arginine	24.7		1		1														
Asparagine	30.7								1										
Aspartate	-								1										
Cysteine	2.1									1									
Glutamate	46.5					1													
Glutamine	-					1													
Glycine	17.6									1									
Histidine	7.5		1					1											
Isoleucine	13.4		1	-1					1										
Leucine	26.9	1	2	-2															
Lysine	18.5		1	-1					1										
Methionine	5.0	-1	1						1	1									
Phenylalanine	81.2			-1	2			1											
Proline	14.8					1													
Serine	15.7									1									
Threonine	15.5								1										
Tryptophan [C]	0.03	-1	-1	2		1	1			1	-1								
Tyrosine	52.4			-1	2			1											
Valine	18.1		2	-1															
Hemicellulose [D]																			
Xylose	53.6							1											
Galactose	5.6											1							
Arabinose	14.7											1							
Glucose	124.3											1							
Mannose	3.9											1							
Rhamnose	0.9												1						
Lignin [D]	42																		1
Cellulose [D]	52.5												1						
Starch [E]	6.1																		1

Metabolite	Amount (mg g ⁻¹ DW)	Precursor demand (mol mol ⁻¹)																
		ACCOA.p	PYR.cp	CO2.p	PEP.cp	AKG.m	P5P.p	E4P.p	OAA.c	3PG.cp	GAP.cp	F6P.cp	G6P.cp	FUM.m	MAL.m	CIT.m	SUCC.m	Starch.p
Soluble sugars [F]	66.7																	
Sucrose	60.4										1	1						
Glucose	2.6											1						
Fructose	3.7										1							
Pigments [G]																		
Chlorophyll	21.9		4	-9		8				4								
Carotenoids	0.7		8	-8						8								
Nucleotides																		
RNA [H]	13.3			2			2	3	1					-2				
DNA [I]	8.2			2			2	3	1					-2				
Lipids [J]	19.2																	
Fatty acids (16:0)	2.5	8																
Fatty acids (18:0)	16.3	9																
Fatty acids (20:0)	0.3	10																
Organic acids	12.8																	
Ascorbate [K]	6.0											1						
Citrate [L]	1.1														1			
Succinate [L]	0.2															1		
Pyruvate [B]	0.6	1																
α-Ketoglutarate [B]	0.3					1												
Malate [L]	4.6														1			

References: [A] C/N combustion, [B] Quantitative LC-MS/MS analysis, [C] Ishihara et al. (2008), [D] Sumiyoshi et al. (2013), [E] Quantitative starch measurement, [F] Quantitative free sugar measurement, [G] Panda and Sakar (2013), [H] Suzuki et al. (2001), [I] Murray and Thompson (1980), [J] Quantitative FAME measurement, [K] Chao et al. (2010), [L] Quantitative GC-MS analysis.

The concentration of protein-bound amino acids was between 0 to 81 mg (g DW)⁻¹, whereas the sucrose content was 60 mg (g DW)⁻¹, compared to 2.6 mg (g DW)⁻¹ and 3.7 mg (g DW)⁻¹ for glucose and fructose, respectively. The most abundant fatty acids were those with C18 chain length with an abundance of 16.3 mg (g DW)⁻¹. Amongst organic acids, ascorbic acid (6.0 mg (g DW)⁻¹), malic acid (4.6 mg (g DW)⁻¹) and citric acid (1.1 mg (g DW)⁻¹) showed the highest concentrations. The remaining organic acids exhibited a concentration of < 1 mg (g DW)⁻¹. The sum of all measured and literature data for biomass components produces an organic carbon content of 85.6% for the rice seedling. The remaining 14.4% were attributed to inorganic compounds, called ash (mineral) content. This is in excellent agreement

with literature values of 13 to 15% for the ash content (Misra et al., 2006), indicating the reliability of the determined biomass composition. The anabolic precursor demand and the determined cellular composition of the rice seedling (Table 5. 4) were used to calculate the carbon requirement for synthesis of one gram biomass (Table 5. 5).

Table 5. 5 Precursor requirements of fifteen-day old, untreated rice seedlings

Anabolic demand of the twelve major biomass precursors in mmol (g DW)⁻¹, as calculated from measured metabolite concentrations and macromolecular compositions (Table 5. 4). The cellular composition of a soil grown rice seedling shoot at the age of 15 days was determined by LC-MS/MS and GC-MS analyses, as well as by quantitative starch, sugar and fatty acid methyl ester measurement. Values for hemicellulose, cellulose, lignin, pigments and nucleotides were taken from literature. DW - dry weight. Metabolite abbreviations are given in Table A9. 1.

Precursor	ACCOA	PYR	PEP	AKG	P5P	E4P	OAA	3PG	GAP	F6P	G6P	SUCCOA
Anabolic demand												
mmol (g DW)⁻¹	0.81	1.28	2.12	0.78	0.49	1.06	0.75	0.44	0.11	0.22	1.29	0.04
C mmol (g DW)⁻¹	1.62	3.83	6.36	3.92	2.46	4.24	3.00	1.33	0.32	1.31	7.73	0.16

As indicated by the data, carbon is primarily channeled to anabolism via glucose 6-phosphate, phosphoenolpyruvate and erythrose 4-phosphate. Additional information, regarding the integration of the experimentally determined biomass composition into the metabolic model is available from (Beckers, 2015).

5.2.2.5 Biomass formation rate

The rate of biomass formation is a quantitative measure of the carbon flow towards anabolism. As external parameter it is routinely included in metabolic flux analysis to constrain the flux solution space. To determine the biomass formation rate, carbon assimilated over a distinct time period, as measured by EA-IRMS, was integrated with the gravimetrically determined increase in plant dry weight (Figure 5. 25). The growth rate was determined by plotting the logarithm of measured dry weights against the harvest time in hours. The slope of the resulting regression represents the specific growth rate of the rice seedlings.

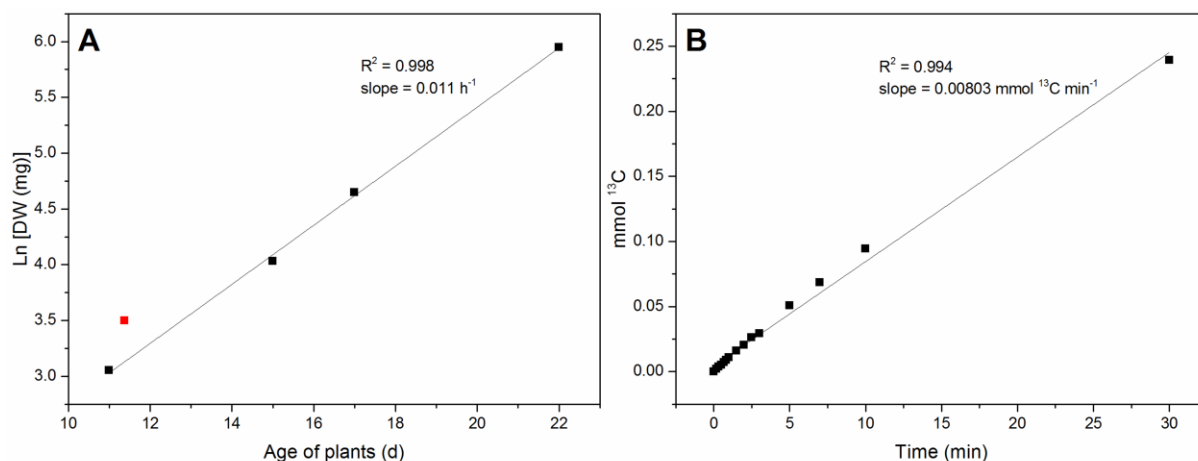


Figure 5.25 Growth rate and CO₂ uptake rate for a rice seedling shoot

(A) The growth rate of a soil grown rice seedling shoot was determined over an 11 day period at a plant age of 11 to 22 days. Two to six shoots were harvested and pooled, depending on the plant size. The plant material was freeze-dried and dry weight per seedling was plotted against the age of the plants, yielding a linear correlation over time and a specific growth rate of 0.011 h^{-1} . A day-time growth rate of 0.026 h^{-1} was calculated using the dry weight increase over nine hours in the light period (red data point). Therefore, 15 individual plant shoots were harvested at 7 am and 4 pm, respectively. (B) Increase of ^{13}C incorporation into seedling shoot biomass revealed a linear regression over time, delivering a CO₂ uptake rate of $0.00803 \text{ mmol (g DW)}^{-1} \text{ min}^{-1}$.

A day-time growth rate of 0.026 h^{-1} was determined by weighing 15 individual rice shoots at 7 am and 4 pm, respectively. In order to assess, whether rice seedlings grow exponentially at the age of 15 days, the growth rate was additionally determined during a longer time period (age 11 to 22 days), including day-night cycles. For the latter, four, six, four and two rice shoots were harvested and pooled at a plant age of 11, 15, 17 and 22 days, respectively. Plants were harvested at 1 pm, i.e. in the middle of the light phase. The natural logarithm of these values plotted against time, resulted in a linear correlation, indicating that plants are growing exponentially, with a growth rate of 0.011 h^{-1} (Figure 5.25). The comparison of the daytime growth rate with the growth rate of the complete 13/11 day-night cycle showed that there was no growth of the seedlings during the dark phase.

The CO₂ uptake rate was determined by EA-IRMS enrichment measurements upon $^{13}\text{CO}_2$ labeling. Soil-grown rice seedlings at the age of 15 days were supplied with an amount of $400 \mu\text{L L}^{-1} \text{ } ^{13}\text{CO}_2$ for 30 minutes and samples were taken at the following time points: 0, 10, 20, 30, 40, 50, 60, 90, 120, 150, 180, 300, 420, 600, 1800 seconds. The ^{13}C enrichment in the rice shoot increased linearly, yielding a CO₂ uptake rate of $0.00803 \text{ mmol CO}_2 \text{ (g DW)}^{-1} \text{ min}^{-1}$ (Figure 5.25 B). The determined growth rate (Figure 5.25 A) was subsequently divided by the CO₂ uptake rate (Figure 5.25 B), giving a biomass yield of $6.59 \text{ g DW (100 mmol CO}_2\text{)}^{-1}$, corresponding to a carbon yield of $2.68 \text{ g C}_{\text{DW}} \text{ (100 C-mmol CO}_2\text{)}^{-1}$, when integrated with the determined carbon percentage of 40.8% (w/w) for dried plant material.

5.2.2.6 Extracellular fluxes

Carbon export flux from the studied seedlings into their roots was assessed by measurement of isotopomer distributions and pool sizes of amino acids and soluble sugars in the root. Soil grown rice seedlings at the age of 15 days were labeled with $400 \mu\text{L L}^{-1} \text{}^{13}\text{CO}_2$ for 30 minutes. Roots were harvested at the following time points: 300 and 1800 seconds. The isotopic enrichment of intracellular metabolites was measured by GC-C-IRMS analyses. The concentrations of amino acids and sucrose was quantified by GC-MS. The enrichment of the respective metabolites and their concentration in the root were used to calculate the amount of carbon exported from the shoot to the root in $\text{mmol } ^{13}\text{C (g DW}_{\text{root}}) \text{ h}^{-1}$ (4.5.7).

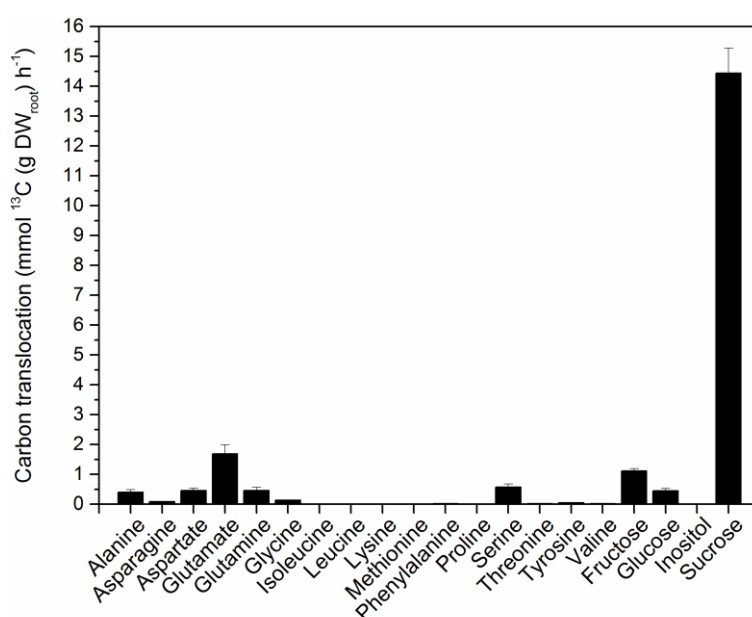


Figure 5. 26 Amount of carbon translocating to the root in form of displayed metabolites

Amount of assimilated carbon that is recovered inside root amino acids and soluble sugars, in $\text{mmol } ^{13}\text{C (g DW}_{\text{root}})^{-1} \text{ h}^{-1}$, as determined by 4.5.7. Soil-grown rice seedlings at the age of 15 days were labeled with $400 \mu\text{L L}^{-1} \text{}^{13}\text{CO}_2$ for 30 minutes. Root samples were taken at the following time points: 300 and 1800 seconds. Isotopic enrichment was determined by GC-IRMS analyses, concentrations were measured by GC-MS. Mean values \pm SD ($n = 4$) are shown.

It became evident that only sucrose was exported to a noteworthy amount ($6 \text{ mmol } ^{13}\text{C (g DW}_{\text{root}}) \text{ h}^{-1}$), indicating a major role of this sugar to provide roots with assimilate (Figure 5. 26, Table A9. 66). Hence, only concentration and mass isotopomer distribution of sucrose (Table A9. 16) were included in the simulation procedure to calculate the export flux from shoot to root.

5.2.3 Anabolic nature of rice seedling metabolism displays high demand for building blocks, supporting growth and development

After the construction and validation of the flux reactor, the development of a diverse set of analytical techniques, assessment of data quality and the optimization of the metabolic model, flux simulations were performed to generate the first metabolic flux map of an agriculturally relevant crop. Central metabolism was widely covered by detecting a broad range of chemically diverse metabolites by several MS techniques (Figure 5. 23). As much as 50 transient isotopomer profiles (Table A9. 16 to Table A9. 65) were obtained and integrated into the network model (Beckers, 2015), comprising metabolite pool sizes (Table 5. 3), the biomass yield (Figure 5. 25), the cellular composition (Table 5. 4), the $^{13}\text{CO}_2$ uptake rate (Figure 5. 25 B) and exact tracer composition (Figure 5. 15 A), as well as the carbon export flux to the root (Figure 5. 26), determined from ^{13}C enrichments and concentrations of exported compounds. All fluxes were normalized to 100 mmol CO_2 uptake and are therefore expressed as mol% of the uptake flux. To minimize the lack-of-fit between experimental and simulated data, free flux and pool size parameters of the network model were iteratively adjusted using a Levenberg-Marquardt algorithm until optimal agreement with experimental data was achieved (Figure 5. 22). The optimal values, received after 50 iterative simulations, were taken as actual flux distribution. Statistical analyses by parameter continuation with a confidence interval of 95% revealed narrow confidence intervals for all fluxes, except for those around pyruvate (Beckers, 2015). This agrees with a high confidence in the obtained fluxes and yielded a comprehensive flux map for the illuminated shoot of a rice seedling (Figure 5. 27). For additional information about the robustness of the model and the influence of individual data sets on the identifiability of fluxes, the reader is kindly referred to (Beckers, 2015).

5.2.3.1 High activity of chloroplast metabolism

Fluxes through CBB cycle and non-oxidative PP pathway were high with flux rates of 182.2 ± 0.3 mol% for glyceraldehyde 3-phosphate dehydrogenase, 69.0 ± 0.2 mol% for sedoheptulose 1,7-bisphosphatase and 35.9 ± 0.1 mol% for transketolase (Figure 5. 27). These high fluxes are explained by the fact that CO_2 , the only carbon source of the examined rice seedlings, is assimilated by the combined activity of the CBB cycle and the non-oxidative PP pathway. Ru-BisCO converted CO_2 and ribulose 1,5-bisphosphate into glyceraldehyde 3-phosphate, the first stable product of CO_2 assimilation (100 ± 0 mol%). High fluxes through the non-oxidative part of the PP pathway enabled efficient regeneration of the photosynthetic carbon acceptor ribulose 1,5-bisphosphate through these reaction steps. As the acceptor is essential to sustain photosynthetic activity, the high fluxes through the non-oxidative pentose phosphate pathway were obviously crucial for fueling photosynthesis.

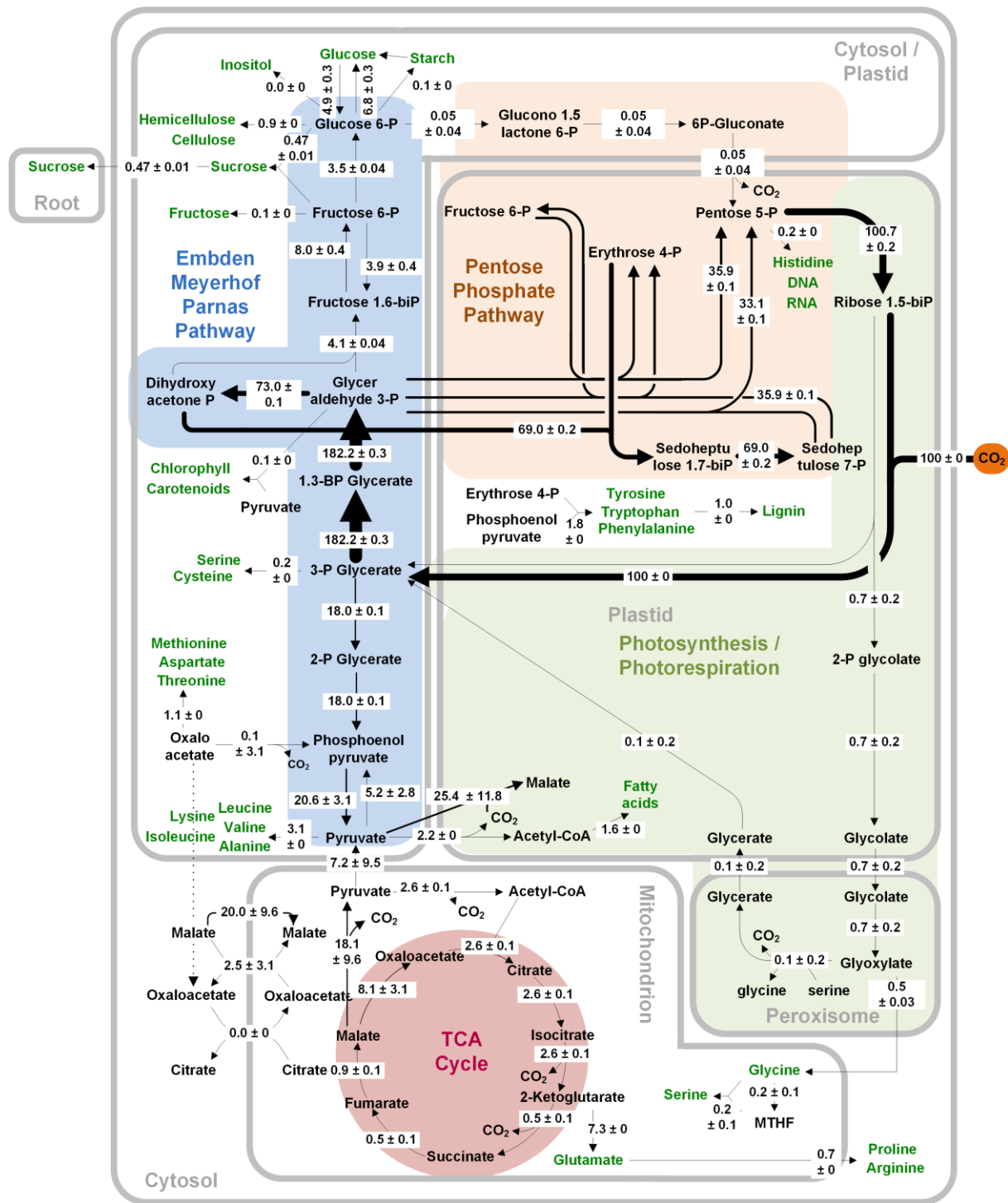


Figure 5. 27 (next page) Metabolic network analysis of a rice shoot at the seedling stage

In vivo carbon flux distribution in the central metabolism of a fifteen-day old, soil grown, illuminated rice seedling, supplied with 400 $\mu\text{L L}^{-1}$ CO₂. Metabolic fluxes are displayed as percentage of substrate uptake as they are normalized to 100 mmol h⁻¹ ¹³CO₂ assimilation. Flux rates with standard errors are given in boxes and are reflected by arrow thickness. Arrows furthermore give the direction of the net flux. Metabolites presented in green represent building blocks for anabolism. Standard errors are derived from the estimated 95% confidence interval as determined by parameter continuation. Flux values are given in Table A9. 67. Figure taken from Beckers (2015).

5.2.3.2 Gluconeogenic nature of EMP pathway

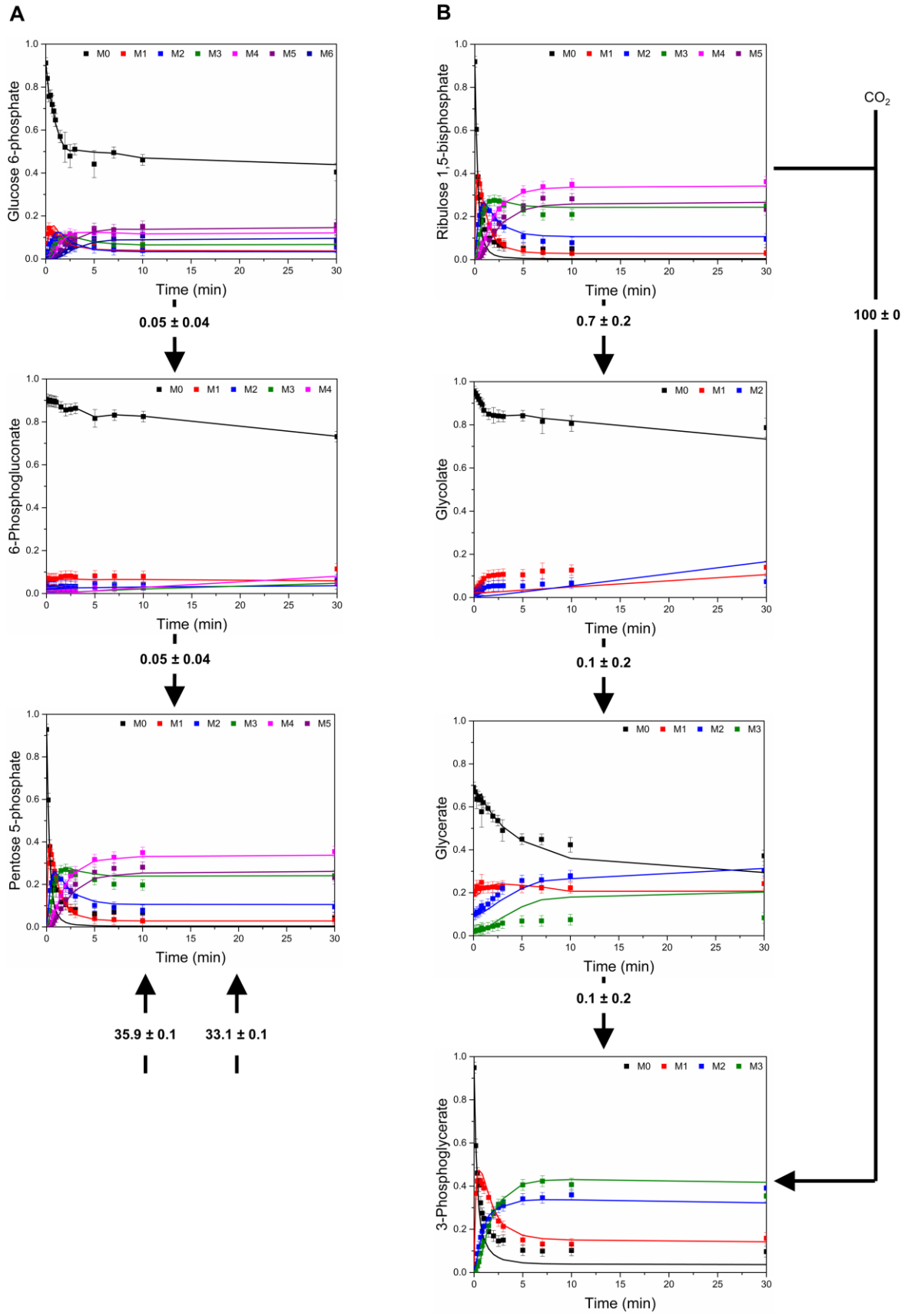
Emanating from 3PG, a flux of 182.2 ± 0.3 mol% for glyceraldehyde 3-phosphate dehydrogenase and of 18 ± 0.1 mol% for phosphopyruvate hydratase was obtained, highlighting a largely gluconeogenic nature of the EMP pathway (Figure 5. 27). Fluxes further upstream of glyceraldehyde 3-phosphate, i.e. 4.1 ± 0.04 mol% for aldolase and fructose-bisphosphatase and 3.5 ± 0.04 mol% for phosphoglucose isomerase support starch and cell wall biosynthesis, as well as sucrose export to the root. The 9:1 ratio of carbon partitioning at the 3PG node underlines a strong anabolic nature of this part of metabolism in the illuminated rice seedling.

5.2.3.3 Low activity of oxidative PP pathway and photorespiration

The oxidative part of the PP pathway exhibited very low flux values (0.05 ± 0.04 mol%). This could reflect efficient inactivation of this pathway in the light to avoid futile interaction with the CBB cycle (Anderson and Duggan, 1976; Hutchings et al., 2005). Flux through reactions of photorespiration was also low (0.1 ± 0.2 mol% to 0.7 ± 0.2 mol%), indicating that the plant was well provided with light and carbon dioxide. That both pathways occurred, albeit at a low activity, was evident from unambiguous incorporation of label into intermediates of the respective pathways (Figure 5. 28). The metabolite 6-phosphogluconate, an intermediate of the oxidative PP pathway, exhibited slow but detectable label incorporation (Figure 5. 28 A, Table A9. 56). Concerning photorespiration, glycolate showed slow enrichment, whereas glycerate was enriched faster (Figure 5. 28 B, Table A9. 64, Table A9. 45). Photorespiration is an essential feature of plant metabolism in the light, as it dissipates excess energy and protects against photoinhibition (Takahashi et al., 2007). It also interacts with secondary pathways, like nitrogen assimilation, respiration and redox signaling (Padmasree et al., 2002; Bauwe et al., 2010). Therefore, even a low activity of photorespiration may be crucial for optimal plant metabolism.

Figure 5. 28 (next page) Label incorporation into intermediates of oxidative pentose phosphate pathway and photorespiration

Experimentally measured (data points) and simulated (solid line) transient mass isotopomer distribution for metabolites of the oxidative pentose phosphate pathway (A) and of photorespiration (B). Flux through the oxidative part of the pentose phosphate pathway (0.05 ± 0.04 mol%) and flux through reactions of photosynthesis (0.1 ± 0.2 to 0.7 ± 0.2 mol%) was very low. Correspondingly, label incorporation into 6-phosphogluconate was slow compared to glucose 6-phosphate and pentose 5-phosphate. Accordingly, label incorporation into glycolate and glycerate was slow compared to ribulose 1,5-bisphosphate and 3-phosphoglycerate. Data points show mass isotopomer data corrected for natural isotope abundance as mean values \pm SD ($n = 5$). Soil-grown rice seedlings (15 days) were labeled with $400 \mu\text{L L}^{-1} \text{ }^{13}\text{CO}_2$ for the following time periods: 0, 10, 20, 30, 40, 50, 60, 90, 120, 150, 180, 300, 420, 600 and 1800 seconds. (M0-M7 – mass isotopomers. The raw data of the measured MIDs of G6P, 6PG, P5P, 3PG, RBP, glycolate and glycerate are given in Table A9. 49, Table A9. 56, Table A9. 59, Table A9. 55, Table A9. 58, Table A9. 64 and Table A9. 45, respectively.



5.2.3.4 Non-cyclic form of TCA cycle supports anabolism

The TCA cycle exhibited low fluxes, especially through enzymes catalyzing the reactions between α -ketoglutarate and malate (Figure 5. 27). This was due to the need for α -ketoglutarate for the formation of glutamate and related amino acids, resulting in a high flux of 7 ± 0 mol% through glutamate dehydrogenase, which practically depleted the cycle. The largely non-cyclic TCA cycle flux resembled the anabolic function of the TCA cycle in the examined metabolic state of the rice plant, similar as for the upper part of the EMP pathway. This anabolic function is achieved by a partly inhibited pyruvate dehydrogenase in the light (Tcherkez et al., 2005). Indeed, flux through this enzyme was low (2.6 ± 0.1). The non-cyclic operation of the TCA cycle highlighted the relevance of carboxylic acid metabolism for anaplerosis in illuminated leaves (Sweetlove et al., 2010). It furthermore provided metabolic flexibility as it minimizes the dependence of the TCA cycle on glycolytic activity (Tronconi et al., 2015).

5.2.3.5 Root carbon supply

As shown above, sucrose is the main substrate for carbon export to the root, other substrates being exported in negligible amounts (Figure 5. 26). Sucrose was exported with a flux of 0.47 ± 0.01 mol%, according to a carbon percentage of 6 C% (Figure 5. 27). Pulse-chase studies revealed a carbon export value of 7 ± 1 C% (Figure 5. 5), which was in great agreement with the data obtained here, despite the fact that the analytical procedures to obtain the data greatly differed in both studies. This excellent agreement enhanced the confidence in the measured values and the associated analytical methods, and further supported the finding that sucrose is the main carbon transport molecule to supply the root.

5.2.3.6 Anabolic demand drives metabolism

The above discussed gluconeogenic nature of the EMP pathway, as well as the non-cyclic form of the TCA cycle revealed a mainly anabolic function of metabolism in the illuminated rice seedling. This is in consistency with the detected exponential growth (Figure 5. 25). As only 0.19 ± 0.11 mol% of the assimilated carbon was respired (Beckers, 2015) and other forms of carbon loss are assumed to be negligible, it can be concluded that the assimilated carbon was almost entirely used for plant metabolic functions. High anabolic fluxes were observed for the biosynthesis of glutamate from α -ketoglutarate (7.3 ± 0 mol%) and for the generation of aromatic amino acids from erythrose 4-phosphate (1.8 ± 0 mol%) as well as their subsequent conversion to lignin (1.0 ± 0 mol%) (Figure 5. 27). Anabolic flux from pyruvate and oxaloacetate towards biosynthesis of amino acids was 3.1 ± 0 mol% and 1.1 ± 0 mol%, respectively. Flux from glucose 6-phosphate towards cellulose and hemicellulose was 0.9 ± 0 mol%. Hence, anabolic fluxes mainly supplied the plant with protein and cell wall components, reflected by

high demands for pyruvate (9.6 C%), glucose 6-phosphate (8.8 C%) and erythrose 4-phosphate (7.2 C%). Cell walls determine plant architecture and play a major role during cell growth and differentiation (Geisler et al., 2008). As the growth rate of seedlings was high, considerable amounts of building blocks for cell wall biosynthesis, as well as for cellular membranes are probably needed (Allen et al., 2007; Schädel et al., 2010; Sumiyoshi et al., 2013). The latter was further represented by a flux of 1.6 ± 0 mol% from acetyl-CoA into fatty acids, the precursors of lipid bilayers. Flux towards starch (0.1 ± 0 mol%) and sucrose (0.47 ± 0.01 mol%) was low. This seemed due to the developmental stage of the examined rice plants. Rice builds large starch and root sucrose storage pools only about two weeks before heading (Yoshida, 1981). As rice plants were examined in the seedling stage, assimilated carbon was obviously directly used for anabolic growth by building cell wall constituents and maintaining nitrogen supply through the non-cyclic form of the TCA cycle.

Anabolic demand as major driver of metabolism, revealed here for an illuminated rice seedling, is fascinating, as heterotrophic plant metabolism is controlled by catabolic reactions to fuel synthesis of storage compounds like oil, starch and protein (Schwender et al., 2003).

5.2.3.7 Malate/pyruvate shuttling sustains the anabolic function of the TCA cycle and balances redox power

Due to the subcellular compartmentation of plant metabolism, intercompartmental transport is necessary to exchange metabolites and redox power between compartments. As cellular membranes are impermeable for direct transfer of ATP and NAD(P)H (Rasmusson et al., 2004), transport occurs indirectly through metabolite shuttles, corresponding to the needs of the cell. In addition to the known MAL/OAA shuttle in the inner mitochondrial membrane (Hoefnagel et al., 1998), the observed fluxes revealed the shuttling of malate and pyruvate between mitochondrion and cytosol/plastid (Figure 5. 27). The latter could be an additional, yet unknown mechanism for the translocation of redox power. Flux analysis revealed that pyruvate, formed as end product of glycolysis, was not directly transported into the mitochondrion, but was rather converted to malate by the activity of plastidic NADP-malic enzyme (Wheeler et al., 2005). The enzyme consumes NADPH and regenerates NADP^+ , the electron acceptor of photosynthetic electron transport, thereby supporting photosynthetic activity and avoiding overreduction (Padmasree et al., 2002). From here, malate was translocated into the mitochondrion by the action of the MAL/OAA shuttle, with a malate net influx of 20 ± 9.6 mol%. The mitochondrial NAD-dependent malic enzyme (Artus and Edwards, 1985) converted malate back into pyruvate, thereby fueling the TCA cycle. This represents an indirect pyruvate transport from chloroplast to mitochondrion with malate as intermediate. The proposed MAL/PYR shuttle channeled reducing power from the cytosol/plastid to the mitochondrion,

which is in accordance to the observed anabolic function of the TCA cycle. So far, a MAL/PYR shuttle, as proposed here, has not been described for plant tissues. However, shuttling of pyruvate and malate between cytosol and mitochondrion has been proposed to occur in pancreatic islets (MacDonald, 1995). The mechanism described by MacDonald is opposed to the one suggested by our data in that pyruvate is imported into the mitochondrion and malate is exported. Accordingly, the generation of redox equivalents in the involved compartments is opposed. Nevertheless, both mechanisms of malate/pyruvate shuttling are used to provide sub-cellular compartments with the required redox power, involving the mitochondrion and malic enzymes. The proposed MAL/PYR shuttle in rice tissue may represent an additional, yet unknown way to balance redox power over several intracellular compartments.

5.2.3.8 Illuminated rice seedlings perform futile cycling to dissipate excess energy from photosynthesis

Three futile cycles were detected in the examined rice seedlings: glucose to glucose 6-phosphate and fructose 6-phosphate to fructose 1,6-bisphosphate cycling, as well as interconversion of phosphoenolpyruvate and pyruvate (Figure 5. 27). In direction of G6P, FBP and PEP the reactions consumed one mole of ATP each. As the metabolites were interconverted, there was no depletion of the cycle, i.e. no net carbon flux, which makes futile cycling especially suitable to dissipate excess energy. Futile cycles are therefore supposed to have a regulatory role in central carbon metabolism, not only to maintain a physiological ATP/NAD(P)H ratio, but also for the fast readjustment of intermediary metabolite levels (Geigenberger and Stitt, 1991; Geigenberger et al., 1997), thereby providing stability to central metabolism (Geigenberger et al., 1997; Rontein et al., 2002). The latter was shown for tomato cells, which exhibited similar flux rates in central carbon metabolism throughout the growth cycle (Rontein et al., 2002). Futile cycling was furthermore described to be important for the homeostasis of carbon and nitrogen metabolism in potato roots (Claeyssen et al., 2013) and was supposed to be an important feature for the optimal operation of central metabolism under stress conditions (Alonso et al., 2005; Alonso et al., 2007b). Evidence for the latter came from the examination of maize root tips. Despite reduced ATP generation under hypoxic conditions, the percentage of ATP consumed by futile cycling was similar under hypoxic and normoxic conditions (Alonso et al., 2007b). Hence, the high cost in ATP of substrate cycles may be important for ideal functioning of plant metabolism (Alonso et al., 2005).

5.2.4 Imazapyr-destructive effect due to altered carbon/nitrogen metabolism with a supposed regulatory role of intracellular pyruvate

To further validate the established INST-MFA approach and to show its feasibility for comprehensive mode-of-action studies, herbicide treatment was performed as proof of concept. Imazapyr was chosen as a widely used herbicide, with well described mechanism of action inhibiting acetolactate synthase (ALS) in branched chain amino acid biosynthesis, as shown by pulse-chase studies (5.1.3.3). These findings should be extended to a more comprehensive, network wide understanding of imazapyr effects by performing INST-MFA. The studies were conducted, using 15-day old, soil-grown rice plants, which were exposed to imazapyr treatment or a control treatment. Four hours after treatment, plants were labeled with $400 \mu\text{L L}^{-1} \text{ }^{13}\text{CO}_2$ for 30 minutes. In total, 150 rice seedlings were labeled in 10 individual experiments, 5 replicate experiments for the imazapyr treatment and the control treatment each (Table A9. 15). The data coverage was equal to that for untreated rice seedlings (5.2.2): 50 transient isotope profiles (Table A9. 16 to Table A9. 65) were obtained and integrated into the network model (Beckers, 2015), including metabolite pool sizes (Table 5. 6), the biomass yield (Figure 5. 25), the cellular composition (Table 5. 7), the $^{13}\text{CO}_2$ uptake rate (Figure 5. 25 B) and exact tracer composition (Table A9. 15), as well as the carbon export flux to the root (Figure 5. 26). To minimize the lack-of-fit between experimental and simulated data, free flux and pool size parameters of the network model were iteratively adjusted using a Levenberg-Marquardt algorithm until optimal agreement with experimental data was achieved. The best fit values, received after 50 iterative adjustments, were taken as actual flux distribution for imazapyr-treated rice seedlings and their respective reference. Parameter continuation with a confidence interval of 95%, revealed narrow confidence intervals for all fluxes, similar to those of the untreated plants (Beckers, 2015). This agrees with a high confidence in the obtained fluxes and yielded a comprehensive flux map with full coverage of the *in vivo*, network wide effect of imazapyr treatment of a rice seedling (Figure 5. 29). The effect of the herbicide imazapyr in reference to the control treatment, revealed significant flux changes as evaluated by a Student's t-test.

5.2.4.1 Fast response: increased protein turnover regenerates branched-chain amino acids

As a result of imazapyr treatment, carbon and nitrogen metabolism changed. This was dramatically represented by the accumulation of storage carbohydrates and increased protein turnover rates (Figure 5. 29).

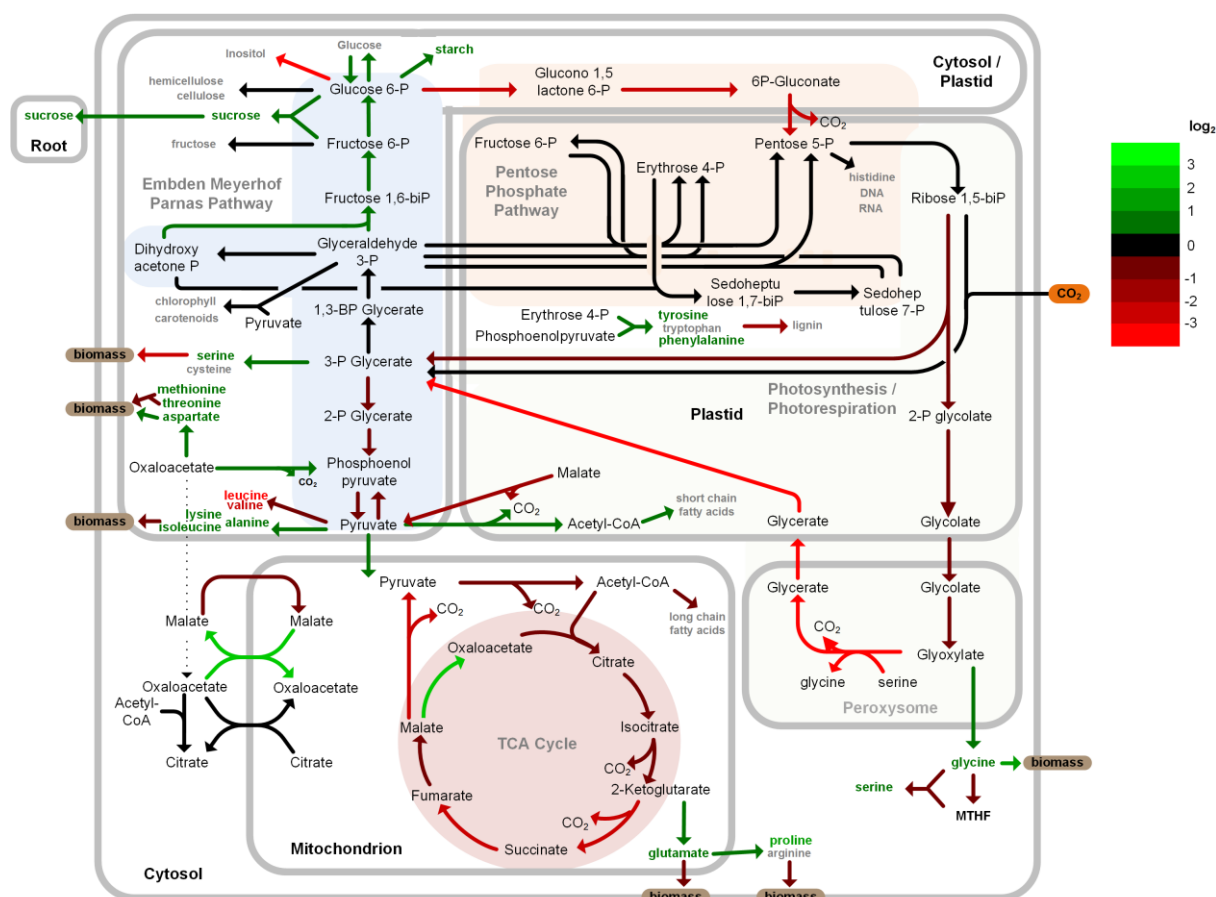


Figure 5.29 Flux map of rice shoot metabolism at seedling stage after imazapyr treatment

In vivo carbon flux distribution in the central metabolism of a fifteen-day old, soil grown, illuminated rice seedling, supplied with $400 \mu\text{L L}^{-1} \text{CO}_2$ after imazapyr treatment. Displayed are the differences in the metabolic flux distribution of an imazapyr-treated rice seedling compared to a control plant, used as reference. Arrows displayed in green and red illustrate an increase or decrease in flux after imazapyr treatment, respectively. Arrows furthermore give the direction of the net flux. Metabolites presented in green (increased intracellular pool size) and red (decreased intracellular pool size) represent building blocks for anabolism. Differences in fluxes were considered significant based on a standard Student's t-test ($P = 0.05$). Flux values are given in Table A9. 68. Figure taken from Beckers (2015).

Considering free amino acids, the metabolic flux into valine and leucine was decreased, perfectly matching the inhibition of AHAS, the enzyme that catalyzes the first step in their biosynthetic pathway (Shaner and Reider, 1986). Also the pool size of both amino acids was considerably smaller (2.7 fold for valine, < LOD for leucine) (Table 5. 6). This reports on the known mode-of-action of the herbicide that was described above by pulse-chase studies (5.1.3.3). Surprisingly, the isoleucine pool size, was slightly increased (1.2 fold), although AHAS is an essential enzyme in the isoleucine biosynthetic pathway as well. The pool sizes of all other amino acids increased or remained constant (Table 5. 6). Strongest increases in pool size were detected for proline (3.3 fold), alanine (1.9 fold), phenylalanine (1.7 fold), glutamate/glutamine (1.7 fold), threonine (1.6 fold) and aspartate/asparagine (1.4 fold).

Table 5. 6 Pool sizes of intracellular metabolites of DMSO- and imazapyr-treated rice seedlings

Pool sizes were determined by GC-MS and LC-MS/MS. EMP and PP pathway intermediates, as well as TCA cycle metabolites (PEP, AKG, P5P, S7P, SUCC, 2PG, FUM, E4P, RBP) exhibited small pool sizes, except for 3PG. Soluble sugars (inositol, glucose, fructose) had pool sizes between 5 to 20 $\mu\text{mol (g DW)}^{-1}$. All amino acids, except for alanine, serine, glycine and threonine showed concentrations below 2 $\mu\text{mol (g DW)}^{-1}$. DW – dry weight. DMSO – control plants treated with a mixture of 0.1% DMSO and 0.1% Dash. LOD – limit of detection.

Pathway	Metabolite	Pool size ($\mu\text{mol g}^{-1}$ DW)		Analytics
		DMSO	Imazapyr	
EMP pathway	Phosphoenolpyruvate	1.06 \pm 0.17	0.93 \pm 0.09	LC-MS/MS
	3-Phosphoglycerate	36.58 \pm 2.31	35.17 \pm 5.71	LC-MS/MS
	2-Phosphoglycerate	1.56 \pm 0.29	1.62 \pm 0.09	LC-MS/MS
PP pathway	Pentose 5-phosphate	1.69 \pm 0.19	1.53 \pm 0.10	LC-MS/MS
	Sedoheptulose 7-phosphate	3.51 \pm 0.46	2.24 \pm 0.13	LC-MS/MS
	Erythrose 4-phosphate	0.17 \pm 0.02	0.07 \pm 0.04	LC-MS/MS
	Ribulose 1.5-bisphosphate	0.21 \pm 0.05	0.17 \pm 0.03	LC-MS/MS
TCA cycle	Succinate	1.48 \pm 0.26	0.77 \pm 0.04	GC-MS
	α -Ketoglutarate	2.13 \pm 0.17	1.72 \pm 0.42	GC-MS
	Fumarate	0.42 \pm 0.01	0.37 \pm 0.02	GC-MS
Amino acids	Alanine	8.12 \pm 0.35	15.76 \pm 0.12	GC-MS
	Valine	0.85 \pm 0.03	0.32 \pm 0.02	GC-MS
	Leucine	0.35 \pm 0.01	< LOD	GC-MS
	Isoleucine	0.27 \pm 0.02	0.33 \pm 0.00	GC-MS
	Glycine	2.84 \pm 0.22	3.90 \pm 0.07	GC-MS
	Proline	0.47 \pm 0.03	1.55 \pm 0.02	GC-MS
	Serine	5.91 \pm 0.38	7.93 \pm 0.04	GC-MS
	Threonine	2.41 \pm 0.17	3.78 \pm 0.03	GC-MS
	Aspartate/Asparagine	17.24 \pm 0.75	23.58 \pm 0.56	GC-MS
	Methionine	0.25 \pm 0.01	0.35 \pm 0.00	GC-MS
	Glutamate/Glutamine	88.08 \pm 4.62	145.07 \pm 3.85	GC-MS
	Phenylalanine	0.35 \pm 0.01	0.58 \pm 0.01	GC-MS
	Tyrosine	0.58 \pm 0.02	0.81 \pm 0.03	GC-MS
Lysine	0.45 \pm 0.02	0.53 \pm 0.01	GC-MS	
Soluble sugars	Glucose	11.86 \pm 1.73	11.28 \pm 0.51	GC-MS
	Fructose	19.02 \pm 2.74	17.70 \pm 0.92	GC-MS
	Inositol	4.74 \pm 0.17	5.33 \pm 0.07	GC-MS

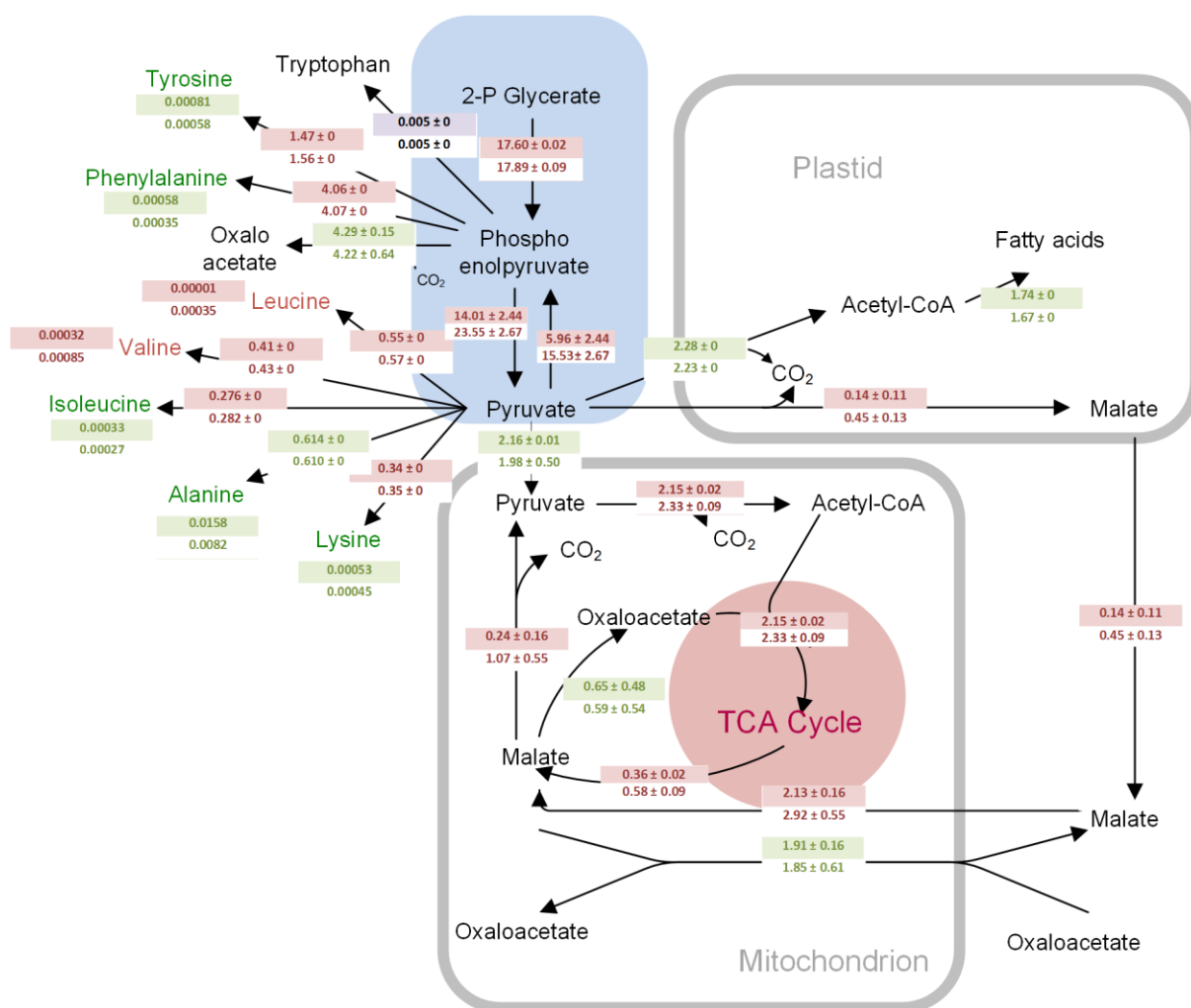


Figure 5. 30 Metabolic flux changes around the pyruvate and phosphoenolpyruvate node imposed by herbicide-treatment

Differences in metabolic flux distribution between imazapyr-treated rice seedlings and DMSO-treated seedlings as a reference. Flux calculation was performed with data from soil grown, illuminated rice seedlings at the age of 15 days that were labeled with 400 $\mu\text{L L}^{-1}$ $^{13}\text{CO}_2$ for 30 minutes. Flux values are given in mol% on the respective arrow. Green and red boxes indicate a significant increase and decrease, respectively, of flux under imazapyr treatment. Differences in fluxes were considered significant based on a standard Student's t-test ($P = 0.05$). Figure taken from Beckers (2015).

Proline concentration increased most prominently, which matches with it being one of the most important compatible solutes, a part of the general stress response (Liang et al., 2013). Threonine is a major precursor of the AHAS synthetic pathway and may have accumulated as consequence of AHAS inhibition. Alanine concentration increased, probably as compensatory reaction for the removal of excess pyruvate, which is another major substrate of AHAS (Gaston et al., 2002). Although most amino acid concentrations increased inside the cell, their de novo biosynthesis decreased (Figure 5. 30). Hence, increases in the amino acid pool sizes were most probably due to an increase in protein turnover to regenerate the branched-chain amino acids valine and leucine as fast response to imazapyr application, which would also explain

the detected increase in isoleucine concentration (Shaner and Reider, 1986; Royuela et al., 2000).

5.2.4.2 Accumulation of storage carbohydrates alters C/N metabolism

Fluxes through the CBB cycle were not altered in response to imazapyr, indicating maintained photosynthetic activity, at least in this early stage of herbicide stress. At the 3-phosphoglycerate node, the flux distribution was equal to the one detected for untreated rice seedlings (Figure 5. 27). Only slightly diminished fluxes were detected between 3-phosphoglycerate and pyruvate (1.02 fold) in imazapyr treated plants. Slightly enhanced fluxes (1.04 fold) were observed between glyceraldehyde 3-phosphate and fructose 6-phosphate. Equally, as for untreated rice seedlings, the flux distribution at the 3PG node displayed the gluconeogenic function of the EMP pathway, supporting the enhanced biosynthesis of starch and sucrose upon imazapyr treatment (Figure 5. 29). Actually, the biomass share of starch and sucrose was enhanced by 1.8 and 1.1 fold, respectively, following imazapyr treatment (Table 5. 7). All other cellular components remained unchanged.

Table 5. 7 Biomass composition of imazapyr-treated rice seedlings

Biomass composition for a rice seedling determined by LC-MS/MS and GC-MS analytics, as well as quantitative starch and fatty acid methyl ester (FAME) measurement. Values for hemicellulose, cellulose, lignin, pigments and nucleotides were taken from literature. DMSO – control plants treated with a mixture of 0.1% DMSO and 0.1% Dash. DW - dry weight.

Metabolite	Amount (mg (g DW) ⁻¹)	
	DMSO	Imazapyr
Amino acids [A, B]		
Alanine	20.3	20.4
Arginine	19.8	19.7
Asparagine	33.2	32.9
Aspartate	-	-
Cysteine	1.9	4.6
Glutamate	46.1	49.5
Glutamine	-	-
Glycine	18.1	17.4
Histidine	7.5	7.4
Isoleucine	13.8	13.5
Leucine	27.6	26.9
Lysine	19.2	18.4
Methionine	5.0	4.9
Phenylalanine	81.3	81.0
Proline	15.2	14.6
Serine	15.9	14.8
Threonine	15.7	15.6
Tryptophan [C]	0.03	0.03
Tyrosine	52.4	49.5
Valine	18.8	18.0
Hemicellulose [D]		

Metabolite	Amount (mg (g DW) ⁻¹)	
	DMSO	Imazapyr
Xylose	53.6	53.6
Galactose	5.6	5.6
Arabinose	14.7	14.7
Glucose	124.3	124.3
Mannose	3.9	3.9
Rhamnose	0.9	0.9
Lignin [D]	42	42
Cellulose [D]	52.5	52.5
Starch [E]	4.1	7.2
Soluble sugars [F]	61.5	70.1
Sucrose	56.0	63.5
Glucose	3.0	2.9
Fructose	3.6	3.7
Pigments [G]		
Chlorophyll	21.9	21.9
Carotenoids	0.7	0.7
Nucleotides [H, I]		
RNA	13.3	13.3
DNA	8.2	8.2
Lipids [J]	19.7	20.6
Fatty acids (16:0)	2.7	2.8
Fatty acids (18:0)	16.6	17.4
Fatty acids (20:0)	0.4	0.4
Organic acids	13.4	13.1
Ascorbate [K]	6.0	6.0
Citrate [L]	1.5	1.4
Succinate [L]	0.2	0.1
Pyruvate [M]	0.5	0.5
α -Ketoglutarate [M]	0.3	0.3
Malate [L]	4.9	4.8

References: [A] C/N combustion, [B] Quantitative LC-MS/MS analysis, [C] Ishihara et al. (2008), [D] Sumiyoshi et al. (2013), [E] Quantitative starch measurement, [F] Quantitative free sugar measurement, [G] Panda and Sakar (2013), [H] Suzuki et al. (2001), [I] Murray and Thompson (1980), [J] Quantitative FAME measurement, [K] Chao et al. (2010), [L] Quantitative GC-MS analysis.

After long term treatment, carbohydrate accumulation is one of the main symptoms of AHAS-inhibiting herbicides. It has been speculated that this is due to a lack of metabolically active sinks at maintained photosynthetic flux (Figure 5. 29) (Zabalza et al., 2004).

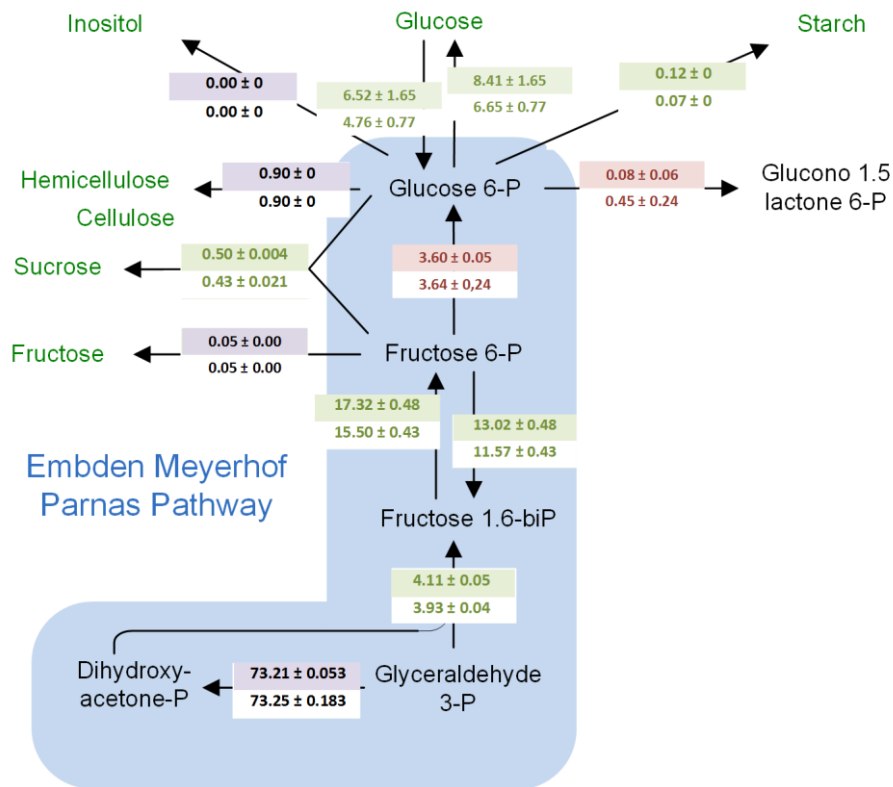


Figure 5. 31 Metabolic flux changes in sugar metabolism imposed by herbicide-treatment

Differences in metabolic flux distribution between imazapyr-treated rice seedlings and DMSO-treated seedlings as a reference. Flux calculation was performed with data from soil grown, illuminated rice seedlings at the age of 15 days that were labeled with $400 \mu\text{L L}^{-1} \text{ }^{13}\text{CO}_2$ for 30 minutes. Flux values are given in mol% on the respective arrow. Green and red boxes indicate a significant increase and decrease, respectively, of flux under imazapyr treatment. Differences in fluxes were considered significant based on a standard Student's t-test ($P = 0.05$). Figure taken from Beckers (2015).

The enhanced sucrose export to the root (1.2 fold), detected for imazapyr-treated plants, was a fast response to the lack of metabolic activity in shoot sinks, e.g. meristematic tissues. As sucrose was probably exported at a higher rate than it could be utilized by the root, carbohydrate subsequently accumulated inside plant leaves as well, because the sucrose gradient necessary for long-distance transport was abolished (Figure 5. 31) (Royuela et al., 2000; Zabalza et al., 2004). Corresponding to carbohydrate accumulation, the oxidative PP pathway exhibited strongly diminished fluxes (5.9 fold) as its precursor, glucose 6-phosphate, was used for starch synthesis, presumably depleting the glucose 6-phosphate pool.

5.2.4.3 Diminished fluxes in TCA cycle, photorespiration and oxidative PP pathway

Regarding the TCA cycle, diminished fluxes were detected for all reactions, except for malate dehydrogenase, which showed an increase by 9.5 fold. Oxoglutarate dehydrogenase and succinate dehydrogenase exhibited 4.8 fold decreased fluxes, respectively. The TCA cycle hence exhibited a lowered activity under herbicide stress, probably related to a reduced anabolic

function. Strongly diminished fluxes were also detected for OPPP (5.9 fold) and photorespiration (up to 9.3 fold). However, it has to be considered that the flux values for these reactions are very low (< 1.1 mol%), both in control and imazapyr-treated plants, indicating a generally low metabolic share of these reactions, which was also observed for untreated rice seedlings (Figure 5. 27). The diminished photorespiratory flux may be due to hypoxic conditions inside the cells of imazapyr-treated plants, which has been shown for the roots of pea plants upon treatment with an imidazolinone herbicide (Zabalza et al., 2011). Anoxia would further explain the reduction of cellular respiration as adaptive response to save oxygen. Reduction of respiratory oxygen loss is probably achieved by the observed increase of fluxes upstream of pyruvate (upper EMP pathway), as well as the decrease downstream of it (TCA cycle) (Figure 5. 29), which hints at a role of pyruvate in respiratory regulation (Zabalza et al., 2009).

5.2.4.4 Growth arrest due to C/N imbalance

Furthermore, anabolic fluxes, e.g. amino acid flux into biomass components, decreased, ultimately causing the generally observed growth arrest of imazapyr-treated plants. The detected increase of free amino acid levels and diminished flux of those free amino acids into biomass components, supports the previously described effect of enhanced protein turnover in imazapyr-treated plants to replenish the pool of branched-chain amino acids (Royuela et al., 2000). Growth inhibition cannot be due to a lack of respiratory substrates, as carbohydrates were found to accumulate inside the cell (Figure 5. 31). Thus, it seems to result from the observed alteration in the ratio of free amino acids and the accumulation of carbohydrates, leading to an imbalance of carbon/nitrogen metabolism.

5.2.4.5 Maintenance of ATP/NADPH balance through enhanced biosynthesis of sucrose, starch and proline

The imbalance between production and consumption of reducing equivalents and energy is increased in plants under stress conditions (Hoefnagel et al., 1998). Under imazapyr stress, photosynthesis was not impaired (Figure 5. 29), while anabolic growth was restricted, leading to a surplus of energy, redox power and assimilated carbon. Hence, the MAL/PYR shuttle, as well as the futile cycles proposed for untreated rice seedlings (5.2.3) to dissipate excess redox power and energy, respectively, could be assumed to be even more active in the stressed plant. In fact, futile cycling between glucose and glucose 6-phosphate exhibited higher flux rates (Figure 5. 31). Interconversion of PEP and pyruvate was, however, diminished (Figure 5. 30). Under normal growth conditions, ATP is extensively used for anabolic reactions (Hoefnagel et al., 1998), which are however impaired in stressed plants. Hence, excess energy

is dissipated by enhanced biosynthesis of starch and sucrose, as well as fatty acids and soluble amino acids, as these metabolites are not associated with growth, which is quickly reduced after imazapyr treatment, but are rather synthesized to store excess energy.

A potential role of the MAL/PYR shuttle in stress response is supported by significant flux changes detected around malate and pyruvate. The net import of malate into the mitochondrion was reduced from 1.07 ± 0.05 mol% to 0.22 ± 0.16 mol% under imazapyr treatment. The lack of substrate correspondingly decreased the NAD-malic enzyme flux by 4.5 fold, thereby reducing the generation of NADH and depriving the TCA cycle of its substrate pyruvate. The latter led to the detected reduction of TCA cycle activity, thereby also reducing the generation of ATP. Probably as compensation, in order to maintain at least minimal TCA cycle activity, pyruvate import into the mitochondrion increased (1.1 fold) and malate dehydrogenase flux was enhanced by 9.5 fold. Malate dehydrogenase catalyzes the conversion of malate to oxaloacetate, which serves as TCA cycle substrate. The reversed flux through the MAL/OAA shuttle decreased mitochondrial NADH concentration, probably to avoid overreduction of the electron transport chain, and concurrently channeled reducing power to the cytosol/plastid. Hence, shuttling of malate and pyruvate between different compartments seems to be important for stressed plants in order to balance redox equivalents and maintain TCA cycle flux. However, it should be considered that flux estimations around malate and oxaloacetate may be corrupted by the fact that malate is a highly interconnected metabolite with low ^{13}C incorporation and oxaloacetate is a very unstable analyte. Therefore, repeating the study with advanced analytics is greatly desired.

The pool size of proline was increased strongest amongst amino acids (Table 5. 6), which can be attributed to its role as compatible solute. However, there probably is another function of increased proline biosynthesis under stress conditions. Proline synthesis is one way of reoxidizing excess NADPH from photosynthesis. Once the stress is removed, ATP, produced when proline is oxidized, may be important for the recovery from stress (Hoefnagel et al., 1998). Hence, proline helps to maintain the ATP/NADPH ratio of plants during and after stress.

The observed early stress phenotype of imazapyr-treated rice seedlings was the result of extensive reprogramming of metabolism from growth to survival. In this study, INST-MFA reveals its incredible potential to examine stress response at the systems level. In addition to pulse-chase studies, which are more suitable for rather superficial fast screening of several phenotypes, INST-MFA provides the possibility to have a detailed look into an interesting phenotype. In this way, the pulse-chase study described the prime target of imazapyr by revealing diminished ^{13}C incorporation into branched-chain amino acids, whereas INST-MFA further revealed an increase in sucrose and starch levels, decreased flux into biomass and compensatory

fluxes to salvage pyruvate at maintained photosynthetic activity. The described techniques are complementary and, taken together, provide a comprehensive toolbox for new phenotyping approaches to reveal the mode-of-action of as yet unknown herbicides.

6 Conclusions and Outlook

Green biotechnology has emerged as a field with a huge potential for industrial production of valuable compounds (Nölke et al., 2003; Xu et al., 2012; Staniek et al., 2013; Sumiyoshi et al., 2013; Lau et al., 2014) and, concerning crop species, has shown to be suitable to enhance nutrient quality and quantity (Ye et al., 2000; Kebeish et al., 2007; Karki et al., 2013; Masuda et al., 2013; Lin et al., 2014; McGrath and Long, 2014) and to provide plants with superior traits (Betz et al., 2000; Jeong et al., 2010; Mao et al., 2013; Chen et al., 2014; Wang et al., 2015), using genetic engineering. Targeted genetic engineering relies on comprehensive understanding of plant metabolic functions and is often hampered by incomplete knowledge.

In this study, a metabolic flux analysis toolbox was developed that was employed to elucidate metabolic functions of *Oryza sativa*, concerning different developmental stages, as well as stress response to high salt and herbicide treatment. The developed toolbox is suitable for precisely controlled isotope labeling experiments of whole plants to track metabolic fluxes *in vivo*. In a first step, pulse-chase studies were used as fast screening tool that were subsequently complemented by the INST-MFA approach to describe interesting phenotypes in more detail. The high technical quality of data obtained under physiologically relevant conditions represents a major improvement of plant metabolic flux profiling. The established setup has a huge potential to be extended to e.g. (i) other plant species, (ii) comprehensive stress response studies, (iii) phenotypic screening of mutants and (iv) mode-of-action studies of herbicides.

Despite the improvements made in the present study to perform comprehensive ^{13}C -based metabolic flux analysis of whole plants, there is still great potential to enhance throughput and resolution of such analyses. An increase in throughput can be achieved by automation of sampling, analytics, data processing and computation. Concerning labeling experiment, more plants could be labeled simultaneously, for example, directly in the greenhouse, which, combined with an automated sampling procedure, would additionally minimize environmental variation and thereby enhance reproducibility (Junker et al., 2015). An autonomous analytical pipeline, comprising extraction, purification, derivatization, chromatography and detection of desired metabolites could further enhance operational capacity (Ngounou Wetie et al., 2012; Núñez et al., 2013; Shubhakar et al., 2015). Data processing, visualization and computation can be sped up by the use of software tools like INCA (Young, 2014) and VANTED (Junker et al., 2006) as well as by the employment of cluster computing (Junker, 2014), respectively.

Subcellular compartmentation considerably increases metabolic flexibility, specialization and regulation and hence poses a major threat to the resolution of intracellular fluxes (Fernie and Morgan, 2013). Resolution can be enhanced by generating compartment-specific information

and integrating this information into a compartmented network model. Such information can be gained by analyzing compartment-specific reporter molecules (Sriram et al., 2004; Schwender, 2008), by performing non-aqueous fractionation (Farré et al., 2002; Benkeblia et al., 2007; Krueger et al., 2011; Tiessen et al., 2012) or by the application of metabolic imaging, using MS (Hölscher et al., 2009; Matros and Mock, 2013), NMR (Borisjuk et al., 2012) or fluorescence resonance energy transfer (FRET)-based techniques (Lalonde et al., 2005; Okumoto et al., 2008). Additionally, widening the analytical spectrum by more sensitive MS and NMR approaches, like capillary-electrophoresis coupled to mass spectrometry (CE-MS) (Monton and Soga, 2007) as well as multinuclear and multidimensional NMR spectroscopy (Fan and Lane, 2008), could enhance metabolic resolution and would allow extending molecular flux studies, e.g. to pathways of secondary metabolism, like phenol, isoprenoid and alkaloid biosynthesis. In addition to subcellular compartmentation, plants furthermore exhibit different tissues, subdivided into several distinct cell types. A metabolic analysis of an organ will therefore always be a mean over different cells (Roscher et al., 2000), which disregards different metabolic phenotypes and may lead to misinterpretation (Shachar-Hill, 2013). Hence, cell- and tissue-specific protocols for metabolic flux analysis are needed, involving flow cytometry or laser microdissection to isolate particular cell types as well as the analysis of cell- or tissue-specific reporter molecules (Kruger and Ratcliffe, 2015).

To most realistically describe plant metabolism, the major aim of plant physiologists is to integrate different omics technologies and provide multi-tissue models of whole plants. Plants have been studied with several omics technologies, including transcriptomics (Vanderschuren et al., 2013), metabolomics and proteomics (Ward et al., 2012; Dong and Chen, 2013). However, to elucidate plant functions on the systems level, it is necessary to integrate multiple omics levels into one network model (Fukushima et al., 2014; Schwender et al., 2015). This is very challenging due to the heterogenic nature of omics data (Schwender et al., 2014), the high interconnectivity of metabolic pathways and the flexibility of biological networks during development and in response to environmental changes (Stitt, 2013). Furthermore, integrating several organs and tissue types is a future prospect of plant systems biology. A recent study, applying a multiscale metabolic modeling approach, demonstrated the high potential of such combined approaches to elucidate metabolic functions on a whole-plant scale (Grafahrend-Belau et al., 2013).

7 Abbreviations

ABA	Abscisic acid
AHAS	Acetohydroxyacid synthase
AP(E)	Atom percent (excess)
ATP	Adenosine triphosphate
BCAA	Branched-chain amino acid
BC	Before Christ
CBB cycle	Calvin-Benson-Bessham cycle
CCM	CO ₂ concentrating mechanism
CE	Capillary electrophoresis
DC	Direct current
DMSO	Dimethyl sulfoxide
DNA	Desoxyribonucleic acid
DW	Dry weight
EA	Elemental analyzer
EI	Electron impact
EMP pathway	Embden-Meyerhof-Parnas pathway
EPDM	Ethylen propylene diene monomer
FAME	Fatty acid methyl ester
FRET	Fluorescence resonance energy transfer
GC	Gas chromatography
GFE	Grain filling early
GFL	Grain filling late
HEPES	4-(2-hydroxyethyl)-1-piperazineethanesulfonic acid
RuBisCO	Ribulose 1.5-bisphosphate carboxylase/oxygenase
INCA	Isotopomer Network Compartmental Analysis
INST-MFA	Isotopically non-stationary metabolic flux analysis

(IR)MS	(Isotope ratio) mass spectrometry
KFP	Kinetic flux profiling
LC	Liquid chromatography
LOD	Limit of detection
MBDSTFA	<i>N</i> -methyl- <i>N</i> - <i>tert</i> -butyldimethylsilyl-trifluoroacetamide
MFA	Metabolic flux analysis
MID	Mass isotopomer distribution
miETC	Mitochondrial electron transport chain
MoA	Mode of action
MTBE	Methyl- <i>tert</i> -butyl-ether
<i>m/z</i>	mass/charge
NAD(P) ⁺	Nicotinamide adenine dinucleotide (phosphate), oxidized
NAD(P)H	Nicotinamide adenine dinucleotide (phosphate), reduced
NMR	Nuclear magnetic resonance
(O)PPP	(Oxidative) pentose phosphate pathway
<i>O. sativa</i>	<i>Oryza sativa</i>
PAR	Photosynthetically active radiation
PVDF	Polyvinylidene fluoride
RNA	Ribonucleic acid
ROS	Reactive oxygen species
SDL	Seedling
TCA	Trichloroacetic acid
TCA cycle	Tricarboxylic acid cycle
TCD	Thermal conductivity detector
TMSH	Trimethylsulfonium hydroxide
VANTED	Visualization and Analysis of Networks containing Experimental Data
VPDB	Vienna Pee Dee Belemnite

8 References

- Abbasi FM, Komatsu S** (2004) A proteomic approach to analyze salt-responsive proteins in rice leaf sheath. *Proteomics* **4**: 2072–2081
- Ahmad P, Ashraf M, Younis M, Hu X, Kumar A, Akram NA, Al-Qurainy F** (2011) Role of transgenic plants in agriculture and biopharming. *Biotechnol Adv* **30**: 524–540
- Ahn S, Tanksley SD** (1993) Comparative linkage maps of the rice and maize genomes. *Proc Natl Acad Sci* **90**: 7980–7984
- Albacete AA, Martínez-Andújar C, Pérez-Alfocea F** (2014) Hormonal and metabolic regulation of source-sink relations under salinity and drought: from plant survival to crop yield stability. *Biotechnol Adv* **32**: 12–30
- Alexandratos N, Bruinsma J** (2012) World agriculture towards 2030/2050: the 2012 revision.
- Allen DK, Evans BS, Libourel IGL** (2014) Analysis of isotopic labeling in peptide fragments by tandem mass spectrometry. *PLoS One* **9**: e91537
- Allen DK, Laclair RW, Ohlrogge JB, Shachar-Hill Y** (2012) Isotope labelling of Rubisco subunits provides *in vivo* information on subcellular biosynthesis and exchange of amino acids between compartments. *Plant, Cell Environ* **35**: 1232–1244
- Allen DK, Libourel IGL, Shachar-Hill Y** (2009a) Metabolic flux analysis in plants: coping with complexity. *Plant Cell Environ* **32**: 1241–1257
- Allen DK, Ohlrogge JB, Shachar-Hill Y** (2009b) The role of light in soybean seed filling metabolism. *Plant J* **58**: 220–234
- Allen DK, Shachar-Hill Y, Ohlrogge JB** (2007) Compartment-specific labeling information in ¹³C metabolic flux analysis of plants. *Phytochemistry* **68**: 2197–2210
- Allen DK, Young JD** (2013) Carbon and nitrogen provisions alter the metabolic flux in developing soybean embryos. *Plant Physiol* **161**: 1458–1475
- Alonso AP, Dale VL, Shachar-Hill Y** (2010) Understanding fatty acid synthesis in developing maize embryos using metabolic flux analysis. *Metab Eng* **12**: 488–497
- Alonso AP, Goffman FD, Ohlrogge JB, Shachar-Hill Y** (2007a) Carbon conversion efficiency and central metabolic fluxes in developing sunflower (*Helianthus annuus* L.) embryos. *Plant J* **52**: 296–308
- Alonso AP, Raymond P, Rolin D, Dieuaide-Noubhani M** (2007b) Substrate cycles in the central metabolism of maize root tips under hypoxia. *Phytochemistry* **68**: 2222–2231
- Alonso AP, Val DL, Shachar-Hill Y** (2011) Central metabolic fluxes in the endosperm of developing maize seeds and their implications for metabolic engineering. *Metab Eng* **13**: 96–107
- Alonso AP, Vigeolas H, Raymond P, Rolin D, Dieuaide-Noubhani M** (2005) A new substrate cycle in plants. Evidence for a high glucose-phosphate-to-glucose turnover from *in vivo* steady-state and pulse-labeling experiments with ¹³C glucose and ¹⁴C glucose. *Plant Physiol* **138**: 2220–2232
- Amaral AI, Teixeira AP, Håkonsen BI, Sonnewald U, Alves PM** (2011) A comprehensive metabolic profile of cultured astrocytes using isotopic transient metabolic flux analysis and ¹³C-labeled glucose. *Front Neuroenergetics* **3**: 5
- Andersen A, Nielsen G, Sorensen H** (1961) Growth chamber for labelling plant material uniformly with radiocarbon. *Physiol Plant* **14**: 378–383

- Anderson LE, Duggan JX** (1976) Light modulation of glucose-6-phosphate dehydrogenase: partial characterization of the light inactivation system and its effects on the properties of the chloroplastic and cytoplasmic forms of the enzyme. *Plant Physiol* **58**: 135–139
- Antoniewicz MR** (2013) Tandem mass spectrometry for measuring stable-isotope labeling. *Curr Opin Biotechnol* **24**: 48–53
- Antoniewicz MR** (2015) Methods and advances in metabolic flux analysis: a mini-review. *J Ind Microbiol Biotechnol* **42**: 317–325
- Antoniewicz MR, Kelleher JK, Stephanopoulos G** (2006) Determination of confidence intervals of metabolic fluxes estimated from stable isotope measurements. *Metab Eng* **8**: 324–337
- Arakawa T, Yu J, Langridge WHR** (2001) Synthesis of a cholera toxin B subunit-rotavirus NSP4 fusion protein in potato. *Plant Cell Rep* **20**: 343–348
- Araújo WL, Ishizaki K, Nunes-Nesi A, Larson TR, Tohge T, Krahnert I, Witt S, Obata T, Schauer N, Graham IA, et al** (2010) Identification of the 2-hydroxyglutarate and isovaleryl-CoA dehydrogenases as alternative electron donors linking lysine catabolism to the electron transport chain of *Arabidopsis* mitochondria. *Plant Cell* **22**: 1549–1563
- Arnon DI** (1971) The light reactions of photosynthesis. *Proc Natl Acad Sci U S A* **68**: 2883–2892
- Artus NN, Edwards GE** (1985) NAD-malic enzyme from plants. *FEBS Lett* **182**: 225–233
- Ashraf S, Singh PK, Yadav DK, Shahnawaz M, Mishra S, Sawant S V., Tuli R** (2005) High level expression of surface glycoprotein of rabies virus in tobacco leaves and its immunoprotective activity in mice. *J Biotechnol* **119**: 1–14
- Balcke GU, Kolle SN, Kamp H, Bethan B, Looser R, Wagner S, Landsiedel R, van Ravenzwaay B** (2011) Linking energy metabolism to dysfunctions in mitochondrial respiration – A metabolomics in vitro approach. *Toxicol Lett* **203**: 200–209
- Bao X, Katz S, Pollard M, Ohlrogge J** (2002) Carbocyclic fatty acids in plants: biochemical and molecular genetic characterization of cyclopropane fatty acid synthesis of *Sterculia foetida*. *Proc Natl Acad Sci U S A* **99**: 7172–7177
- Barker HA, Kamen MD** (1945) Carbon dioxide utilization in the synthesis of acetic acid by *Clostridium thermoaceticum*. *Proc Natl Acad Sci U S A* **31**: 219–225
- Barker HA, Ruben S, Beck J V.** (1940) Radioactive carbon as an indicator of carbon dioxide reduction. IV. The synthesis of acetic acid from carbon dioxide by *Clostridium acidi-urici*. *Proc Natl Acad Sci U S A* **26**: 477–482
- Basu C, Halfhill MD, Mueller TC, Stewart CN** (2004) Weed genomics: New tools to understand weed biology. *Trends Plant Sci* **9**: 391–398
- Basu SK, Dutta M, Goyal A, Bhowmik PK, Kumar J, Nandy S, Scagliusi SM, Prasad R** (2010) Is genetically modified crop the answer for the next green revolution? *GM Crops* **1**: 68–79
- Bauwe H, Hagemann M, Fernie AR** (2010) Photorespiration: players, partners and origin. *Trends Plant Sci* **15**: 330–336
- Baxter CJ, Redestig H, Schauer N, Repsilber D, Patil KR, Nielsen J, Selbig J, Liu J, Fernie AR, Sweetlove LJ** (2007) The metabolic response of heterotrophic *Arabidopsis* cells to oxidative stress. *Plant Physiol* **143**: 312–325
- Beckers V** (2015) Whole plant *in vivo* and *in silico* metabolic flux analysis: towards biotechnological application.
- Benkeblia N, Shinano T, Osaki M** (2007) Metabolite profiling and assessment of metabolome compartmentation of soybean leaves using non-aqueous fractionation and GC-MS

- analysis. *Metabolomics* **3**: 297–305
- Benstein RM, Ludewig K, Wulfert S, Wittek S, Gigolashvili T, Frerigmann H, Gierth M, Flügge U-I, Krueger S** (2013) Arabidopsis Phosphoglycerate Dehydrogenase1 of the Phosphoserine Pathway Is Essential for Development and Required for Ammonium Assimilation and Tryptophan Biosynthesis. *Plant Cell* **25**: 5011–5029
- Berg J, Tymoczko JL, Stryer L** (2006) *Biochemistry*, 6th ed. W. H. Freeman and Company
- Betz FS, Hammond BG, Fuchs RL** (2000) Safety and advantages of *Bacillus thuringiensis*-protected plants to control insect pests. *Regul Toxicol Pharmacol* **32**: 156–173
- Bewley J** (1997) Seed germination and dormancy. *Plant Cell* **9**: 1055–1066
- Beyer P** (2010) Golden rice and “golden” crops for human nutrition. *N Biotechnol* **27**: 478–481
- Beyer P, Al-babili S, Ye X, Lucca P, Schaub P, Welsch R, Rice G** (2002) Golden rice: introducing the β -carotene biosynthesis pathway into rice endosperm by genetic engineering to defeat vitamin A deficiency. *J Nutr* **132**: 506S–510S
- Boatright J, Negre F, Chen X, Kish CM, Wood B, Peel G, Orlova I, Gang D, Rhodes D, Dudareva N** (2004) Understanding in vivo benzenoid metabolism in petunia petal tissue. *Plant Physiol* **135**: 1993–2011
- Bogorad L** (1981) Chloroplasts. *J Cell Biol* **91**: 256s–270s
- Bohmert-Tatarev K, McAvoy S, Daughtry S, Peoples OP, Snell KD** (2011) High levels of bioplastic are produced in fertile transplastomic tobacco plants engineered with a synthetic operon for the production of polyhydroxybutyrate. *Plant Physiol* **155**: 1690–1708
- Bohnert HJ, Gong Q, Li P, Ma S** (2006) Unraveling abiotic stress tolerance mechanisms - Getting genomics going. *Curr Opin Plant Biol* **9**: 180–188
- Borg S, Brinch-Pedersen H, Tauris B, Madsen LH, Darbani B, Noeparvar S, Holm PB** (2012) Wheat ferritins: Improving the iron content of the wheat grain. *J Cereal Sci* **56**: 204–213
- Borisjuk L, Rolletschek H, Neuberger T** (2012) Surveying the plant’s world by magnetic resonance imaging. *Plant J* **70**: 129–146
- Bromand S, Whalen JK, Janzen HH, Schjoerring JK, Ellert BH** (2001) A pulse-labelling method to generate ^{13}C -enriched plant materials. *Plant Soil* **235**: 253–257
- Brunner S, Hurni S, Herren G, Kalinina O, von Burg S, Zeller SL, Schmid B, Winzeler M, Keller B** (2011) Transgenic *Pm3b* wheat lines show resistance to powdery mildew in the field. *Plant Biotechnol J* **9**: 897–910
- Byun MY, Lee J, Cui LH, Kang Y, Oh TK, Park H, Lee H, Kim WT** (2015) Constitutive expression of *DaCBF7*, an Antarctic vascular plant *Deschampsia antarctica* CBF homolog, resulted in improved cold tolerance in transgenic rice plants. *Plant Sci* **236**: 61–74
- Calvin BM** (1956) The Photosynthetic Carbon Cycle. *J Chem Soc* 1895–1915
- Calvin M** (1962) The path of carbon in photosynthesis. *Science* (80-) **135**: 879–889
- Campo S, Baldrich P, Messeguer J, Lalanne E, Coca M, San Segundo B** (2014) Overexpression of a calcium-dependent protein kinase confers salt and drought tolerance in rice by preventing membrane lipid peroxidation. *Plant Physiol* **165**: 688–704
- Cao X, Lu Y, Di D, Zhang Z, Liu H, Tian L, Zhang A, Zhang Y, Shi L, Guo B, et al** (2013) Enhanced virus resistance in transgenic maize expressing a dsRNA-specific endoribonuclease gene from *E. coli*. *PLoS One* **8**: e60829
- Casida JE** (2009) Pest toxicology: The primary mechanisms of pesticide action. *Chem Res Toxicol* **22**: 609–619

- Cegelski L, Schaefer J** (2006) NMR determination of photorespiration in intact leaves using in vivo ^{13}C labeling. *J Magn Reson* **178**: 1–10
- Cegelski L, Schaefer J** (2005) Glycine metabolism in intact leaves by in vivo ^{13}C and ^{15}N labeling. *J Biol Chem* **280**: 39238–39245
- Chang T, Bardenas EA** (1965) The morphology and varietal characteristics of the rice plant. IRRI Publ.
- Chao YY, Hong CY, Kao CH** (2010) The decline in ascorbic acid content is associated with cadmium toxicity of rice seedlings. *Plant Physiol Biochem* **48**: 374–381
- Chen M, Sun L, Wu H, Chen J, Ma Y, Zhang X, Du L, Cheng S, Zhang B, Ye X, et al** (2014) Durable field resistance to wheat yellow mosaic virus in transgenic wheat containing the antisense virus polymerase gene. *Plant Biotechnol J* **12**: 447–456
- Chen M, Zhao Y, Zhuo C, Lu S, Guo Z** (2015) Overexpression of a NF-YC transcription factor from bermudagrass confers tolerance to drought and salinity in transgenic rice. *Plant Biotechnol J* **13**: 482–491
- Chen W, Yang X, Harms GL, Gray WM, Hegeman AD, Cohen JD** (2011) An automated growth enclosure for metabolic labeling of *Arabidopsis thaliana* with ^{13}C -carbon dioxide - an *in vivo* labeling system for proteomics and metabolomics research. *Proteome Sci* **9**: 9–23
- Chen ZY, Brown RL, Damann KE, Cleveland TE** (2010) PR10 expression in maize and its effect on host resistance against *Aspergillus flavus* infection and aflatoxin production. *Mol Plant Pathol* **11**: 69–81
- Chinnusamy V, Jagendorf A, Zhu J-K** (2005) Understanding and improving salt tolerance in plants. *Cell* **45**: 437–448
- Chitteti BR, Peng Z** (2007) Proteome and phosphoproteome differential expression under salinity stress in rice (*Oryza sativa*) roots. *J Proteome Res* **6**: 1718–1727
- Claeysen É, Dorion S, Clendenning A, He JZ, Wally O, Chen J, Auslender EL, Moisan MC, Jolicoeur M, Rivoal J** (2013) The futile cycling of hexose phosphates could account for the fact that hexokinase exerts a high control on glucose phosphorylation but not on glycolytic rate in transgenic potato (*Solanum tuberosum*) roots. *PLoS One* **8**: e53898
- Cliquet JB, Deléens E, Mariotti A** (1990) C and N mobilization from stalk and leaves during kernel filling by C and N tracing in *Zea mays* L. *Plant Physiol* **94**: 1547–1553
- Cock JH, Yoshida S** (1972) Accumulation of ^{14}C carbohydrate before flowering and its subsequent redistribution and respiration in the rice plant. *Proc Crop Sci Soc Japan* **41**: 226–234
- Colón AM, Sengupta N, Rhodes D, Dudareva N, Morgan J** (2010) A kinetic model describes metabolic response to perturbations and distribution of flux control in the benzenoid network of *Petunia hybrida*. *Plant J* **62**: 64–76
- Commandeur U, Twyman RM, Fischer R** (2003) The biosafety of molecular farming in plants. *AgBiotechNet* **5**: 1–9
- Cramer GR, Urano K, Delrot S, Pezzotti M, Shinozaki K** (2011) Effects of abiotic stress on plants: a systems biology perspective. *BMC Plant Biol* **11**: 163
- Cueno ME, Hibi Y, Karamatsu K, Yasutomi Y, Imai K, Laurena AC, Okamoto T** (2010) Preferential expression and immunogenicity of HIV-1 Tat fusion protein expressed in tomato plant. *Transgenic Res* **19**: 889–895
- Dennis D, Miernyk J** (1982) Compartmentation of nonphotosynthetic carbohydrate metabolism. *Annu Rev Plant Physiol* **33**: 27–50
- Dersch LM, Beckers V, Wittmann C** (2015) Green pathways: Metabolic network analysis of

- plant systems. *Metab Eng* **34**: 1–24
- Dhlamini Z, Spillane C, Moss JP, Ruane J, Urquia N, Sonnino A** (2005) Status of research and application of crop biotechnologies in developing countries. Food Agric. Organ. United Nations
- Dieuaide-Noubhani M, Raffard G, Canioni P, Pradet A, Raymond P** (1995) Quantification of compartmented metabolic fluxes in maize root tips using isotope distribution from ^{13}C - or ^{14}C -labeled glucose. *J Biol Chem* **22**: 13147–13159
- Docherty G, Jones V, Evershed RP** (2001) Practical and theoretical considerations in the gas chromatography/combustion/isotope ratio mass spectrometry $\delta^{13}\text{C}$ analysis of small polyfunctional compounds. *Rapid Commun Mass Spectrom* **15**: 730–738
- Dong ZC, Chen Y** (2013) Transcriptomics: Advances and approaches. *Sci China Life Sci* **56**: 960–967
- Dooki AD, Mayer-Posner FJ, Askari H, Zaiee AA, Salekdeh GH** (2006) Proteomic responses of rice young panicles to salinity. *Proteomics* **6**: 6498–6507
- Duke SO** (2012) Why have no new herbicide modes of action appeared in recent years? *Pest Manag Sci* **68**: 505–512
- Dutilleul C, Garmier M, Noctor G, Mathieu C, Foyer CH, Paepe R De** (2003) Leaf mitochondria modulate whole cell redox homeostasis, set antioxidant capacity, and determine stress resistance through altered signaling and diurnal regulation. *Plant Cell* **15**: 1212–1226
- Dyckmans J, Flessa H, Shangguan Z, Beese F** (2000) A dual ^{13}C and ^{15}N long term labelling technique to investigate uptake and translocation of C and N in beech (*Fagus sylvatica* L.). *Isotopes Environ Health Stud* **36**: 63–78
- Eicks M, Knappe S, Flu U** (2002) The plastidic pentose phosphate translocator represents a link between the cytosolic and the plastidic pentose phosphate pathways in plants. *Plant Physiol* **128**: 512–522
- Ellis RJ** (1979) The most abundant protein in the world. *Trends Biochem Sci* **4**: 241–244
- Fan TWM, Lane AN** (2008) Structure-based profiling of metabolites and isotopomers by NMR. *Prog Nucl Magn Reson Spectrosc* **52**: 69–117
- FAO** (2015a) FAOSTAT. <http://faostat.fao.org/site/567/default.aspx#ancor>
- FAO** (2015b) FAOSTAT. <http://faostat.fao.org/site/377/default.aspx#ancor>
- FAO** (2015c) Salt-affected soils. <http://www.fao.org/soils-portal/soil-management/ma>
- Farré EM, Tiessen A, Roessner U, Geigenberger P, Trethewey RN** (2002) Analysis of the compartmentation of glycolytic intermediates, nucleotides, sugars, organic acids, amino acids, and sugar alcohols in potato tubers using a nonaqueous fractionation method. *Plant Physiol* **127**: 685–700
- Fernie AR, Carrari F, Sweetlove LJ** (2004) Respiratory metabolism: glycolysis, the TCA cycle and mitochondrial electron transport. *Curr Opin Plant Biol* **7**: 254–261
- Fernie AR, Morgan JA** (2013) Analysis of metabolic flux using dynamic labelling and metabolic modelling. *Plant, Cell Environ* **36**: 1738–1750
- Ferreira LJ, Azevedo V, Maroco J, Oliveira MM, Santos AP** (2015) Salt tolerant and sensitive rice varieties display differential methylome flexibility under salt stress. *PLoS One* **10**: e0124060
- Fischer R, Emans N** (2000) Molecular farming of pharmaceutical proteins. *Transgenic Res* **9**: 279–299
- Flügge UI, Häusler RE, Ludewig F, Gierth M** (2011) The role of transporters in supplying

- energy to plant plastids. *J Exp Bot* **62**: 2381–2392
- Fraley RT, Rogers SG, Horsch RB, Sanders PR, Flick JS, Adams SP, Bittner ML, Brand L a, Fink CL, Fry JS, et al** (1983) Expression of bacterial genes in plant cells. *Proc Natl Acad Sci U S A* **80**: 4803–4807
- Fukushima A, Kanaya S, Nishida K** (2014) Integrated network analysis and effective tools in plant systems biology. *Front Plant Sci* **5**: 598
- Funayama K, Kojima S, Tabuchi-Kobayashi M, Sawa Y, Nakayama Y, Hayakawa T, Yamaya T** (2013) Cytosolic glutamine synthetase1;2 is responsible for the primary assimilation of ammonium in rice roots. *Plant Cell Physiol* **54**: 934–943
- Furtado A, Lupoi JS, Hoang N, Healey A, Singh S, Simmons BA, Henry RJ** (2014) Modifying plants for biofuel and biomaterial production. *Plant Biotechnol J* **12**: 1246–1258
- Garlick AP, Moore C, Kruger NJ** (2002) Monitoring flux through the oxidative pentose phosphate pathway using [$1-^{14}\text{C}$]gluconate. *Planta* **216**: 265–272
- Garris AJ, Tai TH, Coburn J, Kresovich S, McCouch S** (2005) Genetic structure and diversity in *Oryza sativa* L. *Genetics* **169**: 1631–1638
- Gaston S, Zabalza A, González EM, Arrese-Igor C, Aparicio-Tejo PM, Royuela M** (2002) Imazethapyr, an inhibitor of the branched-chain amino acid biosynthesis, induces aerobic fermentation in pea plants. *Physiol Plant* **114**: 524–532
- Gauthier PPG, Bligny R, Gout E, Mahe A, Nogue S, Hodges M, Tcherkez GGB** (2010) *In folio* isotopic tracing demonstrates that nitrogen assimilation into glutamate is mostly independent from current CO_2 assimilation in illuminated leaves of *Brassica napus*. *New Phytol* **185**: 988–999
- Geigenberger P, Reimholz R, Geiger M, Merlo L, Canale V, Stitt M** (1997) Regulation of sucrose and starch metabolism in potato tubers in response to short-term water deficit. *Planta* **201**: 502–518
- Geigenberger P, Stitt M** (1991) A “futile” cycle of sucrose synthesis and degradation is involved in regulating partitioning between sucrose, starch and respiration in cotyledons of germinating *Ricinus communis* L. seedlings when phloem transport is inhibited. *Planta* **185**: 81–90
- Geisler DA, Sampathkumar A, Mutwil M, Persson S** (2008) Laying down the bricks: logistic aspects of cell wall biosynthesis. *Curr Opin Plant Biol* **11**: 647–652
- Georgiev MI, Eibl R, Zhong JJ** (2013) Hosting the plant cells in vitro: recent trends in bioreactors. *Appl Microbiol Biotechnol* **97**: 3787–3800
- Georgiev MI, Weber J** (2014) Bioreactors for plant cells: Hardware configuration and internal environment optimization as tools for wider commercialization. *Biotechnol Lett* **36**: 1359–1367
- Gerhardt R, Heldt HW** (1984) Measurement of subcellular metabolite levels in leaves by fractionation of freeze-stopped material in nonaqueous media. *Plant Physiol* **75**: 542–547
- Gibson K, Park JS, Nagai Y, Hwang SK, Cho YC, Roh KH, Lee SM, Kim DH, Choi SB, Ito H, et al** (2011) Exploiting leaf starch synthesis as a transient sink to elevate photosynthesis, plant productivity and yields. *Plant Sci* **181**: 275–281
- Gilroy S, Jones DL** (2000) Through form to function: Root hair development and nutrient uptake. *Trends Plant Sci* **5**: 56–60
- Givan C** (1999) Evolving concepts in plant glycolysis: two centuries of progress. *Biol Rev* **74**: 277–309
- Godin J-P, Fay L-B, Hopfgartner G** (2007) Liquid chromatography combined with mass spectrometry for ^{13}C isotopic analysis in life science research. *Mass Spectrom Rev* **26**:

751–774

- Goff SA** (1999) Rice as a model for cereal genomics. *Curr Opin Plant Biol* **2**: 86–89
- Grafahrend-Belau E, Junker A, Eschenroder A, Muller J, Schreiber F, Junker BH** (2013) Multiscale metabolic modeling: Dynamic flux balance analysis on a whole-plant scale. *Plant Physiol* **163**: 637–647
- Griffiths RI, Manefield M, Ostle N, McNamara N, O'Donnell AG, Bailey MJ, Whiteley AS** (2004) $^{13}\text{CO}_2$ pulse labelling of plants in tandem with stable isotope probing: methodological considerations for examining microbial function in the rhizosphere. *J Microbiol Methods* **58**: 119–129
- GRiSP** (2013) Rice Almanac. doi: 10.1093/aob/mcg189
- Grossmann K, Christiansen N, Looser R, Tresch S, Hutzler J, Pollmann S, Ehrhardt T** (2012) Physionomics and metabolomics-two key approaches in herbicidal mode of action discovery. *Pest Manag Sci* **68**: 494–504
- Guo T, Fang Y** (2014) Functional organization and dynamics of the cell nucleus. *Front Plant Sci* **5**: 378
- Han Y, Chen Y, Yin S, Zhang M, Wang W** (2015) Over-expression of *TaEXPB23*, a wheat expansin gene, improves oxidative stress tolerance in transgenic tobacco plants. *J Plant Physiol* **173**: 62–71
- Harada K, Fukusaki E, Bamba T, Sato F, Kobayashi A** (2006) In vivo ^{15}N -enrichment of metabolites in suspension cultured cells and its application to metabolomics. *Biotechnol Prog* **22**: 1003–1011
- Harlan JR, Zohary D** (1966) Distribution of Wild Wheats and Barley - The present distribution of wild forms may provide clues to the regions of early cereal domestication. *Science* (80-) **153**: 1074–1080
- Hasunuma T, Harada K, Miyazawa S, Kondo A, Fukusaki E** (2010) Metabolic turnover analysis by a combination of *in vivo* C-labelling from $^{13}\text{CO}_2$ and metabolic profiling with CE-MS/MS reveals rate-limiting steps of the C3 photosynthetic pathway in *Nicotiana tabacum* leaves. *J Exp Bot* **61**: 1041–1051
- Haupt-Herting S, Klug K, Fock HP** (2001) A new approach to measure gross CO_2 fluxes in leaves. Gross CO_2 assimilation, photorespiration, and mitochondrial respiration in the light in tomato under drought stress. *Plant Physiol* **126**: 388–396
- Häusler RE, Ludewig F, Krueger S** (2014) Amino acids - A life between metabolism and signaling. *Plant Sci* **229**: 225–237
- Heinze E, Yuan Y, Kumar S, Wittmann C, Gehre M, Richnow H-H, Wehrung P, Adam P, Albrecht P** (2008) Analysis of ^{13}C labeling enrichment in microbial culture applying metabolic tracer experiments using gas chromatography-combustion-isotope ratio mass spectrometry. *Anal Biochem* **380**: 202–210
- Heise R, Arrivault S, Szecowka M, Tohge T, Nunes-Nesi A, Stitt M, Nikoloski Z, Fernie AR** (2014) Flux profiling of photosynthetic carbon metabolism in intact plants. *Nat Protoc* **9**: 1803–1024
- Hiei Y, Ohta S, Komari T, Kumashiro T** (1994) Efficient transformation of rice (*Oryza sativa* L.) mediated by *Agrobacterium* and sequence analysis of the boundaries of the T-DNA. *Plant J* **6**: 271–282
- Hildebrandt TM, Nunes Nesi A, Araújo WL, Braun H-P** (2015) Amino Acid Catabolism in Plants. *Mol Plant* **8**: 1563–1579
- Hoang TML, Moghaddam L, Williams B, Khanna H, Dale J, Mundree SG** (2015) Development of salinity tolerance in rice by constitutive-overexpression of genes involved

- in the regulation of programmed cell death. *Front Plant Sci* **6**: 175
- Hoefnagel MHN, Hoefnagel MHN, Atkin OK, Atkin OK, Wiskich JT, Wiskich JT** (1998) Interdependence between chloroplasts and mitochondria in the light and the dark. *Biochim Biophys Acta* **1366**: 235–255
- Hölscher D, Shroff R, Knop K, Gottschaldt M, Crecelius A, Schneider B, Heckel DG, Schubert US, Svatoš A** (2009) Matrix-free UV-laser desorption/ionization (LDI) mass spectrometric imaging at the single-cell level: Distribution of secondary metabolites of *Arabidopsis thaliana* and *Hypericum* species. *Plant J* **60**: 907–918
- Houmar NM, Mainville JL, Bonin CP, Huang S, Luethy MH, Malvar TM** (2007) High-lysine corn generated by endosperm-specific suppression of lysine catabolism using RNAi. *Plant Biotechnol J* **5**: 605–614
- Hu J, Baker A, Bartel B, Linka N, Mullen RT, Reumann S, Zolman BK** (2012) Plant peroxisomes: Biogenesis and function. *Plant Cell* **24**: 2279–2303
- Huang S, Frizzi A, Florida CA, Kruger DE, Luethy MH** (2006) High lysine and high tryptophan transgenic maize resulting from the reduction of both 19- and 22-kD α -zeins. *Plant Mol Biol* **61**: 525–535
- Huege J, Sulpice R, Gibon Y, Lisec J, Koehl K, Kopka J** (2007) GC-EI-TOF-MS analysis of in vivo carbon-partitioning into soluble metabolite pools of higher plants by monitoring isotope dilution after $^{13}\text{C}_2$ labelling. *Phytochemistry* **68**: 2258–2272
- Hurkman WJ, Tanaka CK** (1986) Solubilization of plant membrane proteins for analysis by two-dimensional gel electrophoresis. *Plant Physiol* **81**: 802–806
- Hutchings D, Rawsthorne S, Emes MJ** (2005) Fatty acid synthesis and the oxidative pentose phosphate pathway in developing embryos of oilseed rape (*Brassica napus* L.). *J Exp Bot* **56**: 577–585
- International Rice Genome Sequencing Project** (2005) The map-based sequence of the rice genome. *Nature* **436**: 793–800
- IRRI** (2015a) IRRI research - Why rice? <http://irri.org/our-work/research>
- IRRI** (2015b) Herbicide-resistant rice. <http://irri.org/news/hot-topics/herbicide-resistant>
- Ishihara A, Hashimoto Y, Tanaka C, Dubouzet JG, Nakao T, Matsuda F, Nishioka T, Miyagawa H, Wakasa K** (2008) The tryptophan pathway is involved in the defense responses of rice against pathogenic infection via serotonin production. *Plant J* **54**: 481–495
- Itoh JI, Nonomura KI, Ikeda K, Yamaki S, Inukai Y, Yamagishi H, Kitano H, Nagato Y** (2005) Rice plant development: From zygote to spikelet. *Plant Cell Physiol* **46**: 23–47
- Iyer V, Sriram G, Fulton DB, Zhou R, Westgate ME, Shanks J** (2008) Metabolic flux maps comparing the effect of temperature on protein and oil biosynthesis in developing soybean cotyledons. *Plant, Cell Environ* **31**: 506–517
- Jensen PE, Leister D** (2014) Chloroplast evolution, structure and functions. *F1000Prime Rep* **6**: 1–14
- Jeong JS, Kim YS, Baek KH, Jung H, Ha S-H, Do Choi Y, Kim M, Reuzeau C, Kim J-K** (2010) Root-specific expression of *OsNAC10* improves drought tolerance and grain yield in rice under field drought conditions. *Plant Physiol* **153**: 185–197
- Ji Q, Xu X, Wang K** (2013) Genetic transformation of major cereal crops. *Int J Dev Biol* **57**: 495–508
- Jiang SY, Ma A, Ramamoorthy R, Ramachandran S** (2013) Genome-wide survey on genomic variation, expression divergence, and evolution in two contrasting rice genotypes under high salinity stress. *Genome Biol Evol* **5**: 2032–2050

- Johnson AAT, Kyriacou B, Callahan DL, Carruthers L, Stangoulis J, Lombi E, Tester M** (2011) Constitutive overexpression of the OsNAS gene family reveals single-gene strategies for effective iron- and zinc-biofortification of rice endosperm. *PLoS One*. doi: 10.1371/journal.pone.0024476
- Johnson DHJ, Guerino JJ, Ortlip CJ, Quakenbush LS** (1999) EP0913089 - Synergistic herbicidal composition containing R-imazethapyr and R-imazapyr and method for controlling weeds therewith.
- Jun JH, Song Z, Liu Z, Nikolau BJ, Yeung ES, Lee YJ** (2010) High-spatial and high-mass resolution imaging of surface metabolites of *Arabidopsis thaliana* by laser desorption-ionization mass spectrometry using colloidal silver. *Anal Chem* **82**: 3255–3265
- Junker A, Muraya MM, Weigelt-Fischer K, Arana-Ceballos F, Klukas C, Melchinger AE, Meyer RC, Riewe D, Altmann T** (2015) Optimizing experimental procedures for quantitative evaluation of crop plant performance in high throughput phenotyping systems. *Front Plant Sci* **5**: 770
- Junker BH** (2014) Flux analysis in plant metabolic networks: Increasing throughput and coverage. *Curr Opin Biotechnol* **26**: 183–188
- Junker BH, Klukas C, Schreiber F** (2006) VANTED: A system for advanced data analysis and visualization in the context of biological networks. *BMC Bioinformatics* **7**: 109
- Kader MA, Lindberg S** (2010) Cytosolic calcium and pH signaling in plants under salinity stress. *Plant Signal Behav* **5**: 233–238
- Karasek FW, Clement RE** (2003) *Basic Gas Chromatography-Mass Spectrometry Principles and Techniques*, 3rd ed. Elsevier Science B.V., Amsterdam
- Karki S, Rizal G, Quick WP** (2013) Improvement of photosynthesis in rice (*Oryza sativa* L.) by inserting the C4 pathway. *Rice (N Y)* **6**: 28
- Kato M, Kobayashi K, Ogiso E, Yokoo M** (2004) Photosynthesis and dry-matter production during ripening stage in a female-sterile line of rice. *Plant Prod Sci* **7**: 184–188
- Kawasaki S, Borchert C, Deyholos M, Wang H, Brazille S, Kawai K, Galbraith D, Bohnert HJ** (2001) Gene expression profiles during the initial phase of salt stress in rice. *Plant Cell* **13**: 889–905
- Kebeish R, Niessen M, Thiruveedhi K, Bari R, Hirsch H-J, Rosenkranz R, Stähler N, Schönfeld B, Kreuzaler F, Peterhänsel C** (2007) Chloroplastic photorespiratory bypass increases photosynthesis and biomass production in *Arabidopsis thaliana*. *Nat Biotechnol* **25**: 593–599
- Keegstra K** (2010) Plant cell walls. *Plant Physiol* **154**: 483–486
- Khush G** (2003) Productivity improvements in rice. *Nutr Rev* **61**: 114–116
- Kim DW, Rakwal R, Agrawal GK, Jung YH, Shibato J, Jwa NS, Iwahashi Y, Iwahashi H, Kim DH, Shim IS, et al** (2005) A hydroponic rice seedling culture model system for investigating proteome of salt stress in rice leaf. *Electrophoresis* **26**: 4521–4539
- Kim HK, Choi YH, Verpoorte R** (2011) NMR-based plant metabolomics: Where do we stand, where do we go? *Trends Biotechnol* **29**: 267–275
- Kim Y-S, Kim B-G, Kim T-G, Kang T-J, Yang M-S** (2006) Expression of a cholera toxin B subunit in transgenic lettuce (*Lactuca sativa* L.) using *Agrobacterium*-mediated transformation system. *Plant Cell Tissue Organ Cult* **87**: 203–210
- Kiyomiya S, Nakanishi H, Uchida H, Tsuji A, Nishiyama S, Futatsubashi M, Tsukada H, Ishioka NS, Watanabe S, Ito T, et al** (2001) Real time visualization of ¹³N-translocation in rice under different environmental conditions using positron emitting tracer imaging system. *Plant Physiol* **125**: 1743–1753

- Kleijn RJ, Geertman JMA, Nfor BK, Ras C, Schipper D, Pronk JT, Heijnen JJ, Van Maris AJA, Van Winden WA** (2007) Metabolic flux analysis of a glycerol-overproducing *Saccharomyces cerevisiae* strain based on GC-MS, LC-MS and NMR-derived ^{13}C -labelling data. *FEMS Yeast Res* **7**: 216–231
- Klie S, Krueger S, Krall L, Giavalisco P, Flügge U-I, Willmitzer L, Steinhauser D** (2011) Analysis of the compartmentalized metabolome – a validation of the non-aqueous fractionation technique. *Front Plant Sci* **2**: 55
- Kliphuis AMJ, Klok AJ, Martens DE, Lamers PP, Janssen M, Wijffels RH** (2012) Metabolic modeling of *Chlamydomonas reinhardtii*: Energy requirements for photoautotrophic growth and maintenance. *J Appl Phycol* **24**: 253–266
- Köhler W, Schchtel G, Voleske P** (2012) *Biostatistik - Eine Einführung für Biologen und Agrarwissenschaftler*, 5th ed. doi: 10.1007/s13398-014-0173-7.2
- Kohlstedt M, Becker J, Wittmann C** (2010) Metabolic fluxes and beyond-systems biology understanding and engineering of microbial metabolism. *Appl Microbiol Biotechnol* **88**: 1065–1075
- Koubaa M, Mghaieth S, Thomasset B, Roscher A** (2012) Gas chromatography-mass spectrometry analysis of ^{13}C labeling in sugars for metabolic flux analysis. *Anal Biochem* **425**: 183–188
- Koyama ML, Levesley A, Koebner RMD, Flowers TJ, Yeo AR** (2001) Quantitative trait loci for component physiological traits determining salt tolerance in rice. *Plant Physiol* **125**: 406–422
- Krueger S, Giavalisco P, Krall L, Steinhauser M, Büssis D, Usadel B, Flügge U-I, Willmitzer L, Steinhauser D** (2011) A topological map of the compartmentalized *Arabidopsis thaliana* leaf metabolome. *PLoS One* **6**: e17806
- Kruger NJ, Huddleston JE, Le Lay P, Brown ND, Ratcliffe RG** (2007a) Network flux analysis: impact of ^{13}C -substrates on metabolism in *Arabidopsis thaliana* cell suspension cultures. *Phytochemistry* **68**: 2176–2188
- Kruger NJ, Le Lay P, Ratcliffe RG** (2007b) Vacuolar compartmentation complicates the steady-state analysis of glucose metabolism and forces reappraisal of sucrose cycling in plants. *Phytochemistry* **68**: 2189–2196
- Kruger NJ, Masakapalli SK, Ratcliffe RG** (2012) Strategies for investigating the plant metabolic network with steady-state metabolic flux analysis: Lessons from an *Arabidopsis* cell culture and other systems. *J Exp Bot* **63**: 2309–2323
- Kruger NJ, Ratcliffe RG** (2009) Insights into plant metabolic networks from steady-state metabolic flux analysis. *Biochimie* **91**: 697–702
- Kruger NJ, Ratcliffe RG** (2015) Fluxes through plant metabolic networks: measurements, predictions, insights and challenges. *Biochem J* **456**: 27–38
- Kruger NJ, Von Schaewen A** (2003) The oxidative pentose phosphate pathway: structure and organisation. *Curr Opin Plant Biol* **6**: 236–246
- Kumar GBS, Ganapathi TR, Revathi CJ, Srinivas L, Bapat VA** (2005) Expression of hepatitis B surface antigen in transgenic banana plants. *Planta* **222**: 484–493
- Kumar K, Kumar M, Kim S-R, Ryu H, Cho Y-G** (2013) Insights into genomics of salt stress response in rice. *Rice* **6**: 27
- Kurata N, Moore G, Nagamura Y, Foote T, Yano M, Minobe Y, Gale M** (1994) Conservation of genome structure between rice and wheat. *Nat Biotechnol* **12**: 276–278
- Kusuda H, Koga W, Kusano M, Oikawa A, Saito K, Hirai MY, Yoshida KT** (2015) Ectopic expression of *myo*-inositol 3-phosphate synthase induces a wide range of metabolic

- changes and confers salt tolerance in rice. *Plant Sci* **232**: 49–56
- Lalonde S, Ehrhardt DW, Frommer WB** (2005) Shining light on signaling and metabolic networks by genetically encoded biosensors. *Curr Opin Plant Biol* **8**: 574–581
- Lam H, Coschigano K, Schultz C, Melo-Oliveira R, Tjaden G, Ngai N, Hsieh M, Coruni G** (1995) Use of Arabidopsis mutants and genes to study amide amino acid biosynthesis. *7*: 887–898
- Lau W, Fischbach MA, Osbourn A, Sattely ES** (2014) Key applications of plant metabolic engineering. *PLoS Biol* **12**: e1001879
- Leake JR, Ostle NJ, Rangel-Castro JI, Johnson D** (2006) Carbon fluxes from plants through soil organisms determined by field $^{13}\text{CO}_2$ pulse-labelling in an upland grassland. *Appl Soil Ecol* **33**: 152–175
- Lee TTT, Wang MMC, Hou RCW, Chen L-J, Su R-C, Wang C-S, Tzen JTC** (2003) Enhanced methionine and cysteine levels in transgenic rice seeds by the accumulation of sesame 2S albumin. *Biosci Biotechnol Biochem* **67**: 1699–1705
- Li X, Qian Q, Fu Z, Wang Y, Xiong G, Zeng D, Wang X, Liu X, Teng S, Hiroshi F, et al** (2003) Control of tillering in rice. *Nature* **422**: 618–621
- Liang X, Zhang L, Natarajan SK, Becker DF** (2013) Proline mechanisms of stress survival. *Antioxid Redox Signal* **19**: 998–1011
- Libourel IGL, Gehan JP, Shachar-Hill Y** (2007) Design of substrate label for steady state flux measurements in plant systems using the metabolic network of *Brassica napus* embryos. *Phytochemistry* **68**: 2211–2221
- Lichtenthaler HK** (1998) The stress concept in plants: An introduction. *Ann. N. Y. Acad. Sci.*
- Liepman AH, Olsen LJ** (2003) Alanine aminotransferase homologs catalyze the glutamate:glyoxylate aminotransferase reaction in peroxisomes of Arabidopsis. *Plant Physiol* **131**: 215–227
- Lin HX, Zhu MZ, Yano M, Gao JP, Liang ZW, Su WA, Hu XH, Ren ZH, Chao DY** (2004) QTLs for Na^+ and K^+ uptake of the shoots and roots controlling rice salt tolerance. *Theor Appl Genet* **108**: 253–260
- Lin MT, Occhialini A, Andralojc PJ, Parry MAJ, Hanson MR** (2014) A faster Rubisco with potential to increase photosynthesis in crops. *Nature* **513**: 547–550
- Liu AL, Zou J, Liu CF, Zhou XY, Zhang XW, Luo GY, Chen XB** (2013) Over-expression of *OsHsfA7* enhanced salt and drought tolerance in transgenic rice. *BMB Rep* **46**: 31–36
- Liu C-W, Chang T-S, Hsu Y-K, Wang AZ, Yen H-C, Wu Y-P, Wang C-S, Lai C-C** (2014) Comparative proteomic analysis of early salt stress responsive proteins in roots and leaves of rice. *Proteomics* **14**: 1759–1775
- Liu X, Wang Z, Wang L, Wu R, Phillips J, Deng X** (2009) *LEA* 4 group genes from the resurrection plant *Boea hygrometrica* confer dehydration tolerance in transgenic tobacco. *Plant Sci* **176**: 90–98
- Long L, Gao W, Xu L, Liu M, Luo X, He X, Yang X, Zhang X, Zhu L** (2014) *GbMPK3*, a mitogen-activated protein kinase from cotton, enhances drought and oxidative stress tolerance in tobacco. *Plant Cell Tissue Organ Cult* **116**: 153–162
- Long SP, Marshall-Colon A, Zhu X-G** (2015) Meeting the global food demand of the future by engineering crop photosynthesis and yield potential. *Cell* **161**: 56–66
- Long SP, Zhu XG, Naidu SL, Ort DR** (2006) Can improvement in photosynthesis increase crop yields? *Plant, Cell Environ* **29**: 315–330
- Lonien J, Schwender J** (2009) Analysis of metabolic flux phenotypes for two Arabidopsis

- mutants with severe impairment in seed storage lipid synthesis. *Plant Physiol* **151**: 1617–1634
- Lou X-M, Yao Q-H, Zhang Z, Peng R-H, Xiong A-S, Wang H-K** (2007) Expression of the human hepatitis B virus large surface antigen gene in transgenic tomato plants. *Clin Vaccine Immunol* **14**: 464–469
- Lunn JE** (2007) Compartmentation in plant metabolism. *J Exp Bot* **58**: 35–47
- Ma F, Jazmin LJ, Young JD, Allen DK** (2014) Isotopically nonstationary ^{13}C flux analysis of changes in *Arabidopsis thaliana* leaf metabolism due to high light acclimation. *Proc Natl Acad Sci U S A* **111**: 16967–16972
- Maas EV, Hoffman GJ** (1977) Crop salt tolerance - current assessment. *J Irrig Drain Div* **103**: 115–134
- MacDonald MJ** (1995) Feasibility of a mitochondrial pyruvate malate shuttle in pancreatic islets. *J Biol Chem* **270**: 20051–20058
- Makino A, Mae T, Ohira K** (1984) Relation between nitrogen and ribulose-1,5-bisphosphate carboxylase in rice leaves from emergence through senescence. *Plant Cell Physiol* **25**: 429–437
- Maliga P, Graham I** (2004) Plant biotechnology: Molecular farming and metabolic engineering promise a new generation of high-tech crops. *Curr Opin Plant Biol* **7**: 149–151
- Mandy DE, Goldford JE, Yang H, Allen DK, Libourel IGL** (2014) Metabolic flux analysis using ^{13}C peptide label measurements. *Plant J* **77**: 476–486
- Mao B, Liu X, Hu D, Li D** (2013) Co-expression of RCH10 and AGLU1 confers rice resistance to fungal sheath blight *Rhizoctonia solani* and blast *Magnorpatha oryzae* and reveals impact on seed germination. *World J Microbiol Biotechnol* **30**: 1229–1238
- Martzolff A, Cahoreau E, Cogne G, Peyriga L, Portais JC, Dechandol E, Le Grand F, Massou S, Gonçalves O, Pruvost J, et al** (2012) Photobioreactor design for isotopic non-stationary ^{13}C -metabolic flux analysis (INST ^{13}C -MFA) under photoautotrophic conditions. *Biotechnol Bioeng* **109**: 3030–3040
- Masakapalli SK, Bryant FM, Kruger NJ, Ratcliffe RG** (2013) The metabolic flux phenotype of heterotrophic *Arabidopsis* cells reveals a complex response to changes in nitrogen supply. *Plant J* **74**: 569–582
- Masakapalli SK, Bryant FM, Kruger NJ, Ratcliffe RG** (2014a) The metabolic flux phenotype of heterotrophic *Arabidopsis* cells reveals a flexible balance between the cytosolic and plastidic contributions to carbohydrate oxidation in response to phosphate limitation. *Plant J* **78**: 964–977
- Masakapalli SK, Le Lay P, Huddleston JE, Pollock NL, Kruger NJ, Ratcliffe RG** (2010) Subcellular flux analysis of central metabolism in a heterotrophic *Arabidopsis* cell suspension using steady-state stable isotope labeling. *Plant Physiol* **152**: 602–619
- Masakapalli SK, Ritala A, Dong L, Van Der Krol AR, Oksman-Caldentey KM, Ratcliffe RG, Sweetlove LJ** (2014b) Metabolic flux phenotype of tobacco hairy roots engineered for increased geraniol production. *Phytochemistry* **99**: 73–85
- Masuda H, Aung MS, Nishizawa NK** (2013) Iron biofortification of rice using different transgenic approaches. *Rice (N Y)* **6**: 40
- Matros A, Mock H-P** (2013) Mass spectrometry based imaging techniques for spatially resolved analysis of molecules. *Front Plant Sci* **4**: 89
- Matsuda F, Morino K, Ano R, Kuzawa M, Wakasa K, Miyagawa H** (2005) Metabolic flux analysis of the phenylpropanoid pathway in wound-healing potato tuber tissue using stable isotope-labeled tracer and LC-MS spectroscopy. *Plant Cell Physiol* **46**: 454–466

- McGarvey PB, Hammond J, Dienelt MM, Hooper DC, Fu ZF, Dietzschold B, Koprowski H, Michaels FH** (1995) Expression of the rabies virus glycoprotein in transgenic tomatoes. *Nature* **13**: 1484–1487
- McGrath JM, Long SP** (2014) Can the cyanobacterial carbon-concentrating mechanism increase photosynthesis in crop species? A theoretical analysis. *Plant Physiol* **164**: 2247–2261
- McNeil SD, Nuccio ML, Rhodes D, Shachar-Hill Y, Hanson AD** (2000) Radiotracer and computer modeling evidence that phospho-base methylation is the main route of choline synthesis in tobacco. *Plant Physiol* **123**: 371–380
- Meier-Augenstein W** (1999a) Applied gas chromatography coupled to isotope ratio mass spectrometry. *J Chromatogr A* **842**: 351–371
- Meier-Augenstein W** (1999b) Use of gas chromatography-combustion-isotope ratio mass spectrometry in nutrition and metabolic research. *Curr Opin Clin Nutr Metab Care* **2**: 465–470
- Meng F, Dungait JAJ, Zhang X, He M, Guo Y, Wu W** (2013) Investigation of photosynthate-C allocation 27 days after ^{13}C -pulse labeling of *Zea mays* L. at different growth stages. *Plant Soil* **373**: 755–764
- Misra SC, Randive R, Rao VS, Sheshshayee MS, Serraj R, Monneveux P** (2006) Relationship between carbon isotope discrimination, ash content and grain yield in wheat in the peninsular zone of India. *J Agron Crop Sci* **192**: 352–362
- Moldenhauer K, Slaton N** (2001) Rice growth and development. *In* N Slaton, ed, *Rice Prod. Handb. Coop. Ext. Service, University of Arkansas, Little Rock*, pp 7–14
- Molero G, Aranjuelo I, Teixidor P, Araus JL, Nogués S** (2011) Measurement of ^{13}C and ^{15}N isotope labeling by gas chromatography/combustion/isotope ratio mass spectrometry to study amino acid fluxes in a plant-microbe symbiotic association. *Rapid Commun mass Spectrom* **25**: 599–607
- Molina J, Sikora M, Garud N, Flowers JM, Rubinstein S, Reynolds A, Huang P, Jackson S, Schaal BA, Bustamante CD, et al** (2011) Molecular evidence for a single evolutionary origin of domesticated rice. *Proc Natl Acad Sci U S A* **108**: 8351–8356
- Monton MRN, Soga T** (2007) Metabolome analysis by capillary electrophoresis-mass spectrometry. *J Chromatogr A* **1168**: 237–246
- Munns R, James RA, Läuchli A** (2006) Approaches to increasing the salt tolerance of wheat and other cereals. *J Exp Bot* **57**: 1025–1043
- Munns R, Tester M** (2008) Mechanisms of salinity tolerance. *Annu Rev Plant Biol* **59**: 651–81
- Murashige T, Skoog F** (1962) A revised medium for rapid growth and bio assays with tobacco tissue cultures. *Physiol Plant* **15**: 473–497
- Murray MG, Thompson WF** (1980) Rapid isolation of high molecular weight plant DNA. *Nucleic Acids Res* **8**: 4321–4325
- Nargund S, Sriram G** (2013) Designer labels for plant metabolism: statistical design of isotope labeling experiments for improved quantification of flux in complex plant metabolic networks. *Mol Biosyst* **9**: 99–112
- Ngounou Wetie AG, Sokolowska I, Woods AG, Wormwood KL, Dao S, Patel S, Clarkson BD, Darie CC** (2012) Automated mass spectrometry-based functional assay for the routine analysis of the secretome. *J Lab Autom* **18**: 19–29
- Nochi T, Takagi H, Yuki Y, Yang L, Masumura T, Mejima M, Nakanishi U, Matsumura A, Uozumi A, Hiroi T, et al** (2007) Rice-based mucosal vaccine as a global strategy for cold-chain- and needle-free vaccination. *Proc Natl Acad Sci U S A* **104**: 10986–10991

- Noguchi K, Yoshida K** (2008) Interaction between photosynthesis and respiration in illuminated leaves. *Mitochondrion* **8**: 87–99
- Nöh K, Wiechert W** (2011) The benefits of being transient: isotope-based metabolic flux analysis at the short time scale. *Appl Microbiol Biotechnol* **91**: 1247–1265
- Nölke G, Fischer R, Schillberg S** (2003) Production of therapeutic antibodies in plants. *Curr Top Microbiol Immunol* **3**: 1153–1162
- Nouchi I, Ito O, Harazono Y, Kouchi H** (1994) Acceleration of ^{13}C labelled photosynthate partitioning from leaves to panicles in rice plants exposed to chronic ozone at the reproductive stage. *Environ Pollut* **88**: 253–260
- Nunes-Nesi A, Sulpice R, Gibon Y, Fernie AR** (2008) The enigmatic contribution of mitochondrial function in photosynthesis. *J Exp Bot* **59**: 1675–1684
- Núñez O, Gallart-Ayala H, Martins CPB, Lucci P, Busquets R** (2013) State-of-the-art in fast liquid chromatography-mass spectrometry for bio-analytical applications. *J Chromatogr B* **927**: 3–21
- O’Grady J, Schwender J, Shachar-Hill Y, Morgan JA** (2012) Metabolic cartography: experimental quantification of metabolic fluxes from isotopic labelling studies. *J Exp Bot* **63**: 2293–2308
- Obata T, Kitamoto HK, Nakamura A, Fukuda A, Tanaka Y** (2007) Rice shaker potassium channel OsKAT1 confers tolerance to salinity stress on yeast and rice cells. *Plant Physiol* **144**: 1978–1985
- Oerke E-C** (2006) Crop losses to pests. *J Agric Sci* **144**: 31–43
- Ohta M, Hayashi Y, Nakashima A, Hamada A, Tanaka A, Nakamura T, Hayakawa T** (2002) Introduction of a Na^+/H^+ antiporter gene from the halophyte *Atriplex gmelini* confers salt tolerance to rice. *FEBS Lett* **532**: 279–282
- Okumoto S, Takanaga H, Frommer WB** (2008) Quantitative imaging for discovery and assembly of the metabo-regulome. *New Phytol* **180**: 271–295
- Osaki M, Shinano T** (2001) Plant growth based on interrelation between carbon and nitrogen translocation from leaves. *Photosynthetica* **39**: 197–203
- Padmasree K, Padmavathi L, Raghavendra AS** (2002) Essentiality of mitochondrial oxidative metabolism for photosynthesis: optimization of carbon assimilation and protection against photoinhibition. *Crit Rev Biochem Mol Biol* **37**: 71–119
- Pan Z, Raftery D** (2007) Comparing and combining NMR spectroscopy and mass spectrometry in metabolomics. *Anal Bioanal Chem* **387**: 525–527
- Panda D, Sarkar RK** (2013) Natural leaf senescence: Probed by chlorophyll fluorescence, CO_2 photosynthetic rate and antioxidant enzyme activities during grain filling in different rice cultivars. *Physiol Mol Biol Plants* **19**: 43–51
- Parker R, Flowers TJ, Moore AL, Harpham NVJ** (2006) An accurate and reproducible method for proteome profiling of the effects of salt stress in the rice leaf lamina. *J Exp Bot* **57**: 1109–1118
- Pattanagul W, Thitisaksakul M** (2008) Effect of salinity stress on growth and carbohydrate metabolism in three rice (*Oryza sativa* L.) cultivars differing in salinity tolerance. *Indian J Exp Biol* **46**: 736–742
- Perea Arango I, Loza Rubio E, Rojas Anaya E, Olivera Flores T, Gonzalez De La Vara L, Gómez Lim MA** (2008) Expression of the rabies virus nucleoprotein in plants at high-levels and evaluation of immune responses in mice. *Plant Cell Rep* **27**: 677–685
- Peterhansel C, Niessen M, Kebeish RM** (2008) Metabolic engineering towards the enhancement of photosynthesis. *Photochem Photobiol* **84**: 1317–1323

- Peuke AD, Hartung W, Jeschke WD** (1994) The uptake and flow of C, N and ions between roots and shoots in *Ricinus communis* L. II. Grown with low or high nitrate supply. *J Exp Bot* **45**: 733–740
- Plaxton WC** (1996) The organization and regulation of plant glycolysis. *Annu Rev Plant Physiol Plant Mol Biol* **47**: 185–214
- Plaxton WC, Podestá FE** (2006) The functional organization and control of plant respiration. *CRC Crit Rev Plant Sci* **25**: 159–198
- Price GD, Pengelly JJJ, Forster B, Du J, Whitney SM, von Caemmerer S, Badger MR, Howitt SM, Evans JR** (2013) The cyanobacterial CCM as a source of genes for improving photosynthetic CO₂ fixation in crop species. *J Exp Bot* **63**: 695–709
- Rae BD, Long BM, Whitehead LF, Förster B, Badger MR, Price GD** (2013) Cyanobacterial carboxysomes: Microcompartments that facilitate CO₂ fixation. *J Mol Microbiol Biotechnol* **23**: 300–307
- Ramírez YJP, Tasciotti E, Gutierrez-Ortega A, Donayre Torres AJ, Olivera Flores MT, Giacca M, Gómez Lim MÁ** (2007) Fruit-specific expression of the human immunodeficiency virus type 1 Tat gene in tomato plants and its immunogenic potential in mice. *Clin Vaccine Immunol* **14**: 685–692
- Rasmusson AG, Soole KL, Elthon TE** (2004) Alternative NAD(P)H dehydrogenases of plant mitochondria. *Annu Rev Plant Biol* **55**: 23–39
- Ratcliffe RG, Shachar-Hill Y** (2006) Measuring multiple fluxes through plant metabolic networks. *Plant J* **45**: 490–511
- Rawson BHM, Hofstra G** (1969) Translocation and remobilization of ¹⁴C assimilated at different stages by each leaf of the wheat plant. *Aust J Biol Sci* **22**: 321–331
- Richter EK, Spangenberg JE, Kreuzer M, Leiber F** (2010) Characterization of rapeseed (*Brassica napus*) oils by bulk C, O, H, and fatty acid C stable isotope analyses. *J Agric Food Chem* **58**: 8048–8055
- Ritte G** (2010) ERA-Net PlantGenomics - Verbundvorhaben: Trilaterale Initiative zur Steigerung der Salztoleranz in Reis. Veröffentlichung der Ergebnisse von Forschungsvorhaben im Bmbf-progr. Biol.
- Roessner U, Wagner C, Kopka J, Trethewey RN, Willmitzer L** (2000) Simultaneous analysis of metabolites in potato tuber by gas chromatography-mass spectrometry. *Plant J* **23**: 131–142
- Roessner-Tunali U, Liu J, Leisse A, Balbo I, Perez-Melis A, Willmitzer L, Fernie AR** (2004) Kinetics of labelling of organic and amino acids in potato tubers by gas chromatography-mass spectrometry following incubation in ¹³C labelled isotopes. *Plant J* **39**: 668–679
- Roitsch T** (1999) Source-sink regulation by sugar and stress. *Curr Opin Plant Biol* **2**: 198–206
- Römisch-Margl W, Schramek N, Radykewicz T, Ettenhuber C, Eylert E, Huber C, Römisch-Margl L, Schwarz C, Dobner M, Demmel N, et al** (2007) ¹³CO₂ as a universal metabolic tracer in isotopologue perturbation experiments. *Phytochemistry* **68**: 2273–2289
- Rontein D, Dieuaide-Noubhani M, Dufourc EJ, Raymond P, Rolin D** (2002) The metabolic architecture of plant cells. Stability of central metabolism and flexibility of anabolic pathways during the growth cycle of tomato cells. *J Biol Chem* **277**: 43948–43960
- Roscher A, Emsley L, Raymond P, Roby C** (1998) Unidirectional steady state rates of central metabolism enzymes measured simultaneously in a living plant tissue. *J Biol Chem* **273**: 25053–25061
- Roscher A, Kruger NJ, Ratcliffe RG** (2000) Strategies for metabolic flux analysis in plants

- using isotope labelling. *J Biotechnol* **77**: 81–102
- Rosenthal DM, Locke AM, Khozaei M, Raines CA, Long SP, Ort DR** (2011) Over-expressing the C3 photosynthesis cycle enzyme Sedoheptulose-1-7 Bisphosphatase improves photosynthetic carbon gain and yield under fully open air CO₂ fumigation (FACE). *BMC Plant Biol* **11**: 123
- Roy SJ, Negrão S, Tester M** (2014) Salt resistant crop plants. *Curr Opin Biotechnol* **26**: 115–124
- Royuela M, Gonzalez A, Gonzalez EM, Arrese-Igor C, Aparicio-Tejo PM, Gonzalez-Murua C** (2000) Physiological consequences of continuous, sublethal imazethapyr supply to pea plants. *J Plant Physiol* **157**: 345–354
- Rubio-Infante N, Govea-Alonso DO, Romero-Maldonado A, García-Hernández AL, Ilhuicatzí-Alvarado D, Salazar-González JA, Korban SS, Rosales-Mendoza S, Moreno-Fierros L** (2015) A plant-derived multi-HIV antigen induces broad immune responses in orally immunized mice. *Mol Biotechnol* **57**: 662–674
- Sahi C, Singh A, Kumar K, Blumwald E, Grover A** (2006) Salt stress response in rice : genetics, molecular biology, and comparative genomics. *Funct Integr Genomics* **6**: 263–284
- Saijo Y, Hata S, Kyojuka J, Shimamoto K, Izui K** (2000) Over-expression of a single Ca²⁺-dependent protein kinase confers both cold and salt/drought tolerance on rice plants. *Plant J* **23**: 319–327
- Sakamoto A, Murata A, Murata N** (1998) Metabolic engineering of rice leading to biosynthesis of glycinebetaine and tolerance to salt and cold. *Plant Mol Biol* **38**: 1011–1019
- Salt Tolerance Database on USDA-ARS** (2015) Relative salt tolerance of herbaceous crops. <http://www.usssl.ars.usda.gov/pls/caliche/SALTT42A>
- Sarhadi E, Bazargani MM, Sajise AG, Abdolahi S, Vispo NA, Arceta M, Nejad GM, Singh RK, Salekdeh GH** (2012) Proteomic analysis of rice anthers under salt stress. *Plant Physiol Biochem* **58**: 280–287
- Sasaki T, Yano M, Kurata N** (1996) The Japanese Rice Genome Research Program. *Genome Res* **6**: 661–666
- Schädel C, Blöchl A, Richter A, Hoch G** (2010) Quantification and monosaccharide composition of hemicelluloses from different plant functional types. *Plant Physiol Biochem* **48**: 1–8
- Schaefer J, Kier LD, Stejskal EO** (1980) Characterization of photorespiration in intact leaves using carbon dioxide labeling. *Plant Physiol* **65**: 254–259
- Scheibe R, Backhausen JE, Emmerlich V, Holtgreffe S** (2005) Strategies to maintain redox homeostasis during photosynthesis under changing conditions. *J Exp Bot* **56**: 1481–1489
- Schertl P, Braun H-P** (2014) Respiratory electron transfer pathways in plant mitochondria. *Front Plant Sci* **5**: 163
- Schneider G, Lindqvist Y, Branden C** (1992) RUBISCO: Structure and Mechanism. *Annu Rev Biophys Biomol Struct* **21**: 119–143
- Schoonbeek H, Wang H, Stefanato FL, Craze M, Bowden S, Wallington E, Zipfel C, Ridout CJ** (2015) Rapid report Arabidopsis EF-Tu receptor enhances bacterial disease resistance in transgenic wheat. *New Phytol* **206**: 606–613
- Schwender J** (2008) Metabolic flux analysis as a tool in metabolic engineering of plants. *Curr Opin Biotechnol* **19**: 131–137
- Schwender J, Goffman F, Ohlrogge JB, Shachar-Hill Y** (2004) Rubisco without the Calvin cycle improves the carbon efficiency of developing green seeds. *Nature* **432**: 779–782

- Schwender J, Hay JO** (2012) Predictive Modeling of Biomass Component Tradeoffs in *Brassica napus* Developing Oilseeds Based on in Silico Manipulation of Storage Metabolism. *Plant Physiol* **160**: 1218–1236
- Schwender J, Hebbelmann I, Heinzl N, Hildebrandt TM, Rogers A, Naik D, Klapperstück M, Braun H-P, Schreiber F, Denolf P, et al** (2015) Quantitative multilevel analysis of central metabolism in developing oilseeds of oilseed rape during in vitro culture. *Plant Physiol* **168**: 828–848
- Schwender J, König C, Klapperstück M, Heinzl N, Munz E, Hebbelmann I, Hay JO, Denolf P, De Bodt S, Redestig H, et al** (2014) Transcript abundance on its own cannot be used to infer fluxes in central metabolism. *Front Plant Sci* **5**: 668
- Schwender J, Ohlrogge JB, Shachar-Hill Y** (2003) A flux model of glycolysis and the oxidative pentosephosphate pathway in developing *Brassica napus* embryos. *J Biol Chem* **278**: 29442–22453
- Schwender J, Shachar-Hill Y, Ohlrogge JB** (2006) Mitochondrial metabolism in developing embryos of *Brassica napus*. *J Biol Chem* **281**: 34040–34047
- Shachar-Hill Y** (2013) Metabolic network flux analysis for engineering plant systems. *Curr Opin Biotechnol* **24**: 247–255
- Shaner DL, Reider ML** (1986) Physiological responses of corn (*Zea mays*) to AC 243,997 in combination with valine, leucine, and isoleucine. *Pestic Biochem Physiol* **25**: 248–257
- Shaner DL, Singh BK** (1991) Imidazolinone-induced loss of acetohydroxyacid synthase activity in maize is not due to the enzyme degradation. *Plant Physiol* **97**: 1339–1341
- Sharma AK, Sharma MK** (2009) Plants as bioreactors: Recent developments and emerging opportunities. *Biotechnol Adv* **27**: 811–832
- Sharma MK, Jani D, Thungapathra M, Gautam JK, Meena LS, Singh Y, Ghosh A, Tyagi AK, Sharma AK** (2008) Expression of accessory colonization factor subunit A (ACFA) of *Vibrio cholerae* and ACFA fused to cholera toxin B subunit in transgenic tomato (*Solanum lycopersicum*). *J Biotechnol* **135**: 22–27
- Sharp RE, Poroyko V, Hejlek LG, Spollen WG, Springer GK, Bohnert HJ, Nguyen HT** (2004) Root growth maintenance during water deficits: physiology to functional genomics. *J Exp Bot* **55**: 2343–2351
- Shastri AA, Morgan JA** (2007) A transient isotopic labeling methodology for ¹³C metabolic flux analysis of photoautotrophic microorganisms. *Phytochemistry* **68**: 2302–2312
- Shimamoto K** (1995) The molecular biology of rice. *Science* (80-) **270**: 1772–1773
- Shimamoto K** (1994) Gene expression in transgenic monocots. *Curr Opin Biotechnol* **5**: 158–162
- Shimizu T, Ogamino T, Hiraguri A, Nakazono-Nagaoka E, Uehara-Ichiki T, Nakajima M, Akutsu K, Omura T, Sasaya T** (2013) Strong resistance against *Rice grassy stunt virus* is induced in transgenic rice plants expressing double-stranded RNA of the viral genes for nucleocapsid or movement proteins as targets for RNA interference. *Phytopathology* **103**: 513–519
- Shubhakar A, Reiding KR, Gardner RA, Spencer DIR, Fernandes DL, Wuhrer M** (2015) High-throughput analysis and automation for glycomics studies. *Chromatographia* **78**: 321–333
- Sienkiewicz-Porzucek A, Sulpice R, Osorio S, Krahnert I, Leisse A, Urbanczyk-Wochniak E, Hodges M, Fernie AR, Nunes-Nesi A** (2010) Mild reductions in mitochondrial NAD-dependent isocitrate dehydrogenase activity result in altered nitrate assimilation and pigmentation but do not impact growth. *Mol Plant* **3**: 156–173

- Singla-Pareek SL, Yadav SK, Pareek A, Reddy MK, Sopory SK** (2008) Enhancing salt tolerance in a crop plant by overexpression of glyoxalase II. *Transgenic Res* **17**: 171–180
- Soda N, Kushwaha HR, Soni P, Singla-Pareek SL, Pareek A** (2013) A suite of new genes defining salinity stress tolerance in seedlings of contrasting rice genotypes. *Funct Integr Genomics* **13**: 351–365
- Soh HS, Chung HY, Lee HH, Ajappala H, Jang K, Park J-H, Sim J-S, Lee GY, Lee HJ, Han YH, et al** (2015) Expression and functional validation of heat-labile enterotoxin B (LTB) and cholera toxin B (CTB) subunits in transgenic rice (*Oryza sativa*). *Springerplus* **4**: 148
- Soong JL, Reuss D, Pinney C, Boyack T, Haddix ML, Stewart CE, Cotrufo MF** (2014) Design and operation of a continuous ^{13}C and ^{15}N labeling chamber for uniform or differential, metabolic and structural, plant isotope labeling. *J Vis Exp* **16**: e51117
- Spielbauer G, Margl L, Hannah LC, Römisch W, Ettenhuber C, Bacher A, Gierl A, Eisenreich W, Genschel U** (2006) Robustness of central carbohydrate metabolism in developing maize kernels. *Phytochemistry* **67**: 1460–1475
- Sreenivasulu N, Sopory SK, Kavi Kishor PB** (2007) Deciphering the regulatory mechanisms of abiotic stress tolerance in plants by genomic approaches. *Gene* **388**: 1–13
- Sriram G, Fulton DB, Iyer V, Peterson JM, Zhou R, Westgate ME, Spalding MH, Shanks J** (2004) Quantification of compartmented metabolic fluxes in developing soybean embryos by employing biosynthetically directed fractional ^{13}C labeling, two-dimensional [^{13}C , ^1H] nuclear magnetic resonance, and comprehensive isotop. *Plant Physiol* **136**: 3043–3057
- Sriram G, Fulton DB, Shanks J** (2007a) Flux quantification in central carbon metabolism of *Catharanthus roseus* hairy roots by ^{13}C labeling and comprehensive bondomer balancing. *Phytochemist* **68**: 2243–2257
- Sriram G, Iyer V V, Fulton DB, Shanks J V** (2007b) Identification of hexose hydrolysis products in metabolic flux analytes: A case study of levulinic acid in plant protein hydrolysate. *Metab Eng* **9**: 442–451
- Staniek A, Bouwmeester H, Fraser PD, Kayser O, Martens S, Tissier A, van der Krol S, Wessjohann L, Warzecha H** (2013) Natural products - modifying metabolite pathways in plants. *Biotechnol J* **8**: 1159–1171
- Stitt M** (2013) Systems-integration of plant metabolism: Means, motive and opportunity. *Curr Opin Plant Biol* **16**: 381–388
- Storozhenko S, De Brouwer V, Volckaert M, Navarrete O, Blancquaert D, Zhang G-F, Lambert W, Van Der Straeten D** (2007) Folate fortification of rice by metabolic engineering. *Nat Biotechnol* **25**: 1277–1279
- Su J, Hirji R, Zhang L, He C, Selvaraj G, Wu R** (2006) Evaluation of the stress-inducible production of choline oxidase in transgenic rice as a strategy for producing the stress-protectant glycine betaine. *J Exp Bot* **57**: 1129–1135
- Sui N, Li M, Zhao SJ, Li F, Liang H, Meng QW** (2007) Overexpression of glycerol-3-phosphate acyltransferase gene improves chilling tolerance in tomato. *Planta* **226**: 1097–1108
- Sumiyoshi M, Nakamura A, Nakamura H, Hakata M, Ichikawa H, Hirochika H, Ishii T, Satoh S, Iwai H** (2013) Increase in cellulose accumulation and improvement of saccharification by overexpression of arabinofuranosidase in rice. *PLoS One* **8**: e78269
- Sun D, Wimmers L, Turgeon R** (1988) Scintillation counting of ^{14}C -labeled soluble and insoluble compounds in plant tissue. *Anal Biochem* **169**: 424–427
- Suzuki Y, Makino A, Mae T** (2001) An efficient method for extraction of RNA from rice leaves

- at different ages using benzyl chloride. *J Exp Bot* **52**: 1575–1579
- Sweetlove LJ, Beard KFM, Nunes-Nesi A, Fernie AR, Ratcliffe RG** (2010) Not just a circle: Flux modes in the plant TCA cycle. *Trends Plant Sci* **15**: 462–470
- Sweetlove LJ, Fernie AR** (2013) The spatial organization of metabolism within the plant cell. *Annu Rev Plant Biol* **64**: 723–746
- Szeczowka M, Heise R, Tohge T, Nunes-nesi A, Vosloh D, Huege J, Feil R, Lunn J, Nikoloski Z, Stitt M, et al** (2013) Metabolic fluxes in an illuminated *Arabidopsis* rosette. *Plant Cell* **25**: 694–714
- Szyperski T** (1998) ¹³C-NMR, MS and metabolic flux balancing in biotechnology research. *Q Rev Biophys* **31**: 41–106
- Takahashi S, Bauwe H, Badger M** (2007) Impairment of the photorespiratory pathway accelerates photoinhibition of photosystem II by suppression of repair but not acceleration of damage processes in *Arabidopsis*. *Plant Physiol* **144**: 487–494
- Takeda S, Matsuoka M** (2008) Genetic approaches to crop improvement: responding to environmental and population changes. *Nat Rev Genet* **9**: 444–457
- Tan S, Evans RR, Dahmer ML, Singh BK, Shaner DL** (2005) Imidazolinone-tolerant crops: History, current status and future. *Pest Manag Sci* **61**: 246–257
- Tanaka A, Osaki M** (1983) Growth and behavior of photosynthesized ¹⁴C in various crops in relation to productivity. *Soil Sci Plant Nutr* **29**: 147–158
- Tanaka A, Yamaguchi J** (1968) The growth efficiency in relation to the growth of the rice plant. *Soil Sci Plant Nutr* **14**: 110–116
- Tanaka Y, Hibino T, Hayashi Y, Tanaka A, Kishitani S, Takabe T, Yokota S, Takabe T** (1999) Salt tolerance of transgenic rice overexpressing yeast mitochondrial Mn-SOD in chloroplasts. *Plant Sci* **148**: 131–138
- Tcherkez G, Cornic G, Bligny R, Gout E, Ghashghaie J** (2005) In vivo respiratory metabolism of illuminated leaves. *Plant Physiol* **138**: 1596–1606
- Theerawitaya C, Boriboonkaset T, Cha-Um S, Supaibulwatana K, Kirdmanee C** (2012) Transcriptional regulations of the genes of starch metabolism and physiological changes in response to salt stress rice (*Oryza sativa* L.) seedlings. *Physiol Mol Biol Plants* **18**: 197–208
- Thrower SL** (1962) Translocation of labelled assimilates in the soybean. *Aust J Biol Sci* **15**: 629–649
- Tian D, Yin Z** (2009) Constitutive heterologous expression of *avrXa27* in rice containing the *R* gene *Xa27* confers enhanced resistance to compatible *Xanthomonas oryzae* strains. *Mol Plant Pathol* **10**: 29–39
- Tiessen A, Nerlich A, Faix B, Hümmer C, Fox S, Trafford K, Weber H, Weschke W, Geigenberger P** (2012) Subcellular analysis of starch metabolism in developing barley seeds using a non-aqueous fractionation method. *J Exp Bot* **63**: 2071–2087
- Timischl W** (2013) *Angewandte Statistik*.
- Tiwari S, Verma PC, Singh PK, Tuli R** (2009) Plants as bioreactors for the production of vaccine antigens. *Biotechnol Adv* **27**: 449–467
- Toriyama K, Heong KL, Hardy B** (2004) Rice is life: scientific perspectives for the 21st century. *Proc. World Rice Res. Conf. Tsukuba, Japan*
- Tresch S** (2013) Strategies and future trends to identify the mode of action of phytotoxic compounds. *Plant Sci* **212**: 60–71
- Tronconi MA, Gerrard Wheeler MC, Martinatto A, Zubimendi JP, Andreo CS, Drincovich**

- MF** (2015) Allosteric substrate inhibition of Arabidopsis NAD-dependent malic enzyme 1 is released by fumarate. *Phytochemistry* **111**: 37–47
- Troufflard S, Roscher A, Thomasset B, Barbotin JN, Rawsthorne S, Portais JC** (2007) *In vivo* ¹³C NMR determines metabolic fluxes and steady state in linseed embryos. *Phytochemistry* **68**: 2341–2350
- Turgeon R** (1989) The sink-source transition in leaves. *Annu Rev Plant Physiol Plant Mol Biol* **40**: 119–138
- Twyman RM, Stoger E, Schillberg S, Christou P, Fischer R** (2003) Molecular farming in plants: Host systems and expression technology. *Trends Biotechnol* **21**: 570–578
- UN Department of Economic and Social Affairs** (2015) Population Division. <http://www.un.org/en/development/desa/population/index.shtml>
- Vanderschuren H, Lentz E, Zainuddin I, Gruissem W** (2013) Proteomics of model and crop plant species: Status, current limitations and strategic advances for crop improvement. *J Proteomics* **93**: 5–19
- Vaux DL** (2014) Basic Statistics in Cell Biology. *Annu Rev Cell Dev Biol* **30**: 23–37
- Vendruscolo ECG, Schuster I, Pileggi M, Scapim CA, Molinari HBC, Marur CJ, Vieira LGE** (2007) Stress-induced synthesis of proline confers tolerance to water deficit in transgenic wheat. *J Plant Physiol* **164**: 1367–1376
- Vogeser M, Seger C** (2010) Pitfalls associated with the use of liquid chromatography-tandem mass spectrometry in the clinical laboratory. *Clin Chem* **56**: 1234–1244
- Wakasa K, Hasegawa H, Nemoto H, Matsuda F, Miyazawa H, Tozawa Y, Morino K, Komatsu A, Yamada T, Terakawa T, et al** (2006) High-level tryptophan accumulation in seeds of transgenic rice and its limited effects on agronomic traits and seed metabolite profile. *J Exp Bot* **57**: 3069–3078
- Walk TB, Looser R, Bethan B, Herold MM, Kamlage B, Schmitz O, Van Rawenzwaay B, Mellert W, Coelho PCG, Ehrhardt T, et al** (2007) Means and methods for analyzing a sample by means of chromatography-mass spectrometry.
- Wang CH, Stern I, Gilmour CM, Klungsoyr S, Reed DJ, Bialy JJ, Christensen BE, Cheldelin VH** (1958) Comparative study of glucose catabolism by the radiorespirometric method. *J Bacteriol* **76**: 207–216
- Wang H, Zhang M, Guo R, Shi D, Liu B, Lin X, Yang C** (2012a) Effects of salt stress on ion balance and nitrogen metabolism of old and young leaves in rice (*Oryza sativa* L.). *BMC Plant Biol* **12**: 194
- Wang X, Han H, Yan J, Chen F, Wei W** (2015) A new AP2/ERF transcription factor from the oil plant *Jatropha curcas* confers salt and drought tolerance to transgenic tobacco. *Appl Biochem Biotechnol* **176**: 582–597
- Wang Y, Li J** (2005) The plant architecture of rice (*Oryza sativa*). *Plant Mol Biol* **59**: 75–84
- Wang Y, Li J** (2011) Branching in rice. *Curr Opin Plant Biol* **14**: 94–99
- Wang Z, Chen Z, Cheng J, Lai Y, Wang J, Bao Y, Huang J, Zhang H** (2012b) QTL analysis of Na⁺ and K⁺ concentrations in roots and shoots under different levels of NaCl stress in rice (*Oryza sativa* L.). *PLoS One* **7**: e51202
- Ward JA, Ponnala L, Weber CA** (2012) Strategies for transcriptome analysis in nonmodel plants. *Am J Bot* **99**: 267–276
- Watanabe M, Balazadeh S, Tohge T, Erban A, Giavalisco P, Kopka J, Mueller-Roeber B, Fernie AR, Hoefgen R** (2013) Comprehensive dissection of spatiotemporal metabolic shifts in primary, secondary, and lipid metabolism during developmental senescence in Arabidopsis. *Plant Physiol* **162**: 1290–1310

- Weber APM, Linka N** (2011) Connecting the plastid: transporters of the plastid envelope and their role in linking plastidial with cytosolic metabolism. *Annu Rev Plant Biol* **62**: 53–77
- Weichert N, Hauptmann V, Menzel M, Schallau K, Gunkel P, Hertel TC, Pietzsch M, Spohn U, Conrad U** (2014) Transglutamination allows production and characterization of native-sized ELPylated spider silk proteins from transgenic plants. *Plant Biotechnol J* **12**: 265–275
- Wheeler MCG, Drincovich FM, Andreo CS, Flugge U-I, Tronconi MA, Maurino VG** (2005) A comprehensive analysis of the NADP-malic enzyme gene family of *Arabidopsis*. *Plant Physiol* **139**: 39–51
- WHO** (2015) Micronutrient deficiencies. <http://www.who.int/nutrition/topics/vad/en/>
- Wiechert W** (2001) ¹³C metabolic flux analysis. *Metab Eng* **3**: 195–206
- Wiechert W, De Graaf AA** (1996) In vivo stationary flux analysis by ¹³C labeling experiments. *Adv Biochem Eng Biotechnol* **54**: 109–154
- Wiechert W, Nöh K** (2013) Isotopically non-stationary metabolic flux analysis: complex yet highly informative. *Curr Opin Biotechnol* **24**: 979–986
- Wienkoop S, Weiss J, May P, Kempa S, Irgang S, Recuenco-Munoz L, Pietzke M, Schwemmer T, Rupprecht J, Egelhofer V, et al** (2010) Targeted proteomics for *Chlamydomonas reinhardtii* combined with rapid subcellular protein fractionation, metabolomics and metabolic flux analyses. *Mol Biosyst* **6**: 1018–1031
- Wilkinson S, Davies WJ** (2002) ABA-based chemical signalling: the co-ordination of responses to stress in plants. *Plant, Cell Environ* **25**: 195–210
- Williams TCR, Miguet L, Masakapalli SK, Kruger NJ, Sweetlove LJ, Ratcliffe RG** (2008) Metabolic network fluxes in heterotrophic *Arabidopsis* cells: Stability of the flux distribution under different oxygenation conditions. *Plant Physiol* **148**: 704–718
- Wilson JB** (1988) A review of evidence on the control of shoot:root ratio, in relation to models. *Ann Bot* **61**: 433–449
- Winnik WM, Kitchin KT** (2008) Measurement of oxidative stress parameters using liquid chromatography – tandem mass spectroscopy (LC–MS/MS). *Toxicol Appl Pharmacol* **233**: 100–106
- Wittmann C** (2007) Fluxome analysis using GC-MS. *Microb Cell Fact* **6**: 6
- Wittmann C, Heinzle E** (1999) Mass spectrometry for metabolic flux analysis. *Biotechnol Bioeng* **62**: 739–750
- Wu H, Ye H, Yao R, Zhang T, Xiong L** (2015) OsJAZ9 acts as a transcriptional regulator in jasmonate signaling and modulates salt stress tolerance in rice. *Plant Sci* **232**: 1–12
- Wu WX, Liu W, Lu HH, Chen YX, Medha D, Janice T** (2009) Use of ¹³C labeling to assess carbon partitioning in transgenic and nontransgenic (parental) rice and their rhizosphere soil microbial communities. *FEMS Microbiol Ecol* **67**: 93–102
- Xu J, Dolan MC, Medrano G, Cramer CL, Weathers PJ** (2012) Green factory: Plants as bioproduction platforms for recombinant proteins. *Biotechnol Adv* **30**: 1171–1184
- Xu K, Xu X, Fukao T, Canlas P, Maghirang-Rodriguez R, Heuer S, Ismail AM, Bailey-Serres J, Ronald PC, Mackill DJ** (2006) *Sub1A* is an ethylene-response-factor-like gene that confers submergence tolerance to rice. *Nature* **442**: 705–708
- Yamada N, Theerawitaya C, Cha-um S, Kirdmanee C, Takabe T** (2014) Expression and functional analysis of putative vacuolar Ca²⁺-transporters (CAXs and ACAs) in roots of salt tolerant and sensitive rice cultivars. *Protoplasma* **251**: 1067–1075
- Yang X-C, Hwa C-M** (2008) Genetic modification of plant architecture and variety improvement

- in rice. *Heredity (Edinb)* **101**: 396–404
- Ye X, Al-Babili S, Klöti A, Zhang J, Lucca P, Beyer P, Potrykus I** (2000) Engineering the provitamin A (β -carotene) biosynthetic pathway into (carotenoid-free) rice endosperm. *Science* **287**: 303–305
- Yoshida S** (1981) *Fundamentals of rice crop science*. IRRI Publications, Los Baños, Philippines
- Youm JW, Won YS, Jeon JH, Ryu CJ, Choi YK, Kim HC, Kim BD, Joung H, Kim HS** (2007) Oral immunogenicity of potato-derived HBsAg middle protein in BALB/c mice. *Vaccine* **25**: 577–584
- Young JD** (2014) INCA: A computational platform for isotopically nonstationary metabolic flux analysis. *Bioinformatics* **30**: 1333–1335
- Young JD, Shastri AA, Stephanopoulos G, Morgan JA** (2011) Mapping photoautotrophic metabolism with isotopically nonstationary ^{13}C flux analysis. *Metab Eng* **13**: 656–665
- Young JD, Walther JL, Antoniewicz MR, Yoo H, Stephanopoulos G** (2008) An elementary metabolite unit (EMU) based method of isotopically nonstationary flux analysis. *Biotechnol Bioeng* **99**: 686–699
- Yuan Y, Yang TH, Heinzle E** (2010) ^{13}C metabolic flux analysis for larger scale cultivation using gas chromatography-combustion-isotope ratio mass spectrometry. *Metab Eng* **12**: 392–400
- Zabalza A, van Dongen JT, Froehlich A, Oliver SN, Faix B, Gupta KJ, Schmäzlin E, Igal M, Orcaray L, Royuela M, et al** (2009) Regulation of respiration and fermentation to control the plant internal oxygen concentration. *Plant Physiol* **149**: 1087–1098
- Zabalza A, Orcaray L, Gaston S, Royuela M** (2004) Carbohydrate accumulation in leaves of plants treated with the herbicide chlorsulfuron or imazethapyr is due to a decrease in sink strength. *J Agric Food Chem* **52**: 7601–7606
- Zabalza A, Orcaray L, Igal M, Schauer N, Fernie AR, Geigenberger P, van Dongen JT, Royuela M** (2011) Unraveling the role of fermentation in the mode of action of acetolactate synthase inhibitors by metabolic profiling. *J Plant Physiol* **168**: 1568–1575
- Zhang C, Hicks GR, Raikhel N** (2014) Plant vacuole morphology and vacuolar trafficking. *Front Plant Sci* **5**: 476
- Zheng X, Chen B, Lu G, Han B** (2009) Overexpression of a NAC transcription factor enhances rice drought and salt tolerance. *Biochem Biophys Res Commun* **379**: 985–989
- Zhu X-G, Long SP, Ort DR** (2010) Improving photosynthetic efficiency for greater yield. *Annu Rev Plant Biol* **61**: 235–261
- Zimmermann M, Sauer U, Zamboni N** (2014) Quantification and Mass Isotopomer Profiling of α -Keto Acids in Central Carbon Metabolism. *Anal Chem* **86**: 3232–3237
- Zohary D, Hopf M, Weiss E** (2012) *Domestication of plants in the old world*, 4th ed. Oxford University Press, Oxford
- Zou J, Liu C, Liu A, Zou D, Chen X** (2012) Overexpression of *OsHsp17.0* and *OsHsp23.7* enhances drought and salt tolerance in rice. *J Plant Physiol* **169**: 628–635

9 Appendix

Table A9. 1 Metabolite abbreviations

Abbreviation	Full name
2PG	2-Phosphoglycerate
3PG	3-Phosphoglycerate
6PG	6-Phosphoglyconate
AcCoA	Acetyl-CoA
AKG/2OG	α -Ketoglutarate
C16	Palmitic acid
C18	Stearic acid
C20	Arachidic acid
CIT	Citrate
DHAP	Dihydroxyacetone phosphate
E4P	Erythrose 4-phosphate
F6P	Fructose 6-phosphate
FBP	Fructose 1,6-bisphosphate
FRC	Fructose
FUM	Fumarate
G6P	Glucose 6-phosphate
GAP	Glyceraldehyde 3-phosphate
GLC	Glucose
GLL6P	6-Phosphogluconolactone
GLYCER	Glycerate
GLYCO	Glycolate
GLYOX	Glyoxylate
ICIT	Isocitrate
INO	Inositol
MAL	Malate
MTHF	5,10-Methylenetetrahydrofolate
OAA	Oxaloacetate
P5P	Pentose 5-phosphate
PEP	Phosphoenolpyruvate
PYR	Pyruvate
RBP	Ribulose 1,5-bisphosphate
R5P	Ribose 5-phosphate
Ru5P	Ribulose 5-phosphate
S7P	Sedoheptulose 7-phosphate
SBP	Sedoheptulose 1,7-bisphosphate
SUC(C)	Succinate
SUCR	Sucrose

Table A9. 2 Raw data of Figure 5. 3, validation of labeling system

Enrichment values are provided as mean values ($n = 3$) and are expressed as $\delta^{13}\text{C}$ (‰). Abbreviations: SD (standard deviation), AM (arithmetic mean), d $^{13}\text{C}/^{12}\text{C}$ ($\delta^{13}\text{C}$), 10 – 180 min (time of labeling pulse).

	Description	Measured data		Corrected data		t-Test	
		AM	SD	AM	SD	Description	p-value
Time/ $^{13}\text{C}\text{O}_2$	400ppm_10min	136.29	5.97	165.74	5.97	400ppm vs 700ppm, 10 min	0.001
	400ppm_60min	1366.90	236.88	1396.35	236.88	400ppm vs 700ppm, 60 min	0.025
	400ppm_180min	2446.17	29.28	2475.62	29.28	400ppm vs 700ppm, 180 min	0.007
	700ppm_10min	294.67	26.54	324.12	26.54		
	700ppm_60min	2267.22	281.16	2267.22	281.16		
	700ppm_180min	4738.03	278.00	4767.48	278.00		
	Control	-29.45	0.16				
Number of plants	1	1145.31	0.00	1175.49	0.89	1 vs 3	0.578
	3	985.26	155.48	1015.44	155.48	1 vs 6	0.313
	6	1352.22	64.52	1382.40	64.53	1 vs 12	0.997
	12	1167.34	112.42	1197.52	112.42		
	Control	-30.18	0.89				
Impact of daytime	9:30 AM	419.95	38.10			9:30 vs 13:30	0.912
	10:30 AM	392.09	23.62			10:30 vs 13:30	0.270
	11:30 AM	472.47	18.07			11:30 vs 13:30	0.911
	12:30 AM	475.37	6.08			12:30 vs 13:30	0.906
	1:30 PM	446.17	26.50			14:30 vs 13:30	0.999
	2:30 PM	432.50	6.79			15:30 vs 13:30	1.000
	3:30 PM	438.17	21.98			16:30 vs 13:30	0.978
	4:30 PM	466.10	20.01				

Table A9. 3 Raw data of Figure 5. 5 and Figure 5. 8, comparing ¹³C with ¹⁵N labeling of rice seedlings

Enrichment values are provided as mean values ($n = 3$) and are expressed as δ -values (‰), corrected for natural labeling. Mean values \pm SD ($n = 3$) are listed. A Student's t-test was applied to determine significant differences at $P \leq 0.05$ between means of stressed and untreated plants. Abbreviations: C (unlabeled control), SD (standard deviation), AM (arithmetic mean), t0 – t48 (harvest time after labeling in hours).

Description	No treatment				Salt stress				t-Test ρ -value
	Measured data		Corrected data		Measured data		Corrected data		
	AM	SD	AM	SD	AM	SD	AM	SD	
Shoot_13C_C	-30.43	0.16			-30.43	0.16			
Shoot_13C_t0	419.30	43.49	449.73	43.49	369.20	8.62	399.63	8.62	0.122
Shoot_13C_t2	283.14	11.31	313.57	11.31	247.79	20.30	278.21	20.30	0.058
Shoot_13C_t4	258.19	10.48	288.62	10.48	219.21	40.46	249.64	40.46	0.182
Shoot_13C_t24	160.11	7.59	190.54	7.59	134.04	18.72	164.46	18.72	0.089
Shoot_13C_t48	106.79	8.65	137.22	8.65	115.39	4.13	145.81	4.14	0.196
Shoot_15N_C	-5.80	0.30			-5.80	0.30			
Shoot_15N_t0	181.09	22.71	211.51	22.71	28.92	6.12	59.35	6.13	0.000
Shoot_15N_t2	742.06	20.75	772.49	20.76	305.72	36.71	336.14	36.72	0.000
Shoot_15N_t4	722.59	26.59	753.02	26.59	368.36	140.30	398.79	140.30	0.013
Shoot_15N_t24	658.58	70.38	689.01	70.38	272.93	39.75	303.36	39.75	0.001
Shoot_15N_t48	597.10	31.45	627.53	31.46	362.02	20.14	392.45	20.14	0.000
Root_13C_C	-27.45	0.50			-27.45	0.50			
Root_13C_t0	-13.34	3.09	14.11	3.13	-22.33	0.61	5.12	0.79	0.008
Root_13C_t2	152.70	32.41	180.15	32.42	171.48	26.73	198.94	26.73	0.482
Root_13C_t4	142.99	9.03	170.44	9.05	134.08	41.64	161.53	41.65	0.736
Root_13C_t24	131.21	13.92	158.67	13.92	76.78	29.49	104.23	29.49	0.045
Root_13C_t48	91.85	5.01	119.30	5.03	80.19	8.65	107.64	8.67	0.113
Root_15N_C	17.10	21.19			17.10	21.19			
Root_15N_t0	4157.95	24.26	4185.41	32.21	2464.35	159.35	2491.81	160.75	0.000
Root_15N_t2	767.91	17.10	795.36	27.23	865.69	52.90	893.15	56.99	0.038
Root_15N_t4	663.40	14.90	690.85	25.90	585.29	129.77	612.75	131.49	0.359
Root_15N_t24	588.31	44.34	615.76	49.14	448.40	63.10	475.86	66.56	0.035
Root_15N_t48	480.55	38.43	508.00	43.89	410.71	23.33	438.16	31.52	0.055

Table A9. 4 Raw data of Figure 5. 6, comparing ^{13}C labeling of seedlings grown on soil with seedlings grown on hydroponic medium

Enrichment values are provided as mean values ($n = 3$) and are expressed as atom percent excess, corrected for natural isotopes. Normalised values were used for graphical representation. Values were normalised to the highest value of the data set (Soil, Phe, t24), which was set 100%. Negative values were set zero. Student's t-test was performed to assess significant differences between amino acid mean values of seedlings grown on soil and hydroponically grown seedlings at $P \leq 0.05$. Abbreviations: Soil (soil-grown plants), Hydr (hydroponically grown plants), SD (standard deviation), AM (arithmetic mean), C (Control), $\delta^{13}\text{C}/12\text{C}$ ($\delta^{13}\text{C}$), t0 – t48 (harvest time after labeling in hours), I to III (number of biological replicate), at% (atom percent), APE (atom percent excess), Norm (%) (normalised values expressed in percent). Amino acid abbreviations are corresponding to three letter code.

	Soil					Hydroponic					t-Test <i>p</i> -value	
	d $^{13}\text{C}/^{12}\text{C}$ (‰)		APE (%)		Norm (%)	d $^{13}\text{C}/^{12}\text{C}$ (‰)		APE (%)		Norm (%)		
AS	AM	SD	AM	SD	Norm (%)	AM	SD	AM	SD	Norm (%)		
t0	Ala	-8.20	2.93	0.024	0.003	22.78	-16.58	1.34	0.016	0.001	15.23	0.023
	Gly	-8.43	0.95	0.024	0.001	22.70	-5.15	0.72	0.028	0.001	26.40	0.014
	Val	-30.32	0.62	0.004	0.001	3.63	-31.81	1.06	0.004	0.001	3.51	0.835
	Leu	-22.83	1.56	0.013	0.002	12.30	-28.65	0.61	0.008	0.001	7.32	0.013
	Ile	-28.70	0.17	0.006	0.000	5.20	-30.49	1.02	0.004	0.001	3.67	0.054
	Pro	-35.71	0.48	-0.004	0.001	-3.56	-36.21	1.03	-0.003	0.001	-3.22	0.687
	Ser	-13.74	0.90	0.022	0.001	20.59	-2.48	1.27	0.033	0.001	30.45	0.000
	Thr	-37.94	0.92	-0.004	0.001	-3.42	-34.80	0.84	-0.002	0.001	-2.05	0.131
	Phe	-15.21	6.37	0.024	0.007	22.10	-20.31	0.25	0.016	0.000	14.76	0.155
	Asp	-24.88	2.36	0.010	0.003	9.43	-28.63	0.28	0.004	0.000	3.91	0.008
	Glu	-33.72	0.38	0.000	0.000	0.46	-33.65	0.57	-0.002	0.001	-2.11	0.004
	Lys	-23.58	2.37	0.011	0.003	10.41	-27.68	0.37	0.005	0.000	4.40	0.015
	His	-9.34	5.05	0.024	0.006	22.23	-19.15	0.30	0.014	0.000	12.85	0.026
Tyr						-21.18	0.19	0.012	0.000	11.22		
t2	Ala	14.20	2.44	0.049	0.003	45.62	8.33	1.35	0.044	0.001	40.65	0.236
	Gly	8.99	1.17	0.043	0.001	40.47	2.80	0.45	0.037	0.000	34.51	0.074
	Val	1.79	1.55	0.039	0.002	36.40	-7.40	1.82	0.030	0.002	28.42	0.047
	Leu	13.27	0.95	0.053	0.001	49.14	-2.39	0.78	0.037	0.001	34.12	0.005

	Soil					Hydroponic						
	d 13C/12C (‰)		APE (%)		Norm (%)	d 13C/12C (‰)		APE (%)		Norm (%)	t-Test	
AS	AM	SD	AM	SD		AM	SD	AM	SD		p-value	
Ile	-7.92	1.17	0.028	0.001	26.41	-15.39	0.86	0.020	0.001	19.09	0.015	
Pro	-24.14	0.86	0.009	0.001	8.25	-28.61	0.66	0.005	0.001	4.54	0.011	
Ser	3.91	1.06	0.041	0.001	38.60	1.18	1.11	0.037	0.001	34.19	0.165	
Thr	-18.71	1.96	0.017	0.002	16.22	-25.89	1.03	0.008	0.001	7.04	0.004	
Phe	28.28	1.61	0.071	0.002	66.48	14.45	0.39	0.054	0.000	50.22	0.012	
Asp	-11.01	1.95	0.025	0.002	23.59	-20.18	0.89	0.013	0.001	12.53	0.004	
Glu	-19.04	2.05	0.017	0.002	15.43	-25.72	0.74	0.006	0.001	5.98	0.003	
Lys	-5.99	1.25	0.030	0.001	28.37	-14.68	0.76	0.019	0.001	17.66	0.004	
His	1.32	0.69	0.035	0.001	33.11	5.27	0.24	0.040	0.000	37.76	0.069	
Tyr	11.01	0.90	0.048	0.001	44.92	4.17	0.70	0.040	0.001	37.09	0.041	
t4	Ala	24.49	1.10	0.060	0.001	56.12	14.50	0.31	0.050	0.000	46.94	0.023
	Gly	11.69	1.17	0.046	0.001	43.23	8.77	2.39	0.043	0.003	40.61	0.331
	Val	16.48	1.08	0.055	0.001	51.38	3.48	4.40	0.043	0.004	40.55	0.703
	Leu	26.34	2.31	0.067	0.003	62.46	9.75	3.60	0.050	0.004	46.51	0.015
	Ile	3.89	1.41	0.041	0.002	38.46	-2.84	3.20	0.034	0.003	31.90	0.068
	Pro	-8.20	0.44	0.026	0.000	24.52	-9.61	4.19	0.026	0.005	23.94	0.815
	Ser	9.40	0.25	0.047	0.000	44.20	3.49	1.99	0.039	0.002	36.54	0.019
	Thr	-7.69	1.24	0.029	0.001	27.46	-13.66	4.67	0.021	0.005	19.52	0.043
	Phe	43.45	2.11	0.088	0.002	81.94	28.90	2.16	0.070	0.002	64.95	0.021
	Asp	-2.66	0.94	0.034	0.001	32.11	-6.78	3.33	0.028	0.004	26.20	0.062
	Glu	-4.45	1.55	0.032	0.002	30.33	-4.81	4.18	0.029	0.005	27.33	0.276
	Lys	3.06	0.96	0.040	0.001	37.60	-3.08	3.32	0.032	0.004	29.50	0.030
	His	12.16	1.72	0.047	0.002	44.17	6.83	6.00	0.042	0.007	39.36	0.354
Tyr	20.75	2.12	0.059	0.002	54.85	13.80	0.55	0.050	0.001	46.91	0.068	
t24	Ala	24.45	2.99	0.060	0.003	56.08	19.04	1.36	0.055	0.001	51.57	0.111

	Soil					Hydroponic						
	d 13C/12C (‰)		APE (%)		Norm (%)	d 13C/12C (‰)		APE (%)		Norm (%)	t-Test	
AS	AM	SD	AM	SD		AM	SD	AM	SD		p-value	
Gly	9.49	2.56	0.044	0.003	40.98	9.24	0.64	0.044	0.001	41.09	0.899	
Val	27.62	3.51	0.066	0.003	61.73	23.94	0.91	0.064	0.001	59.74	0.429	
Leu	33.48	3.34	0.075	0.004	69.75	28.42	1.98	0.070	0.002	65.54	0.187	
Ile	22.59	3.35	0.062	0.004	57.54	24.97	1.66	0.064	0.002	60.25	0.256	
Pro	19.19	2.72	0.056	0.003	52.46	26.27	1.95	0.065	0.002	60.53	0.044	
Ser	11.46	2.20	0.050	0.002	46.31	6.35	0.82	0.042	0.001	39.46	0.007	
Thr	7.96	0.91	0.046	0.001	43.42	9.73	1.05	0.046	0.001	43.39	0.998	
Phe	61.18	6.04	0.107	0.007	100.00	54.72	3.02	0.098	0.003	91.28	0.130	
Asp	8.26	0.60	0.046	0.001	43.24	12.31	1.02	0.049	0.001	45.68	0.300	
Glu	14.13	1.44	0.053	0.002	49.29	24.14	2.15	0.061	0.002	56.86	0.078	
Lys	17.75	4.78	0.056	0.005	52.59	19.08	1.73	0.056	0.002	52.11	0.899	
His	19.32	2.12	0.055	0.002	51.47	17.67	1.37	0.054	0.001	50.41	0.681	
Tyr	32.45	3.54	0.071	0.004	66.78	31.33	2.67	0.069	0.003	64.78	0.630	
t48	Ala	9.07	1.25	0.043	0.001	40.39	3.90	0.62	0.039	0.001	36.12	0.065
	Gly	0.00	1.21	0.034	0.001	31.31	-1.77	0.57	0.032	0.001	29.85	0.321
	Val	19.67	0.12	0.057	0.003	53.04	11.54	0.23	0.050	0.001	46.99	0.036
	Leu	21.89	2.97	0.062	0.003	57.93	13.52	1.19	0.054	0.001	50.35	0.032
	Ile	24.88	3.32	0.064	0.004	59.87	15.85	1.84	0.055	0.002	50.95	0.005
	Pro	23.16	3.86	0.060	0.004	56.51	18.62	1.72	0.056	0.002	52.73	0.120
	Ser	2.15	1.74	0.039	0.002	36.81	-7.69	0.84	0.027	0.001	25.14	0.002
	Thr	3.76	2.82	0.042	0.003	39.14	-1.76	1.95	0.034	0.002	31.67	0.000
	Phe	38.33	2.71	0.082	0.003	76.71	34.43	1.64	0.076	0.002	70.59	0.088
	Asp	3.37	2.31	0.041	0.003	38.25	1.40	0.98	0.037	0.001	34.55	0.005
	Glu	6.56	2.31	0.044	0.003	41.56	9.76	1.23	0.045	0.001	42.18	0.586
Lys	14.45	3.22	0.053	0.004	49.22	11.80	1.51	0.048	0.002	44.68	0.066	

	Soil					Hydroponic					
	d 13C/12C (‰)		APE (%)		Norm (%)	d 13C/12C (‰)		APE (%)		Norm (%)	t-Test
AS	AM	SD	AM	SD		AM	SD	AM	SD		p-value
His	15.22	2.71	0.051	0.003	47.29	9.87	1.12	0.045	0.001	42.45	0.064
Tyr	15.54	1.49	0.053	0.002	49.54	15.84	1.46	0.052	0.002	48.99	0.792
C	Ala	-30.51	0.19			-31.50	0.24				
	Gly	-30.67	0.05			-31.02	0.39				
	Val	-33.76	0.24			-35.27	0.04				
	Leu	-34.88	0.56			-35.82	0.02				
	Ile	-33.80	0.30			-34.09	0.14				
	Pro	-32.22	0.51			-33.06	0.12				
	Ser	-33.91	0.34			-32.31	0.30				
	Thr	-34.59	0.20			-32.79	0.43				
	Phe	-36.87	0.31			-34.77	0.19				
	Asp	-34.11	0.51			-32.45	0.15				
	Glu	-34.16	0.60			-31.58	0.33				
	Lys	-33.78	0.92			-31.99	0.22				
	His	-31.12	1.99			-31.73	0.38				
Tyr	-33.01	0.86			-32.17	0.39					

Table A9. 5 Raw data of Figure 5. 7, comparing shoot and root ¹³C and ¹⁵N labeling.

Enrichment values are provided as mean values ($n = 3$) and are expressed as atom percent excess, corrected for natural isotopes. Delta values were converted to atom% enrichment (Eq. 2), subsequently corrected for the amount of carbon and nitrogen atoms in the respective amino acid. Corrected values were used to calculate the atom percent excess of the individual amino acids (Eq. 3). Abbreviations: SD (standard deviation), AM (arithmetic mean), AA (amino acid), $\delta^{13}\text{C}$, APE (atom percent excess), $t_0 - t_4$ (harvest time after labeling in hours. Amino acid abbreviations are corresponding to three letter code.

		13C				15N					
		d 13C/12C (‰)		APE (%)		d 15N/14N (‰)		APE (%)		t-Test	
AS		AM	SD	AM	SD	AM	SD	AM	SD	p-value	
t ₀	Shoot	Ala	-16.58	1.34	0.049	0.004	249.64	1.25	-0.021	0.000	0.000
		Gly	-5.15	0.72	0.057	0.002	228.52	3.91	-0.018	0.001	0.000
		Pro	-36.21	1.03	-0.017	0.006	187.87	4.17	0.018	0.002	0.000
		Ser	-2.48	1.27	0.098	0.004	428.89	8.30	0.025	0.003	0.000
		Asp	-28.63	0.28	0.017	0.001	341.99	5.86	0.005	0.002	0.001
		Glu	-33.65	0.57	-0.011	0.003	319.06	3.47	-0.001	0.001	0.005
	Root	Ala	-34.86	1.00	-0.010	0.003	325.94	30.06	0.007	0.011	0.074
		Gly	-33.61	0.95	-0.005	0.002	211.19	13.69	-0.024	0.005	0.009
		Pro	-34.28	0.94	-0.005	0.005	159.93	6.50	0.008	0.002	0.053
		Ser	-32.48	0.74	-0.008	0.002	668.51	184.63	0.112	0.067	0.042
		Asp	-34.57	1.01	-0.010	0.004	619.41	222.83	0.106	0.081	0.074
		Glu	-34.42	0.86	-0.002	0.005	768.43	170.11	0.163	0.062	0.015
t ₂	Shoot	Ala	8.33	1.35	0.131	0.004	572.41	8.34	0.096	0.003	0.000
		Gly	2.80	0.45	0.074	0.001	504.90	2.47	0.083	0.001	0.000
		Pro	-28.61	0.66	0.024	0.004	438.11	6.82	0.109	0.002	0.000
		Ser	1.18	1.11	0.110	0.004	562.65	9.36	0.074	0.003	0.000
		Asp	-20.18	0.89	0.054	0.004	575.14	3.90	0.090	0.001	0.000
		Glu	-25.72	0.74	0.032	0.004	542.81	11.11	0.081	0.004	0.000
	Root	Ala	20.38	1.63	0.171	0.005	842.02	6.07	0.194	0.002	0.002
		Gly	1.55	1.32	0.072	0.003	563.39	25.39	0.104	0.009	0.004
		Pro	-12.97	1.05	0.112	0.006	531.44	29.40	0.143	0.011	0.011
		Ser	8.91	0.35	0.127	0.001	622.57	29.40	0.096	0.011	0.007
		Asp	-3.13	1.61	0.128	0.007	745.42	15.24	0.151	0.006	0.010
		Glu	0.75	1.67	0.190	0.009	727.81	39.49	0.148	0.014	0.013
t ₄	Shoot	Ala	14.50	0.31	0.151	0.001	613.20	41.97	0.111	0.015	0.011
		Gly	8.77	2.39	0.087	0.005	628.79	5.20	0.128	0.002	0.000
		Pro	-9.61	4.19	0.128	0.023	559.64	12.37	0.153	0.004	0.135
		Ser	3.49	1.99	0.117	0.007	638.37	15.98	0.102	0.006	0.035
		Asp	-6.78	3.33	0.112	0.015	634.79	10.81	0.111	0.004	0.923
		Glu	-4.81	4.18	0.146	0.023	623.73	13.90	0.110	0.005	0.056
	Root	Ala	23.10	5.30	0.180	0.017	737.27	104.12	0.156	0.038	0.383
		Gly	1.75	4.94	0.072	0.011	677.87	48.16	0.146	0.017	0.003
		Pro	7.02	2.89	0.221	0.016	682.04	25.43	0.198	0.009	0.094
		Ser	7.18	4.04	0.122	0.013	711.01	12.34	0.128	0.004	0.491

		13C				15N					
		d 13C/12C (‰)		APE (%)		d 15N/14N (‰)		APE (%)		t-Test	
AS		AM	SD	AM	SD	AM	SD	AM	SD	p-value	
	Asp	7.39	3.15	0.174	0.014	757.97	7.80	0.156	0.003	0.097	
	Glu	17.32	3.32	0.280	0.018	771.76	10.18	0.164	0.004	0.000	
Control	Shoot	Ala	-31.50	0.24			307.44	3.76			
		Gly	-31.02	0.39			276.80	3.63			
		Pro	-33.06	0.12			138.60	37.71			
		Ser	-32.31	0.30			359.18	1.41			
		Asp	-32.45	0.15			328.78	6.01			
		Glu	-31.58	0.33			320.86	4.88			
	Root	Ala	-31.76	0.26			307.44	3.76			
		Gly	-31.29	0.21			276.80	3.63			
		Pro	-33.41	0.37			138.60	37.71			
		Ser	-29.99	0.64			359.18	1.41			
		Asp	-32.32	0.49			328.78	6.01			
		Glu	-33.97	3.73			320.86	4.88			

Table A9. 6 Raw data of Figure 5. 9 A, displaying ^{13}C enrichment of imazapyr-treated rice seedlings, immediately after the labeling pulse.

Enrichment values are provided as mean values ($n = 3$) and are expressed as $\delta^{13}\text{C}$ (‰), corrected for natural isotopes. Abbreviations: SD (standard deviation), AM (arithmetic mean), C (unlabeled control), IMA (Imazapyr treatment), DMSO (control treatment).

Imazapyr - Assimilation					
Description	Measured data		Corrected data		t-Test <i>p</i>-value
	AM	SD	AM	SD	
Shoot_DMSO	567.16	15.34	594.60	15.51	0.554
Shoot_IMA	558.33	18.10	585.77	26.45	
Shoot_C	-27.44	0.42			

Table A9. 7 Raw data of Figure 5. 9 B, displaying ^{13}C enrichment of imazapyr-treated rice seedlings after a two-hour chase period.

Enrichment values are provided as mean values ($n = 3$) and are expressed $\delta^{13}\text{C}$ (‰), corrected for natural isotopes. Values of the imazapyr-treated plants were normalised to those of plants treated with the control solution (DMSO). Abbreviations: SD (standard deviation), AM (arithmetic mean), AA (amino acid), Control (unlabeled Imazapyr- or DMSO-treated plant). Amino acid abbreviations are corresponding to three letter code.

AA	Imazapyr						DMSO						Normalized data	t-Test p -value	
	Control		Sample				Control		Sample						
	Measured data AM	SD	Measured data AM	SD	Corrected data AM	SD	Measured data AM	SD	Measured data AM	SD	Corrected data AM	SD			SD
Ala	-32.54	0.20	18.54	1.89	51.08	1.89	-32.54	0.20	42.32	5.71	74.86	5.71	68.23	2.52	0.002
Gly	-32.95	0.19	9.68	2.54	42.63	2.54	-32.95	0.19	24.20	3.32	57.15	3.32	74.59	4.45	0.004
Val	-36.15	0.66	-34.44	0.80	1.71	0.80	-36.15	0.66	5.18	6.23	41.33	6.23	4.14	1.93	0.000
Leu	-36.36	0.26	-34.17	0.52	2.19	0.52	-36.36	0.26	17.21	1.40	53.57	1.40	4.09	0.98	0.000
Ile	-34.70	0.54	-30.90	0.52	3.80	0.52	-34.70	0.54	-1.65	3.29	33.04	3.29	11.50	1.59	0.000
Pro	-32.26	0.37	-28.83	0.40	3.43	0.40	-32.26	0.37	-14.05	2.30	18.21	2.30	18.82	2.22	0.000
Ser	-32.28	0.09	5.78	3.79	38.06	3.79	-32.28	0.09	25.17	1.47	57.45	1.47	66.25	6.60	0.001
Thr	-33.44	0.16	-22.84	2.41	10.60	2.41	-33.44	0.16	0.44	2.79	33.88	2.79	31.30	7.13	0.000
Phe	-35.85	0.19	-18.79	2.53	17.05	2.53	-35.85	0.19	22.53	1.18	58.38	1.18	29.21	4.34	0.000
Asp	-32.84	0.08	-10.74	3.90	22.10	3.90	-32.84	0.08	11.91	3.64	44.75	3.64	49.40	8.71	0.002
Glu	-32.52	0.18	-16.33	3.17	16.19	3.17	-32.52	0.18	-3.10	2.42	29.42	2.42	55.03	10.77	0.005
Lys	-32.80	0.27	-27.12	0.45	5.68	0.45	-32.80	0.27	-3.79	2.80	29.00	2.80	19.57	1.56	0.000
His	-33.06	0.35	-27.31	0.99	5.75	0.99	-33.06	0.35	-2.20	3.25	30.86	3.25	18.65	3.19	0.000
Tyr	-33.64	0.19	-20.39	3.78	13.25	3.78	-33.64	0.19	6.03	2.83	39.67	2.83	33.40	9.53	0.001

Table A9. 8 Raw data of Figure 5. 10 B, comparing ¹³C labeling of plants in the flowering stage with plants in grain filling early and grain filling late.

Enrichment values are provided as mean values ($n = 3$) and are expressed as δ -values (‰), corrected for natural labeling. Mean values \pm SD ($n = 3$) are listed. ANOVA with Tukey's test was applied to determine significant differences at $P \leq 0.05$ between means of the different tissue types. Abbreviations: C (unlabeled control), SD (standard deviation), AM (arithmetic mean), t0 – t48 (harvest time after labeling in hours).

	Description	Measured data		Corrected data		t-Test	
		AM	SD	AM	SD	Description	p-value
Flowering	Leaf_C	-30.92	0.36	259.04	41.60	Flag leaf vs Leaf	0.855
	Leaf	228.12	41.60			Stem vs Panicle	1.000
	Flag leaf_C	-30.19	0.75	237.95	49.78	Flag leaf vs Stem	0.000
	Flag leaf	207.76	49.77			Flag leaf vs Panicle	0.000
	Stem_C	-30.14	0.31	-0.26	1.66	Leaf vs Stem	0.000
	Stem	-30.40	1.63			Leaf vs Panicle	0.000
	Panicle_C	-29.55	0.39	-0.63	1.69		
	Panicle	-30.18	1.65				
Grain filling early	Leaf_C	-28.60	0.70	191.93	7.88	Flag leaf vs Leaf	0.336
	Leaf	163.33	7.85			Stem vs Panicle	1.000
	Flag leaf_C	-28.51	0.69	213.20	22.83	Flag leaf vs Stem	0.000
	Flag leaf	184.69	22.82			Flag leaf vs Panicle	0.000
	Stem_C	-27.00	0.40	-0.01	0.53	Leaf vs Stem	0.000
	Stem	-27.01	0.34			Leaf vs Panicle	0.000
	Panicle_C	-26.95	0.74	8.67	1.10		
	Panicle	-18.28	0.82				
Grain filling late	Leaf_C	-30.86	3.58	168.76	12.09	Flag leaf vs Leaf	0.000
	Leaf	137.90	11.54			Stem vs Panicle	0.997
	Flag leaf_C	-30.48	4.90	273.28	28.44	Flag leaf vs Stem	0.000
	Flag leaf	242.80	28.01			Flag leaf vs Panicle	0.000
	Stem_C	-31.02	5.01	1.66	5.15	Leaf vs Stem	0.000
	Stem	-29.35	1.20			Leaf vs Panicle	0.000
	Panicle_C	-31.64	5.66	4.12	6.05		
	Panicle	-27.52	2.12				

Table A9. 9 Raw data of Figure 5. 10 D, comparing ^{13}C labeling of the different tissue types of plants in the late grain filling stage.

Enrichment values are provided as mean values ($n = 3$) and are expressed as δ -values (‰), corrected for natural labeling. Mean values \pm SD ($n = 3$) are listed. ANOVA with Tukey's test was applied to determine significant differences at $P \leq 0.05$ between means of the different tissue types. Abbreviations: C (unlabeled control), SD (standard deviation), AM (arithmetic mean), t0 – t48 (harvest time after labeling in hours).

Organ	Description	Measured data		Corrected data		t-Test		
		AM	SD	AM	SD	Time point	Description	<i>p</i> -value
Leaf	C	-30.06	0.21			t0	Flag leaf vs Leaf	0.000
	t0	100.02	18.48	130.08	18.48		Stem vs Panicle	0.000
	t2	46.90	9.06	76.96	9.07		Flag leaf vs Stem	0.000
	t4	28.28	17.28	58.34	17.28		Flag leaf vs Panicle	0.003
	t24	-6.81	3.32	23.25	3.33		Leaf vs Stem	0.975
	t48	-7.32	1.35	22.74	1.37		Leaf vs Panicle	0.005
	Flag leaf	C	-30.21	0.45				t2
t0		274.96	55.51	305.18	55.51	Stem vs Panicle	0.000	
t2		137.45	16.04	167.66	16.05	Flag leaf vs Stem	0.000	
t4		57.82	28.96	88.04	28.97	Flag leaf vs Panicle	0.000	
t24		1.49	6.16	31.70	6.18	Leaf vs Stem	0.959	
t48		-0.55	1.87	29.66	1.92	Leaf vs Panicle	0.000	
Stem		C	-29.98	0.91			t4	
	t0	-29.79	0.24	0.18	0.94	Stem vs Panicle		0.009
	t2	-14.71	5.99	15.27	6.06	Flag leaf vs Stem		0.225
	t4	-7.42	6.99	22.56	7.05	Flag leaf vs Panicle		0.150
	t24	-9.92	3.41	20.06	3.53	Leaf vs Stem		0.175
	t48	20.01	14.03	49.99	14.06	Leaf vs Panicle		0.999
	Panicle	C	-30.03	0.41				t24
t0		-20.00	2.68	10.03	2.71	Stem vs Panicle	0.524	
t2		-10.83	2.33	19.19	2.37	Flag leaf vs Stem	0.000	
t4		26.66	11.17	56.69	11.18	Flag leaf vs Panicle	0.979	
t24		64.02	18.55	94.05	18.55	Leaf vs Stem	0.000	
t48		45.49	19.57	75.52	19.57	Leaf vs Panicle	0.000	
						t48	Flag leaf vs Leaf	
					Stem vs Panicle		0.245	
					Flag leaf vs Stem		0.007	
					Flag leaf vs Panicle		0.094	
					Leaf vs Stem		0.120	
					Leaf vs Panicle		0.003	

Table A9. 10 Raw data of Figure 5. 11, comparing ^{13}C labeling of a seedling shoot with the leaf of a plant in the late grain filling stage.

Enrichment values are provided as mean values ($n = 3$) and are expressed as atom percent excess, corrected for natural isotopes. Normalised values were used for graphical representation. Values were normalised to the highest value of the data set (Soil, Phe, t24), which was set 100%. Negative values were set zero. Student's t-test was performed to assess significant differences at $P \leq 0.05$ between amino acid mean values of a seedling shoot and the leaf of a plant in the late grain filling stage. Abbreviations: SDL (seedling), GFL (grain filling late), SD (standard deviation), AM (arithmetic mean), C (Control), d 13C/12C ($\delta^{13}\text{C}$), t0 – t48 (harvest time after labeling in hours), at% (atom percent), APE (atom percent excess), Norm (%) (normalised values expressed in percent). Amino acid abbreviations are corresponding to three letter code.

	SDL shoot					Leaf GFL					t-Test	
	d 13C/12C (‰)		APE (%)		Norm (%)	d 13C/12C (‰)		APE (%)		Norm (%)	p -value	
AS	AM	SD	AM	SD		AM	SD	AM	SD			
t0	Ala	-8.20	2.93	0.024	0.003	22.78	-14.57	7.29	0.019	0.008	17.73	0.269
	Gly	-8.43	0.95	0.024	0.001	22.70	-25.12	0.37	0.007	0.000	6.48	0.000
	Val	-30.32	0.62	0.004	0.001	3.63	-33.59	0.96	0.001	0.001	1.32	0.031
	Leu	-22.83	1.56	0.013	0.002	12.30	-34.18	1.00	0.001	0.001	0.55	0.001
	Ile	-28.70	0.17	0.006	0.000	5.20	-32.93	0.08	0.000	0.000	0.35	0.000
	Pro	-35.71	0.48	-0.004	0.001	-3.56	-31.64	0.34	0.001	0.000	0.81	0.000
	Ser	-13.74	0.90	0.022	0.001	20.59	-19.45	2.97	0.012	0.003	11.45	0.002
	Thr	-37.94	0.92	-0.004	0.001	-3.42	-29.88	1.35	0.001	0.001	1.32	0.005
	Phe	-15.21	6.37	0.024	0.007	22.10	-33.00	0.61	0.001	0.001	0.86	0.007
	Asp	-24.88	2.36	0.010	0.003	9.43	-28.11	2.06	0.002	0.002	2.18	0.009
	Glu	-33.72	0.38	0.000	0.000	0.46	-30.84	0.66	0.001	0.001	0.71	0.621
	Lys	-23.58	2.37	0.011	0.003	10.41	-31.57	0.51	0.001	0.001	0.95	0.003
	His	-9.34	5.05	0.024	0.006	22.23	-24.78	1.61	0.008	0.002	7.69	0.006
	Tyr						-20.12	7.74	0.013	0.008	12.01	
t2	Ala	14.20	2.44	0.049	0.003	45.62	-18.17	0.75	0.015	0.001	14.07	0.000
	Gly	8.99	1.17	0.043	0.001	40.47	-21.92	0.75	0.010	0.001	9.76	0.000
	Val	1.79	1.55	0.039	0.002	36.40	-33.41	0.18	0.002	0.000	1.50	0.000
	Leu	13.27	0.95	0.053	0.001	49.14	-33.76	0.28	0.001	0.000	0.98	0.000
	Ile	-7.92	1.17	0.028	0.001	26.41	-32.40	0.23	0.001	0.000	0.89	0.000

	SDL shoot					Leaf GFL					t-Test	
AS	d 13C/12C (‰)		APE (%)		Norm (%)	d 13C/12C (‰)		APE (%)		Norm (%)	p-value	
	AM	SD	AM	SD		AM	SD	AM	SD			
Pro	-24.14	0.86	0.009	0.001	8.25	-31.40	0.30	0.001	0.000	1.06	0.000	
Ser	3.91	1.06	0.041	0.001	38.60	-17.68	1.58	0.014	0.002	13.27	0.000	
Thr	-18.71	1.96	0.017	0.002	16.22	-30.45	0.34	0.001	0.000	0.75	0.000	
Phe	28.28	1.61	0.071	0.002	66.48	-32.42	0.38	0.002	0.000	1.46	0.000	
Asp	-11.01	1.95	0.025	0.002	23.59	-25.59	1.03	0.005	0.001	4.75	0.000	
Glu	-19.04	2.05	0.017	0.002	15.43	-29.36	0.35	0.002	0.000	2.22	0.001	
Lys	-5.99	1.25	0.030	0.001	28.37	-30.80	0.10	0.002	0.000	1.73	0.000	
His	1.32	0.69	0.035	0.001	33.11	-30.35	2.55	0.002	0.003	2.00	0.000	
Tyr	11.01	0.90	0.048	0.001	44.92	-29.16	0.66	0.003	0.001	2.78	0.000	
t4	Ala	24.49	1.10	0.060	0.001	56.12	-21.40	3.12	0.012	0.003	10.76	0.000
	Gly	11.69	1.17	0.046	0.001	43.23	-22.12	0.60	0.010	0.001	9.55	0.000
	Val	16.48	1.08	0.055	0.001	51.38	-33.50	0.48	0.001	0.000	1.40	0.000
	Leu	26.34	2.31	0.067	0.003	62.46	-33.53	0.36	0.001	0.000	1.21	0.000
	Ile	3.89	1.41	0.041	0.002	38.46	-32.52	0.21	0.001	0.000	0.77	0.000
	Pro	-8.20	0.44	0.026	0.000	24.52	-31.87	0.45	0.001	0.000	0.57	0.000
	Ser	9.40	0.25	0.047	0.000	44.20	-19.79	1.07	0.012	0.001	11.11	0.000
	Thr	-7.69	1.24	0.029	0.001	27.46	-29.27	0.47	0.002	0.001	1.95	0.000
	Phe	43.45	2.11	0.088	0.002	81.94	-31.31	0.43	0.003	0.000	2.59	0.000
	Asp	-2.66	0.94	0.034	0.001	32.11	-26.13	0.27	0.004	0.000	4.20	0.000
	Glu	-4.45	1.55	0.032	0.002	30.33	-29.10	0.27	0.003	0.000	2.49	0.000
	Lys	3.06	0.96	0.040	0.001	37.60	-30.63	0.25	0.002	0.000	1.90	0.000
	His	12.16	1.72	0.047	0.002	44.17	-29.99	1.03	0.003	0.001	2.38	0.000
Tyr	20.75	2.12	0.059	0.002	54.85	-27.80	0.36	0.004	0.000	4.17	0.000	
t24	Ala	24.45	2.99	0.060	0.003	56.08	-16.54	2.67	0.017	0.003	15.72	0.000
	Gly	9.49	2.56	0.044	0.003	40.98	-22.85	0.70	0.009	0.001	8.81	0.000

	SDL shoot					Leaf GFL					t-Test
AS	d 13C/12C (‰)		APE (%)		Norm (%)	d 13C/12C (‰)		APE (%)		Norm (%)	p-value
	AM	SD	AM	SD		AM	SD	AM	SD		
Val	27.62	3.51	0.066	0.003	61.73	-33.44	0.33	0.001	0.001	1.01	0.000
Leu	33.48	3.34	0.075	0.004	69.75	-34.02	0.39	0.001	0.000	0.72	0.000
Ile	22.59	3.35	0.062	0.004	57.54	-32.56	0.29	0.001	0.000	0.73	0.000
Pro	19.19	2.72	0.056	0.003	52.46	-31.35	0.14	0.001	0.000	1.11	0.000
Ser	11.46	2.20	0.050	0.002	46.31	-19.77	1.48	0.012	0.002	11.13	0.000
Thr	7.96	0.91	0.046	0.001	43.42	-27.77	0.36	0.004	0.000	3.48	0.000
Phe	61.18	6.04	0.107	0.007	100.00	-32.23	0.37	0.002	0.000	1.65	0.000
Asp	8.26	0.60	0.046	0.001	43.24	-23.59	0.58	0.007	0.001	6.80	0.000
Glu	14.13	1.44	0.053	0.002	49.29	-25.80	0.45	0.006	0.000	5.86	0.000
Lys	17.75	4.78	0.056	0.005	52.59	-30.76	0.50	0.002	0.001	1.77	0.000
His	19.32	2.12	0.055	0.002	51.47	-29.75	0.64	0.003	0.001	2.62	0.000
Tyr	32.45	3.54	0.071	0.004	66.78	-28.94	0.80	0.003	0.001	3.01	0.000
Ala	9.07	1.25	0.043	0.001	40.39	-16.85	1.03	0.017	0.001	15.41	0.000
Gly	0.00	1.21	0.034	0.001	31.31	-22.85	0.80	0.009	0.001	8.80	0.000
Val	19.67	0.12	0.057	0.003	53.04	-31.11	0.81	0.004	0.001	3.60	0.000
Leu	21.89	2.97	0.062	0.003	57.93	-32.51	0.37	0.002	0.000	2.25	0.000
Ile	24.88	3.32	0.064	0.004	59.87	-31.06	0.27	0.002	0.000	2.26	0.000
Pro	23.16	3.86	0.060	0.004	56.51	-29.09	0.23	0.004	0.000	3.41	0.000
t48 Ser	2.15	1.74	0.039	0.002	36.81	-20.66	0.49	0.011	0.001	10.22	0.000
Thr	3.76	2.82	0.042	0.003	39.14	-26.06	0.61	0.006	0.001	5.22	0.000
Phe	38.33	2.71	0.082	0.003	76.71	-29.99	0.54	0.004	0.001	3.94	0.000
Asp	3.37	2.31	0.041	0.003	38.25	-21.35	0.47	0.010	0.001	9.08	0.000
Glu	6.56	2.31	0.044	0.003	41.56	-20.47	0.51	0.012	0.001	11.30	0.000
Lys	14.45	3.22	0.053	0.004	49.22	-28.16	0.25	0.005	0.000	4.42	0.000
His	15.22	2.71	0.051	0.003	47.29	-27.41	1.65	0.005	0.002	5.02	0.000

	SDL shoot					Leaf GFL					t-Test
AS	d 13C/12C (‰)		APE (%)		Norm (%)	d 13C/12C (‰)		APE (%)		Norm (%)	p-value
	AM	SD	AM	SD		AM	SD	AM	SD		
Tyr	15.54	1.49	0.053	0.002	49.54	-25.91	0.69	0.007	0.001	6.10	0.000
C	Ala	-30.51	0.19			-31.95	0.37				
	Gly	-30.67	0.05			-31.48	0.25				
	Val	-33.76	0.24			-34.85	0.71				
	Leu	-34.88	0.56			-34.72	0.18				
	Ile	-33.80	0.30			-33.27	0.16				
	Pro	-32.22	0.51			-32.43	0.28				
	Ser	-33.91	0.34			-30.67	0.35				
	Thr	-34.59	0.20			-31.18	0.86				
	Phe	-36.87	0.31			-33.85	0.24				
	Asp	-34.11	0.51			-30.24	0.23				
	Glu	-34.16	0.60			-31.54	0.23				
	Lys	-33.78	0.92			-32.49	0.50				
	His	-31.12	1.99			-32.32	2.12				
Tyr	-33.01	0.86			-31.89	0.44					

Table A9. 11 Raw data of Figure 5. 12, comparing ^{13}C labeling of the different tissue types of a plant in the late grain filling stage.

Enrichment values are provided as mean values ($n = 3$) and are expressed as atom percent excess, corrected for natural isotopes. Normalised values were used for graphical representation. Values were normalised to the highest value of the data set (Phe, Panicle), which was set 100%. Negative values were set zero. ANOVA with Tukey's test was performed to assess significant differences between mean values of amino acids from leaf (L), flag leaf (FL), stem (S) and panicle (P) at $P \leq 0.05$. Abbreviations: SD (standard deviation), AM (arithmetic mean), AA (amino acid), $\delta^{13}\text{C}/12\text{C}$ ($\delta^{13}\text{C}$), I to III (number of biological replicate), at% (atom percent), APE (atom percent excess), Norm (%) (normalised values expressed in percent). Amino acid abbreviations are corresponding to three letter code.

		Control		Sample				
		$\delta^{13}\text{C}/12\text{C}$ (‰)		$\delta^{13}\text{C}/12\text{C}$ (‰)		APE (%)		
	AS	AM	SD	AM	SD	AM	SD	Norm (%)
Leaf	Ala	-31.95	0.37	-16.54	2.67	0.017	0.003	39.80
	Gly	-31.48	0.25	-22.85	0.70	0.009	0.001	22.29
	Val	-34.89	0.51	-33.89	0.82	0.001	0.001	2.57
	Leu	-34.72	0.18	-34.02	0.39	0.001	0.000	1.81
	Ile	-33.27	0.16	-32.56	0.29	0.001	0.000	1.84
	Pro	-32.43	0.28	-31.35	0.14	0.001	0.000	2.80
	Ser	-30.67	0.35	-19.77	1.48	0.012	0.002	28.17
	Thr	-31.18	0.86	-27.77	0.36	0.004	0.000	8.81
	Phe	-33.85	0.24	-32.23	0.37	0.002	0.000	4.17
	Asp	-30.24	0.23	-23.59	0.58	0.007	0.001	17.21
	Glu	-31.54	0.23	-25.80	0.45	0.006	0.000	14.84
	Lys	-32.49	0.50	-30.76	0.50	0.002	0.001	4.48
	His	-32.32	2.12	-29.75	0.64	0.003	0.001	6.63
	Tyr	-31.89	0.44	-28.94	0.80	0.003	0.001	7.61
Flag leaf	Ala	-31.46	0.63	-15.45	0.33	0.017	0.000	41.38
	Gly	-31.43	0.64	-22.02	0.59	0.010	0.001	24.31
	Val	-34.86	0.72	-32.86	1.13	0.002	0.001	5.16
	Leu	-34.98	0.46	-33.25	0.96	0.002	0.001	4.48
	Ile	-33.13	0.25	-31.99	0.52	0.001	0.001	2.95
	Pro	-32.18	0.42	-31.18	0.47	0.001	0.001	2.59
	Ser	-30.74	0.61	-19.46	0.27	0.012	0.000	29.14
	Thr	-31.11	0.60	-27.05	0.26	0.004	0.000	10.50
	Phe	-34.52	0.26	-31.64	1.10	0.003	0.001	7.45
	Asp	-30.73	0.58	-23.58	0.22	0.008	0.000	18.48
	Glu	-31.69	0.55	-23.35	1.49	0.009	0.002	21.55
	Lys	-32.19	0.57	-30.23	0.30	0.002	0.000	5.08
	His	-29.85	1.67	-27.17	1.08	0.003	0.001	6.92
	Tyr	-32.39	0.71	-28.63	0.41	0.004	0.000	9.71
Stem	Ala	-32.14	1.46	-26.99	0.14	0.006	0.000	13.29
	Gly	-32.50	1.16	-29.86	0.73	0.003	0.001	6.84
	Val	-33.53	1.59	-31.82	0.47	0.002	0.001	5.58
	Leu	-34.23	1.37	-33.10	0.83	0.001	0.001	2.93

		Control		Sample				
		d 13C/12C (‰)		d 13C/12C (‰)		APE (%)		
AS		AM	SD	AM	SD	AM	SD	Norm (%)
Ile		-32.43	1.53	-30.60	1.44	0.002	0.002	4.72
Pro		-32.01	0.95	-28.84	0.99	0.003	0.001	8.19
Ser		-30.53	1.44	-27.56	1.90	0.003	0.002	7.66
Thr		-31.00	1.31	-29.50	0.74	0.002	0.001	3.86
Phe		-32.23	1.80	-28.40	2.24	0.004	0.002	9.90
Asp		-31.14	1.36	-26.51	0.33	0.005	0.000	11.95
Glu		-31.17	0.89	-27.11	0.24	0.004	0.000	10.50
Lys		-31.94	1.37	-30.09	0.58	0.002	0.001	4.78
His		-30.15	1.05	-27.48	1.43	0.003	0.002	6.89
Tyr		-33.10	1.50	-26.27	1.66	0.007	0.002	17.66
Ala	Panicle	-31.31	1.19	-2.88	3.55	0.031	0.004	73.43
Gly		-30.07	1.34	-14.76	1.67	0.017	0.002	39.55
Val		-33.89	1.36	-18.21	2.65	0.017	0.002	40.88
Leu		-34.64	1.20	-12.45	3.10	0.024	0.003	57.34
Ile		-32.56	0.82	-19.16	1.19	0.015	0.001	34.62
Pro		-32.48	0.86	-18.09	2.52	0.016	0.003	37.19
Ser		-30.50	1.17	-11.12	2.13	0.021	0.002	50.06
Thr		-31.81	0.74	-21.13	0.73	0.012	0.001	27.59
Phe		-34.22	1.19	4.49	2.52	0.042	0.003	100.00
Asp		-32.29	2.05	-14.29	1.34	0.020	0.001	46.52
Glu		-32.20	1.04	-9.43	2.13	0.025	0.002	58.84
Lys		-32.21	0.71	-18.92	1.58	0.015	0.002	34.35
His		-29.89	0.53	-13.43	2.15	0.018	0.002	42.53
Tyr		-32.39	0.41	-2.65	1.81	0.032	0.002	76.84
t-Test		AS	FL vs L	S vs L	P vs L	S vs FL	P vs FL	P vs F
	Ala	0.923	0.000	0.000	0.000	0.000	0.000	
	Gly	0.560	0.000	0.000	0.000	0.000	0.000	
	Val	0.578	0.505	0.000	0.999	0.000	0.000	
	Leu	0.667	0.968	0.000	0.891	0.000	0.000	
	Ile	0.911	0.419	0.000	0.770	0.000	0.000	
	Pro	1.000	0.144	0.000	0.129	0.000	0.000	
	Ser	0.972	0.000	0.000	0.000	0.000	0.000	
	Thr	0.365	0.004	0.000	0.001	0.000	0.000	
	Phe	0.701	0.285	0.000	0.832	0.000	0.000	
	Asp	0.662	0.006	0.000	0.002	0.000	0.000	
	Glu	0.095	0.358	0.000	0.009	0.000	0.000	
	Lys	0.974	0.997	0.000	0.995	0.000	0.000	
	His	0.998	0.999	0.000	1.000	0.000	0.000	
	Tyr	0.861	0.022	0.000	0.065	0.000	0.000	

Table A9. 12 Raw data of Figure 5. 13, statistical significance between measured amino acid enrichments.

Atom percent excess values, corrected for natural isotopes and normalised to the highest value of the respective data set, were used for statistical analysis. ANOVA with Tukey's test was performed to assess significant differences between mean values of ^{13}C incorporation into amino acids of leaf, flag leaf, stem and panicle of a plant in the late grain filling stage and the shoot of a seedling after a 24 hour chase period at $P \leq 0.05$. Abbreviations: AA (amino acid). Amino acid abbreviations are corresponding to three letter code.

AA	Leaf	Flag leaf	Stem	Panicle	Seedling shoot
Asp-Ala	0.000	0.000	1.000	0.000	0.000
Glu-Ala	0.000	0.000	0.998	0.000	0.000
Lys-Ala	0.000	0.000	0.129	0.000	0.122
His-Ala	0.000	0.000	0.494	0.000	0.016
Tyr-Ala	0.000	0.000	0.891	0.924	0.000
Gly-Ala	0.000	0.000	0.466	0.000	0.000
Val-Ala	0.000	0.000	0.226	0.000	0.001
Leu-Ala	0.000	0.000	0.027	0.000	0.000
Ile-Ala	0.000	0.000	0.119	0.000	0.984
Pro-Ala	0.000	0.000	0.803	0.000	0.114
Ser-Ala	0.000	0.000	0.641	0.000	0.000
Thr-Ala	0.000	0.000	0.062	0.000	0.000
Phe-Ala	0.000	0.000	0.993	0.000	0.000
Glu-Asp	0.981	0.960	1.000	0.000	0.000
Lys-Asp	0.000	0.000	0.332	0.001	0.000
His-Asp	0.000	0.001	0.814	0.852	0.000
Tyr-Asp	0.000	0.020	0.605	0.000	0.000
Gly-Asp	0.231	0.322	0.789	0.150	0.674
Val-Asp	0.000	0.000	0.502	0.407	0.000
Leu-Asp	0.000	0.000	0.088	0.003	0.000
Ile-Asp	0.000	0.000	0.310	0.001	0.000
Pro-Asp	0.000	0.000	0.975	0.012	0.000
Ser-Asp	0.000	0.002	0.912	0.945	0.314
Thr-Asp	0.003	0.043	0.181	0.000	1.000
Phe-Asp	0.000	0.001	1.000	0.000	0.000
Lys-Glu	0.000	0.000	0.652	0.000	0.260
His-Glu	0.003	0.000	0.979	0.000	0.792
Tyr-Glu	0.014	0.000	0.294	0.000	0.000
Gly-Glu	0.012	0.991	0.972	0.000	0.000
Val-Glu	0.000	0.000	0.823	0.000	0.000
Leu-Glu	0.000	0.000	0.245	1.000	0.000
Ile-Glu	0.000	0.000	0.626	0.000	0.000
Pro-Glu	0.000	0.000	1.000	0.000	0.274
Ser-Glu	0.000	0.079	0.996	0.026	0.291
Thr-Glu	0.067	0.001	0.431	0.000	0.001
Phe-Glu	0.000	0.000	1.000	0.000	0.000

AA	Leaf	Flag leaf	Stem	Panicle	Seedling shoot
His-Lys	0.993	1.000	1.000	0.050	1.000
Tyr-Lys	0.846	0.659	0.002	0.000	0.000
Gly-Lys	0.000	0.000	1.000	0.549	0.000
Val-Lys	0.997	1.000	1.000	0.231	0.000
Leu-Lys	0.944	1.000	1.000	0.000	0.000
Ile-Lys	0.947	0.999	1.000	1.000	0.006
Pro-Lys	0.999	0.995	0.985	0.992	1.000
Ser-Lys	0.000	0.000	0.998	0.000	0.000
Thr-Lys	0.445	0.449	1.000	0.196	0.000
Phe-Lys	1.000	0.996	0.743	0.000	0.000
Tyr-His	1.000	0.987	0.016	0.000	0.000
Gly-His	0.000	0.000	1.000	0.983	0.000
Val-His	0.567	1.000	1.000	1.000	0.000
Leu-His	0.302	0.996	0.954	0.000	0.000
Ile-His	0.307	0.833	1.000	0.069	0.001
Pro-His	0.637	0.742	1.000	0.483	1.000
Ser-His	0.000	0.000	1.000	0.096	0.004
Thr-His	0.986	0.929	0.995	0.000	0.000
Phe-His	0.977	1.000	0.992	0.000	0.000
Gly-Tyr	0.000	0.000	0.015	0.000	0.000
Val-Tyr	0.223	0.712	0.005	0.000	0.005
Leu-Tyr	0.092	0.506	0.000	0.000	0.324
Ile-Tyr	0.094	0.152	0.002	0.000	0.000
Pro-Tyr	0.270	0.108	0.053	0.000	0.000
Ser-Tyr	0.000	0.000	0.028	0.000	0.000
Thr-Tyr	1.000	1.000	0.001	0.000	0.000
Phe-Tyr	0.750	0.998	0.229	0.000	0.000
Val-Gly	0.000	0.000	1.000	1.000	0.000
Leu-Gly	0.000	0.000	0.964	0.000	0.000
Ile-Gly	0.000	0.000	1.000	0.638	0.000
Pro-Gly	0.000	0.000	1.000	0.997	0.000
Ser-Gly	0.088	0.617	1.000	0.004	0.003
Thr-Gly	0.000	0.000	0.997	0.001	0.579
Phe-Gly	0.000	0.000	0.989	0.000	0.000
Leu-Val	1.000	1.000	0.999	0.000	0.000
Ile-Val	1.000	0.998	1.000	0.292	0.034
Pro-Val	1.000	0.991	0.999	0.904	0.000
Ser-Val	0.000	0.000	1.000	0.017	0.000
Thr-Val	0.058	0.502	1.000	0.000	0.000
Phe-Val	0.999	0.998	0.888	0.000	0.000
Ile-Leu	1.000	1.000	1.000	0.000	0.000
Pro-Leu	1.000	1.000	0.748	0.000	0.000
Ser-Leu	0.000	0.000	0.884	0.128	0.000

AA	Leaf	Flag leaf	Stem	Panicle	Seedling shoot
Thr-Leu	0.020	0.315	1.000	0.000	0.000
Phe-Leu	0.978	0.977	0.313	0.000	0.000
Pro-Ile	1.000	1.000	0.981	0.997	0.005
Ser-Ile	0.000	0.000	0.997	0.000	0.000
Thr-Ile	0.021	0.077	1.000	0.151	0.000
Phe-Ile	0.979	0.686	0.718	0.000	0.000
Ser-Pro	0.000	0.000	1.000	0.000	0.000
Thr-Pro	0.073	0.053	0.915	0.013	0.000
Phe-Pro	1.000	0.579	1.000	0.000	0.000
Thr-Ser	0.000	0.000	0.977	0.000	0.394
Phe-Ser	0.000	0.000	0.999	0.000	0.000
Phe-Thr	0.341	0.980	0.522	0.000	0.000

Table A9. 13 GC-MS acquisition parameters

Acquisition parameters for determination of the mass isotopomer distribution of listed analytes with corresponding mass fragments and mass isotopomers.

Analyte	Mass fragment	Mass isotopomer
INO	318-322	M0-M4
PYR	174-176	M0-M2
SUCR	361-367	M0-M6
CIT/ICIT	273-278	M0-M5
GLYCER	189-191	M0-M2
	292-295	M0-M3
GLYCO	147-149	M0-M2
	133-135	M0-M2
GLC	205-207	M0-M2
	319-323	M0-M4
FRC	217-220	M0-M3
	307-310	M0-M3
SER	204-206	M0-M2
	218-220	M0-M2
ASP	232-235	M0-M3
MAL	233-236	M0-M3
VAL	218-220	M0-M2
SUC	247-251	M0-M4
FUM	245-249	M0-M4
AKG	304-309	M0-M5
	288-293	M0-M5
F6P	357-259	M0-M2
	387-390	M0-M3
G6P	357-359	M0-M2
	387-390	M0-M3
S7P	387-390	M0-M3
ALA	116-118	M0-M2
LEU	158-163	M0-M5
ILE	218-220	M0-M2
	232-235	M0-M3
GLY	174-175	M0-M1
THR	320-323	M0-M3
PRO	156-160	M0-M4
PHE	218-220	M0-M2
GLN	156-160	M0-M4

Table A9. 14 LC-MS/MS acquisition parameters

Acquisition parameters for determination of the mass isotopomer distribution of listed analytes with corresponding parent ion (Q1 mass), daughter ion (Q3 mass), collision energy (CE).

Analyte	Mass isotopomer	Q1 mass	Q3 mass	CE
G6P	M0	259	97	-20
	M1	260	97	-20
	M2	261	97	-20
	M3	262	97	-20
	M4	263	97	-20
	M5	264	97	-20
	M6	265	97	-20
DHAP	M0	169	97	-14
	M1	170	97	-14
	M2	171	97	-14
	M3	172	97	-14
MAL	M0	133	115	-14
	M1	134	116	-14
	M2	135	117	-14
	M3	136	118	-14
	M4	137	119	-14
PEP	M0	167	79	-18
	M1	168	79	-18
	M2	169	79	-18
	M3	170	79	-18
GAP	M0	169	79	-12
	M1	170	79	-12
	M2	171	79	-12
	M3	172	79	-12
AKG	M0	145	101	-12
	M1	146	101	-12
	M1	146	102	-12
	M2	147	102	-12
	M2	147	103	-12
	M3	148	103	-12
	M3	148	104	-12
	M4	149	104	-12
	M4	149	105	-12
	M5	150	105	-12
R5P	M0	229	79	-54
	M1	230	79	-54
	M2	231	79	-54
	M3	232	79	-54
	M4	233	79	-54

Analyte	Mass isotopomer	Q1 mass	Q3 mass	CE
	M5	234	79	-54
PYR	M0	87	43	-13
	M1	88	43	-13
	M1	88	44	-13
	M2	89	45	-13
	M2	89	44	-13
	M3	90	45	-13
6PG	M0	275	97	-22
	M1	276	97	-22
	M2	277	97	-22
	M3	278	97	-22
	M4	279	97	-22
	M5	280	97	-22
	M6	281	97	-22
FBP	M0	339	97	-24
	M1	340	97	-24
	M2	341	97	-24
	M3	342	97	-24
	M4	343	97	-24
	M5	344	97	-24
	M6	345	97	-24
S7P	M0	289	97	-26
	M1	290	97	-26
	M2	291	97	-26
	M3	292	97	-26
	M4	293	97	-26
	M5	294	97	-26
	M6	295	97	-26
	M7	296	97	-26
SUC	M0	117	73	-16
	M1	118	73	-16
	M1	118	74	-16
	M2	119	74	-16
	M2	119	75	-16
	M3	120	75	-16
	M3	120	76	-16
	M4	121	76	-16
2PG	M0	185	79	-20
	M1	186	79	-20
	M2	187	79	-20
	M3	188	79	-20
3PG	M0	185	79	-40
	M1	186	79	-40

Analyte	Mass isotopomer	Q1 mass	Q3 mass	CE
	M2	187	79	-40
	M3	188	79	-40
F6P	M0	259	97	-20
	M1	260	97	-20
	M2	261	97	-20
	M3	262	97	-20
	M4	263	97	-20
	M5	264	97	-20
	M6	265	97	-20
FUM	M0	115	71	-10
	M1	116	71	-10
	M1	116	72	-10
	M2	117	72	-10
	M2	117	73	-10
	M3	118	73	-10
	M3	118	74	-10
	M4	119	74	-10
ICIT	M0	191	173	-12
	M1	192	174	-12
	M2	193	175	-12
	M3	194	176	-12
	M4	195	177	-12
	M5	196	178	-12
	M6	197	179	-12
RU5P	M0	229	97	-15
	M1	230	97	-15
	M2	231	97	-15
	M3	232	97	-15
	M4	233	97	-15
	M5	234	97	-15
OAA	M0	131	87	-12
	M1	132	87	-12
	M1	132	88	-12
	M2	133	88	-12
	M2	133	89	-12
	M3	134	89	-12
	M3	134	90	-12
	M4	135	90	-12
CIT	M0	191	87	-22
	M1	192	87	-22
	M1	192	88	-22
	M2	193	87	-22
	M2	193	88	-22

Analyte	Mass isotopomer	Q1 mass	Q3 mass	CE
	M2	193	89	-22
	M3	194	87	-22
	M3	194	88	-22
	M3	194	89	-22
	M3	194	90	-22
	M4	195	88	-22
	M4	195	89	-22
	M4	195	90	-22
	M5	196	89	-22
	M5	196	90	-22
	M6	197	90	-22
E4P	M0	199	97	-16
	M1	200	97	-16
	M2	201	97	-16
	M3	202	97	-16
	M4	203	97	-16
GLYOX	M0	73	45	-12
	M1	74	45	-12
	M1	74	46	-12
	M2	75	46	-12
RBP	M0	309	79	-83
	M1	310	79	-83
	M2	311	79	-83
	M3	312	79	-83
	M4	313	79	-83
	M5	314	79	-83
ACCOA	M0	403	79	-78
	M1	404	79	-78
	M2	405	79	-78
	M3	406	79	-78
	M4	407	79	-78
	M5	408	79	-78
	M6	409	79	-78
	M7	410	79	-78
	M8	411	79	-78
	M9	412	79	-78
	M10	413	79	-78
	M11	414	79	-78
GLYCO	M1	75	45	-14
	M2	76	45	-14
	M2	76	46	-14
	M3	77	46	-14
GLYCER	M0	105	75	-16

Analyte	Mass isotopomer	Q1 mass	Q3 mass	CE
	M1	106	75	-16
	M1	106	76	-16
	M2	107	76	-16
	M2	107	77	-16
	M3	108	77	-16

Table A9. 15 Tracer composition inside the reactor during labeling of untreated rice seedlings, DMSO-treated rice seedlings and imazapyr-treated rice seedlings, measured by online-MS

Mean values ($n = 5$) of isotopomer abundance are listed. Abbreviations: SD (standard deviation), AM (arithmetic mean).

Time (s)	No treatment				DMSO				Imazapyr			
	[M] ⁺		[M+1] ⁺		[M] ⁺		[M+1] ⁺		[M] ⁺		[M+1] ⁺	
	AM	SD	AM	SD	AM	SD	AM	SD	AM	SD	AM	SD
0	0.943	0.007	0.057	0.007	0.964	0.007	0.036	0.007	0.969	0.003	0.031	0.003
13	0.105	0.127	0.895	0.127	0.220	0.214	0.780	0.214	0.062	0.017	0.938	0.017
25	0.050	0.012	0.950	0.012	0.067	0.024	0.933	0.024	0.062	0.008	0.938	0.008
38	0.052	0.011	0.948	0.011	0.060	0.016	0.940	0.016	0.061	0.009	0.939	0.009
50	0.053	0.011	0.947	0.011	0.060	0.016	0.940	0.016	0.062	0.009	0.938	0.009
63	0.055	0.011	0.945	0.011	0.061	0.016	0.939	0.016	0.065	0.010	0.935	0.010
75	0.058	0.011	0.942	0.011	0.065	0.017	0.935	0.017	0.066	0.009	0.934	0.009
88	0.061	0.011	0.939	0.011	0.065	0.017	0.935	0.017	0.069	0.011	0.931	0.011
100	0.062	0.010	0.938	0.010	0.067	0.017	0.933	0.017	0.070	0.009	0.930	0.009
113	0.065	0.011	0.935	0.011	0.069	0.016	0.931	0.016	0.073	0.010	0.927	0.010
125	0.067	0.012	0.933	0.012	0.071	0.017	0.929	0.017	0.074	0.010	0.926	0.010
138	0.068	0.012	0.932	0.012	0.072	0.017	0.928	0.017	0.075	0.010	0.925	0.010
150	0.070	0.012	0.930	0.012	0.073	0.017	0.927	0.017	0.075	0.009	0.925	0.009
163	0.070	0.012	0.930	0.012	0.074	0.017	0.926	0.017	0.076	0.009	0.924	0.009
176	0.071	0.011	0.929	0.011	0.075	0.017	0.925	0.017	0.078	0.010	0.922	0.010
188	0.072	0.012	0.928	0.012	0.076	0.016	0.924	0.016	0.080	0.010	0.920	0.010
201	0.073	0.012	0.927	0.012	0.076	0.017	0.924	0.017	0.079	0.010	0.921	0.010
213	0.074	0.012	0.926	0.012	0.077	0.016	0.923	0.016	0.081	0.010	0.919	0.010
226	0.076	0.012	0.924	0.012	0.078	0.017	0.922	0.017	0.083	0.011	0.917	0.011
238	0.077	0.013	0.923	0.013	0.080	0.017	0.920	0.017	0.084	0.010	0.916	0.010
251	0.076	0.012	0.924	0.012	0.080	0.016	0.920	0.016	0.083	0.010	0.917	0.010

Time (s)	No treatment				DMSO				Imazapyr			
	[M] ⁺		[M+1] ⁺		[M] ⁺		[M+1] ⁺		[M] ⁺		[M+1] ⁺	
	AM	SD	AM	SD	AM	SD	AM	SD	AM	SD	AM	SD
263	0.078	0.012	0.922	0.012	0.081	0.016	0.919	0.016	0.084	0.009	0.916	0.009
276	0.080	0.012	0.920	0.012	0.083	0.017	0.917	0.017	0.086	0.010	0.914	0.010
288	0.082	0.012	0.918	0.012	0.083	0.016	0.917	0.016	0.087	0.010	0.913	0.010
301	0.081	0.013	0.919	0.013	0.084	0.017	0.916	0.017	0.087	0.010	0.913	0.010
314	0.082	0.013	0.918	0.013	0.084	0.016	0.916	0.016	0.087	0.010	0.913	0.010
326	0.084	0.012	0.916	0.012	0.086	0.016	0.914	0.016	0.090	0.010	0.910	0.010
339	0.086	0.012	0.914	0.012	0.087	0.017	0.913	0.017	0.091	0.011	0.909	0.011
351	0.088	0.013	0.912	0.013	0.087	0.018	0.913	0.018	0.092	0.010	0.908	0.010
364	0.089	0.013	0.911	0.013	0.089	0.017	0.911	0.017	0.093	0.009	0.907	0.009
376	0.089	0.013	0.911	0.013	0.089	0.018	0.911	0.018	0.093	0.009	0.907	0.009
389	0.089	0.013	0.911	0.013	0.089	0.017	0.911	0.017	0.093	0.010	0.907	0.010
401	0.090	0.013	0.910	0.013	0.090	0.017	0.910	0.017	0.094	0.009	0.906	0.009
414	0.091	0.014	0.909	0.014	0.091	0.017	0.909	0.017	0.094	0.009	0.906	0.009
426	0.091	0.013	0.909	0.013	0.092	0.018	0.908	0.018	0.095	0.010	0.905	0.010
439	0.091	0.012	0.909	0.012	0.092	0.018	0.908	0.018	0.095	0.009	0.905	0.009
451	0.092	0.013	0.908	0.013	0.092	0.017	0.908	0.017	0.095	0.010	0.905	0.010
464	0.093	0.013	0.907	0.013	0.094	0.018	0.906	0.018	0.096	0.009	0.904	0.009
477	0.092	0.014	0.908	0.014	0.093	0.017	0.907	0.017	0.096	0.010	0.904	0.010
489	0.093	0.013	0.907	0.013	0.094	0.017	0.906	0.017	0.097	0.009	0.903	0.009
502	0.093	0.013	0.907	0.013	0.094	0.018	0.906	0.018	0.098	0.008	0.902	0.008
514	0.094	0.015	0.906	0.015	0.095	0.017	0.905	0.017	0.098	0.010	0.902	0.010
527	0.097	0.014	0.903	0.014	0.097	0.018	0.903	0.018	0.100	0.010	0.900	0.010
539	0.099	0.013	0.901	0.013	0.098	0.017	0.902	0.017	0.102	0.011	0.898	0.011
552	0.100	0.014	0.900	0.014	0.100	0.017	0.900	0.017	0.104	0.010	0.896	0.010
564	0.102	0.014	0.898	0.014	0.100	0.018	0.900	0.018	0.105	0.011	0.895	0.011

	No treatment				DMSO				Imazapyr			
	[M] ⁺		[M+1] ⁺		[M] ⁺		[M+1] ⁺		[M] ⁺		[M+1] ⁺	
Time (s)	AM	SD	AM	SD	AM	SD	AM	SD	AM	SD	AM	SD
577	0.102	0.014	0.898	0.014	0.101	0.017	0.899	0.017	0.106	0.012	0.894	0.012
589	0.102	0.016	0.898	0.016	0.101	0.017	0.899	0.017	0.106	0.012	0.894	0.012
602	0.102	0.015	0.898	0.015	0.102	0.018	0.898	0.018	0.108	0.011	0.892	0.011
615	0.104	0.015	0.896	0.015	0.103	0.018	0.897	0.018	0.108	0.012	0.892	0.012
627	0.104	0.015	0.896	0.015	0.103	0.018	0.897	0.018	0.108	0.011	0.892	0.011
640	0.105	0.016	0.895	0.016	0.103	0.017	0.897	0.017	0.109	0.011	0.891	0.011
652	0.105	0.014	0.895	0.014	0.103	0.018	0.897	0.018	0.110	0.012	0.890	0.012
665	0.105	0.015	0.895	0.015	0.104	0.018	0.896	0.018	0.109	0.011	0.891	0.011
677	0.106	0.014	0.894	0.014	0.105	0.018	0.895	0.018	0.110	0.011	0.890	0.011
690	0.106	0.015	0.894	0.015	0.105	0.018	0.895	0.018	0.110	0.011	0.890	0.011
702	0.107	0.016	0.893	0.016	0.106	0.018	0.894	0.018	0.111	0.011	0.889	0.011
715	0.108	0.015	0.892	0.015	0.107	0.017	0.893	0.017	0.112	0.012	0.888	0.012
727	0.110	0.015	0.890	0.015	0.108	0.017	0.892	0.017	0.113	0.011	0.887	0.011
740	0.111	0.016	0.889	0.016	0.111	0.016	0.889	0.016	0.113	0.010	0.887	0.010
752	0.112	0.015	0.888	0.015	0.111	0.015	0.889	0.015	0.115	0.010	0.885	0.010
765	0.114	0.016	0.886	0.016	0.113	0.015	0.887	0.015	0.115	0.011	0.885	0.011
778	0.114	0.016	0.886	0.016	0.113	0.016	0.887	0.016	0.115	0.010	0.885	0.010
790	0.115	0.017	0.885	0.017	0.113	0.016	0.887	0.016	0.116	0.011	0.884	0.011
803	0.116	0.016	0.884	0.016	0.114	0.015	0.886	0.015	0.116	0.011	0.884	0.011
815	0.116	0.017	0.884	0.017	0.114	0.015	0.886	0.015	0.117	0.010	0.883	0.010
828	0.117	0.017	0.883	0.017	0.115	0.015	0.885	0.015	0.118	0.010	0.882	0.010
840	0.118	0.017	0.882	0.017	0.115	0.015	0.885	0.015	0.118	0.011	0.882	0.011
853	0.118	0.017	0.882	0.017	0.116	0.015	0.884	0.015	0.118	0.011	0.882	0.011
865	0.118	0.018	0.882	0.018	0.116	0.014	0.884	0.014	0.118	0.010	0.882	0.010
878	0.119	0.018	0.881	0.018	0.117	0.015	0.883	0.015	0.119	0.010	0.881	0.010

	No treatment				DMSO				Imazapyr			
	[M] ⁺		[M+1] ⁺		[M] ⁺		[M+1] ⁺		[M] ⁺		[M+1] ⁺	
Time (s)	AM	SD	AM	SD	AM	SD	AM	SD	AM	SD	AM	SD
890	0.119	0.017	0.881	0.017	0.117	0.014	0.883	0.014	0.119	0.010	0.881	0.010
903	0.120	0.018	0.880	0.018	0.118	0.015	0.882	0.015	0.119	0.011	0.881	0.011
915	0.120	0.017	0.880	0.017	0.119	0.015	0.881	0.015	0.122	0.010	0.878	0.010
928	0.120	0.017	0.880	0.017	0.119	0.015	0.881	0.015	0.121	0.009	0.879	0.009
941	0.121	0.018	0.879	0.018	0.119	0.015	0.881	0.015	0.122	0.009	0.878	0.009
953	0.122	0.018	0.878	0.018	0.120	0.015	0.880	0.015	0.122	0.010	0.878	0.010
966	0.122	0.017	0.878	0.017	0.120	0.015	0.880	0.015	0.123	0.009	0.877	0.009
978	0.122	0.018	0.878	0.018	0.120	0.015	0.880	0.015	0.123	0.009	0.877	0.009
991	0.123	0.018	0.877	0.018	0.121	0.015	0.879	0.015	0.124	0.009	0.876	0.009
1003	0.124	0.018	0.876	0.018	0.120	0.014	0.880	0.014	0.124	0.009	0.876	0.009
1016	0.124	0.018	0.876	0.018	0.123	0.014	0.877	0.014	0.125	0.009	0.875	0.009
1028	0.126	0.019	0.874	0.019	0.124	0.014	0.876	0.014	0.127	0.009	0.873	0.009
1041	0.128	0.018	0.872	0.018	0.127	0.015	0.873	0.015	0.129	0.009	0.871	0.009
1053	0.130	0.019	0.870	0.019	0.128	0.016	0.872	0.016	0.131	0.010	0.869	0.010
1066	0.131	0.020	0.869	0.020	0.129	0.016	0.871	0.016	0.132	0.010	0.868	0.010
1079	0.131	0.020	0.869	0.020	0.130	0.015	0.870	0.015	0.132	0.010	0.868	0.010
1091	0.131	0.019	0.869	0.019	0.131	0.016	0.869	0.016	0.133	0.009	0.867	0.009
1104	0.132	0.020	0.868	0.020	0.131	0.015	0.869	0.015	0.134	0.010	0.866	0.010
1116	0.133	0.019	0.867	0.019	0.133	0.016	0.867	0.016	0.133	0.011	0.867	0.011
1129	0.135	0.019	0.865	0.019	0.133	0.016	0.867	0.016	0.134	0.010	0.866	0.010
1141	0.134	0.020	0.866	0.020	0.132	0.016	0.868	0.016	0.135	0.010	0.865	0.010
1154	0.135	0.020	0.865	0.020	0.134	0.015	0.866	0.015	0.136	0.010	0.864	0.010
1166	0.135	0.019	0.865	0.019	0.134	0.017	0.866	0.017	0.136	0.010	0.864	0.010
1179	0.136	0.019	0.864	0.019	0.135	0.016	0.865	0.016	0.137	0.010	0.863	0.010
1191	0.137	0.019	0.863	0.019	0.135	0.015	0.865	0.015	0.137	0.009	0.863	0.009

Time (s)	No treatment				DMSO				Imazapyr			
	[M] ⁺		[M+1] ⁺		[M] ⁺		[M+1] ⁺		[M] ⁺		[M+1] ⁺	
	AM	SD	AM	SD	AM	SD	AM	SD	AM	SD	AM	SD
1204	0.136	0.019	0.864	0.019	0.136	0.014	0.864	0.014	0.137	0.009	0.863	0.009
1216	0.137	0.019	0.863	0.019	0.136	0.015	0.864	0.015	0.137	0.010	0.863	0.010
1229	0.137	0.019	0.863	0.019	0.136	0.015	0.864	0.015	0.138	0.010	0.862	0.010
1242	0.137	0.018	0.863	0.018	0.136	0.016	0.864	0.016	0.138	0.010	0.862	0.010
1254	0.139	0.018	0.861	0.018	0.137	0.015	0.863	0.015	0.139	0.010	0.861	0.010
1267	0.139	0.019	0.861	0.019	0.138	0.015	0.862	0.015	0.139	0.009	0.861	0.009
1279	0.140	0.018	0.860	0.018	0.138	0.015	0.862	0.015	0.140	0.010	0.860	0.010
1292	0.140	0.019	0.860	0.019	0.139	0.016	0.861	0.016	0.140	0.011	0.860	0.011
1304	0.141	0.018	0.859	0.018	0.138	0.015	0.862	0.015	0.141	0.010	0.859	0.010
1317	0.141	0.019	0.859	0.019	0.139	0.015	0.861	0.015	0.140	0.010	0.860	0.010
1329	0.141	0.018	0.859	0.018	0.140	0.015	0.860	0.015	0.140	0.010	0.860	0.010
1342	0.143	0.019	0.857	0.019	0.140	0.016	0.860	0.016	0.141	0.010	0.859	0.010
1354	0.141	0.018	0.859	0.018	0.141	0.015	0.859	0.015	0.142	0.011	0.858	0.011
1367	0.143	0.019	0.857	0.019	0.141	0.015	0.859	0.015	0.142	0.010	0.858	0.010
1380	0.143	0.019	0.857	0.019	0.142	0.016	0.858	0.016	0.142	0.010	0.858	0.010
1392	0.144	0.019	0.856	0.019	0.142	0.015	0.858	0.015	0.143	0.010	0.857	0.010
1405	0.145	0.019	0.855	0.019	0.143	0.015	0.857	0.015	0.143	0.010	0.857	0.010
1417	0.145	0.019	0.855	0.019	0.143	0.015	0.857	0.015	0.144	0.010	0.856	0.010
1430	0.144	0.018	0.856	0.018	0.144	0.015	0.856	0.015	0.144	0.010	0.856	0.010
1442	0.146	0.018	0.854	0.018	0.143	0.015	0.857	0.015	0.144	0.010	0.856	0.010
1455	0.146	0.018	0.854	0.018	0.144	0.014	0.856	0.014	0.145	0.010	0.855	0.010
1467	0.146	0.019	0.854	0.019	0.144	0.015	0.856	0.015	0.145	0.010	0.855	0.010
1480	0.147	0.018	0.853	0.018	0.145	0.015	0.855	0.015	0.145	0.010	0.855	0.010
1492	0.148	0.019	0.852	0.019	0.145	0.016	0.855	0.016	0.146	0.009	0.854	0.009
1505	0.148	0.018	0.852	0.018	0.146	0.016	0.854	0.016	0.146	0.010	0.854	0.010

Time (s)	No treatment				DMSO				Imazapyr			
	[M] ⁺		[M+1] ⁺		[M] ⁺		[M+1] ⁺		[M] ⁺		[M+1] ⁺	
	AM	SD	AM	SD	AM	SD	AM	SD	AM	SD	AM	SD
1517	0.148	0.018	0.852	0.018	0.146	0.015	0.854	0.015	0.147	0.009	0.853	0.009
1530	0.148	0.019	0.852	0.019	0.146	0.015	0.854	0.015	0.147	0.010	0.853	0.010
1543	0.149	0.019	0.851	0.019	0.147	0.015	0.853	0.015	0.148	0.011	0.852	0.011
1555	0.149	0.018	0.851	0.018	0.147	0.016	0.853	0.016	0.148	0.010	0.852	0.010
1568	0.150	0.018	0.850	0.018	0.148	0.015	0.852	0.015	0.148	0.009	0.852	0.009
1580	0.150	0.018	0.850	0.018	0.149	0.016	0.851	0.016	0.149	0.010	0.851	0.010
1593	0.150	0.018	0.850	0.018	0.149	0.014	0.851	0.014	0.149	0.010	0.851	0.010
1605	0.151	0.019	0.849	0.019	0.149	0.014	0.851	0.014	0.149	0.010	0.851	0.010
1618	0.151	0.018	0.849	0.018	0.150	0.015	0.850	0.015	0.150	0.010	0.850	0.010
1630	0.151	0.018	0.849	0.018	0.150	0.015	0.850	0.015	0.151	0.010	0.849	0.010
1643	0.152	0.018	0.848	0.018	0.150	0.014	0.850	0.014	0.150	0.010	0.850	0.010
1655	0.153	0.018	0.847	0.018	0.151	0.015	0.849	0.015	0.151	0.011	0.849	0.011
1668	0.153	0.019	0.847	0.019	0.151	0.014	0.849	0.014	0.152	0.010	0.848	0.010
1681	0.154	0.017	0.846	0.017	0.151	0.015	0.849	0.015	0.152	0.009	0.848	0.009
1693	0.154	0.019	0.846	0.019	0.151	0.015	0.849	0.015	0.152	0.010	0.848	0.010
1706	0.154	0.019	0.846	0.019	0.152	0.015	0.848	0.015	0.153	0.010	0.847	0.010
1718	0.154	0.018	0.846	0.018	0.152	0.014	0.848	0.014	0.153	0.010	0.847	0.010
1731	0.154	0.019	0.846	0.019	0.153	0.015	0.847	0.015	0.153	0.010	0.847	0.010
1743	0.156	0.019	0.844	0.019	0.153	0.014	0.847	0.014	0.153	0.011	0.847	0.011
1756	0.155	0.018	0.845	0.018	0.154	0.015	0.846	0.015	0.154	0.011	0.846	0.011
1768	0.156	0.019	0.844	0.019	0.154	0.014	0.846	0.014	0.154	0.011	0.846	0.011
1781	0.156	0.019	0.844	0.019	0.154	0.015	0.846	0.015	0.155	0.010	0.845	0.010
1793	0.157	0.018	0.843	0.018	0.154	0.014	0.846	0.014	0.155	0.010	0.845	0.010
1806	0.157	0.018	0.843	0.018	0.155	0.015	0.845	0.015	0.155	0.010	0.845	0.010

Table A9. 16 Mass isotopomer distribution of root sucrose, measured by GC-IRMS

Mean values ($n = 5$) of isotopomer abundance are listed. Abbreviations: SD (standard deviation), AM (arithmetic mean).

Labeling time (s)	Isotopomer	No treatment		DMSO		Imazapyr	
		AM	SD	AM	SD	AM	SD
300	[M] ⁺	0.593	0.541	0.593	0.541	0.986	0.004
	[M+1] ⁺	0.006	0.005	0.006	0.005	0.014	0.004
600	[M] ⁺	0.590	0.539	0.591	0.539	0.982	0.005
	[M+1] ⁺	0.009	0.008	0.008	0.008	0.017	0.005
1800	[M] ⁺	0.536	0.489	0.534	0.487	0.918	0.030
	[M+1] ⁺	0.063	0.057	0.065	0.060	0.081	0.030

Table A9. 17 Mass isotopomer distribution of fructose 2, measured by GC-IRMS

Mean values ($n = 5$) of isotopomer abundance are listed. Abbreviations: SD (standard deviation), AM (arithmetic mean).

Labeling time (s)	Isotopomer	No treatment		DMSO		Imazapyr	
		AM	SD	AM	SD	AM	SD
0	[M] ⁺	0.989	0.000	0.989	0.000	0.989	0.000
	[M+1] ⁺	0.011	0.000	0.011	0.000	0.011	0.000
10	[M] ⁺	0.989	0.000	0.988	0.001	0.988	0.001
	[M+1] ⁺	0.011	0.000	0.012	0.001	0.012	0.001
20	[M] ⁺	0.988	0.001	0.987	0.001	0.986	0.003
	[M+1] ⁺	0.012	0.001	0.013	0.001	0.014	0.003
30	[M] ⁺	0.988	0.001	0.987	0.001	0.987	0.002
	[M+1] ⁺	0.012	0.001	0.013	0.001	0.013	0.002
40	[M] ⁺	0.988	0.001	0.987	0.001	0.986	0.002
	[M+1] ⁺	0.012	0.001	0.013	0.001	0.014	0.002
50	[M] ⁺	0.987	0.001	0.984	0.003	0.986	0.002
	[M+1] ⁺	0.013	0.001	0.016	0.003	0.014	0.002
60	[M] ⁺	0.987	0.001	0.984	0.004	0.985	0.001
	[M+1] ⁺	0.013	0.001	0.016	0.004	0.015	0.001
90	[M] ⁺	0.986	0.001	0.982	0.002	0.985	0.001
	[M+1] ⁺	0.014	0.001	0.018	0.002	0.015	0.001
120	[M] ⁺	0.986	0.002	0.983	0.002	0.979	0.004
	[M+1] ⁺	0.014	0.002	0.017	0.002	0.021	0.004
150	[M] ⁺	0.985	0.001	0.983	0.004	0.982	0.003
	[M+1] ⁺	0.015	0.001	0.017	0.004	0.018	0.003
180	[M] ⁺	0.983	0.005	0.980	0.008	0.980	0.003
	[M+1] ⁺	0.017	0.005	0.020	0.008	0.020	0.003
300	[M] ⁺	0.982	0.002	0.978	0.005	0.977	0.010
	[M+1] ⁺	0.018	0.002	0.022	0.005	0.023	0.010
420	[M] ⁺	0.983	0.002	0.977	0.008	0.980	0.003

Labeling time (s)	Isotopomer	No treatment		DMSO		Imazapyr	
		AM	SD	AM	SD	AM	SD
600	[M+1] ⁺	0.017	0.002	0.023	0.008	0.020	0.003
	[M] ⁺	0.981	0.004	0.980	0.003	0.979	0.003
	[M+1] ⁺	0.019	0.004	0.020	0.003	0.021	0.003
1800	[M] ⁺	0.971	0.006	0.956	0.027	0.959	0.015
	[M+1] ⁺	0.029	0.006	0.044	0.027	0.041	0.015

Table A9. 18 Mass isotopomer distribution of fructose 1, measured by GC-IRMS

Mean values ($n = 5$) of isotopomer abundance are listed. Abbreviations: SD (standard deviation), AM (arithmetic mean).

Labeling time (s)	Isotopomer	No treatment		DMSO		Imazapyr	
		AM	SD	AM	SD	AM	SD
0	[M] ⁺	0.989	0.000	0.989	0.000	0.989	0.000
	[M+1] ⁺	0.011	0.000	0.011	0.000	0.011	0.000
10	[M] ⁺	0.989	0.000	0.988	0.001	0.988	0.001
	[M+1] ⁺	0.011	0.000	0.012	0.001	0.012	0.001
20	[M] ⁺	0.988	0.001	0.987	0.001	0.986	0.003
	[M+1] ⁺	0.012	0.001	0.013	0.001	0.014	0.003
30	[M] ⁺	0.988	0.001	0.986	0.001	0.986	0.002
	[M+1] ⁺	0.012	0.001	0.014	0.001	0.014	0.002
40	[M] ⁺	0.987	0.001	0.987	0.001	0.985	0.001
	[M+1] ⁺	0.013	0.001	0.013	0.001	0.015	0.001
50	[M] ⁺	0.986	0.001	0.984	0.003	0.985	0.001
	[M+1] ⁺	0.014	0.001	0.016	0.003	0.015	0.001
60	[M] ⁺	0.987	0.001	0.984	0.004	0.985	0.001
	[M+1] ⁺	0.013	0.001	0.016	0.004	0.015	0.001
90	[M] ⁺	0.986	0.001	0.982	0.002	0.984	0.001
	[M+1] ⁺	0.014	0.001	0.018	0.002	0.016	0.001
120	[M] ⁺	0.985	0.002	0.983	0.003	0.979	0.005
	[M+1] ⁺	0.015	0.002	0.017	0.003	0.021	0.005
150	[M] ⁺	0.984	0.001	0.982	0.004	0.982	0.003
	[M+1] ⁺	0.016	0.001	0.018	0.004	0.018	0.003
180	[M] ⁺	0.982	0.005	0.980	0.009	0.980	0.003
	[M+1] ⁺	0.018	0.005	0.020	0.009	0.020	0.003
300	[M] ⁺	0.982	0.002	0.979	0.006	0.977	0.010
	[M+1] ⁺	0.018	0.002	0.021	0.006	0.023	0.010
420	[M] ⁺	0.983	0.002	0.977	0.008	0.980	0.003
	[M+1] ⁺	0.017	0.002	0.023	0.008	0.020	0.003
600	[M] ⁺	0.981	0.004	0.980	0.003	0.979	0.003
	[M+1] ⁺	0.019	0.004	0.020	0.003	0.021	0.003
1800	[M] ⁺	0.968	0.006	0.957	0.031	0.959	0.017

Labeling time (s)	Isotopomer	No treatment		DMSO		Imazapyr	
		AM	SD	AM	SD	AM	SD
	[M+1] ⁺	0.032	0.006	0.043	0.031	0.041	0.017

Table A9. 19 Mass isotopomer distribution of glucose, measured by GC-IRMS

Mean values ($n = 5$) of isotopomer abundance are listed. Abbreviations: SD (standard deviation), AM (arithmetic mean).

Labeling time (s)	Isotopomer	No treatment		DMSO		Imazapyr	
		AM	SD	AM	SD	AM	SD
0	[M] ⁺	0.989	0.000	0.989	0.000	0.989	0.000
	[M+1] ⁺	0.011	0.000	0.011	0.000	0.011	0.000
10	[M] ⁺	0.989	0.000	0.989	0.000	0.989	0.000
	[M+1] ⁺	0.011	0.000	0.011	0.000	0.011	0.000
20	[M] ⁺	0.989	0.001	0.989	0.001	0.988	0.001
	[M+1] ⁺	0.011	0.001	0.011	0.001	0.012	0.001
30	[M] ⁺	0.989	0.000	0.988	0.001	0.988	0.001
	[M+1] ⁺	0.011	0.000	0.012	0.001	0.012	0.001
40	[M] ⁺	0.988	0.000	0.988	0.000	0.987	0.001
	[M+1] ⁺	0.012	0.000	0.012	0.000	0.013	0.001
50	[M] ⁺	0.988	0.001	0.987	0.002	0.987	0.001
	[M+1] ⁺	0.012	0.001	0.013	0.002	0.013	0.001
60	[M] ⁺	0.988	0.001	0.986	0.003	0.987	0.001
	[M+1] ⁺	0.012	0.001	0.014	0.003	0.013	0.001
90	[M] ⁺	0.987	0.001	0.984	0.003	0.986	0.001
	[M+1] ⁺	0.013	0.001	0.016	0.003	0.014	0.001
120	[M] ⁺	0.986	0.001	0.983	0.004	0.981	0.003
	[M+1] ⁺	0.014	0.001	0.017	0.004	0.019	0.003
150	[M] ⁺	0.985	0.001	0.982	0.005	0.982	0.003
	[M+1] ⁺	0.015	0.001	0.018	0.005	0.018	0.003
180	[M] ⁺	0.984	0.005	0.980	0.008	0.980	0.002
	[M+1] ⁺	0.016	0.005	0.020	0.008	0.020	0.002
300	[M] ⁺	0.982	0.002	0.977	0.006	0.977	0.009
	[M+1] ⁺	0.018	0.002	0.023	0.006	0.023	0.009
420	[M] ⁺	0.983	0.002	0.976	0.008	0.979	0.003
	[M+1] ⁺	0.017	0.002	0.024	0.008	0.021	0.003
600	[M] ⁺	0.980	0.005	0.977	0.003	0.974	0.006
	[M+1] ⁺	0.020	0.005	0.023	0.003	0.026	0.006
1800	[M] ⁺	0.968	0.005	0.948	0.030	0.948	0.016
	[M+1] ⁺	0.032	0.005	0.052	0.030	0.052	0.016

Table A9. 20 Mass isotopomer distribution of inositol, measured by GC-IRMS

Mean values ($n = 5$) of isotopomer abundance are listed. Abbreviations: SD (standard deviation), AM (arithmetic mean).

Labeling time (s)	Isotopomer	No treatment		DMSO		Imazapyr	
		AM	SD	AM	SD	AM	SD
0	[M] ⁺	0.989	0.000	0.989	0.000	0.989	0.000
	[M+1] ⁺	0.011	0.000	0.011	0.000	0.011	0.000
10	[M] ⁺	0.989	0.000	0.989	0.000	0.989	0.000
	[M+1] ⁺	0.011	0.000	0.011	0.000	0.011	0.000
20	[M] ⁺	0.989	0.000	0.989	0.000	0.989	0.000
	[M+1] ⁺	0.011	0.000	0.011	0.000	0.011	0.000
30	[M] ⁺	0.989	0.000	0.989	0.000	0.989	0.000
	[M+1] ⁺	0.011	0.000	0.011	0.000	0.011	0.000
40	[M] ⁺	0.988	0.000	0.989	0.000	0.989	0.000
	[M+1] ⁺	0.012	0.000	0.011	0.000	0.011	0.000
50	[M] ⁺	0.988	0.001	0.989	0.000	0.989	0.000
	[M+1] ⁺	0.012	0.001	0.011	0.000	0.011	0.000
60	[M] ⁺	0.988	0.001	0.989	0.000	0.989	0.001
	[M+1] ⁺	0.012	0.001	0.011	0.000	0.011	0.001
90	[M] ⁺	0.987	0.000	0.989	0.001	0.989	0.001
	[M+1] ⁺	0.013	0.000	0.011	0.001	0.011	0.001
120	[M] ⁺	0.986	0.001	0.989	0.002	0.989	0.001
	[M+1] ⁺	0.014	0.001	0.011	0.002	0.011	0.001
150	[M] ⁺	0.988	0.005	0.989	0.001	0.989	0.001
	[M+1] ⁺	0.012	0.005	0.011	0.001	0.011	0.001
180	[M] ⁺	0.985	0.001	0.989	0.001	0.989	0.001
	[M+1] ⁺	0.015	0.001	0.011	0.001	0.011	0.001
300	[M] ⁺	0.985	0.002	0.988	0.001	0.987	0.003
	[M+1] ⁺	0.015	0.002	0.012	0.001	0.013	0.003
420	[M] ⁺	0.984	0.001	0.987	0.000	0.987	0.000
	[M+1] ⁺	0.016	0.001	0.013	0.000	0.013	0.000
600	[M] ⁺	0.983	0.001	0.986	0.000	0.986	0.000
	[M+1] ⁺	0.017	0.001	0.014	0.000	0.014	0.000
1800	[M] ⁺	0.971	0.003	0.973	0.001	0.973	0.001
	[M+1] ⁺	0.029	0.003	0.027	0.001	0.027	0.001

Table A9. 21 Mass isotopomer distribution of valine, measured by GC-IRMS

Mean values ($n = 5$) of isotopomer abundance are listed. Abbreviations: SD (standard deviation), AM (arithmetic mean).

Labeling time (s)	Isotopomer	No treatment		DMSO		Imazapyr	
		AM	SD	AM	SD	AM	SD
0	[M] ⁺	0.989	0.000	0.990	0.000	0.990	0.000

Labeling time (s)	Isotopomer	No treatment		DMSO		Imazapyr	
		AM	SD	AM	SD	AM	SD
10	[M+1] ⁺	0.011	0.000	0.010	0.000	0.010	0.000
	[M] ⁺	0.989	0.000	0.990	0.000	0.990	0.000
20	[M+1] ⁺	0.011	0.000	0.010	0.000	0.010	0.000
	[M] ⁺	0.989	0.000	0.990	0.000	0.990	0.000
30	[M+1] ⁺	0.011	0.000	0.010	0.000	0.010	0.000
	[M] ⁺	0.989	0.000	0.990	0.000	0.990	0.000
40	[M+1] ⁺	0.011	0.000	0.010	0.000	0.010	0.000
	[M] ⁺	0.989	0.000	0.990	0.000	0.990	0.000
50	[M+1] ⁺	0.011	0.000	0.010	0.000	0.010	0.000
	[M] ⁺	0.989	0.000	0.990	0.000	0.990	0.000
60	[M+1] ⁺	0.011	0.000	0.010	0.000	0.010	0.000
	[M] ⁺	0.989	0.000	0.990	0.000	0.990	0.000
90	[M+1] ⁺	0.011	0.000	0.011	0.000	0.011	0.001
	[M] ⁺	0.989	0.000	0.989	0.000	0.989	0.001
120	[M+1] ⁺	0.012	0.000	0.011	0.000	0.011	0.001
	[M] ⁺	0.988	0.000	0.989	0.000	0.989	0.001
150	[M+1] ⁺	0.013	0.001	0.012	0.001	0.010	0.000
	[M] ⁺	0.987	0.001	0.988	0.001	0.990	0.000
180	[M+1] ⁺	0.014	0.001	0.014	0.001	0.010	0.000
	[M] ⁺	0.986	0.001	0.986	0.001	0.990	0.000
300	[M+1] ⁺	0.021	0.002	0.021	0.001	0.012	0.002
	[M] ⁺	0.979	0.002	0.979	0.001	0.988	0.002
420	[M+1] ⁺	0.030	0.004	0.031	0.004	0.012	0.002
	[M] ⁺	0.970	0.004	0.969	0.004	0.988	0.002
600	[M+1] ⁺	0.046	0.006	0.048	0.005	0.015	0.005
	[M] ⁺	0.954	0.006	0.952	0.005	0.985	0.005
1800	[M+1] ⁺	0.096	0.011	0.131	0.013	0.024	0.018
	[M] ⁺	0.904	0.011	0.869	0.013	0.976	0.018

Table A9. 22 Mass isotopomer distribution of tyrosine, measured by GC-IRMS

Mean values ($n = 5$) of isotopomer abundance are listed. Abbreviations: SD (standard deviation), AM (arithmetic mean).

Labeling time (s)	Isotopomer	No treatment		DMSO		Imazapyr	
		AM	SD	AM	SD	AM	SD
0	[M] ⁺	0.9893	0.0000	0.9892	0.0001	0.989	0.000
	[M+1] ⁺	0.0107	0.0000	0.0108	0.0001	0.011	0.000
10	[M] ⁺	0.9892	0.0000	0.9888	0.0005	0.989	0.000
	[M+1] ⁺	0.0108	0.0000	0.0112	0.0005	0.011	0.000
20	[M] ⁺	0.9891	0.0001	0.9886	0.0008	0.989	0.000

Labeling time (s)	Isotopomer	No treatment		DMSO		Imazapyr	
		AM	SD	AM	SD	AM	SD
30	[M+1] ⁺	0.0109	0.0001	0.0114	0.0008	0.011	0.000
	[M] ⁺	0.9891	0.0000	0.9883	0.0005	0.988	0.001
40	[M+1] ⁺	0.0109	0.0000	0.0117	0.0005	0.012	0.001
	[M] ⁺	0.9889	0.0000	0.9878	0.0012	0.988	0.001
50	[M+1] ⁺	0.0111	0.0000	0.0122	0.0012	0.012	0.001
	[M] ⁺	0.9887	0.0001	0.9877	0.0014	0.988	0.001
60	[M+1] ⁺	0.0113	0.0001	0.0123	0.0014	0.012	0.001
	[M] ⁺	0.9878	0.0003	0.9876	0.0012	0.988	0.001
90	[M+1] ⁺	0.0122	0.0003	0.0124	0.0012	0.012	0.001
	[M] ⁺	0.9864	0.0003	0.9853	0.0013	0.987	0.002
120	[M+1] ⁺	0.0136	0.0003	0.0147	0.0013	0.013	0.002
	[M] ⁺	0.9848	0.0012	0.9846	0.0011	0.987	0.000
150	[M+1] ⁺	0.0152	0.0012	0.0154	0.0011	0.013	0.000
	[M] ⁺	0.9831	0.0010	0.9829	0.0023	0.986	0.001
180	[M+1] ⁺	0.0169	0.0010	0.0171	0.0023	0.014	0.001
	[M] ⁺	0.9825	0.0019	0.9815	0.0021	0.986	0.001
300	[M+1] ⁺	0.0175	0.0019	0.0185	0.0021	0.014	0.001
	[M] ⁺	0.9712	0.0030	0.9721	0.0024	0.983	0.003
420	[M+1] ⁺	0.0288	0.0030	0.0279	0.0024	0.017	0.003
	[M] ⁺	0.9661	0.0038	0.9647	0.0052	0.979	0.002
600	[M+1] ⁺	0.0339	0.0038	0.0353	0.0052	0.021	0.002
	[M] ⁺	0.9539	0.0089	0.9546	0.0025	0.975	0.005
1800	[M+1] ⁺	0.0461	0.0089	0.0454	0.0025	0.025	0.005
	[M] ⁺	0.9117	0.0048	0.8833	0.0336	0.937	0.013
	[M+1] ⁺	0.0883	0.0048	0.1167	0.0336	0.063	0.013

Table A9. 23 Mass isotopomer distribution of serine, measured by GC-IRMS

Mean values ($n = 5$) of isotopomer abundance are listed. Abbreviations: SD (standard deviation), AM (arithmetic mean).

Labeling time (s)	Isotopomer	No treatment		DMSO		Imazapyr	
		AM	SD	AM	SD	AM	SD
0	[M] ⁺	0.989	0.000	0.989	0.001	0.989	0.000
	[M+1] ⁺	0.011	0.000	0.011	0.001	0.011	0.000
10	[M] ⁺	0.989	0.000	0.989	0.001	0.989	0.000
	[M+1] ⁺	0.011	0.000	0.011	0.001	0.011	0.000
20	[M] ⁺	0.986	0.001	0.985	0.000	0.986	0.001
	[M+1] ⁺	0.014	0.001	0.015	0.000	0.014	0.001
30	[M] ⁺	0.981	0.002	0.978	0.002	0.980	0.002
	[M+1] ⁺	0.019	0.002	0.022	0.002	0.020	0.002
40	[M] ⁺	0.970	0.002	0.970	0.003	0.971	0.005

Labeling time (s)	Isotopomer	No treatment		DMSO		Imazapyr	
		AM	SD	AM	SD	AM	SD
50	[M+1] ⁺	0.030	0.002	0.030	0.003	0.029	0.005
	[M] ⁺	0.961	0.004	0.956	0.003	0.962	0.003
60	[M+1] ⁺	0.039	0.004	0.044	0.003	0.038	0.003
	[M] ⁺	0.940	0.005	0.944	0.005	0.953	0.006
90	[M+1] ⁺	0.060	0.005	0.056	0.005	0.047	0.006
	[M] ⁺	0.903	0.007	0.903	0.010	0.921	0.012
120	[M+1] ⁺	0.097	0.007	0.097	0.010	0.079	0.012
	[M] ⁺	0.876	0.010	0.879	0.020	0.893	0.011
150	[M+1] ⁺	0.124	0.010	0.121	0.020	0.107	0.011
	[M] ⁺	0.839	0.008	0.852	0.009	0.865	0.015
180	[M+1] ⁺	0.161	0.008	0.148	0.009	0.135	0.015
	[M] ⁺	0.839	0.033	0.822	0.011	0.847	0.012
300	[M+1] ⁺	0.161	0.033	0.178	0.011	0.153	0.012
	[M] ⁺	0.749	0.013	0.753	0.007	0.797	0.049
420	[M+1] ⁺	0.251	0.013	0.247	0.007	0.203	0.049
	[M] ⁺	0.697	0.015	0.713	0.012	0.745	0.026
600	[M+1] ⁺	0.303	0.015	0.287	0.012	0.255	0.026
	[M] ⁺	0.655	0.021	0.668	0.013	0.716	0.023
1800	[M+1] ⁺	0.345	0.021	0.332	0.013	0.284	0.023
	[M] ⁺	0.602	0.013	0.611	0.007	0.654	0.029
	[M+1] ⁺	0.398	0.013	0.389	0.007	0.346	0.029

Table A9. 24 Mass isotopomer distribution of sucrose, measured by GC-IRMS

Mean values ($n = 5$) of isotopomer abundance are listed. Abbreviations: SD (standard deviation), AM (arithmetic mean).

Labeling time (s)	Isotopomer	No treatment		DMSO		Imazapyr	
		AM	SD	AM	SD	AM	SD
0	[M] ⁺	0.989	0.000	0.989	0.000	0.989	0.000
	[M+1] ⁺	0.011	0.000	0.011	0.000	0.011	0.000
10	[M] ⁺	0.989	0.000	0.989	0.000	0.989	0.000
	[M+1] ⁺	0.011	0.000	0.011	0.000	0.011	0.000
20	[M] ⁺	0.989	0.000	0.989	0.000	0.989	0.000
	[M+1] ⁺	0.011	0.000	0.011	0.000	0.011	0.000
30	[M] ⁺	0.989	0.000	0.989	0.000	0.989	0.000
	[M+1] ⁺	0.011	0.000	0.011	0.000	0.011	0.000
40	[M] ⁺	0.989	0.000	0.989	0.000	0.989	0.000
	[M+1] ⁺	0.011	0.000	0.011	0.000	0.011	0.000
50	[M] ⁺	0.989	0.000	0.988	0.000	0.989	0.000
	[M+1] ⁺	0.011	0.000	0.012	0.000	0.011	0.000
60	[M] ⁺	0.988	0.000	0.988	0.000	0.988	0.000

Labeling time (s)	Isotopomer	No treatment		DMSO		Imazapyr	
		AM	SD	AM	SD	AM	SD
90	[M+1] ⁺	0.012	0.000	0.012	0.000	0.012	0.000
	[M] ⁺	0.986	0.000	0.986	0.000	0.986	0.000
	[M+1] ⁺	0.014	0.000	0.014	0.000	0.014	0.000
120	[M] ⁺	0.984	0.001	0.982	0.001	0.984	0.000
	[M+1] ⁺	0.016	0.001	0.018	0.001	0.016	0.000
150	[M] ⁺	0.980	0.001	0.980	0.001	0.980	0.001
	[M+1] ⁺	0.020	0.001	0.020	0.001	0.020	0.001
180	[M] ⁺	0.977	0.001	0.977	0.002	0.978	0.001
	[M+1] ⁺	0.023	0.001	0.023	0.002	0.022	0.001
300	[M] ⁺	0.961	0.002	0.961	0.005	0.962	0.004
	[M+1] ⁺	0.039	0.002	0.039	0.005	0.038	0.004
420	[M] ⁺	0.946	0.005	0.948	0.006	0.951	0.003
	[M+1] ⁺	0.054	0.005	0.052	0.006	0.049	0.003
600	[M] ⁺	0.922	0.007	0.924	0.007	0.927	0.008
	[M+1] ⁺	0.078	0.007	0.076	0.007	0.073	0.008
1800	[M] ⁺	0.808	0.014	0.802	0.007	0.819	0.021
	[M+1] ⁺	0.192	0.014	0.198	0.007	0.181	0.021

Table A9. 25 Mass isotopomer distribution of malate, measured by GC-IRMS

Mean values ($n = 5$) of isotopomer abundance are listed. Abbreviations: SD (standard deviation), AM (arithmetic mean).

Labeling time (s)	Isotopomer	No treatment		DMSO		Imazapyr	
		AM	SD	AM	SD	AM	SD
0	[M] ⁺	0.989	0.000	0.989	0.000	0.989	0.000
	[M+1] ⁺	0.011	0.000	0.011	0.000	0.011	0.000
10	[M] ⁺	0.989	0.000	0.989	0.000	0.989	0.000
	[M+1] ⁺	0.011	0.000	0.011	0.000	0.011	0.000
20	[M] ⁺	0.989	0.000	0.988	0.000	0.988	0.000
	[M+1] ⁺	0.011	0.000	0.012	0.000	0.012	0.000
30	[M] ⁺	0.988	0.000	0.988	0.000	0.988	0.000
	[M+1] ⁺	0.012	0.000	0.012	0.000	0.012	0.000
40	[M] ⁺	0.988	0.000	0.987	0.000	0.988	0.000
	[M+1] ⁺	0.012	0.000	0.013	0.000	0.012	0.000
50	[M] ⁺	0.988	0.000	0.987	0.000	0.987	0.000
	[M+1] ⁺	0.012	0.000	0.013	0.000	0.013	0.000
60	[M] ⁺	0.987	0.000	0.986	0.001	0.987	0.000
	[M+1] ⁺	0.013	0.000	0.014	0.001	0.013	0.000
90	[M] ⁺	0.987	0.000	0.985	0.001	0.986	0.001
	[M+1] ⁺	0.013	0.000	0.015	0.001	0.014	0.001
120	[M] ⁺	0.986	0.001	0.983	0.001	0.985	0.001

Labeling time (s)	Isotopomer	No treatment		DMSO		Imazapyr	
		AM	SD	AM	SD	AM	SD
150	[M+1] ⁺	0.014	0.001	0.017	0.001	0.015	0.001
	[M] ⁺	0.985	0.000	0.983	0.001	0.985	0.001
	[M+1] ⁺	0.015	0.000	0.017	0.001	0.015	0.001
180	[M] ⁺	0.984	0.001	0.982	0.002	0.983	0.001
	[M+1] ⁺	0.016	0.001	0.018	0.002	0.017	0.001
300	[M] ⁺	0.980	0.001	0.977	0.002	0.978	0.002
	[M+1] ⁺	0.020	0.001	0.023	0.002	0.022	0.002
420	[M] ⁺	0.976	0.002	0.972	0.003	0.974	0.002
	[M+1] ⁺	0.024	0.002	0.028	0.003	0.026	0.002
600	[M] ⁺	0.968	0.002	0.961	0.002	0.964	0.003
	[M+1] ⁺	0.032	0.002	0.039	0.002	0.036	0.003
1800	[M] ⁺	0.933	0.005	0.892	0.011	0.897	0.010
	[M+1] ⁺	0.067	0.005	0.108	0.011	0.103	0.010

Table A9. 26 Mass isotopomer distribution of lysine, measured by GC-IRMS

Mean values ($n = 5$) of isotopomer abundance are listed. Abbreviations: SD (standard deviation), AM (arithmetic mean).

Labeling time (s)	Isotopomer	No treatment		DMSO		Imazapyr	
		AM	SD	AM	SD	AM	SD
0	[M] ⁺	0.9893	0.0000	0.9892	0.0003	0.989	0.000
	[M+1] ⁺	0.0107	0.0000	0.0108	0.0003	0.011	0.000
10	[M] ⁺	0.9891	0.0001	0.9894	0.0002	0.989	0.000
	[M+1] ⁺	0.0109	0.0001	0.0106	0.0002	0.011	0.000
20	[M] ⁺	0.9889	0.0003	0.9894	0.0001	0.989	0.000
	[M+1] ⁺	0.0111	0.0003	0.0106	0.0001	0.011	0.000
30	[M] ⁺	0.9886	0.0001	0.9894	0.0001	0.989	0.000
	[M+1] ⁺	0.0114	0.0001	0.0106	0.0001	0.011	0.000
40	[M] ⁺	0.9882	0.0002	0.9893	0.0001	0.989	0.000
	[M+1] ⁺	0.0118	0.0002	0.0107	0.0001	0.011	0.000
50	[M] ⁺	0.9882	0.0005	0.9891	0.0002	0.989	0.000
	[M+1] ⁺	0.0118	0.0005	0.0109	0.0002	0.011	0.000
60	[M] ⁺	0.9873	0.0004	0.9891	0.0002	0.989	0.000
	[M+1] ⁺	0.0127	0.0004	0.0109	0.0002	0.011	0.000
90	[M] ⁺	0.9858	0.0007	0.9879	0.0005	0.989	0.001
	[M+1] ⁺	0.0142	0.0007	0.0121	0.0005	0.011	0.001
120	[M] ⁺	0.9853	0.0017	0.9879	0.0008	0.989	0.000
	[M+1] ⁺	0.0147	0.0017	0.0121	0.0008	0.011	0.000
150	[M] ⁺	0.9839	0.0015	0.9874	0.0011	0.989	0.000
	[M+1] ⁺	0.0161	0.0015	0.0126	0.0011	0.011	0.000
180	[M] ⁺	0.9842	0.0025	0.9851	0.0011	0.989	0.000

Labeling time (s)	Isotopomer	No treatment		DMSO		Imazapyr	
		AM	SD	AM	SD	AM	SD
300	[M+1] ⁺	0.0158	0.0025	0.0149	0.0011	0.011	0.000
	[M] ⁺	0.9786	0.0059	0.9799	0.0023	0.987	0.001
	[M+1] ⁺	0.0214	0.0059	0.0201	0.0023	0.013	0.001
420	[M] ⁺	0.9675	0.0040	0.9728	0.0012	0.984	0.002
	[M+1] ⁺	0.0325	0.0040	0.0272	0.0012	0.016	0.002
600	[M] ⁺	0.9537	0.0077	0.9589	0.0028	0.982	0.002
	[M+1] ⁺	0.0463	0.0077	0.0411	0.0028	0.018	0.002
1800	[M] ⁺	0.9185	0.0123	0.8960	0.0180	0.952	0.018
	[M+1] ⁺	0.0815	0.0123	0.1040	0.0180	0.048	0.018

Table A9. 27 Mass isotopomer distribution of glycine, measured by GC-IRMS

Mean values ($n = 5$) of isotopomer abundance are listed. Abbreviations: SD (standard deviation), AM (arithmetic mean).

Labeling time (s)	Isotopomer	No treatment		DMSO		Imazapyr	
		AM	SD	AM	SD	AM	SD
0	[M] ⁺	0.989	0.001	0.989	0.001	0.989	0.000
	[M+1] ⁺	0.011	0.001	0.011	0.001	0.011	0.000
10	[M] ⁺	0.985	0.001	0.985	0.001	0.985	0.001
	[M+1] ⁺	0.015	0.001	0.015	0.001	0.015	0.001
20	[M] ⁺	0.969	0.004	0.967	0.004	0.968	0.002
	[M+1] ⁺	0.031	0.004	0.033	0.004	0.032	0.002
30	[M] ⁺	0.953	0.004	0.945	0.008	0.945	0.010
	[M+1] ⁺	0.047	0.004	0.055	0.008	0.055	0.010
40	[M] ⁺	0.922	0.006	0.925	0.010	0.928	0.010
	[M+1] ⁺	0.078	0.006	0.075	0.010	0.072	0.010
50	[M] ⁺	0.907	0.012	0.906	0.008	0.908	0.008
	[M+1] ⁺	0.093	0.012	0.094	0.008	0.092	0.008
60	[M] ⁺	0.882	0.013	0.889	0.015	0.898	0.017
	[M+1] ⁺	0.118	0.013	0.111	0.015	0.102	0.017
90	[M] ⁺	0.851	0.024	0.852	0.013	0.858	0.018
	[M+1] ⁺	0.149	0.024	0.148	0.013	0.142	0.018
120	[M] ⁺	0.821	0.027	0.822	0.022	0.835	0.022
	[M+1] ⁺	0.179	0.027	0.178	0.022	0.165	0.022
150	[M] ⁺	0.793	0.036	0.796	0.013	0.802	0.017
	[M+1] ⁺	0.207	0.036	0.204	0.013	0.198	0.017
180	[M] ⁺	0.792	0.030	0.772	0.026	0.794	0.027
	[M+1] ⁺	0.208	0.030	0.228	0.026	0.206	0.027
300	[M] ⁺	0.738	0.029	0.740	0.025	0.754	0.043
	[M+1] ⁺	0.262	0.029	0.260	0.025	0.246	0.043
420	[M] ⁺	0.714	0.044	0.695	0.019	0.713	0.012

Labeling time (s)	Isotopomer	No treatment		DMSO		Imazapyr	
		AM	SD	AM	SD	AM	SD
600	[M+1] ⁺	0.286	0.044	0.305	0.019	0.287	0.012
	[M] ⁺	0.669	0.023	0.682	0.026	0.706	0.040
	[M+1] ⁺	0.331	0.023	0.318	0.026	0.294	0.040
1800	[M] ⁺	0.627	0.051	0.617	0.017	0.647	0.038
	[M+1] ⁺	0.373	0.051	0.383	0.017	0.353	0.038

Table A9. 28 Mass isotopomer distribution of glutamine, measured by GC-IRMS

Mean values ($n = 5$) of isotopomer abundance are listed. Abbreviations: SD (standard deviation), AM (arithmetic mean).

Labeling time (s)	Isotopomer	No treatment		DMSO		Imazapyr	
		AM	SD	AM	SD	AM	SD
0	[M] ⁺	0.989	0.000	0.989	0.000	0.989	0.000
	[M+1] ⁺	0.011	0.000	0.011	0.000	0.011	0.000
10	[M] ⁺	0.989	0.000	0.989	0.000	0.989	0.000
	[M+1] ⁺	0.011	0.000	0.011	0.000	0.011	0.000
20	[M] ⁺	0.989	0.000	0.989	0.000	0.989	0.000
	[M+1] ⁺	0.011	0.000	0.011	0.000	0.011	0.000
30	[M] ⁺	0.989	0.000	0.989	0.000	0.989	0.000
	[M+1] ⁺	0.011	0.000	0.011	0.000	0.011	0.000
40	[M] ⁺	0.989	0.000	0.989	0.000	0.989	0.000
	[M+1] ⁺	0.011	0.000	0.011	0.000	0.011	0.000
50	[M] ⁺	0.989	0.000	0.989	0.000	0.989	0.000
	[M+1] ⁺	0.011	0.000	0.011	0.000	0.011	0.000
60	[M] ⁺	0.989	0.000	0.989	0.000	0.989	0.000
	[M+1] ⁺	0.011	0.000	0.011	0.000	0.011	0.000
90	[M] ⁺	0.989	0.000	0.989	0.000	0.989	0.000
	[M+1] ⁺	0.011	0.000	0.011	0.000	0.011	0.000
120	[M] ⁺	0.989	0.000	0.989	0.000	0.989	0.000
	[M+1] ⁺	0.011	0.000	0.011	0.000	0.011	0.000
150	[M] ⁺	0.989	0.000	0.989	0.000	0.989	0.000
	[M+1] ⁺	0.011	0.000	0.011	0.000	0.011	0.000
180	[M] ⁺	0.989	0.000	0.989	0.000	0.989	0.000
	[M+1] ⁺	0.011	0.000	0.011	0.000	0.011	0.000
300	[M] ⁺	0.988	0.001	0.988	0.000	0.989	0.000
	[M+1] ⁺	0.012	0.001	0.012	0.000	0.011	0.000
420	[M] ⁺	0.988	0.000	0.987	0.001	0.988	0.000
	[M+1] ⁺	0.012	0.000	0.013	0.001	0.012	0.000
600	[M] ⁺	0.987	0.000	0.985	0.001	0.987	0.001
	[M+1] ⁺	0.013	0.000	0.015	0.001	0.013	0.001
1800	[M] ⁺	0.976	0.004	0.961	0.003	0.971	0.004

[M+1] ⁺	0.024	0.004	0.039	0.003	0.029	0.004
--------------------	-------	-------	-------	-------	-------	-------

Table A9. 29 Mass isotopomer distribution of glutamate, measured by GC-IRMS

Mean values ($n = 5$) of isotopomer abundance are listed. Abbreviations: SD (standard deviation), AM (arithmetic mean).

Labeling time (s)	Isotopomer	No treatment		DMSO		Imazapyr	
		AM	SD	AM	SD	AM	SD
0	[M] ⁺	0.989	0.000	0.989	0.000	0.989	0.000
	[M+1] ⁺	0.011	0.000	0.011	0.000	0.011	0.000
10	[M] ⁺	0.989	0.000	0.989	0.000	0.989	0.000
	[M+1] ⁺	0.011	0.000	0.011	0.000	0.011	0.000
20	[M] ⁺	0.989	0.000	0.989	0.000	0.989	0.000
	[M+1] ⁺	0.011	0.000	0.011	0.000	0.011	0.000
30	[M] ⁺	0.989	0.000	0.989	0.000	0.989	0.000
	[M+1] ⁺	0.011	0.000	0.011	0.000	0.011	0.000
40	[M] ⁺	0.989	0.000	0.989	0.000	0.989	0.000
	[M+1] ⁺	0.011	0.000	0.011	0.000	0.011	0.000
50	[M] ⁺	0.989	0.000	0.989	0.000	0.989	0.000
	[M+1] ⁺	0.011	0.000	0.011	0.000	0.011	0.000
60	[M] ⁺	0.989	0.000	0.989	0.000	0.989	0.000
	[M+1] ⁺	0.011	0.000	0.011	0.000	0.011	0.000
90	[M] ⁺	0.989	0.000	0.989	0.000	0.989	0.000
	[M+1] ⁺	0.011	0.000	0.011	0.000	0.011	0.000
120	[M] ⁺	0.989	0.000	0.989	0.000	0.989	0.000
	[M+1] ⁺	0.011	0.000	0.011	0.000	0.011	0.000
150	[M] ⁺	0.989	0.000	0.989	0.000	0.988	0.000
	[M+1] ⁺	0.011	0.000	0.011	0.000	0.012	0.000
180	[M] ⁺	0.988	0.000	0.988	0.000	0.988	0.000
	[M+1] ⁺	0.012	0.000	0.012	0.000	0.012	0.000
300	[M] ⁺	0.987	0.001	0.987	0.000	0.987	0.001
	[M+1] ⁺	0.013	0.001	0.013	0.000	0.013	0.001
420	[M] ⁺	0.987	0.000	0.985	0.001	0.985	0.001
	[M+1] ⁺	0.013	0.000	0.015	0.001	0.015	0.001
600	[M] ⁺	0.985	0.000	0.981	0.001	0.983	0.002
	[M+1] ⁺	0.015	0.000	0.019	0.001	0.017	0.002
1800	[M] ⁺	0.969	0.004	0.943	0.005	0.956	0.005
	[M+1] ⁺	0.031	0.004	0.057	0.005	0.044	0.005

Table A9. 30 Mass isotopomer distribution of aspartate, measured by GC-IRMS

Mean values ($n = 5$) of isotopomer abundance are listed. Abbreviations: SD (standard deviation), AM (arithmetic mean).

Labeling time (s)	Isotopomer	No treatment		DMSO		Imazapyr	
		AM	SD	AM	SD	AM	SD
0	[M] ⁺	0.989	0.000	0.989	0.000	0.989	0.000
	[M+1] ⁺	0.011	0.000	0.011	0.000	0.011	0.000
10	[M] ⁺	0.989	0.000	0.989	0.000	0.989	0.000
	[M+1] ⁺	0.011	0.000	0.011	0.000	0.011	0.000
20	[M] ⁺	0.989	0.000	0.988	0.000	0.989	0.000
	[M+1] ⁺	0.011	0.000	0.012	0.000	0.011	0.000
30	[M] ⁺	0.988	0.000	0.988	0.000	0.988	0.000
	[M+1] ⁺	0.012	0.000	0.012	0.000	0.012	0.000
40	[M] ⁺	0.988	0.000	0.987	0.000	0.988	0.000
	[M+1] ⁺	0.012	0.000	0.013	0.000	0.012	0.000
50	[M] ⁺	0.987	0.000	0.986	0.000	0.987	0.001
	[M+1] ⁺	0.013	0.000	0.014	0.000	0.013	0.001
60	[M] ⁺	0.986	0.001	0.985	0.001	0.986	0.001
	[M+1] ⁺	0.014	0.001	0.015	0.001	0.014	0.001
90	[M] ⁺	0.983	0.001	0.981	0.003	0.983	0.002
	[M+1] ⁺	0.017	0.001	0.019	0.003	0.017	0.002
120	[M] ⁺	0.980	0.001	0.977	0.001	0.980	0.002
	[M+1] ⁺	0.020	0.001	0.023	0.001	0.020	0.002
150	[M] ⁺	0.977	0.001	0.974	0.002	0.977	0.004
	[M+1] ⁺	0.023	0.001	0.026	0.002	0.023	0.004
180	[M] ⁺	0.976	0.003	0.970	0.003	0.975	0.003
	[M+1] ⁺	0.024	0.003	0.030	0.003	0.025	0.003
300	[M] ⁺	0.959	0.004	0.952	0.004	0.960	0.008
	[M+1] ⁺	0.041	0.004	0.048	0.004	0.040	0.008
420	[M] ⁺	0.940	0.006	0.932	0.008	0.938	0.006
	[M+1] ⁺	0.060	0.006	0.068	0.008	0.062	0.006
600	[M] ⁺	0.909	0.008	0.895	0.005	0.903	0.011
	[M+1] ⁺	0.091	0.008	0.105	0.005	0.097	0.011
1800	[M] ⁺	0.824	0.019	0.771	0.009	0.793	0.019
	[M+1] ⁺	0.176	0.019	0.229	0.009	0.207	0.019

Table A9. 31 Mass isotopomer distribution of asparagine, measured by GC-IRMS

Mean values ($n = 5$) of isotopomer abundance are listed. Abbreviations: SD (standard deviation), AM (arithmetic mean).

Labeling time (s)	Isotopomer	No treatment		DMSO		Imazapyr	
		AM	SD	AM	SD	AM	SD
0	[M] ⁺	0.989	0.000	0.989	0.000	0.989	0.000

Labeling time (s)	Isotopomer	No treatment		DMSO		Imazapyr	
		AM	SD	AM	SD	AM	SD
10	[M+1] ⁺	0.011	0.000	0.011	0.000	0.011	0.000
	[M] ⁺	0.989	0.000	0.989	0.000	0.989	0.000
20	[M+1] ⁺	0.011	0.000	0.011	0.000	0.011	0.000
	[M] ⁺	0.989	0.000	0.988	0.001	0.988	0.001
30	[M+1] ⁺	0.011	0.000	0.012	0.001	0.012	0.001
	[M] ⁺	0.988	0.000	0.988	0.000	0.987	0.002
40	[M+1] ⁺	0.012	0.000	0.012	0.000	0.013	0.002
	[M] ⁺	0.988	0.000	0.987	0.002	0.987	0.001
50	[M+1] ⁺	0.012	0.000	0.013	0.002	0.013	0.001
	[M] ⁺	0.988	0.001	0.987	0.001	0.987	0.001
60	[M+1] ⁺	0.012	0.001	0.013	0.001	0.013	0.001
	[M] ⁺	0.988	0.001	0.985	0.002	0.986	0.002
90	[M+1] ⁺	0.012	0.001	0.015	0.002	0.014	0.002
	[M] ⁺	0.987	0.001	0.985	0.001	0.984	0.004
120	[M+1] ⁺	0.013	0.001	0.015	0.001	0.016	0.004
	[M] ⁺	0.987	0.001	0.982	0.001	0.984	0.004
150	[M+1] ⁺	0.013	0.001	0.018	0.001	0.016	0.004
	[M] ⁺	0.985	0.002	0.985	0.003	0.985	0.002
180	[M+1] ⁺	0.015	0.002	0.015	0.003	0.015	0.002
	[M] ⁺	0.986	0.001	0.981	0.002	0.985	0.002
300	[M+1] ⁺	0.014	0.001	0.019	0.002	0.015	0.002
	[M] ⁺	0.983	0.004	0.979	0.002	0.983	0.003
420	[M+1] ⁺	0.017	0.004	0.021	0.002	0.017	0.003
	[M] ⁺	0.984	0.002	0.981	0.004	0.984	0.002
600	[M+1] ⁺	0.016	0.002	0.019	0.004	0.016	0.002
	[M] ⁺	0.983	0.002	0.981	0.002	0.981	0.005
1800	[M+1] ⁺	0.017	0.002	0.019	0.002	0.019	0.005
	[M] ⁺	0.978	0.004	0.971	0.005	0.974	0.005
	[M+1] ⁺	0.022	0.004	0.029	0.005	0.026	0.005

Table A9. 32 Mass isotopomer distribution of alanine, measured by GC-IRMS

Mean values ($n = 5$) of isotopomer abundance are listed. Abbreviations: SD (standard deviation), AM (arithmetic mean).

Labeling time (s)	Isotopomer	No treatment		DMSO		Imazapyr	
		AM	SD	AM	SD	AM	SD
0	[M] ⁺	0.989	0.000	0.989	0.000	0.989	0.000
	[M+1] ⁺	0.011	0.000	0.011	0.000	0.011	0.000
10	[M] ⁺	0.987	0.000	0.986	0.001	0.988	0.000
	[M+1] ⁺	0.013	0.000	0.014	0.001	0.012	0.000
20	[M] ⁺	0.982	0.007	0.983	0.002	0.986	0.001

Labeling time (s)	Isotopomer	No treatment		DMSO		Imazapyr	
		AM	SD	AM	SD	AM	SD
30	[M+1] ⁺	0.018	0.007	0.017	0.002	0.014	0.001
	[M] ⁺	0.983	0.001	0.980	0.002	0.983	0.001
	[M+1] ⁺	0.017	0.001	0.020	0.002	0.017	0.001
40	[M] ⁺	0.980	0.002	0.978	0.001	0.981	0.002
	[M+1] ⁺	0.020	0.002	0.022	0.001	0.019	0.002
50	[M] ⁺	0.975	0.002	0.971	0.004	0.979	0.002
	[M+1] ⁺	0.025	0.002	0.029	0.004	0.021	0.002
60	[M] ⁺	0.976	0.004	0.968	0.006	0.976	0.002
	[M+1] ⁺	0.024	0.004	0.032	0.006	0.024	0.002
90	[M] ⁺	0.965	0.003	0.951	0.005	0.967	0.005
	[M+1] ⁺	0.035	0.003	0.049	0.005	0.033	0.005
120	[M] ⁺	0.953	0.008	0.934	0.006	0.953	0.006
	[M+1] ⁺	0.047	0.008	0.066	0.006	0.047	0.006
150	[M] ⁺	0.934	0.009	0.905	0.011	0.939	0.011
	[M+1] ⁺	0.066	0.009	0.095	0.011	0.061	0.011
180	[M] ⁺	0.927	0.010	0.890	0.013	0.929	0.016
	[M+1] ⁺	0.073	0.010	0.110	0.013	0.071	0.016
300	[M] ⁺	0.867	0.013	0.830	0.007	0.888	0.026
	[M+1] ⁺	0.133	0.013	0.170	0.007	0.112	0.026
420	[M] ⁺	0.837	0.021	0.781	0.018	0.856	0.024
	[M+1] ⁺	0.163	0.021	0.219	0.018	0.144	0.024
600	[M] ⁺	0.792	0.019	0.752	0.030	0.839	0.033
	[M+1] ⁺	0.208	0.019	0.248	0.030	0.161	0.033
1800	[M] ⁺	0.741	0.033	0.673	0.016	0.738	0.028
	[M+1] ⁺	0.259	0.033	0.327	0.016	0.262	0.028

Table A9. 33 Mass isotopomer distribution of serine_204, measured by GC-MS

Mean values ($n = 5$) of isotopomer abundance are listed. Abbreviations: SD (standard deviation), AM (arithmetic mean).

Labeling time (s)	Isotopomer	No treatment		DMSO		Imazapyr	
		AM	SD	AM	SD	AM	SD
0	[M] ⁺	0.775	0.008	0.780	0.003	0.778	0.005
	[M+1] ⁺	0.156	0.003	0.154	0.002	0.154	0.003
	[M+2] ⁺	0.069	0.004	0.067	0.001	0.068	0.002
10	[M] ⁺	0.776	0.006	0.779	0.002	0.772	0.011
	[M+1] ⁺	0.155	0.003	0.154	0.002	0.156	0.005
	[M+2] ⁺	0.068	0.003	0.067	0.001	0.072	0.006
20	[M] ⁺	0.773	0.004	0.775	0.003	0.759	0.037
	[M+1] ⁺	0.159	0.002	0.157	0.002	0.163	0.014
	[M+2] ⁺	0.068	0.002	0.068	0.001	0.079	0.023

Labeling time (s)	Isotopomer	No treatment		DMSO		Imazapyr	
		AM	SD	AM	SD	AM	SD
30	[M] ⁺	0.768	0.003	0.766	0.003	0.762	0.010
	[M+1] ⁺	0.164	0.002	0.165	0.003	0.165	0.005
	[M+2] ⁺	0.069	0.001	0.069	0.001	0.072	0.006
40	[M] ⁺	0.749	0.005	0.755	0.003	0.753	0.012
	[M+1] ⁺	0.178	0.003	0.173	0.003	0.173	0.006
	[M+2] ⁺	0.073	0.002	0.072	0.001	0.074	0.005
50	[M] ⁺	0.739	0.006	0.737	0.006	0.646	0.218
	[M+1] ⁺	0.185	0.004	0.186	0.004	0.173	0.015
	[M+2] ⁺	0.076	0.002	0.077	0.002	0.181	0.233
60	[M] ⁺	0.719	0.006	0.723	0.010	0.732	0.012
	[M+1] ⁺	0.199	0.004	0.196	0.007	0.188	0.007
	[M+2] ⁺	0.082	0.002	0.081	0.003	0.080	0.005
90	[M] ⁺	0.674	0.009	0.676	0.014	0.699	0.018
	[M+1] ⁺	0.226	0.006	0.223	0.009	0.208	0.011
	[M+2] ⁺	0.099	0.003	0.101	0.005	0.093	0.007
120	[M] ⁺	0.644	0.016	0.648	0.021	0.667	0.015
	[M+1] ⁺	0.240	0.009	0.235	0.013	0.224	0.009
	[M+2] ⁺	0.117	0.008	0.117	0.009	0.110	0.006
150	[M] ⁺	0.606	0.011	0.619	0.011	0.635	0.021
	[M+1] ⁺	0.256	0.007	0.248	0.006	0.236	0.012
	[M+2] ⁺	0.138	0.004	0.133	0.005	0.129	0.009
180	[M] ⁺	0.608	0.042	0.584	0.013	0.618	0.014
	[M+1] ⁺	0.250	0.024	0.259	0.007	0.242	0.009
	[M+2] ⁺	0.142	0.019	0.156	0.006	0.140	0.005
300	[M] ⁺	0.497	0.018	0.497	0.012	0.558	0.060
	[M+1] ⁺	0.283	0.008	0.279	0.009	0.250	0.024
	[M+2] ⁺	0.220	0.010	0.224	0.006	0.191	0.036
420	[M] ⁺	0.438	0.018	0.446	0.010	0.498	0.037
	[M+1] ⁺	0.289	0.008	0.281	0.006	0.264	0.015
	[M+2] ⁺	0.273	0.013	0.273	0.008	0.238	0.023
600	[M] ⁺	0.375	0.024	0.397	0.025	0.457	0.030
	[M+1] ⁺	0.291	0.008	0.280	0.014	0.264	0.011
	[M+2] ⁺	0.334	0.018	0.322	0.014	0.278	0.020
1800	[M] ⁺	0.253	0.019	0.281	0.015	0.355	0.029
	[M+1] ⁺	0.326	0.005	0.312	0.010	0.293	0.006
	[M+2] ⁺	0.421	0.024	0.406	0.011	0.352	0.024

Table A9. 34 Mass isotopomer distribution of serine_218, measured by GC-MS

Mean values ($n = 5$) of isotopomer abundance are listed. Abbreviations: SD (standard deviation), AM (arithmetic mean).

Labeling time (s)	Isotopomer	No treatment		DMSO		Imazapyr	
		AM	SD	AM	SD	AM	SD
0	[M] ⁺	0.775	0.007	0.778	0.001	0.776	0.004
	[M+1] ⁺	0.154	0.002	0.153	0.001	0.153	0.001
	[M+2] ⁺	0.071	0.005	0.069	0.001	0.070	0.003
10	[M] ⁺	0.775	0.006	0.777	0.001	0.770	0.010
	[M+1] ⁺	0.155	0.002	0.154	0.001	0.156	0.003
	[M+2] ⁺	0.070	0.004	0.069	0.001	0.074	0.007
20	[M] ⁺	0.772	0.004	0.773	0.001	0.758	0.035
	[M+1] ⁺	0.157	0.001	0.157	0.001	0.161	0.010
	[M+2] ⁺	0.071	0.003	0.070	0.001	0.082	0.025
30	[M] ⁺	0.768	0.003	0.767	0.003	0.764	0.010
	[M+1] ⁺	0.159	0.001	0.160	0.002	0.160	0.004
	[M+2] ⁺	0.073	0.002	0.073	0.002	0.076	0.006
40	[M] ⁺	0.753	0.005	0.758	0.002	0.756	0.010
	[M+1] ⁺	0.167	0.001	0.164	0.001	0.164	0.004
	[M+2] ⁺	0.080	0.003	0.078	0.002	0.079	0.007
50	[M] ⁺	0.745	0.005	0.744	0.005	0.641	0.238
	[M+1] ⁺	0.170	0.002	0.170	0.002	0.271	0.231
	[M+2] ⁺	0.085	0.003	0.086	0.003	0.088	0.009
60	[M] ⁺	0.729	0.005	0.731	0.008	0.739	0.010
	[M+1] ⁺	0.176	0.002	0.175	0.003	0.171	0.003
	[M+2] ⁺	0.095	0.003	0.094	0.005	0.090	0.007
90	[M] ⁺	0.692	0.008	0.693	0.011	0.712	0.016
	[M+1] ⁺	0.188	0.005	0.185	0.004	0.179	0.006
	[M+2] ⁺	0.120	0.004	0.122	0.007	0.110	0.010
120	[M] ⁺	0.665	0.016	0.668	0.018	0.685	0.012
	[M+1] ⁺	0.194	0.006	0.190	0.007	0.185	0.004
	[M+2] ⁺	0.142	0.010	0.142	0.012	0.130	0.008
150	[M] ⁺	0.630	0.008	0.642	0.010	0.656	0.018
	[M+1] ⁺	0.202	0.004	0.195	0.005	0.191	0.007
	[M+2] ⁺	0.168	0.006	0.163	0.006	0.153	0.011
180	[M] ⁺	0.630	0.037	0.610	0.011	0.639	0.012
	[M+1] ⁺	0.199	0.011	0.202	0.006	0.196	0.005
	[M+2] ⁺	0.171	0.027	0.188	0.006	0.166	0.007
300	[M] ⁺	0.522	0.014	0.522	0.012	0.576	0.056
	[M+1] ⁺	0.225	0.003	0.218	0.008	0.207	0.015
	[M+2] ⁺	0.253	0.013	0.260	0.005	0.217	0.041
420	[M] ⁺	0.458	0.018	0.466	0.009	0.516	0.033
	[M+1] ⁺	0.237	0.007	0.229	0.005	0.220	0.008

Labeling time (s)	Isotopomer	No treatment		DMSO		Imazapyr	
		AM	SD	AM	SD	AM	SD
600	[M+2] ⁺	0.304	0.013	0.305	0.010	0.265	0.025
	[M] ⁺	0.392	0.022	0.412	0.024	0.471	0.027
	[M+1] ⁺	0.249	0.005	0.238	0.010	0.228	0.008
	[M+2] ⁺	0.359	0.022	0.349	0.017	0.300	0.021
1800	[M] ⁺	0.266	0.018	0.294	0.014	0.364	0.027
	[M+1] ⁺	0.300	0.008	0.286	0.010	0.270	0.006
	[M+2] ⁺	0.434	0.025	0.420	0.010	0.365	0.024

Table A9. 35 Mass isotopomer distribution of succinate, measured by GC-MS

Mean values ($n = 5$) of isotopomer abundance are listed. Abbreviations: SD (standard deviation), AM (arithmetic mean).

Labeling time (s)	Isotopomer	No treatment		DMSO		Imazapyr	
		AM	SD	AM	SD	AM	SD
0	[M] ⁺	0.634	0.013	0.641	0.004	0.644	0.002
	[M+1] ⁺	0.240	0.009	0.235	0.002	0.234	0.001
	[M+2] ⁺	0.096	0.003	0.095	0.002	0.093	0.001
	[M+3] ⁺	0.022	0.001	0.022	0.001	0.022	0.000
	[M+4] ⁺	0.006	0.000	0.006	0.000	0.006	0.000
	[M+5] ⁺	0.001	0.000	0.001	0.000	0.001	0.000
	[M+6] ⁺	0.000	0.000	0.000	0.000	0.000	0.000
10	[M] ⁺	0.635	0.012	0.641	0.005	0.641	0.004
	[M+1] ⁺	0.240	0.009	0.235	0.002	0.233	0.002
	[M+2] ⁺	0.096	0.003	0.095	0.002	0.094	0.002
	[M+3] ⁺	0.022	0.001	0.022	0.001	0.023	0.001
	[M+4] ⁺	0.006	0.000	0.006	0.000	0.007	0.001
	[M+5] ⁺	0.001	0.000	0.001	0.000	0.001	0.001
	[M+6] ⁺	0.000	0.000	0.000	0.000	0.001	0.000
20	[M] ⁺	0.642	0.004	0.640	0.004	0.636	0.014
	[M+1] ⁺	0.235	0.003	0.235	0.001	0.232	0.006
	[M+2] ⁺	0.094	0.001	0.095	0.002	0.094	0.002
	[M+3] ⁺	0.022	0.000	0.022	0.001	0.024	0.004
	[M+4] ⁺	0.006	0.000	0.006	0.000	0.010	0.008
	[M+5] ⁺	0.001	0.000	0.001	0.000	0.003	0.005
	[M+6] ⁺	0.000	0.000	0.000	0.000	0.002	0.004
30	[M] ⁺	0.635	0.018	0.640	0.005	0.641	0.006
	[M+1] ⁺	0.240	0.012	0.235	0.001	0.233	0.003
	[M+2] ⁺	0.096	0.005	0.095	0.002	0.094	0.003
	[M+3] ⁺	0.022	0.001	0.022	0.001	0.023	0.001
	[M+4] ⁺	0.006	0.000	0.006	0.000	0.007	0.002
	[M+5] ⁺	0.001	0.000	0.001	0.000	0.001	0.001
	[M+6] ⁺	0.000	0.000	0.000	0.000	0.001	0.001

Labeling time (s)	Isotopomer	No treatment		DMSO		Imazapyr	
		AM	SD	AM	SD	AM	SD
40	[M] ⁺	0.640	0.004	0.642	0.005	0.641	0.004
	[M+1] ⁺	0.236	0.003	0.234	0.002	0.234	0.002
	[M+2] ⁺	0.094	0.001	0.094	0.002	0.094	0.002
	[M+3] ⁺	0.022	0.000	0.022	0.001	0.023	0.001
	[M+4] ⁺	0.006	0.000	0.006	0.000	0.007	0.001
	[M+5] ⁺	0.001	0.000	0.001	0.000	0.001	0.001
	[M+6] ⁺	0.000	0.000	0.000	0.000	0.001	0.000
50	[M] ⁺	0.642	0.001	0.639	0.004	0.641	0.006
	[M+1] ⁺	0.234	0.002	0.235	0.001	0.233	0.002
	[M+2] ⁺	0.094	0.001	0.095	0.002	0.094	0.002
	[M+3] ⁺	0.022	0.000	0.023	0.001	0.023	0.001
	[M+4] ⁺	0.006	0.000	0.006	0.000	0.007	0.001
	[M+5] ⁺	0.001	0.000	0.001	0.000	0.001	0.001
	[M+6] ⁺	0.000	0.000	0.000	0.000	0.001	0.000
60	[M] ⁺	0.638	0.006	0.639	0.005	0.640	0.005
	[M+1] ⁺	0.236	0.004	0.235	0.002	0.234	0.002
	[M+2] ⁺	0.095	0.001	0.095	0.002	0.095	0.002
	[M+3] ⁺	0.023	0.000	0.023	0.001	0.023	0.001
	[M+4] ⁺	0.006	0.000	0.007	0.000	0.007	0.001
	[M+5] ⁺	0.001	0.000	0.001	0.000	0.001	0.001
	[M+6] ⁺	0.000	0.000	0.000	0.000	0.001	0.000
90	[M] ⁺	0.631	0.011	0.636	0.004	0.638	0.006
	[M+1] ⁺	0.239	0.008	0.234	0.001	0.233	0.002
	[M+2] ⁺	0.097	0.003	0.096	0.002	0.095	0.003
	[M+3] ⁺	0.024	0.000	0.024	0.001	0.024	0.001
	[M+4] ⁺	0.007	0.000	0.008	0.000	0.008	0.001
	[M+5] ⁺	0.001	0.000	0.002	0.000	0.002	0.000
	[M+6] ⁺	0.001	0.000	0.001	0.000	0.001	0.000
120	[M] ⁺	0.629	0.010	0.633	0.006	0.635	0.006
	[M+1] ⁺	0.237	0.007	0.232	0.002	0.232	0.003
	[M+2] ⁺	0.097	0.003	0.096	0.002	0.096	0.003
	[M+3] ⁺	0.025	0.000	0.026	0.001	0.025	0.001
	[M+4] ⁺	0.009	0.001	0.009	0.001	0.009	0.000
	[M+5] ⁺	0.002	0.000	0.002	0.000	0.002	0.000
	[M+6] ⁺	0.001	0.000	0.001	0.000	0.001	0.000
150	[M] ⁺	0.631	0.004	0.630	0.004	0.631	0.006
	[M+1] ⁺	0.233	0.003	0.232	0.002	0.231	0.002
	[M+2] ⁺	0.096	0.001	0.096	0.002	0.096	0.002
	[M+3] ⁺	0.026	0.000	0.027	0.001	0.026	0.001
	[M+4] ⁺	0.010	0.000	0.011	0.001	0.011	0.000
	[M+5] ⁺	0.003	0.000	0.003	0.000	0.003	0.000
	[M+6] ⁺	0.001	0.000	0.002	0.000	0.002	0.000

Labeling time (s)	Isotopomer	No treatment		DMSO		Imazapyr	
		AM	SD	AM	SD	AM	SD
180	[M] ⁺	0.629	0.002	0.625	0.002	0.629	0.005
	[M+1] ⁺	0.231	0.002	0.232	0.001	0.230	0.003
	[M+2] ⁺	0.096	0.001	0.097	0.001	0.096	0.002
	[M+3] ⁺	0.027	0.000	0.028	0.001	0.027	0.001
	[M+4] ⁺	0.012	0.000	0.012	0.001	0.012	0.001
	[M+5] ⁺	0.003	0.000	0.004	0.000	0.004	0.000
	[M+6] ⁺	0.002	0.000	0.002	0.000	0.002	0.000
300	[M] ⁺	0.612	0.004	0.610	0.005	0.612	0.005
	[M+1] ⁺	0.227	0.003	0.226	0.002	0.226	0.002
	[M+2] ⁺	0.097	0.001	0.097	0.002	0.097	0.002
	[M+3] ⁺	0.032	0.001	0.033	0.001	0.032	0.001
	[M+4] ⁺	0.019	0.001	0.020	0.002	0.019	0.002
	[M+5] ⁺	0.008	0.000	0.008	0.001	0.008	0.001
	[M+6] ⁺	0.005	0.000	0.006	0.001	0.006	0.001
420	[M] ⁺	0.599	0.009	0.597	0.003	0.602	0.007
	[M+1] ⁺	0.225	0.006	0.221	0.002	0.223	0.001
	[M+2] ⁺	0.097	0.003	0.096	0.002	0.096	0.002
	[M+3] ⁺	0.035	0.002	0.036	0.001	0.035	0.002
	[M+4] ⁺	0.025	0.002	0.027	0.002	0.025	0.002
	[M+5] ⁺	0.011	0.001	0.012	0.001	0.011	0.001
	[M+6] ⁺	0.008	0.001	0.010	0.001	0.009	0.001
600	[M] ⁺	0.577	0.012	0.577	0.008	0.578	0.011
	[M+1] ⁺	0.217	0.004	0.214	0.003	0.215	0.003
	[M+2] ⁺	0.096	0.002	0.095	0.002	0.096	0.002
	[M+3] ⁺	0.041	0.003	0.041	0.002	0.041	0.003
	[M+4] ⁺	0.036	0.005	0.037	0.004	0.037	0.004
	[M+5] ⁺	0.018	0.003	0.019	0.002	0.019	0.002
	[M+6] ⁺	0.015	0.002	0.017	0.002	0.015	0.002
1800	[M] ⁺	0.468	0.014	0.459	0.021	0.475	0.021
	[M+1] ⁺	0.178	0.005	0.174	0.007	0.179	0.007
	[M+2] ⁺	0.092	0.002	0.089	0.002	0.091	0.002
	[M+3] ⁺	0.071	0.006	0.070	0.006	0.067	0.006
	[M+4] ⁺	0.095	0.007	0.100	0.011	0.092	0.011
	[M+5] ⁺	0.054	0.004	0.058	0.007	0.053	0.007
	[M+6] ⁺	0.042	0.004	0.049	0.007	0.043	0.005

Table A9. 36 Mass isotopomer distribution of sucrose, measured by GC-MS

Mean values ($n = 5$) of isotopomer abundance are listed. Abbreviations: SD (standard deviation), AM (arithmetic mean).

Labeling time (s)	Isotopomer	No treatment		DMSO		Imazapyr	
		AM	SD	AM	SD	AM	SD
0	[M] ⁺	0.642	0.018	0.652	0.004	0.654	0.002
	[M+1] ⁺	0.219	0.011	0.212	0.001	0.211	0.001
	[M+2] ⁺	0.107	0.005	0.105	0.002	0.103	0.002
	[M+3] ⁺	0.023	0.001	0.023	0.001	0.023	0.000
	[M+4] ⁺	0.007	0.000	0.007	0.000	0.007	0.000
	[M+5] ⁺	0.001	0.000	0.001	0.000	0.001	0.000
	[M+6] ⁺	0.000	0.000	0.000	0.000	0.000	0.000
10	[M] ⁺	0.642	0.017	0.652	0.004	0.653	0.004
	[M+1] ⁺	0.219	0.011	0.212	0.001	0.211	0.001
	[M+2] ⁺	0.107	0.005	0.104	0.002	0.104	0.002
	[M+3] ⁺	0.023	0.001	0.023	0.001	0.023	0.001
	[M+4] ⁺	0.007	0.000	0.007	0.000	0.007	0.001
	[M+5] ⁺	0.001	0.000	0.001	0.000	0.002	0.001
	[M+6] ⁺	0.000	0.000	0.000	0.000	0.001	0.001
20	[M] ⁺	0.652	0.006	0.651	0.004	0.648	0.011
	[M+1] ⁺	0.213	0.004	0.213	0.001	0.209	0.004
	[M+2] ⁺	0.104	0.002	0.105	0.002	0.103	0.003
	[M+3] ⁺	0.023	0.000	0.023	0.001	0.024	0.002
	[M+4] ⁺	0.007	0.000	0.007	0.000	0.009	0.004
	[M+5] ⁺	0.001	0.000	0.001	0.000	0.004	0.006
	[M+6] ⁺	0.000	0.000	0.000	0.000	0.003	0.005
30	[M] ⁺	0.642	0.024	0.651	0.004	0.652	0.006
	[M+1] ⁺	0.219	0.015	0.212	0.001	0.211	0.002
	[M+2] ⁺	0.107	0.007	0.105	0.002	0.104	0.003
	[M+3] ⁺	0.023	0.002	0.023	0.001	0.023	0.001
	[M+4] ⁺	0.007	0.000	0.007	0.000	0.007	0.001
	[M+5] ⁺	0.001	0.000	0.001	0.000	0.002	0.001
	[M+6] ⁺	0.000	0.000	0.000	0.000	0.001	0.001
40	[M] ⁺	0.650	0.006	0.653	0.005	0.652	0.004
	[M+1] ⁺	0.214	0.004	0.211	0.001	0.211	0.001
	[M+2] ⁺	0.104	0.002	0.104	0.003	0.104	0.002
	[M+3] ⁺	0.023	0.000	0.023	0.001	0.023	0.001
	[M+4] ⁺	0.007	0.000	0.007	0.000	0.007	0.001
	[M+5] ⁺	0.001	0.000	0.001	0.000	0.002	0.001
	[M+6] ⁺	0.000	0.000	0.000	0.000	0.001	0.001
50	[M] ⁺	0.652	0.002	0.650	0.004	0.653	0.005
	[M+1] ⁺	0.212	0.002	0.212	0.001	0.211	0.001
	[M+2] ⁺	0.104	0.001	0.105	0.002	0.104	0.003

Labeling time (s)	Isotopomer	No treatment		DMSO		Imazapyr	
		AM	SD	AM	SD	AM	SD
	[M+3] ⁺	0.023	0.000	0.024	0.001	0.023	0.001
	[M+4] ⁺	0.007	0.000	0.007	0.000	0.007	0.001
	[M+5] ⁺	0.001	0.000	0.002	0.000	0.002	0.001
	[M+6] ⁺	0.001	0.000	0.001	0.000	0.001	0.001
60	[M] ⁺	0.648	0.008	0.650	0.004	0.651	0.005
	[M+1] ⁺	0.214	0.005	0.212	0.001	0.211	0.001
	[M+2] ⁺	0.105	0.002	0.105	0.003	0.104	0.002
	[M+3] ⁺	0.023	0.000	0.024	0.001	0.024	0.001
	[M+4] ⁺	0.007	0.000	0.007	0.000	0.007	0.001
	[M+5] ⁺	0.001	0.000	0.002	0.000	0.002	0.001
	[M+6] ⁺	0.001	0.000	0.001	0.000	0.001	0.001
90	[M] ⁺	0.640	0.016	0.648	0.003	0.650	0.005
	[M+1] ⁺	0.218	0.010	0.211	0.001	0.210	0.001
	[M+2] ⁺	0.107	0.005	0.105	0.002	0.104	0.003
	[M+3] ⁺	0.025	0.001	0.024	0.001	0.024	0.001
	[M+4] ⁺	0.008	0.000	0.008	0.000	0.008	0.000
	[M+5] ⁺	0.002	0.000	0.002	0.000	0.002	0.000
	[M+6] ⁺	0.001	0.000	0.001	0.000	0.001	0.000
120	[M] ⁺	0.639	0.014	0.646	0.005	0.648	0.006
	[M+1] ⁺	0.216	0.009	0.210	0.001	0.209	0.003
	[M+2] ⁺	0.106	0.004	0.104	0.002	0.104	0.003
	[M+3] ⁺	0.025	0.001	0.025	0.001	0.025	0.001
	[M+4] ⁺	0.009	0.000	0.009	0.001	0.009	0.000
	[M+5] ⁺	0.003	0.000	0.003	0.000	0.003	0.000
	[M+6] ⁺	0.001	0.000	0.002	0.000	0.001	0.000
150	[M] ⁺	0.643	0.005	0.644	0.004	0.645	0.005
	[M+1] ⁺	0.211	0.004	0.209	0.001	0.209	0.001
	[M+2] ⁺	0.105	0.001	0.105	0.002	0.104	0.003
	[M+3] ⁺	0.025	0.000	0.026	0.001	0.026	0.001
	[M+4] ⁺	0.010	0.000	0.010	0.000	0.010	0.000
	[M+5] ⁺	0.004	0.000	0.004	0.000	0.004	0.000
	[M+6] ⁺	0.002	0.000	0.002	0.000	0.002	0.000
180	[M] ⁺	0.643	0.004	0.640	0.002	0.644	0.006
	[M+1] ⁺	0.209	0.003	0.209	0.001	0.208	0.002
	[M+2] ⁺	0.104	0.001	0.105	0.001	0.104	0.003
	[M+3] ⁺	0.026	0.000	0.026	0.001	0.026	0.001
	[M+4] ⁺	0.011	0.000	0.011	0.001	0.011	0.001
	[M+5] ⁺	0.005	0.000	0.005	0.001	0.005	0.000
	[M+6] ⁺	0.003	0.000	0.003	0.000	0.003	0.000
300	[M] ⁺	0.628	0.005	0.627	0.004	0.629	0.004
	[M+1] ⁺	0.206	0.003	0.205	0.001	0.205	0.002
	[M+2] ⁺	0.104	0.001	0.104	0.002	0.104	0.002

Labeling time (s)	Isotopomer	No treatment		DMSO		Imazapyr	
		AM	SD	AM	SD	AM	SD
	[M+3] ⁺	0.028	0.001	0.029	0.001	0.028	0.001
	[M+4] ⁺	0.015	0.001	0.016	0.001	0.016	0.001
	[M+5] ⁺	0.010	0.000	0.011	0.001	0.011	0.001
	[M+6] ⁺	0.007	0.000	0.009	0.001	0.008	0.001
420	[M] ⁺	0.616	0.011	0.617	0.003	0.621	0.006
	[M+1] ⁺	0.205	0.007	0.201	0.002	0.202	0.001
	[M+2] ⁺	0.103	0.004	0.102	0.002	0.102	0.002
	[M+3] ⁺	0.030	0.001	0.030	0.001	0.029	0.001
	[M+4] ⁺	0.019	0.001	0.019	0.001	0.018	0.001
	[M+5] ⁺	0.015	0.002	0.017	0.001	0.015	0.001
	[M+6] ⁺	0.011	0.001	0.014	0.001	0.012	0.001
600	[M] ⁺	0.598	0.011	0.600	0.006	0.601	0.009
	[M+1] ⁺	0.199	0.005	0.195	0.003	0.196	0.002
	[M+2] ⁺	0.101	0.002	0.100	0.002	0.100	0.002
	[M+3] ⁺	0.032	0.002	0.031	0.001	0.032	0.002
	[M+4] ⁺	0.025	0.003	0.025	0.002	0.025	0.003
	[M+5] ⁺	0.025	0.004	0.027	0.003	0.026	0.003
	[M+6] ⁺	0.020	0.003	0.023	0.003	0.021	0.002
1800	[M] ⁺	0.505	0.012	0.496	0.019	0.511	0.019
	[M+1] ⁺	0.167	0.004	0.163	0.006	0.167	0.006
	[M+2] ⁺	0.089	0.001	0.087	0.003	0.089	0.003
	[M+3] ⁺	0.043	0.004	0.041	0.002	0.041	0.003
	[M+4] ⁺	0.059	0.006	0.059	0.007	0.056	0.007
	[M+5] ⁺	0.078	0.006	0.084	0.011	0.075	0.010
	[M+6] ⁺	0.061	0.005	0.070	0.010	0.061	0.008

Table A9. 37 Mass isotopomer distribution of threonine, measured by GC-MS

Mean values ($n = 5$) of isotopomer abundance are listed. Abbreviations: SD (standard deviation), AM (arithmetic mean).

Labeling time (s)	Isotopomer	No treatment		DMSO		Imazapyr	
		AM	SD	AM	SD	AM	SD
0	[M] ⁺	0.681	0.001	0.683	0.003	0.684	0.001
	[M+1] ⁺	0.199	0.000	0.199	0.002	0.198	0.000
	[M+2] ⁺	0.097	0.002	0.099	0.001	0.099	0.001
	[M+3] ⁺	0.022	0.003	0.020	0.002	0.020	0.000
10	[M] ⁺	0.682	0.002	0.682	0.003	0.682	0.003
	[M+1] ⁺	0.199	0.001	0.200	0.003	0.200	0.004
	[M+2] ⁺	0.098	0.001	0.098	0.001	0.098	0.001
	[M+3] ⁺	0.021	0.001	0.020	0.001	0.020	0.001
20	[M] ⁺	0.682	0.000	0.683	0.002	0.681	0.003
	[M+1] ⁺	0.200	0.001	0.199	0.001	0.199	0.002

Labeling time (s)	Isotopomer	No treatment		DMSO		Imazapyr	
		AM	SD	AM	SD	AM	SD
30	[M+2] ⁺	0.099	0.001	0.098	0.001	0.099	0.002
	[M+3] ⁺	0.020	0.001	0.020	0.001	0.021	0.002
	[M] ⁺	0.684	0.004	0.683	0.003	0.681	0.003
	[M+1] ⁺	0.198	0.003	0.200	0.004	0.201	0.003
	[M+2] ⁺	0.098	0.001	0.098	0.001	0.098	0.001
40	[M+3] ⁺	0.020	0.000	0.019	0.001	0.020	0.001
	[M] ⁺	0.682	0.001	0.684	0.002	0.681	0.004
	[M+1] ⁺	0.199	0.001	0.199	0.002	0.202	0.005
	[M+2] ⁺	0.099	0.001	0.097	0.001	0.098	0.001
	[M+3] ⁺	0.020	0.001	0.020	0.001	0.019	0.001
50	[M] ⁺	0.683	0.001	0.684	0.001	0.685	0.002
	[M+1] ⁺	0.199	0.001	0.198	0.001	0.198	0.002
	[M+2] ⁺	0.098	0.001	0.098	0.001	0.098	0.001
	[M+3] ⁺	0.020	0.001	0.020	0.000	0.019	0.002
	[M] ⁺	0.682	0.002	0.685	0.005	0.681	0.004
60	[M+1] ⁺	0.199	0.002	0.198	0.003	0.201	0.006
	[M+2] ⁺	0.098	0.000	0.098	0.001	0.099	0.003
	[M+3] ⁺	0.020	0.001	0.019	0.001	0.019	0.001
	[M] ⁺	0.682	0.000	0.679	0.009	0.682	0.002
	[M+1] ⁺	0.200	0.001	0.204	0.015	0.200	0.002
90	[M+2] ⁺	0.098	0.001	0.099	0.006	0.099	0.001
	[M+3] ⁺	0.021	0.001	0.019	0.002	0.020	0.001
	[M] ⁺	0.681	0.002	0.687	0.011	0.680	0.003
	[M+1] ⁺	0.200	0.002	0.197	0.009	0.201	0.004
	[M+2] ⁺	0.098	0.000	0.098	0.001	0.098	0.001
120	[M+3] ⁺	0.021	0.001	0.018	0.003	0.020	0.001
	[M] ⁺	0.682	0.001	0.682	0.003	0.683	0.002
	[M+1] ⁺	0.200	0.001	0.198	0.004	0.199	0.001
	[M+2] ⁺	0.098	0.001	0.099	0.004	0.098	0.000
	[M+3] ⁺	0.020	0.002	0.021	0.002	0.020	0.001
150	[M] ⁺	0.682	0.002	0.680	0.003	0.682	0.005
	[M+1] ⁺	0.200	0.001	0.201	0.004	0.201	0.004
	[M+2] ⁺	0.098	0.001	0.099	0.001	0.099	0.002
	[M+3] ⁺	0.020	0.001	0.020	0.001	0.019	0.001
	[M] ⁺	0.682	0.000	0.680	0.006	0.680	0.002
180	[M+1] ⁺	0.200	0.000	0.203	0.007	0.201	0.002
	[M+2] ⁺	0.098	0.001	0.098	0.001	0.099	0.001
	[M+3] ⁺	0.020	0.001	0.019	0.000	0.020	0.001
	[M] ⁺	0.682	0.001	0.682	0.001	0.682	0.003
	[M+1] ⁺	0.200	0.001	0.199	0.001	0.199	0.002
300	[M+2] ⁺	0.098	0.000	0.099	0.001	0.099	0.000
	[M+3] ⁺	0.020	0.001	0.020	0.001	0.020	0.001
	[M] ⁺	0.682	0.001	0.682	0.001	0.682	0.003
	[M+1] ⁺	0.200	0.001	0.199	0.001	0.199	0.002
	[M+2] ⁺	0.098	0.000	0.099	0.001	0.099	0.000
420	[M+3] ⁺	0.021	0.001	0.020	0.001	0.020	0.001

Labeling time (s)	Isotopomer	No treatment		DMSO		Imazapyr	
		AM	SD	AM	SD	AM	SD
600	[M] ⁺	0.681	0.001	0.682	0.003	0.683	0.001
	[M+1] ⁺	0.199	0.001	0.198	0.001	0.198	0.001
	[M+2] ⁺	0.098	0.001	0.100	0.001	0.099	0.000
	[M+3] ⁺	0.021	0.001	0.021	0.002	0.020	0.000
1800	[M] ⁺	0.660	0.002	0.654	0.005	0.665	0.004
	[M+1] ⁺	0.198	0.001	0.198	0.003	0.201	0.005
	[M+2] ⁺	0.105	0.001	0.107	0.002	0.103	0.001
	[M+3] ⁺	0.036	0.002	0.042	0.004	0.032	0.004

Table A9. 38 Mass isotopomer distribution of valine, measured by GC-MS

Mean values ($n = 5$) of isotopomer abundance are listed. Abbreviations: SD (standard deviation), AM (arithmetic mean).

Labeling time (s)	Isotopomer	No treatment		DMSO		Imazapyr	
		AM	SD	AM	SD	AM	SD
0	[M] ⁺	0.758	0.004	0.761	0.005	0.761	0.004
	[M+1] ⁺	0.172	0.003	0.169	0.004	0.167	0.002
	[M+2] ⁺	0.070	0.001	0.070	0.001	0.072	0.004
10	[M] ⁺	0.759	0.003	0.761	0.005	0.760	0.015
	[M+1] ⁺	0.170	0.003	0.169	0.004	0.170	0.013
	[M+2] ⁺	0.070	0.001	0.070	0.001	0.071	0.002
20	[M] ⁺	0.759	0.003	0.762	0.008	0.753	0.026
	[M+1] ⁺	0.171	0.003	0.168	0.006	0.169	0.013
	[M+2] ⁺	0.070	0.000	0.070	0.002	0.078	0.015
30	[M] ⁺	0.759	0.003	0.762	0.004	0.761	0.014
	[M+1] ⁺	0.171	0.003	0.169	0.003	0.168	0.006
	[M+2] ⁺	0.070	0.001	0.069	0.001	0.071	0.008
40	[M] ⁺	0.758	0.003	0.760	0.005	0.763	0.015
	[M+1] ⁺	0.171	0.003	0.170	0.004	0.168	0.010
	[M+2] ⁺	0.070	0.000	0.070	0.001	0.069	0.005
50	[M] ⁺	0.759	0.003	0.761	0.004	0.756	0.011
	[M+1] ⁺	0.171	0.003	0.169	0.003	0.175	0.013
	[M+2] ⁺	0.070	0.000	0.070	0.001	0.069	0.004
60	[M] ⁺	0.758	0.003	0.761	0.007	0.760	0.010
	[M+1] ⁺	0.172	0.004	0.170	0.005	0.169	0.006
	[M+2] ⁺	0.070	0.001	0.070	0.002	0.070	0.004
90	[M] ⁺	0.756	0.004	0.758	0.008	0.764	0.011
	[M+1] ⁺	0.173	0.004	0.170	0.006	0.167	0.009
	[M+2] ⁺	0.071	0.000	0.072	0.006	0.069	0.003
120	[M] ⁺	0.756	0.004	0.758	0.004	0.768	0.016
	[M+1] ⁺	0.173	0.004	0.171	0.004	0.164	0.011
	[M+2] ⁺	0.071	0.001	0.071	0.001	0.068	0.005

Labeling time (s)	Isotopomer	No treatment		DMSO		Imazapyr	
		AM	SD	AM	SD	AM	SD
150	[M] ⁺	0.755	0.003	0.756	0.005	0.764	0.012
	[M+1] ⁺	0.174	0.003	0.172	0.004	0.167	0.009
	[M+2] ⁺	0.072	0.001	0.072	0.002	0.069	0.003
180	[M] ⁺	0.754	0.003	0.758	0.007	0.763	0.011
	[M+1] ⁺	0.174	0.002	0.171	0.005	0.166	0.007
	[M+2] ⁺	0.072	0.000	0.072	0.002	0.070	0.005
300	[M] ⁺	0.748	0.003	0.750	0.012	0.761	0.009
	[M+1] ⁺	0.176	0.003	0.173	0.007	0.169	0.007
	[M+2] ⁺	0.076	0.001	0.077	0.005	0.070	0.002
420	[M] ⁺	0.741	0.003	0.738	0.008	0.752	0.013
	[M+1] ⁺	0.178	0.003	0.177	0.005	0.186	0.031
	[M+2] ⁺	0.081	0.002	0.085	0.003	0.062	0.019
600	[M] ⁺	0.606	0.270	0.726	0.008	0.761	0.015
	[M+1] ⁺	0.260	0.176	0.179	0.005	0.168	0.008
	[M+2] ⁺	0.134	0.094	0.095	0.004	0.071	0.007
1800	[M] ⁺	0.686	0.004	0.658	0.021	0.746	0.020
	[M+1] ⁺	0.190	0.002	0.199	0.019	0.178	0.017
	[M+2] ⁺	0.124	0.005	0.143	0.013	0.076	0.011

Table A9. 39 Mass isotopomer distribution of pyruvate, measured by GC-MS

Mean values ($n = 5$) of isotopomer abundance are listed. Abbreviations: SD (standard deviation), AM (arithmetic mean).

Labeling time (s)	Isotopomer	No treatment		DMSO		Imazapyr	
		AM	SD	AM	SD	AM	SD
0	[M] ⁺	0.852	0.007	0.859	0.007	0.859	0.004
	[M+1] ⁺	0.108	0.004	0.104	0.006	0.103	0.005
	[M+2] ⁺	0.040	0.004	0.037	0.003	0.038	0.002
10	[M] ⁺	0.783	0.008	0.778	0.030	0.790	0.016
	[M+1] ⁺	0.169	0.006	0.174	0.026	0.160	0.016
	[M+2] ⁺	0.048	0.003	0.048	0.005	0.050	0.002
20	[M] ⁺	0.753	0.037	0.735	0.034	0.753	0.024
	[M+1] ⁺	0.189	0.031	0.202	0.026	0.180	0.017
	[M+2] ⁺	0.058	0.007	0.063	0.008	0.067	0.016
30	[M] ⁺	0.705	0.007	0.706	0.046	0.740	0.027
	[M+1] ⁺	0.220	0.007	0.217	0.032	0.188	0.019
	[M+2] ⁺	0.076	0.002	0.077	0.014	0.072	0.009
40	[M] ⁺	0.719	0.070	0.688	0.043	0.725	0.021
	[M+1] ⁺	0.188	0.081	0.224	0.028	0.194	0.016
	[M+2] ⁺	0.093	0.013	0.088	0.015	0.081	0.006
50	[M] ⁺	0.698	0.065	0.684	0.046	0.708	0.019
	[M+1] ⁺	0.210	0.042	0.219	0.031	0.199	0.015

Labeling time (s)	Isotopomer	No treatment		DMSO		Imazapyr	
		AM	SD	AM	SD	AM	SD
60	[M+2] ⁺	0.092	0.022	0.097	0.015	0.094	0.005
	[M] ⁺	0.654	0.012	0.671	0.041	0.703	0.042
	[M+1] ⁺	0.234	0.007	0.221	0.024	0.199	0.028
	[M+2] ⁺	0.112	0.005	0.109	0.017	0.099	0.014
90	[M] ⁺	0.641	0.022	0.663	0.053	0.702	0.039
	[M+1] ⁺	0.225	0.017	0.208	0.028	0.186	0.020
	[M+2] ⁺	0.134	0.007	0.129	0.025	0.113	0.019
120	[M] ⁺	0.649	0.018	0.674	0.036	0.719	0.028
	[M+1] ⁺	0.205	0.008	0.191	0.013	0.169	0.016
	[M+2] ⁺	0.145	0.010	0.135	0.025	0.111	0.013
150	[M] ⁺	0.648	0.013	0.667	0.043	0.703	0.016
	[M+1] ⁺	0.195	0.008	0.187	0.021	0.167	0.008
	[M+2] ⁺	0.157	0.005	0.147	0.023	0.130	0.010
180	[M] ⁺	0.680	0.066	0.673	0.032	0.699	0.018
	[M+1] ⁺	0.173	0.024	0.173	0.016	0.164	0.008
	[M+2] ⁺	0.146	0.042	0.153	0.017	0.137	0.012
300	[M] ⁺	0.652	0.019	0.663	0.026	0.700	0.066
	[M+1] ⁺	0.163	0.006	0.160	0.013	0.149	0.019
	[M+2] ⁺	0.185	0.015	0.178	0.018	0.151	0.048
420	[M] ⁺	0.634	0.017	0.647	0.045	0.680	0.031
	[M+1] ⁺	0.160	0.004	0.155	0.014	0.146	0.011
	[M+2] ⁺	0.206	0.017	0.199	0.034	0.174	0.020
600	[M] ⁺	0.626	0.006	0.653	0.034	0.654	0.032
	[M+1] ⁺	0.151	0.003	0.120	0.049	0.147	0.008
	[M+2] ⁺	0.224	0.007	0.226	0.053	0.198	0.025
1800	[M] ⁺	0.536	0.018	0.546	0.048	0.615	0.079
	[M+1] ⁺	0.174	0.010	0.166	0.011	0.134	0.067
	[M+2] ⁺	0.290	0.011	0.287	0.038	0.251	0.017

Table A9. 40 Mass isotopomer distribution of proline, measured by GC-MS

Mean values ($n = 5$) of isotopomer abundance are listed. Abbreviations: SD (standard deviation), AM (arithmetic mean).

Labeling time (s)	Isotopomer	No treatment		DMSO		Imazapyr	
		AM	SD	AM	SD	AM	SD
0	[M] ⁺	0.842	0.002	0.840	0.005	0.840	0.004
	[M+1] ⁺	0.113	0.001	0.113	0.001	0.114	0.001
	[M+2] ⁺	0.040	0.001	0.042	0.004	0.042	0.002
	[M+3] ⁺	0.004	0.000	0.004	0.001	0.004	0.000
	[M+4] ⁺	0.001	0.000	0.001	0.000	0.001	0.000
10	[M] ⁺	0.842	0.001	0.838	0.005	0.840	0.004
	[M+1] ⁺	0.113	0.001	0.113	0.001	0.114	0.001

Labeling time (s)	Isotopomer	No treatment		DMSO		Imazapyr	
		AM	SD	AM	SD	AM	SD
20	[M+2] ⁺	0.040	0.001	0.044	0.004	0.042	0.003
	[M+3] ⁺	0.004	0.000	0.004	0.000	0.004	0.000
	[M+4] ⁺	0.001	0.000	0.001	0.000	0.001	0.000
	[M] ⁺	0.842	0.001	0.838	0.005	0.837	0.003
	[M+1] ⁺	0.113	0.001	0.113	0.001	0.114	0.001
30	[M+2] ⁺	0.040	0.001	0.044	0.004	0.044	0.002
	[M+3] ⁺	0.004	0.000	0.004	0.001	0.004	0.000
	[M+4] ⁺	0.001	0.000	0.001	0.000	0.001	0.000
	[M] ⁺	0.841	0.003	0.838	0.004	0.838	0.003
	[M+1] ⁺	0.113	0.001	0.114	0.003	0.114	0.001
40	[M+2] ⁺	0.041	0.003	0.042	0.004	0.043	0.002
	[M+3] ⁺	0.004	0.000	0.004	0.000	0.004	0.000
	[M+4] ⁺	0.001	0.000	0.001	0.000	0.001	0.000
	[M] ⁺	0.840	0.002	0.841	0.007	0.840	0.003
	[M+1] ⁺	0.114	0.001	0.112	0.001	0.114	0.001
50	[M+2] ⁺	0.041	0.002	0.042	0.005	0.042	0.003
	[M+3] ⁺	0.004	0.000	0.004	0.001	0.004	0.000
	[M+4] ⁺	0.001	0.000	0.001	0.000	0.001	0.000
	[M] ⁺	0.840	0.002	0.839	0.005	0.840	0.005
	[M+1] ⁺	0.113	0.001	0.113	0.001	0.113	0.001
60	[M+2] ⁺	0.042	0.002	0.043	0.005	0.042	0.003
	[M+3] ⁺	0.004	0.000	0.004	0.001	0.004	0.000
	[M+4] ⁺	0.001	0.000	0.001	0.000	0.001	0.000
	[M] ⁺	0.841	0.002	0.838	0.005	0.840	0.003
	[M+1] ⁺	0.113	0.001	0.113	0.001	0.114	0.001
90	[M+2] ⁺	0.041	0.002	0.044	0.004	0.042	0.002
	[M+3] ⁺	0.004	0.000	0.004	0.001	0.004	0.000
	[M+4] ⁺	0.001	0.000	0.001	0.000	0.001	0.000
	[M] ⁺	0.842	0.001	0.836	0.009	0.841	0.003
	[M+1] ⁺	0.114	0.001	0.113	0.001	0.114	0.002
120	[M+2] ⁺	0.040	0.001	0.044	0.004	0.041	0.002
	[M+3] ⁺	0.004	0.000	0.004	0.001	0.004	0.000
	[M+4] ⁺	0.001	0.000	0.004	0.006	0.001	0.000
	[M] ⁺	0.841	0.002	0.840	0.004	0.841	0.004
	[M+1] ⁺	0.113	0.001	0.113	0.001	0.114	0.002
150	[M+2] ⁺	0.041	0.002	0.042	0.004	0.041	0.003
	[M+3] ⁺	0.004	0.000	0.004	0.000	0.004	0.000
	[M+4] ⁺	0.001	0.000	0.001	0.000	0.001	0.000
	[M] ⁺	0.841	0.003	0.837	0.005	0.840	0.004
150	[M+1] ⁺	0.114	0.001	0.113	0.001	0.114	0.001
	[M+2] ⁺	0.041	0.003	0.044	0.005	0.042	0.002
	[M+3] ⁺	0.004	0.000	0.004	0.001	0.004	0.000
	[M+4] ⁺	0.001	0.000	0.001	0.000	0.001	0.000

Labeling time (s)	Isotopomer	No treatment		DMSO		Imazapyr	
		AM	SD	AM	SD	AM	SD
180	[M+4] ⁺	0.001	0.000	0.001	0.000	0.001	0.000
	[M] ⁺	0.841	0.002	0.837	0.004	0.841	0.003
	[M+1] ⁺	0.114	0.001	0.114	0.002	0.114	0.002
	[M+2] ⁺	0.041	0.002	0.044	0.004	0.041	0.002
	[M+3] ⁺	0.004	0.000	0.004	0.001	0.004	0.000
300	[M+4] ⁺	0.001	0.000	0.001	0.000	0.001	0.000
	[M] ⁺	0.839	0.004	0.836	0.005	0.839	0.003
	[M+1] ⁺	0.114	0.001	0.114	0.001	0.114	0.002
	[M+2] ⁺	0.042	0.003	0.045	0.004	0.043	0.003
	[M+3] ⁺	0.004	0.001	0.004	0.001	0.004	0.000
420	[M+4] ⁺	0.001	0.000	0.001	0.000	0.001	0.000
	[M] ⁺	0.838	0.002	0.835	0.003	0.835	0.005
	[M+1] ⁺	0.114	0.001	0.115	0.001	0.115	0.002
	[M+2] ⁺	0.042	0.002	0.045	0.003	0.045	0.004
	[M+3] ⁺	0.004	0.001	0.005	0.000	0.004	0.001
600	[M+4] ⁺	0.001	0.000	0.002	0.000	0.001	0.000
	[M] ⁺	0.835	0.005	0.829	0.003	0.831	0.005
	[M+1] ⁺	0.115	0.001	0.116	0.001	0.116	0.001
	[M+2] ⁺	0.045	0.004	0.049	0.003	0.047	0.004
	[M+3] ⁺	0.004	0.001	0.005	0.000	0.005	0.001
1800	[M+4] ⁺	0.004	0.001	0.010	0.003	0.006	0.001
	[M] ⁺	0.809	0.012	0.779	0.015	0.800	0.003
	[M+1] ⁺	0.120	0.001	0.123	0.002	0.121	0.001
	[M+2] ⁺	0.058	0.008	0.074	0.008	0.063	0.002
	[M+3] ⁺	0.009	0.002	0.015	0.003	0.011	0.001

Table A9. 41 Mass isotopomer distribution of phenylalanine, measured by GC-MS

Mean values ($n = 5$) of isotopomer abundance are listed. Abbreviations: SD (standard deviation), AM (arithmetic mean).

Labeling time (s)	Isotopomer	No treatment		DMSO		Imazapyr	
		AM	SD	AM	SD	AM	SD
0	[M] ⁺	0.770	0.007	0.764	0.028	0.774	0.005
	[M+1] ⁺	0.158	0.007	0.163	0.018	0.156	0.004
	[M+2] ⁺	0.072	0.002	0.073	0.010	0.070	0.002
10	[M] ⁺	0.773	0.003	0.773	0.007	0.773	0.006
	[M+1] ⁺	0.158	0.004	0.156	0.006	0.157	0.007
	[M+2] ⁺	0.068	0.003	0.070	0.003	0.070	0.002
20	[M] ⁺	0.774	0.007	0.775	0.003	0.771	0.016
	[M+1] ⁺	0.157	0.005	0.155	0.002	0.157	0.009
	[M+2] ⁺	0.069	0.002	0.070	0.002	0.072	0.007

Labeling time (s)	Isotopomer	No treatment		DMSO		Imazapyr	
		AM	SD	AM	SD	AM	SD
30	[M] ⁺	0.768	0.008	0.768	0.013	0.768	0.011
	[M+1] ⁺	0.162	0.006	0.161	0.012	0.160	0.007
	[M+2] ⁺	0.070	0.004	0.071	0.002	0.072	0.005
40	[M] ⁺	0.767	0.004	0.767	0.013	0.769	0.009
	[M+1] ⁺	0.162	0.004	0.163	0.011	0.159	0.005
	[M+2] ⁺	0.070	0.001	0.070	0.003	0.072	0.004
50	[M] ⁺	0.767	0.006	0.759	0.010	0.768	0.006
	[M+1] ⁺	0.162	0.003	0.169	0.008	0.161	0.007
	[M+2] ⁺	0.071	0.005	0.072	0.002	0.071	0.002
60	[M] ⁺	0.757	0.007	0.758	0.006	0.766	0.006
	[M+1] ⁺	0.169	0.005	0.168	0.005	0.161	0.006
	[M+2] ⁺	0.074	0.003	0.074	0.002	0.073	0.004
90	[M] ⁺	0.738	0.003	0.734	0.009	0.764	0.006
	[M+1] ⁺	0.181	0.003	0.180	0.008	0.164	0.005
	[M+2] ⁺	0.080	0.000	0.086	0.005	0.073	0.001
120	[M] ⁺	0.719	0.023	0.734	0.016	0.757	0.006
	[M+1] ⁺	0.193	0.018	0.182	0.012	0.166	0.004
	[M+2] ⁺	0.088	0.007	0.084	0.004	0.078	0.003
150	[M] ⁺	0.705	0.019	0.715	0.009	0.755	0.008
	[M+1] ⁺	0.196	0.011	0.191	0.008	0.169	0.006
	[M+2] ⁺	0.099	0.009	0.094	0.003	0.076	0.003
180	[M] ⁺	0.725	0.020	0.699	0.013	0.744	0.009
	[M+1] ⁺	0.181	0.011	0.199	0.010	0.173	0.008
	[M+2] ⁺	0.094	0.010	0.102	0.008	0.082	0.003
300	[M] ⁺	0.664	0.021	0.660	0.013	0.736	0.017
	[M+1] ⁺	0.202	0.010	0.202	0.009	0.172	0.008
	[M+2] ⁺	0.133	0.012	0.138	0.005	0.091	0.010
420	[M] ⁺	0.644	0.013	0.654	0.012	0.725	0.007
	[M+1] ⁺	0.201	0.004	0.199	0.006	0.176	0.004
	[M+2] ⁺	0.155	0.009	0.147	0.008	0.099	0.004
600	[M] ⁺	0.614	0.012	0.636	0.020	0.710	0.006
	[M+1] ⁺	0.206	0.006	0.197	0.009	0.178	0.003
	[M+2] ⁺	0.180	0.008	0.166	0.015	0.112	0.007
1800	[M] ⁺	0.537	0.021	0.541	0.015	0.626	0.023
	[M+1] ⁺	0.226	0.009	0.227	0.009	0.201	0.006
	[M+2] ⁺	0.237	0.016	0.231	0.010	0.172	0.019

Table A9. 42 Mass isotopomer distribution of malate, measured by GC-MS

Mean values ($n = 5$) of isotopomer abundance are listed. Abbreviations: SD (standard deviation), AM (arithmetic mean).

Labeling time (s)	Isotopomer	No treatment		DMSO		Imazapyr	
		AM	SD	AM	SD	AM	SD
0	[M] ⁺	1.000	0.000	1.000	0.000	1.000	0.001
	[M+1] ⁺	0.000	0.000	0.000	0.000	0.000	0.000
	[M+2] ⁺	0.000	0.000	0.000	0.000	0.000	0.000
	[M+3] ⁺	0.000	0.000	0.000	0.000	0.000	0.000
	[M+4] ⁺	0.000	0.000	0.000	0.000	0.000	0.000
10	[M] ⁺	1.000	0.000	1.000	0.000	1.000	0.000
	[M+1] ⁺	0.000	0.000	0.000	0.000	0.000	0.000
	[M+2] ⁺	0.000	0.000	0.000	0.000	0.000	0.000
	[M+3] ⁺	0.000	0.000	0.000	0.000	0.000	0.000
	[M+4] ⁺	0.000	0.000	0.000	0.000	0.000	0.000
20	[M] ⁺	1.000	0.000	1.000	0.000	1.000	0.000
	[M+1] ⁺	0.000	0.000	0.000	0.000	0.000	0.000
	[M+2] ⁺	0.000	0.000	0.000	0.000	0.000	0.000
	[M+3] ⁺	0.000	0.000	0.000	0.000	0.000	0.000
	[M+4] ⁺	0.000	0.000	0.000	0.000	0.000	0.000
30	[M] ⁺	1.000	0.000	1.000	0.000	1.000	0.000
	[M+1] ⁺	0.000	0.000	0.000	0.000	0.000	0.000
	[M+2] ⁺	0.000	0.000	0.000	0.000	0.000	0.000
	[M+3] ⁺	0.000	0.000	0.000	0.000	0.000	0.000
	[M+4] ⁺	0.000	0.000	0.000	0.000	0.000	0.000
40	[M] ⁺	1.000	0.000	1.000	0.000	1.000	0.000
	[M+1] ⁺	0.000	0.000	0.000	0.000	0.000	0.000
	[M+2] ⁺	0.000	0.000	0.000	0.000	0.000	0.000
	[M+3] ⁺	0.000	0.000	0.000	0.000	0.000	0.000
	[M+4] ⁺	0.000	0.000	0.000	0.000	0.000	0.000
50	[M] ⁺	1.000	0.000	1.000	0.000	1.000	0.000
	[M+1] ⁺	0.000	0.000	0.000	0.000	0.000	0.000
	[M+2] ⁺	0.000	0.000	0.000	0.000	0.000	0.000
	[M+3] ⁺	0.000	0.000	0.000	0.000	0.000	0.000
	[M+4] ⁺	0.000	0.000	0.000	0.000	0.000	0.000
60	[M] ⁺	1.000	0.000	1.000	0.000	1.000	0.000
	[M+1] ⁺	0.000	0.000	0.000	0.000	0.000	0.000
	[M+2] ⁺	0.000	0.000	0.000	0.000	0.000	0.000
	[M+3] ⁺	0.000	0.000	0.000	0.000	0.000	0.000
	[M+4] ⁺	0.000	0.000	0.000	0.000	0.000	0.000
90	[M] ⁺	1.000	0.000	1.000	0.000	1.000	0.000
	[M+1] ⁺	0.000	0.000	0.000	0.000	0.000	0.000
	[M+2] ⁺	0.000	0.000	0.000	0.000	0.000	0.000

Labeling time (s)	Isotopomer	No treatment		DMSO		Imazapyr	
		AM	SD	AM	SD	AM	SD
	[M+3] ⁺	0.000	0.000	0.000	0.000	0.000	0.000
	[M+4] ⁺	0.000	0.000	0.000	0.000	0.000	0.000
120	[M] ⁺	1.000	0.000	1.000	0.000	1.000	0.000
	[M+1] ⁺	0.000	0.000	0.000	0.000	0.000	0.000
	[M+2] ⁺	0.000	0.000	0.000	0.000	0.000	0.000
	[M+3] ⁺	0.000	0.000	0.000	0.000	0.000	0.000
	[M+4] ⁺	0.000	0.000	0.000	0.000	0.000	0.000
150	[M] ⁺	1.000	0.000	1.000	0.000	1.000	0.000
	[M+1] ⁺	0.000	0.000	0.000	0.000	0.000	0.000
	[M+2] ⁺	0.000	0.000	0.000	0.000	0.000	0.000
	[M+3] ⁺	0.000	0.000	0.000	0.000	0.000	0.000
	[M+4] ⁺	0.000	0.000	0.000	0.000	0.000	0.000
180	[M] ⁺	1.000	0.000	1.000	0.000	1.000	0.000
	[M+1] ⁺	0.000	0.000	0.000	0.000	0.000	0.000
	[M+2] ⁺	0.000	0.000	0.000	0.000	0.000	0.000
	[M+3] ⁺	0.000	0.000	0.000	0.000	0.000	0.000
	[M+4] ⁺	0.000	0.000	0.000	0.000	0.000	0.000
300	[M] ⁺	1.000	0.000	1.000	0.000	1.000	0.000
	[M+1] ⁺	0.000	0.000	0.000	0.000	0.000	0.000
	[M+2] ⁺	0.000	0.000	0.000	0.000	0.000	0.000
	[M+3] ⁺	0.000	0.000	0.000	0.000	0.000	0.000
	[M+4] ⁺	0.000	0.000	0.000	0.000	0.000	0.000
420	[M] ⁺	1.000	0.000	1.000	0.000	0.995	0.011
	[M+1] ⁺	0.000	0.000	0.000	0.000	0.000	0.000
	[M+2] ⁺	0.000	0.000	0.000	0.000	0.001	0.002
	[M+3] ⁺	0.000	0.000	0.000	0.000	0.000	0.001
	[M+4] ⁺	0.000	0.000	0.000	0.000	0.004	0.008
600	[M] ⁺	1.000	0.000	1.000	0.000	1.000	0.000
	[M+1] ⁺	0.000	0.000	0.000	0.000	0.000	0.000
	[M+2] ⁺	0.000	0.000	0.000	0.000	0.000	0.000
	[M+3] ⁺	0.000	0.000	0.000	0.000	0.000	0.000
	[M+4] ⁺	0.000	0.000	0.000	0.000	0.000	0.000
1800	[M] ⁺	1.000	0.000	0.999	0.001	1.000	0.000
	[M+1] ⁺	0.000	0.000	0.000	0.000	0.000	0.000
	[M+2] ⁺	0.000	0.000	0.000	0.000	0.000	0.000
	[M+3] ⁺	0.000	0.000	0.001	0.001	0.000	0.000
	[M+4] ⁺	0.000	0.000	0.000	0.000	0.000	0.000

Table A9. 43 Mass isotopomer distribution of leucine, measured by GC-MS

Mean values ($n = 5$) of isotopomer abundance are listed. Abbreviations: SD (standard deviation), AM (arithmetic mean).

Labeling time (s)	Isotopomer	Wild type		DMSO		Imazapyr	
		AM	SD	AM	SD	AM	SD
0	[M] ⁺	0.805	0.018	0.744	0.143	0.574	0.189
	[M+1] ⁺	0.138	0.018	0.197	0.125	0.317	0.175
	[M+2] ⁺	0.040	0.002	0.044	0.010	0.065	0.016
	[M+3] ⁺	0.013	0.016	0.013	0.011	0.034	0.037
	[M+4] ⁺	0.003	0.004	0.002	0.002	0.009	0.013
	[M+5] ⁺	0.001	0.000	0.001	0.003	0.002	0.003
10	[M] ⁺	0.795	0.020	0.727	0.119	0.543	0.327
	[M+1] ⁺	0.141	0.014	0.213	0.105	0.334	0.284
	[M+2] ⁺	0.040	0.003	0.047	0.009	0.063	0.024
	[M+3] ⁺	0.018	0.018	0.010	0.004	0.045	0.045
	[M+4] ⁺	0.004	0.005	0.001	0.001	0.012	0.014
	[M+5] ⁺	0.002	0.001	0.001	0.003	0.003	0.006
20	[M] ⁺	0.801	0.025	0.610	0.335	0.539	0.315
	[M+1] ⁺	0.144	0.021	0.308	0.286	0.326	0.276
	[M+2] ⁺	0.038	0.003	0.062	0.029	0.068	0.028
	[M+3] ⁺	0.013	0.010	0.014	0.014	0.049	0.044
	[M+4] ⁺	0.003	0.003	0.002	0.002	0.015	0.018
	[M+5] ⁺	0.002	0.001	0.003	0.007	0.003	0.006
30	[M] ⁺	0.782	0.017	0.727	0.099	0.464	0.255
	[M+1] ⁺	0.155	0.019	0.211	0.085	0.398	0.239
	[M+2] ⁺	0.040	0.004	0.050	0.012	0.080	0.026
	[M+3] ⁺	0.017	0.015	0.010	0.006	0.044	0.022
	[M+4] ⁺	0.004	0.004	0.002	0.002	0.011	0.011
	[M+5] ⁺	0.002	0.001	0.001	0.002	0.003	0.006
40	[M] ⁺	0.795	0.018	0.640	0.283	0.495	0.314
	[M+1] ⁺	0.142	0.007	0.264	0.238	0.387	0.271
	[M+2] ⁺	0.039	0.002	0.056	0.030	0.071	0.038
	[M+3] ⁺	0.017	0.019	0.031	0.027	0.036	0.026
	[M+4] ⁺	0.004	0.005	0.007	0.008	0.008	0.008
	[M+5] ⁺	0.002	0.001	0.003	0.005	0.003	0.005
50	[M] ⁺	0.793	0.031	0.724	0.089	0.564	0.313
	[M+1] ⁺	0.144	0.018	0.208	0.072	0.305	0.255
	[M+2] ⁺	0.038	0.004	0.053	0.014	0.066	0.042
	[M+3] ⁺	0.019	0.019	0.012	0.005	0.047	0.029
	[M+4] ⁺	0.005	0.006	0.002	0.002	0.014	0.010
	[M+5] ⁺	0.002	0.001	0.001	0.002	0.004	0.007
60	[M] ⁺	0.762	0.065	0.600	0.330	0.541	0.221
	[M+1] ⁺	0.158	0.025	0.301	0.252	0.321	0.176

Labeling time (s)	Isotopomer	Wild type		DMSO		Imazapyr	
		AM	SD	AM	SD	AM	SD
	[M+2] ⁺	0.045	0.010	0.069	0.042	0.063	0.028
	[M+3] ⁺	0.025	0.027	0.021	0.025	0.056	0.063
	[M+4] ⁺	0.007	0.008	0.005	0.006	0.016	0.017
	[M+5] ⁺	0.003	0.002	0.003	0.007	0.003	0.005
90	[M] ⁺	0.795	0.010	0.741	0.068	0.573	0.159
	[M+1] ⁺	0.143	0.017	0.182	0.049	0.296	0.123
	[M+2] ⁺	0.041	0.003	0.054	0.012	0.067	0.018
	[M+3] ⁺	0.015	0.017	0.015	0.010	0.046	0.030
	[M+4] ⁺	0.004	0.005	0.005	0.003	0.016	0.011
	[M+5] ⁺	0.002	0.001	0.003	0.004	0.001	0.003
120	[M] ⁺	0.786	0.031	0.741	0.096	0.492	0.325
	[M+1] ⁺	0.143	0.014	0.180	0.063	0.341	0.242
	[M+2] ⁺	0.041	0.004	0.051	0.017	0.087	0.046
	[M+3] ⁺	0.021	0.020	0.018	0.011	0.056	0.028
	[M+4] ⁺	0.006	0.006	0.009	0.007	0.021	0.012
	[M+5] ⁺	0.003	0.002	0.002	0.003	0.004	0.008
150	[M] ⁺	0.778	0.032	0.721	0.068	0.519	0.318
	[M+1] ⁺	0.147	0.011	0.193	0.047	0.321	0.218
	[M+2] ⁺	0.042	0.004	0.056	0.013	0.080	0.045
	[M+3] ⁺	0.024	0.023	0.018	0.009	0.052	0.033
	[M+4] ⁺	0.007	0.007	0.010	0.007	0.024	0.020
	[M+5] ⁺	0.003	0.002	0.001	0.002	0.005	0.009
180	[M] ⁺	0.790	0.037	0.672	0.135	0.517	0.289
	[M+1] ⁺	0.136	0.024	0.214	0.079	0.300	0.187
	[M+2] ⁺	0.043	0.006	0.067	0.025	0.077	0.041
	[M+3] ⁺	0.021	0.023	0.029	0.020	0.071	0.042
	[M+4] ⁺	0.006	0.006	0.015	0.012	0.030	0.022
	[M+5] ⁺	0.003	0.002	0.002	0.003	0.005	0.009
300	[M] ⁺	0.767	0.023	0.573	0.319	0.619	0.255
	[M+1] ⁺	0.148	0.010	0.240	0.147	0.234	0.140
	[M+2] ⁺	0.050	0.005	0.083	0.045	0.067	0.038
	[M+3] ⁺	0.023	0.017	0.057	0.063	0.050	0.046
	[M+4] ⁺	0.008	0.005	0.041	0.053	0.029	0.034
	[M+5] ⁺	0.003	0.001	0.007	0.013	0.002	0.002
420	[M] ⁺	0.736	0.013	0.727	0.029	0.459	0.310
	[M+1] ⁺	0.150	0.014	0.161	0.012	0.281	0.134
	[M+2] ⁺	0.060	0.003	0.063	0.008	0.088	0.048
	[M+3] ⁺	0.037	0.022	0.028	0.009	0.091	0.056
	[M+4] ⁺	0.013	0.003	0.018	0.008	0.067	0.064
	[M+5] ⁺	0.004	0.001	0.002	0.002	0.014	0.015
600	[M] ⁺	0.609	0.206	0.563	0.310	0.463	0.361
	[M+1] ⁺	0.172	0.046	0.200	0.101	0.258	0.130

Labeling time (s)	Isotopomer	Wild type		DMSO		Imazapyr	
		AM	SD	AM	SD	AM	SD
	[M+2] ⁺	0.081	0.027	0.082	0.033	0.091	0.054
	[M+3] ⁺	0.070	0.057	0.075	0.079	0.094	0.082
	[M+4] ⁺	0.053	0.067	0.068	0.085	0.080	0.083
	[M+5] ⁺	0.015	0.015	0.011	0.014	0.014	0.017
1800	[M] ⁺	0.590	0.136	0.428	0.291	0.479	0.309
	[M+1] ⁺	0.153	0.009	0.203	0.080	0.225	0.077
	[M+2] ⁺	0.085	0.016	0.101	0.025	0.083	0.043
	[M+3] ⁺	0.083	0.051	0.121	0.080	0.103	0.090
	[M+4] ⁺	0.070	0.054	0.119	0.096	0.094	0.093
	[M+5] ⁺	0.020	0.008	0.027	0.013	0.016	0.017

Table A9. 44 Mass isotopomer distribution of isoleucine, measured by GC-MS

Mean values ($n = 5$) of isotopomer abundance are listed. Abbreviations: SD (standard deviation), AM (arithmetic mean).

Labeling time (s)	Isotopomer	No treatment		DMSO		Imazapyr	
		AM	SD	AM	SD	AM	SD
0	[M] ⁺	0.776	0.001	0.771	0.004	0.776	0.008
	[M+1] ⁺	0.157	0.002	0.161	0.003	0.157	0.007
	[M+2] ⁺	0.067	0.002	0.068	0.002	0.068	0.002
10	[M] ⁺	0.771	0.004	0.779	0.010	0.746	0.060
	[M+1] ⁺	0.159	0.002	0.153	0.008	0.189	0.073
	[M+2] ⁺	0.070	0.002	0.068	0.005	0.065	0.014
20	[M] ⁺	0.769	0.004	0.777	0.016	0.755	0.023
	[M+1] ⁺	0.161	0.003	0.154	0.010	0.186	0.056
	[M+2] ⁺	0.071	0.002	0.069	0.009	0.059	0.033
30	[M] ⁺	0.770	0.003	0.772	0.008	0.771	0.003
	[M+1] ⁺	0.158	0.003	0.158	0.012	0.161	0.005
	[M+2] ⁺	0.072	0.005	0.070	0.004	0.068	0.003
40	[M] ⁺	0.772	0.004	0.770	0.005	0.771	0.009
	[M+1] ⁺	0.158	0.002	0.158	0.008	0.158	0.010
	[M+2] ⁺	0.070	0.002	0.072	0.004	0.071	0.002
50	[M] ⁺	0.769	0.004	0.769	0.010	0.761	0.017
	[M+1] ⁺	0.160	0.004	0.158	0.007	0.180	0.049
	[M+2] ⁺	0.071	0.002	0.074	0.004	0.059	0.033
60	[M] ⁺	0.769	0.009	0.757	0.020	0.769	0.002
	[M+1] ⁺	0.160	0.004	0.173	0.028	0.157	0.005
	[M+2] ⁺	0.071	0.007	0.070	0.010	0.074	0.005
90	[M] ⁺	0.770	0.005	0.770	0.007	0.770	0.006
	[M+1] ⁺	0.160	0.004	0.157	0.010	0.161	0.008
	[M+2] ⁺	0.069	0.002	0.073	0.006	0.069	0.002
120	[M] ⁺	0.763	0.007	0.769	0.006	0.769	0.007

Labeling time (s)	Isotopomer	No treatment		DMSO		Imazapyr	
		AM	SD	AM	SD	AM	SD
150	[M+1] ⁺	0.164	0.004	0.158	0.003	0.157	0.008
	[M+2] ⁺	0.073	0.006	0.073	0.006	0.074	0.003
	[M] ⁺	0.767	0.007	0.772	0.003	0.772	0.009
180	[M+1] ⁺	0.160	0.005	0.157	0.005	0.157	0.010
	[M+2] ⁺	0.073	0.003	0.070	0.005	0.071	0.005
	[M] ⁺	0.767	0.003	0.763	0.009	0.769	0.006
300	[M+1] ⁺	0.162	0.002	0.160	0.007	0.159	0.006
	[M+2] ⁺	0.071	0.001	0.076	0.008	0.072	0.005
	[M] ⁺	0.768	0.005	0.733	0.080	0.767	0.009
420	[M+1] ⁺	0.159	0.003	0.180	0.046	0.160	0.009
	[M+2] ⁺	0.073	0.004	0.087	0.034	0.073	0.003
	[M] ⁺	0.768	0.005	0.771	0.008	0.742	0.056
600	[M+1] ⁺	0.160	0.004	0.156	0.009	0.203	0.092
	[M+2] ⁺	0.072	0.004	0.073	0.003	0.054	0.036
	[M] ⁺	0.768	0.012	0.757	0.028	0.757	0.023
1800	[M+1] ⁺	0.158	0.009	0.165	0.023	0.182	0.055
	[M+2] ⁺	0.074	0.005	0.078	0.011	0.061	0.034
	[M] ⁺	0.756	0.011	0.727	0.042	0.736	0.063
1800	[M+1] ⁺	0.166	0.008	0.175	0.028	0.203	0.097
	[M+2] ⁺	0.078	0.003	0.098	0.014	0.061	0.034

Table A9. 45 Mass isotopomer distribution of glycerate_292, measured by GC-MS

Mean values ($n = 5$) of isotopomer abundance are listed. Abbreviations: SD (standard deviation), AM (arithmetic mean).

Labeling time (s)	Isotopomer	No treatment		DMSO		Imazapyr	
		AM	SD	AM	SD	AM	SD
0	[M] ⁺	0.690	0.006	0.693	0.001	0.689	0.007
	[M+1] ⁺	0.192	0.002	0.191	0.001	0.192	0.002
	[M+2] ⁺	0.098	0.004	0.097	0.000	0.099	0.004
	[M+3] ⁺	0.019	0.001	0.019	0.000	0.019	0.002
10	[M] ⁺	0.669	0.003	0.628	0.035	0.632	0.019
	[M+1] ⁺	0.207	0.003	0.238	0.025	0.230	0.018
	[M+2] ⁺	0.102	0.003	0.108	0.006	0.112	0.006
	[M+3] ⁺	0.022	0.001	0.027	0.004	0.027	0.002
20	[M] ⁺	0.635	0.044	0.607	0.054	0.609	0.044
	[M+1] ⁺	0.229	0.029	0.248	0.034	0.237	0.025
	[M+2] ⁺	0.110	0.009	0.116	0.013	0.124	0.023
	[M+3] ⁺	0.026	0.006	0.030	0.007	0.031	0.008
30	[M] ⁺	0.647	0.016	0.601	0.033	0.601	0.034
	[M+1] ⁺	0.219	0.009	0.246	0.019	0.243	0.022
	[M+2] ⁺	0.109	0.005	0.122	0.010	0.124	0.008

Labeling time (s)	Isotopomer	No treatment		DMSO		Imazapyr	
		AM	SD	AM	SD	AM	SD
40	[M+3] ⁺	0.025	0.002	0.031	0.005	0.032	0.004
	[M] ⁺	0.633	0.026	0.594	0.029	0.583	0.049
	[M+1] ⁺	0.223	0.014	0.245	0.016	0.249	0.029
	[M+2] ⁺	0.116	0.009	0.128	0.009	0.133	0.014
	[M+3] ⁺	0.027	0.004	0.033	0.004	0.035	0.007
50	[M] ⁺	0.577	0.072	0.556	0.050	0.574	0.048
	[M+1] ⁺	0.248	0.037	0.257	0.026	0.246	0.024
	[M+2] ⁺	0.138	0.024	0.147	0.017	0.142	0.018
	[M+3] ⁺	0.036	0.011	0.040	0.008	0.037	0.007
60	[M] ⁺	0.620	0.026	0.553	0.049	0.570	0.047
	[M+1] ⁺	0.222	0.013	0.253	0.024	0.244	0.024
	[M+2] ⁺	0.127	0.009	0.153	0.018	0.147	0.016
	[M+3] ⁺	0.031	0.004	0.041	0.007	0.039	0.007
90	[M] ⁺	0.593	0.024	0.518	0.046	0.547	0.018
	[M+1] ⁺	0.224	0.008	0.247	0.017	0.238	0.008
	[M+2] ⁺	0.147	0.012	0.185	0.022	0.171	0.007
	[M+3] ⁺	0.037	0.004	0.050	0.008	0.045	0.003
120	[M] ⁺	0.556	0.026	0.491	0.064	0.500	0.046
	[M+1] ⁺	0.227	0.010	0.241	0.017	0.241	0.014
	[M+2] ⁺	0.173	0.011	0.211	0.035	0.204	0.024
	[M+3] ⁺	0.044	0.004	0.057	0.012	0.055	0.008
150	[M] ⁺	0.536	0.014	0.483	0.043	0.504	0.025
	[M+1] ⁺	0.225	0.004	0.235	0.010	0.229	0.008
	[M+2] ⁺	0.190	0.008	0.222	0.025	0.211	0.013
	[M+3] ⁺	0.049	0.003	0.059	0.008	0.056	0.005
180	[M] ⁺	0.490	0.050	0.464	0.042	0.500	0.028
	[M+1] ⁺	0.231	0.014	0.231	0.008	0.227	0.006
	[M+2] ⁺	0.220	0.028	0.240	0.027	0.216	0.017
	[M+3] ⁺	0.059	0.009	0.064	0.008	0.057	0.005
300	[M] ⁺	0.450	0.020	0.422	0.043	0.424	0.033
	[M+1] ⁺	0.225	0.005	0.223	0.004	0.226	0.005
	[M+2] ⁺	0.257	0.013	0.280	0.032	0.276	0.022
	[M+3] ⁺	0.068	0.004	0.075	0.009	0.074	0.007
420	[M] ⁺	0.448	0.020	0.403	0.033	0.412	0.008
	[M+1] ⁺	0.223	0.004	0.222	0.002	0.223	0.002
	[M+2] ⁺	0.260	0.012	0.296	0.025	0.288	0.004
	[M+3] ⁺	0.069	0.004	0.079	0.007	0.077	0.001
600	[M] ⁺	0.424	0.034	0.391	0.015	0.392	0.020
	[M+1] ⁺	0.223	0.009	0.221	0.004	0.224	0.004
	[M+2] ⁺	0.279	0.019	0.306	0.013	0.303	0.013
	[M+3] ⁺	0.074	0.007	0.082	0.004	0.081	0.004
1800	[M] ⁺	0.372	0.026	0.326	0.026	0.355	0.031

Labeling time (s)	Isotopomer	No treatment		DMSO		Imazapyr	
		AM	SD	AM	SD	AM	SD
	[M+1] ⁺	0.242	0.011	0.245	0.006	0.242	0.006
	[M+2] ⁺	0.303	0.014	0.336	0.016	0.316	0.020
	[M+3] ⁺	0.083	0.005	0.093	0.005	0.087	0.006

Table A9. 46 Mass isotopomer distribution of glycerate₁₈₉, measured by GC-MS

Mean values ($n = 5$) of isotopomer abundance are listed. Abbreviations: SD (standard deviation), AM (arithmetic mean).

Labeling time (s)	Isotopomer	No treatment		DMSO		Imazapyr	
		AM	SD	AM	SD	AM	SD
0	[M] ⁺	0.748	0.005	0.751	0.001	0.748	0.006
	[M+1] ⁺	0.166	0.003	0.165	0.001	0.166	0.001
	[M+2] ⁺	0.086	0.003	0.084	0.001	0.086	0.005
10	[M] ⁺	0.744	0.004	0.741	0.006	0.733	0.011
	[M+1] ⁺	0.168	0.003	0.170	0.003	0.172	0.002
	[M+2] ⁺	0.088	0.002	0.089	0.003	0.095	0.009
20	[M] ⁺	0.733	0.012	0.726	0.017	0.711	0.039
	[M+1] ⁺	0.174	0.007	0.178	0.008	0.182	0.011
	[M+2] ⁺	0.093	0.006	0.096	0.009	0.107	0.028
30	[M] ⁺	0.731	0.006	0.714	0.014	0.710	0.012
	[M+1] ⁺	0.175	0.004	0.184	0.006	0.185	0.005
	[M+2] ⁺	0.094	0.003	0.102	0.008	0.105	0.008
40	[M] ⁺	0.716	0.013	0.702	0.012	0.692	0.020
	[M+1] ⁺	0.183	0.006	0.189	0.005	0.192	0.008
	[M+2] ⁺	0.101	0.007	0.109	0.008	0.115	0.013
50	[M] ⁺	0.681	0.033	0.668	0.025	0.676	0.026
	[M+1] ⁺	0.199	0.012	0.204	0.008	0.200	0.009
	[M+2] ⁺	0.120	0.021	0.128	0.018	0.125	0.017
60	[M] ⁺	0.694	0.014	0.657	0.023	0.664	0.021
	[M+1] ⁺	0.196	0.005	0.209	0.005	0.205	0.006
	[M+2] ⁺	0.110	0.009	0.134	0.018	0.131	0.016
90	[M] ⁺	0.654	0.017	0.600	0.026	0.620	0.006
	[M+1] ⁺	0.219	0.005	0.233	0.004	0.227	0.004
	[M+2] ⁺	0.128	0.012	0.167	0.025	0.153	0.009
120	[M] ⁺	0.610	0.016	0.543	0.065	0.564	0.029
	[M+1] ⁺	0.236	0.004	0.255	0.013	0.246	0.004
	[M+2] ⁺	0.153	0.014	0.201	0.054	0.189	0.029
150	[M] ⁺	0.580	0.012	0.534	0.028	0.550	0.020
	[M+1] ⁺	0.250	0.004	0.260	0.003	0.256	0.009
	[M+2] ⁺	0.170	0.010	0.206	0.032	0.195	0.017
180	[M] ⁺	0.535	0.036	0.506	0.034	0.542	0.025
	[M+1] ⁺	0.260	0.004	0.266	0.004	0.256	0.006

Labeling time (s)	Isotopomer	No treatment		DMSO		Imazapyr	
		AM	SD	AM	SD	AM	SD
300	[M+2] ⁺	0.205	0.037	0.229	0.036	0.203	0.022
	[M] ⁺	0.489	0.021	0.460	0.042	0.462	0.030
	[M+1] ⁺	0.260	0.007	0.259	0.003	0.258	0.004
	[M+2] ⁺	0.251	0.017	0.281	0.042	0.280	0.027
420	[M] ⁺	0.490	0.020	0.442	0.035	0.451	0.007
	[M+1] ⁺	0.250	0.005	0.252	0.006	0.253	0.004
	[M+2] ⁺	0.260	0.017	0.306	0.035	0.296	0.008
600	[M] ⁺	0.466	0.035	0.431	0.016	0.432	0.021
	[M+1] ⁺	0.246	0.009	0.246	0.006	0.250	0.007
	[M+2] ⁺	0.288	0.027	0.323	0.020	0.319	0.018
1800	[M] ⁺	0.414	0.028	0.356	0.040	0.394	0.033
	[M+1] ⁺	0.266	0.014	0.274	0.012	0.264	0.007
	[M+2] ⁺	0.320	0.019	0.371	0.029	0.342	0.027

Table A9. 47 Mass isotopomer distribution of glutamate, measured by GC-MS

Mean values ($n = 5$) of isotopomer abundance are listed. Abbreviations: SD (standard deviation), AM (arithmetic mean).

Labeling time (s)	Isotopomer	No treatment		DMSO		Imazapyr	
		AM	SD	AM	SD	AM	SD
0	[M] ⁺	0.817	0.005	0.785	0.062	0.825	0.003
	[M+1] ⁺	0.127	0.003	0.120	0.015	0.124	0.001
	[M+2] ⁺	0.044	0.002	0.044	0.008	0.041	0.001
	[M+3] ⁺	0.008	0.001	0.010	0.005	0.007	0.001
	[M+4] ⁺	0.004	0.001	0.041	0.080	0.003	0.001
10	[M] ⁺	0.820	0.006	0.800	0.057	0.820	0.013
	[M+1] ⁺	0.125	0.002	0.120	0.009	0.126	0.006
	[M+2] ⁺	0.043	0.002	0.040	0.003	0.041	0.003
	[M+3] ⁺	0.008	0.002	0.007	0.003	0.008	0.003
	[M+4] ⁺	0.004	0.000	0.033	0.066	0.004	0.002
20	[M] ⁺	0.822	0.002	0.808	0.031	0.818	0.016
	[M+1] ⁺	0.125	0.001	0.122	0.008	0.125	0.004
	[M+2] ⁺	0.043	0.001	0.041	0.003	0.044	0.006
	[M+3] ⁺	0.007	0.000	0.007	0.001	0.009	0.006
	[M+4] ⁺	0.004	0.001	0.021	0.039	0.003	0.001
30	[M] ⁺	0.821	0.006	0.812	0.032	0.818	0.014
	[M+1] ⁺	0.125	0.002	0.120	0.008	0.126	0.003
	[M+2] ⁺	0.043	0.002	0.040	0.004	0.044	0.005
	[M+3] ⁺	0.007	0.001	0.006	0.002	0.009	0.005
	[M+4] ⁺	0.004	0.001	0.022	0.041	0.004	0.001
40	[M] ⁺	0.821	0.005	0.800	0.035	0.826	0.010
	[M+1] ⁺	0.126	0.002	0.121	0.011	0.123	0.006

Labeling time (s)	Isotopomer	No treatment		DMSO		Imazapyr	
		AM	SD	AM	SD	AM	SD
50	[M+2] ⁺	0.042	0.001	0.045	0.009	0.040	0.002
	[M+3] ⁺	0.007	0.002	0.010	0.008	0.008	0.002
	[M+4] ⁺	0.004	0.000	0.025	0.046	0.003	0.001
	[M] ⁺	0.817	0.005	0.813	0.021	0.817	0.017
	[M+1] ⁺	0.127	0.002	0.122	0.004	0.126	0.007
60	[M+2] ⁺	0.043	0.002	0.041	0.002	0.044	0.006
	[M+3] ⁺	0.009	0.002	0.008	0.002	0.009	0.004
	[M+4] ⁺	0.004	0.000	0.016	0.026	0.004	0.002
	[M] ⁺	0.817	0.006	0.813	0.025	0.821	0.014
	[M+1] ⁺	0.127	0.002	0.122	0.006	0.124	0.006
90	[M+2] ⁺	0.044	0.002	0.041	0.002	0.043	0.004
	[M+3] ⁺	0.009	0.003	0.007	0.001	0.009	0.005
	[M+4] ⁺	0.004	0.000	0.017	0.030	0.003	0.001
	[M] ⁺	0.823	0.002	0.804	0.038	0.822	0.009
	[M+1] ⁺	0.125	0.002	0.117	0.010	0.125	0.002
120	[M+2] ⁺	0.041	0.001	0.041	0.002	0.042	0.004
	[M+3] ⁺	0.007	0.001	0.011	0.007	0.008	0.003
	[M+4] ⁺	0.003	0.000	0.026	0.044	0.003	0.000
	[M] ⁺	0.819	0.004	0.804	0.024	0.818	0.017
	[M+1] ⁺	0.126	0.003	0.122	0.007	0.127	0.005
150	[M+2] ⁺	0.043	0.002	0.045	0.008	0.043	0.004
	[M+3] ⁺	0.009	0.002	0.011	0.007	0.009	0.007
	[M+4] ⁺	0.004	0.000	0.017	0.026	0.004	0.002
	[M] ⁺	0.818	0.005	0.808	0.024	0.820	0.015
	[M+1] ⁺	0.126	0.002	0.124	0.011	0.127	0.007
180	[M+2] ⁺	0.044	0.002	0.041	0.003	0.042	0.003
	[M+3] ⁺	0.008	0.001	0.012	0.005	0.007	0.003
	[M+4] ⁺	0.004	0.001	0.015	0.024	0.004	0.001
	[M] ⁺	0.819	0.007	0.819	0.021	0.815	0.019
	[M+1] ⁺	0.126	0.002	0.123	0.007	0.126	0.005
300	[M+2] ⁺	0.043	0.002	0.044	0.007	0.043	0.005
	[M+3] ⁺	0.008	0.002	0.010	0.008	0.011	0.008
	[M+4] ⁺	0.004	0.001	0.004	0.001	0.004	0.002
	[M] ⁺	0.817	0.008	0.813	0.028	0.819	0.010
	[M+1] ⁺	0.126	0.002	0.117	0.014	0.126	0.004
420	[M+2] ⁺	0.044	0.004	0.041	0.004	0.042	0.002
	[M+3] ⁺	0.008	0.003	0.010	0.004	0.009	0.004
	[M+4] ⁺	0.004	0.001	0.018	0.032	0.004	0.001
	[M] ⁺	0.817	0.008	0.813	0.028	0.819	0.010
	[M+1] ⁺	0.126	0.002	0.117	0.014	0.126	0.004
420	[M+2] ⁺	0.042	0.002	0.042	0.004	0.043	0.002
	[M+3] ⁺	0.008	0.002	0.008	0.004	0.008	0.002
	[M] ⁺	0.819	0.005	0.810	0.022	0.818	0.008
	[M+1] ⁺	0.127	0.002	0.124	0.006	0.127	0.003

Labeling time (s)	Isotopomer	No treatment		DMSO		Imazapyr	
		AM	SD	AM	SD	AM	SD
600	[M+4] ⁺	0.004	0.000	0.016	0.026	0.004	0.001
	[M] ⁺	0.815	0.009	0.772	0.081	0.818	0.004
	[M+1] ⁺	0.127	0.002	0.155	0.074	0.128	0.002
	[M+2] ⁺	0.045	0.004	0.047	0.007	0.044	0.001
	[M+3] ⁺	0.009	0.003	0.010	0.004	0.007	0.001
	[M+4] ⁺	0.004	0.000	0.016	0.027	0.004	0.000
1800	[M] ⁺	0.797	0.009	0.774	0.017	0.787	0.016
	[M+1] ⁺	0.134	0.004	0.140	0.005	0.134	0.005
	[M+2] ⁺	0.053	0.004	0.060	0.007	0.057	0.005
	[M+3] ⁺	0.011	0.001	0.017	0.004	0.014	0.006
	[M+4] ⁺	0.006	0.001	0.009	0.003	0.007	0.002

Table A9. 48 Mass isotopomer distribution of fumarate, measured by GC-MS

Mean values ($n = 5$) of isotopomer abundance are listed. Abbreviations: SD (standard deviation), AM (arithmetic mean).

Labeling time (s)	Isotopomer	No treatment		DMSO		Imazapyr	
		AM	SD	AM	SD	AM	SD
0	[M] ⁺	0.738	0.021	0.746	0.004	0.722	0.052
	[M+1] ⁺	0.163	0.019	0.163	0.014	0.172	0.035
	[M+2] ⁺	0.080	0.003	0.076	0.007	0.090	0.024
	[M+3] ⁺	0.019	0.003	0.014	0.002	0.014	0.007
	[M+4] ⁺	0.000	0.000	0.001	0.003	0.003	0.005
	10	[M] ⁺	0.734	0.020	0.751	0.011	0.746
[M+1] ⁺		0.163	0.021	0.155	0.005	0.141	0.058
[M+2] ⁺		0.085	0.004	0.079	0.001	0.088	0.014
[M+3] ⁺		0.017	0.004	0.012	0.006	0.016	0.003
[M+4] ⁺		0.001	0.002	0.002	0.004	0.010	0.022
20		[M] ⁺	0.741	0.019	0.746	0.006	0.756
	[M+1] ⁺	0.161	0.018	0.160	0.006	0.122	0.082
	[M+2] ⁺	0.081	0.004	0.080	0.004	0.094	0.011
	[M+3] ⁺	0.017	0.004	0.013	0.006	0.019	0.006
	[M+4] ⁺	0.000	0.001	0.002	0.004	0.009	0.020
	30	[M] ⁺	0.733	0.029	0.746	0.006	0.748
[M+1] ⁺		0.165	0.017	0.159	0.005	0.147	0.066
[M+2] ⁺		0.080	0.005	0.079	0.003	0.086	0.007
[M+3] ⁺		0.019	0.006	0.014	0.003	0.016	0.008
[M+4] ⁺		0.003	0.007	0.002	0.005	0.003	0.007
40		[M] ⁺	0.730	0.031	0.739	0.017	0.753
	[M+1] ⁺	0.170	0.027	0.158	0.015	0.144	0.051
	[M+2] ⁺	0.082	0.001	0.079	0.006	0.085	0.008
	[M+3] ⁺	0.018	0.005	0.015	0.005	0.016	0.007

Labeling time (s)	Isotopomer	No treatment		DMSO		Imazapyr	
		AM	SD	AM	SD	AM	SD
50	[M+4] ⁺	0.000	0.000	0.009	0.020	0.003	0.007
	[M] ⁺	0.735	0.025	0.750	0.008	0.742	0.054
	[M+1] ⁺	0.164	0.022	0.155	0.004	0.143	0.054
	[M+2] ⁺	0.083	0.007	0.081	0.001	0.089	0.011
	[M+3] ⁺	0.016	0.004	0.013	0.005	0.016	0.008
60	[M+4] ⁺	0.001	0.003	0.002	0.004	0.010	0.023
	[M] ⁺	0.725	0.029	0.738	0.015	0.762	0.072
	[M+1] ⁺	0.169	0.025	0.165	0.019	0.120	0.068
	[M+2] ⁺	0.087	0.004	0.081	0.002	0.088	0.006
	[M+3] ⁺	0.018	0.005	0.013	0.004	0.017	0.004
90	[M+4] ⁺	0.000	0.000	0.002	0.004	0.013	0.030
	[M] ⁺	0.721	0.021	0.722	0.034	0.740	0.060
	[M+1] ⁺	0.174	0.019	0.174	0.022	0.148	0.061
	[M+2] ⁺	0.085	0.002	0.087	0.015	0.090	0.014
	[M+3] ⁺	0.019	0.002	0.015	0.002	0.015	0.006
120	[M+4] ⁺	0.001	0.002	0.002	0.004	0.007	0.017
	[M] ⁺	0.736	0.028	0.754	0.062	0.742	0.056
	[M+1] ⁺	0.165	0.019	0.139	0.067	0.154	0.065
	[M+2] ⁺	0.080	0.007	0.084	0.007	0.085	0.006
	[M+3] ⁺	0.018	0.006	0.015	0.004	0.017	0.007
150	[M+4] ⁺	0.001	0.003	0.009	0.019	0.003	0.007
	[M] ⁺	0.731	0.023	0.734	0.010	0.742	0.062
	[M+1] ⁺	0.167	0.019	0.160	0.012	0.148	0.058
	[M+2] ⁺	0.082	0.005	0.082	0.005	0.090	0.017
	[M+3] ⁺	0.019	0.004	0.016	0.003	0.017	0.004
180	[M+4] ⁺	0.001	0.003	0.008	0.018	0.003	0.007
	[M] ⁺	0.733	0.032	0.735	0.008	0.733	0.058
	[M+1] ⁺	0.162	0.025	0.165	0.007	0.151	0.057
	[M+2] ⁺	0.084	0.008	0.081	0.005	0.094	0.017
	[M+3] ⁺	0.020	0.006	0.015	0.006	0.017	0.008
300	[M+4] ⁺	0.001	0.002	0.003	0.007	0.006	0.013
	[M] ⁺	0.722	0.033	0.736	0.013	0.737	0.016
	[M+1] ⁺	0.171	0.021	0.164	0.006	0.165	0.017
	[M+2] ⁺	0.087	0.008	0.080	0.006	0.080	0.002
	[M+3] ⁺	0.020	0.006	0.018	0.004	0.015	0.008
420	[M+4] ⁺	0.001	0.002	0.003	0.006	0.003	0.007
	[M] ⁺	0.708	0.026	0.731	0.020	0.744	0.056
	[M+1] ⁺	0.169	0.026	0.152	0.016	0.146	0.068
	[M+2] ⁺	0.094	0.011	0.088	0.007	0.090	0.012
	[M+3] ⁺	0.028	0.003	0.019	0.007	0.020	0.009
600	[M+4] ⁺	0.002	0.003	0.010	0.022	0.000	0.000
	[M] ⁺	0.694	0.025	0.703	0.028	0.724	0.053

Labeling time (s)	Isotopomer	No treatment		DMSO		Imazapyr	
		AM	SD	AM	SD	AM	SD
	[M+1] ⁺	0.174	0.015	0.169	0.025	0.151	0.050
	[M+2] ⁺	0.091	0.007	0.089	0.010	0.096	0.020
	[M+3] ⁺	0.029	0.007	0.023	0.008	0.024	0.009
	[M+4] ⁺	0.013	0.008	0.015	0.034	0.005	0.011
1800	[M] ⁺	0.651	0.037	0.673	0.022	0.704	0.069
	[M+1] ⁺	0.173	0.012	0.165	0.007	0.128	0.062
	[M+2] ⁺	0.096	0.012	0.102	0.015	0.109	0.017
	[M+3] ⁺	0.045	0.009	0.052	0.007	0.052	0.004
	[M+4] ⁺	0.036	0.009	0.009	0.019	0.007	0.016

Table A9. 49 Mass isotopomer distribution of glucose 6-phosphate, measured by GC-MS

Mean values ($n = 5$) of isotopomer abundance are listed. Abbreviations: SD (standard deviation), AM (arithmetic mean).

Labeling time (s)	Isotopomer	No treatment		DMSO		Imazapyr	
		AM	SD	AM	SD	AM	SD
0	[M] ⁺	0.661	0.029	0.661	0.021	0.706	0.075
	[M+1] ⁺	0.209	0.018	0.234	0.079	0.192	0.015
	[M+2] ⁺	0.130	0.016	0.106	0.059	0.102	0.075
10	[M] ⁺	0.662	0.029	0.701	0.037	0.654	0.032
	[M+1] ⁺	0.207	0.012	0.208	0.015	0.251	0.088
	[M+2] ⁺	0.130	0.026	0.091	0.051	0.095	0.056
20	[M] ⁺	0.622	0.087	0.684	0.059	0.664	0.032
	[M+1] ⁺	0.202	0.026	0.211	0.008	0.236	0.046
	[M+2] ⁺	0.176	0.106	0.105	0.059	0.100	0.057
30	[M] ⁺	0.673	0.027	0.661	0.020	0.610	0.051
	[M+1] ⁺	0.202	0.013	0.240	0.041	0.281	0.110
	[M+2] ⁺	0.126	0.021	0.099	0.057	0.109	0.062
40	[M] ⁺	0.634	0.035	0.672	0.099	0.649	0.095
	[M+1] ⁺	0.224	0.039	0.231	0.106	0.228	0.036
	[M+2] ⁺	0.142	0.026	0.097	0.064	0.123	0.072
50	[M] ⁺	0.618	0.046	0.646	0.018	0.608	0.048
	[M+1] ⁺	0.197	0.039	0.245	0.046	0.263	0.050
	[M+2] ⁺	0.185	0.035	0.110	0.061	0.128	0.075
60	[M] ⁺	0.606	0.024	0.670	0.081	0.676	0.106
	[M+1] ⁺	0.236	0.012	0.212	0.017	0.197	0.041
	[M+2] ⁺	0.158	0.016	0.118	0.066	0.127	0.072
90	[M] ⁺	0.559	0.019	0.623	0.101	0.568	0.028
	[M+1] ⁺	0.247	0.015	0.225	0.016	0.271	0.075
	[M+2] ⁺	0.195	0.020	0.152	0.085	0.161	0.091
120	[M] ⁺	0.522	0.023	0.553	0.057	0.529	0.043
	[M+1] ⁺	0.242	0.019	0.260	0.059	0.296	0.133

Labeling time (s)	Isotopomer	No treatment		DMSO		Imazapyr	
		AM	SD	AM	SD	AM	SD
150	[M+2] ⁺	0.236	0.031	0.187	0.107	0.175	0.101
	[M] ⁺	0.528	0.043	0.567	0.060	0.559	0.096
	[M+1] ⁺	0.243	0.017	0.251	0.044	0.250	0.015
	[M+2] ⁺	0.229	0.031	0.182	0.103	0.191	0.108
180	[M] ⁺	0.487	0.050	0.557	0.062	0.579	0.207
	[M+1] ⁺	0.257	0.039	0.253	0.047	0.198	0.083
	[M+2] ⁺	0.256	0.027	0.189	0.107	0.223	0.127
300	[M] ⁺	0.467	0.072	0.535	0.085	0.538	0.076
	[M+1] ⁺	0.240	0.032	0.255	0.038	0.257	0.041
	[M+2] ⁺	0.294	0.047	0.210	0.120	0.205	0.115
420	[M] ⁺	0.483	0.041	0.537	0.142	0.559	0.118
	[M+1] ⁺	0.246	0.011	0.240	0.022	0.249	0.021
	[M+2] ⁺	0.272	0.036	0.222	0.125	0.192	0.128
600	[M] ⁺	0.427	0.032	0.581	0.134	0.451	0.040
	[M+1] ⁺	0.256	0.013	0.214	0.074	0.313	0.169
	[M+2] ⁺	0.318	0.028	0.205	0.126	0.236	0.133
1800	[M] ⁺	0.414	0.017	0.502	0.078	0.497	0.106
	[M+1] ⁺	0.273	0.023	0.273	0.052	0.279	0.051
	[M+2] ⁺	0.314	0.026	0.225	0.126	0.225	0.135

Table A9. 50 Mass isotopomer distribution of citrate, measured by GC-MS

Mean values ($n = 5$) of isotopomer abundance are listed. Abbreviations: SD (standard deviation), AM (arithmetic mean).

Labeling time (s)	Isotopomer	No treatment		DMSO		Imazapyr	
		AM	SD	AM	SD	AM	SD
0	[M] ⁺	0.745	0.003	0.748	0.005	0.748	0.005
	[M+1] ⁺	0.169	0.003	0.165	0.002	0.165	0.002
	[M+2] ⁺	0.073	0.001	0.071	0.004	0.072	0.003
	[M+3] ⁺	0.011	0.001	0.011	0.002	0.010	0.002
	[M+4] ⁺	0.002	0.000	0.002	0.000	0.002	0.000
	[M+5] ⁺	0.000	0.000	0.002	0.003	0.002	0.003
10	[M] ⁺	0.745	0.001	0.744	0.004	0.744	0.007
	[M+1] ⁺	0.167	0.000	0.167	0.002	0.165	0.003
	[M+2] ⁺	0.074	0.001	0.074	0.001	0.074	0.003
	[M+3] ⁺	0.011	0.001	0.011	0.002	0.011	0.001
	[M+4] ⁺	0.003	0.000	0.003	0.000	0.003	0.000
	[M+5] ⁺	0.000	0.000	0.002	0.003	0.003	0.005
20	[M] ⁺	0.745	0.001	0.746	0.002	0.742	0.008
	[M+1] ⁺	0.167	0.000	0.167	0.001	0.165	0.006
	[M+2] ⁺	0.074	0.000	0.073	0.001	0.073	0.001
	[M+3] ⁺	0.011	0.001	0.011	0.001	0.011	0.001

Labeling time (s)	Isotopomer	No treatment		DMSO		Imazapyr	
		AM	SD	AM	SD	AM	SD
30	[M+4] ⁺	0.002	0.000	0.002	0.000	0.003	0.001
	[M+5] ⁺	0.000	0.000	0.001	0.000	0.006	0.010
	[M] ⁺	0.745	0.001	0.745	0.002	0.743	0.003
	[M+1] ⁺	0.168	0.001	0.167	0.001	0.167	0.001
	[M+2] ⁺	0.073	0.000	0.073	0.001	0.074	0.001
	[M+3] ⁺	0.012	0.001	0.011	0.001	0.011	0.001
40	[M+4] ⁺	0.002	0.001	0.002	0.000	0.003	0.001
	[M+5] ⁺	0.000	0.000	0.001	0.002	0.002	0.004
	[M] ⁺	0.744	0.004	0.739	0.015	0.745	0.001
	[M+1] ⁺	0.169	0.004	0.166	0.006	0.167	0.001
	[M+2] ⁺	0.073	0.000	0.072	0.001	0.072	0.003
	[M+3] ⁺	0.011	0.000	0.011	0.002	0.012	0.000
50	[M+4] ⁺	0.002	0.000	0.002	0.000	0.002	0.000
	[M+5] ⁺	0.000	0.000	0.010	0.018	0.002	0.003
	[M] ⁺	0.745	0.001	0.744	0.002	0.741	0.005
	[M+1] ⁺	0.167	0.001	0.168	0.003	0.167	0.002
	[M+2] ⁺	0.074	0.000	0.073	0.000	0.075	0.003
	[M+3] ⁺	0.012	0.000	0.011	0.001	0.011	0.001
60	[M+4] ⁺	0.002	0.000	0.003	0.000	0.003	0.000
	[M+5] ⁺	0.000	0.000	0.001	0.001	0.004	0.004
	[M] ⁺	0.745	0.001	0.745	0.005	0.744	0.005
	[M+1] ⁺	0.167	0.000	0.168	0.005	0.166	0.002
	[M+2] ⁺	0.074	0.001	0.072	0.002	0.073	0.001
	[M+3] ⁺	0.011	0.000	0.011	0.001	0.011	0.001
90	[M+4] ⁺	0.002	0.000	0.002	0.000	0.002	0.000
	[M+5] ⁺	0.000	0.000	0.001	0.002	0.004	0.006
	[M] ⁺	0.745	0.001	0.748	0.007	0.745	0.006
	[M+1] ⁺	0.167	0.000	0.164	0.004	0.166	0.001
	[M+2] ⁺	0.074	0.001	0.071	0.005	0.073	0.002
	[M+3] ⁺	0.011	0.000	0.011	0.002	0.011	0.002
120	[M+4] ⁺	0.002	0.000	0.003	0.001	0.002	0.000
	[M+5] ⁺	0.000	0.000	0.003	0.005	0.002	0.003
	[M] ⁺	0.742	0.004	0.743	0.006	0.745	0.004
	[M+1] ⁺	0.170	0.005	0.167	0.005	0.165	0.004
	[M+2] ⁺	0.074	0.001	0.073	0.003	0.073	0.003
	[M+3] ⁺	0.011	0.000	0.011	0.001	0.011	0.002
150	[M+4] ⁺	0.002	0.000	0.003	0.001	0.003	0.001
	[M+5] ⁺	0.000	0.000	0.003	0.005	0.002	0.003
	[M] ⁺	0.744	0.001	0.744	0.003	0.743	0.002
	[M+1] ⁺	0.168	0.001	0.167	0.001	0.166	0.002
	[M+2] ⁺	0.074	0.001	0.073	0.003	0.075	0.001
	[M+3] ⁺	0.012	0.001	0.012	0.001	0.012	0.001

Labeling time (s)	Isotopomer	No treatment		DMSO		Imazapyr	
		AM	SD	AM	SD	AM	SD
180	[M+4] ⁺	0.003	0.000	0.003	0.000	0.003	0.000
	[M+5] ⁺	0.000	0.000	0.001	0.001	0.001	0.001
	[M] ⁺	0.743	0.002	0.742	0.001	0.742	0.010
	[M+1] ⁺	0.168	0.001	0.167	0.001	0.165	0.005
	[M+2] ⁺	0.075	0.001	0.075	0.001	0.074	0.006
	[M+3] ⁺	0.012	0.000	0.012	0.000	0.011	0.002
300	[M+4] ⁺	0.003	0.001	0.003	0.000	0.003	0.000
	[M+5] ⁺	0.000	0.001	0.002	0.002	0.005	0.006
	[M] ⁺	0.740	0.001	0.739	0.003	0.735	0.004
	[M+1] ⁺	0.169	0.001	0.168	0.001	0.169	0.004
	[M+2] ⁺	0.076	0.001	0.076	0.002	0.077	0.002
	[M+3] ⁺	0.013	0.001	0.013	0.001	0.013	0.000
420	[M+4] ⁺	0.003	0.000	0.003	0.000	0.003	0.000
	[M+5] ⁺	0.000	0.000	0.001	0.001	0.002	0.002
	[M] ⁺	0.743	0.011	0.735	0.004	0.736	0.003
	[M+1] ⁺	0.165	0.007	0.166	0.003	0.167	0.001
	[M+2] ⁺	0.076	0.003	0.078	0.001	0.077	0.002
	[M+3] ⁺	0.013	0.000	0.014	0.001	0.014	0.001
600	[M+4] ⁺	0.003	0.000	0.004	0.000	0.004	0.000
	[M+5] ⁺	0.001	0.000	0.003	0.004	0.002	0.003
	[M] ⁺	0.734	0.004	0.731	0.006	0.729	0.010
	[M+1] ⁺	0.170	0.003	0.167	0.001	0.170	0.006
	[M+2] ⁺	0.078	0.001	0.079	0.002	0.080	0.003
	[M+3] ⁺	0.013	0.001	0.014	0.002	0.016	0.002
1800	[M+4] ⁺	0.004	0.000	0.005	0.001	0.005	0.000
	[M+5] ⁺	0.001	0.000	0.004	0.004	0.002	0.000
	[M] ⁺	0.718	0.005	0.702	0.005	0.701	0.012
	[M+1] ⁺	0.170	0.001	0.168	0.002	0.168	0.004
	[M+2] ⁺	0.085	0.002	0.090	0.002	0.091	0.004
	[M+3] ⁺	0.019	0.002	0.023	0.001	0.024	0.003
1800	[M+4] ⁺	0.007	0.001	0.011	0.002	0.011	0.002
	[M+5] ⁺	0.003	0.001	0.006	0.001	0.006	0.001

Table A9. 51 Mass isotopomer distribution of aspartate, measured by GC-MS

Mean values ($n = 5$) of isotopomer abundance are listed. Abbreviations: SD (standard deviation), AM (arithmetic mean).

Labeling time (s)	Isotopomer	No treatment		DMSO		Imazapyr	
		AM	SD	AM	SD	AM	SD
0	[M] ⁺	0.761	0.003	0.763	0.001	0.762	0.001
	[M+1] ⁺	0.158	0.001	0.158	0.000	0.158	0.000
	[M+2] ⁺	0.069	0.001	0.068	0.000	0.069	0.000

Labeling time (s)	Isotopomer	No treatment		DMSO		Imazapyr	
		AM	SD	AM	SD	AM	SD
10	[M+3] ⁺	0.012	0.002	0.011	0.000	0.012	0.001
	[M] ⁺	0.762	0.002	0.763	0.001	0.761	0.002
	[M+1] ⁺	0.158	0.001	0.158	0.001	0.158	0.001
	[M+2] ⁺	0.068	0.001	0.068	0.001	0.069	0.001
	[M+3] ⁺	0.011	0.001	0.011	0.000	0.012	0.001
20	[M] ⁺	0.762	0.001	0.762	0.001	0.756	0.013
	[M+1] ⁺	0.159	0.001	0.159	0.001	0.159	0.001
	[M+2] ⁺	0.068	0.000	0.069	0.001	0.071	0.005
	[M+3] ⁺	0.011	0.001	0.011	0.000	0.015	0.008
30	[M] ⁺	0.761	0.001	0.761	0.001	0.759	0.004
	[M+1] ⁺	0.159	0.001	0.160	0.001	0.159	0.001
	[M+2] ⁺	0.068	0.000	0.069	0.001	0.069	0.001
	[M+3] ⁺	0.011	0.000	0.011	0.000	0.012	0.002
40	[M] ⁺	0.760	0.001	0.760	0.002	0.759	0.003
	[M+1] ⁺	0.160	0.001	0.160	0.001	0.160	0.002
	[M+2] ⁺	0.068	0.000	0.069	0.001	0.069	0.001
	[M+3] ⁺	0.011	0.000	0.011	0.000	0.012	0.001
50	[M] ⁺	0.760	0.001	0.758	0.002	0.759	0.003
	[M+1] ⁺	0.160	0.001	0.161	0.001	0.160	0.002
	[M+2] ⁺	0.069	0.000	0.069	0.001	0.069	0.001
	[M+3] ⁺	0.011	0.000	0.011	0.000	0.012	0.001
60	[M] ⁺	0.759	0.001	0.757	0.002	0.758	0.003
	[M+1] ⁺	0.161	0.001	0.162	0.001	0.161	0.002
	[M+2] ⁺	0.069	0.000	0.070	0.001	0.070	0.001
	[M+3] ⁺	0.011	0.000	0.012	0.001	0.012	0.001
90	[M] ⁺	0.756	0.002	0.752	0.004	0.755	0.004
	[M+1] ⁺	0.162	0.002	0.164	0.003	0.162	0.002
	[M+2] ⁺	0.069	0.000	0.071	0.001	0.070	0.001
	[M+3] ⁺	0.012	0.000	0.013	0.001	0.012	0.001
120	[M] ⁺	0.754	0.003	0.750	0.002	0.752	0.005
	[M+1] ⁺	0.163	0.002	0.165	0.001	0.163	0.003
	[M+2] ⁺	0.070	0.001	0.072	0.001	0.071	0.001
	[M+3] ⁺	0.013	0.001	0.014	0.001	0.013	0.001
150	[M] ⁺	0.751	0.003	0.747	0.002	0.749	0.006
	[M+1] ⁺	0.164	0.002	0.165	0.001	0.164	0.003
	[M+2] ⁺	0.071	0.000	0.072	0.001	0.072	0.002
	[M+3] ⁺	0.014	0.000	0.015	0.001	0.015	0.002
180	[M] ⁺	0.751	0.002	0.742	0.002	0.747	0.006
	[M+1] ⁺	0.163	0.001	0.167	0.001	0.164	0.003
	[M+2] ⁺	0.071	0.001	0.074	0.000	0.073	0.002
	[M+3] ⁺	0.014	0.001	0.017	0.001	0.016	0.002
300	[M] ⁺	0.736	0.002	0.727	0.004	0.736	0.009

Labeling time (s)	Isotopomer	No treatment		DMSO		Imazapyr	
		AM	SD	AM	SD	AM	SD
	[M+1] ⁺	0.165	0.001	0.167	0.001	0.165	0.003
	[M+2] ⁺	0.077	0.001	0.079	0.001	0.077	0.003
	[M+3] ⁺	0.022	0.001	0.026	0.002	0.023	0.004
420	[M] ⁺	0.721	0.004	0.710	0.007	0.715	0.007
	[M+1] ⁺	0.165	0.001	0.167	0.001	0.166	0.002
	[M+2] ⁺	0.082	0.002	0.085	0.002	0.084	0.002
	[M+3] ⁺	0.031	0.002	0.037	0.004	0.035	0.004
600	[M] ⁺	0.693	0.004	0.679	0.002	0.683	0.006
	[M+1] ⁺	0.164	0.001	0.165	0.001	0.165	0.002
	[M+2] ⁺	0.093	0.002	0.097	0.001	0.096	0.002
	[M+3] ⁺	0.050	0.003	0.060	0.002	0.056	0.006
1800	[M] ⁺	0.597	0.015	0.543	0.024	0.561	0.014
	[M+1] ⁺	0.163	0.003	0.159	0.001	0.162	0.003
	[M+2] ⁺	0.134	0.005	0.154	0.011	0.146	0.005
	[M+3] ⁺	0.107	0.013	0.145	0.013	0.131	0.012

Table A9. 52 Mass isotopomer distribution of alanine, measured by GC-MS

Mean values ($n = 5$) of isotopomer abundance are listed. Abbreviations: SD (standard deviation), AM (arithmetic mean).

Labeling time (s)	Isotopomer	No treatment		DMSO		Imazapyr	
		AM	SD	AM	SD	AM	SD
0	[M] ⁺	0.847	0.010	0.846	0.007	0.856	0.006
	[M+1] ⁺	0.111	0.005	0.112	0.004	0.106	0.005
	[M+2] ⁺	0.043	0.005	0.042	0.003	0.039	0.002
10	[M] ⁺	0.849	0.007	0.849	0.003	0.850	0.007
	[M+1] ⁺	0.110	0.004	0.111	0.002	0.109	0.003
	[M+2] ⁺	0.041	0.003	0.040	0.001	0.041	0.004
20	[M] ⁺	0.846	0.008	0.842	0.004	0.846	0.020
	[M+1] ⁺	0.112	0.005	0.115	0.002	0.110	0.008
	[M+2] ⁺	0.042	0.003	0.043	0.002	0.044	0.012
30	[M] ⁺	0.848	0.007	0.842	0.005	0.851	0.008
	[M+1] ⁺	0.112	0.004	0.114	0.003	0.108	0.005
	[M+2] ⁺	0.041	0.003	0.043	0.002	0.041	0.004
40	[M] ⁺	0.844	0.008	0.838	0.006	0.848	0.005
	[M+1] ⁺	0.114	0.005	0.116	0.003	0.110	0.003
	[M+2] ⁺	0.042	0.003	0.045	0.002	0.042	0.003
50	[M] ⁺	0.842	0.009	0.832	0.006	0.848	0.008
	[M+1] ⁺	0.114	0.005	0.119	0.003	0.110	0.005
	[M+2] ⁺	0.044	0.004	0.049	0.003	0.042	0.003
60	[M] ⁺	0.840	0.009	0.832	0.009	0.844	0.006
	[M+1] ⁺	0.115	0.005	0.118	0.005	0.111	0.003

Labeling time (s)	Isotopomer	No treatment		DMSO		Imazapyr	
		AM	SD	AM	SD	AM	SD
90	[M+2] ⁺	0.045	0.004	0.050	0.004	0.044	0.003
	[M] ⁺	0.832	0.011	0.811	0.022	0.835	0.006
	[M+1] ⁺	0.118	0.006	0.123	0.008	0.115	0.003
	[M+2] ⁺	0.049	0.005	0.066	0.016	0.050	0.003
120	[M] ⁺	0.819	0.010	0.802	0.019	0.826	0.006
	[M+1] ⁺	0.123	0.005	0.127	0.006	0.118	0.004
	[M+2] ⁺	0.058	0.005	0.071	0.013	0.056	0.002
150	[M] ⁺	0.805	0.006	0.775	0.017	0.810	0.011
	[M+1] ⁺	0.127	0.002	0.137	0.006	0.123	0.005
	[M+2] ⁺	0.067	0.004	0.088	0.012	0.067	0.006
180	[M] ⁺	0.795	0.017	0.756	0.014	0.806	0.016
	[M+1] ⁺	0.130	0.008	0.142	0.005	0.123	0.008
	[M+2] ⁺	0.075	0.009	0.102	0.010	0.070	0.008
300	[M] ⁺	0.735	0.011	0.688	0.017	0.759	0.029
	[M+1] ⁺	0.148	0.003	0.159	0.006	0.136	0.012
	[M+2] ⁺	0.117	0.009	0.153	0.012	0.104	0.017
420	[M] ⁺	0.700	0.018	0.632	0.022	0.719	0.022
	[M+1] ⁺	0.159	0.006	0.174	0.006	0.149	0.007
	[M+2] ⁺	0.142	0.014	0.195	0.018	0.132	0.015
600	[M] ⁺	0.631	0.017	0.585	0.031	0.683	0.046
	[M+1] ⁺	0.179	0.004	0.185	0.013	0.158	0.015
	[M+2] ⁺	0.190	0.014	0.229	0.020	0.159	0.030
1800	[M] ⁺	0.535	0.054	0.459	0.050	0.560	0.030
	[M+1] ⁺	0.214	0.017	0.229	0.020	0.200	0.011
	[M+2] ⁺	0.251	0.039	0.312	0.032	0.240	0.021

Table A9. 53 Mass isotopomer distribution of 2-oxoglutaric acid, measured by GC-MS

Mean values ($n = 5$) of isotopomer abundance are listed. Abbreviations: SD (standard deviation), AM (arithmetic mean).

Labeling time (s)	Isotopomer	No treatment		DMSO		Imazapyr	
		AM	SD	AM	SD	AM	SD
0	[M] ⁺	0.708	0.036	0.736	0.009	0.728	0.014
	[M+1] ⁺	0.172	0.010	0.168	0.009	0.169	0.007
	[M+2] ⁺	0.081	0.015	0.075	0.009	0.087	0.015
	[M+3] ⁺	0.016	0.007	0.013	0.003	0.015	0.003
	[M+4] ⁺	0.016	0.022	0.001	0.001	0.001	0.001
	[M+5] ⁺	0.006	0.008	0.008	0.017	0.000	0.000
10	[M] ⁺	0.703	0.031	0.735	0.011	0.729	0.012
	[M+1] ⁺	0.168	0.005	0.172	0.006	0.169	0.005
	[M+2] ⁺	0.087	0.005	0.077	0.004	0.086	0.009
	[M+3] ⁺	0.018	0.006	0.014	0.002	0.014	0.004

Labeling time (s)	Isotopomer	No treatment		DMSO		Imazapyr	
		AM	SD	AM	SD	AM	SD
20	[M+4] ⁺	0.017	0.025	0.001	0.001	0.001	0.001
	[M+5] ⁺	0.007	0.009	0.002	0.004	0.000	0.001
	[M] ⁺	0.667	0.081	0.730	0.017	0.721	0.019
	[M+1] ⁺	0.164	0.013	0.176	0.010	0.169	0.005
	[M+2] ⁺	0.112	0.065	0.078	0.007	0.089	0.013
	[M+3] ⁺	0.026	0.021	0.014	0.003	0.017	0.005
30	[M+4] ⁺	0.020	0.020	0.001	0.001	0.001	0.001
	[M+5] ⁺	0.011	0.010	0.002	0.003	0.002	0.004
	[M] ⁺	0.700	0.033	0.734	0.007	0.727	0.017
	[M+1] ⁺	0.164	0.006	0.170	0.006	0.177	0.015
	[M+2] ⁺	0.090	0.005	0.080	0.005	0.080	0.003
	[M+3] ⁺	0.019	0.005	0.014	0.001	0.014	0.002
40	[M+4] ⁺	0.020	0.023	0.001	0.001	0.002	0.003
	[M+5] ⁺	0.008	0.010	0.000	0.001	0.000	0.001
	[M] ⁺	0.703	0.023	0.737	0.016	0.726	0.012
	[M+1] ⁺	0.164	0.006	0.169	0.005	0.171	0.007
	[M+2] ⁺	0.091	0.006	0.076	0.010	0.086	0.009
	[M+3] ⁺	0.018	0.003	0.017	0.005	0.016	0.003
50	[M+4] ⁺	0.017	0.020	0.002	0.002	0.001	0.001
	[M+5] ⁺	0.006	0.008	0.000	0.000	0.000	0.001
	[M] ⁺	0.693	0.037	0.730	0.011	0.724	0.021
	[M+1] ⁺	0.162	0.008	0.173	0.007	0.167	0.002
	[M+2] ⁺	0.093	0.003	0.081	0.005	0.088	0.016
	[M+3] ⁺	0.021	0.006	0.015	0.004	0.018	0.006
60	[M+4] ⁺	0.021	0.027	0.001	0.001	0.001	0.002
	[M+5] ⁺	0.010	0.012	0.000	0.000	0.002	0.003
	[M] ⁺	0.707	0.030	0.732	0.010	0.723	0.016
	[M+1] ⁺	0.163	0.007	0.173	0.008	0.172	0.007
	[M+2] ⁺	0.089	0.010	0.079	0.005	0.086	0.007
	[M+3] ⁺	0.020	0.004	0.014	0.002	0.018	0.005
90	[M+4] ⁺	0.016	0.021	0.001	0.002	0.001	0.001
	[M+5] ⁺	0.006	0.008	0.000	0.000	0.000	0.000
	[M] ⁺	0.701	0.032	0.736	0.008	0.722	0.013
	[M+1] ⁺	0.165	0.004	0.169	0.004	0.172	0.008
	[M+2] ⁺	0.087	0.007	0.078	0.004	0.087	0.007
	[M+3] ⁺	0.019	0.006	0.015	0.003	0.017	0.005
120	[M+4] ⁺	0.020	0.023	0.001	0.002	0.001	0.001
	[M+5] ⁺	0.009	0.010	0.000	0.000	0.000	0.001
	[M] ⁺	0.697	0.031	0.736	0.014	0.729	0.011
	[M+1] ⁺	0.167	0.006	0.169	0.004	0.169	0.005
	[M+2] ⁺	0.091	0.006	0.077	0.006	0.084	0.007
	[M+3] ⁺	0.021	0.006	0.015	0.003	0.015	0.003

Labeling time (s)	Isotopomer	No treatment		DMSO		Imazapyr	
		AM	SD	AM	SD	AM	SD
	[M+4] ⁺	0.017	0.022	0.001	0.001	0.001	0.001
	[M+5] ⁺	0.007	0.009	0.003	0.006	0.002	0.004
150	[M] ⁺	0.696	0.039	0.734	0.010	0.729	0.011
	[M+1] ⁺	0.163	0.005	0.170	0.003	0.172	0.006
	[M+2] ⁺	0.095	0.014	0.081	0.007	0.083	0.008
	[M+3] ⁺	0.021	0.006	0.014	0.003	0.015	0.003
	[M+4] ⁺	0.019	0.022	0.001	0.001	0.001	0.001
	[M+5] ⁺	0.008	0.010	0.000	0.000	0.000	0.001
180	[M] ⁺	0.681	0.057	0.731	0.015	0.717	0.017
	[M+1] ⁺	0.162	0.008	0.172	0.005	0.171	0.008
	[M+2] ⁺	0.097	0.007	0.082	0.011	0.090	0.009
	[M+3] ⁺	0.022	0.007	0.013	0.002	0.019	0.007
	[M+4] ⁺	0.028	0.038	0.001	0.002	0.001	0.002
	[M+5] ⁺	0.012	0.016	0.000	0.000	0.002	0.004
300	[M] ⁺	0.699	0.027	0.732	0.009	0.712	0.021
	[M+1] ⁺	0.167	0.007	0.172	0.004	0.171	0.006
	[M+2] ⁺	0.090	0.011	0.080	0.005	0.096	0.019
	[M+3] ⁺	0.020	0.004	0.015	0.003	0.019	0.006
	[M+4] ⁺	0.018	0.021	0.001	0.001	0.001	0.001
	[M+5] ⁺	0.007	0.009	0.002	0.003	0.000	0.000
420	[M] ⁺	0.699	0.029	0.729	0.010	0.725	0.015
	[M+1] ⁺	0.166	0.007	0.170	0.004	0.171	0.002
	[M+2] ⁺	0.087	0.005	0.083	0.007	0.088	0.011
	[M+3] ⁺	0.021	0.004	0.017	0.004	0.016	0.003
	[M+4] ⁺	0.021	0.025	0.001	0.002	0.001	0.002
	[M+5] ⁺	0.006	0.007	0.000	0.001	0.000	0.001
600	[M] ⁺	0.691	0.035	0.726	0.006	0.711	0.027
	[M+1] ⁺	0.166	0.009	0.172	0.004	0.178	0.013
	[M+2] ⁺	0.091	0.008	0.084	0.005	0.092	0.012
	[M+3] ⁺	0.022	0.005	0.016	0.003	0.017	0.003
	[M+4] ⁺	0.023	0.027	0.002	0.002	0.001	0.001
	[M+5] ⁺	0.008	0.009	0.000	0.000	0.000	0.000
1800	[M] ⁺	0.680	0.029	0.687	0.018	0.683	0.019
	[M+1] ⁺	0.168	0.008	0.175	0.007	0.174	0.007
	[M+2] ⁺	0.098	0.013	0.099	0.006	0.103	0.008
	[M+3] ⁺	0.024	0.005	0.026	0.004	0.027	0.008
	[M+4] ⁺	0.022	0.020	0.010	0.005	0.009	0.006
	[M+5] ⁺	0.008	0.010	0.004	0.003	0.003	0.002

Table A9. 54 Mass isotopomer distribution of sedoheptulose 7-phosphate, measured by LC-MS

Mean values ($n = 5$) of isotopomer abundance are listed. Abbreviations: SD (standard deviation), AM (arithmetic mean).

Labeling time (s)	Isotopomer	No treatment		DMSO		Imazapyr	
		AM	SD	AM	SD	AM	SD
0	[M] ⁺	0.893	0.010	0.866	0.021	0.773	0.209
	[M+1] ⁺	0.080	0.006	0.086	0.016	0.071	0.028
	[M+2] ⁺	0.020	0.002	0.032	0.002	0.030	0.006
	[M+3] ⁺	0.001	0.000	0.002	0.000	0.008	0.012
	[M+4] ⁺	0.002	0.001	0.003	0.003	0.021	0.042
	[M+5] ⁺	0.001	0.001	0.000	0.000	0.045	0.097
	[M+6] ⁺	0.002	0.001	0.008	0.005	0.027	0.038
	[M+7] ⁺	0.001	0.001	0.002	0.002	0.026	0.051
10	[M] ⁺	0.303	0.019	0.269	0.035	0.264	0.034
	[M+1] ⁺	0.339	0.008	0.345	0.017	0.345	0.014
	[M+2] ⁺	0.255	0.014	0.266	0.026	0.262	0.019
	[M+3] ⁺	0.084	0.010	0.093	0.017	0.097	0.022
	[M+4] ⁺	0.015	0.003	0.017	0.003	0.020	0.006
	[M+5] ⁺	0.003	0.001	0.004	0.001	0.004	0.002
	[M+6] ⁺	0.001	0.000	0.005	0.002	0.005	0.002
	[M+7] ⁺	0.001	0.000	0.003	0.001	0.003	0.001
20	[M] ⁺	0.166	0.026	0.146	0.014	0.142	0.020
	[M+1] ⁺	0.260	0.009	0.251	0.030	0.242	0.020
	[M+2] ⁺	0.311	0.006	0.307	0.012	0.308	0.013
	[M+3] ⁺	0.181	0.012	0.199	0.021	0.196	0.018
	[M+4] ⁺	0.060	0.011	0.066	0.012	0.074	0.014
	[M+5] ⁺	0.018	0.005	0.021	0.007	0.026	0.006
	[M+6] ⁺	0.004	0.001	0.007	0.001	0.009	0.001
	[M+7] ⁺	0.002	0.000	0.003	0.001	0.004	0.001
30	[M] ⁺	0.130	0.008	0.103	0.015	0.103	0.013
	[M+1] ⁺	0.190	0.019	0.174	0.013	0.163	0.022
	[M+2] ⁺	0.296	0.007	0.289	0.009	0.274	0.016
	[M+3] ⁺	0.228	0.016	0.249	0.009	0.250	0.018
	[M+4] ⁺	0.103	0.008	0.112	0.006	0.130	0.014
	[M+5] ⁺	0.041	0.006	0.052	0.007	0.058	0.014
	[M+6] ⁺	0.009	0.001	0.016	0.003	0.017	0.003
	[M+7] ⁺	0.003	0.000	0.006	0.001	0.006	0.001
40	[M] ⁺	0.110	0.013	0.090	0.015	0.088	0.007
	[M+1] ⁺	0.124	0.013	0.123	0.012	0.123	0.012
	[M+2] ⁺	0.251	0.011	0.245	0.008	0.236	0.013
	[M+3] ⁺	0.251	0.007	0.259	0.009	0.252	0.003
	[M+4] ⁺	0.154	0.011	0.162	0.006	0.168	0.010
	[M+5] ⁺	0.080	0.011	0.085	0.006	0.092	0.010

Labeling time (s)	Isotopomer	No treatment		DMSO		Imazapyr	
		AM	SD	AM	SD	AM	SD
50	[M+6] ⁺	0.023	0.004	0.027	0.003	0.030	0.005
	[M+7] ⁺	0.007	0.001	0.009	0.001	0.011	0.002
	[M] ⁺	0.102	0.006	0.077	0.014	0.077	0.015
	[M+1] ⁺	0.090	0.003	0.085	0.004	0.086	0.011
	[M+2] ⁺	0.202	0.013	0.198	0.009	0.191	0.017
	[M+3] ⁺	0.242	0.009	0.253	0.008	0.256	0.009
	[M+4] ⁺	0.187	0.009	0.192	0.007	0.193	0.010
	[M+5] ⁺	0.120	0.006	0.129	0.007	0.129	0.014
60	[M+6] ⁺	0.042	0.003	0.048	0.004	0.049	0.008
	[M+7] ⁺	0.015	0.002	0.017	0.002	0.019	0.004
	[M] ⁺	0.084	0.004	0.071	0.017	0.079	0.009
	[M+1] ⁺	0.073	0.007	0.072	0.008	0.070	0.006
	[M+2] ⁺	0.174	0.013	0.167	0.015	0.168	0.012
	[M+3] ⁺	0.243	0.004	0.240	0.010	0.228	0.007
	[M+4] ⁺	0.205	0.008	0.205	0.008	0.207	0.009
	[M+5] ⁺	0.144	0.014	0.156	0.012	0.155	0.013
90	[M+6] ⁺	0.057	0.006	0.064	0.008	0.067	0.007
	[M+7] ⁺	0.021	0.004	0.024	0.002	0.028	0.005
	[M] ⁺	0.077	0.004	0.057	0.011	0.070	0.012
	[M+1] ⁺	0.042	0.006	0.040	0.006	0.040	0.004
	[M+2] ⁺	0.110	0.010	0.097	0.007	0.101	0.003
	[M+3] ⁺	0.193	0.010	0.182	0.008	0.177	0.006
	[M+4] ⁺	0.226	0.003	0.219	0.009	0.217	0.009
	[M+5] ⁺	0.196	0.012	0.216	0.014	0.212	0.007
120	[M+6] ⁺	0.107	0.007	0.127	0.011	0.124	0.005
	[M+7] ⁺	0.048	0.008	0.063	0.007	0.060	0.004
	[M] ⁺	0.086	0.018	0.072	0.026	0.064	0.013
	[M+1] ⁺	0.035	0.013	0.041	0.026	0.029	0.004
	[M+2] ⁺	0.082	0.019	0.081	0.038	0.072	0.007
	[M+3] ⁺	0.150	0.017	0.147	0.027	0.139	0.006
	[M+4] ⁺	0.207	0.011	0.200	0.015	0.207	0.004
	[M+5] ⁺	0.222	0.022	0.221	0.032	0.232	0.004
150	[M+6] ⁺	0.145	0.022	0.152	0.042	0.166	0.010
	[M+7] ⁺	0.073	0.016	0.087	0.031	0.092	0.006
	[M] ⁺	0.075	0.011	0.066	0.015	0.068	0.011
	[M+1] ⁺	0.023	0.002	0.025	0.003	0.027	0.003
	[M+2] ⁺	0.052	0.006	0.052	0.005	0.057	0.003
	[M+3] ⁺	0.115	0.012	0.112	0.007	0.106	0.008
	[M+4] ⁺	0.197	0.009	0.188	0.010	0.183	0.007
	[M+5] ⁺	0.242	0.005	0.241	0.013	0.239	0.007
[M+6] ⁺	0.192	0.008	0.195	0.010	0.201	0.013	
[M+7] ⁺	0.104	0.015	0.122	0.018	0.121	0.008	

Labeling time (s)	Isotopomer	No treatment		DMSO		Imazapyr	
		AM	SD	AM	SD	AM	SD
180	[M] ⁺	0.091	0.013	0.072	0.017	0.061	0.005
	[M+1] ⁺	0.022	0.002	0.023	0.005	0.023	0.003
	[M+2] ⁺	0.044	0.002	0.045	0.006	0.052	0.005
	[M+3] ⁺	0.096	0.008	0.087	0.007	0.094	0.007
	[M+4] ⁺	0.178	0.009	0.168	0.012	0.175	0.006
	[M+5] ⁺	0.235	0.011	0.234	0.006	0.239	0.007
	[M+6] ⁺	0.213	0.006	0.228	0.020	0.223	0.005
	[M+7] ⁺	0.120	0.020	0.142	0.017	0.132	0.008
300	[M] ⁺	0.085	0.015	0.069	0.015	0.151	0.172
	[M+1] ⁺	0.017	0.002	0.018	0.004	0.033	0.030
	[M+2] ⁺	0.027	0.005	0.031	0.004	0.052	0.042
	[M+3] ⁺	0.062	0.010	0.060	0.009	0.071	0.023
	[M+4] ⁺	0.141	0.012	0.134	0.011	0.125	0.015
	[M+5] ⁺	0.237	0.011	0.224	0.009	0.201	0.072
	[M+6] ⁺	0.267	0.013	0.281	0.020	0.227	0.113
	[M+7] ⁺	0.163	0.023	0.183	0.021	0.141	0.068
420	[M] ⁺	0.086	0.013	0.074	0.016	0.153	0.173
	[M+1] ⁺	0.015	0.002	0.018	0.002	0.016	0.008
	[M+2] ⁺	0.020	0.002	0.024	0.001	0.042	0.017
	[M+3] ⁺	0.046	0.004	0.048	0.006	0.056	0.010
	[M+4] ⁺	0.124	0.009	0.118	0.010	0.120	0.010
	[M+5] ⁺	0.238	0.012	0.225	0.010	0.194	0.085
	[M+6] ⁺	0.288	0.014	0.300	0.010	0.252	0.070
	[M+7] ⁺	0.183	0.018	0.194	0.020	0.166	0.035
600	[M] ⁺	0.084	0.008	0.070	0.009	0.085	0.025
	[M+1] ⁺	0.015	0.003	0.017	0.002	0.019	0.003
	[M+2] ⁺	0.017	0.004	0.023	0.004	0.028	0.005
	[M+3] ⁺	0.042	0.007	0.041	0.005	0.050	0.006
	[M+4] ⁺	0.116	0.013	0.108	0.011	0.117	0.008
	[M+5] ⁺	0.239	0.014	0.224	0.012	0.225	0.012
	[M+6] ⁺	0.303	0.019	0.312	0.015	0.292	0.015
	[M+7] ⁺	0.184	0.026	0.205	0.021	0.184	0.018
1800	[M] ⁺	0.079	0.010	0.064	0.018	0.059	0.009
	[M+1] ⁺	0.025	0.002	0.028	0.005	0.024	0.002
	[M+2] ⁺	0.029	0.006	0.037	0.003	0.034	0.003
	[M+3] ⁺	0.062	0.010	0.061	0.008	0.062	0.005
	[M+4] ⁺	0.150	0.013	0.147	0.009	0.151	0.010
	[M+5] ⁺	0.258	0.007	0.259	0.004	0.261	0.006
	[M+6] ⁺	0.273	0.022	0.273	0.011	0.281	0.018
	[M+7] ⁺	0.124	0.021	0.133	0.010	0.128	0.010

Table A9. 55 Mass isotopomer distribution of 3-phosphoglycerate, measured by LC-MS

Mean values ($n = 5$) of isotopomer abundance are listed. Abbreviations: SD (standard deviation), AM (arithmetic mean).

Labeling time (s)	Isotopomer	No treatment		DMSO		Imazapyr	
		AM	SD	AM	SD	AM	SD
0	[M] ⁺	0.949	0.007	0.949	0.006	0.825	0.263
	[M+1] ⁺	0.039	0.005	0.040	0.007	0.047	0.012
	[M+2] ⁺	0.010	0.002	0.010	0.001	0.080	0.151
	[M+3] ⁺	0.002	0.001	0.001	0.001	0.048	0.100
10	[M] ⁺	0.587	0.031	0.549	0.032	0.555	0.031
	[M+1] ⁺	0.366	0.027	0.399	0.027	0.390	0.024
	[M+2] ⁺	0.037	0.005	0.041	0.005	0.045	0.004
	[M+3] ⁺	0.009	0.002	0.010	0.002	0.011	0.003
20	[M] ⁺	0.461	0.019	0.420	0.033	0.433	0.027
	[M+1] ⁺	0.423	0.015	0.454	0.014	0.430	0.020
	[M+2] ⁺	0.087	0.008	0.092	0.012	0.101	0.008
	[M+3] ⁺	0.029	0.004	0.033	0.008	0.036	0.005
30	[M] ⁺	0.405	0.030	0.343	0.016	0.331	0.031
	[M+1] ⁺	0.427	0.013	0.458	0.008	0.458	0.016
	[M+2] ⁺	0.119	0.011	0.135	0.006	0.143	0.016
	[M+3] ⁺	0.049	0.008	0.064	0.010	0.068	0.014
40	[M] ⁺	0.323	0.030	0.301	0.016	0.293	0.015
	[M+1] ⁺	0.425	0.022	0.440	0.014	0.440	0.009
	[M+2] ⁺	0.162	0.007	0.164	0.008	0.169	0.008
	[M+3] ⁺	0.089	0.011	0.095	0.012	0.098	0.014
50	[M] ⁺	0.275	0.008	0.255	0.013	0.255	0.022
	[M+1] ⁺	0.411	0.005	0.419	0.008	0.409	0.018
	[M+2] ⁺	0.191	0.009	0.196	0.007	0.204	0.015
	[M+3] ⁺	0.123	0.007	0.131	0.005	0.132	0.012
60	[M] ⁺	0.250	0.017	0.222	0.008	0.227	0.024
	[M+1] ⁺	0.391	0.008	0.403	0.011	0.390	0.009
	[M+2] ⁺	0.213	0.005	0.217	0.009	0.221	0.012
	[M+3] ⁺	0.146	0.013	0.158	0.008	0.162	0.012
90	[M] ⁺	0.189	0.009	0.166	0.011	0.170	0.008
	[M+1] ⁺	0.348	0.012	0.328	0.008	0.317	0.013
	[M+2] ⁺	0.247	0.004	0.256	0.004	0.261	0.014
	[M+3] ⁺	0.216	0.020	0.251	0.013	0.252	0.009
120	[M] ⁺	0.169	0.008	0.142	0.018	0.149	0.006
	[M+1] ⁺	0.272	0.012	0.266	0.013	0.264	0.008
	[M+2] ⁺	0.278	0.010	0.280	0.010	0.284	0.010
	[M+3] ⁺	0.281	0.018	0.312	0.024	0.303	0.012
150	[M] ⁺	0.146	0.007	0.140	0.012	0.133	0.013
	[M+1] ⁺	0.238	0.015	0.235	0.011	0.229	0.011

Labeling time (s)	Isotopomer	No treatment		DMSO		Imazapyr	
		AM	SD	AM	SD	AM	SD
180	[M+2] ⁺	0.301	0.007	0.297	0.010	0.296	0.010
	[M+3] ⁺	0.315	0.017	0.327	0.017	0.343	0.018
	[M] ⁺	0.150	0.016	0.133	0.018	0.133	0.008
	[M+1] ⁺	0.213	0.008	0.201	0.013	0.206	0.010
	[M+2] ⁺	0.309	0.009	0.312	0.007	0.313	0.002
300	[M+3] ⁺	0.328	0.026	0.354	0.021	0.348	0.019
	[M] ⁺	0.103	0.013	0.104	0.011	0.119	0.046
	[M+1] ⁺	0.151	0.013	0.140	0.011	0.143	0.007
	[M+2] ⁺	0.341	0.013	0.336	0.013	0.332	0.014
420	[M+3] ⁺	0.406	0.019	0.420	0.028	0.406	0.035
	[M] ⁺	0.099	0.008	0.090	0.015	0.107	0.016
	[M+1] ⁺	0.132	0.008	0.122	0.007	0.156	0.061
	[M+2] ⁺	0.346	0.007	0.336	0.008	0.331	0.018
600	[M+3] ⁺	0.423	0.014	0.452	0.016	0.406	0.062
	[M] ⁺	0.102	0.012	0.088	0.007	0.091	0.008
	[M+1] ⁺	0.131	0.008	0.114	0.008	0.122	0.010
	[M+2] ⁺	0.360	0.018	0.339	0.008	0.359	0.007
1800	[M+3] ⁺	0.407	0.029	0.459	0.011	0.428	0.014
	[M] ⁺	0.096	0.007	0.088	0.020	0.088	0.007
	[M+1] ⁺	0.158	0.015	0.150	0.008	0.148	0.005
	[M+2] ⁺	0.392	0.012	0.390	0.006	0.390	0.010
	[M+3] ⁺	0.354	0.025	0.372	0.016	0.373	0.005

Table A9. 56 Mass isotopomer distribution of 6-phosphogluconate, measured by LC-MS

Mean values ($n = 5$) of isotopomer abundance are listed. Abbreviations: SD (standard deviation), AM (arithmetic mean).

Labeling time (s)	Isotopomer	No treatment		DMSO		Imazapyr	
		AM	SD	AM	SD	AM	SD
0	[M] ⁺	0.905	0.016	0.846	0.014	0.745	0.242
	[M+1] ⁺	0.057	0.004	0.067	0.007	0.084	0.033
	[M+2] ⁺	0.034	0.013	0.072	0.019	0.080	0.040
	[M+3] ⁺	0.003	0.001	0.007	0.006	0.023	0.040
	[M+4] ⁺	0.001	0.000	0.007	0.004	0.068	0.131
10	[M] ⁺	0.895	0.010	0.870	0.012	0.849	0.024
	[M+1] ⁺	0.071	0.005	0.064	0.005	0.068	0.008
	[M+2] ⁺	0.028	0.004	0.056	0.013	0.066	0.018
	[M+3] ⁺	0.004	0.003	0.004	0.002	0.008	0.003
	[M+4] ⁺	0.003	0.001	0.005	0.005	0.008	0.004
20	[M] ⁺	0.901	0.005	0.841	0.037	0.850	0.021
	[M+1] ⁺	0.064	0.006	0.071	0.012	0.064	0.003
	[M+2] ⁺	0.029	0.003	0.067	0.017	0.065	0.017

Labeling time (s)	Isotopomer	No treatment		DMSO		Imazapyr	
		AM	SD	AM	SD	AM	SD
30	[M+3] ⁺	0.003	0.002	0.012	0.005	0.013	0.003
	[M+4] ⁺	0.002	0.001	0.009	0.011	0.008	0.006
	[M] ⁺	0.898	0.008	0.848	0.015	0.843	0.009
	[M+1] ⁺	0.066	0.007	0.070	0.009	0.072	0.011
	[M+2] ⁺	0.030	0.002	0.064	0.014	0.066	0.013
	[M+3] ⁺	0.003	0.001	0.010	0.005	0.013	0.003
40	[M+4] ⁺	0.002	0.001	0.009	0.003	0.006	0.004
	[M] ⁺	0.894	0.007	0.858	0.013	0.832	0.021
	[M+1] ⁺	0.069	0.004	0.071	0.004	0.075	0.008
	[M+2] ⁺	0.030	0.003	0.050	0.009	0.064	0.009
	[M+3] ⁺	0.005	0.001	0.013	0.004	0.014	0.004
	[M+4] ⁺	0.003	0.001	0.008	0.002	0.016	0.011
50	[M] ⁺	0.897	0.011	0.838	0.022	0.839	0.010
	[M+1] ⁺	0.067	0.005	0.073	0.009	0.078	0.005
	[M+2] ⁺	0.028	0.002	0.060	0.013	0.057	0.008
	[M+3] ⁺	0.004	0.004	0.014	0.003	0.016	0.005
	[M+4] ⁺	0.004	0.001	0.016	0.006	0.010	0.005
	[M] ⁺	0.892	0.011	0.847	0.013	0.833	0.017
60	[M+1] ⁺	0.069	0.004	0.072	0.009	0.077	0.008
	[M+2] ⁺	0.028	0.007	0.056	0.009	0.059	0.015
	[M+3] ⁺	0.007	0.003	0.016	0.001	0.018	0.011
	[M+4] ⁺	0.004	0.002	0.010	0.002	0.012	0.007
	[M] ⁺	0.870	0.014	0.838	0.013	0.817	0.013
	[M+1] ⁺	0.079	0.003	0.079	0.011	0.078	0.010
90	[M+2] ⁺	0.035	0.009	0.047	0.010	0.068	0.012
	[M+3] ⁺	0.009	0.004	0.019	0.005	0.021	0.008
	[M+4] ⁺	0.008	0.003	0.017	0.003	0.016	0.005
	[M] ⁺	0.855	0.028	0.779	0.137	0.812	0.027
	[M+1] ⁺	0.081	0.009	0.071	0.005	0.078	0.010
	[M+2] ⁺	0.034	0.006	0.075	0.051	0.058	0.009
120	[M+3] ⁺	0.015	0.007	0.036	0.040	0.023	0.009
	[M+4] ⁺	0.014	0.007	0.039	0.045	0.028	0.013
	[M] ⁺	0.859	0.009	0.827	0.013	0.800	0.010
	[M+1] ⁺	0.081	0.004	0.080	0.010	0.073	0.007
	[M+2] ⁺	0.034	0.003	0.050	0.006	0.061	0.003
	[M+3] ⁺	0.015	0.001	0.022	0.007	0.033	0.016
150	[M+4] ⁺	0.011	0.003	0.021	0.007	0.034	0.008
	[M] ⁺	0.863	0.006	0.819	0.027	0.809	0.031
	[M+1] ⁺	0.078	0.007	0.080	0.010	0.079	0.007
	[M+2] ⁺	0.034	0.005	0.051	0.007	0.056	0.004
	[M+3] ⁺	0.015	0.001	0.022	0.009	0.030	0.015
	[M+4] ⁺	0.010	0.002	0.028	0.010	0.026	0.012

Labeling time (s)	Isotopomer	No treatment		DMSO		Imazapyr	
		AM	SD	AM	SD	AM	SD
300	[M] ⁺	0.816	0.041	0.791	0.011	0.791	0.014
	[M+1] ⁺	0.082	0.011	0.085	0.007	0.088	0.009
	[M+2] ⁺	0.047	0.013	0.056	0.009	0.059	0.015
	[M+3] ⁺	0.027	0.009	0.028	0.004	0.034	0.008
	[M+4] ⁺	0.028	0.011	0.040	0.006	0.028	0.010
420	[M] ⁺	0.831	0.013	0.796	0.029	0.660	0.289
	[M+1] ⁺	0.081	0.006	0.083	0.013	0.089	0.011
	[M+2] ⁺	0.042	0.007	0.062	0.010	0.113	0.137
	[M+3] ⁺	0.025	0.006	0.024	0.011	0.083	0.116
	[M+4] ⁺	0.021	0.003	0.035	0.017	0.054	0.029
600	[M] ⁺	0.825	0.012	0.793	0.028	0.775	0.031
	[M+1] ⁺	0.080	0.008	0.091	0.014	0.078	0.012
	[M+2] ⁺	0.042	0.003	0.053	0.012	0.066	0.018
	[M+3] ⁺	0.026	0.006	0.027	0.010	0.030	0.007
	[M+4] ⁺	0.028	0.004	0.036	0.009	0.051	0.010
1800	[M] ⁺	0.731	0.020	0.696	0.029	0.669	0.032
	[M+1] ⁺	0.114	0.008	0.117	0.014	0.112	0.019
	[M+2] ⁺	0.064	0.008	0.085	0.006	0.097	0.021
	[M+3] ⁺	0.046	0.007	0.052	0.008	0.056	0.009
	[M+4] ⁺	0.045	0.004	0.049	0.014	0.066	0.016

Table A9. 57 Mass isotopomer distribution of pyruvate, measured by LC-MS

Mean values ($n = 5$) of isotopomer abundance are listed. Abbreviations: SD (standard deviation), AM (arithmetic mean).

Labeling time (s)	Isotopomer	No treatment		DMSO		Imazapyr	
		AM	SD	AM	SD	AM	SD
0	[M] ⁺	0.886	0.013	0.860	0.042	0.906	0.023
	[M+1] ⁺	0.036	0.003	0.040	0.002	0.035	0.005
	[M+2] ⁺	0.052	0.006	0.065	0.021	0.042	0.012
	[M+3] ⁺	0.026	0.005	0.035	0.020	0.017	0.009
10	[M] ⁺	0.850	0.009	0.849	0.015	0.855	0.017
	[M+1] ⁺	0.089	0.007	0.069	0.016	0.069	0.019
	[M+2] ⁺	0.042	0.005	0.052	0.008	0.051	0.013
	[M+3] ⁺	0.018	0.005	0.030	0.012	0.025	0.016
20	[M] ⁺	0.810	0.041	0.821	0.018	0.812	0.040
	[M+1] ⁺	0.129	0.030	0.093	0.030	0.096	0.028
	[M+2] ⁺	0.044	0.009	0.057	0.016	0.061	0.021
	[M+3] ⁺	0.017	0.005	0.029	0.018	0.031	0.018
30	[M] ⁺	0.774	0.011	0.809	0.027	0.820	0.019
	[M+1] ⁺	0.147	0.024	0.105	0.017	0.103	0.023
	[M+2] ⁺	0.053	0.013	0.057	0.017	0.052	0.015

Labeling time (s)	Isotopomer	No treatment		DMSO		Imazapyr	
		AM	SD	AM	SD	AM	SD
40	[M+3] ⁺	0.026	0.009	0.029	0.020	0.024	0.013
	[M] ⁺	0.739	0.024	0.794	0.027	0.801	0.027
	[M+1] ⁺	0.162	0.019	0.122	0.026	0.112	0.024
	[M+2] ⁺	0.065	0.007	0.056	0.015	0.057	0.025
	[M+3] ⁺	0.034	0.006	0.027	0.017	0.029	0.023
50	[M] ⁺	0.727	0.038	0.776	0.042	0.807	0.015
	[M+1] ⁺	0.174	0.014	0.121	0.052	0.114	0.015
	[M+2] ⁺	0.067	0.018	0.065	0.016	0.053	0.007
	[M+3] ⁺	0.031	0.015	0.038	0.019	0.025	0.008
60	[M] ⁺	0.718	0.031	0.777	0.019	0.789	0.041
	[M+1] ⁺	0.178	0.020	0.122	0.036	0.122	0.045
	[M+2] ⁺	0.070	0.014	0.065	0.013	0.060	0.010
	[M+3] ⁺	0.034	0.013	0.036	0.014	0.029	0.010
90	[M] ⁺	0.728	0.019	0.771	0.036	0.775	0.028
	[M+1] ⁺	0.159	0.008	0.115	0.031	0.124	0.017
	[M+2] ⁺	0.074	0.010	0.074	0.011	0.070	0.011
	[M+3] ⁺	0.039	0.010	0.040	0.012	0.031	0.009
120	[M] ⁺	0.724	0.026	0.779	0.044	0.793	0.029
	[M+1] ⁺	0.146	0.015	0.102	0.028	0.104	0.029
	[M+2] ⁺	0.084	0.008	0.077	0.017	0.069	0.004
	[M+3] ⁺	0.045	0.008	0.042	0.014	0.034	0.005
150	[M] ⁺	0.721	0.018	0.799	0.031	0.767	0.030
	[M+1] ⁺	0.137	0.009	0.092	0.021	0.096	0.016
	[M+2] ⁺	0.093	0.008	0.072	0.008	0.087	0.015
	[M+3] ⁺	0.049	0.007	0.038	0.007	0.049	0.018
180	[M] ⁺	0.695	0.058	0.771	0.049	0.766	0.031
	[M+1] ⁺	0.142	0.024	0.099	0.026	0.101	0.019
	[M+2] ⁺	0.106	0.021	0.086	0.015	0.087	0.011
	[M+3] ⁺	0.057	0.015	0.044	0.009	0.046	0.009
300	[M] ⁺	0.734	0.021	0.754	0.025	0.774	0.057
	[M+1] ⁺	0.101	0.006	0.087	0.010	0.082	0.018
	[M+2] ⁺	0.107	0.010	0.101	0.011	0.093	0.023
	[M+3] ⁺	0.058	0.008	0.058	0.010	0.051	0.019
420	[M] ⁺	0.700	0.040	0.733	0.046	0.644	0.231
	[M+1] ⁺	0.103	0.012	0.092	0.016	0.104	0.058
	[M+2] ⁺	0.126	0.018	0.114	0.021	0.153	0.102
	[M+3] ⁺	0.071	0.014	0.062	0.014	0.099	0.073
600	[M] ⁺	0.686	0.021	0.760	0.048	0.742	0.043
	[M+1] ⁺	0.093	0.010	0.076	0.014	0.082	0.015
	[M+2] ⁺	0.138	0.007	0.104	0.022	0.111	0.020
	[M+3] ⁺	0.083	0.006	0.060	0.016	0.065	0.014
1800	[M] ⁺	0.583	0.035	0.660	0.061	0.655	0.077

Labeling time (s)	Isotopomer	No treatment		DMSO		Imazapyr	
		AM	SD	AM	SD	AM	SD
	[M+1] ⁺	0.115	0.009	0.098	0.026	0.102	0.030
	[M+2] ⁺	0.187	0.017	0.153	0.027	0.154	0.033
	[M+3] ⁺	0.115	0.011	0.089	0.011	0.089	0.016

Table A9. 58 Mass isotopomer distribution of ribulose 1,5-bisphosphate, measured by LC-MS

Mean values ($n = 5$) of isotopomer abundance are listed. Abbreviations: SD (standard deviation), AM (arithmetic mean).

Labeling time (s)	Isotopomer	No treatment		DMSO		Imazapyr	
		AM	SD	AM	SD	AM	SD
0	[M] ⁺	0.919	0.004	0.916	0.011	0.779	0.303
	[M+1] ⁺	0.059	0.005	0.063	0.009	0.058	0.003
	[M+2] ⁺	0.017	0.002	0.019	0.001	0.048	0.064
	[M+3] ⁺	0.002	0.001	0.001	0.000	0.015	0.028
	[M+4] ⁺	0.002	0.002	0.002	0.000	0.058	0.122
	[M+5] ⁺	0.001	0.001	0.000	0.000	0.042	0.090
10	[M] ⁺	0.605	0.021	0.572	0.043	0.565	0.040
	[M+1] ⁺	0.286	0.015	0.307	0.024	0.301	0.014
	[M+2] ⁺	0.080	0.007	0.090	0.013	0.094	0.015
	[M+3] ⁺	0.023	0.002	0.026	0.005	0.027	0.008
	[M+4] ⁺	0.004	0.003	0.005	0.002	0.009	0.003
	[M+5] ⁺	0.002	0.002	0.001	0.001	0.003	0.002
20	[M] ⁺	0.384	0.009	0.355	0.023	0.349	0.040
	[M+1] ⁺	0.361	0.005	0.364	0.011	0.350	0.015
	[M+2] ⁺	0.163	0.003	0.176	0.009	0.186	0.016
	[M+3] ⁺	0.073	0.007	0.083	0.015	0.085	0.012
	[M+4] ⁺	0.015	0.001	0.017	0.005	0.023	0.004
	[M+5] ⁺	0.004	0.001	0.004	0.002	0.007	0.002
30	[M] ⁺	0.290	0.014	0.256	0.020	0.265	0.033
	[M+1] ⁺	0.352	0.015	0.339	0.014	0.320	0.015
	[M+2] ⁺	0.205	0.008	0.220	0.004	0.218	0.014
	[M+3] ⁺	0.117	0.012	0.136	0.012	0.143	0.018
	[M+4] ⁺	0.028	0.005	0.036	0.007	0.040	0.010
	[M+5] ⁺	0.009	0.002	0.012	0.004	0.014	0.005
40	[M] ⁺	0.217	0.021	0.209	0.013	0.208	0.013
	[M+1] ⁺	0.300	0.018	0.294	0.010	0.294	0.010
	[M+2] ⁺	0.236	0.011	0.235	0.009	0.234	0.003
	[M+3] ⁺	0.174	0.020	0.181	0.011	0.179	0.012
	[M+4] ⁺	0.054	0.007	0.059	0.005	0.060	0.006
	[M+5] ⁺	0.020	0.004	0.022	0.003	0.026	0.004
50	[M] ⁺	0.183	0.005	0.165	0.012	0.168	0.012
	[M+1] ⁺	0.257	0.005	0.251	0.011	0.255	0.015

Labeling time (s)	Isotopomer	No treatment		DMSO		Imazapyr	
		AM	SD	AM	SD	AM	SD
	[M+2] ⁺	0.237	0.003	0.238	0.005	0.236	0.004
	[M+3] ⁺	0.213	0.005	0.225	0.008	0.217	0.010
	[M+4] ⁺	0.077	0.001	0.084	0.003	0.084	0.011
	[M+5] ⁺	0.033	0.002	0.037	0.004	0.040	0.006
60	[M] ⁺	0.140	0.012	0.141	0.010	0.156	0.018
	[M+1] ⁺	0.230	0.008	0.222	0.010	0.212	0.012
	[M+2] ⁺	0.247	0.005	0.239	0.007	0.242	0.014
	[M+3] ⁺	0.238	0.007	0.240	0.010	0.232	0.011
	[M+4] ⁺	0.098	0.006	0.104	0.009	0.106	0.015
	[M+5] ⁺	0.046	0.007	0.053	0.007	0.051	0.008
90	[M] ⁺	0.100	0.007	0.103	0.014	0.111	0.018
	[M+1] ⁺	0.161	0.014	0.148	0.008	0.142	0.007
	[M+2] ⁺	0.227	0.012	0.203	0.013	0.211	0.010
	[M+3] ⁺	0.271	0.014	0.271	0.007	0.261	0.009
	[M+4] ⁺	0.150	0.007	0.167	0.009	0.168	0.010
	[M+5] ⁺	0.091	0.012	0.108	0.014	0.107	0.008
120	[M] ⁺	0.081	0.005	0.075	0.015	0.085	0.006
	[M+1] ⁺	0.117	0.010	0.102	0.013	0.110	0.007
	[M+2] ⁺	0.190	0.007	0.172	0.011	0.181	0.008
	[M+3] ⁺	0.275	0.008	0.274	0.010	0.269	0.004
	[M+4] ⁺	0.203	0.009	0.215	0.013	0.209	0.008
	[M+5] ⁺	0.133	0.013	0.160	0.020	0.146	0.009
150	[M] ⁺	0.067	0.007	0.077	0.009	0.068	0.007
	[M+1] ⁺	0.088	0.007	0.083	0.006	0.076	0.001
	[M+2] ⁺	0.171	0.010	0.154	0.006	0.153	0.007
	[M+3] ⁺	0.272	0.006	0.259	0.009	0.253	0.010
	[M+4] ⁺	0.234	0.009	0.237	0.009	0.250	0.014
	[M+5] ⁺	0.167	0.013	0.190	0.013	0.200	0.011
180	[M] ⁺	0.063	0.004	0.071	0.008	0.066	0.010
	[M+1] ⁺	0.072	0.007	0.065	0.005	0.069	0.005
	[M+2] ⁺	0.152	0.012	0.136	0.011	0.146	0.007
	[M+3] ⁺	0.253	0.008	0.244	0.013	0.248	0.004
	[M+4] ⁺	0.262	0.014	0.268	0.007	0.263	0.007
	[M+5] ⁺	0.197	0.018	0.218	0.018	0.208	0.018
300	[M] ⁺	0.052	0.005	0.055	0.007	0.062	0.012
	[M+1] ⁺	0.043	0.004	0.042	0.004	0.047	0.009
	[M+2] ⁺	0.106	0.004	0.097	0.008	0.104	0.018
	[M+3] ⁺	0.230	0.008	0.211	0.015	0.213	0.014
	[M+4] ⁺	0.318	0.007	0.318	0.009	0.312	0.018
	[M+5] ⁺	0.250	0.018	0.277	0.028	0.262	0.031
420	[M] ⁺	0.049	0.006	0.052	0.004	0.102	0.090
	[M+1] ⁺	0.033	0.003	0.030	0.004	0.049	0.031

Labeling time (s)	Isotopomer	No treatment		DMSO		Imazapyr	
		AM	SD	AM	SD	AM	SD
	[M+2] ⁺	0.086	0.007	0.079	0.004	0.124	0.079
	[M+3] ⁺	0.208	0.013	0.196	0.010	0.200	0.008
	[M+4] ⁺	0.339	0.013	0.336	0.009	0.277	0.127
	[M+5] ⁺	0.285	0.019	0.307	0.016	0.248	0.071
600	[M] ⁺	0.051	0.007	0.047	0.004	0.051	0.009
	[M+1] ⁺	0.029	0.004	0.027	0.003	0.028	0.003
	[M+2] ⁺	0.079	0.009	0.067	0.006	0.073	0.006
	[M+3] ⁺	0.210	0.010	0.186	0.009	0.192	0.007
	[M+4] ⁺	0.350	0.011	0.355	0.007	0.356	0.009
	[M+5] ⁺	0.282	0.021	0.318	0.022	0.300	0.015
1800	[M] ⁺	0.030	0.003	0.030	0.005	0.031	0.005
	[M+1] ⁺	0.031	0.005	0.030	0.003	0.030	0.004
	[M+2] ⁺	0.095	0.011	0.086	0.008	0.089	0.007
	[M+3] ⁺	0.249	0.019	0.235	0.009	0.238	0.006
	[M+4] ⁺	0.362	0.009	0.369	0.005	0.370	0.013
	[M+5] ⁺	0.233	0.028	0.249	0.018	0.242	0.007

Table A9. 59 Mass isotopomer distribution of pentose 5-phosphate, measured by LC-MS

Mean values ($n = 5$) of isotopomer abundance are listed. Abbreviations: SD (standard deviation), AM (arithmetic mean).

Labeling time (s)	Isotopomer	No treatment		DMSO		Imazapyr	
		AM	SD	AM	SD	AM	SD
0	[M] ⁺	0.929	0.008	0.918	0.025	0.766	0.369
	[M+1] ⁺	0.058	0.006	0.063	0.022	0.079	0.050
	[M+2] ⁺	0.010	0.002	0.009	0.003	0.029	0.045
	[M+3] ⁺	0.001	0.000	0.004	0.003	0.008	0.015
	[M+4] ⁺	0.001	0.002	0.005	0.006	0.107	0.236
	[M+5] ⁺	0.001	0.001	0.001	0.001	0.010	0.023
10	[M] ⁺	0.597	0.032	0.588	0.052	0.575	0.057
	[M+1] ⁺	0.299	0.023	0.305	0.047	0.315	0.025
	[M+2] ⁺	0.078	0.006	0.073	0.019	0.082	0.027
	[M+3] ⁺	0.019	0.003	0.026	0.010	0.024	0.011
	[M+4] ⁺	0.005	0.003	0.007	0.007	0.003	0.001
	[M+5] ⁺	0.001	0.001	0.002	0.001	0.001	0.001
20	[M] ⁺	0.378	0.032	0.340	0.035	0.356	0.038
	[M+1] ⁺	0.360	0.012	0.374	0.009	0.367	0.026
	[M+2] ⁺	0.171	0.011	0.180	0.011	0.183	0.021
	[M+3] ⁺	0.075	0.015	0.087	0.017	0.074	0.023
	[M+4] ⁺	0.013	0.006	0.014	0.014	0.015	0.005
	[M+5] ⁺	0.003	0.001	0.005	0.003	0.005	0.002
30	[M] ⁺	0.302	0.033	0.259	0.025	0.264	0.019

Labeling time (s)	Isotopomer	No treatment		DMSO		Imazapyr	
		AM	SD	AM	SD	AM	SD
	[M+1] ⁺	0.340	0.014	0.323	0.017	0.329	0.019
	[M+2] ⁺	0.208	0.016	0.222	0.016	0.224	0.005
	[M+3] ⁺	0.118	0.015	0.157	0.021	0.143	0.023
	[M+4] ⁺	0.024	0.004	0.029	0.008	0.031	0.008
	[M+5] ⁺	0.008	0.002	0.010	0.003	0.010	0.004
40	[M] ⁺	0.229	0.012	0.215	0.020	0.205	0.012
	[M+1] ⁺	0.295	0.016	0.293	0.020	0.280	0.018
	[M+2] ⁺	0.237	0.013	0.235	0.032	0.258	0.027
	[M+3] ⁺	0.172	0.016	0.175	0.020	0.181	0.017
	[M+4] ⁺	0.051	0.004	0.062	0.008	0.056	0.009
	[M+5] ⁺	0.017	0.004	0.020	0.004	0.020	0.006
50	[M] ⁺	0.191	0.008	0.164	0.009	0.173	0.008
	[M+1] ⁺	0.263	0.002	0.255	0.017	0.256	0.020
	[M+2] ⁺	0.240	0.011	0.221	0.043	0.237	0.010
	[M+3] ⁺	0.206	0.008	0.238	0.032	0.220	0.011
	[M+4] ⁺	0.069	0.006	0.084	0.013	0.077	0.011
	[M+5] ⁺	0.032	0.002	0.039	0.012	0.037	0.009
60	[M] ⁺	0.174	0.034	0.160	0.016	0.147	0.006
	[M+1] ⁺	0.220	0.011	0.211	0.015	0.218	0.008
	[M+2] ⁺	0.236	0.007	0.242	0.022	0.257	0.045
	[M+3] ⁺	0.231	0.013	0.242	0.022	0.233	0.023
	[M+4] ⁺	0.094	0.010	0.094	0.014	0.097	0.016
	[M+5] ⁺	0.046	0.006	0.052	0.006	0.048	0.016
90	[M] ⁺	0.118	0.033	0.139	0.076	0.106	0.018
	[M+1] ⁺	0.160	0.011	0.138	0.010	0.146	0.007
	[M+2] ⁺	0.224	0.002	0.194	0.017	0.205	0.012
	[M+3] ⁺	0.265	0.019	0.284	0.024	0.275	0.013
	[M+4] ⁺	0.147	0.013	0.141	0.036	0.165	0.007
	[M+5] ⁺	0.086	0.013	0.104	0.015	0.103	0.008
120	[M] ⁺	0.105	0.025	0.074	0.022	0.087	0.007
	[M+1] ⁺	0.111	0.010	0.103	0.012	0.100	0.005
	[M+2] ⁺	0.189	0.006	0.176	0.019	0.183	0.015
	[M+3] ⁺	0.271	0.007	0.279	0.015	0.267	0.015
	[M+4] ⁺	0.197	0.014	0.207	0.019	0.203	0.010
	[M+5] ⁺	0.129	0.020	0.162	0.019	0.160	0.009
150	[M] ⁺	0.080	0.011	0.089	0.016	0.064	0.010
	[M+1] ⁺	0.084	0.008	0.077	0.014	0.074	0.008
	[M+2] ⁺	0.165	0.013	0.153	0.019	0.151	0.010
	[M+3] ⁺	0.258	0.008	0.270	0.011	0.270	0.006
	[M+4] ⁺	0.240	0.017	0.222	0.012	0.247	0.010
	[M+5] ⁺	0.173	0.019	0.190	0.020	0.194	0.015
180	[M] ⁺	0.082	0.017	0.072	0.018	0.064	0.009

Labeling time (s)	Isotopomer	No treatment		DMSO		Imazapyr	
		AM	SD	AM	SD	AM	SD
	[M+1] ⁺	0.069	0.007	0.061	0.011	0.064	0.008
	[M+2] ⁺	0.144	0.012	0.133	0.010	0.141	0.012
	[M+3] ⁺	0.245	0.007	0.249	0.020	0.245	0.009
	[M+4] ⁺	0.260	0.018	0.260	0.013	0.270	0.014
	[M+5] ⁺	0.201	0.025	0.225	0.020	0.215	0.016
300	[M] ⁺	0.062	0.013	0.059	0.008	0.050	0.014
	[M+1] ⁺	0.039	0.003	0.039	0.008	0.048	0.013
	[M+2] ⁺	0.101	0.005	0.092	0.019	0.092	0.010
	[M+3] ⁺	0.223	0.011	0.218	0.019	0.228	0.017
	[M+4] ⁺	0.317	0.010	0.308	0.012	0.306	0.041
	[M+5] ⁺	0.257	0.018	0.284	0.039	0.277	0.037
420	[M] ⁺	0.069	0.010	0.054	0.013	0.089	0.074
	[M+1] ⁺	0.035	0.006	0.033	0.003	0.084	0.112
	[M+2] ⁺	0.092	0.005	0.083	0.010	0.085	0.012
	[M+3] ⁺	0.201	0.008	0.187	0.026	0.168	0.066
	[M+4] ⁺	0.328	0.013	0.327	0.018	0.314	0.042
	[M+5] ⁺	0.275	0.020	0.317	0.033	0.260	0.084
600	[M] ⁺	0.067	0.013	0.049	0.005	0.048	0.011
	[M+1] ⁺	0.028	0.005	0.025	0.005	0.029	0.004
	[M+2] ⁺	0.078	0.009	0.063	0.008	0.072	0.005
	[M+3] ⁺	0.197	0.012	0.196	0.016	0.197	0.008
	[M+4] ⁺	0.350	0.013	0.347	0.007	0.351	0.009
	[M+5] ⁺	0.281	0.023	0.320	0.027	0.303	0.022
1800	[M] ⁺	0.043	0.007	0.033	0.010	0.028	0.005
	[M+1] ⁺	0.034	0.006	0.029	0.002	0.027	0.004
	[M+2] ⁺	0.095	0.012	0.080	0.007	0.086	0.008
	[M+3] ⁺	0.241	0.017	0.232	0.016	0.237	0.013
	[M+4] ⁺	0.354	0.011	0.363	0.007	0.372	0.010
	[M+5] ⁺	0.232	0.031	0.263	0.022	0.249	0.012

Table A9. 60 Mass isotopomer distribution of 2-phosphoglycerate, measured by LC-MS

Mean values ($n = 5$) of isotopomer abundance are listed. Abbreviations: SD (standard deviation), AM (arithmetic mean).

Labeling time (s)	Isotopomer	No treatment		DMSO		Imazapyr	
		AM	SD	AM	SD	AM	SD
0	[M] ⁺	0.956	0.004	0.948	0.006	0.823	0.262
	[M+1] ⁺	0.036	0.001	0.037	0.002	0.082	0.096
	[M+2] ⁺	0.007	0.003	0.014	0.004	0.055	0.085
	[M+3] ⁺	0.001	0.001	0.001	0.001	0.040	0.081
10	[M] ⁺	0.749	0.043	0.718	0.045	0.695	0.068
	[M+1] ⁺	0.222	0.035	0.247	0.036	0.263	0.056

Labeling time (s)	Isotopomer	No treatment		DMSO		Imazapyr	
		AM	SD	AM	SD	AM	SD
	[M+2] ⁺	0.024	0.007	0.029	0.009	0.036	0.010
	[M+3] ⁺	0.005	0.002	0.006	0.003	0.007	0.004
20	[M] ⁺	0.643	0.055	0.594	0.036	0.580	0.077
	[M+1] ⁺	0.288	0.040	0.325	0.020	0.322	0.054
	[M+2] ⁺	0.053	0.011	0.060	0.014	0.073	0.017
	[M+3] ⁺	0.017	0.006	0.021	0.006	0.025	0.008
30	[M] ⁺	0.585	0.048	0.497	0.097	0.527	0.054
	[M+1] ⁺	0.301	0.036	0.354	0.062	0.331	0.031
	[M+2] ⁺	0.077	0.007	0.101	0.024	0.093	0.010
	[M+3] ⁺	0.037	0.009	0.047	0.016	0.049	0.015
40	[M] ⁺	0.511	0.045	0.494	0.032	0.447	0.057
	[M+1] ⁺	0.316	0.026	0.331	0.016	0.355	0.030
	[M+2] ⁺	0.111	0.014	0.111	0.009	0.122	0.020
	[M+3] ⁺	0.061	0.006	0.064	0.010	0.076	0.013
50	[M] ⁺	0.414	0.019	0.416	0.046	0.413	0.067
	[M+1] ⁺	0.357	0.015	0.349	0.020	0.338	0.024
	[M+2] ⁺	0.133	0.005	0.139	0.025	0.147	0.026
	[M+3] ⁺	0.095	0.009	0.096	0.010	0.102	0.021
60	[M] ⁺	0.410	0.042	0.407	0.026	0.349	0.059
	[M+1] ⁺	0.329	0.021	0.323	0.011	0.338	0.015
	[M+2] ⁺	0.155	0.009	0.153	0.010	0.178	0.030
	[M+3] ⁺	0.106	0.017	0.117	0.014	0.135	0.017
90	[M] ⁺	0.368	0.029	0.313	0.010	0.316	0.044
	[M+1] ⁺	0.283	0.026	0.287	0.012	0.277	0.010
	[M+2] ⁺	0.182	0.014	0.202	0.009	0.205	0.018
	[M+3] ⁺	0.166	0.020	0.198	0.010	0.202	0.023
120	[M] ⁺	0.300	0.057	0.258	0.063	0.263	0.038
	[M+1] ⁺	0.263	0.007	0.256	0.011	0.247	0.009
	[M+2] ⁺	0.216	0.028	0.226	0.026	0.240	0.017
	[M+3] ⁺	0.220	0.034	0.260	0.033	0.250	0.015
150	[M] ⁺	0.283	0.022	0.302	0.030	0.241	0.076
	[M+1] ⁺	0.224	0.016	0.217	0.011	0.209	0.018
	[M+2] ⁺	0.238	0.015	0.226	0.015	0.256	0.030
	[M+3] ⁺	0.255	0.019	0.255	0.021	0.295	0.040
180	[M] ⁺	0.278	0.046	0.266	0.048	0.265	0.062
	[M+1] ⁺	0.199	0.005	0.193	0.005	0.199	0.014
	[M+2] ⁺	0.250	0.011	0.246	0.024	0.250	0.037
	[M+3] ⁺	0.272	0.037	0.296	0.024	0.285	0.029
300	[M] ⁺	0.222	0.042	0.213	0.015	0.241	0.049
	[M+1] ⁺	0.151	0.008	0.148	0.010	0.150	0.010
	[M+2] ⁺	0.284	0.024	0.274	0.020	0.284	0.022
	[M+3] ⁺	0.343	0.024	0.365	0.023	0.325	0.059

Labeling time (s)	Isotopomer	No treatment		DMSO		Imazapyr	
		AM	SD	AM	SD	AM	SD
420	[M] ⁺	0.219	0.014	0.199	0.016	0.174	0.060
	[M+1] ⁺	0.128	0.012	0.121	0.003	0.120	0.007
	[M+2] ⁺	0.285	0.011	0.283	0.021	0.363	0.151
	[M+3] ⁺	0.368	0.013	0.397	0.024	0.343	0.121
600	[M] ⁺	0.207	0.021	0.200	0.022	0.173	0.039
	[M+1] ⁺	0.118	0.008	0.105	0.006	0.107	0.004
	[M+2] ⁺	0.303	0.013	0.293	0.016	0.311	0.016
	[M+3] ⁺	0.372	0.015	0.402	0.007	0.409	0.035
1800	[M] ⁺	0.170	0.018	0.153	0.023	0.147	0.017
	[M+1] ⁺	0.139	0.008	0.135	0.005	0.142	0.014
	[M+2] ⁺	0.342	0.009	0.344	0.019	0.350	0.014
	[M+3] ⁺	0.349	0.024	0.368	0.015	0.360	0.024

Table A9. 61 Mass isotopomer distribution of phosphoenolpyruvate, measured by LC-MS

Mean values ($n = 5$) of isotopomer abundance are listed. Abbreviations: SD (standard deviation), AM (arithmetic mean).

Labeling time (s)	Isotopomer	No treatment		DMSO		Imazapyr	
		AM	SD	AM	SD	AM	SD
0	[M] ⁺	0.916	0.011	0.926	0.020	0.778	0.245
	[M+1] ⁺	0.033	0.002	0.038	0.004	0.045	0.029
	[M+2] ⁺	0.048	0.011	0.032	0.020	0.156	0.201
	[M+3] ⁺	0.003	0.002	0.004	0.002	0.021	0.016
10	[M] ⁺	0.707	0.029	0.700	0.034	0.674	0.043
	[M+1] ⁺	0.246	0.025	0.267	0.029	0.231	0.025
	[M+2] ⁺	0.042	0.005	0.029	0.005	0.087	0.042
	[M+3] ⁺	0.005	0.001	0.004	0.002	0.009	0.006
20	[M] ⁺	0.592	0.010	0.578	0.034	0.578	0.026
	[M+1] ⁺	0.324	0.012	0.342	0.031	0.319	0.032
	[M+2] ⁺	0.068	0.007	0.062	0.004	0.079	0.015
	[M+3] ⁺	0.016	0.004	0.018	0.007	0.024	0.006
30	[M] ⁺	0.538	0.037	0.491	0.019	0.491	0.038
	[M+1] ⁺	0.349	0.021	0.379	0.009	0.354	0.037
	[M+2] ⁺	0.083	0.013	0.091	0.004	0.113	0.018
	[M+3] ⁺	0.030	0.005	0.040	0.007	0.043	0.006
40	[M] ⁺	0.449	0.021	0.436	0.015	0.430	0.012
	[M+1] ⁺	0.360	0.033	0.383	0.005	0.368	0.036
	[M+2] ⁺	0.134	0.016	0.118	0.008	0.134	0.034
	[M+3] ⁺	0.056	0.008	0.063	0.007	0.068	0.007
50	[M] ⁺	0.397	0.014	0.368	0.018	0.392	0.030
	[M+1] ⁺	0.359	0.017	0.373	0.030	0.354	0.029
	[M+2] ⁺	0.160	0.007	0.163	0.028	0.157	0.020

Labeling time (s)	Isotopomer	No treatment		DMSO		Imazapyr	
		AM	SD	AM	SD	AM	SD
60	[M+3] ⁺	0.083	0.004	0.096	0.010	0.097	0.016
	[M] ⁺	0.355	0.038	0.354	0.023	0.335	0.095
	[M+1] ⁺	0.362	0.009	0.369	0.015	0.280	0.092
	[M+2] ⁺	0.175	0.037	0.164	0.023	0.284	0.179
	[M+3] ⁺	0.108	0.011	0.113	0.012	0.101	0.019
90	[M] ⁺	0.300	0.022	0.265	0.024	0.281	0.045
	[M+1] ⁺	0.315	0.016	0.314	0.014	0.284	0.014
	[M+2] ⁺	0.220	0.036	0.217	0.015	0.252	0.053
	[M+3] ⁺	0.165	0.015	0.204	0.019	0.183	0.012
120	[M] ⁺	0.280	0.030	0.245	0.040	0.281	0.021
	[M+1] ⁺	0.259	0.019	0.262	0.012	0.235	0.024
	[M+2] ⁺	0.234	0.025	0.227	0.009	0.241	0.046
	[M+3] ⁺	0.227	0.021	0.266	0.023	0.244	0.032
150	[M] ⁺	0.260	0.009	0.247	0.035	0.252	0.037
	[M+1] ⁺	0.231	0.016	0.208	0.006	0.177	0.079
	[M+2] ⁺	0.240	0.013	0.256	0.027	0.274	0.030
	[M+3] ⁺	0.269	0.018	0.289	0.020	0.297	0.053
180	[M] ⁺	0.265	0.021	0.253	0.041	0.262	0.008
	[M+1] ⁺	0.201	0.012	0.187	0.012	0.180	0.019
	[M+2] ⁺	0.259	0.020	0.249	0.039	0.263	0.038
	[M+3] ⁺	0.275	0.022	0.311	0.012	0.295	0.021
300	[M] ⁺	0.208	0.034	0.202	0.011	0.231	0.019
	[M+1] ⁺	0.140	0.005	0.128	0.010	0.126	0.016
	[M+2] ⁺	0.286	0.019	0.290	0.010	0.308	0.056
	[M+3] ⁺	0.366	0.022	0.380	0.014	0.335	0.055
420	[M] ⁺	0.205	0.008	0.190	0.025	0.186	0.040
	[M+1] ⁺	0.115	0.005	0.109	0.009	0.088	0.037
	[M+2] ⁺	0.296	0.013	0.301	0.017	0.393	0.189
	[M+3] ⁺	0.383	0.018	0.400	0.011	0.334	0.116
600	[M] ⁺	0.189	0.022	0.181	0.022	0.203	0.019
	[M+1] ⁺	0.104	0.012	0.099	0.005	0.093	0.019
	[M+2] ⁺	0.313	0.023	0.294	0.023	0.340	0.041
	[M+3] ⁺	0.393	0.008	0.427	0.013	0.364	0.015
1800	[M] ⁺	0.153	0.014	0.142	0.027	0.138	0.020
	[M+1] ⁺	0.136	0.017	0.128	0.006	0.115	0.014
	[M+2] ⁺	0.359	0.012	0.360	0.027	0.401	0.063
	[M+3] ⁺	0.352	0.026	0.370	0.012	0.347	0.046

Table A9. 62 Mass isotopomer distribution of fructose 1,5-bisphosphate, measured by LC-MS

Mean values ($n = 5$) of isotopomer abundance are listed. Abbreviations: SD (standard deviation), AM (arithmetic mean).

Labeling time (s)	Isotopomer	No treatment		DMSO		Imazapyr	
		AM	SD	AM	SD	AM	SD
0	[M] ⁺	0.854	0.039	0.852	0.032	0.748	0.239
	[M+1] ⁺	0.091	0.037	0.074	0.005	0.092	0.047
	[M+2] ⁺	0.021	0.006	0.027	0.006	0.030	0.012
	[M+3] ⁺	0.002	0.001	0.003	0.002	0.015	0.021
	[M+4] ⁺	0.002	0.002	0.003	0.001	0.012	0.016
	[M+5] ⁺	0.004	0.002	0.004	0.003	0.024	0.040
	[M+6] ⁺	0.026	0.026	0.037	0.034	0.079	0.109
10	[M] ⁺	0.558	0.038	0.480	0.026	0.514	0.058
	[M+1] ⁺	0.278	0.024	0.311	0.015	0.289	0.027
	[M+2] ⁺	0.117	0.015	0.149	0.021	0.135	0.030
	[M+3] ⁺	0.022	0.004	0.031	0.004	0.028	0.010
	[M+4] ⁺	0.007	0.001	0.008	0.002	0.009	0.006
	[M+5] ⁺	0.004	0.002	0.002	0.001	0.005	0.003
	[M+6] ⁺	0.014	0.012	0.018	0.016	0.021	0.013
20	[M] ⁺	0.499	0.018	0.410	0.014	0.390	0.043
	[M+1] ⁺	0.253	0.025	0.268	0.021	0.281	0.017
	[M+2] ⁺	0.152	0.021	0.195	0.009	0.196	0.017
	[M+3] ⁺	0.053	0.005	0.071	0.006	0.077	0.015
	[M+4] ⁺	0.021	0.004	0.026	0.004	0.029	0.007
	[M+5] ⁺	0.006	0.001	0.006	0.003	0.009	0.002
	[M+6] ⁺	0.017	0.015	0.024	0.016	0.018	0.010
30	[M] ⁺	0.418	0.024	0.376	0.024	0.389	0.034
	[M+1] ⁺	0.241	0.026	0.230	0.014	0.223	0.005
	[M+2] ⁺	0.189	0.019	0.202	0.015	0.195	0.018
	[M+3] ⁺	0.088	0.010	0.105	0.006	0.104	0.016
	[M+4] ⁺	0.040	0.007	0.049	0.004	0.052	0.011
	[M+5] ⁺	0.011	0.002	0.015	0.004	0.017	0.004
	[M+6] ⁺	0.013	0.010	0.023	0.012	0.020	0.011
40	[M] ⁺	0.387	0.030	0.339	0.010	0.346	0.028
	[M+1] ⁺	0.211	0.031	0.204	0.011	0.204	0.013
	[M+2] ⁺	0.190	0.021	0.209	0.007	0.203	0.012
	[M+3] ⁺	0.108	0.020	0.130	0.006	0.124	0.005
	[M+4] ⁺	0.064	0.012	0.074	0.004	0.075	0.009
	[M+5] ⁺	0.019	0.006	0.024	0.001	0.026	0.003
	[M+6] ⁺	0.021	0.015	0.019	0.011	0.022	0.009
50	[M] ⁺	0.365	0.028	0.304	0.020	0.287	0.045
	[M+1] ⁺	0.176	0.026	0.179	0.014	0.176	0.014
	[M+2] ⁺	0.183	0.018	0.192	0.018	0.203	0.015

Labeling time (s)	Isotopomer	No treatment		DMSO		Imazapyr	
		AM	SD	AM	SD	AM	SD
	[M+3] ⁺	0.139	0.020	0.147	0.014	0.159	0.023
	[M+4] ⁺	0.082	0.013	0.101	0.010	0.106	0.015
	[M+5] ⁺	0.030	0.005	0.039	0.003	0.042	0.009
	[M+6] ⁺	0.025	0.014	0.038	0.029	0.027	0.007
60	[M] ⁺	0.356	0.045	0.269	0.021	0.290	0.038
	[M+1] ⁺	0.166	0.027	0.169	0.011	0.151	0.007
	[M+2] ⁺	0.170	0.014	0.196	0.011	0.188	0.016
	[M+3] ⁺	0.140	0.013	0.161	0.008	0.158	0.014
	[M+4] ⁺	0.101	0.015	0.121	0.009	0.124	0.016
	[M+5] ⁺	0.042	0.008	0.050	0.006	0.051	0.007
	[M+6] ⁺	0.025	0.009	0.032	0.009	0.038	0.006
90	[M] ⁺	0.259	0.021	0.189	0.018	0.226	0.030
	[M+1] ⁺	0.129	0.018	0.110	0.010	0.110	0.001
	[M+2] ⁺	0.166	0.017	0.159	0.008	0.154	0.012
	[M+3] ⁺	0.172	0.012	0.185	0.007	0.181	0.014
	[M+4] ⁺	0.151	0.012	0.183	0.013	0.170	0.007
	[M+5] ⁺	0.079	0.006	0.106	0.014	0.099	0.005
	[M+6] ⁺	0.043	0.008	0.068	0.008	0.060	0.005
120	[M] ⁺	0.249	0.044	0.193	0.031	0.184	0.028
	[M+1] ⁺	0.117	0.025	0.078	0.010	0.089	0.003
	[M+2] ⁺	0.132	0.007	0.126	0.018	0.133	0.007
	[M+3] ⁺	0.165	0.014	0.168	0.019	0.178	0.008
	[M+4] ⁺	0.165	0.024	0.190	0.027	0.194	0.015
	[M+5] ⁺	0.106	0.021	0.133	0.025	0.137	0.008
	[M+6] ⁺	0.067	0.011	0.112	0.043	0.085	0.006
150	[M] ⁺	0.234	0.038	0.174	0.033	0.196	0.051
	[M+1] ⁺	0.096	0.011	0.069	0.010	0.070	0.006
	[M+2] ⁺	0.110	0.009	0.105	0.007	0.105	0.008
	[M+3] ⁺	0.153	0.013	0.163	0.006	0.152	0.008
	[M+4] ⁺	0.180	0.012	0.205	0.016	0.196	0.020
	[M+5] ⁺	0.139	0.019	0.170	0.018	0.166	0.021
	[M+6] ⁺	0.088	0.012	0.115	0.016	0.115	0.014
180	[M] ⁺	0.238	0.010	0.190	0.029	0.182	0.024
	[M+1] ⁺	0.082	0.011	0.067	0.009	0.076	0.011
	[M+2] ⁺	0.094	0.009	0.088	0.005	0.101	0.007
	[M+3] ⁺	0.148	0.009	0.147	0.007	0.154	0.008
	[M+4] ⁺	0.183	0.003	0.197	0.014	0.193	0.013
	[M+5] ⁺	0.159	0.008	0.185	0.017	0.177	0.011
	[M+6] ⁺	0.096	0.016	0.127	0.016	0.117	0.011
300	[M] ⁺	0.250	0.019	0.186	0.047	0.198	0.061
	[M+1] ⁺	0.091	0.026	0.055	0.007	0.061	0.021
	[M+2] ⁺	0.076	0.009	0.067	0.006	0.096	0.062

Labeling time (s)	Isotopomer	No treatment		DMSO		Imazapyr	
		AM	SD	AM	SD	AM	SD
	[M+3] ⁺	0.115	0.004	0.120	0.015	0.124	0.013
	[M+4] ⁺	0.162	0.016	0.189	0.025	0.174	0.030
	[M+5] ⁺	0.184	0.026	0.220	0.013	0.196	0.078
	[M+6] ⁺	0.123	0.022	0.164	0.013	0.151	0.035
420	[M] ⁺	0.254	0.026	0.190	0.033	0.225	0.051
	[M+1] ⁺	0.069	0.013	0.055	0.006	0.067	0.030
	[M+2] ⁺	0.057	0.005	0.060	0.008	0.064	0.010
	[M+3] ⁺	0.097	0.006	0.107	0.012	0.097	0.018
	[M+4] ⁺	0.172	0.011	0.180	0.015	0.158	0.045
	[M+5] ⁺	0.210	0.013	0.233	0.012	0.213	0.031
	[M+6] ⁺	0.140	0.017	0.173	0.012	0.176	0.038
600	[M] ⁺	0.210	0.081	0.203	0.037	0.190	0.064
	[M+1] ⁺	0.061	0.032	0.048	0.008	0.049	0.012
	[M+2] ⁺	0.053	0.009	0.050	0.006	0.055	0.006
	[M+3] ⁺	0.103	0.011	0.093	0.011	0.105	0.009
	[M+4] ⁺	0.191	0.030	0.176	0.021	0.187	0.028
	[M+5] ⁺	0.237	0.053	0.251	0.012	0.247	0.031
	[M+6] ⁺	0.144	0.029	0.180	0.011	0.167	0.019
1800	[M] ⁺	0.153	0.034	0.128	0.019	0.121	0.038
	[M+1] ⁺	0.075	0.017	0.062	0.008	0.052	0.015
	[M+2] ⁺	0.066	0.009	0.066	0.010	0.064	0.006
	[M+3] ⁺	0.128	0.013	0.125	0.014	0.126	0.012
	[M+4] ⁺	0.216	0.012	0.223	0.008	0.228	0.024
	[M+5] ⁺	0.239	0.032	0.257	0.022	0.261	0.025
	[M+6] ⁺	0.123	0.021	0.139	0.015	0.147	0.010

Table A9. 63 Mass isotopomer distribution of glucose 6-phosphate, measured by LC-MS

Mean values ($n = 5$) of isotopomer abundance are listed. Abbreviations: SD (standard deviation), AM (arithmetic mean).

Labeling time (s)	Isotopomer	No treatment		DMSO		Imazapyr	
		AM	SD	AM	SD	AM	SD
0	[M] ⁺	0.912	0.001	0.908	0.011	0.732	0.392
	[M+1] ⁺	0.073	0.001	0.072	0.011	0.062	0.023
	[M+2] ⁺	0.013	0.001	0.015	0.002	0.022	0.017
	[M+3] ⁺	0.001	0.000	0.001	0.000	0.041	0.090
	[M+4] ⁺	0.001	0.000	0.001	0.000	0.052	0.114
	[M+5] ⁺	0.000	0.000	0.000	0.000	0.019	0.041
	[M+6] ⁺	0.001	0.000	0.004	0.003	0.072	0.154
10	[M] ⁺	0.840	0.022	0.831	0.016	0.825	0.017
	[M+1] ⁺	0.117	0.014	0.120	0.012	0.122	0.012
	[M+2] ⁺	0.035	0.006	0.039	0.005	0.042	0.005

Labeling time (s)	Isotopomer	No treatment		DMSO		Imazapyr	
		AM	SD	AM	SD	AM	SD
	[M+3] ⁺	0.005	0.001	0.005	0.001	0.006	0.001
	[M+4] ⁺	0.001	0.000	0.002	0.000	0.002	0.000
	[M+5] ⁺	0.000	0.000	0.000	0.000	0.000	0.000
	[M+6] ⁺	0.001	0.000	0.003	0.002	0.003	0.001
20	[M] ⁺	0.756	0.008	0.770	0.030	0.772	0.032
	[M+1] ⁺	0.143	0.006	0.131	0.010	0.130	0.018
	[M+2] ⁺	0.070	0.003	0.067	0.012	0.065	0.011
	[M+3] ⁺	0.021	0.002	0.020	0.008	0.020	0.004
	[M+4] ⁺	0.007	0.001	0.007	0.004	0.008	0.001
	[M+5] ⁺	0.001	0.000	0.001	0.000	0.002	0.000
	[M+6] ⁺	0.001	0.000	0.003	0.001	0.003	0.001
30	[M] ⁺	0.762	0.024	0.731	0.027	0.705	0.017
	[M+1] ⁺	0.127	0.010	0.128	0.012	0.134	0.010
	[M+2] ⁺	0.068	0.009	0.081	0.011	0.090	0.007
	[M+3] ⁺	0.027	0.005	0.035	0.006	0.042	0.005
	[M+4] ⁺	0.012	0.003	0.017	0.004	0.021	0.004
	[M+5] ⁺	0.003	0.001	0.004	0.002	0.005	0.001
	[M+6] ⁺	0.002	0.000	0.004	0.001	0.004	0.001
40	[M] ⁺	0.719	0.042	0.728	0.025	0.672	0.034
	[M+1] ⁺	0.122	0.013	0.120	0.007	0.129	0.011
	[M+2] ⁺	0.082	0.014	0.078	0.009	0.096	0.009
	[M+3] ⁺	0.044	0.008	0.040	0.007	0.055	0.009
	[M+4] ⁺	0.024	0.005	0.023	0.005	0.032	0.005
	[M+5] ⁺	0.007	0.002	0.007	0.002	0.010	0.001
	[M+6] ⁺	0.003	0.001	0.005	0.001	0.006	0.001
50	[M] ⁺	0.689	0.020	0.671	0.054	0.661	0.015
	[M+1] ⁺	0.114	0.000	0.117	0.005	0.118	0.009
	[M+2] ⁺	0.086	0.007	0.090	0.015	0.096	0.004
	[M+3] ⁺	0.056	0.007	0.059	0.015	0.061	0.004
	[M+4] ⁺	0.037	0.004	0.040	0.012	0.041	0.005
	[M+5] ⁺	0.013	0.002	0.014	0.005	0.015	0.003
	[M+6] ⁺	0.006	0.001	0.009	0.004	0.008	0.002
60	[M] ⁺	0.647	0.030	0.641	0.056	0.622	0.022
	[M+1] ⁺	0.116	0.003	0.117	0.007	0.114	0.009
	[M+2] ⁺	0.093	0.010	0.093	0.014	0.097	0.007
	[M+3] ⁺	0.069	0.008	0.068	0.015	0.074	0.006
	[M+4] ⁺	0.050	0.010	0.051	0.014	0.057	0.004
	[M+5] ⁺	0.018	0.003	0.019	0.006	0.023	0.001
	[M+6] ⁺	0.008	0.002	0.011	0.003	0.012	0.001
90	[M] ⁺	0.570	0.029	0.556	0.029	0.561	0.048
	[M+1] ⁺	0.100	0.011	0.103	0.004	0.100	0.007
	[M+2] ⁺	0.095	0.004	0.092	0.005	0.090	0.011

Labeling time (s)	Isotopomer	No treatment		DMSO		Imazapyr	
		AM	SD	AM	SD	AM	SD
	[M+3] ⁺	0.091	0.012	0.089	0.006	0.088	0.014
	[M+4] ⁺	0.082	0.014	0.086	0.010	0.086	0.012
	[M+5] ⁺	0.041	0.007	0.047	0.007	0.048	0.005
	[M+6] ⁺	0.021	0.005	0.027	0.005	0.027	0.002
120	[M] ⁺	0.520	0.070	0.470	0.084	0.498	0.034
	[M+1] ⁺	0.089	0.006	0.084	0.004	0.092	0.006
	[M+2] ⁺	0.083	0.014	0.088	0.015	0.087	0.006
	[M+3] ⁺	0.097	0.016	0.106	0.021	0.099	0.008
	[M+4] ⁺	0.105	0.024	0.119	0.026	0.105	0.010
	[M+5] ⁺	0.068	0.013	0.081	0.016	0.074	0.009
	[M+6] ⁺	0.037	0.008	0.052	0.014	0.045	0.008
150	[M] ⁺	0.479	0.054	0.510	0.061	0.469	0.018
	[M+1] ⁺	0.084	0.005	0.085	0.003	0.085	0.008
	[M+2] ⁺	0.076	0.008	0.073	0.005	0.075	0.009
	[M+3] ⁺	0.104	0.017	0.096	0.006	0.096	0.004
	[M+4] ⁺	0.116	0.014	0.112	0.013	0.114	0.006
	[M+5] ⁺	0.090	0.009	0.062	0.060	0.096	0.009
	[M+6] ⁺	0.052	0.006	0.062	0.015	0.064	0.006
180	[M] ⁺	0.510	0.026	0.489	0.066	0.477	0.015
	[M+1] ⁺	0.077	0.005	0.077	0.003	0.084	0.006
	[M+2] ⁺	0.063	0.005	0.063	0.006	0.070	0.009
	[M+3] ⁺	0.089	0.010	0.086	0.011	0.093	0.005
	[M+4] ⁺	0.109	0.007	0.111	0.020	0.108	0.006
	[M+5] ⁺	0.093	0.011	0.100	0.018	0.101	0.010
	[M+6] ⁺	0.058	0.005	0.073	0.019	0.067	0.008
300	[M] ⁺	0.441	0.063	0.459	0.037	0.547	0.137
	[M+1] ⁺	0.066	0.007	0.069	0.003	0.074	0.002
	[M+2] ⁺	0.052	0.002	0.055	0.010	0.052	0.007
	[M+3] ⁺	0.082	0.010	0.078	0.008	0.064	0.021
	[M+4] ⁺	0.121	0.019	0.110	0.005	0.087	0.032
	[M+5] ⁺	0.142	0.025	0.131	0.021	0.102	0.047
	[M+6] ⁺	0.096	0.019	0.098	0.023	0.073	0.033
420	[M] ⁺	0.495	0.027	0.465	0.038	0.431	0.111
	[M+1] ⁺	0.061	0.004	0.067	0.003	0.066	0.009
	[M+2] ⁺	0.043	0.002	0.049	0.004	0.089	0.089
	[M+3] ⁺	0.066	0.004	0.070	0.005	0.067	0.014
	[M+4] ⁺	0.108	0.011	0.106	0.007	0.100	0.020
	[M+5] ⁺	0.136	0.014	0.142	0.019	0.113	0.034
	[M+6] ⁺	0.092	0.007	0.102	0.015	0.135	0.096
600	[M] ⁺	0.461	0.023	0.465	0.030	0.442	0.040
	[M+1] ⁺	0.060	0.005	0.065	0.003	0.066	0.004
	[M+2] ⁺	0.039	0.001	0.045	0.008	0.049	0.006

Labeling time (s)	Isotopomer	No treatment		DMSO		Imazapyr	
		AM	SD	AM	SD	AM	SD
1800	[M+3] ⁺	0.067	0.007	0.063	0.009	0.071	0.006
	[M+4] ⁺	0.114	0.012	0.105	0.011	0.113	0.013
	[M+5] ⁺	0.151	0.008	0.147	0.007	0.151	0.017
	[M+6] ⁺	0.107	0.009	0.110	0.009	0.108	0.013
	[M] ⁺	0.404	0.040	0.389	0.041	0.375	0.016
	[M+1] ⁺	0.076	0.009	0.080	0.005	0.076	0.004
	[M+2] ⁺	0.055	0.003	0.061	0.006	0.063	0.005
	[M+3] ⁺	0.087	0.005	0.086	0.009	0.093	0.007
	[M+4] ⁺	0.132	0.010	0.131	0.014	0.137	0.009
	[M+5] ⁺	0.159	0.022	0.160	0.017	0.163	0.005
	[M+6] ⁺	0.086	0.021	0.093	0.010	0.093	0.006

Table A9. 64 Mass isotopomer distribution of glycolate, measured by LC-MS

Mean values ($n = 5$) of isotopomer abundance are listed. Abbreviations: SD (standard deviation), AM (arithmetic mean).

Labeling time (s)	Isotopomer	No treatment		DMSO		Imazapyr	
		AM	SD	AM	SD	AM	SD
0	[M] ⁺	0.954	0.008	0.957	0.006	0.963	0.005
	[M+1] ⁺	0.031	0.005	0.028	0.004	0.025	0.004
	[M+2] ⁺	0.015	0.003	0.014	0.002	0.012	0.001
10	[M] ⁺	0.944	0.007	0.949	0.001	0.942	0.006
	[M+1] ⁺	0.037	0.005	0.034	0.002	0.039	0.003
	[M+2] ⁺	0.019	0.002	0.017	0.001	0.019	0.002
20	[M] ⁺	0.932	0.004	0.931	0.003	0.919	0.008
	[M+1] ⁺	0.046	0.003	0.046	0.002	0.055	0.006
	[M+2] ⁺	0.022	0.002	0.023	0.001	0.026	0.003
30	[M] ⁺	0.919	0.011	0.919	0.011	0.908	0.010
	[M+1] ⁺	0.054	0.007	0.055	0.007	0.062	0.007
	[M+2] ⁺	0.028	0.004	0.026	0.004	0.030	0.004
40	[M] ⁺	0.902	0.020	0.909	0.014	0.890	0.008
	[M+1] ⁺	0.065	0.013	0.061	0.008	0.073	0.006
	[M+2] ⁺	0.033	0.007	0.031	0.005	0.037	0.002
50	[M] ⁺	0.894	0.020	0.893	0.014	0.883	0.011
	[M+1] ⁺	0.071	0.013	0.071	0.009	0.077	0.008
	[M+2] ⁺	0.035	0.007	0.037	0.005	0.040	0.003
60	[M] ⁺	0.867	0.023	0.891	0.022	0.864	0.020
	[M+1] ⁺	0.088	0.015	0.073	0.014	0.091	0.013
	[M+2] ⁺	0.045	0.008	0.036	0.008	0.045	0.007
90	[M] ⁺	0.849	0.017	0.863	0.014	0.837	0.024
	[M+1] ⁺	0.100	0.011	0.091	0.010	0.108	0.014
	[M+2] ⁺	0.051	0.006	0.046	0.005	0.056	0.010

Labeling time (s)	Isotopomer	No treatment		DMSO		Imazapyr	
		AM	SD	AM	SD	AM	SD
120	[M] ⁺	0.844	0.037	0.865	0.034	0.838	0.025
	[M+1] ⁺	0.103	0.025	0.089	0.022	0.108	0.016
	[M+2] ⁺	0.054	0.012	0.046	0.012	0.054	0.009
150	[M] ⁺	0.841	0.027	0.858	0.020	0.818	0.021
	[M+1] ⁺	0.105	0.018	0.094	0.013	0.118	0.014
	[M+2] ⁺	0.054	0.009	0.048	0.007	0.063	0.008
180	[M] ⁺	0.839	0.013	0.846	0.023	0.834	0.019
	[M+1] ⁺	0.107	0.010	0.102	0.015	0.108	0.012
	[M+2] ⁺	0.054	0.003	0.051	0.008	0.058	0.008
300	[M] ⁺	0.842	0.020	0.819	0.014	0.821	0.061
	[M+1] ⁺	0.105	0.013	0.119	0.009	0.119	0.040
	[M+2] ⁺	0.053	0.007	0.061	0.005	0.061	0.021
420	[M] ⁺	0.816	0.056	0.829	0.029	0.760	0.139
	[M+1] ⁺	0.122	0.037	0.112	0.020	0.151	0.075
	[M+2] ⁺	0.062	0.019	0.059	0.010	0.089	0.064
600	[M] ⁺	0.806	0.036	0.830	0.039	0.787	0.027
	[M+1] ⁺	0.127	0.024	0.111	0.025	0.140	0.017
	[M+2] ⁺	0.067	0.012	0.059	0.015	0.073	0.010
1800	[M] ⁺	0.787	0.044	0.751	0.033	0.741	0.037
	[M+1] ⁺	0.140	0.029	0.164	0.021	0.171	0.023
	[M+2] ⁺	0.073	0.015	0.085	0.012	0.088	0.014

Table A9. 65 Mass isotopomer distribution of fructose 6-phosphate, measured by LC-MS

Mean values ($n = 5$) of isotopomer abundance are listed. Abbreviations: SD (standard deviation), AM (arithmetic mean).

Labeling time (s)	Isotopomer	No treatment		DMSO		Imazapyr	
		AM	SD	AM	SD	AM	SD
0	[M] ⁺	0.911	0.007	0.889	0.019	0.745	0.307
	[M+1] ⁺	0.071	0.006	0.074	0.007	0.079	0.014
	[M+2] ⁺	0.013	0.001	0.019	0.003	0.053	0.067
	[M+3] ⁺	0.001	0.000	0.001	0.001	0.036	0.074
	[M+4] ⁺	0.002	0.001	0.005	0.002	0.032	0.058
	[M+5] ⁺	0.000	0.000	0.001	0.001	0.016	0.033
	[M+6] ⁺	0.001	0.000	0.011	0.014	0.039	0.063
10	[M] ⁺	0.625	0.043	0.585	0.021	0.599	0.040
	[M+1] ⁺	0.245	0.027	0.254	0.009	0.244	0.017
	[M+2] ⁺	0.105	0.012	0.121	0.018	0.115	0.019
	[M+3] ⁺	0.018	0.004	0.023	0.004	0.022	0.009
	[M+4] ⁺	0.005	0.001	0.007	0.002	0.008	0.003
	[M+5] ⁺	0.001	0.000	0.002	0.000	0.002	0.001
	[M+6] ⁺	0.001	0.000	0.008	0.007	0.009	0.006

Labeling time (s)	Isotopomer	No treatment		DMSO		Imazapyr	
		AM	SD	AM	SD	AM	SD
20	[M] ⁺	0.519	0.022	0.454	0.042	0.477	0.043
	[M+1] ⁺	0.227	0.011	0.243	0.028	0.232	0.008
	[M+2] ⁺	0.168	0.012	0.197	0.017	0.178	0.021
	[M+3] ⁺	0.057	0.006	0.068	0.007	0.069	0.014
	[M+4] ⁺	0.023	0.004	0.026	0.005	0.028	0.007
	[M+5] ⁺	0.004	0.001	0.006	0.002	0.007	0.002
	[M+6] ⁺	0.002	0.000	0.007	0.003	0.008	0.004
30	[M] ⁺	0.453	0.022	0.401	0.043	0.436	0.056
	[M+1] ⁺	0.208	0.015	0.222	0.022	0.198	0.007
	[M+2] ⁺	0.189	0.014	0.197	0.023	0.182	0.025
	[M+3] ⁺	0.093	0.006	0.104	0.011	0.104	0.018
	[M+4] ⁺	0.042	0.007	0.053	0.006	0.055	0.014
	[M+5] ⁺	0.010	0.002	0.015	0.003	0.016	0.003
	[M+6] ⁺	0.004	0.000	0.009	0.002	0.010	0.003
40	[M] ⁺	0.427	0.052	0.373	0.049	0.398	0.046
	[M+1] ⁺	0.169	0.009	0.182	0.013	0.173	0.012
	[M+2] ⁺	0.184	0.020	0.194	0.023	0.184	0.017
	[M+3] ⁺	0.120	0.018	0.130	0.013	0.122	0.014
	[M+4] ⁺	0.070	0.014	0.084	0.006	0.081	0.015
	[M+5] ⁺	0.021	0.005	0.025	0.003	0.026	0.004
	[M+6] ⁺	0.008	0.002	0.013	0.002	0.016	0.003
50	[M] ⁺	0.413	0.038	0.356	0.045	0.370	0.029
	[M+1] ⁺	0.141	0.008	0.145	0.012	0.152	0.015
	[M+2] ⁺	0.173	0.018	0.183	0.023	0.173	0.008
	[M+3] ⁺	0.132	0.010	0.143	0.019	0.144	0.013
	[M+4] ⁺	0.092	0.010	0.106	0.010	0.102	0.012
	[M+5] ⁺	0.034	0.004	0.041	0.003	0.037	0.006
	[M+6] ⁺	0.014	0.001	0.026	0.014	0.022	0.003
60	[M] ⁺	0.361	0.013	0.331	0.030	0.360	0.042
	[M+1] ⁺	0.135	0.011	0.137	0.009	0.133	0.005
	[M+2] ⁺	0.163	0.009	0.174	0.015	0.161	0.009
	[M+3] ⁺	0.153	0.010	0.151	0.012	0.151	0.013
	[M+4] ⁺	0.120	0.014	0.126	0.007	0.118	0.017
	[M+5] ⁺	0.047	0.005	0.053	0.006	0.050	0.009
	[M+6] ⁺	0.021	0.003	0.029	0.005	0.027	0.001
90	[M] ⁺	0.330	0.027	0.289	0.040	0.300	0.033
	[M+1] ⁺	0.100	0.007	0.097	0.006	0.098	0.005
	[M+2] ⁺	0.139	0.015	0.135	0.014	0.133	0.011
	[M+3] ⁺	0.157	0.007	0.157	0.013	0.157	0.008
	[M+4] ⁺	0.152	0.009	0.166	0.015	0.161	0.008
	[M+5] ⁺	0.082	0.005	0.096	0.010	0.096	0.006
	[M+6] ⁺	0.040	0.004	0.060	0.008	0.054	0.003

Labeling time (s)	Isotopomer	No treatment		DMSO		Imazapyr	
		AM	SD	AM	SD	AM	SD
120	[M] ⁺	0.321	0.029	0.288	0.038	0.294	0.026
	[M+1] ⁺	0.082	0.004	0.083	0.011	0.086	0.006
	[M+2] ⁺	0.110	0.007	0.109	0.010	0.110	0.012
	[M+3] ⁺	0.147	0.009	0.147	0.003	0.147	0.006
	[M+4] ⁺	0.168	0.013	0.171	0.017	0.168	0.010
	[M+5] ⁺	0.109	0.012	0.122	0.024	0.118	0.008
	[M+6] ⁺	0.062	0.006	0.082	0.016	0.077	0.004
150	[M] ⁺	0.293	0.031	0.299	0.027	0.293	0.054
	[M+1] ⁺	0.066	0.005	0.070	0.004	0.068	0.003
	[M+2] ⁺	0.088	0.011	0.091	0.010	0.090	0.007
	[M+3] ⁺	0.142	0.017	0.135	0.013	0.135	0.014
	[M+4] ⁺	0.172	0.009	0.172	0.006	0.170	0.014
	[M+5] ⁺	0.150	0.002	0.135	0.005	0.145	0.018
	[M+6] ⁺	0.090	0.014	0.097	0.005	0.098	0.013
180	[M] ⁺	0.322	0.028	0.291	0.029	0.269	0.017
	[M+1] ⁺	0.062	0.006	0.063	0.003	0.068	0.007
	[M+2] ⁺	0.073	0.007	0.077	0.011	0.087	0.007
	[M+3] ⁺	0.126	0.010	0.127	0.008	0.134	0.007
	[M+4] ⁺	0.169	0.011	0.165	0.011	0.171	0.007
	[M+5] ⁺	0.154	0.016	0.162	0.009	0.162	0.010
	[M+6] ⁺	0.094	0.013	0.115	0.012	0.110	0.009
300	[M] ⁺	0.303	0.014	0.279	0.016	0.366	0.188
	[M+1] ⁺	0.054	0.004	0.055	0.005	0.061	0.011
	[M+2] ⁺	0.053	0.005	0.061	0.012	0.062	0.011
	[M+3] ⁺	0.104	0.005	0.103	0.011	0.092	0.027
	[M+4] ⁺	0.162	0.006	0.160	0.013	0.139	0.049
	[M+5] ⁺	0.193	0.008	0.198	0.015	0.162	0.074
	[M+6] ⁺	0.132	0.016	0.144	0.023	0.118	0.051
420	[M] ⁺	0.294	0.034	0.279	0.028	0.277	0.079
	[M+1] ⁺	0.045	0.003	0.052	0.004	0.055	0.005
	[M+2] ⁺	0.043	0.001	0.054	0.008	0.061	0.017
	[M+3] ⁺	0.086	0.007	0.094	0.011	0.084	0.026
	[M+4] ⁺	0.159	0.009	0.155	0.013	0.148	0.009
	[M+5] ⁺	0.224	0.029	0.207	0.009	0.166	0.062
	[M+6] ⁺	0.148	0.010	0.159	0.014	0.207	0.144
600	[M] ⁺	0.301	0.039	0.270	0.027	0.280	0.041
	[M+1] ⁺	0.043	0.006	0.048	0.002	0.050	0.004
	[M+2] ⁺	0.040	0.004	0.048	0.010	0.054	0.006
	[M+3] ⁺	0.082	0.006	0.087	0.012	0.091	0.011
	[M+4] ⁺	0.157	0.010	0.155	0.012	0.158	0.016
	[M+5] ⁺	0.230	0.018	0.219	0.013	0.212	0.012
	[M+6] ⁺	0.147	0.023	0.173	0.016	0.154	0.011

Labeling time (s)	Isotopomer	No treatment		DMSO		Imazapyr	
		AM	SD	AM	SD	AM	SD
1800	[M] ⁺	0.262	0.020	0.263	0.034	0.248	0.038
	[M+1] ⁺	0.057	0.005	0.065	0.005	0.063	0.006
	[M+2] ⁺	0.053	0.006	0.064	0.008	0.065	0.009
	[M+3] ⁺	0.109	0.017	0.112	0.013	0.112	0.017
	[M+4] ⁺	0.183	0.004	0.174	0.015	0.179	0.017
	[M+5] ⁺	0.222	0.019	0.204	0.011	0.212	0.004
	[M+6] ⁺	0.114	0.017	0.118	0.007	0.122	0.005

Table A9. 66 Amount of carbon translocating to the root in form of displayed metabolites

Amount of assimilated carbon that is recovered inside root amino acids and soluble sugars, in mmol ^{13}C (g DW_{root})⁻¹ h⁻¹, as determined by 4.5.7. Soil-grown rice seedlings at the age of 15 days were labeled with 400 $\mu\text{L L}^{-1}$ $^{13}\text{CO}_2$ for 30 minutes. Root samples were taken at the following time points: 300 and 1800 seconds. Isotopic enrichment was determined by GC-IRMS analyses, concentrations were measured by GC-MS. Enrichment values are provided as mean values ($n = 4$) with corresponding standard deviations. Abbreviations: SD (standard deviation), AM (arithmetic mean), $\delta^{13}\text{C}$ (‰), 300s and 1800s (harvest time after labeling in seconds), DW (dry weight), R (ratio of $^{13}\text{C}/^{12}\text{C}$), ^{12}C (portion of ^{12}C), ^{13}C (portion of ^{13}C). Metabolite abbreviations can be found in Table A9. 1. Amino acid abbreviations are corresponding to three letter code.

Analyte	Analyte concentration (mmol (g DW _{root}) ⁻¹)	300s						1800s						Exported carbon (mmol ^{13}C (gDW _{root}) ⁻¹ h ⁻¹)
		$\delta^{13}\text{C}$ (‰)		R _{sample}	^{12}C	^{13}C	$\delta^{13}\text{C}$ (‰)		R _{sample}	^{12}C	^{13}C			
		AM	SD				AM	SD						
ALA	0.0107	7.10	19.75	0.0113	0.9889	0.0111	5109.29	1126.25	0.0683	0.9361	0.0639	0.4060		
ASN	0.0184	-32.58	18.48	0.0108	0.9893	0.0107	400.14	84.99	0.0157	0.9846	0.0154	0.0834		
ASP	0.0184	10.44	16.29	0.0113	0.9888	0.0112	2477.32	403.19	0.0389	0.9626	0.0374	0.4642		
GLU	0.1146	-22.38	2.02	0.0109	0.9892	0.0108	1115.08	204.48	0.0236	0.9769	0.0231	1.6887		
GLN	0.0444	-25.54	2.39	0.0109	0.9892	0.0108	768.12	191.12	0.0198	0.9806	0.0194	0.4579		
GLY	0.0036	317.72	114.05	0.0147	0.9855	0.0145	8176.94	652.79	0.1026	0.9069	0.0931	0.1357		
ILE	0.0003	-24.95	7.94	0.0109	0.9892	0.0108	479.36	130.17	0.0165	0.9837	0.0163	0.0024		
LEU	0.0004	-36.18	12.91	0.0108	0.9893	0.0107	602.86	176.81	0.0179	0.9824	0.0176	0.0041		
LYS	0.0005	-9.28	5.77	0.0111	0.9890	0.0110	2024.35	348.02	0.0338	0.9673	0.0327	0.0141		
MET	0.0003	20.07	27.47	0.0114	0.9887	0.0113	2821.09	1024.12	0.0427	0.9590	0.0410	0.0117		
PHE	0.0004	-13.85	3.58	0.0110	0.9891	0.0109	2124.89	342.08	0.0349	0.9662	0.0338	0.0202		
PRO	0.0007	-19.02	3.79	0.0110	0.9892	0.0108	241.91	125.92	0.0139	0.9863	0.0137	0.0024		
SER	0.0073	109.72	64.76	0.0124	0.9877	0.0123	11507.49	2172.58	0.1398	0.8773	0.1227	0.5764		
THR	0.0031	-31.58	2.52	0.0108	0.9893	0.0107	706.90	126.81	0.0191	0.9813	0.0187	0.0237		
TYR	0.0006	-1.43	11.34	0.0112	0.9890	0.0110	3338.63	424.09	0.0485	0.9537	0.0463	0.0471		
VAL	0.0011	-28.05	2.83	0.0109	0.9893	0.0107	1660.40	381.80	0.0297	0.9711	0.0289	0.0241		
FRC	0.0618	-27.77	2.44	0.0109	0.9892	0.0108	1132.87	84.63	0.0238	0.9767	0.0233	1.1157		
GLC	0.0079	-22.27	3.86	0.0109	0.9892	0.0108	3746.32	630.23	0.0531	0.9496	0.0504	0.4499		
INO	0.0008	-34.49	3.35	0.0108	0.9893	0.0107	840.89	108.13	0.0206	0.9798	0.0202	0.0109		

Analyte	Analyte concentration (mmol (g DW _{root}) ⁻¹)	300s					1800s					Exported carbon (mmol ¹³ C (gDW _{root}) ⁻¹ h ⁻¹)
		d 13C/12C (‰)		R _{sample}	¹² C	¹³ C	d 13C/12C (‰)		R _{sample}	¹² C	¹³ C	
		AM	SD				AM	SD				
SUCR	0.0538	-22.53	1.85	0.0109	0.9892	0.0108	9383.68	604.39	0.1161	0.8960	0.1040	14.4379

Table A9. 67 Flux values of untreated rice seedlings

Flux values of a 15 day old soil-grown rice seedling, as determined by ¹³C INST-MFA. The flux values are expressed as mmol (100 mmol CO₂)⁻¹ (mol%). The boundaries of the 95% confidence intervals and the standard deviation were derived by parameter continuation. Abbreviations: r (reaction), net (net flux), exch (exchange flux), val (flux value), lb (lower boundary), ub (upper boundary), std (standard deviation). The biomass formation equation (R6) is as follows: 0.1543*P_{YR}.cp + 0.2704*A_{KG}.m + 0.4111*P_{5P}.p + 0.1299*O_{AA}.c + 0.0433*3P_G.cp + 0.0198*F_{6P}.cp + 0.3397*G_{6P}.cp + 0.1445*G_{AP}.cp + 0.0055*C_{IT}.m + 0.0012*S_{UCC}.m + 0.0342*M_{AL}.m + 0.0206*F_{RC}.cp + 0.6429*G_{LC}.cp + 0.1765*sucrose.cp + 0.0377*starch.p + 0.2064*alanine.c + 0.1417*arginine.c + 0.2143*aspar.c + 0.0171*cysteine.p + 0.2719*glutamate.m + 0.2305*glycine.p + 0.0483*histidine.p + 0.1019*isoleucine.p + 0.2043*leucine.p + 0.1225*lysine.p + 0.0334*methionine.p + 0.4913*phenylalanine.p + 0.1275*proline.c + 0.1422*serine.p + 0.1266*threonine.p + 0.2885*tyrosine.p + 0.1537*valine.p + 0.054*tryptophane.p + 0.0098*C₁₆.p + 0.0573*C₁₈.p + 0.001075*C₂₀.p -> biomass.

Reaction number	Reaction	No treatment			
		val	lb	ub	std
'R1'	CO ₂ in.p -> CO ₂ EX.p	91.52	91.41	91.85	0.11
'R2'	12CO ₂ in.p -> CO ₂ in.p	5.90	5.41	6.21	0.20
'R3'	13CO ₂ in.p -> CO ₂ in.p	85.56	85.19	86.02	0.21
'R4'	CO ₂ .p -> CO ₂ EX.p	8.48	8.15	8.59	0.11
'R5'	CO ₂ .p -> CO ₂ sink.s	0.19	0.00	0.43	0.11
'R6'	Biomass formation	2.68	2.68	2.68	0.00
'R7 net'	G _{6P} .cp -> F _{6P} .cp	-3.49	-3.60	-3.45	0.04
'R7 exch'	F _{6P} .cp -> G _{6P} .cp	NaN	127.10	Inf	FALSE
'R8 net'	F _{BP} .cp -> F _{6P} .cp	4.08	4.04	4.18	0.04
'R8 exch'	F _{6P} .cp -> F _{BP} .cp	3.89	3.53	5.01	0.38
'R9 net'	F _{BP} .cp -> D _{HAP} .cp + G _{AP} .cp	-4.08	-4.18	-4.04	0.04
'R9 exch'	D _{HAP} .cp + G _{AP} .cp -> F _{BP} .cp	0.56	0.00	1.22	0.31
'R10 net'	G _{AP} .cp -> D _{HAP} .cp	73.00	72.86	73.42	0.14
'R10 exch'	D _{HAP} .cp -> G _{AP} .cp	NaN	0.00	Inf	FALSE
'R11 net'	G _{AP} .cp -> 3P _G .cp	-182.16	-183.21	-181.85	0.35
'R11 exch'	3P _G .cp -> G _{AP} .cp	427.30	320.11	1013.80	176.96
'R12 net'	3P _G .cp -> 2P _G .cp	18.02	17.81	18.11	0.08

Reaction number	Reaction	No treatment			
		val	lb	ub	std
'R12 exch'	2PG.cp -> 3PG.cp	21.08	16.90	24.22	1.87
'R13 net'	2PG.cp -> PEP.cp	18.02	17.81	18.11	0.08
'R13 exch'	PEP.cp -> 2PG.cp	NaN	1251.27	Inf	FALSE
'R14 net'	PYR.cp -> PEP.cp	-15.42	-19.52	-7.34	3.11
'R14 exch'	PEP.cp -> PYR.cp	5.21	0.00	10.87	2.77
'R15'	PYR.cp -> ACCOA.p + CO2.p	2.17	2.17	2.17	0.00
'R16'	G6P.cp -> 6PG.cp	0.05	0.00	0.15	0.04
'R17'	6PG.cp -> P5P.p + CO2.p	0.05	0.00	0.15	0.04
'R18 net'	GAP.cp + S7P.p -> E4P.p + F6P.p	35.90	35.80	36.10	0.08
'R18 exch'	E4P.p + F6P.p -> GAP.cp + S7P.p	NaN	30.55	Inf	FALSE
'R19 net'	E4P.p + P5P.p -> F6P.p + GAP.cp	-35.90	-36.10	-35.80	0.08
'R19 exch'	F6P.p + GAP.cp -> E4P.p + P5P.p	NaN	112.00	Inf	FALSE
'R20 net'	GAP.cp + S7P.p -> P5P.p + P5P.p	33.06	32.97	33.27	0.08
'R20 exch'	P5P.p + P5P.p -> GAP.cp + S7P.p	0.57	0.00	1.02	0.26
'R21'	P5P.p -> RBP.p	100.70	100.50	101.30	0.20
'R22'	CO2EX.p + RBP.p -> 3PG.cp + 3PG.cp	100.00	100.00	100.00	0.00
'R23'	DHAP.cp + E4P.p -> S7P.p	68.96	68.77	69.37	0.15
'R24'	RBP.p -> GLYCO.pg + 3PG.cp	0.70	0.50	1.30	0.20
'R25'	GLYCO.pg -> GLYOX.g	0.70	0.50	1.30	0.20
'R26'	GLYOX.g + serine.p -> glycine.p + GLYCER.pg	0.13	0.00	0.86	0.22
'R27'	GLYCER.pg -> 3PG.cp	0.13	0.00	0.86	0.22
'R28'	sucrose.r -> zzzzzzzzzzzzzSink	0.47	0.46	0.49	0.01
R29 net'	OAA.c -> CO2.p + PEP.cp	-0.10	-7.08	5.10	3.11
R29 exch'	OAA.c <- CO2.p + PEP.cp	22.84	13.83	28.09	3.64

Reaction number	Reaction	No treatment			
		val	lb	ub	std
'R30 net'	MAL.p -> PYR.cp + CO2.p	-25.42	-45.25	0.88	11.77
'R30 exch'	PYR.cp + CO2.p -> MAL.p	21.38	11.05	33.84	5.81
'R31 net'	MAL.m -> MAL.c	-19.92	-39.56	-1.83	9.62
'R31 exch'	MAL.c -> MAL.m	NaN	0.00	Inf	FALSE
'R32 net'	PYR.m -> PYR.cp	7.22	-2.71	34.63	9.52
'R32 exch'	PYR.cp -> PYR.m	NaN	0.00	Inf	FALSE
'R33 net'	OAA.m + CIT.c -> OAA.c + CIT.m	0.00	0.00	0.00	0.00
'R33 exch'	OAA.c + CIT.m -> OAA.m + CIT.c	0.60	0.00	1.89	0.48
'R34 net'	MAL.m + OAA.c -> MAL.c + OAA.m	-2.49	-9.48	2.71	3.11
'R34 exch'	MAL.c + OAA.m -> MAL.m + OAA.c	10.12	5.02	18.82	3.52
'R35 net'	MAL.c -> MAL.p	-25.42	-45.25	0.88	11.77
'R35 exch'	MAL.p -> MAL.c	NaN	0.00	NaN	FALSE
'R36'	PYR.m -> ACCOA.m + CO2.p	2.62	2.40	2.71	0.08
'R37'	OAA.m + ACCOA.m -> CIT.m	2.62	2.40	2.71	0.08
'R38 net'	CIT.m -> AKG.m + CO2.p	2.60	2.39	2.69	0.08
'R38 exch'	AKG.m + CO2.p -> CIT.m	NaN	0.00	Inf	FALSE
'R39'	AKG.m -> SUCC.m + CO2.p	0.50	0.29	0.59	0.08
'R40'	SUCC.m -> FUM.m	0.50	0.28	0.59	0.08
'R41'	FUM.m -> MAL.m	0.88	0.66	0.97	0.08
'R42'	MAL.m -> OAA.m	8.08	0.00	12.19	3.11
'R43'	MAL.m -> CO2.p + PYR.m	18.09	0.00	37.73	9.62
'R44'	G6P.cp -> starch.p	0.10	0.10	0.10	0.00
'R45'	G6P.cp -> INO.cp	0.00	0.00	0.00	0.00
'R46'	G6P.cp -> GLC.cp	6.85	6.31	7.42	0.28

Reaction number	Reaction	No treatment			
		val	lb	ub	std
'R47'	GLC.cp -> G6P.cp	4.96	4.42	5.54	0.28
'R48'	F6P.cp -> FRC.cp	0.06	0.06	0.06	0.00
'R49'	G6P.cp + F6P.cp -> sucrose.cp	0.48	0.47	0.50	0.01
'R50'	sucrose.cp -> sucrose.r	0.47	0.46	0.49	0.01
'R51'	8*ACCOA.p -> C16.p	0.03	0.03	0.03	0.00
'R52'	9*ACCOA.p -> C18.p	0.15	0.15	0.15	0.00
'R53'	10*ACCOA.p -> C20.p	0.00	0.00	0.00	0.00
'R54'	3PG.cp -> serine.p	0.10	0.03	0.33	0.08
'R55'	3PG.cp -> cysteine.p	0.05	0.05	0.05	0.00
'R56'	3PG.cp -> glycine.p + CO2.p	0.32	0.22	0.61	0.10
'R57'	GLYOX.g -> glycine.p	0.51	0.44	0.54	0.03
'R58'	glycine.p -> zzMTHF.p + CO2.p	0.21	0.07	0.65	0.15
'R59'	glycine.p + zzMTHF.p -> serine.p	0.21	0.07	0.65	0.15
'R60'	PYR.cp + glutamate.m -> alanine.c + AKG.m	0.58	0.58	0.58	0.00
'R61'	PYR.cp + PYR.cp + glutamate.m -> valine.p + AKG.m + CO2.p	0.41	0.41	0.41	0.00
'R62'	PYR.cp + PYR.cp + ACCOA.p + glutamate.m -> leucine.p + CO2.p + CO2.p + AKG.m	0.55	0.55	0.55	0.00
'R63'	OAA.c + glutamate.m -> aspar.c + AKG.m	0.24	0.00	0.62	0.16
'R64'	OAA.c -> aspar.c	0.39	0.00	0.62	0.16
'R65'	P5P.p + CO2.p + glutamate.m -> histidine.p + AKG.m	0.13	0.13	0.13	0.00
'R66'	AKG.m -> proline.c	0.34	0.34	0.34	0.00
'R67'	AKG.m + glutamate.m + OAA.c + CO2.p -> arginine.c + AKG.m + FUM.m	0.38	0.38	0.38	0.00
'R68'	OAA.c + PYR.cp + glutamate.m -> lysine.p + CO2.p + AKG.m	0.33	0.33	0.33	0.00
'R69'	OAA.c -> threonine.p	0.35	0.35	0.35	0.00
'R70'	OAA.c + PYR.cp + glutamate.m -> isoleucine.p + CO2.p + AKG.m	0.27	0.27	0.27	0.00

Reaction number	Reaction	No treatment			
		val	lb	ub	std
'R71'	OAA.c + 3PG.cp + CO2.p -> methionine.p + PYR.cp	0.09	0.09	0.09	0.00
'R72'	E4P.p + PEP.cp + PEP.cp + glutamate.m -> tyrosine.p + CO2.p + AKG.m	0.77	0.77	0.77	0.00
'R73'	E4P.p + PEP.cp + PEP.cp + glutamate.m -> phenylalanine.p + CO2.p + AKG.m	2.06	2.06	2.06	0.00
'R74'	AKG.m -> glutamate.m	6.58	6.34	6.97	0.16
'R75'	E4P.p + PEP.cp + PEP.cp + P5P.p + 3PG.cp + glutamate.m -> CO2.p + tryptophane.p + PYR.cp + GAP.cp + AKG.m	0.00	0.00	0.00	0.00

Table A9. 68 Flux values of DMSO-treated rice seedlings and imazapyr-treated rice seedlings

Flux values of a 15 day old soil-grown rice seedling, as determined by ¹³C INST-MFA. The flux values are expressed as mmol (100 mmol CO₂)⁻¹ (mol%). The boundaries of the 95% confidence intervals and the standard deviation were derived by parameter continuation. Abbreviations: r (reaction), net (net flux), exch (exchange flux), val (flux value), lb (lower boundary), ub (upper boundary), std (standard deviation). The biomass formation equation (R6) is as follows: 0.1543*PYR.cp + 0.2704*AKG.m + 0.4111*P5P.p + 0.1299*OAA.c + 0.0433*3PG.cp + 0.0198*F6P.cp + 0.3397*G6P.cp + 0.1445*GAP.cp + 0.0055*CIT.m + 0.0012*SUCC.m + 0.0342*MAL.m + 0.0206*FRC.cp + 0.6429*GLC.cp + 0.1765*sucrose.cp + 0.0377*starch.p + 0.2064*alanine.c + 0.1417*arginine.c + 0.2143*aspar.c + 0.0171*cysteine.p + 0.2719*glutamate.m + 0.2305*glycine.p + 0.0483*histidine.p + 0.1019*isoleucine.p + 0.2043*leucine.p + 0.1225*lysine.p + 0.0334*methionine.p + 0.4913*phenylalanine.p + 0.1275*proline.c + 0.1422*serine.p + 0.1266*threonine.p + 0.2885*tyrosine.p + 0.1537*valine.p + 0.054*tryptophane.p + 0.0098*C16.p + 0.0573*C18.p + 0.001075*C20.p -> biomass.

Reaction number	Reaction	DMSO				IMAZAPYR			
		val	lb	ub	std	val	lb	ub	std
'R1'	CO2in.p -> CO2EX.p	93.13	91.82	95.37	0.90	92.78	92.62	93.28	0.17
'R2'	12CO2in.p -> CO2in.p	5.02	3.99	5.73	0.44	5.11	4.58	5.53	0.24
'R3'	13CO2in.p -> CO2in.p	88.33	86.41	90.20	0.97	87.66	87.11	88.25	0.29
'R4'	CO2.p -> CO2EX.p	6.87	4.63	8.18	0.90	7.22	6.72	7.38	0.17
'R5'	CO2.p -> CO2sink.s	2.31	0.00	3.55	0.91	0.29	0.00	0.65	0.17
'R6'	Biomass formation	2.68	2.68	2.68	0.00	2.68	2.68	2.68	0.00
'R7 net'	G6P.cp -> F6P.cp	-3.64	-4.32	-3.38	0.24	-3.60	-3.69	-3.50	0.05
'R7 exch'	F6P.cp -> G6P.cp								
'R8 net'	FBP.cp -> F6P.cp	4.05	3.93	4.10	0.04	4.21	4.11	4.30	0.05
'R8 exch'	F6P.cp -> FBP.cp								
'R9 net'	FBP.cp -> DHAP.cp + GAP.cp	-4.05	-4.10	-3.93	0.04	-4.21	-4.30	-4.11	0.05
'R9 exch'	DHAP.cp + GAP.cp -> FBP.cp								
'R10 net'	GAP.cp -> DHAP.cp	73.26	72.92	73.64	0.18	73.21	73.13	73.34	0.05
'R10 exch'	DHAP.cp -> GAP.cp								
'R11 net'	GAP.cp -> 3PG.cp	-182.68	-183.82	-182.04	0.45	-182.67	-182.97	-182.45	0.13
'R11 exch'	3PG.cp -> GAP.cp								
'R12 net'	3PG.cp -> 2PG.cp	17.89	17.62	17.95	0.09	17.60	17.55	17.62	0.02

Reaction number	Reaction	DMSO				IMAZAPYR			
		val	lb	ub	std	val	lb	ub	std
'R12 exch'	2PG.cp -> 3PG.cp								
'R13 net'	2PG.cp -> PEP.cp	17.89	17.62	17.95	0.09	17.60	17.55	17.62	0.02
'R13 exch'	PEP.cp -> 2PG.cp								
'R14 net'	PYR.cp -> PEP.cp	-8.13	-9.64	-7.54	0.54	-8.04	-8.88	-7.55	0.34
'R14 exch'	PEP.cp -> PYR.cp	15.53	8.43	18.89	2.67	5.96	4.80	14.37	2.44
'R15'	PYR.cp -> ACCOA.p + CO2.p	2.23	2.23	2.23	0.00	2.29	2.29	2.29	0.00
'R16'	G6P.cp -> 6PG.cp	0.45	0.00	0.94	0.24	0.08	0.00	0.22	0.06
'R17'	6PG.cp -> P5P.p + CO2.p	0.45	0.00	0.94	0.24	0.08	0.00	0.22	0.06
'R18 net'	GAP.cp + S7P.p -> E4P.p + F6P.p	35.98	35.63	36.26	0.16	35.91	35.84	36.00	0.04
'R18 exch'	E4P.p + F6P.p -> GAP.cp + S7P.p								
'R19 net'	E4P.p + P5P.p -> F6P.p + GAP.cp	-35.98	-36.26	-35.63	0.16	-35.91	-36.00	-35.84	0.04
'R19 exch'	F6P.p + GAP.cp -> E4P.p + P5P.p								
'R20 net'	GAP.cp + S7P.p -> P5P.p + P5P.p	33.16	32.82	33.45	0.16	33.14	33.07	33.23	0.04
'R20 exch'	P5P.p + P5P.p -> GAP.cp + S7P.p								
'R21'	P5P.p -> RBP.p	101.09	100.76	101.84	0.28	100.98	100.83	101.15	0.08
'R22'	CO2EX.p + RBP.p -> 3PG.cp + 3PG.cp	100.00	100.00	100.00	0.00	100.00	100.00	100.00	0.00
'R23'	DHAP.cp + E4P.p -> S7P.p	69.14	68.45	69.71	0.32	69.05	68.91	69.23	0.08
'R24'	RBP.p -> GLYCO.pg + 3PG.cp	1.09	0.76	1.84	0.28	0.98	0.83	1.15	0.08
'R25'	GLYCO.pg -> GLYOX.g	1.09	0.76	1.84	0.28	0.98	0.83	1.15	0.08
'R26'	GLYOX.g + serine.p -> glycine.p + GLYCER.pg	0.54	0.00	1.01	0.26	0.06	0.00	0.22	0.06
'R27'	GLYCER.pg -> 3PG.cp	0.54	0.00	1.01	0.26	0.06	0.00	0.22	0.06
'R28'	sucrose.r -> zzzzzzzzzzzzzSink	0.43	0.43	0.51	0.02	0.50	0.50	0.51	0.00
R29 net'	OAA.c -> CO2.p + PEP.cp	-4.22	-4.80	-2.28	0.64	-4.29	-4.55	-3.93	0.16
R29 exch'	OAA.c <- CO2.p + PEP.cp								

Reaction number	Reaction	DMSO				IMAZAPYR			
		val	lb	ub	std	val	lb	ub	std
'R30 net'	MAL.p -> PYR.cp + CO2.p	0.45	0.01	0.54	0.13	0.14	-0.13	0.29	0.11
'R30 exch'	PYR.cp + CO2.p -> MAL.p								
'R31 net'	MAL.m -> MAL.c	-2.92	-4.00	-1.85	0.55	-2.13	-2.53	-1.89	0.16
'R31 exch'	MAL.c -> MAL.m								
'R32 net'	PYR.m -> PYR.cp	-1.98	-2.40	-0.43	0.50	-2.16	-2.17	-2.15	0.01
'R32 exch'	PYR.cp -> PYR.m								
'R33 net'	OAA.m + CIT.c -> OAA.c + CIT.m	0.00	0.00	0.00	0.00	0.00	0.00	0.00	0.00
'R33 exch'	OAA.c + CIT.m -> OAA.m + CIT.c								
'R34 net'	MAL.m + OAA.c -> MAL.c + OAA.m	1.85	0.02	2.39	0.61	1.91	1.56	2.17	0.16
'R34 exch'	MAL.c + OAA.m -> MAL.m + OAA.c								
'R35 net'	MAL.c -> MAL.p	0.45	0.01	0.54	0.13	0.14	-0.13	0.29	0.11
'R35 exch'	MAL.p -> MAL.c								
'R36'	PYR.m -> ACCOA.m + CO2.p	2.33	2.05	2.39	0.09	2.15	2.10	2.17	0.02
'R37'	OAA.m + ACCOA.m -> CIT.m	2.33	2.05	2.39	0.09	2.15	2.10	2.17	0.02
'R38 net'	CIT.m -> AKG.m + CO2.p	2.31	2.03	2.37	0.09	2.13	2.08	2.16	0.02
'R38 exch'	AKG.m + CO2.p -> CIT.m								
'R39'	AKG.m -> SUCC.m + CO2.p	0.28	0.00	0.34	0.09	0.06	0.00	0.08	0.02
'R40'	SUCC.m -> FUM.m	0.27	0.00	0.34	0.09	0.06	0.00	0.08	0.02
'R41'	FUM.m -> MAL.m	0.58	0.30	0.64	0.09	0.36	0.30	0.38	0.02
'R42'	MAL.m -> OAA.m	0.59	0.00	2.11	0.54	0.65	0.00	1.89	0.48
'R43'	MAL.m -> CO2.p + PYR.m	1.07	0.00	2.16	0.55	0.24	0.00	0.64	0.16
'R44'	G6P.cp -> starch.p	0.07	0.07	0.07	0.00	0.12	0.12	0.12	0.00
'R45'	G6P.cp -> INO.cp	0.00	0.00	0.00	0.00	0.00	0.00	0.00	0.00
'R46'	G6P.cp -> GLC.cp	6.65	5.47	8.50	0.77	8.41	5.57	12.05	1.65

Reaction number	Reaction	DMSO				IMAZAPYR			
		val	lb	ub	std	val	lb	ub	std
'R47'	GLC.cp -> G6P.cp	4.76	3.58	6.61	0.77	6.52	3.68	10.16	1.65
'R48'	F6P.cp -> FRC.cp	0.05	0.05	0.05	0.00	0.05	0.05	0.05	0.00
'R49'	G6P.cp + F6P.cp -> sucrose.cp	0.49	0.43	0.51	0.02	0.51	0.50	0.51	0.00
'R50'	sucrose.cp -> sucrose.r	0.43	0.43	0.51	0.02	0.50	0.50	0.51	0.00
'R51'	8*ACCOA.p -> C16.p	0.03	0.03	0.03	0.00	0.03	0.03	0.03	0.00
'R52'	9*ACCOA.p -> C18.p	0.16	0.16	0.16	0.00	0.16	0.16	0.16	0.00
'R53'	10*ACCOA.p -> C20.p	0.00	0.00	0.00	0.00	0.00	0.00	0.00	0.00
'R54'	3PG.cp -> serine.p	0.31	0.10	0.51	0.10	0.13	0.09	0.19	0.03
'R55'	3PG.cp -> cysteine.p	0.04	0.04	0.04	0.00	0.10	0.10	0.10	0.00
'R56'	3PG.cp -> glycine.p + CO2.p	0.56	0.32	0.83	0.13	0.33	0.29	0.34	0.01
'R57'	GLYOX.g -> glycine.p	0.76	0.65	0.91	0.07	0.88	0.83	0.94	0.03
'R58'	glycine.p -> zzMTHF.p + CO2.p	0.54	0.26	0.94	0.17	0.33	0.28	0.44	0.04
'R59'	glycine.p + zzMTHF.p -> serine.p	0.54	0.26	0.94	0.17	0.33	0.28	0.44	0.04
'R60'	PYR.cp + glutamate.m -> alanine.c + AKG.m	0.61	0.61	0.61	0.00	0.61	0.61	0.61	0.00
'R61'	PYR.cp + PYR.cp + glutamate.m -> valine.p + AKG.m + CO2.p	0.43	0.43	0.43	0.00	0.41	0.41	0.41	0.00
'R62'	PYR.cp + PYR.cp + ACCOA.p + glutamate.m -> leucine.p + CO2.p + CO2.p + AKG.m	0.56	0.56	0.56	0.00	0.55	0.55	0.55	0.00
'R63'	OAA.c + glutamate.m -> aspar.c + AKG.m	0.45	0.00	0.67	0.17	0.15	0.00	0.67	0.17
'R64'	OAA.c -> aspar.c	0.22	0.00	0.67	0.17	0.52	0.00	0.67	0.17
'R65'	P5P.p + CO2.p + glutamate.m -> histidine.p + AKG.m	0.13	0.13	0.13	0.00	0.13	0.13	0.13	0.00
'R66'	AKG.m -> proline.c	0.35	0.35	0.35	0.00	0.34	0.34	0.34	0.00
'R67'	AKG.m + glutamate.m + OAA.c + CO2.p -> arginine.c + AKG.m + FUM.m	0.30	0.30	0.30	0.00	0.30	0.30	0.30	0.00
'R68'	OAA.c + PYR.cp + glutamate.m -> lysine.p + CO2.p + AKG.m	0.35	0.35	0.35	0.00	0.34	0.34	0.34	0.00
'R69'	OAA.c -> threonine.p	0.35	0.35	0.35	0.00	0.35	0.35	0.35	0.00

Reaction number	Reaction	DMSO				IMAZAPYR			
		val	lb	ub	std	val	lb	ub	std
'R70'	OAA.c + PYR.cp + glutamate.m -> isoleucine.p + CO2.p + AKG.m	0.28	0.28	0.28	0.00	0.28	0.28	0.28	0.00
'R71'	OAA.c + 3PG.cp + CO2.p -> methionine.p + PYR.cp	0.09	0.09	0.09	0.00	0.09	0.09	0.09	0.00
'R72'	E4P.p + PEP.cp + PEP.cp + glutamate.m -> tyrosine.p + CO2.p + AKG.m	0.78	0.78	0.78	0.00	0.73	0.73	0.73	0.00
'R73'	E4P.p + PEP.cp + PEP.cp + glutamate.m -> phenylalanine.p + CO2.p + AKG.m	2.04	2.04	2.04	0.00	2.03	2.03	2.03	0.00
'R74'	AKG.m -> glutamate.m	6.77	6.33	7.00	0.17	6.43	6.28	6.95	0.17
'R75'	E4P.p + PEP.cp + PEP.cp + P5P.p + 3PG.cp + glutamate.m -> CO2.p + tryptophane.p + PYR.cp + GAP.cp + AKG.m	0.00	0.00	0.00	0.00	0.00	0.00	0.00	0.00